A·S·P·E·N

Center for Physics

ASPEN WINTER CONFERENCE ON GRAVITATIONAL WAVES AND THEIR DETECTION

JANUARY 26-FEBRUARY 1, 1997

ADVANCED DETECTOR RESEARCH AND DEVELOPMENT

EDITOR: SYDNEY MESHKOV

LIGO-G970195-00-M

PROGRAM
ASPEN WINTER CONFERENCE ON GRAVITATIONAL WAVES AND THEIR DETECTION

Aspen Center for Physics
January 26 - February 1, 1997

Monday AM: Status of Present Detectors
January 27 Chair: S. Meshkov

8:00	S. Meshkov(Caltech) Jane Kelly(ACP)	Welcome
8:10	A. Giazotto(Pisa)	Status of Virgo
8.35	Discussion	
8:45	J. Hough(Glasgow)	Status of GEO 600
9:10	Discussion	
9:20	Coffee Break	
9:35	D. Shoemaker(MIT)	Status of LIGO
10:00	Discussion	
10:10	W. Hamilton(LSU)	Status of Bar Detectors
10:35	Discussion	

Monday PM: A. Advanced Interferometers and Detectors
January 27 Chair: R. Schilling

4:30	M. Fejer(Stanford)	Topologies for Advanced Detectors
4:55	Discussion	
5:05	R. Flaminio(Annecy)	Virgo Plans for a Long Term R&D Program
5:30	Discussion	
5:40	Coffee Break	

B. Collaboration Formation for Advanced Detectors I
Chair: M. Coles

6:00	G. Sanders(Caltech)	Introductory Remarks
6:30	Discussion	
6:40	Round Table Discussion	Finn, Flaminio, Gustafson, Reitze, Ruediger, Sanders, Stebbins, Ward

Tuesday AM: A. Advanced Interferometry
January 28 Chair: R. Drever

8:00	A. Ruediger(Garching)	The Sagnac Interferometer - Pro and Con
8:25	Discussion	
8:35	D. Schnier(Garching)	Resonance Coincidence Method-A New Locking Scheme for Narrow Band Dual Recycling
9:00	Discussion	
9:10	Coffee Break	
9:25	S. Kawamura(Caltech)	Signal Recycling and Resonant Sideband Extraction
9:40	Discussion	
9:50	V. Braginsky(Moscow)	Recent Results of the MSU Group
10:15	Discussion	
10:25	R. Schilling(Garching)	Transfer Function of Interferometric GW Detectors at Higher Frequencies
10:50	Discussion	

Tuesday PM Suspensions and Seismic Isolation I
January 28 Chair: R. Stebbins

4:30	S. Richman(JILA)	Progress on Low-Frequency Active Seismic Isolation
4:55	Discussion	
5:05	J. Giaime(JILA)	Improvements to the JILA Isolation Platform
5:30	Discussion	
5:40	D. DeBra(Stanford)	Strategies for Vibration Isolation and Alignment
6:05	Discussion	
6:15	Coffee Break	
6:30	S. Kawamura(Caltech)	The Initial LIGO Suspension and Isolation
6:45	Discussion	
6:55	G. Gonzales(MIT)	Advanced LIGO Suspensions and Seismic Isolation
7:10	Discussion	
7:20	Round Table Discussion	Braccini, DeBra, DeSalvo, Drever, Kawamura, Robertson, Stebbins

Wednesday AM LIGO Research Community(LRC)
January 29 Chair: S. Finn

8:00	J. Munch(Adelaide)	ACIGA Prototype and Activities
8:30	Discussion	
8:45	D. Berley(NSF)	The View From NSF
9:15	Discussion	
9:30	Coffee Break	
9:45	Meeting of LIGO Research Community and Discussion	
1:30	Meeting of LIGO Research Community(continued)	

Wednesday PM A. Lasers
January 29 Chair: R. Byer

4:30	S. Rowan(Glasgow)	Excess Intensity Noise at High Frequencies in Nd:YAG Laser Amplifiers
4:50	Discussion	
5:00	W. Tulloch(Stanford)	Conceptual Design of a 100W Diode Laser Pumped Nd:YAG Laser for GW Interferometry
5:20	Discussion	
5:30	Coffee Break	

B. Optical Elements
Chair: P. Saulson

5:45	D. Reitze(Florida)	Design Considerations for LIGO Input Optics
6:10	Discussion	
6:20	W. Kells(Caltech)	LIGO Optic Quality and Improvement R&D
6:45	Discussion	

C. Advanced Concepts
Chair: J. Hall

6:55	R. Drever(Caltech)	Coupled Suspensions, Magnetic Levitation, and Other Ideas
7:20	Discussion	
7:30	J. Wilson(Livermore)	General Relativistic Numerical Hydrodynamics for Neutron Star Binaries
7:50	Discussion	

Thursday AM — Suspensions and Seismic Isolation II
January 30 — Chair: J. Hough

8:00	S. Braccini(Pisa)	Virgo Superattenuator System
8:25	Discussion	
8:35	L. Holloway(Illinois)	A Pre-Isolation Stage for the Virgo Superattenuator
9:00	Discussion	
9:10	R. DeSalvo(INFN-Pisa)	Noise in the Virgo Superattenuators
9:35	Discussion	
9:55	S. Rowan(Glasgow)	Measurements on Fused Quartz Pendulums for Gravitational Wave Detectors
10:20	Discussion	
10:30	N. Robertson(Glasgow)	Suspension Design for GEO 600
10:55	Discussion	
11:05	P. Saulson(Syracuse)	A Few Advances in Understanding Thermal Noise
11:30	Discussion	

Thursday PM — Status of Present Detectors II
January 30 — Chair: R. Flaminio

4:30	M. Barton(ICRR-Tokyo)	A 2D X-Pendulum Vibration Isolation System
4:55	Discussion	
5:05	G. Mathews(Notre Dame)	GR Numerical Results Relevant to Gravity Wave Detectors
5:30	Discussion	

Thursday Evening: Public Lecture, Wheeler Opera House
Chair: S. Meshkov

8:00	G. Sanders(Caltech)	Listening to Einstein's Universe

Friday AM — Signal Processing and Data Analysis of Existing and Future Data I
January 31 — Chair: N. Robertson

8:00	S. Vitale(Trento)	Data Analysis for Resonant Detectors-AURIGA Data Analysis
8:25	Discussion	
8:35	W. Johnson(LSU)	Lessons Learned from Allegro and Others
9:00	Discussion	
9:10	Coffee Break	
9:25	P. Astone(Rome)	Interactive Method for the GW Periodic Sources Search
9:50	Discussion	
10:00	A. Wiseman(Caltech)	Future of Coalescing Binary Data Analysis
10:25	Discussion	
10:35	C. Cutler(Penn State)	GW Pulsar Searches
11:00	Discussion	

Friday PM — Signal Processing and Data Analysis of Existing and Future Data II
January 31 — Chair: M. Cerdonio

4:30	S. Finn(Northwestern)	Report on GWDAW Meeting
4:55	Discussion	
5:05	B. Allen(Caltech)	GRASP(Gravitational Radiation Analysis and Simulation Package)
5:30	Discussion	
6:00	Coffee Break	
6:15	P. Brady(Caltech)	Continuous Wave Sources: Hierarchical Searches and Stepping
6:40	Discussion	
6:50	M. Cerdonio(Padova)	(Almost) Isotropic Sky Coverage for GW Bursts of the Upcoming World Network of Interferometric and Bar Detectors
7:15	Discussion	

Saturday AM — A. Advanced Detectors in the Future
February 1 — Chair: A. Giazotto

8:00	R. Stebbins(JILA)	A NASA-Led Version of LISA
8:30	Discussion	
8:40	M. Choptuik(UT-Austin)	Binary Black Hole Grand Challenge Update
9:10	Discussion	
9:20	Coffee Break	

B. Collaboration Formation for Advanced Detectors II
Chair: H. Ward

9:35	S. Finn(Northwestern)	Summary of Opinions Expressed at Meeting
10:05	Discussion	
10:15	P. Saulson(Syracuse)	Where Do We Go From Here?
10:40	Discussion	

Monday AM: Status of Present Detectors
January 27 Chair: S. Meshkov

8:00	S. Meshkov(Caltech) Jane Kelly(ACP)	Welcome
8:10	A. Giazotto(Pisa)	Status of Virgo
8.35	Discussion	
8:45	J. Hough(Glasgow)	Status of GEO 600
9:10	Discussion	
9:20	Coffee Break	
9:35	D. Shoemaker(MIT)	Status of LIGO
10:00	Discussion	
10:10	W. Hamilton(LSU)	Status of Bar Detectors
10:35	Discussion	

GIAZOTTO

VIRGO COLLABORATION
FRANCE

LAPP Annecy

Physicists		*Engineers*	*Technicians*	*Administrant*
B. Caron	B. Mours	M. Axeline	D. Boget	C. Lemarec
A. Dominjon	V. Sannibale	F. Bellachia	B. Bourdas	
C. Drezen	M. Yvert	C. Ginard	P.-Y. David	
R. Flaminio		J.-C. Lacotte	L. Derome	
X. Grave		J. Lecoq	G. Gaillard	
F. Marion		B. Lieunard	L. Giacobone	
L. Massonnet		S. Lieunard	R. Hermel	
C. Mehmel		P. Mugnier	J.-C. Lemarec	
R. Morand			R. Sottile	

Laser Optics Orsay

Physicists		*Engineers*	*Technicians*	*Administrant*
M. Barsuglia	C. Nary Man	Y. Acker	P. Bindzi	E. Rouillere
B. Bhawal	M. Pham-Tu	R. Bartlet	J.-C. Lucenay	
A. Brillet	M. Taubman	J. Cachenaut	T. Redon	
F. Bondu	E. Tournier	F. Cleva		
H. Heitmann	J.Y. Vinet	V. Reita		
J.-M. Innocent				
L. Latrach				

IPN Lyon

Physicists	*Engineers*
J.M. Mackowski	L. Dognin
L. Pinard	P. Ganau
	C. Michel
	M. Napolitano

ESPCI Paris

Physicists
C. Boccara
P. Gleyzes
J.P. Roger
V. Loriette

LAL Orsay

Physicists	*Engineers*	*Technicians*	
V. Brisson	C. Arnault	R. Combeau	G. Lissillour
F. Cavalier	J.L. Beney	P. Corona	R. Marie
M. Davier	R. Bilhaut	J.P. Coulon	J.C. Marrucho
P. Hello	R. Chiche	S. Cuzon	P. Rivoirard
P. Heusse	M. Dialinas	M. Dehamme	M. Taurigna
F. Ledlberder	A. Ducorps	C. Eder	
P. Marin	A. Hrisoho	C. Garnier	
	A. Reboux	M. Gaspard	
	P. Roudier	E. Jules	

VIRGO COLLABORATION
ITALY

INFN Frascati

Physicists	*Technicians*	*Administrant*
D. Babusci	E. Cima	S. Giromini
S. Bellucci	M. Iannarelli	
S. Candusso	D. Orecchini	
G. Giordano	E. Turri	
G. Matone		

INFN Firenze

Physicists
E. Bougleaux
M. Mazzoni
P. Peifer
R. Stanga

INFN Napoli

Physicist	
F. Barone	M. Flagiello
E. Calloni	M. Longo
L. Di Fiore	M. Lops
F. Garufi	S. Marano
A. Grado	
L. Milano	
S. Solimeno	

INFN Perugia

Physicists
G. Cagnoli
M. Punturo
L. Gammaitoni
J. Kovalik
F. Marchesoni

INFN Pisa

Physicists		*Engineers*	*Technicians*	*Administrant*
M. Beccaria	A. Giassi	A. Basti	L. Berretta	P. Benfatti
M. Bernardini	P. La Penna	D. Enard	E. Carboni	C. Tofani
S. Braccini	G. Losurdo	A. Gaddi	R. Coeci	P. Villani
C. Bradaschia	M. Maggiore	A. Gennai	G. De Carolis	
G. Cella	S. Mancini	H.B. Pan	A. Di Secco	
A. Ciampa	F. Palla	A. Pasqualetti	M. Iacoponi	
E. Cuoco	D. Passuello	P. Popolizio	F. Paoletti	
G. Curci	R. Poggiani	F. Raffaelli	E. Pucciarelli	
R. De Salvo	A. Viceré		A. Ragonesi	
R. Del Fabbro	Z. Zhou		R. Ruberti	
A. Di Virgilio				
I. Ferrante				
F. Fidecaro				
A. Giazotto				

INFN Roma

Physicists	*Engineers*	*Technicians*	*Administrant*
V. Ferrari	F. Bronzini	L. Andreanelli	L. Rizzo
E. Majorana		M.Perciballi	
P. Puppo		E. Serrani	
P. Rapagnani		G. Capradossi	
F. Ricci		A. Mattei	
		F. Pellegrino	

Organisation structure of VIRGO

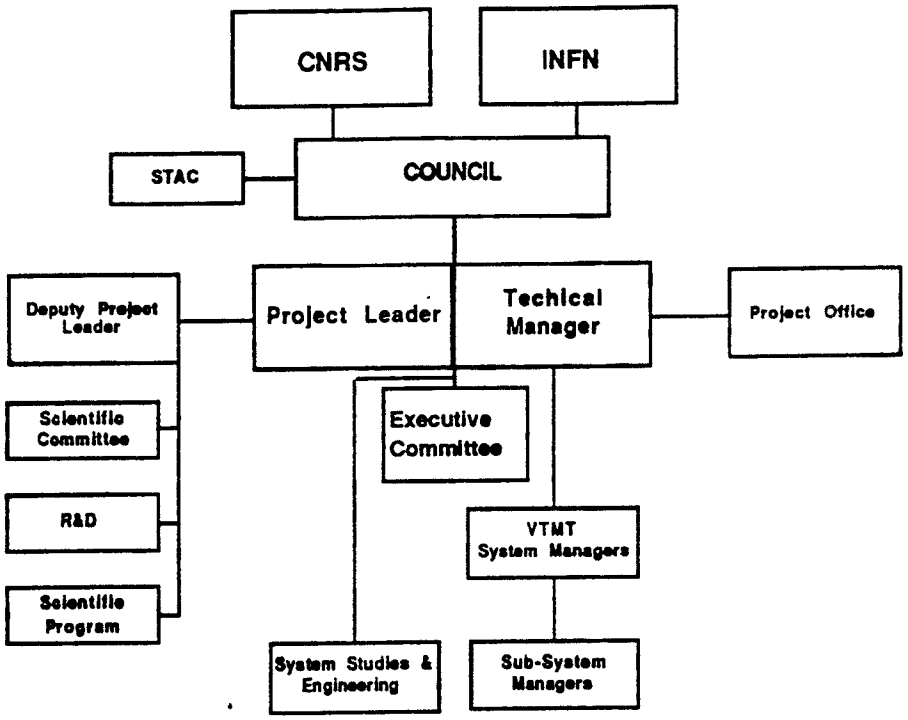

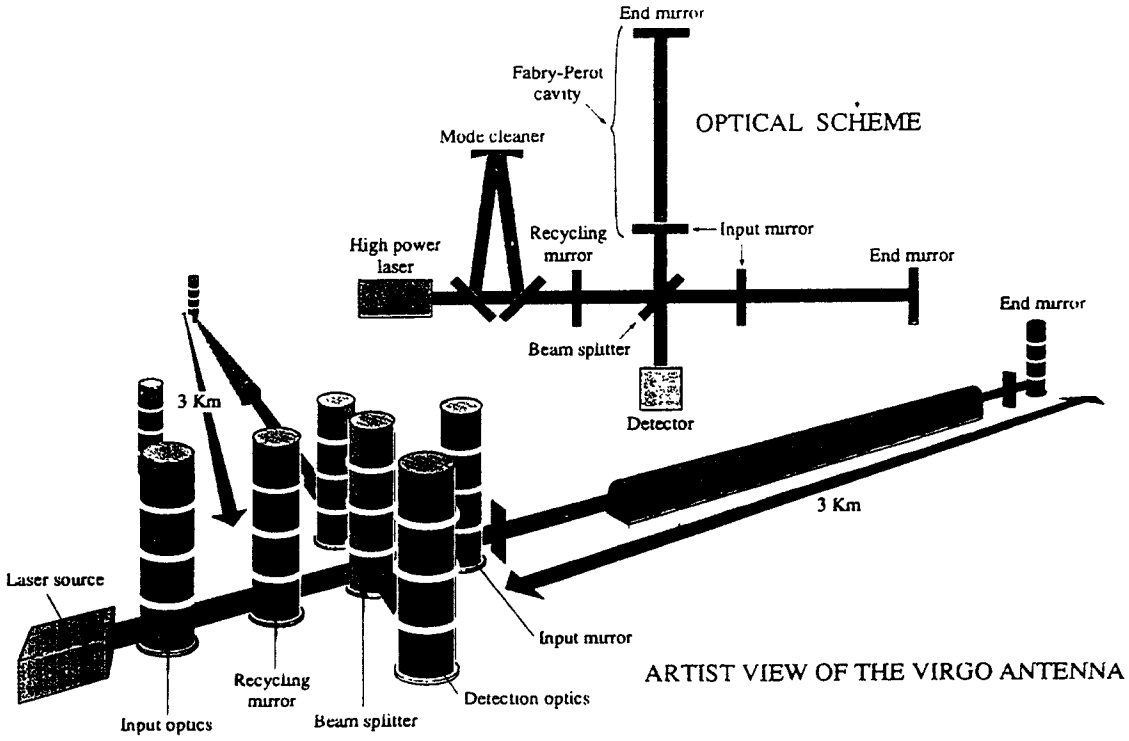

ARTIST VIEW OF THE VIRGO ANTENNA

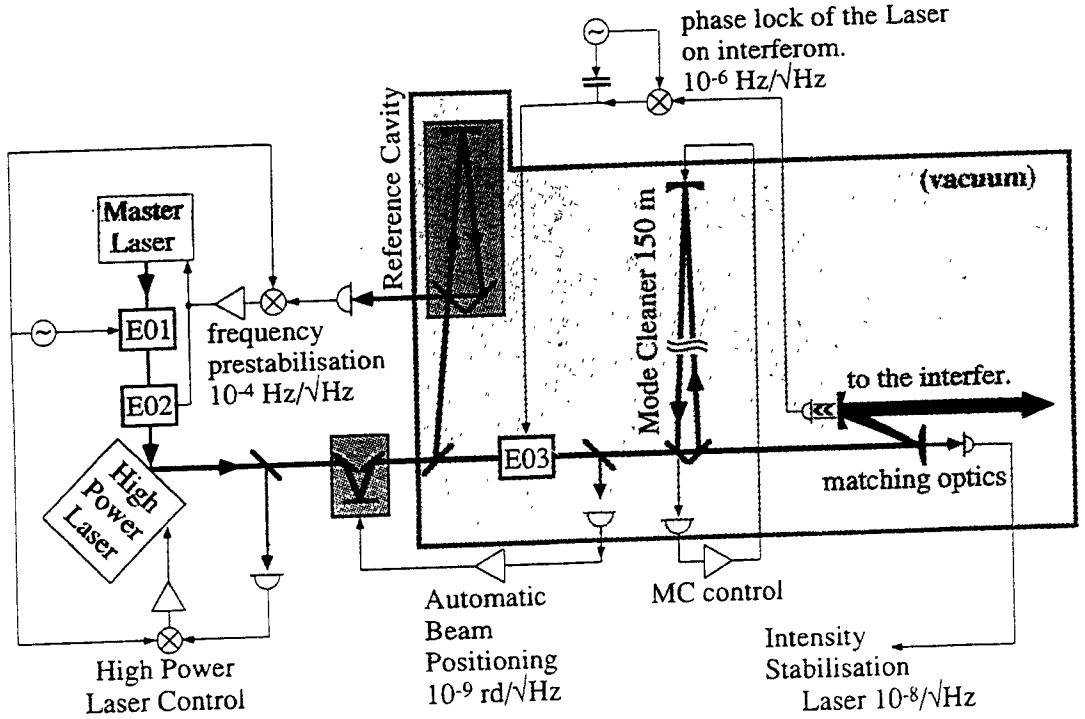

Stabilised High Power LASER and Input Optics.

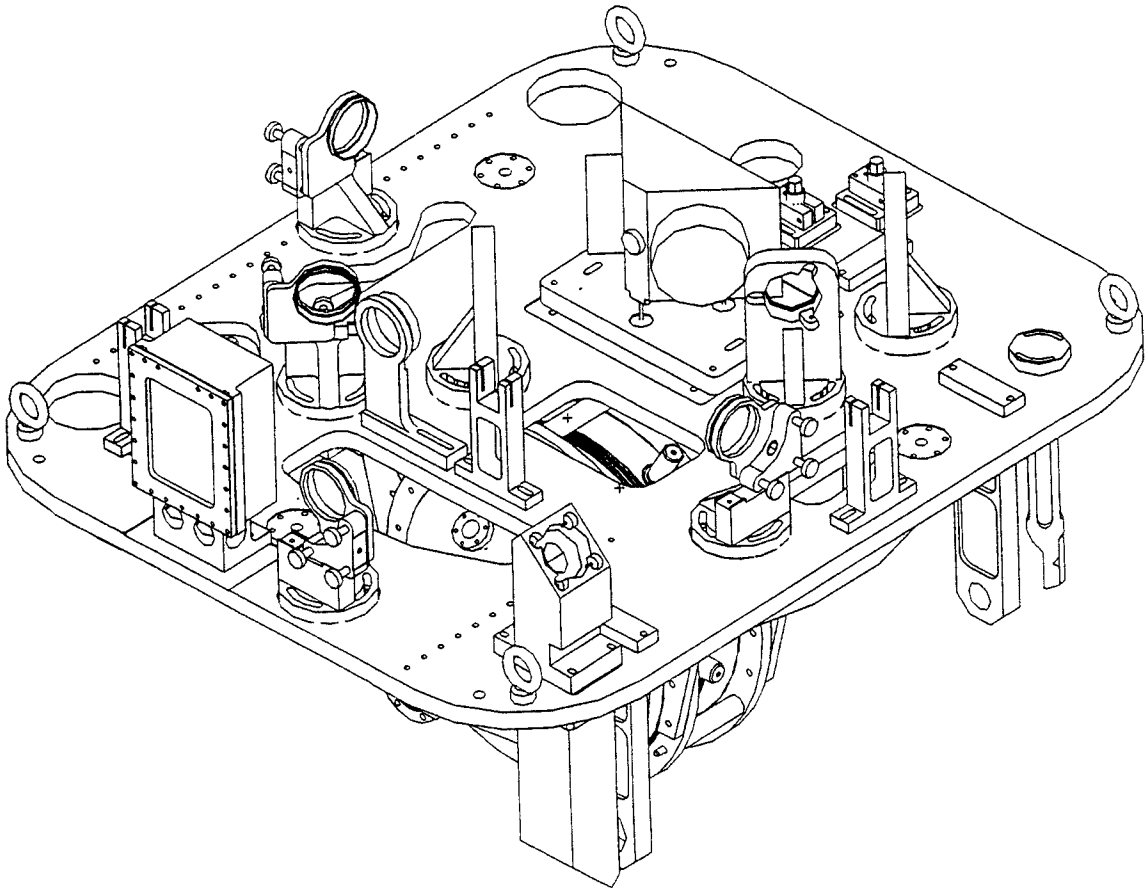

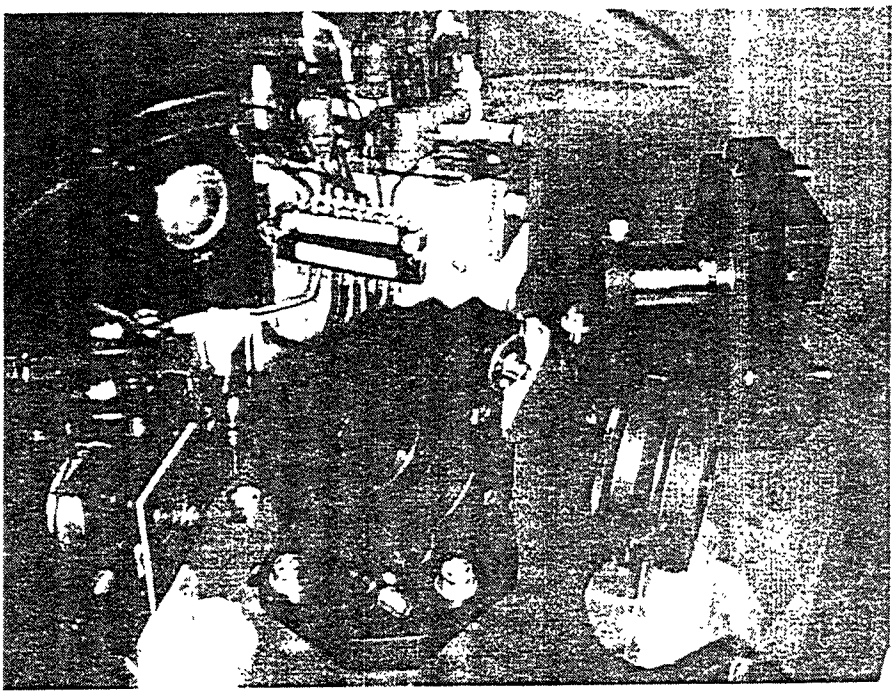

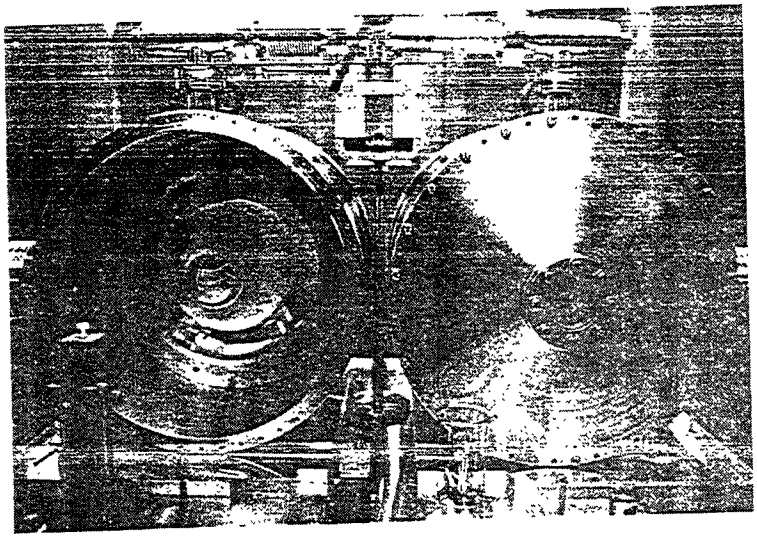

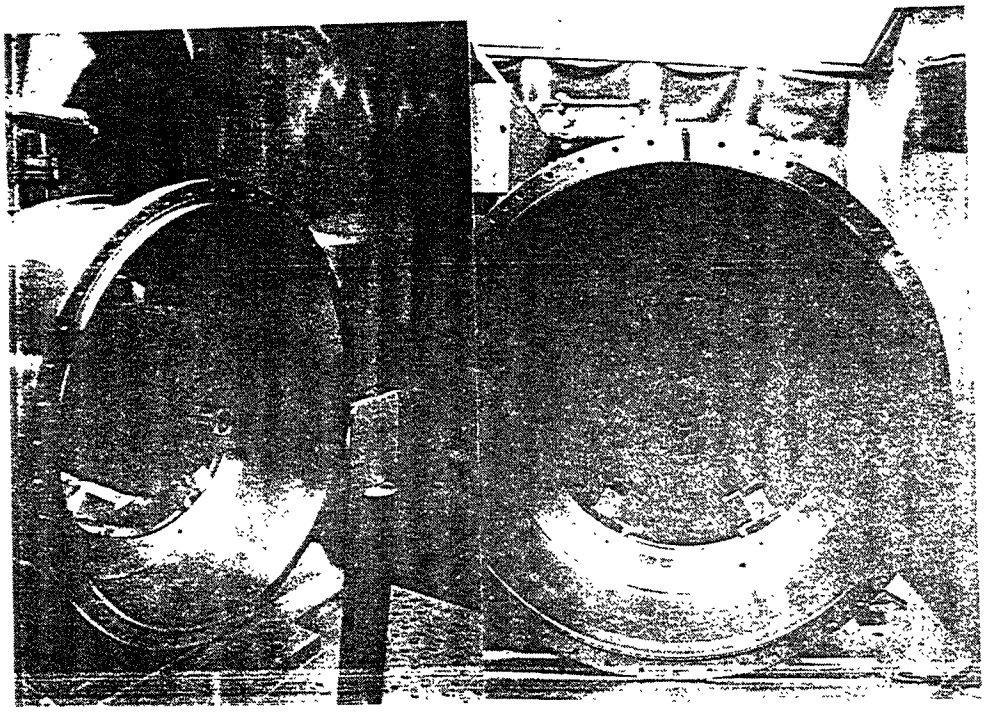

MIRRORS

	Diam./Thick.(mm)		
FP Cavity Input	350	/ 100	Suprasil 312
FP Cavity Output	350	/ 200	ULE
Beam Splitter	230	/ 5 5	Suprasil 311
Recycling	120	/ 3 0	Suprasil 312

Substrate Absorption < 2 ppm/cm

COATINGS

Results obtained in 1995 by the Lyon Group using DIBS on 80 mm Diam. Mirrors:

Absorption < 0.5 ppm

Scattering < 0.6 ppm

Band Centering < 10 nm

Values inside Virgo Spec.

Currently under design the large coater for 300 mm coatings production.

P521 22x30/10

VACUUM PIPE

Diam. 1200 mm

Lengh 2 x 3000 m

Material: Stainless Steel 304 L

Non corrugated tube totally welded with reiforcing rings

Thickness 4 mm

Module lengh 15 m

Module bake-out in air at 400 C

Bellows: One per module (elastic regime)

Residual pressure 10-(9) mbar for H2

Outgassing rate: 5 10-(14) mbar.l/cm2.s for H2

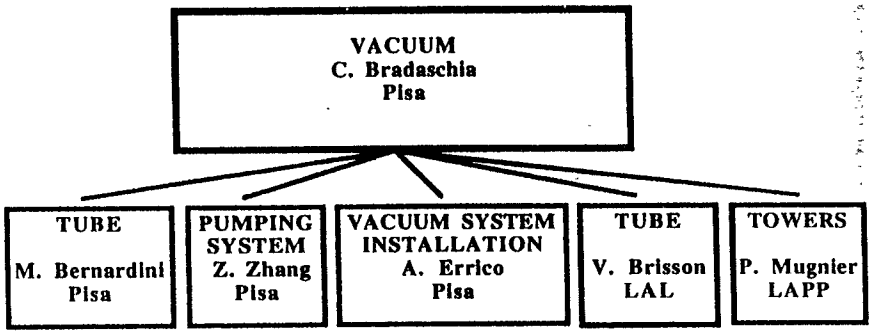

Pisa Vacuum Group

M. Bernardini (Phys.)
C. Bradaschia (Phys.)
A. Errico (Eng.)
H.B.Pan (Eng.)
A Pasqualetti (Eng.)
R. Cosci (Techn.)
A. Ragonesi (Techn.)

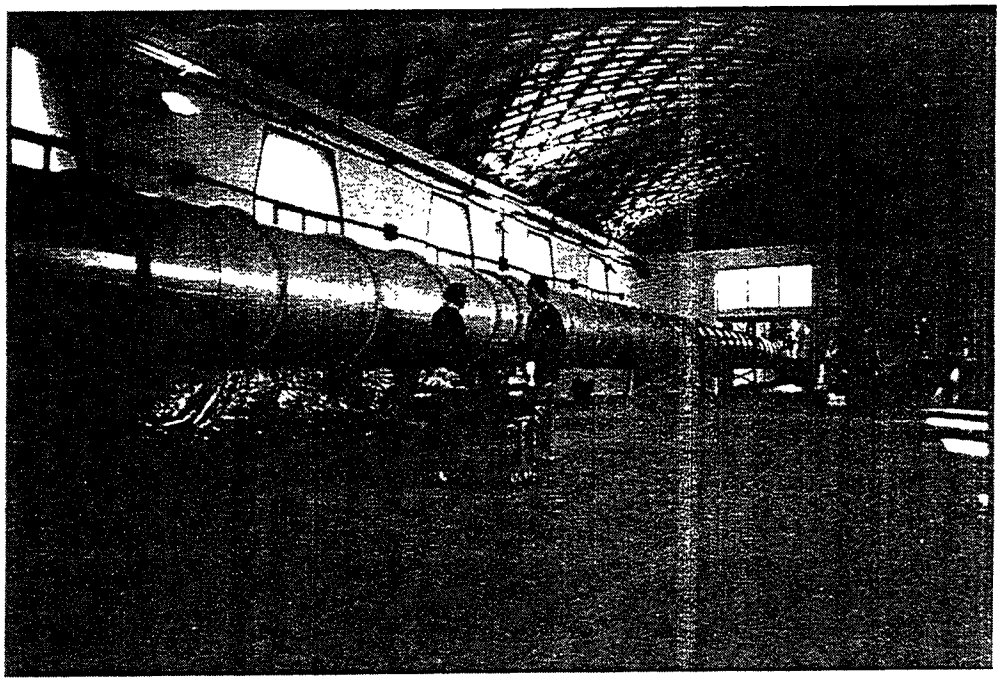

PLASTIBOR
P52L 22x30/10

Fig. 9/a

LONGITUDINAL SECTION

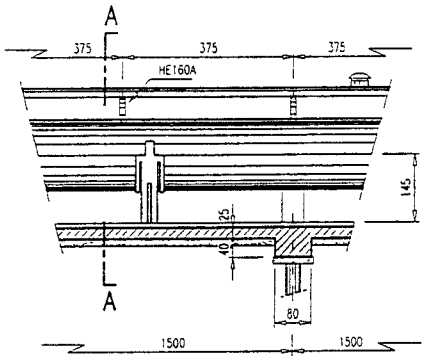

SECTION A–A

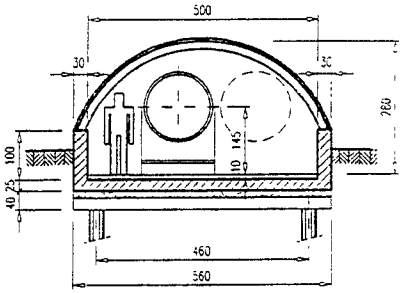

TRANSVERSAL SECTION

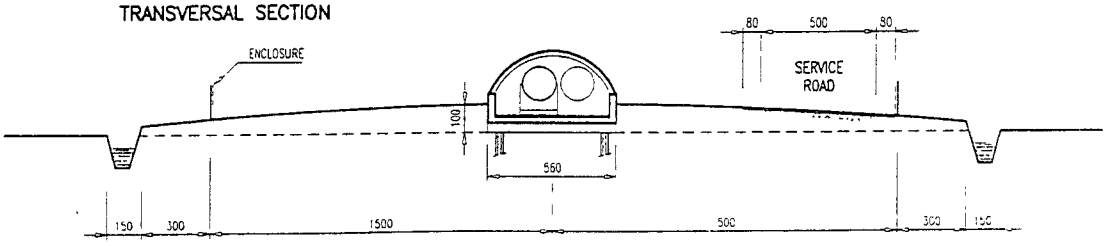

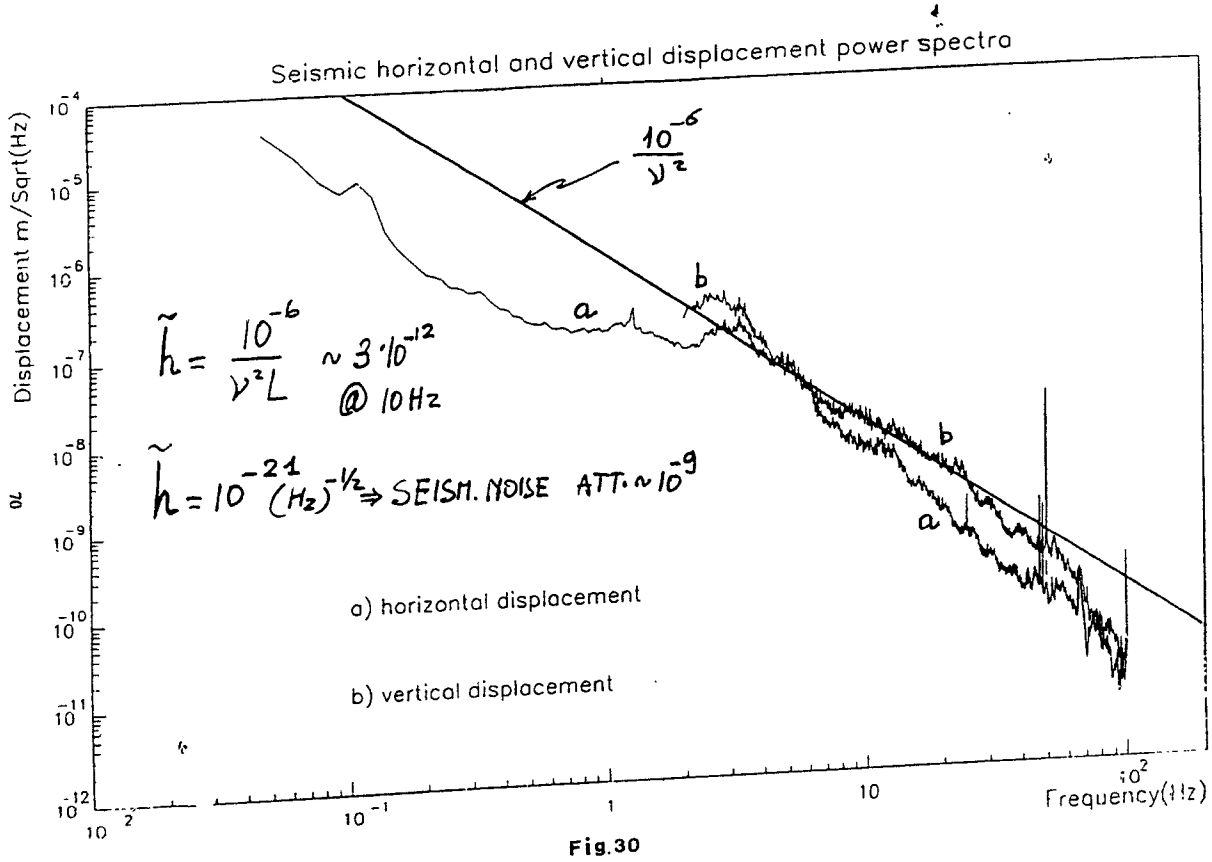

Fig.30

PREISOLATOR WHY?

PASSIVE OPERATION

1) SMOOTHEST SUSP. POINT MOTION:
DOES NOT EXCITE S.A. NORMAL
MODES $\Rightarrow$ LESS ITF UNLOCKS

2) REDUCES MIRROR RMS MOTION
TO $\lesssim 1\,\mu$

6D ACTIVE OPERATION

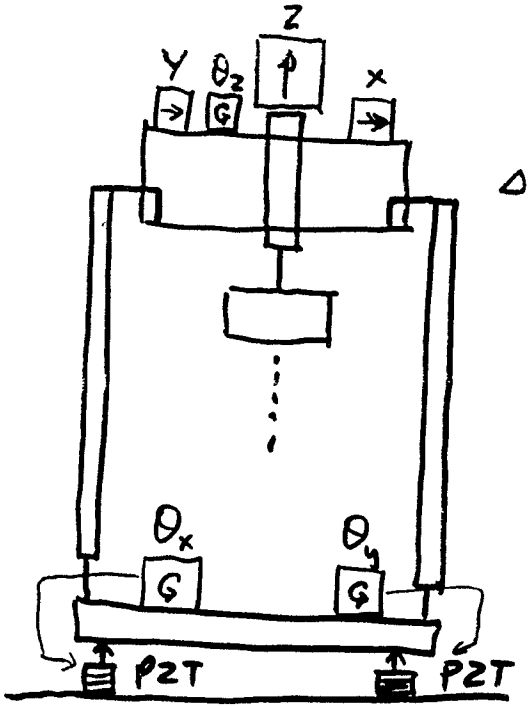

SENS. ACC.

$\Delta Z, \Delta X \sim 10^{-12} \frac{\omega^2 - \omega_0^2}{\omega^2}$ $m/\sqrt{Hz}$

$\Delta\theta \sim 10^{-11} \frac{\omega^2 - \omega_0^2}{\omega^2}$ $rad/\sqrt{Hz}$

SEISMIC DISPL.

$X, Y, Z \sim 10^{-3}$ m @ 30 m Hz

INDEPENDENT ACCELER.:

Z , θ_x θ_y

CORRELATED ACCELER.

Y, X, θ_z : ONLY!! (3×3)

NOT EASY BUT SIMPLEST CONF.

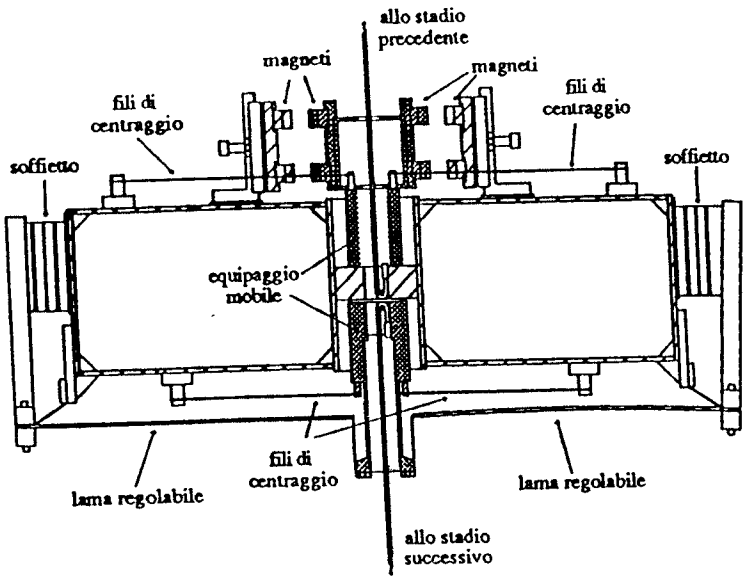

b)

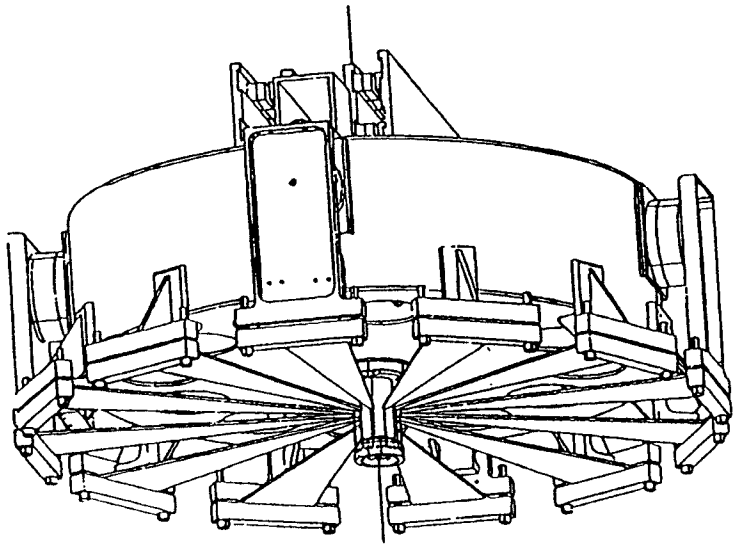

MARAGING 35 C

estimated creep rates for the trained Maraging blades: 0.01±0.02 microns/hour

0.03±0.03 microns/hour

0.03±0.05 microns/hour

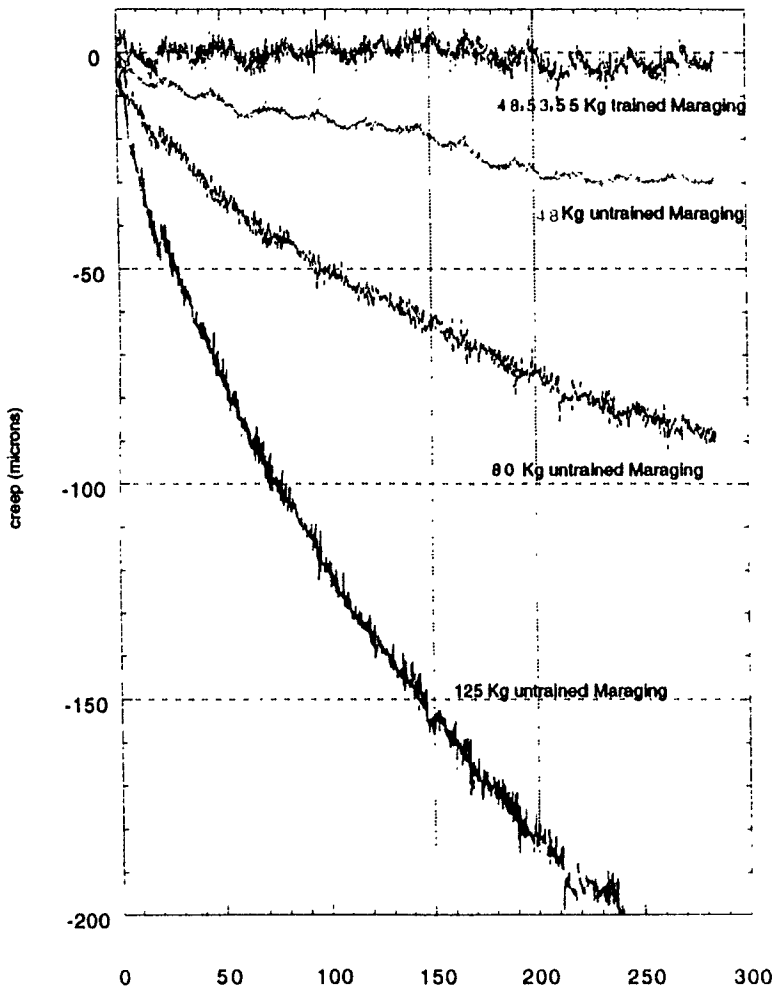

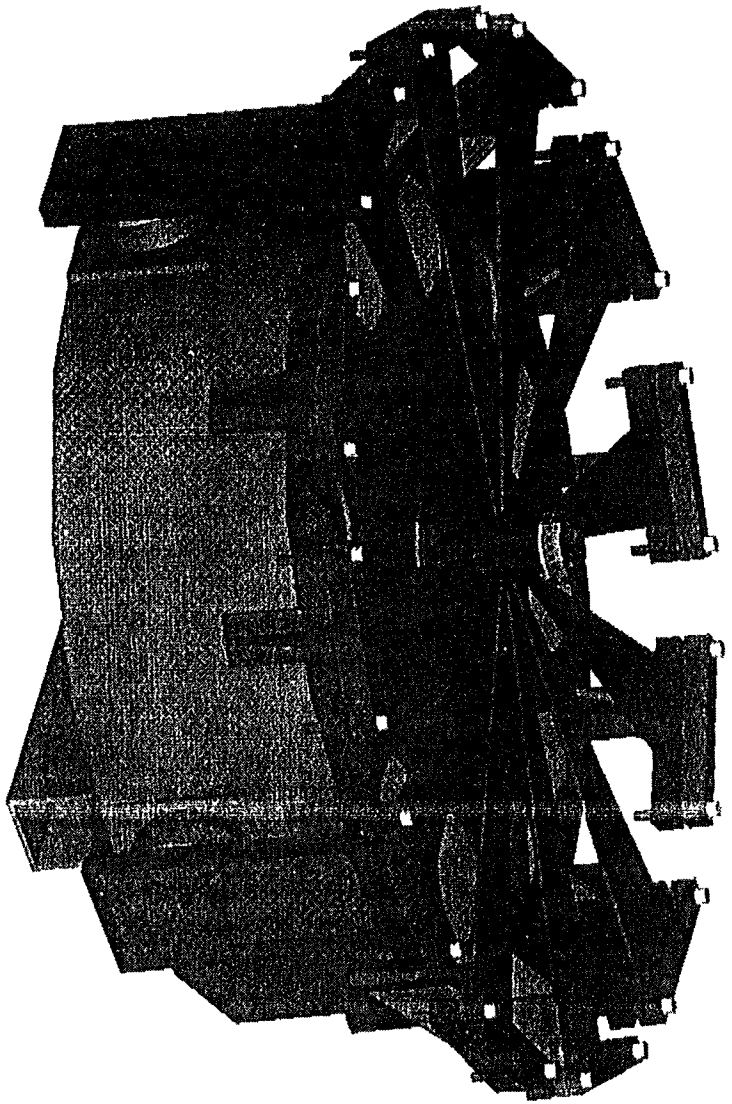

VIRGO Seismic Attenuation ($V-H-10^{-2}$)

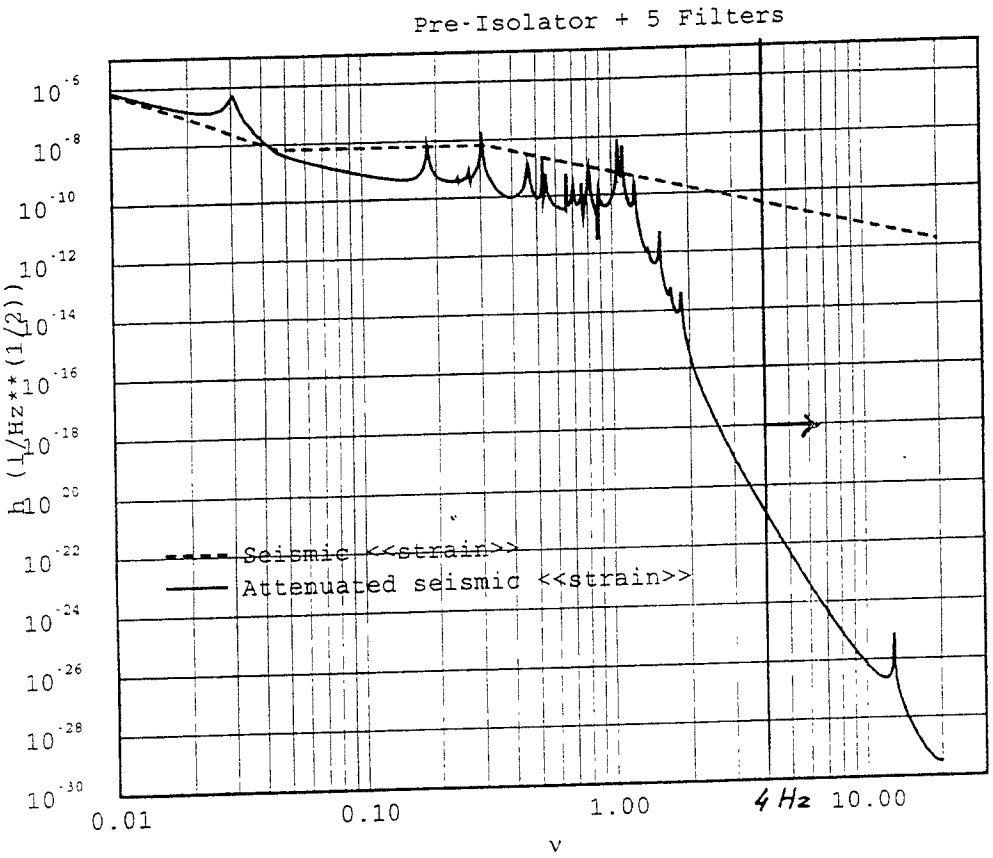

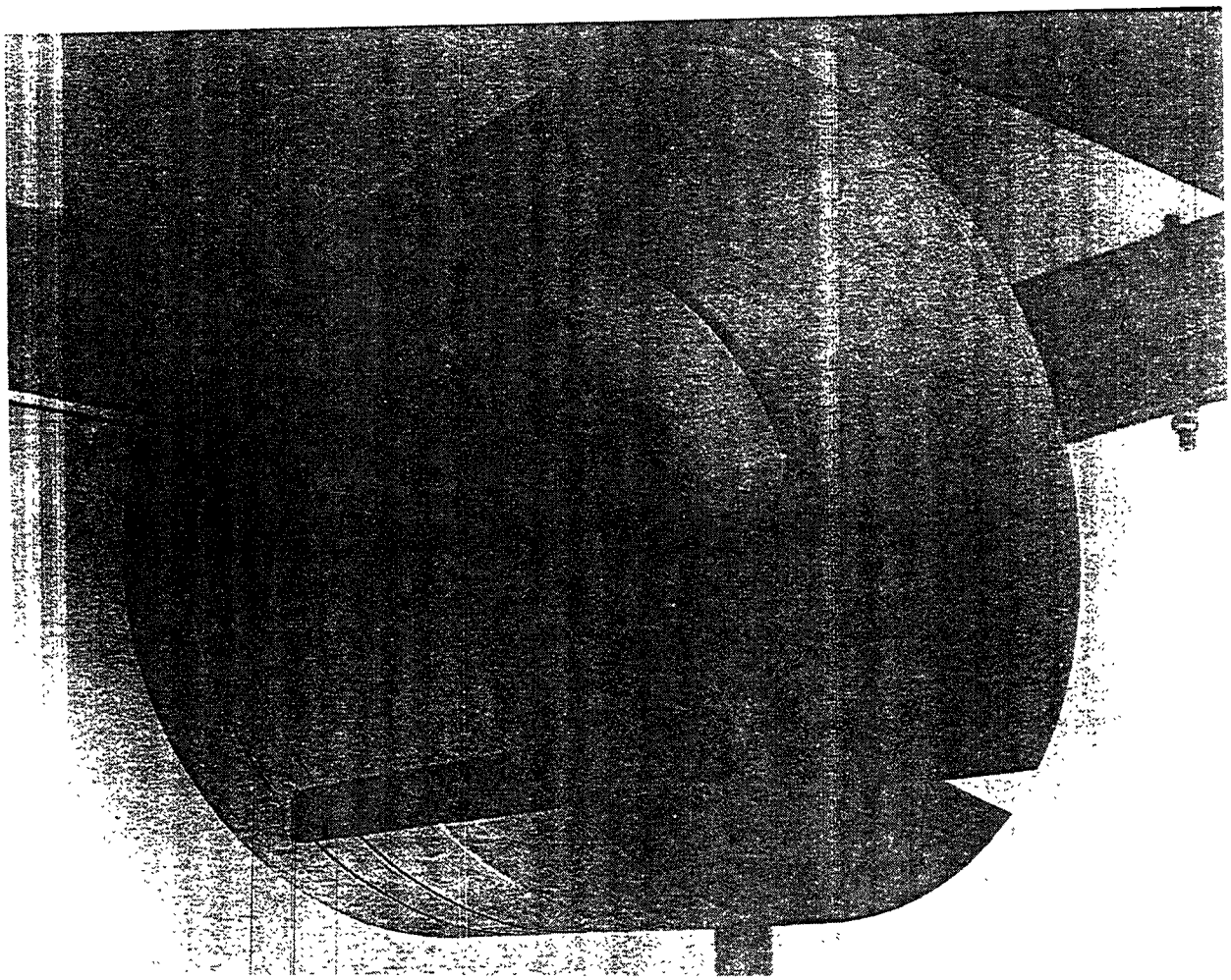

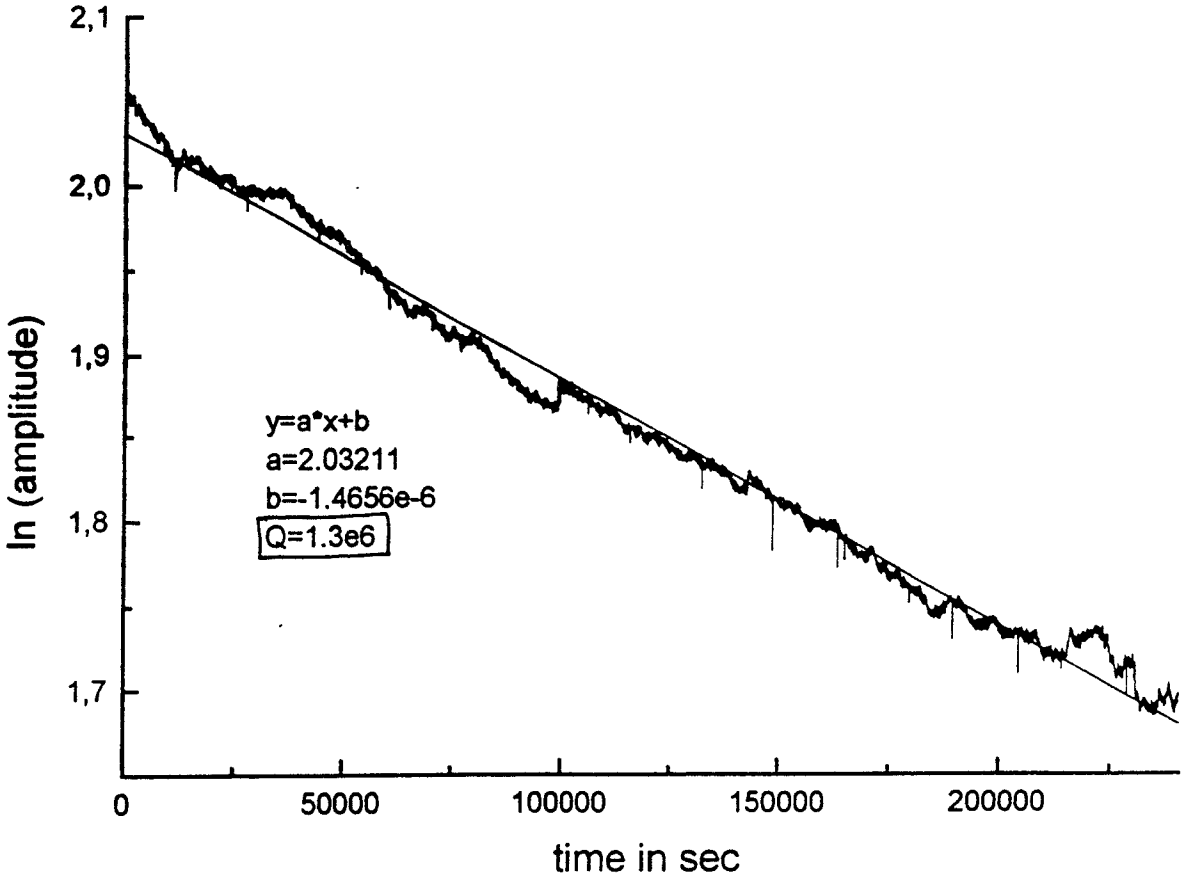
2,1
2,0
1,9
1,8
1,7
ln (amplitude)
y=a*x+b
a=2.03211
b=-1.4656e-6
Q=1.3e6
0
50000
100000
150000
200000
time in sec

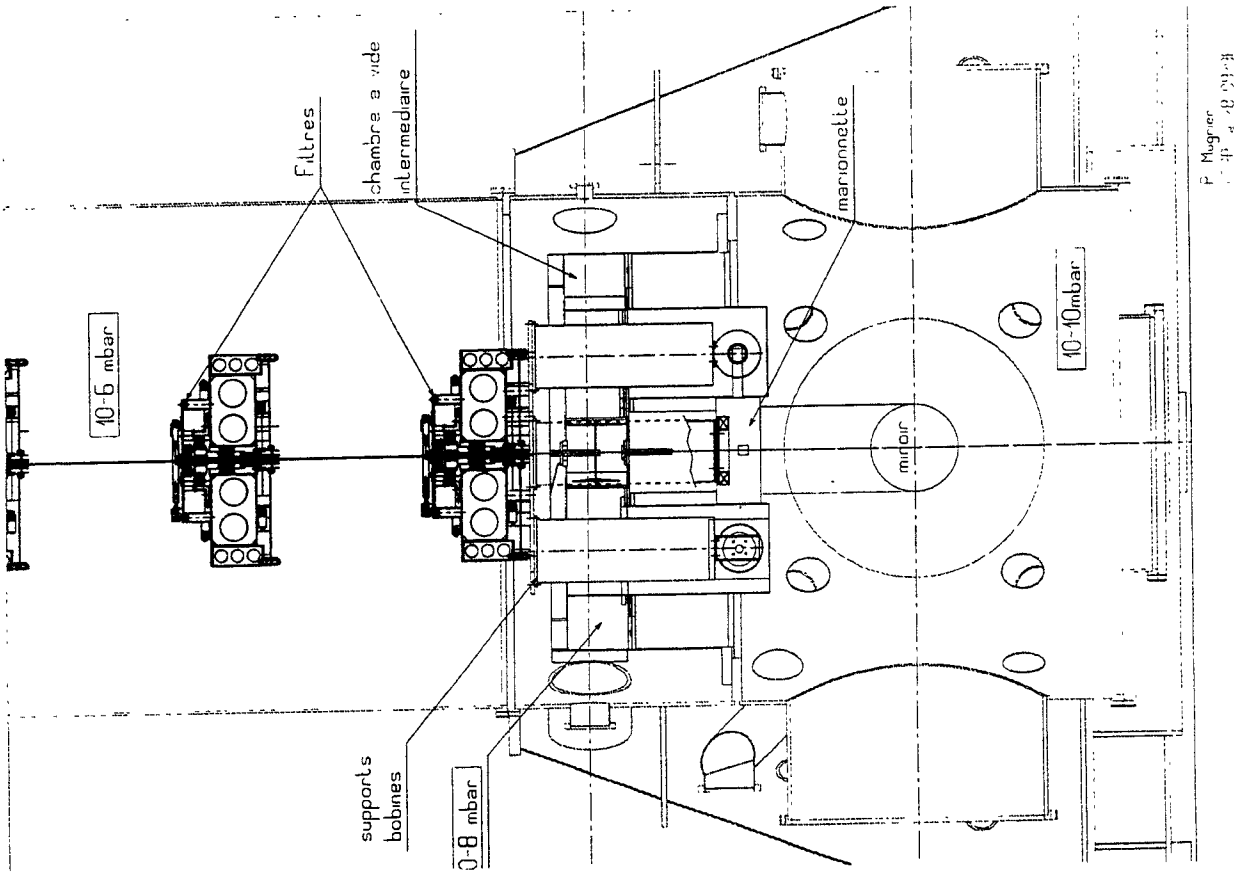
Filtres
chambre à vide intermediaire
marionnette
10-6 mbar
10-10mbar
miroir
supports bobines
10-8 mbar

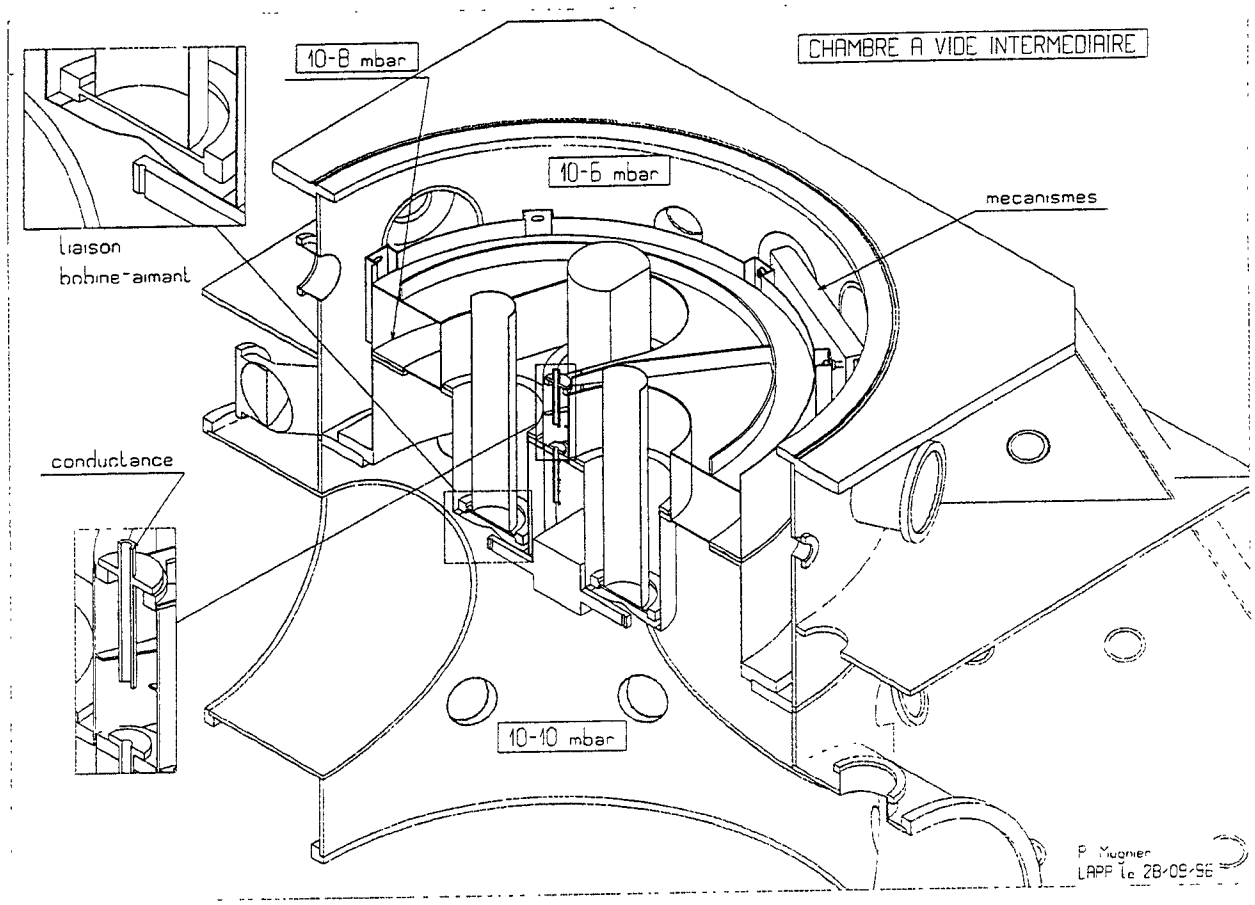
CHAMBRE A VIDE INTERMEDIAIRE
10-8 mbar
10-6 mbar
10-10 mbar
liaison
bobine-aimant
conductance
mecanismes
P. Mugnier
LAPP le 28-09-96

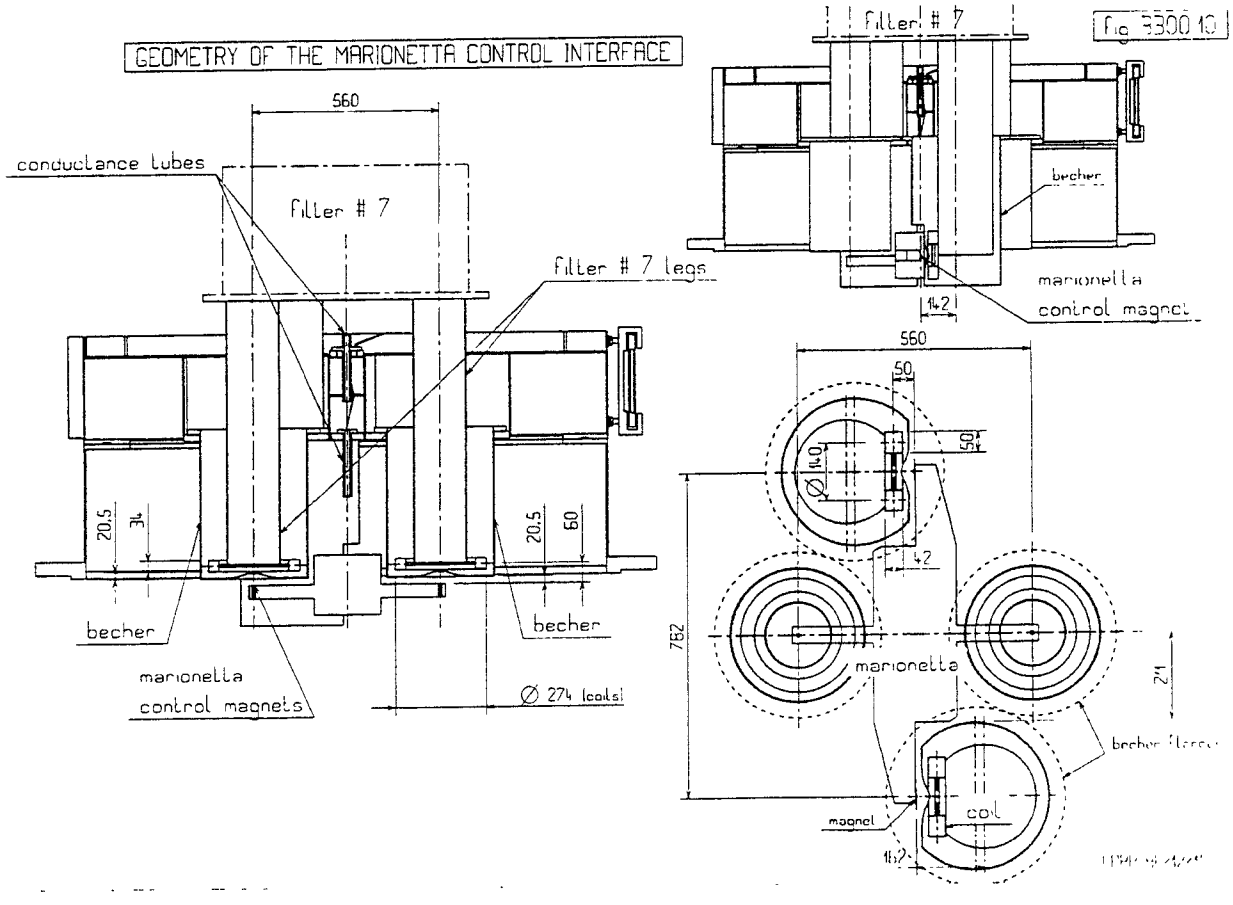
GEOMETRY OF THE MARIONETTA CONTROL INTERFACE
fig 3300.10
560
conductance tubes
filter # 7
filter # 7 legs
20.5
34
20.5
60
becher
becher
marionetta
control magnets
Ø 274 (coils)
filter # 7
becher
marionetta
control magnet
142
560
50
50
140
42
782
marionetta
211
becher flange
magnet
coil
182

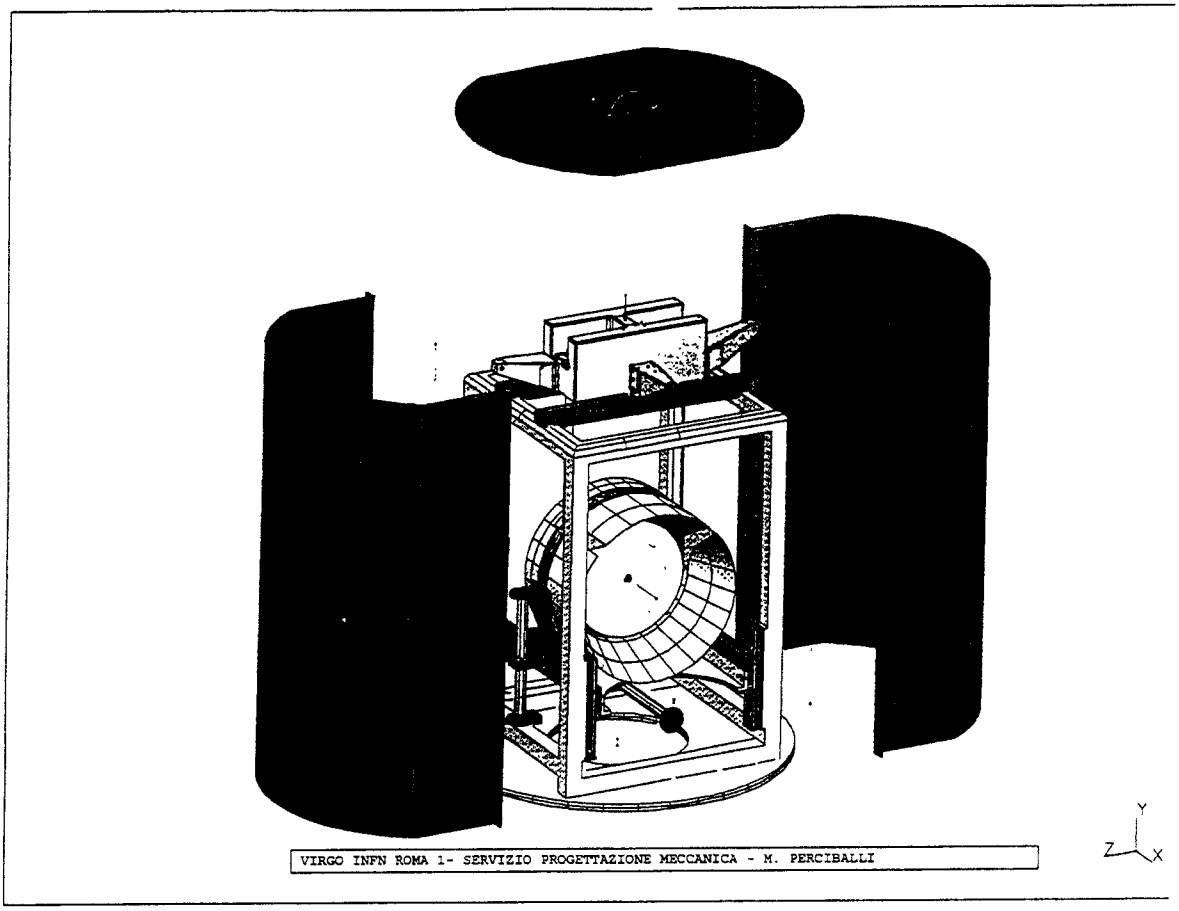
VIRGO INFN ROMA 1- SERVIZIO PROGETTAZIONE MECCANICA - M. PERCIBALLI
Y
Z
X

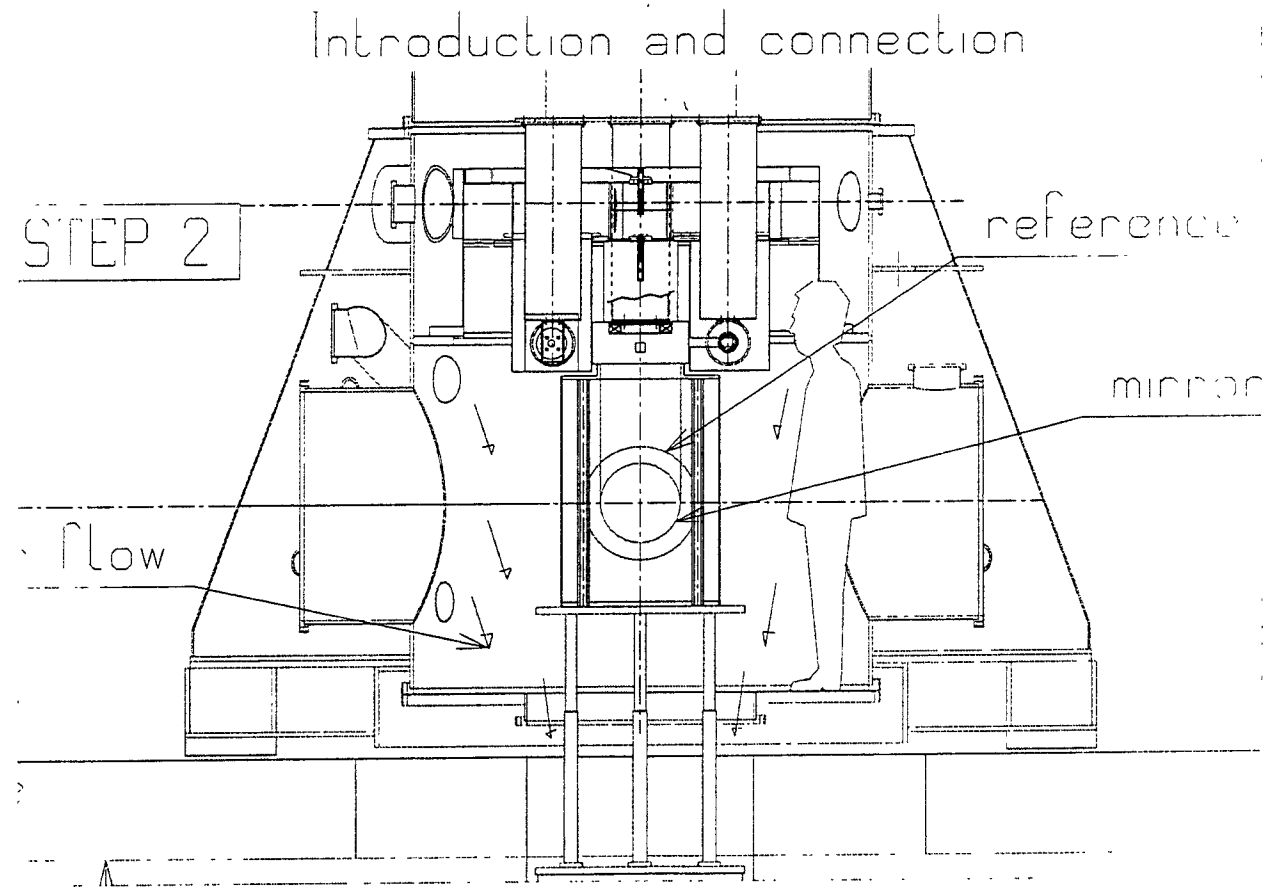
Introduction and connection
STEP 2
reference
mirror
low

BAFFLES

Tube noise (no Baffle) $\sim 10^{-22} \left(\frac{10}{\nu}\right)^2 \frac{1}{\sqrt{Hz}}$

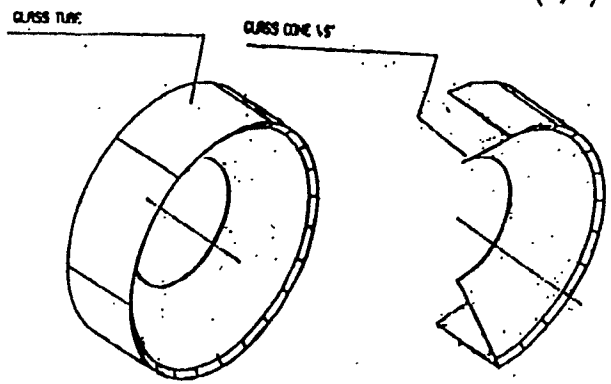

BLACK GLASS :
Transmission 10-7 @ 1 μ
Total Diffusion < 10–5
Reflectivity < 10-3 **0°-45°**

Total Number of Baffles: 160

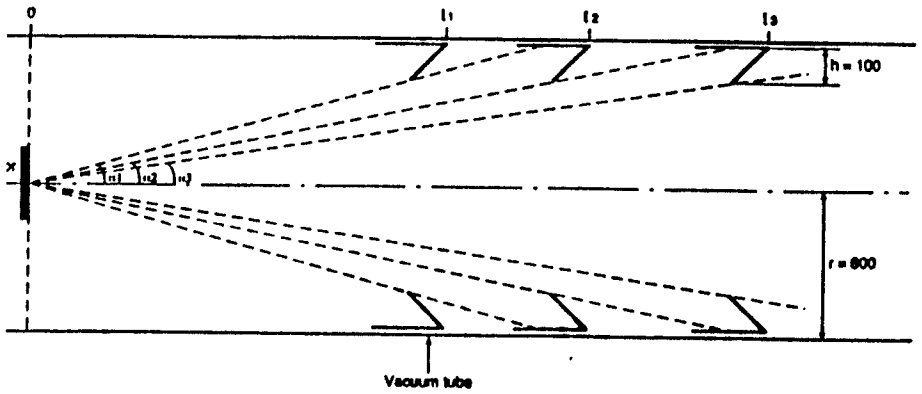

Expected noise < $10^{-24} \frac{1}{\sqrt{Hz}}$

NOISES

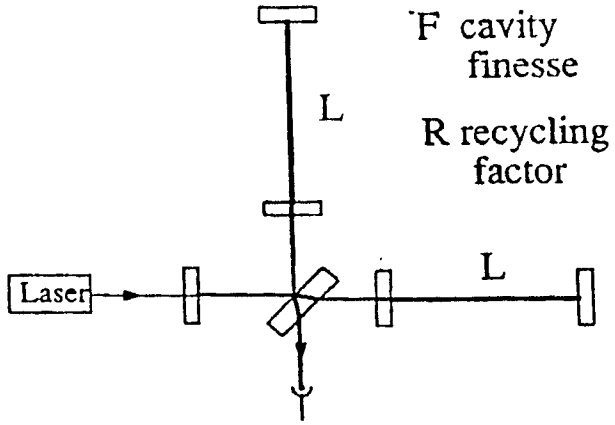

1) Phase Noise: $\Phi_n = \frac{1}{\sqrt{n_{phot}}}$

$$\tilde{h}_n = \frac{\lambda}{8\,FL}\sqrt{1+\left(\frac{2\omega FL}{\pi\ c}\right)^2}\sqrt{\frac{h\upsilon}{RW}} \quad \Rightarrow \quad \text{large } F \cdot L \cdot \sqrt{R}$$

2) Thermal Noise:

$$\tilde{h}_n = \frac{1}{\omega^2 L}\sqrt{\frac{16\,kT\,\omega_p}{MQ}} \quad \Rightarrow \quad \text{large } L \cdot \sqrt{M} \cdot \sqrt{Q}$$

$$\boxed{\omega^2 \text{small} \ \Rightarrow \ L \approx Km}$$

3) Seismic Noise:

$$\tilde{h}_n = \frac{2\tilde{x}_s}{L} \quad \text{with} \quad \tilde{x}_s \approx \frac{10^{-7}}{\upsilon^2} \quad \text{main contribution!}$$

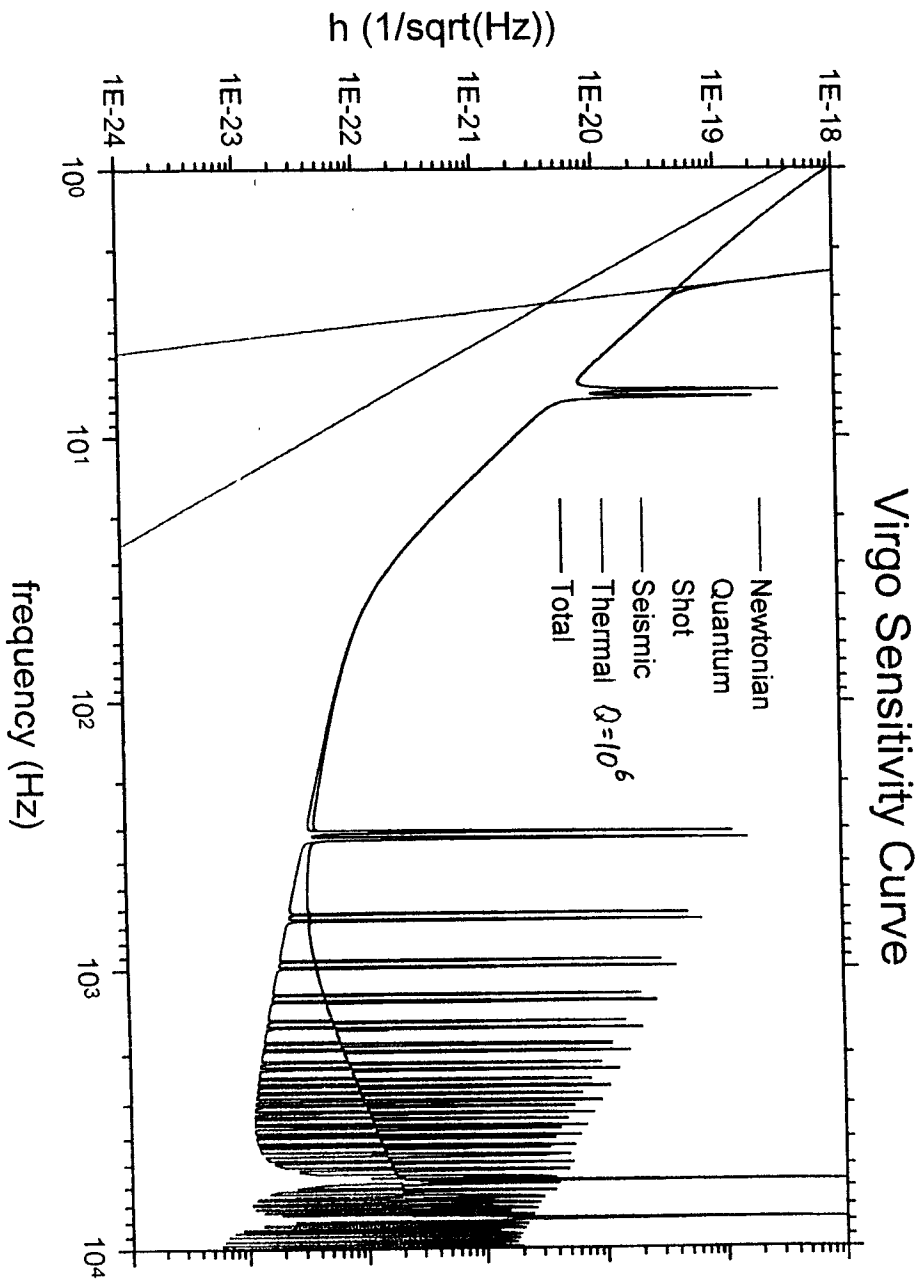

4) Newtonian Noise:
Seismic Noise vibrates masses sourrounding mirrors, creating a variable Newtonian Force on the mirrors.

$$\tilde{h}_n = \frac{1}{L}\frac{7\cdot 10^{-2} G\rho}{\nu^2}\cdot\frac{10^{-7}}{\nu^2} = \frac{4\cdot 10^{-19}}{\nu^4}$$

5) Quantum Limit:
Limits the position measurement precision of a mass M in a time $t=1/\nu$.

$$\tilde{h}_n = \frac{1}{L\,\omega}\sqrt{\frac{4\hbar}{M}} = \frac{1.5\cdot 10^{-22}}{\nu}$$

Virgo Sensitivity Curve evaluated with:
$L=3000$ m, $Q_{pendulum}=$, $Q_{mirror}=10^6$, $P_{laser}=20$ W, $F=100$, $R=50$

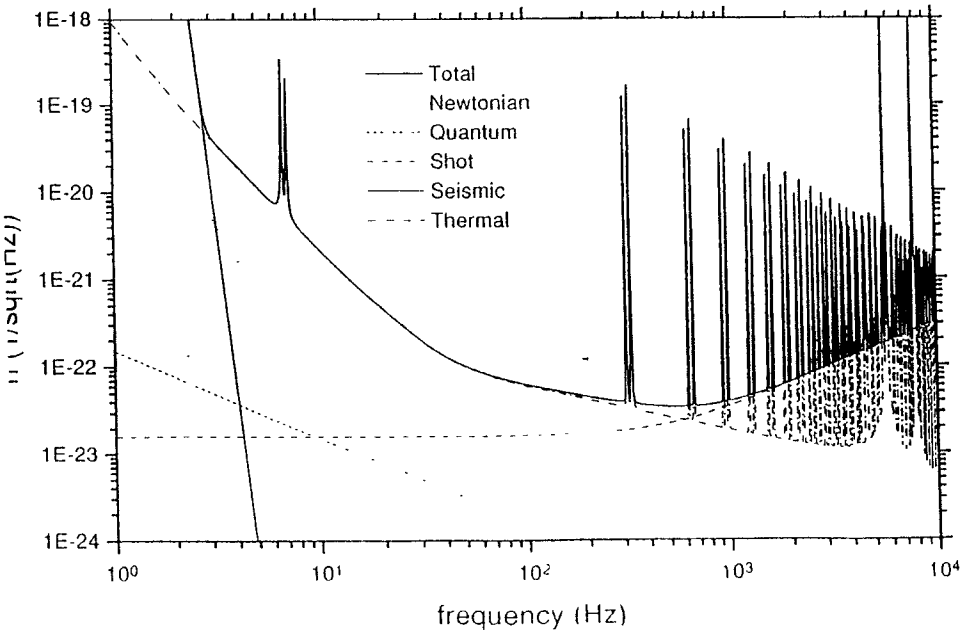

VIRGO General Planning

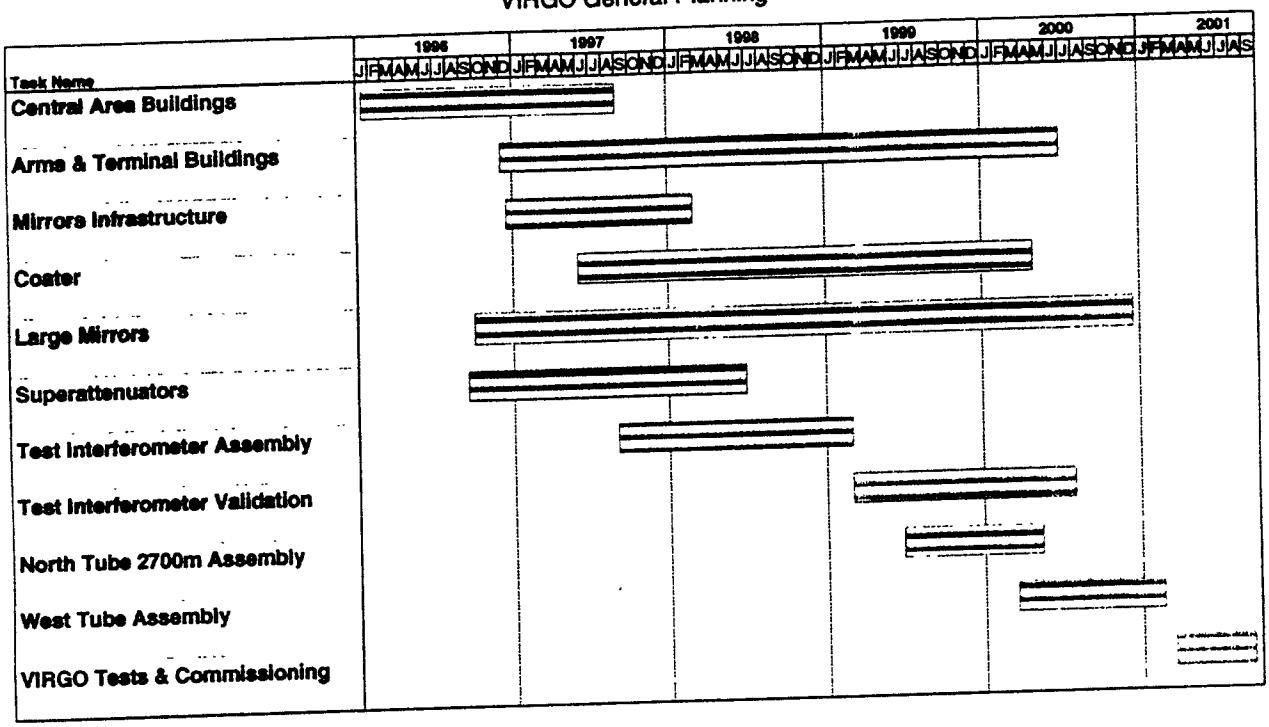

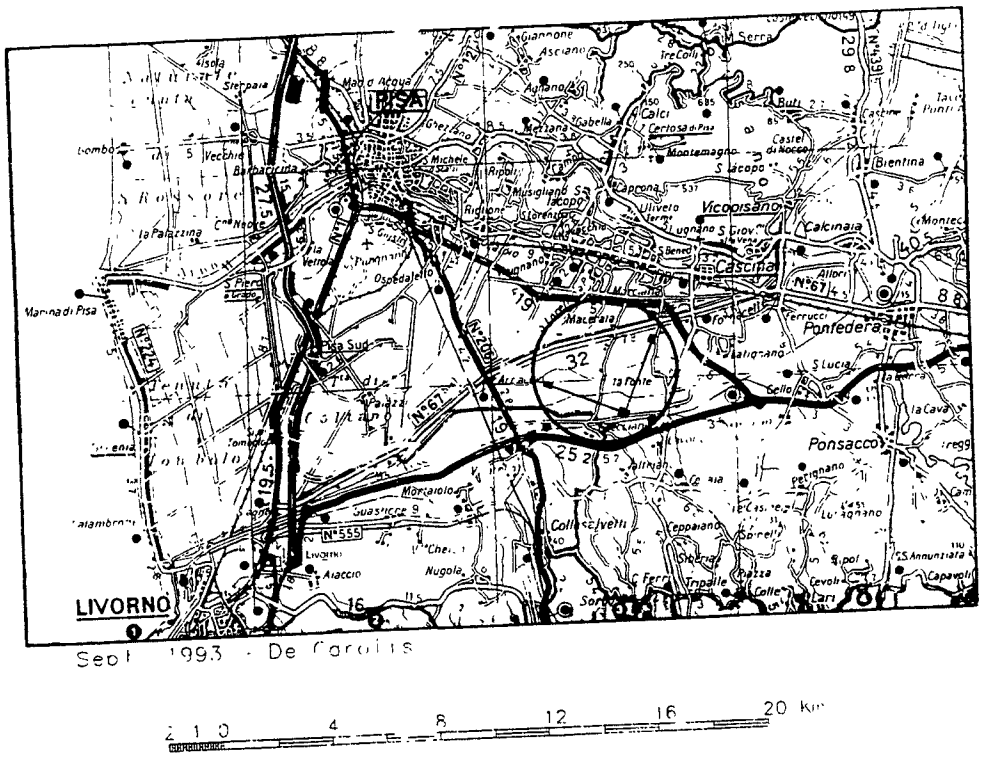

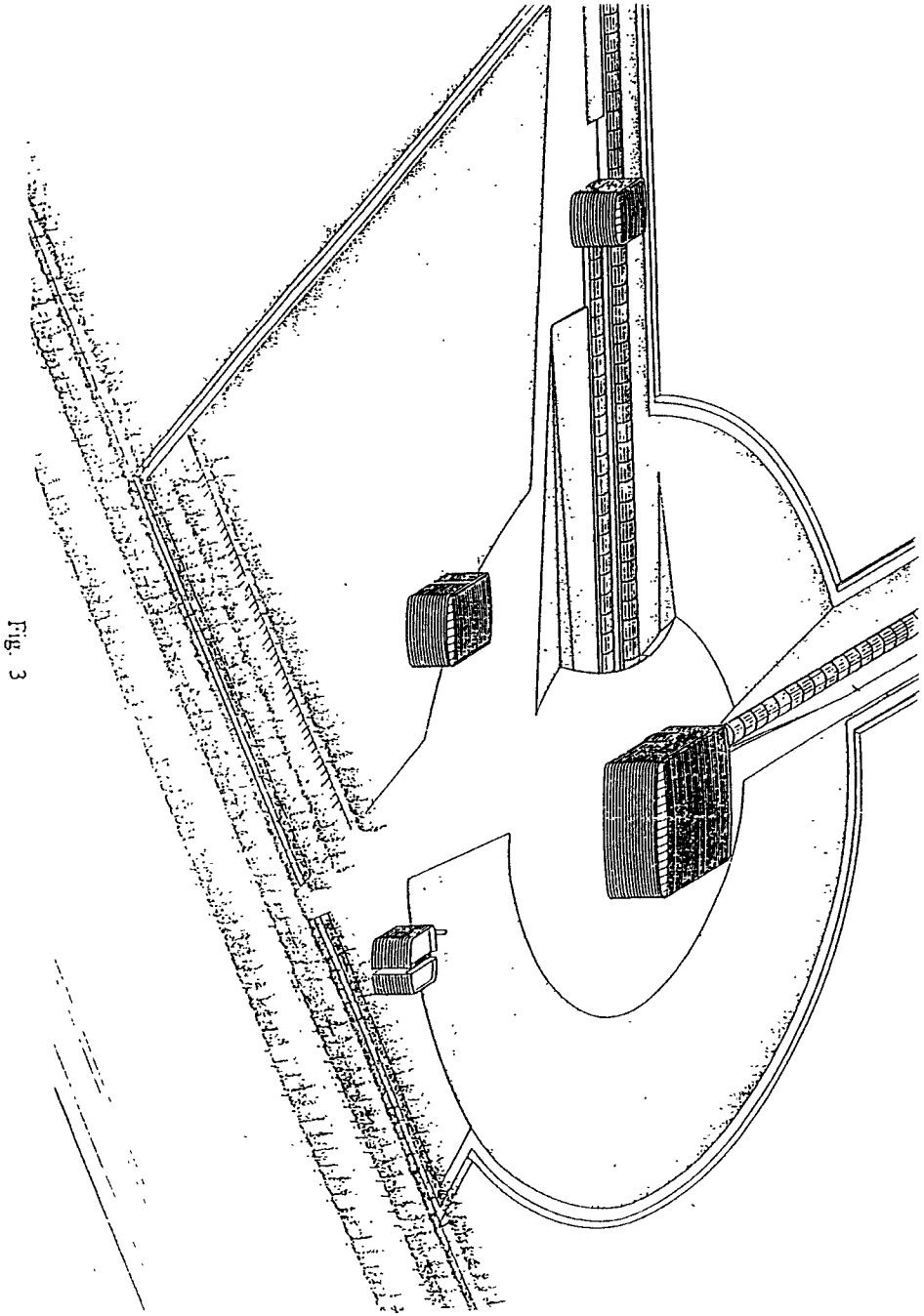

Fig. 3

A = CENTRAL BUIDING
B = CONTROL BUILDING
C = SERVICE BUILDING
D = MODE CLEANER
E = ASSEMBLY BUILDING
F = TERMINAL BUILDING

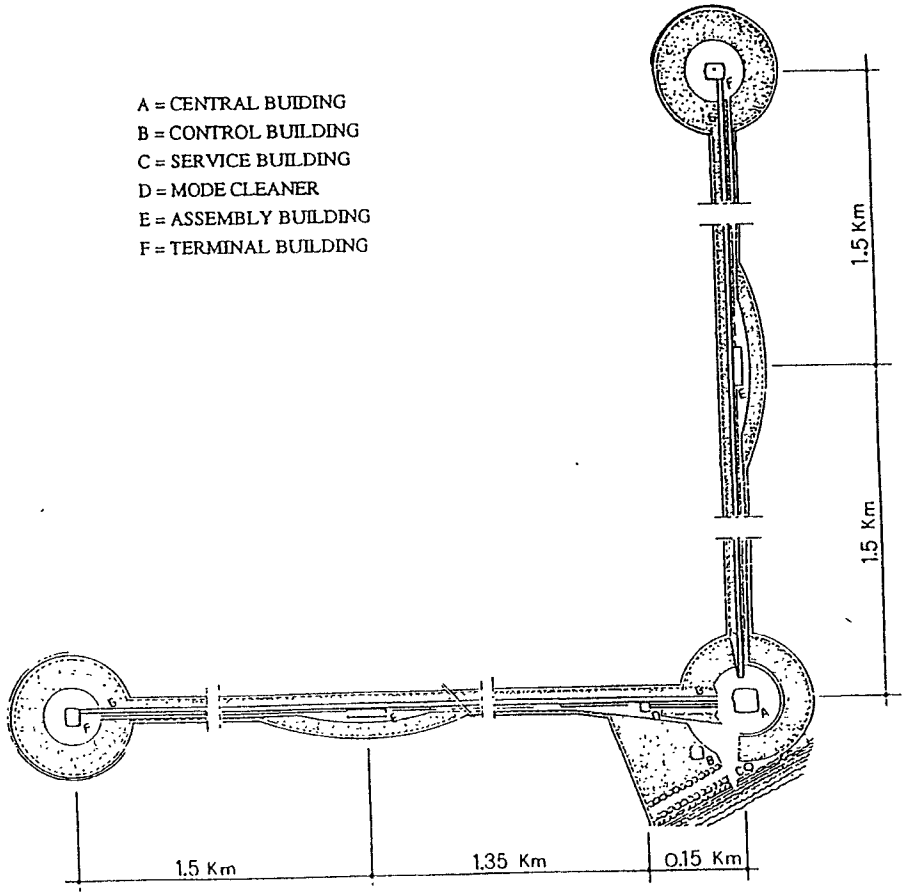

Fig. 2

Stato dei lavori a Cascina, 10 settembre 1996

Edificio Centrale

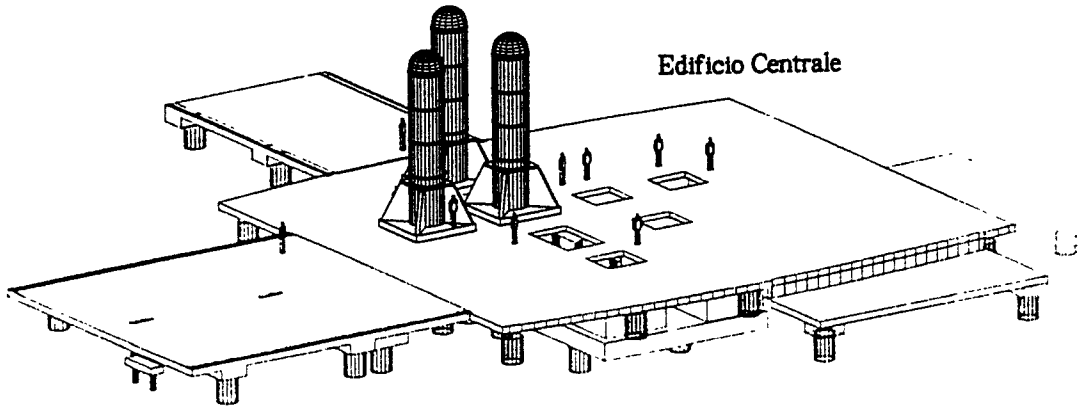

Edificio Tecnologico

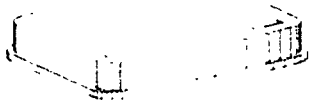

Edificio Controllo

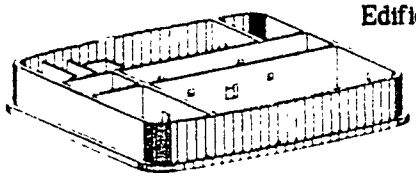

P.I G. De Carolis VIRGO

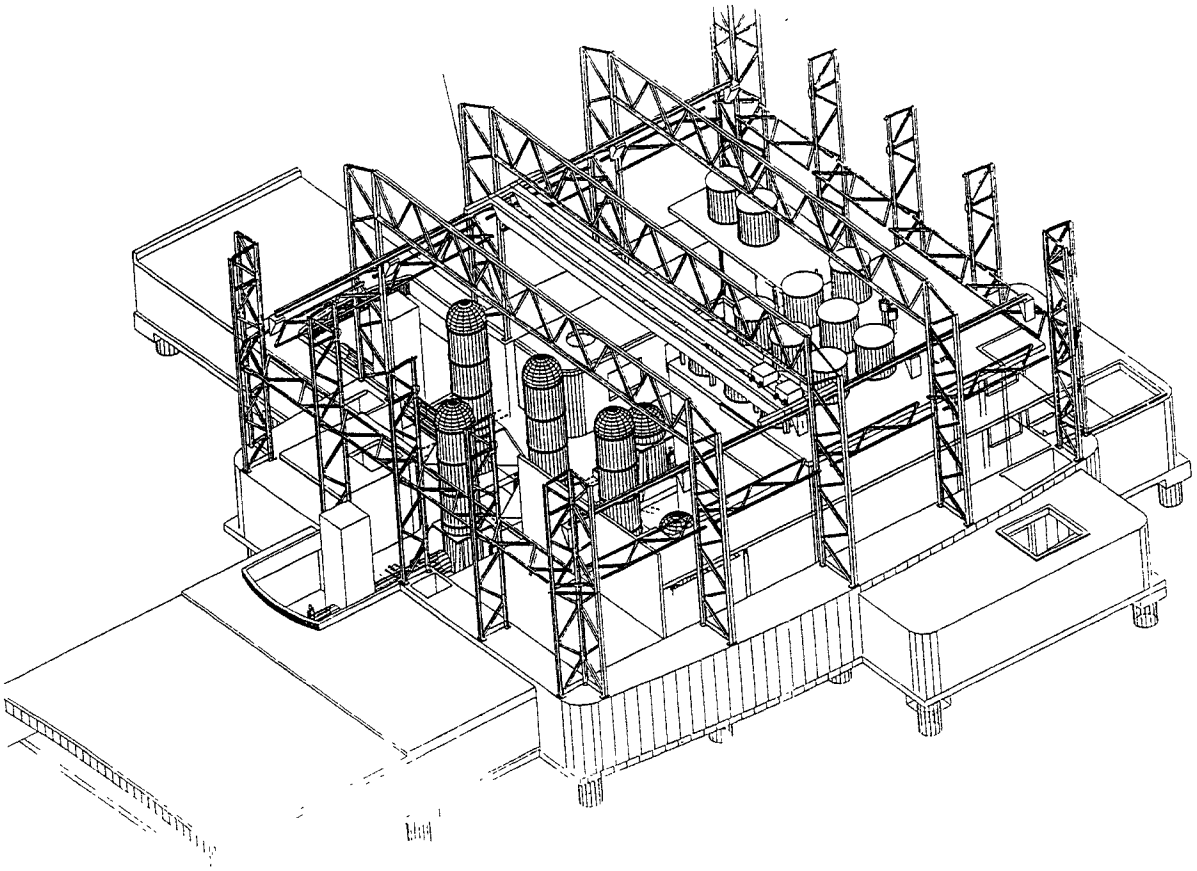

CONTROL BUILDING

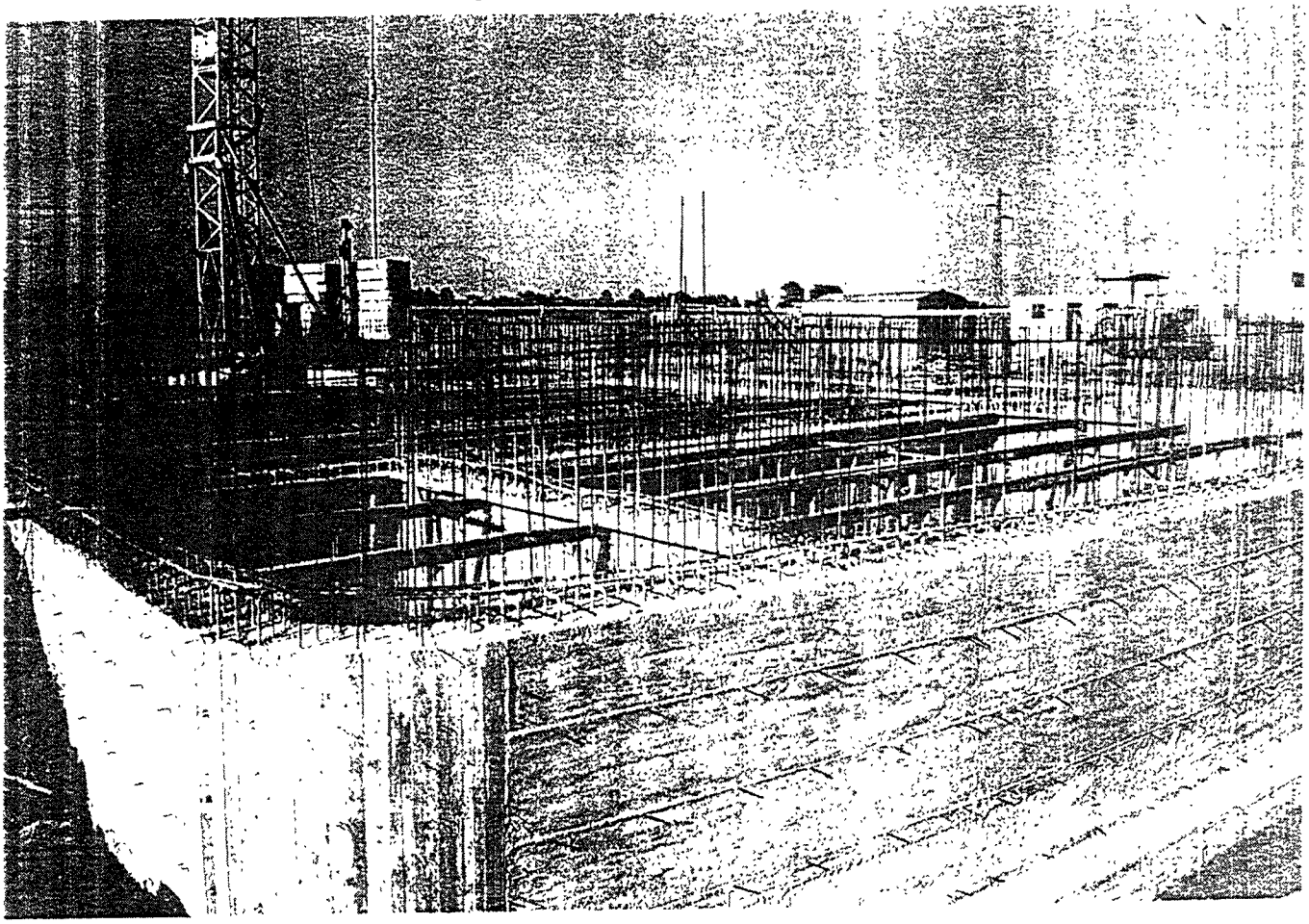

TECHNICAL BUILDING

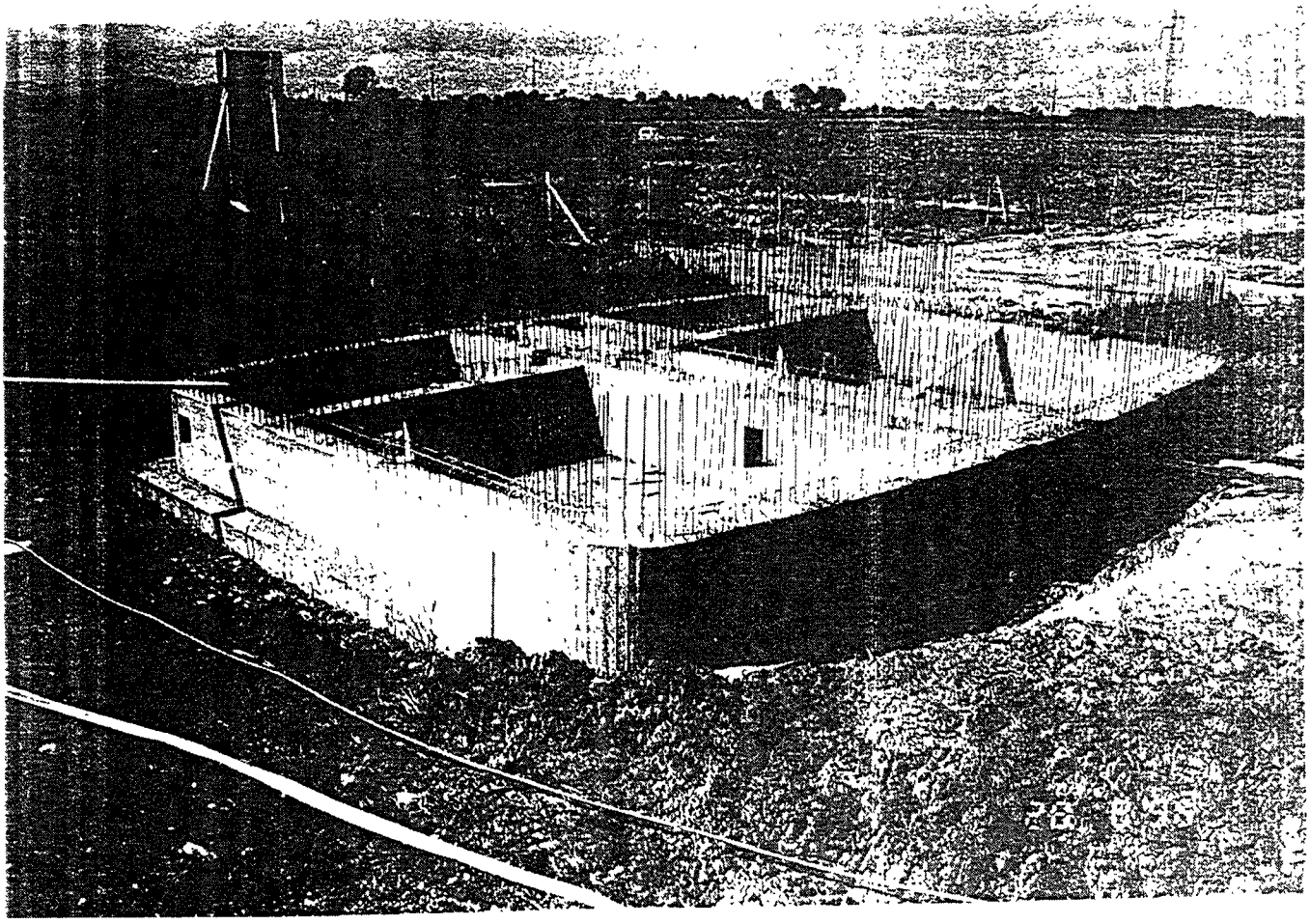

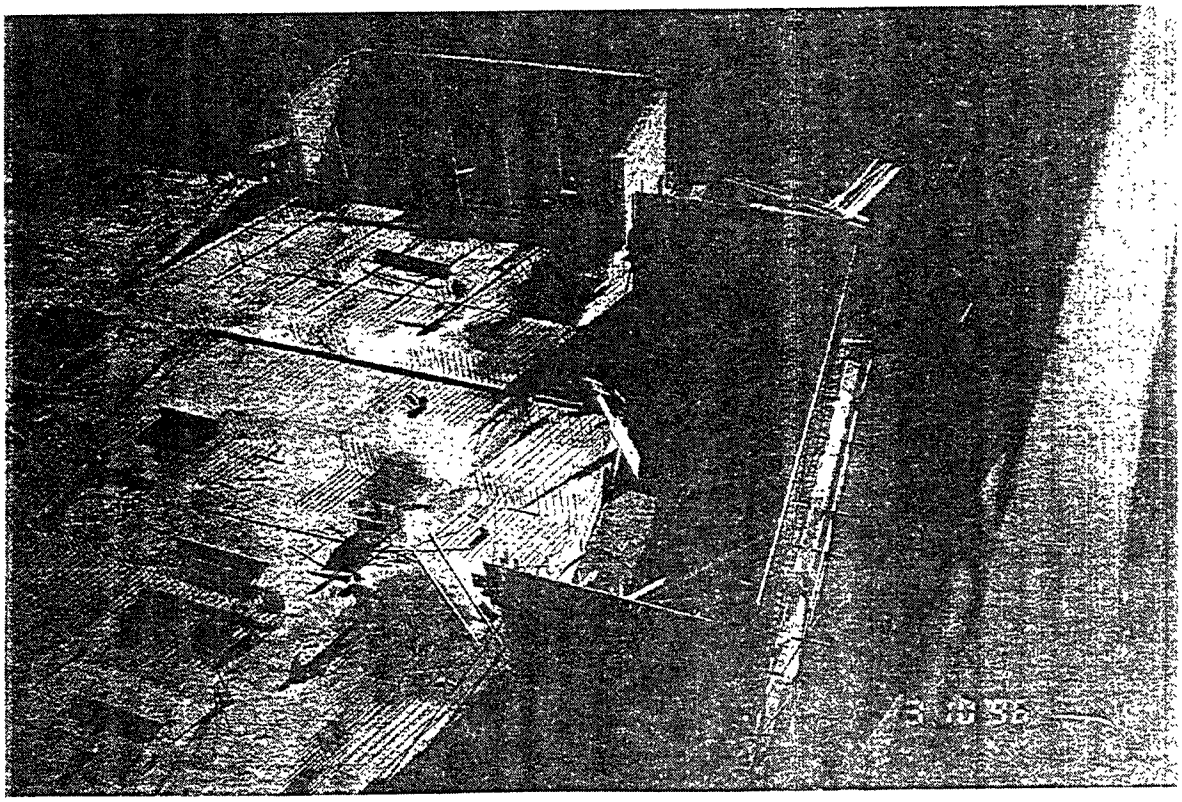

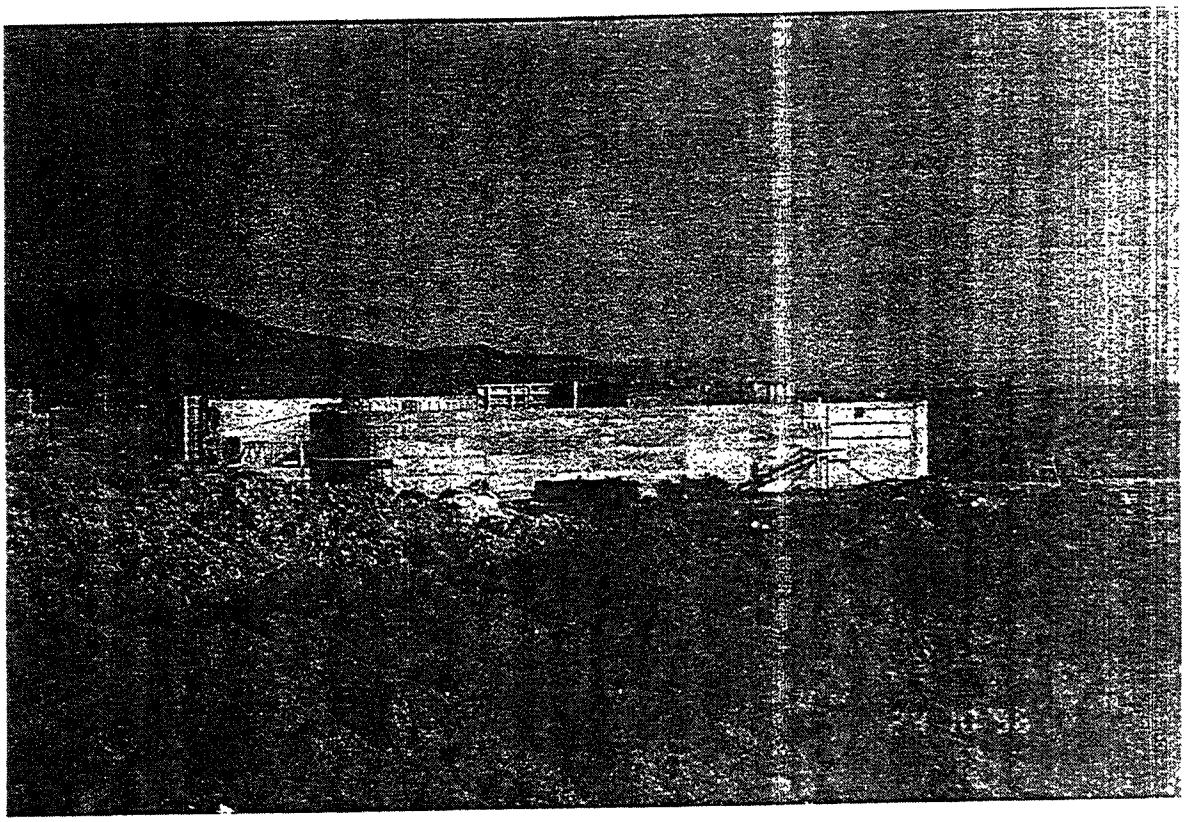

CENTRAL BUILDING - NORTH ARM

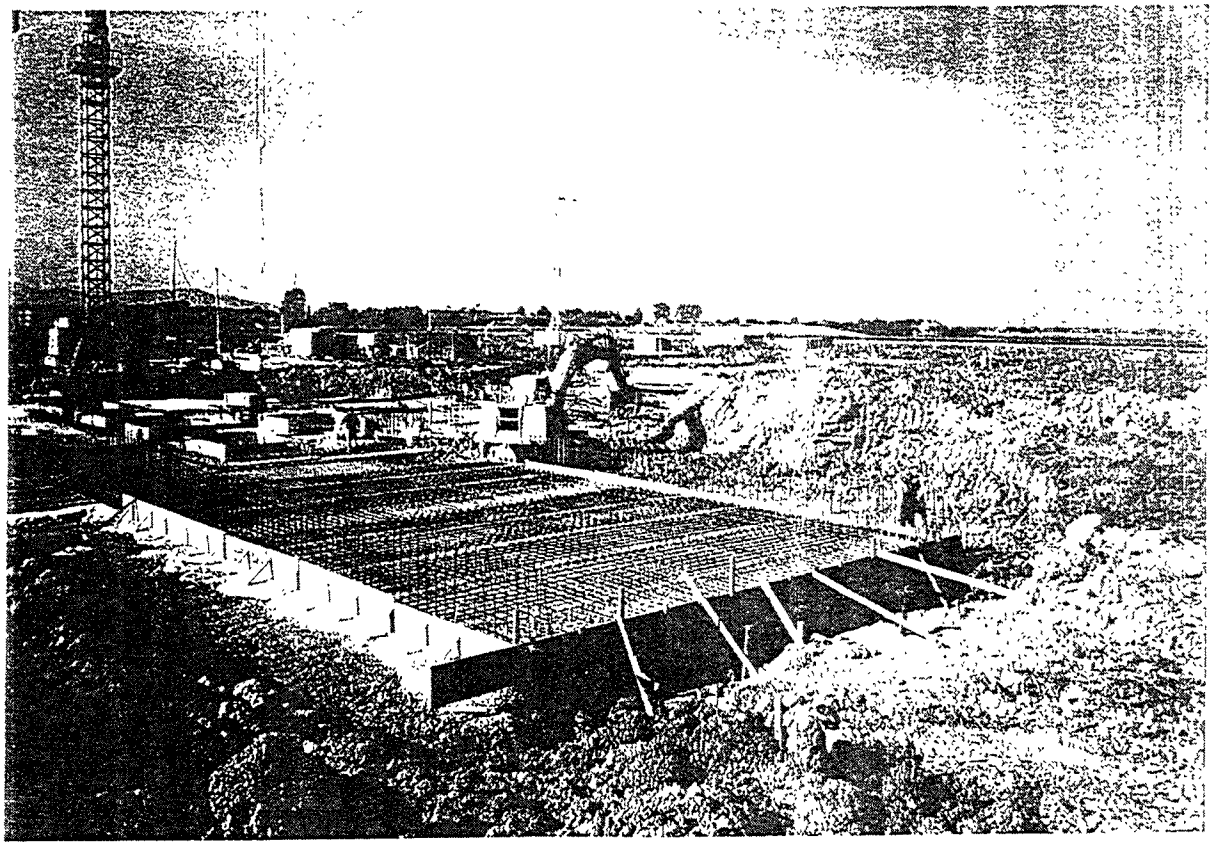

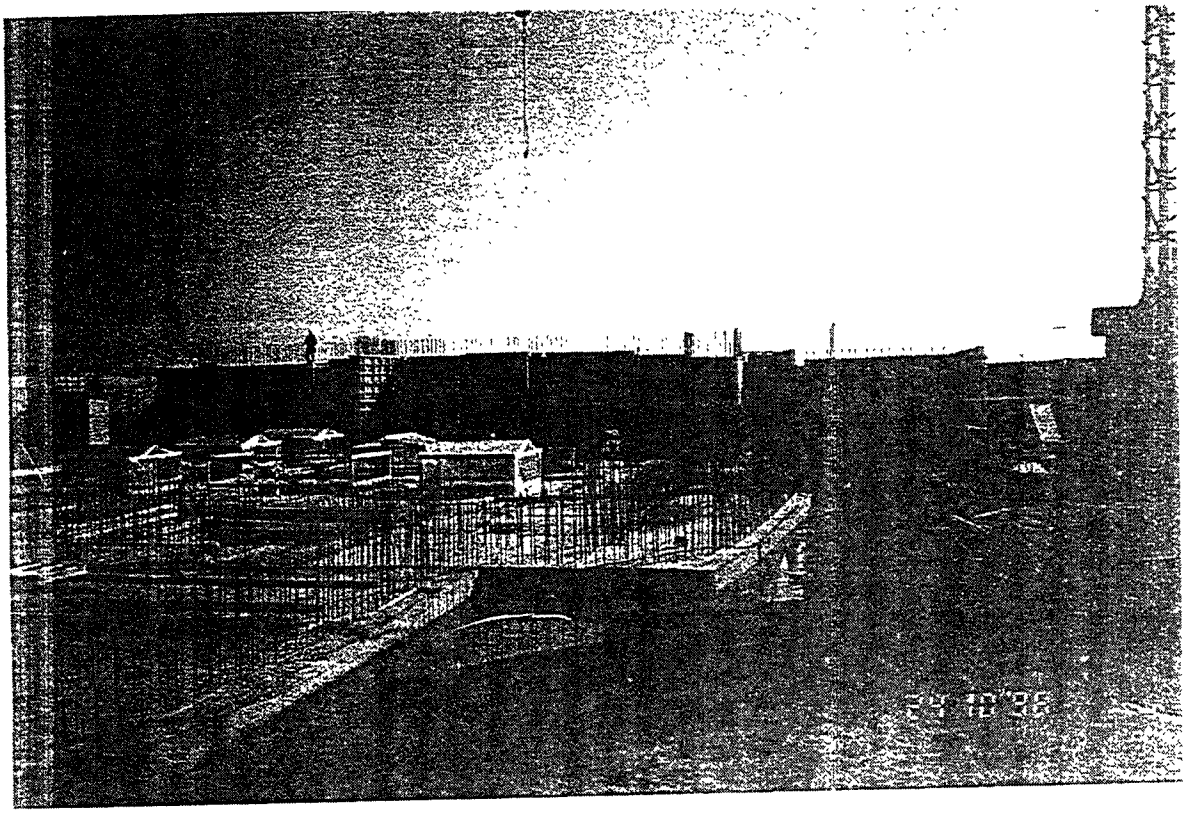
24 10'96

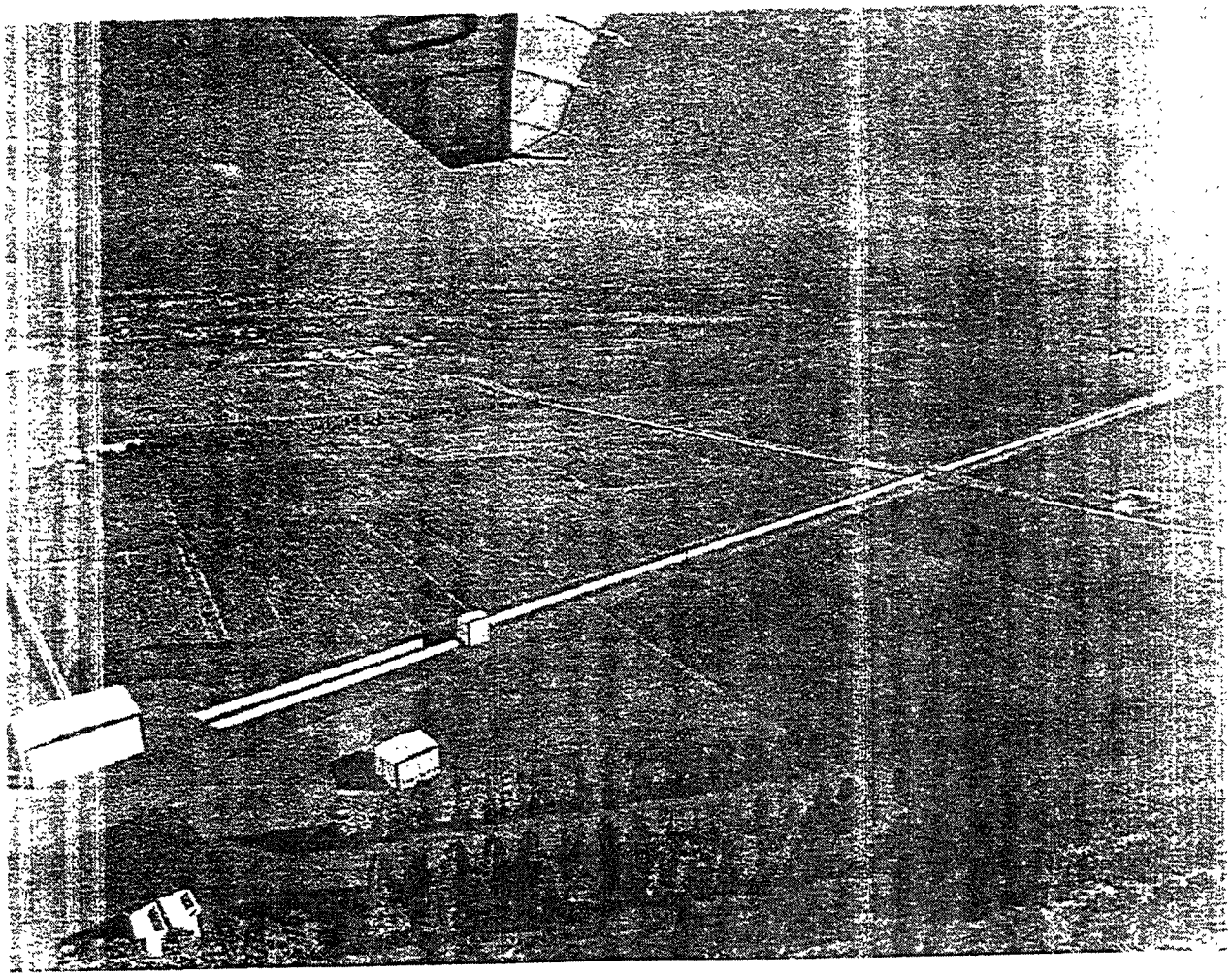

GEO 600: Current Status

J. Hough
University of Glasgow
for the GEO Team

Aspen, January 1997

GEO 600 – background

- Based on experiences with prototype systems at :
  - Garching (3m / 30m delay lines)
  - Glasgow (10m Fabry-Perot)
- Descoped version of original GEO proposal for a 3km interferometer
- Main personnel :
  - **Hannover**
    Danzmann, Aufmuth, Lück, Rinkleff, Schrempel, Welling, Willke + colleagues
  - **Garching**
    Mizuno, Rüdiger, Schilling, Schnier, Winkler + colleagues
  - **Glasgow**
    Hough, Newton, Plissi, N.Robertson, D.Robertson, Rowan, Skeldon, Strain, Ward + colleagues
  - **Cardiff / Potsdam**
    Schutz + colleagues

GEO 600 – rationale

- 600m baseline, low cost, high performance system
- planned sensitivity close to that of first stage LIGO or VIRGO above a few hundred Hertz
- construction on a timescale equivalent to that of the longer detectors
- can participate in coincidence experiments with LIGO and VIRGO
- can undertake meaningful stand-alone pulsar searches
- will allow development of advanced interferometric techniques

Interferometer outline

- The main detector is a recycled Michelson interferometer with :
  - 600m arm length
  - power recycling with a factor of 1500
  - signal recycling tunable in bandwidth and centre frequency
  - external modulation for signal recovery

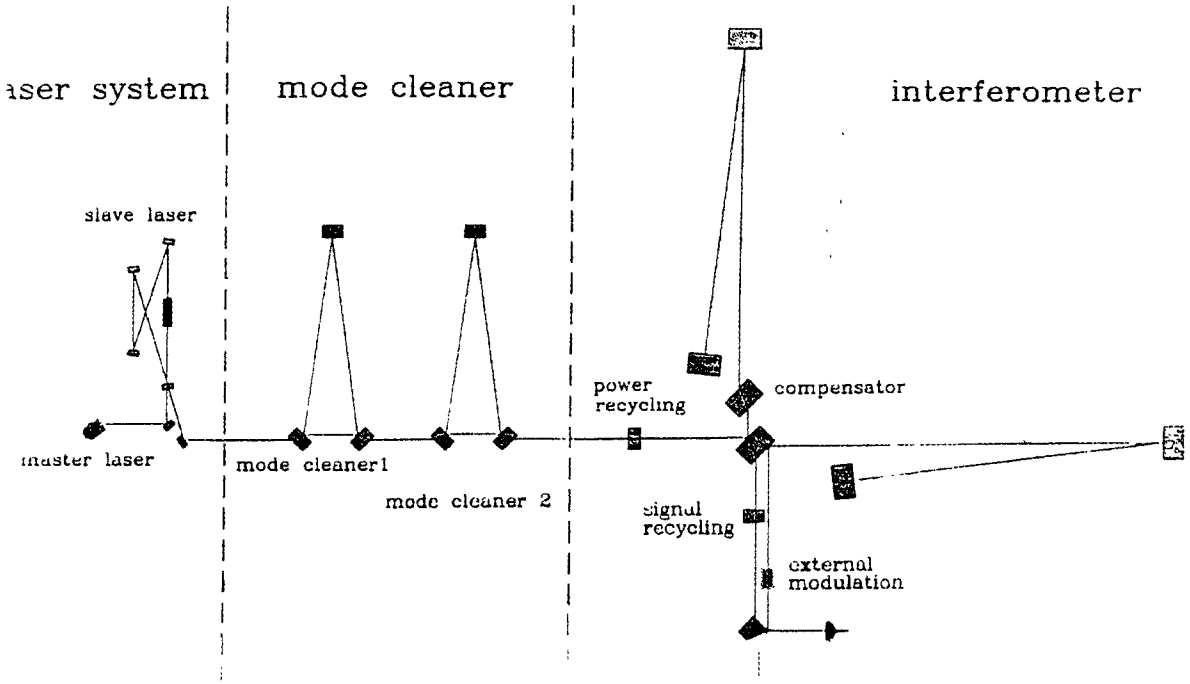
laser system
mode cleaner
interferometer
slave laser
master laser
mode cleaner1
mode cleaner 2
power recycling
compensator
signal recycling
external modulation

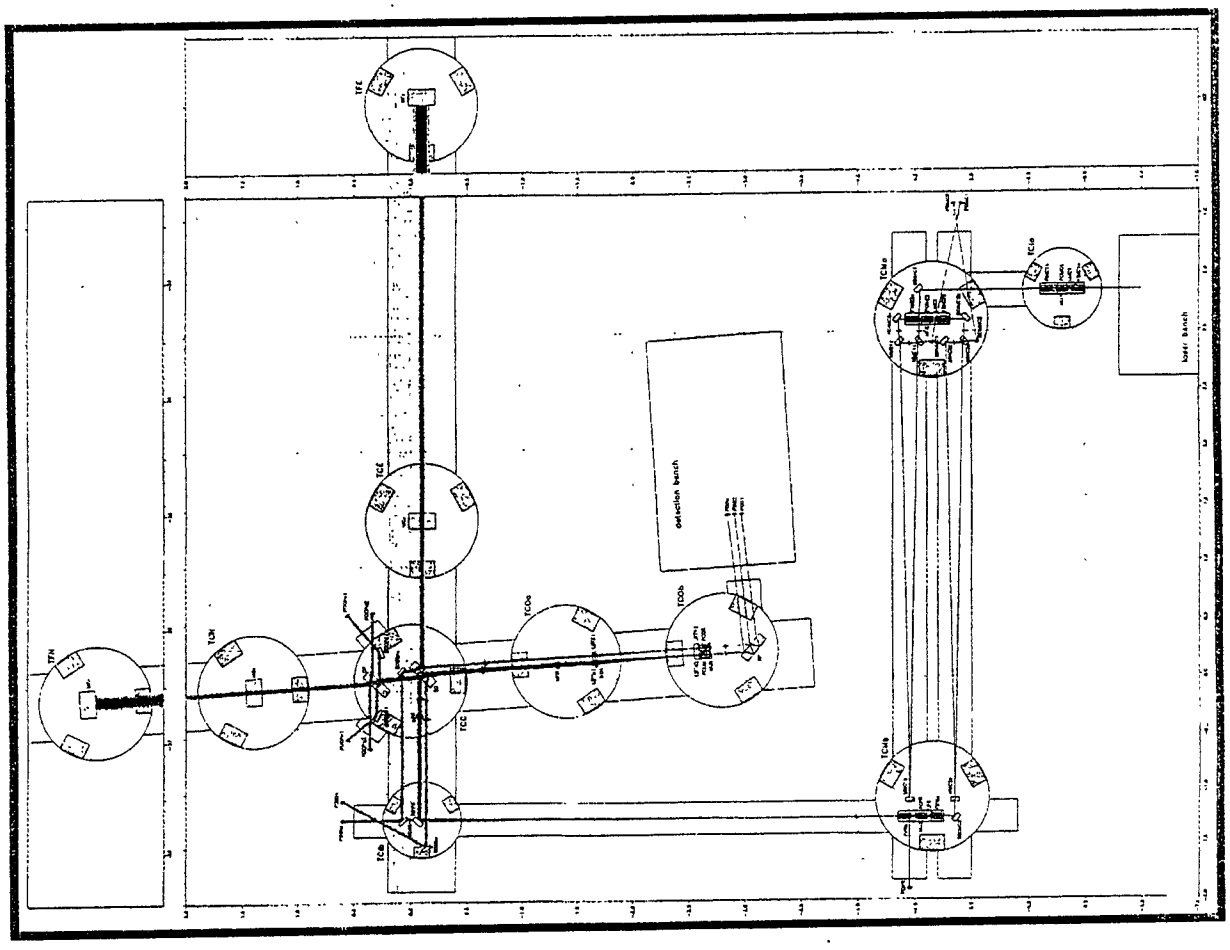

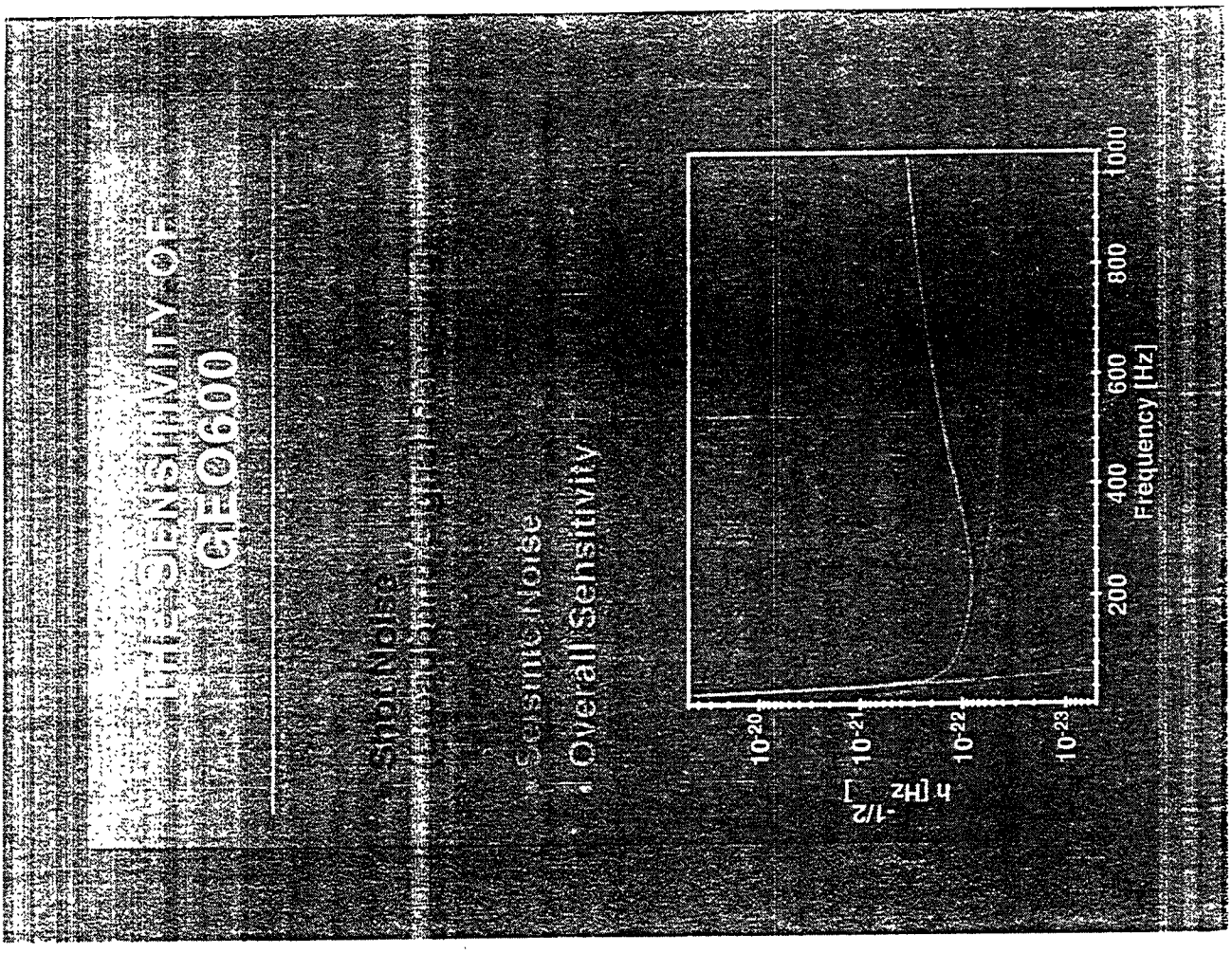

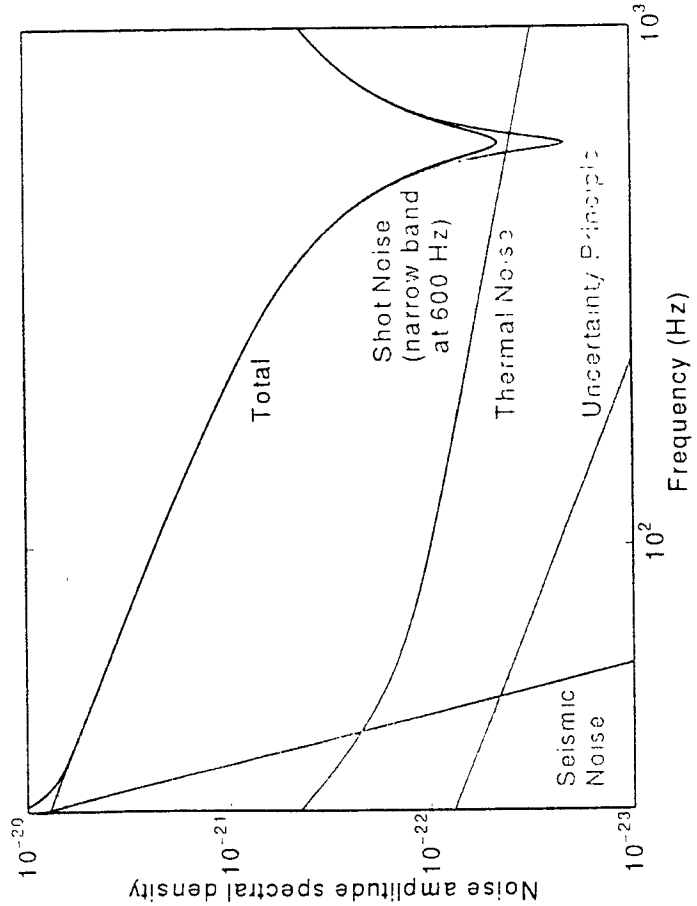

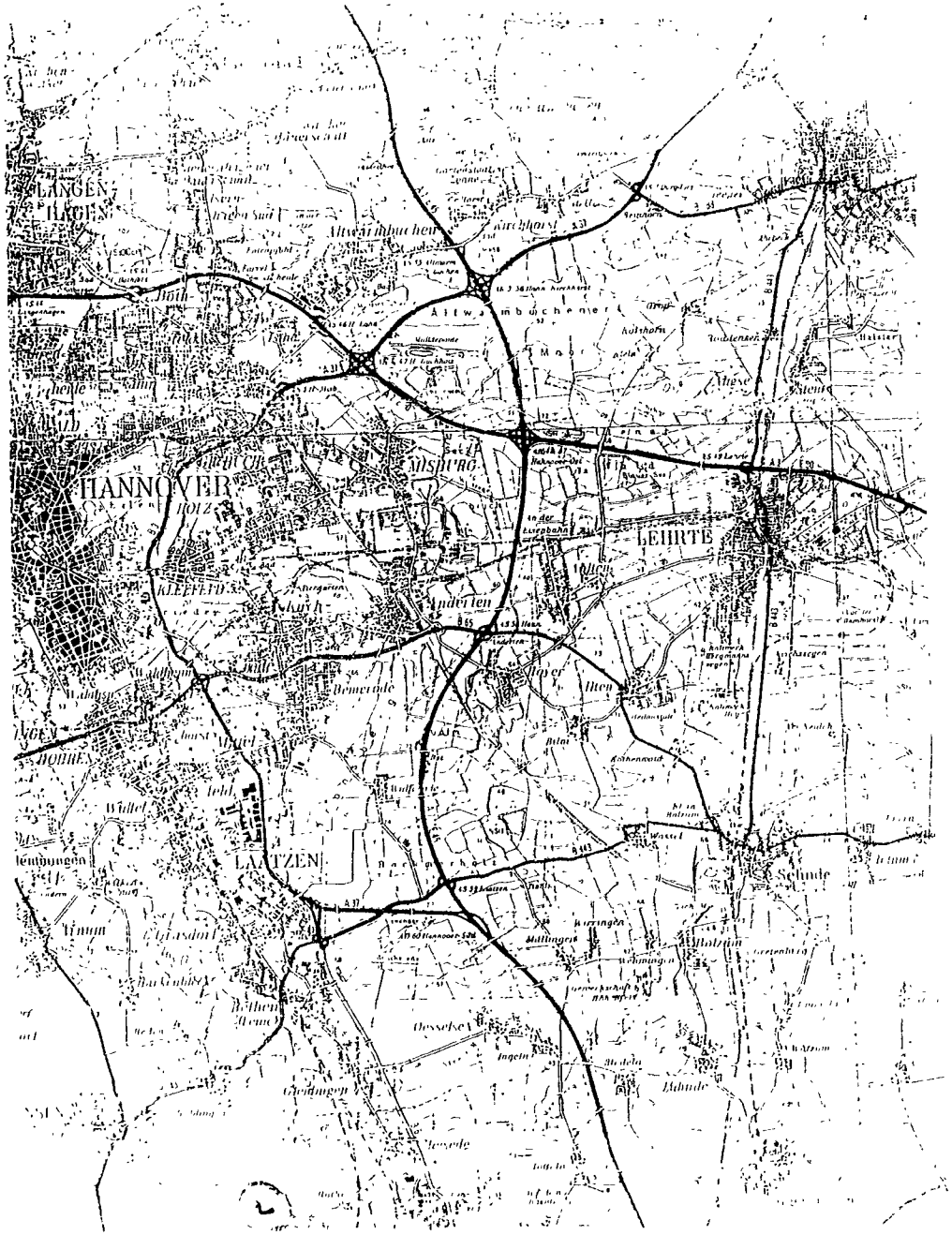
HANNOVER
LEHRTE
LAATZEN

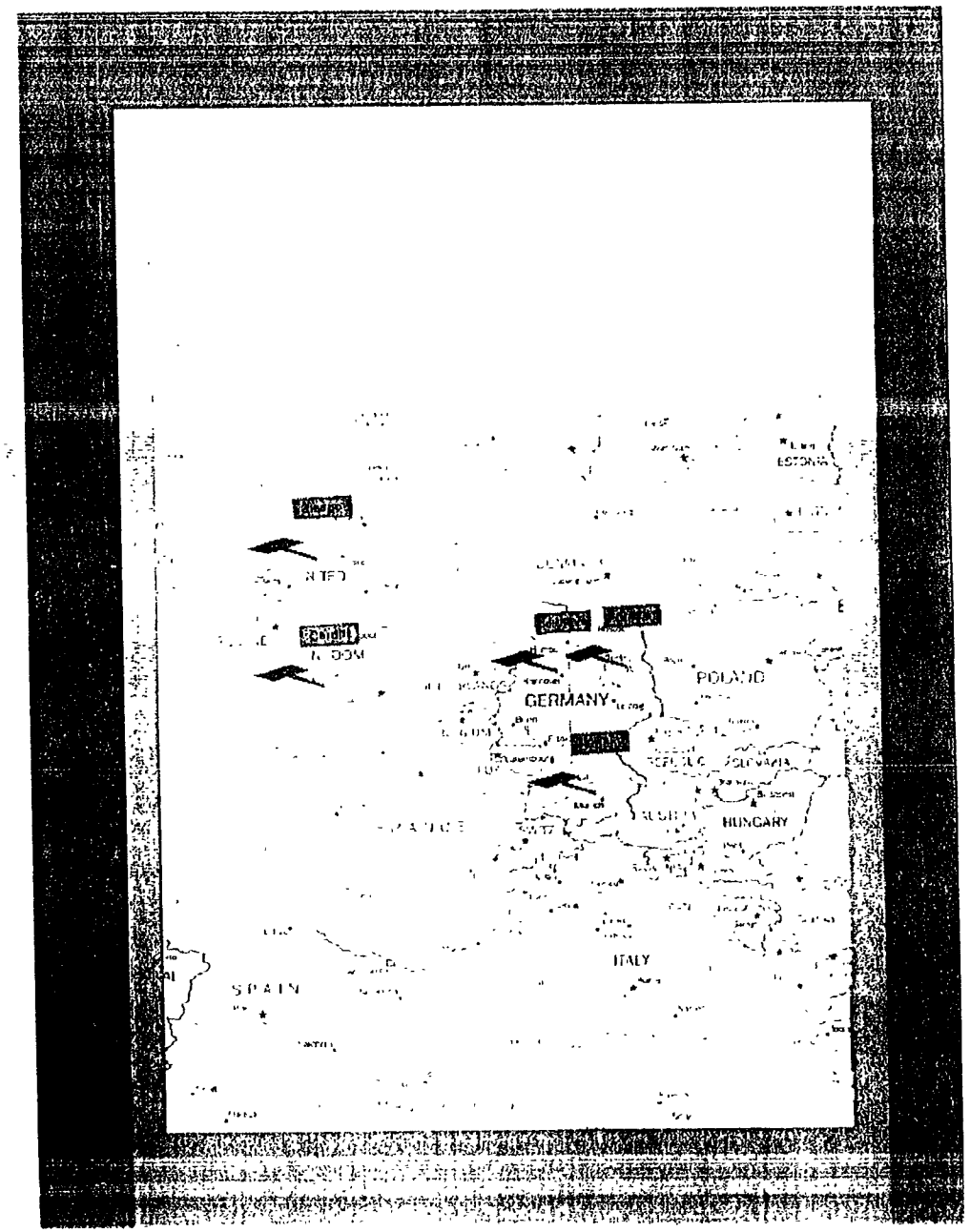
POLAND
GERMANY
HUNGARY
ITALY
SPAIN

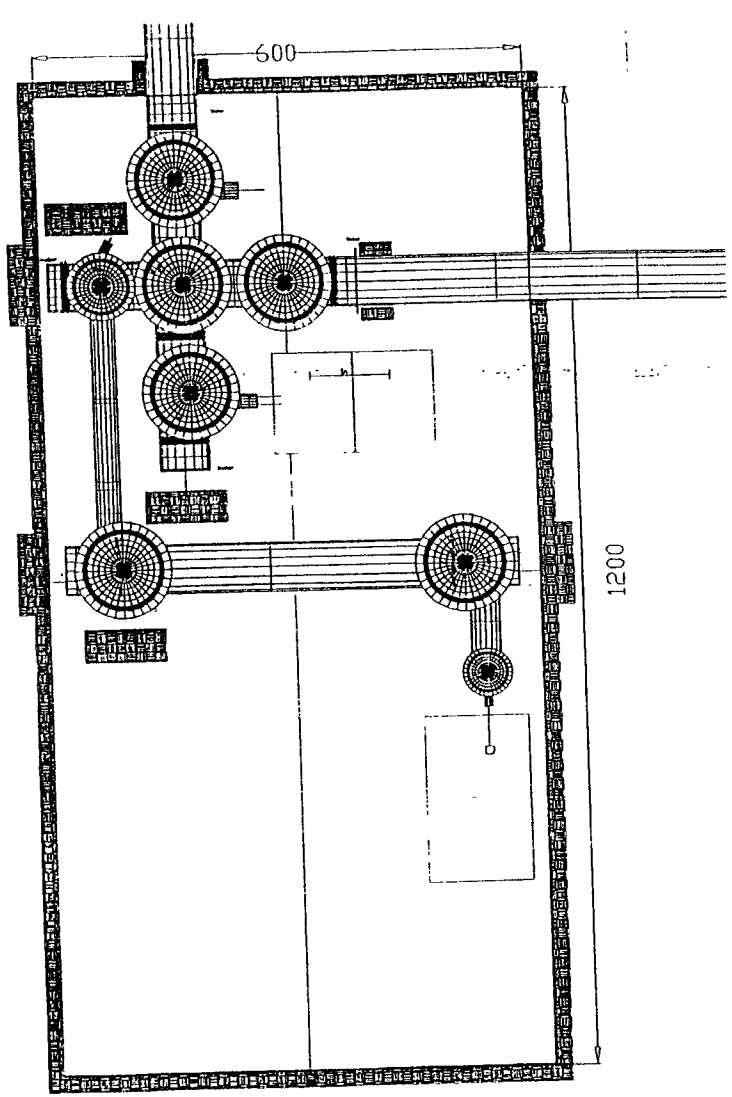

Figure A.5.4: *Scale plan of the centre station and part of one of the interferometer arms*

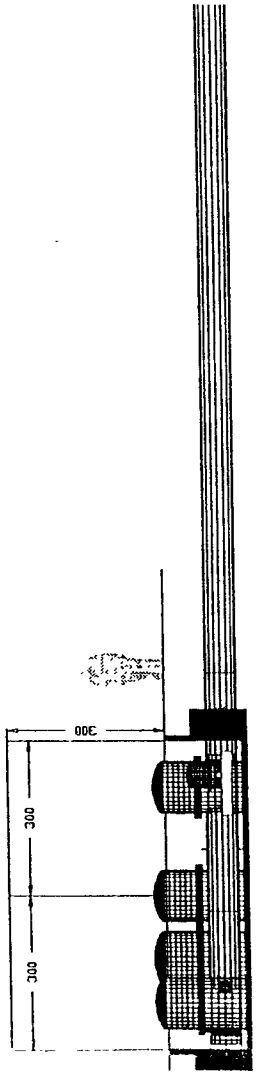

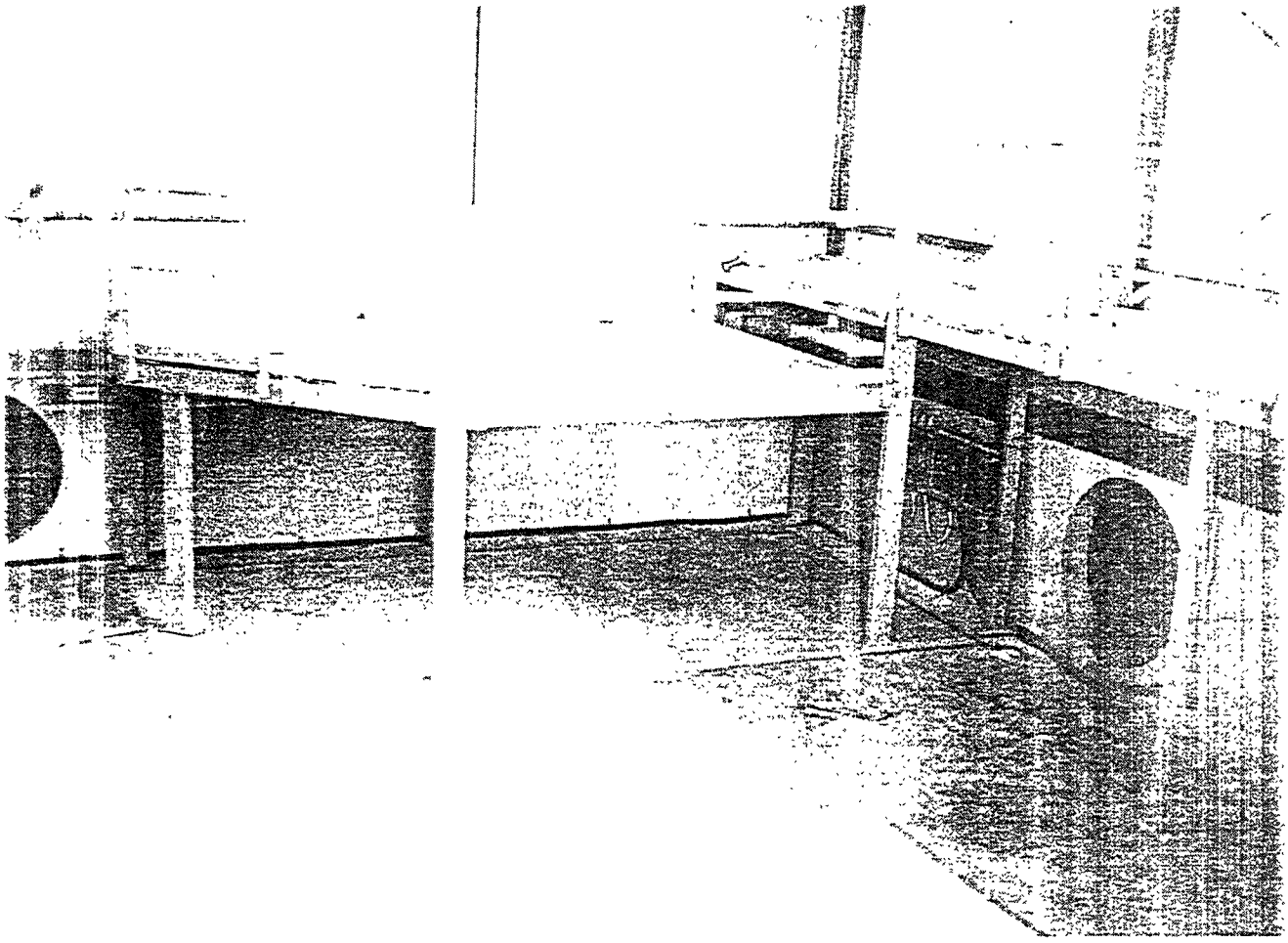

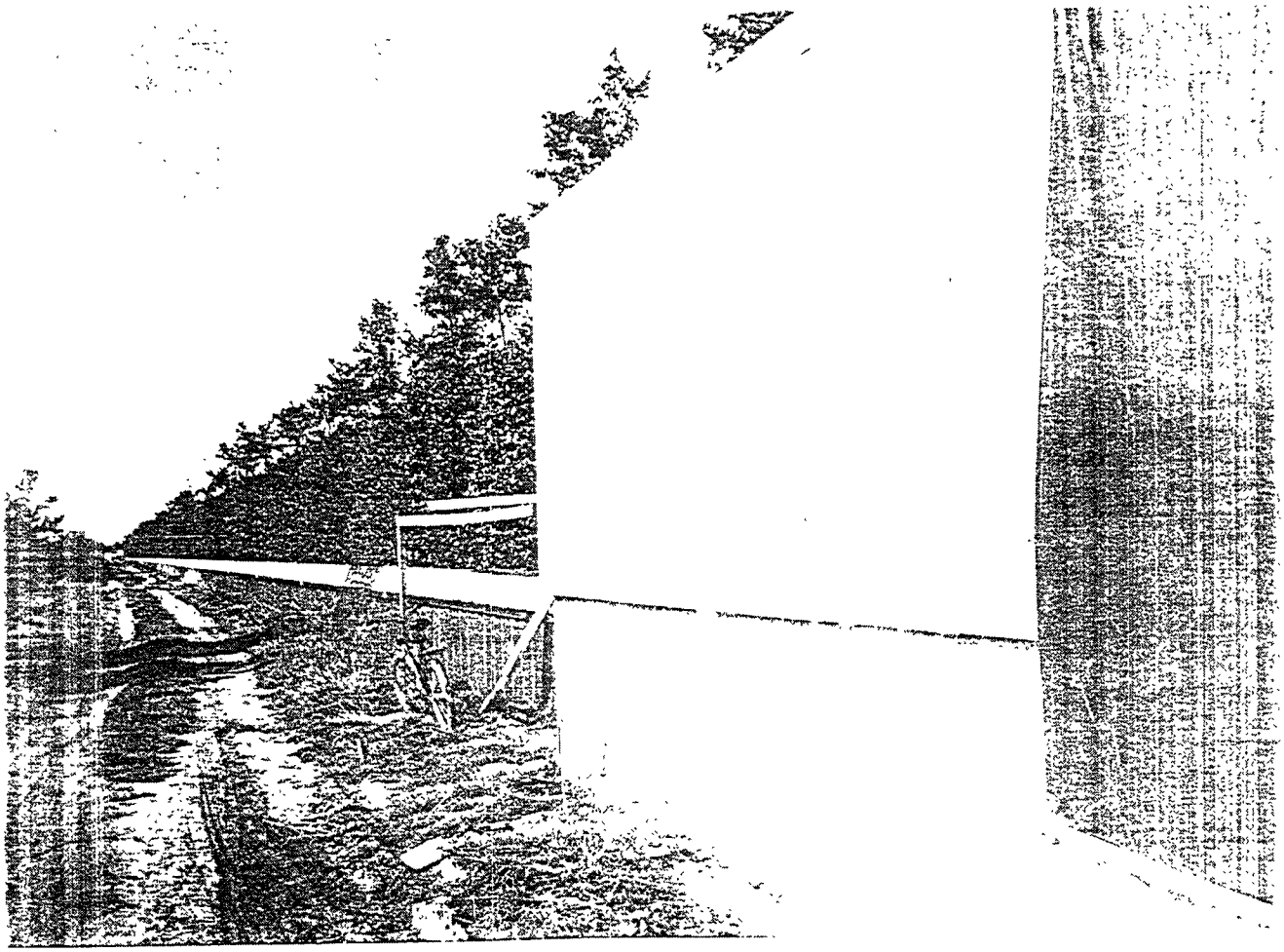

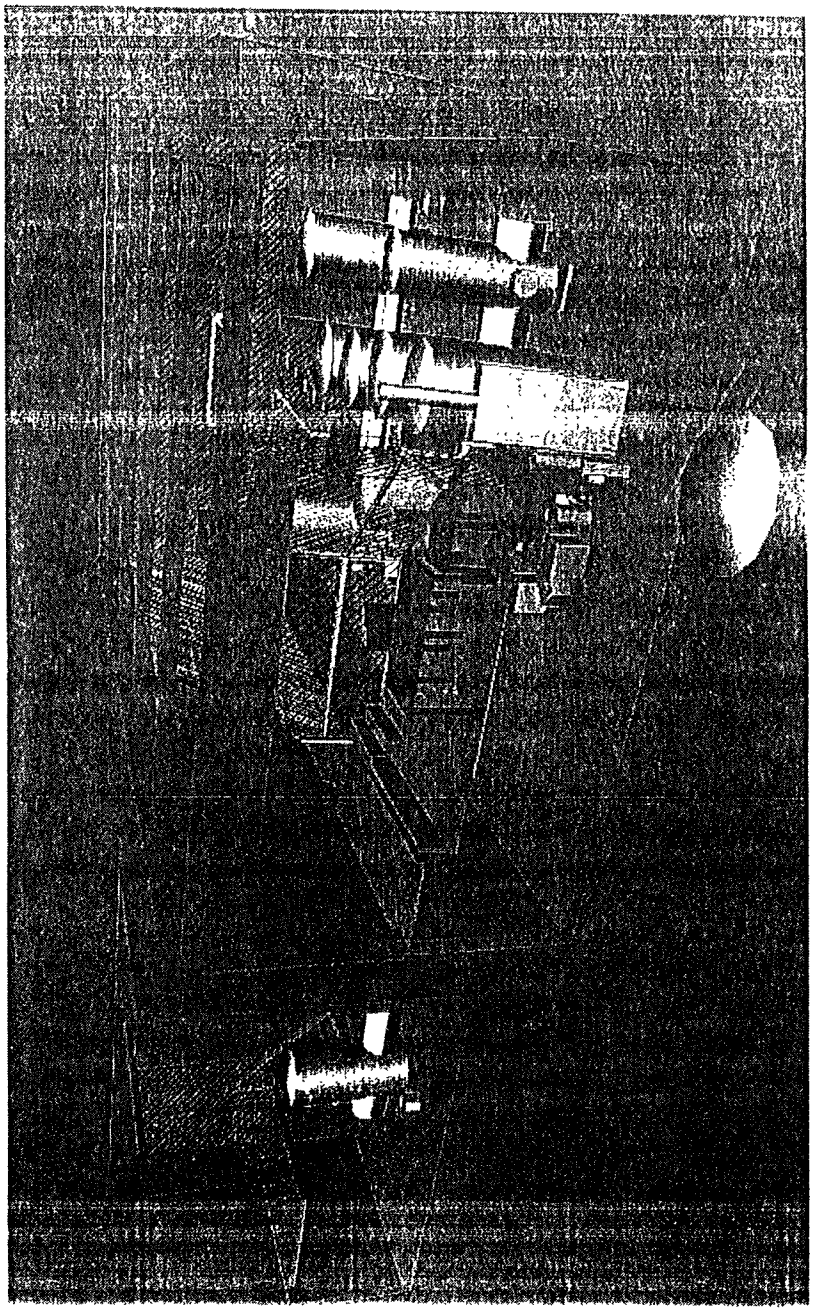

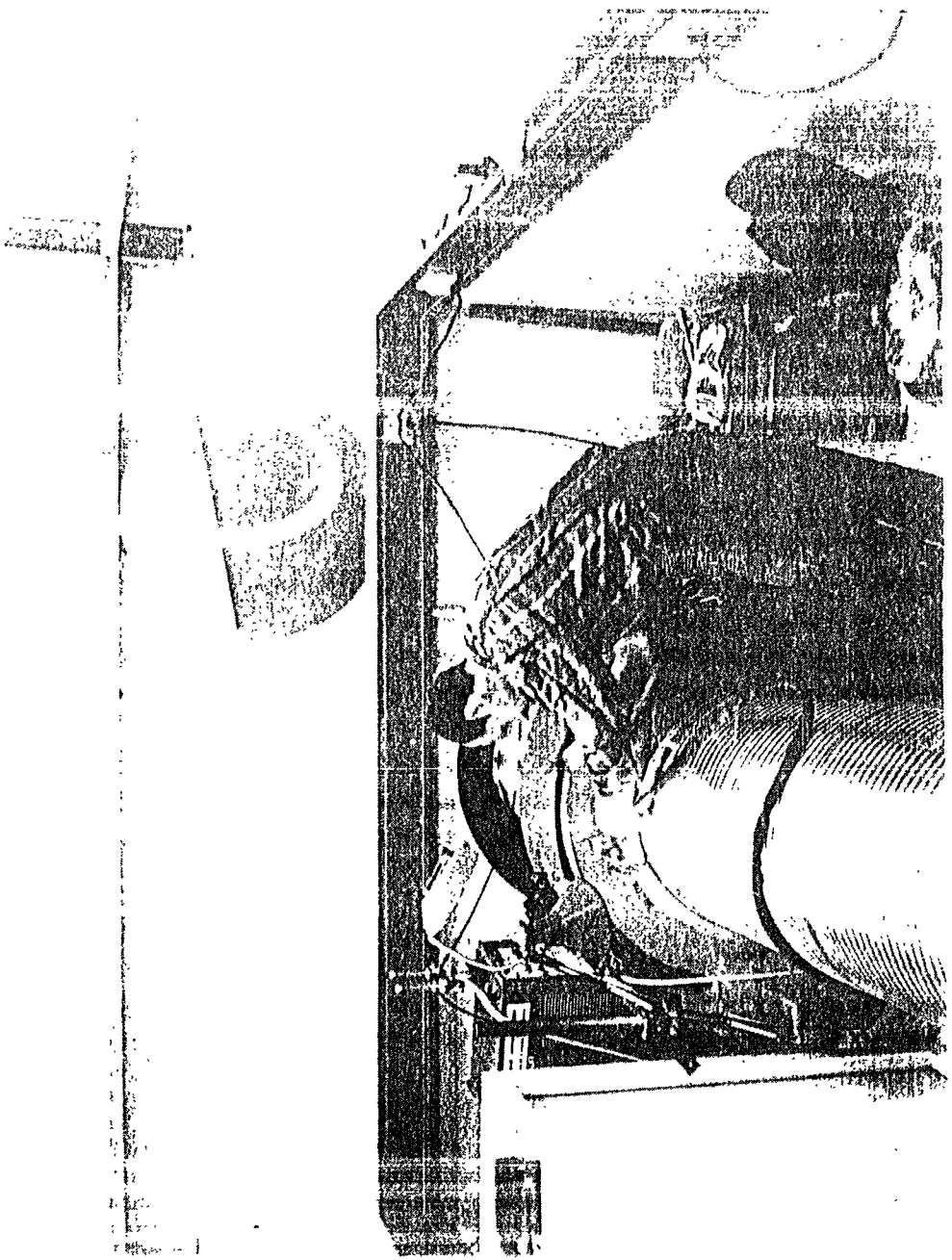

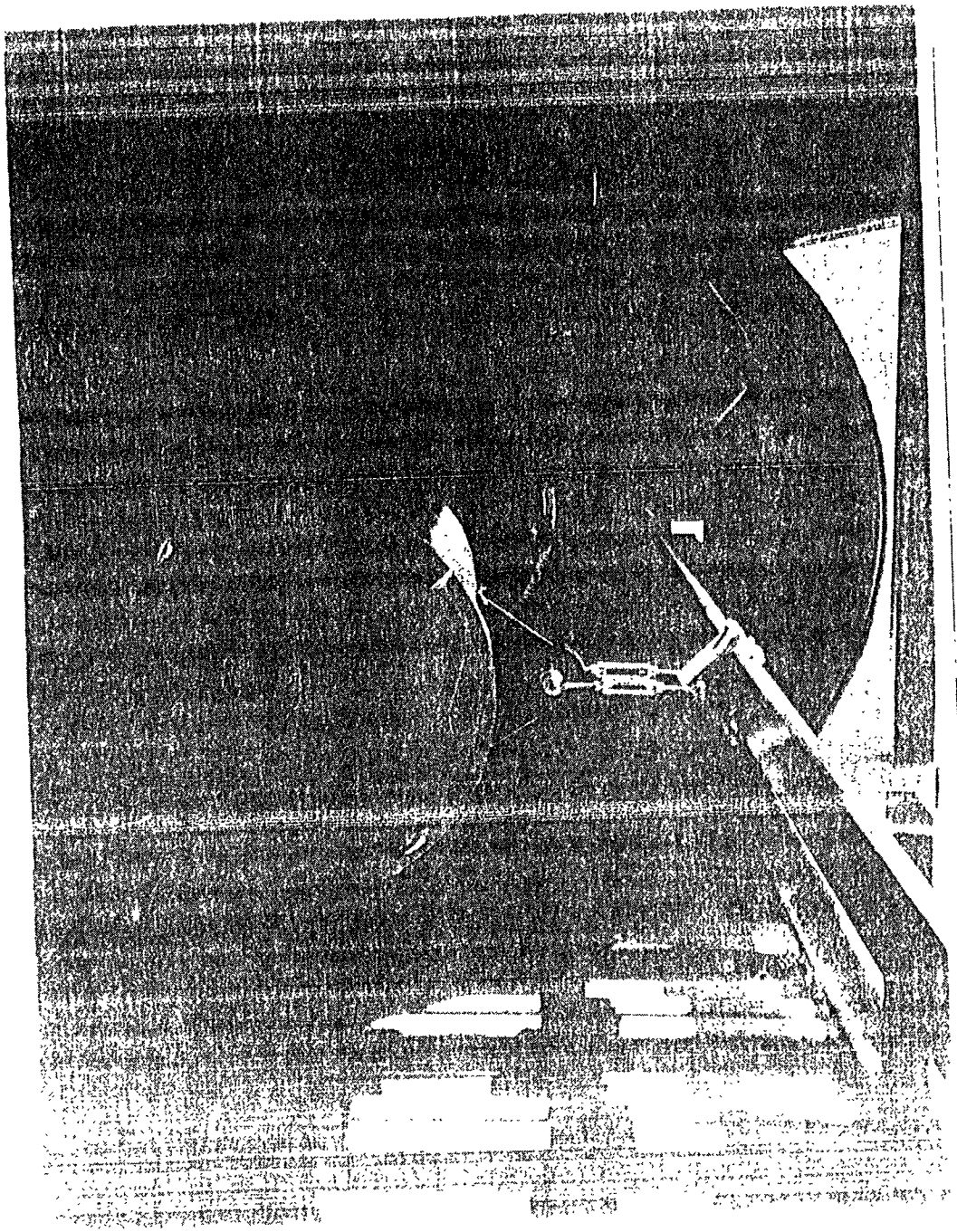

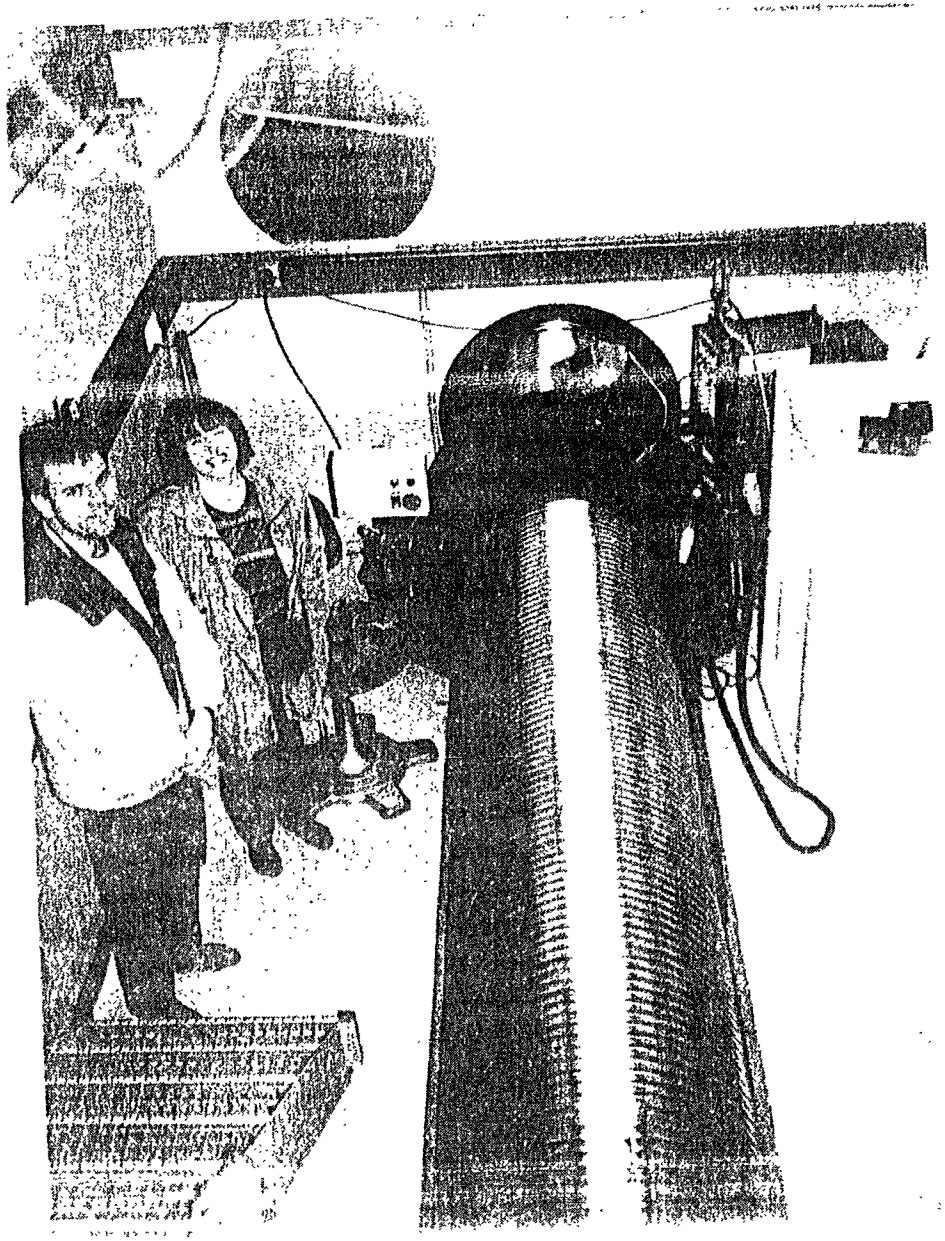

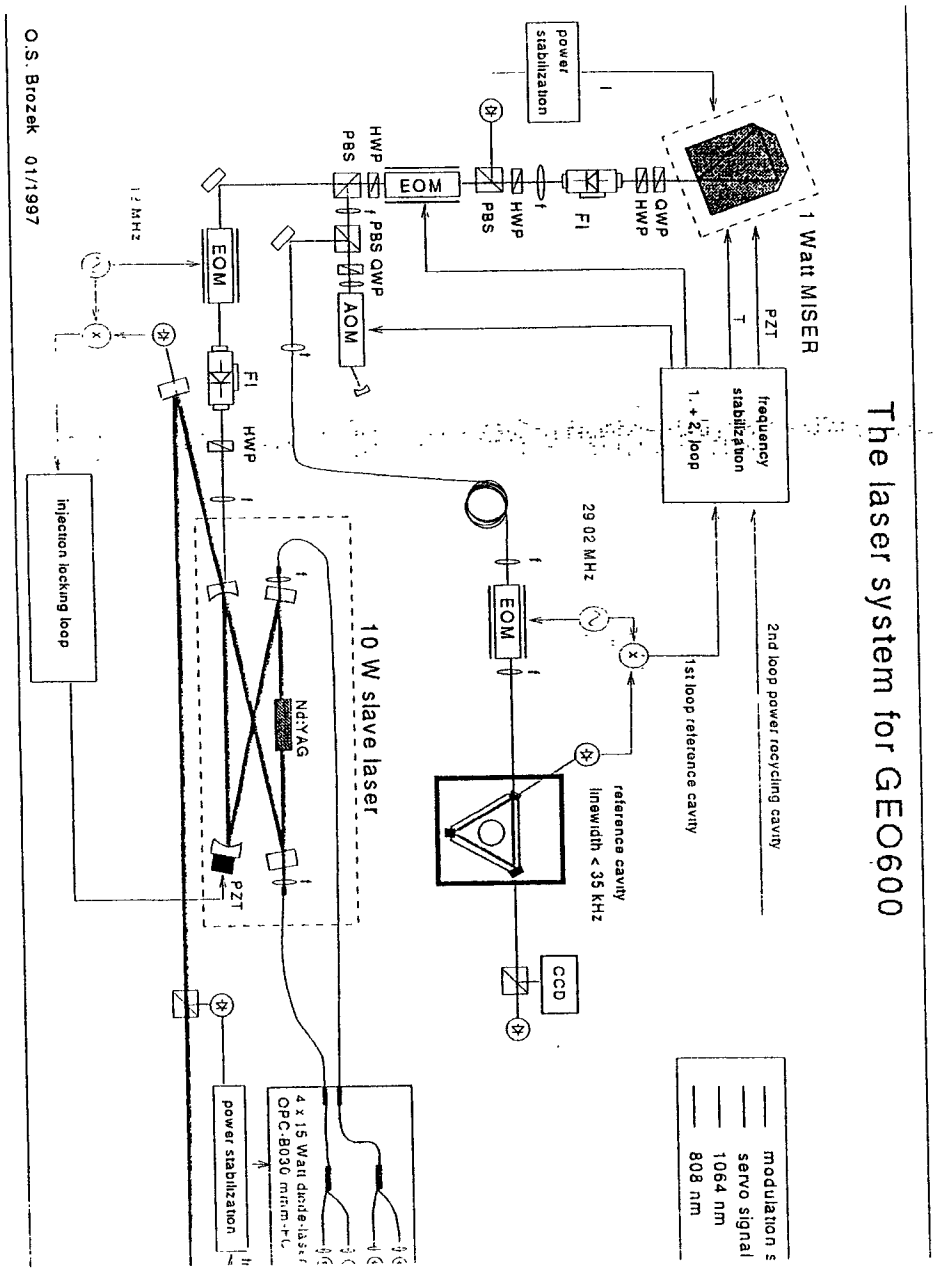

GEO 600 specifications – 1

- Arms
  - 2 x 600m, bearing NNW and ENE, near Ruthe, close to Hannover
- Laser system
  - Nd:YAG, diode-pumped, 1064nm, master/slave system with injection lock
  - 10 Watt output power
  - frequency stabilised
  - intensity stabilised
- Mode cleaners
  - twin suspended mirror ring cavities
  - length 8m, finesse 1900, linewidth 20kHz
  - 50dB suppression of beam jitter per cavity

GEO 600 specifications – 2

- Optics
  - 25cm diameter, 15cm thick OH^--free fused silica, absorption < 1ppm/cm
- Mirrors
  - ionsputtered, absorption loss < 1ppm/cm
- Power recycling
  - up to 10kW of circulating power
- Signal recycling
  - up to 1000 - fold signal power enhancement
  - tunability from 50Hz to 1500Hz, with bandwidth from 5Hz to 500Hz

GEO 600 specifications – 3

- Seismic isolation / suspension
  - 2-layer stacks plus 2 vertical springs
  - double pendulums with reaction masses where required
  - lower stage monolithic fused silica
- Vacuum
  - 60cm diameter pipes
  - 5×10^{-8} mbar for Hydrogen, 5×10^{-9} mbar for other gases
  - hydrocarbon-free
- Sensitivity
  - depending on chosen bandwidth

    $h \sim 2 \times 10^{-22} / Hz^{-1/2}$ to

    $h \sim 3 \times 10^{-23} / Hz^{-1/2}$

GEO 600 collaboration

- Garching (30m prototype)
  - power recycling
  - signal recycling
  - auto-alignment
- Glasgow (10m prototype)
  - seismic isolation
  - monolithic pendulum suspensions
  - computer control
- Hannover (600m detector)
  - buildings
  - vacuum system
  - laser system
- Cardiff / Potsdam
  - data acquisition
  - data analysis

Timetable

- 1996
  - vacuum system
- 1997
  - mode-cleaners, laser bench
- 1998
  - investigations with a 1200m long cavity formed from single arm
- 1999
  - 600m Michelson interferometer
- 2000
  - final optics

DATA TAKING

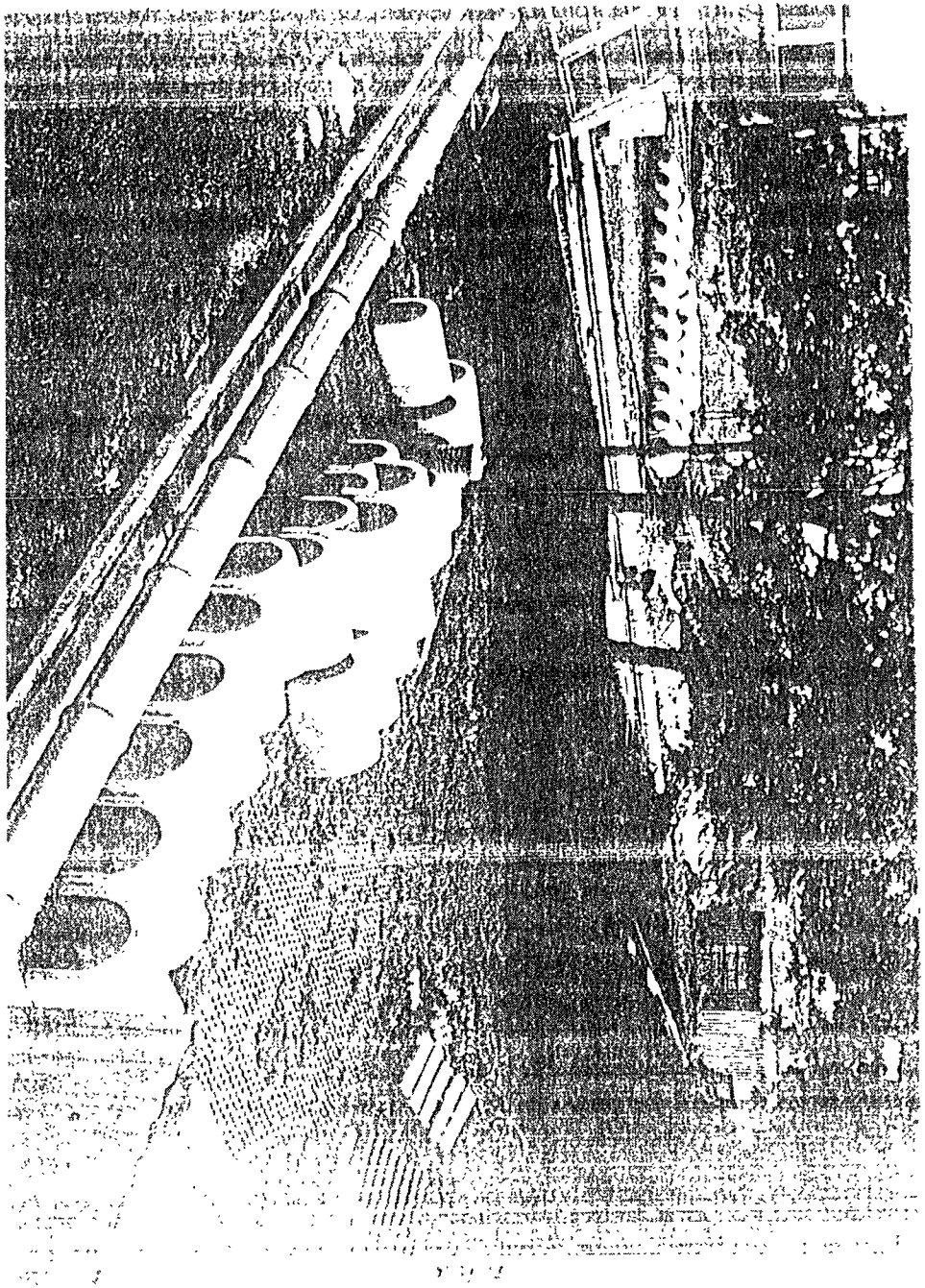

Technological developments

- Garching
- Hannover
- Glasgow

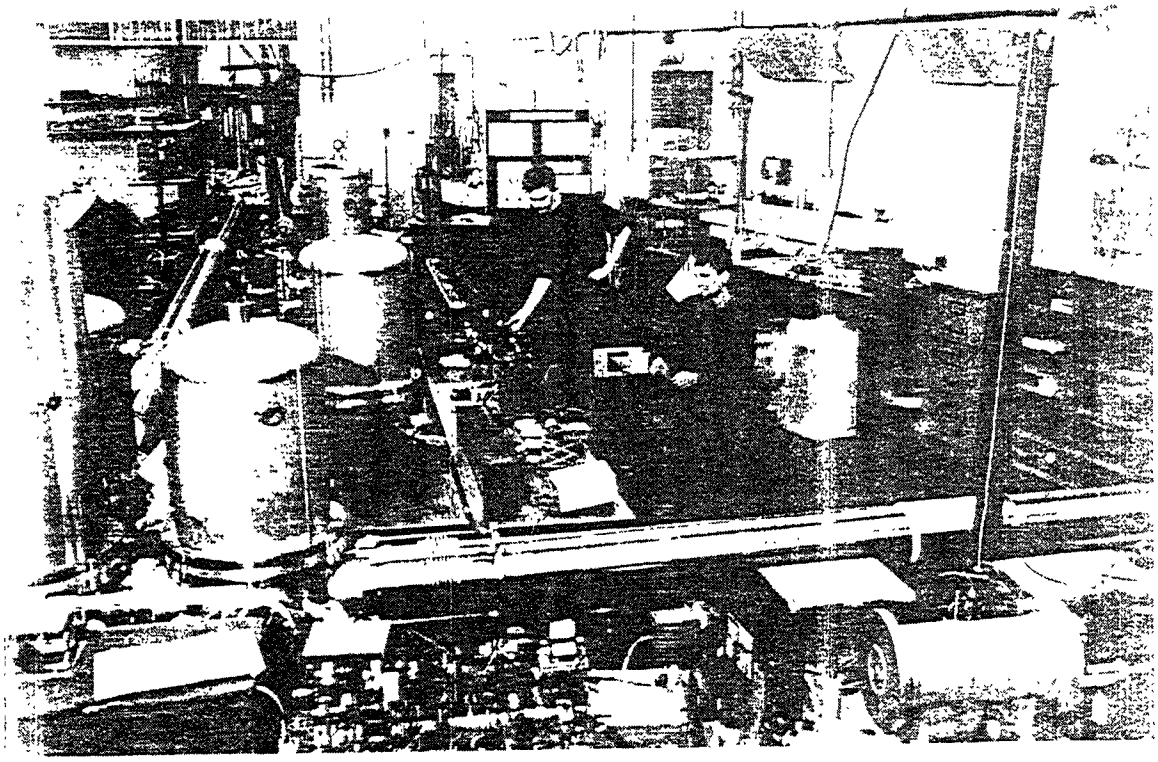

GLASGOW 10 m PROTOTYPE DETECTOR

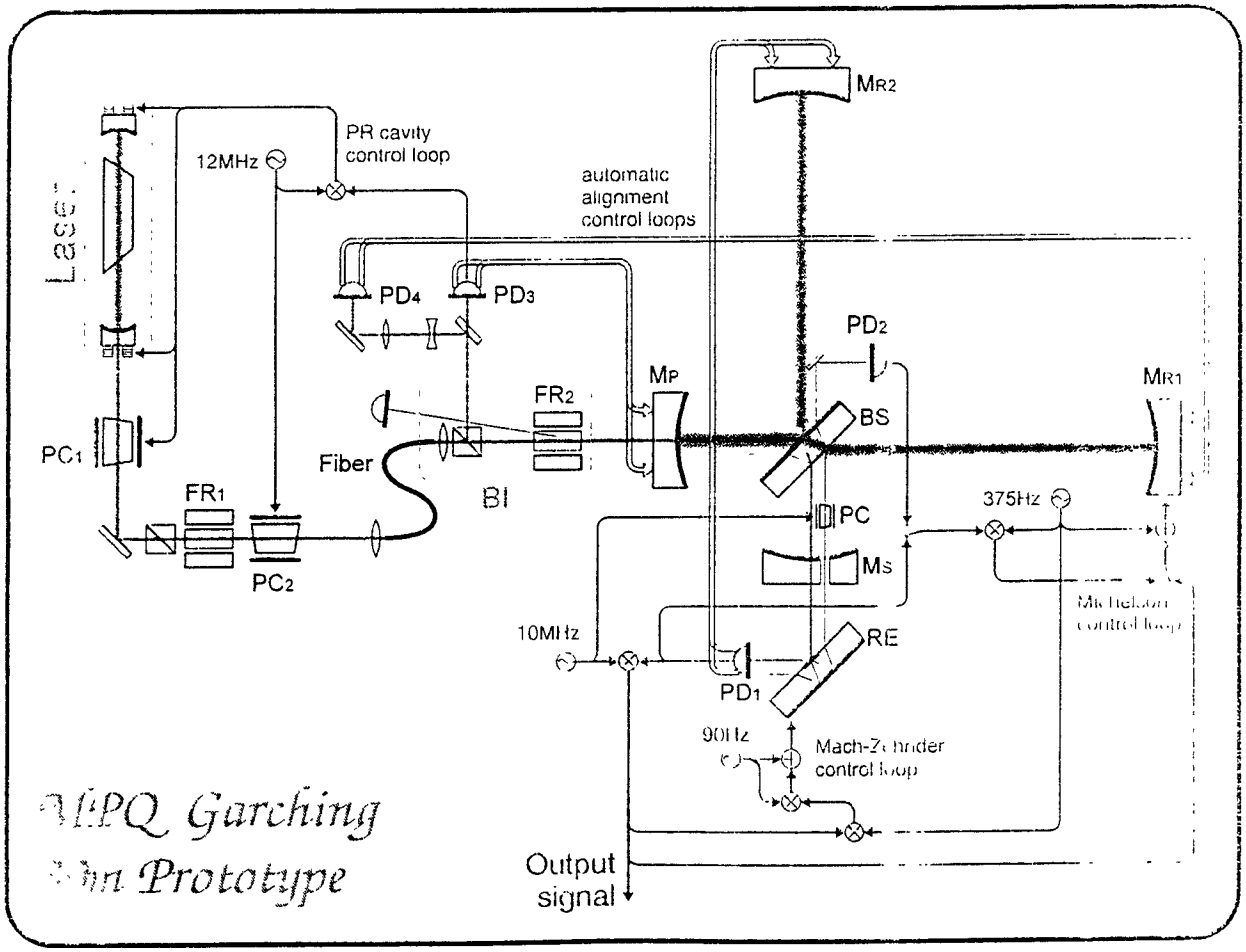

MPQ Garching
10m Prototype

Power Recycling

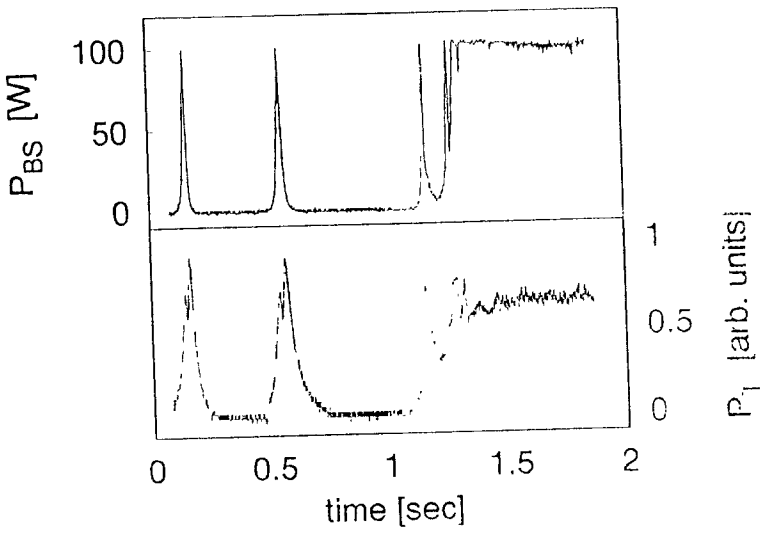

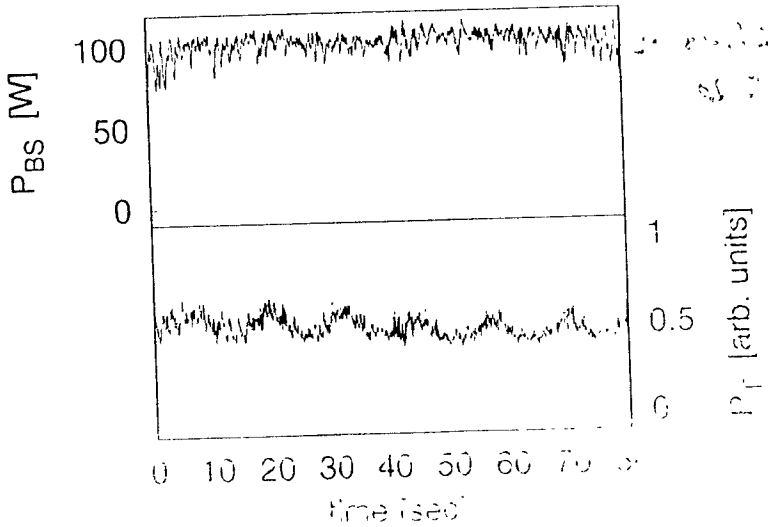

External Modulation

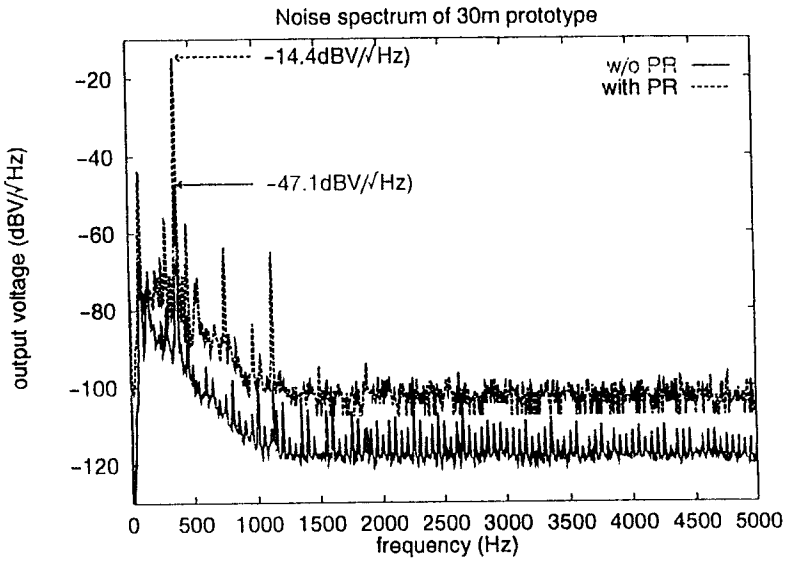

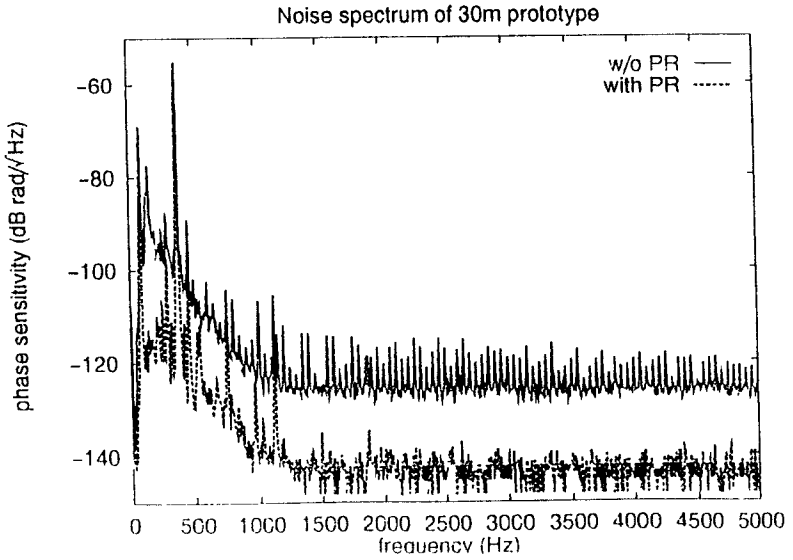

LIGO Overview

Aspen '97

D. Shoemaker

27 January 97

Organization of presentation

- Detector research and design
- Facilities status
- Schedule

LIGO Interferometer Design

Philosophy of initial design

- conservative: designs tested, many in sensitive interferometers
- minimum of extrapolation required
  - › displacement, phase sensitivity demonstrated
- some systems revised from first design
  - › Argon laser, Viton springs

Role of R&D in process

- modeling helps target important/difficult design questions
- small-scale experiments test models in some regimes
- in general, test in sensitive interferometer follows
- actual LIGO design then possible

Subsystems breakdown

- Length Control
- Alignment Control
- Pre-Stabilized Laser
- Input Optics
- Core Optics Components, Support
- Suspension
- Seismic Isolation
- Physics Environment Monitor
- Control and Data System

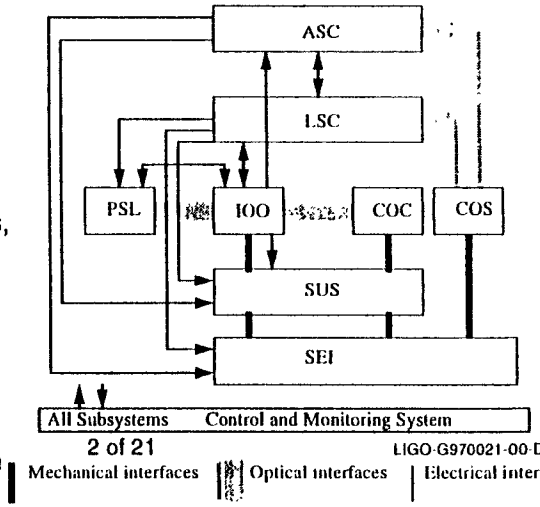

Length Sensing/Control

Phase modulation key to obtaining signals

- Pound-Drever-Hall reflection locking techniques
- Asymmetry in Michelson to give differential signals

Designs tightly coupled to work on 40m, Phase Noise Ifo.

- acquisition and operation are both challenges
- modeling crucial, due to scaling required from lab to LIGO
- recycling experiment on 40m will give system test

Largely digital servoloop to be used

- transmission of signals over 4km eased (dynamic range!)

Reconfiguration of 40m as recycled Fabry-Perot Michelson

- significant activity in '97
- gives data directly to interferometer length control design
- allows tests of models in dynamic regime

40 m Recycling

Theory:

Optical and Servo Topology for the Recycled 40-m Interferometer

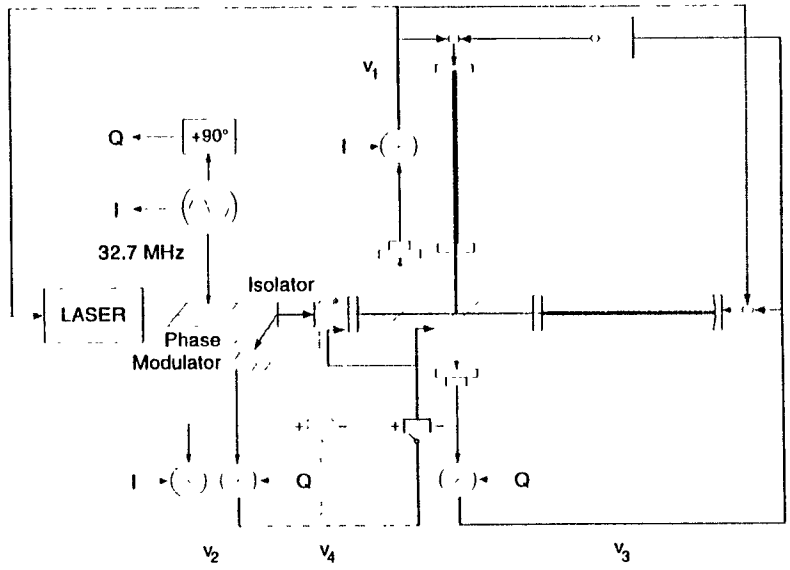

40 m Recycling

Practice:

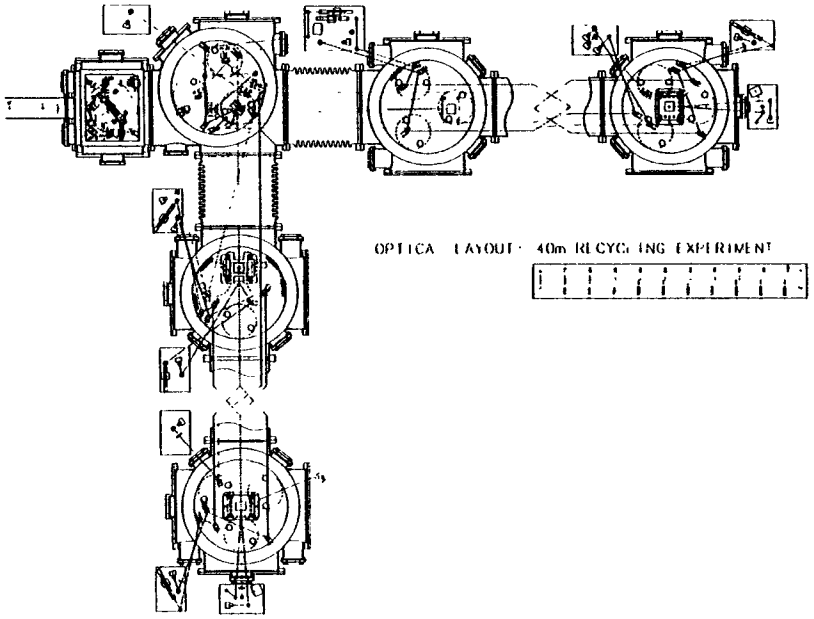

Alignment Sensing/Control

Alignment of cavities to laser beam

- effective use of laser power
- avoid spurious effects from undesired modes
- performance requirement of $\sim 10^{-8}$ rad
- elegant model using expansion in modes of cavities

Sensing analogous to length sensing

- add spatial resolution to photodetectors
- look in near field/far field to separate translations, angles

Experimental test on table-top

- model verified

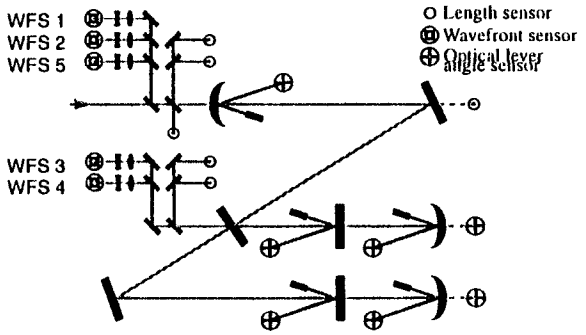

Alignment Sensing/Control

Model and prototypes tested on table-top system

- beautiful confirmation of Modal Model
  - predictions for placement of sensors, telescopes
  - predictions for signal decomposition at ports
- digital acquisition/control demonstrated
  - each quadrant digitized
  - all 'matrix operations' in software
  - all dithering of elements, read-in of monitors, data
  - servoloop transfer function
- wavefront sensor head, demodulation system shaken down
  - basically ready for production

Many aspects to complete design

- initial alignment
  - get the beam down the tube (10^{-4} rad)
  - get close enough for length control (10^{-7} rad)
- ; pre-operational; operational alignment
- centering: <1mm to limit noise coupling

R&D: Phase Noise Research

Goal: to demonstrate required initial LIGO phase sensitivity

- test models for shot-noise, sensing system
- develop photodetector technology
- uncover laser, servo, scattered light problems/solutions

Simplified optical system to minimize position sensitivity

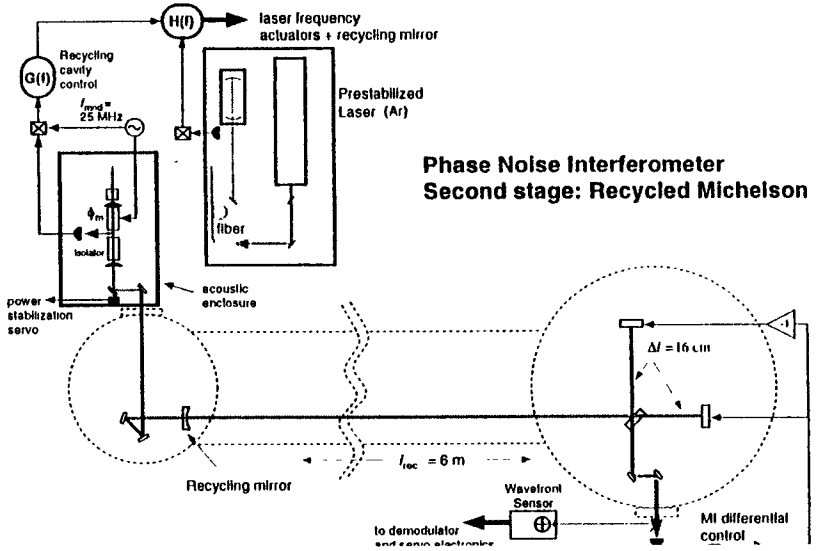

R&D: Phase noise research

Comparison of recycled, unrecycled cases

- high-frequency noise, 4×10^{-10} rad/$\sqrt{\text{Hz}}$, shot noise limited
- low-frequency noise from parasitics, frequency noise....

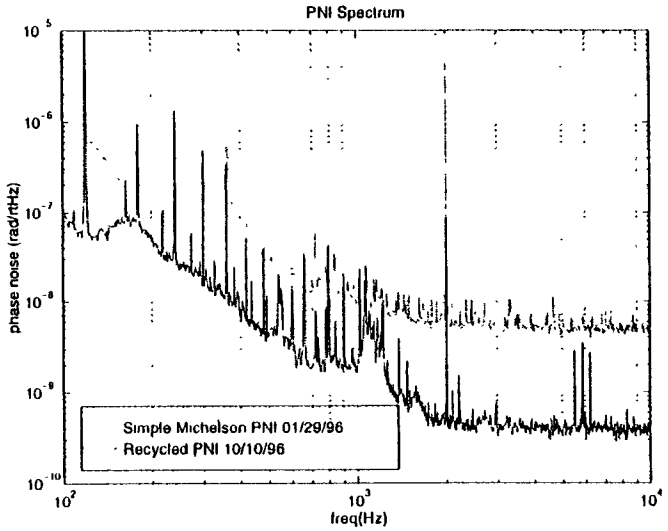

Next phase: conversion to Nd:YAG/1064 nm

- experiment will run to ~Jan 98
- tests low-power IR laser in characterized testbed

Pre-stabilized laser

Laser Source

- being developed and produced by Lightwave, Inc.
- monolithic Nd:YAG oscillator, followed by amplifier; 10 W output
- first units to be delivered in Oct 97

Stabilization

- based on rich experience with Argon Ion lasers
- modifications for Nd:YAG; e.g., filter cavity (Stanford)
- development underway using available 700 mW laser
- initial prototype for test in Phase Noise Ifo., in coming months

Input Optics

Under development in collaboration with Univ. Florida

- helped by clean interfaces, frequent visits, good communication

Principal components

- phase modulation system (multiple sidebands required)
- 3-mirror Fabry-Perot suspended mode cleaner
- matching telescope to main optics; reflective

Core Optics

'Pathfinder' process

- exploring/developing polishing, metrology, coating technologies
- significant progress on all fronts

Substrates: fused quartz, 25cm x 10 cm

- Heraeus low-OH material where absorption critical
- Corning for other applications

Polishing

- Three firms qualified for LIGO polishing
- 1 nm surface figure over 10cm required, and possible!

Coating

- REO and LIGO cooperating in measurement, characterization
- use AR coating reflectivity designs to study uniformity

Metrology

- NIST is the independent contractor for Pathfinder
- comparisons with vendor metrology; probably the limiting technology

Core Optics Support

- baffling, in-vacuum relay mirrors, etc.

Polished Surfaces

<1 nm over a 20cm diameter!

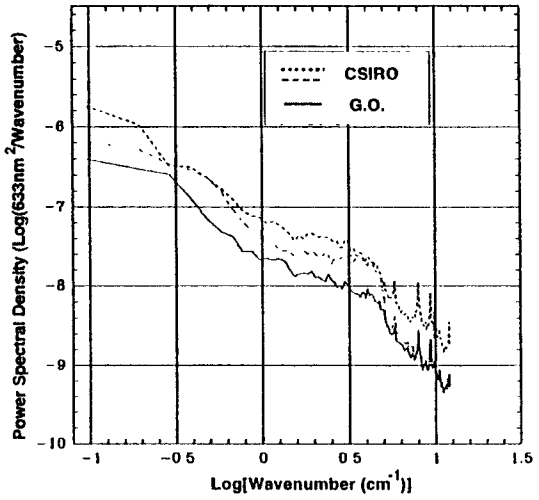

One dimensional power spectra from NIST metrology of curved surfaces Z(0,0),Z(1,1) Z(2,0),Z(2,2),Z(3,1),Z(3,3),Z(4,0) removed

Coating

Use properties of AR coating to advantage

- reflectivity very strong function of thickness near zero reflection
- tune layer thickness to study uniformity, scan samples

Synthesize complete coating from these measurements

- fit to complete the surface
- make fictive 40-layer coating
- give feedback to REO on nature of problems

Rapidly approaching design flatness

40 layer HR coating phase map

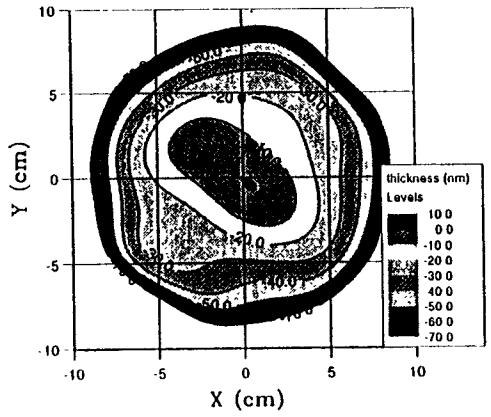

Suspensions

Two basic flavors:

- Small Optic Suspensions: Input Optics components
- Large Optic Suspensions: Core Optics

Prototypes in construction/test

- challenges in fiber attachment (Q), initial balancing
- also in control electronics: severe dynamic range requirements
- tests in 40m interferometer for control, noise performance

Seismic Isolation

Design contracted to Hytec, Inc.

- requirements developed by LIGO
- design makes incremental changes in initial design
- principal change in springs: Constrained Layer Damping

Requirements in control, GW band

- resonances create servo-control challenges, but...
- attenuation in signal band crucial

Preliminary design well advanced

- actuators for drift, tidal, microseismic peak also in development

Coil and Leaf Spring concepts

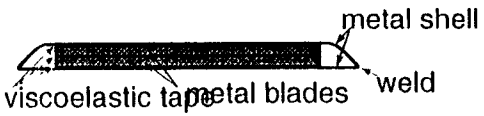

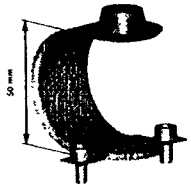

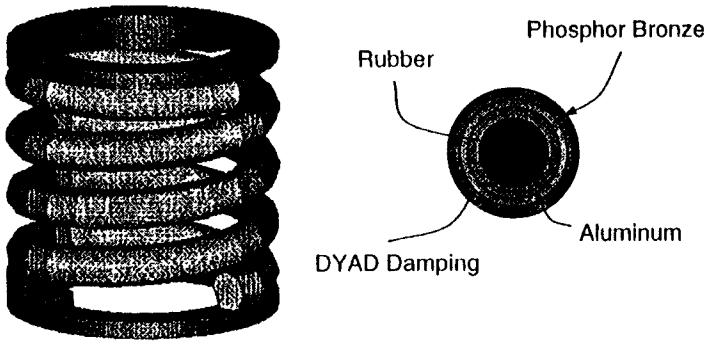

Control and Data System

Backbone of the Interferometer

- electronics standards and design
- communications between subsystems
- all centralized control, monitor, operator consoles
- timing
- software up to the data analysis

Data Acquisition

- order of 5 MB/sec per interferometer total data rate
- data assembled into frames, short and long term storage

On-line Diagnostics

- interferometer console to allow quick-look, scripts

Prototyping and design well advanced

- much R&D now using CDS electronics
- several subsystems tests (laser)
- data acquisition/frame builder in test

Physics Environment Monitor

All probable paths from environment to interferometer

- seismic (low 'drift' frequencies to GW band)
- acoustic
- electromagnetic: lightening, RFI, magnetic fields
- temperature humidity, wind, rain, etc.

Characterization of transfer functions

- stimulus-response

System separate from interferometer

- to be used for veto, correlation, regressions
- principally commercial instruments

Early to the sites

- portable carts to enable measurements as buildings go up
- measure changes in the environment
- early data on correlations between sites

R&D Plans for '97

R&D for initial interferometer: ends in '97

- all designs finished, fabrication underway
- 40m recycling
  - length control acquisition
  - length control operational mode
  - tests of CDS electronics, data acquisition, etc.
- Phase noise measurements
  - characterization of Nd:YAG laser
  - guidance to Pre-Stabilized Laser design
  - experience with infra-red optics, components
- Suspension tests in 40m
  - control and mechanical stability
  - internally-generated noise mechanisms
  - installation practice
- Thermal noise research
  - measurements of Q for suspended test mass optics
- Temporal, spatial modeling
  - to support design activities; integration of models

Beam Tube

Beam Tube slabs in place

- a short interstate, laid in a week

Tubes in full production

- all activity is at Hanford for now; Livingston in Spring '98
- an enormous steel mill/factory churning away
- some 190 tube sections formed, 52 installed; no leaks!

Baffles baffling

- designed to limit scattered light
- coated with powdered glass and 'fired' to reduce backscatter
- some spalling; tiny glass missiles launched through beam
- solutions under study

Covers covering (cowering?)

- over 2200 manufactured, awaiting installation

Installation and bakeout finished by end-98; LA end-99

Civil Construction

Hanford

- slab just poured and cured for LVEA (large vertex building)
- structural steel frame going up
- other buildings nearing completion

Livingston

- heavy equipment now arriving

Schedule

- Hanford occupancy fall '97
- Livingston occupancy spring '98

Vacuum Equipment

Main chambers (BSC)

- 5 chambers largely finished (~1/2 WA complement)
- other 10 in various states of construction

Input/Output chambers (HAM)

- 8 chambers look like chambers
- material for the other 11 on hand

Other elements (spool pieces, valves, pumps) keeping up

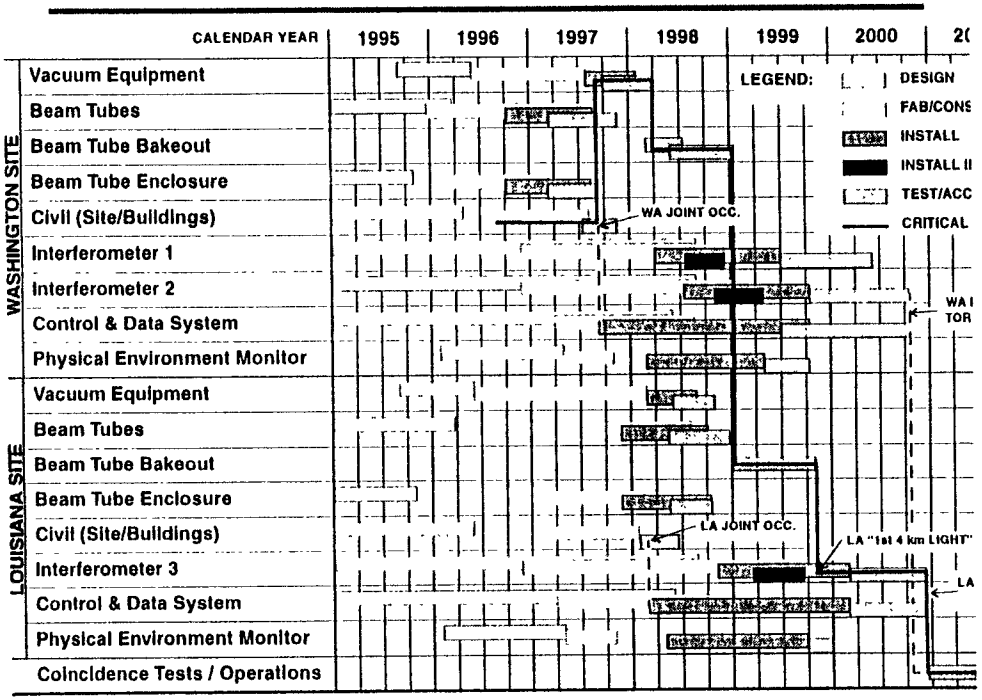
CALENDAR YEAR
1995
1996
1997
1998
1999
2000
WASHINGTON SITE
Vacuum Equipment
Beam Tubes
Beam Tube Bakeout
Beam Tube Enclosure
Civil (Site/Buildings)
Interferometer 1
Interferometer 2
Control & Data System
Physical Environment Monitor
LOUISIANA SITE
Vacuum Equipment
Beam Tubes
Beam Tube Bakeout
Beam Tube Enclosure
Civil (Site/Buildings)
Interferometer 3
Control & Data System
Physical Environment Monitor
Coincidence Tests / Operations
LEGEND:
DESIGN
FAB/CONS
INSTALL
INSTALL II
TEST/ACC
CRITICAL
WA JOINT OCC.
LA JOINT OCC.
LA "1st 4 km LIGHT"

Monday PM: A. Advanced Interferometers and Detectors
January 27 Chair: R. Schilling

4:30	M. Fejer(Stanford)	Topologies for Advanced Detectors
4:55	Discussion	
5:05	R. Flaminio(Annecy)	Virgo Plans for a Long Term R&D Program
5:30	Discussion	
5:40	Coffee Break	

B. Collaboration Formation for Advanced Detectors I
Chair: M. Coles

6:00	G. Sanders(Caltech)	Introductory Remarks
6:30	Discussion	
6:40	Round Table Discussion	Finn, Flaminio, Gustafson, Reitze, Ruediger, Sanders, Stebbins, Ward

Topologies for Advanced Interferometers

Ke-Xun Sun, Peter Byersdorf, Eric Gustafson
R. L. Byer, and M. M. Fejer

E. L. Ginzton Laboratory

Stanford University

Receiver Sensitivity

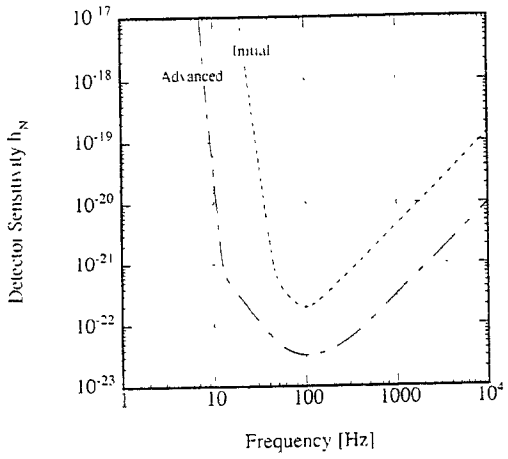

Phase Noise
- more powerful laser
- recycling
- low-loss optical components

Thermal Noise
- higher Q materials and suspensions
- improved fabrication techniques

Seismic Noise and System Control
- active and passive isolation

System Control

Interferometer topology influences many of these choices

is addressed briefly in the next section. A complete summary of prior work is available as a supplement to this proposal.

Table 1.1
Assumptions for Initial and Advanced LIGO Interferometers

Parameter	Initial LIGO	Advanced LIGO
Effective Optical Power(1)	2 watts (2)	60 watts (3)
Laser Wavelength (4)	514 nm	532 nm
Power Recycling Factor	30	200
Cavity Storage Time	880 μsec	1.3 msec
Arm Length	4000 m	4000 m
Mirror Mass	10 kg	100 kg
Mirror Diameter	25 cm	48 cm
Mirror Internal Q (5)	10^5	$3x10^7$
Single Pendulum Q	$8x10^5$	NA
Double Pendulum Q	NA	10^8
Stack Transmission at 100 Hz	-110 db	<< -230 db
Stack Transmission at 10 Hz	NA	-110 db
Strain Sensitivity ($1/\sqrt{Hz}$) at 100 Hz	$2x10^{-23}$	$4x10^{-24}$

(1) The effective optical power is the product of the optical power at the input to the interferometer multiplied by the detector quantum efficiency.
(2) A 5 watt Argon ion laser is reduced to 2 watts of effective power by losses in the modulators, optical isolators, beam expanding telescope and the mode cleaner.
(3) For the advanced receiver, improved losses, and increased quantum efficiency are assumed to result in an effective power of 60 watts from a frequency-doubled 100-watt Nd:YAG laser.
(4) These wavelengths are based on an Argon-ion laser for the initial interferometer and frequency-doubled Nd:YAG laser for the advanced interferometer and do not reflect the LIGO plans to change the laser to Nd:YAG at 1064 nm, a change which is reflected in Table 4.1.
(5) The earlier LIGO sensitivity estimates were based on viscous damping in the test masses and suspensions. Our estimates assume structural damping consistent with the current LIGO measurements (Whitcomb 1994).

2. A Brief Review of Prior NSF Supported Work

For the interferometric measurement of optical phase, advanced gravitational-wave receivers require an efficient laser that provides hundreds of watts of optical power with low amplitude noise, frequency noise and spatial mode noise, in a diffraction-limited beam. During the past 5 years the NSF funded research program (PHY-89 13017, PHY-92 15157) directed by Professor Robert L Byer has accomplished the following: 1) frequency stabilized the output of diode-laser-pumped nonplanar ring oscillators (NPROs) to high-finesse Fabry-Perot interferometers, thus reducing laser frequency noise at all frequencies of interest to LIGO (10 Hz to 10 kHz), 2) designed and characterized a medium-power (5.5 W) injection-locked diode-laser-pumped laser as a first step toward meeting the laser requirements for the initial LIGO interferometers, 3) measured the spectral density of frequency noise of an injection-locked laser,

Interferometer Topology

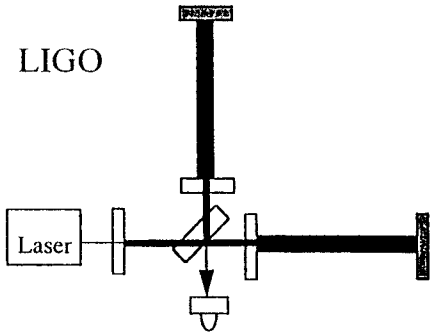

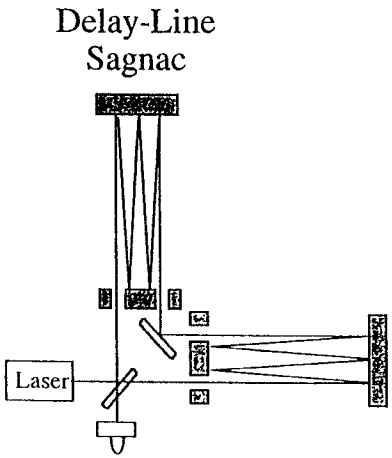

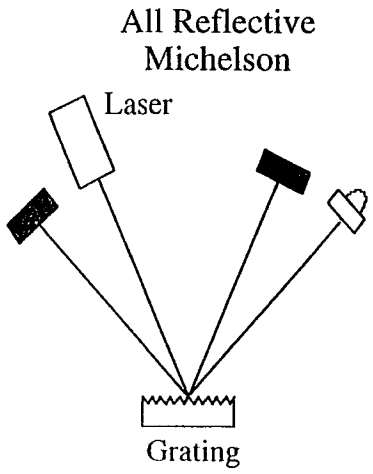

Interferometer Topologies

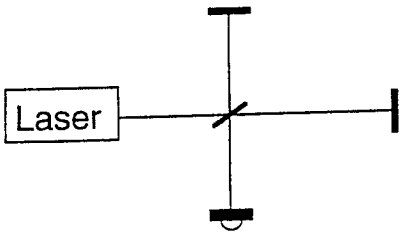

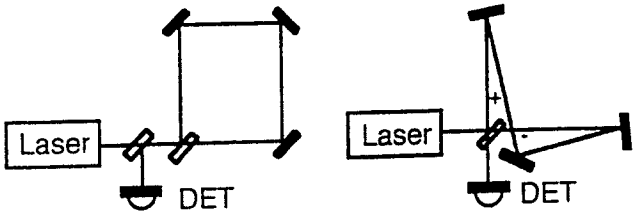

Power Recycled F-P Michelson

Laser
- ultra-narrow linewidth
- moderate power

Controls
- multiply-nested loops

Optical Components
- thermooptic sensitivity

Single Pass Sagnac

Laser
- broadband
- high power

Controls
- many fewer loops

Optical Components
- some reduced sensitivity

Common path Interferometers simplify some engineering problems

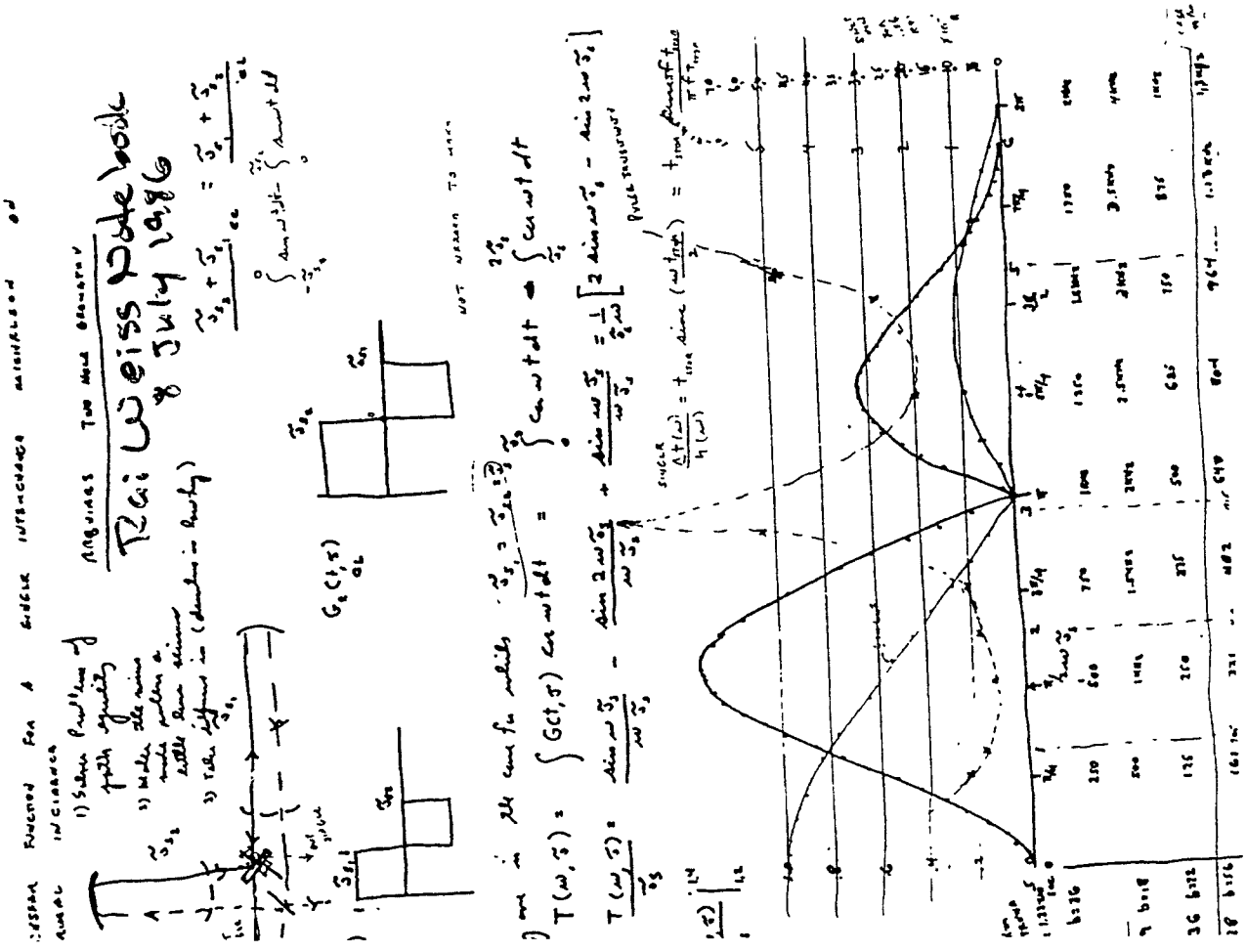

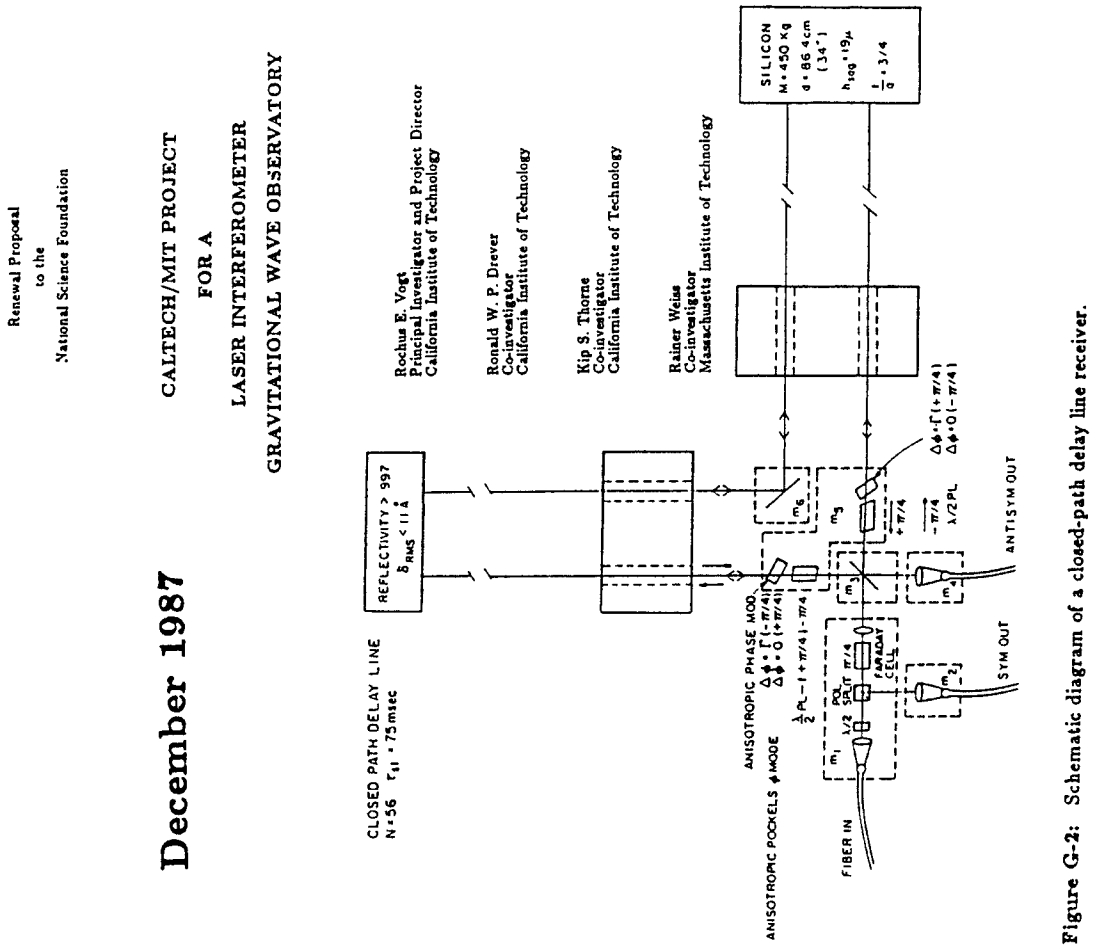

Figure G-2: Schematic diagram of a closed-path delay line receiver.

Sagnac vs. Michelson: Responsivity

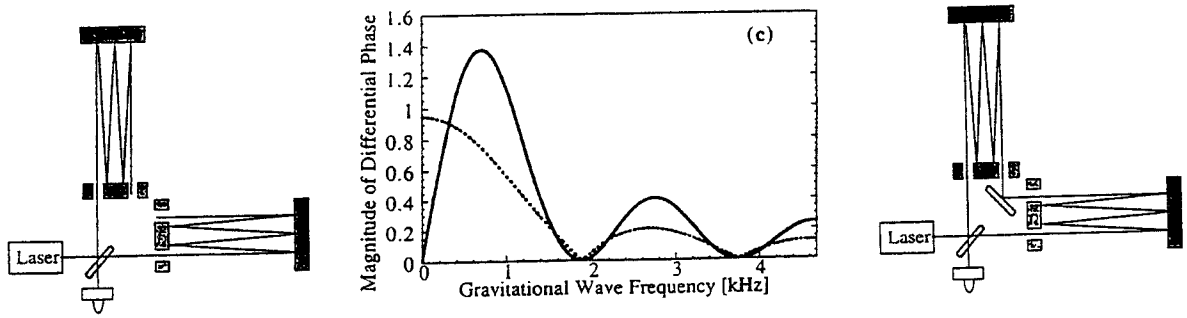

$$\tau_s = 2NL/c$$

Responsivity:	$R_M(f) = 2(f_l/f)\sin(\pi\tau_s f)$	$R_S(f) = 4(f_l/f)\sin^2(\pi\tau_s f)$
Peak frequency:	$f_{\max} = 0$	$f_{\max} = 0.37/\tau_s$
DC Response:	$R(0) = 2\pi f_l \tau_s$	$R(0) = 0$
Peak Responsivity:	$R_S(f_{\max})/R_M(f_{\max}) = 1.84$	

Sagnac vs Michelson: Sensitivity

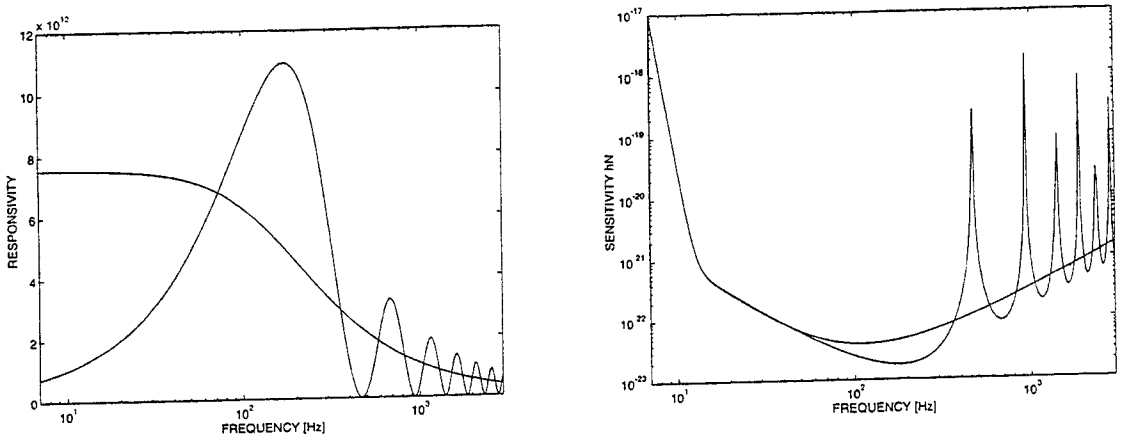

$$\Delta\phi(f) = R(f)[\Delta L_{gw}(f) + \Delta L_{noise}(f)] + \Delta\phi_{noise}$$

$$R(f) > \frac{\Delta\phi_{noise}}{\Delta L_{noise}} \Rightarrow \Delta L_{noise} \text{ limits resolution}$$

Laser power and storage time can affect low-frequency sensitivity for SI

Experimental Setup for a Zero-Area Sagnac Interferometer

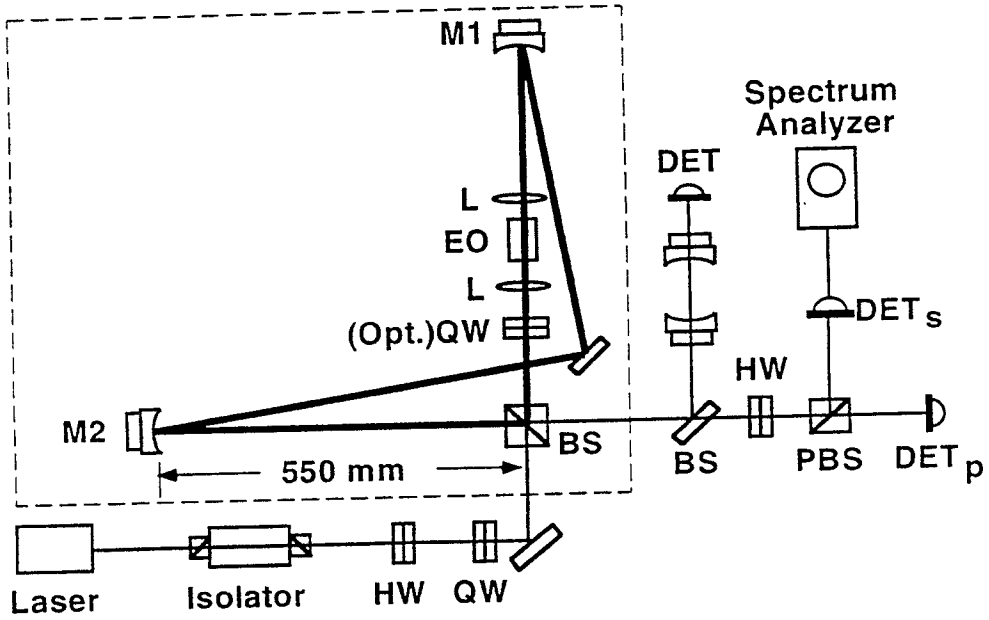

Signal Extraction with Post-Modulation

- Shift detection to frequencies above technical noise
- Retain simple polarization-based signal extraction
- Modulator after dark port
  - only low optical power handling

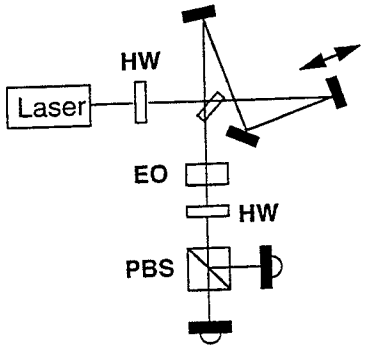

90 MHz EOM
Detect 10 - 1000 Hz mirror displacements
Phase noise several dB > SNL above acoustic noise
  – electronics, not fundamental

Compare Sagnac to Possible Advanced FPM

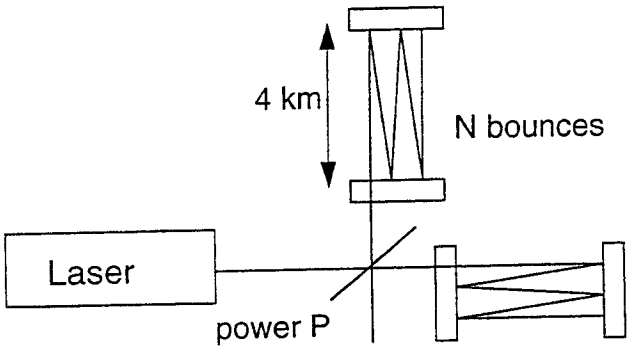

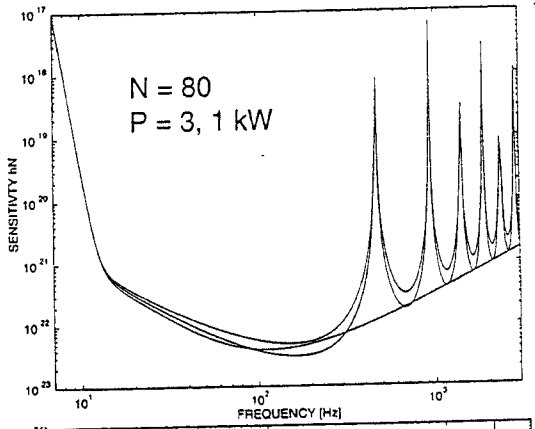

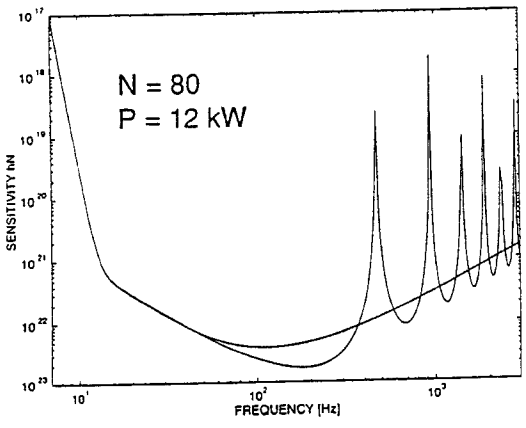

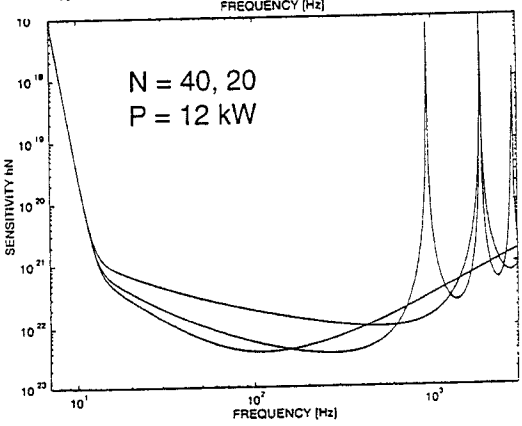

Key Issues for Advanced Sagnac Interferometer

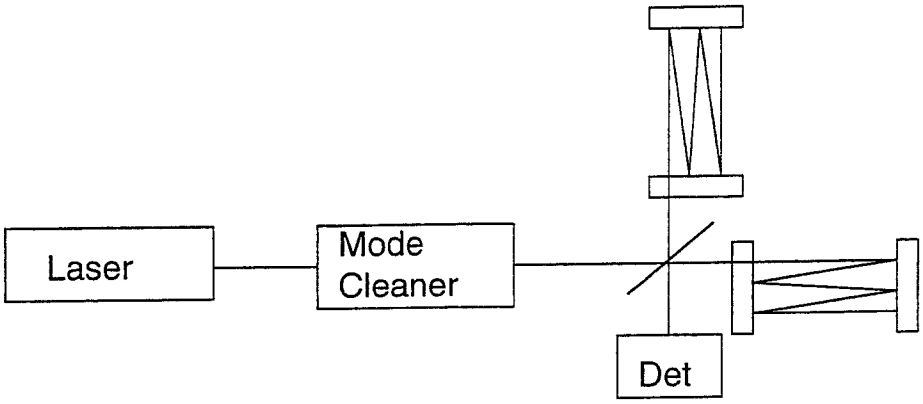

- Responsivity: How to obtain required storage time?
  - delay-line design that fits
  - scattered light issues
- Phase noise: How to obtain required power on beamsplitter?
  - laser design for high power
  - mode cleaner for broadband laser

Obtaining Required Responsivity

- Recycling schemes
  - signal recycling
  - resonant sideband extraction

  Require narrowband laser
- Increase storage time
  - Fabry-Perot arms

  Require narrowband laser
  - delay lines

  Realistic mirror size?
- Delay line scaling
  - mirror size an issue

    must fit in system

    must be fabricatable
  - tolerable clipping a key parameter

    low coherence source helps
  - double-pass designs useful

Obtaining Required Phase Sensitivity

- Power recycling
  Requires ultrastable 100 W laser

- Single-pass interferometer
  Requires broadband ≈ 10 kW laser

- High power lasers
  Today: 350 W Yb:YAG, $M^2 = 1.1$ (Giesen)
  10 – 15 years: Photons will be cheap 1 - 10kW

- High power laser designs
  - power scaling with oscillator/amplifer configuration
  - broadband: Noise modulation on oscillator
    Pseudothermal fiber ASE source
  - spatial mode control: Active mirror
    Hollow fiber mode filter

Thermally-Induced Optical Effects in High-Power Laser Interferometers

- **Thermal lensing due to refractive index changes**
- **Birefringence due to mechanical stresses**
- **Mirror curvature changes due to thermal expansion**

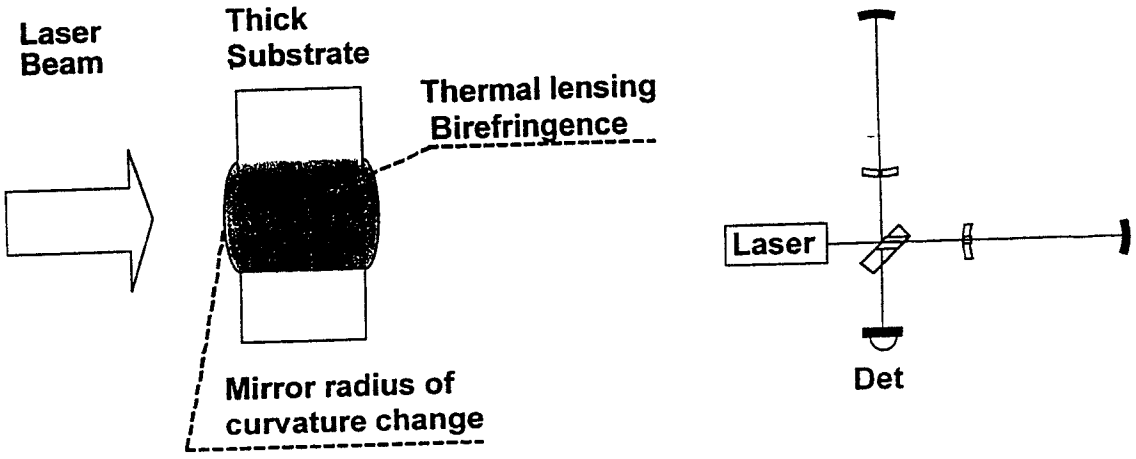

REFLECTIVE ELEMENTS

- INPUT COUPLER

TRANSMISSIVE

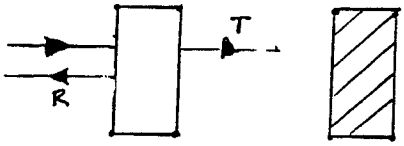

partial reflector

REFLECTIVE

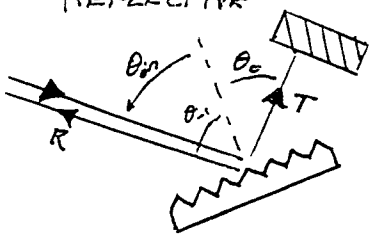

Littrow grating

- BEAM SPLITTER

TRANSMISSIVE

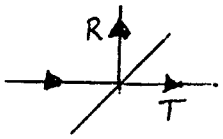

REFLECTIVE:

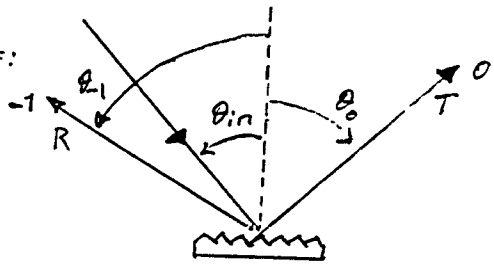

Michelson Interferometer Using a Grating Beam Splitter

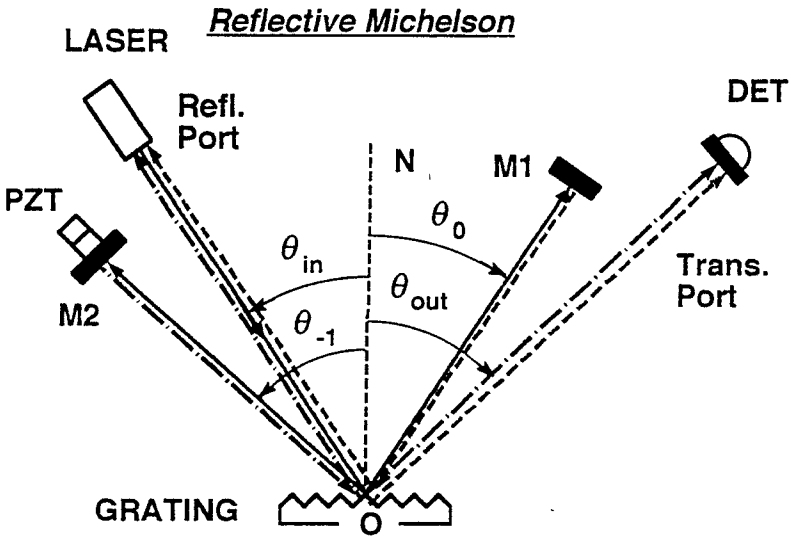

Reflective Michelson

Transmissive Michelson (for comparison)

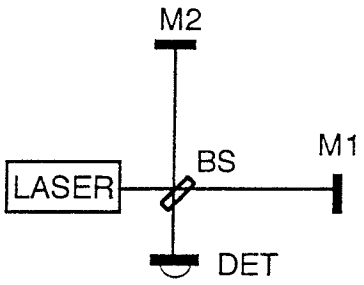

θ_{in}= 32.5°, θ_{out}= 47.6°

$\eta_{-1} = \eta_0$ = 48.2%

High Contrast Ratio Michelson Interferometry

Contrast ratio ~0.99 with an off-shelf grating of 1200 line/mm

K. X. Sun

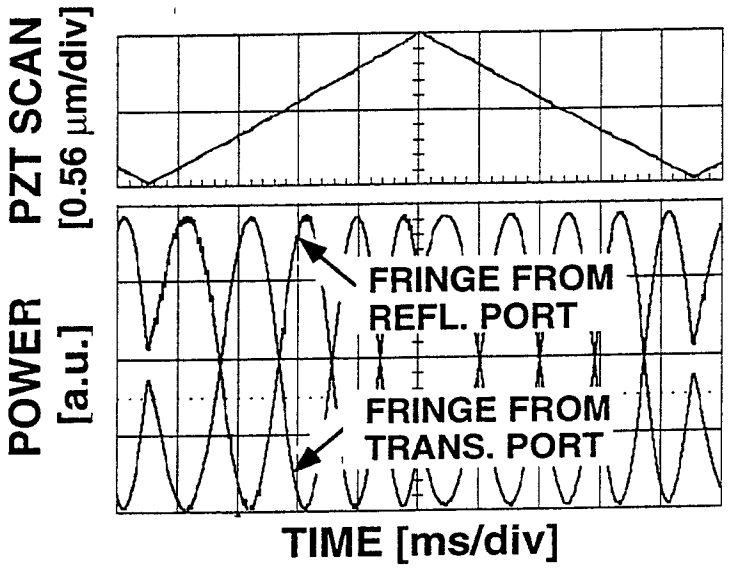

Also built: Sagnac, Finesse ≈ 90 Fabry Perot

Future Work

- Delay line designs
- Scattered light effects
- Interferometry with broadband sources
- SNL signal extraction at higher powers
- Sagnac alignment control
- Spatial mode control and filtering of input radiation
- All-reflective interferometers
- Operation with power-scaled lasers
- Thermal effects in Sagnac interferometers
- Compare scaling with other topologies

Summary

- Sagnac interferometer provides common path advantages
  - zero DC response: looser low frequency control tolerances
  - white light interferometer: broadband laser
  - tolerant of some types of optical perturbations
- Polarization-based signal extraction scheme
  - generates common path local oscillator
  - SNL detection retaining these advantages
- Recycling schemes or FP arms eliminate most of these advantages
- Key Issues
  - high power laser design
  - delay line design

Aspen '97

VIRGO plans for a long term R and D program

R. Flaminio
(L.A.P.P. Annecy)

for the

VIRGO collaboration

VIRGO Long Term R&D activity

Prospect

- Two possibilities:

1) VIRGO and/or LIGO detect some signals.
   New detectors will be built.
   Upgrades for astrophysical research will be needed

2) VIRGO and LIGO reach the expected sensitivity but no detection is achieved
   Upgrades will be required to increase sensitivity

- In both cases a long term R&D activity is required

VIRGO sensitivity

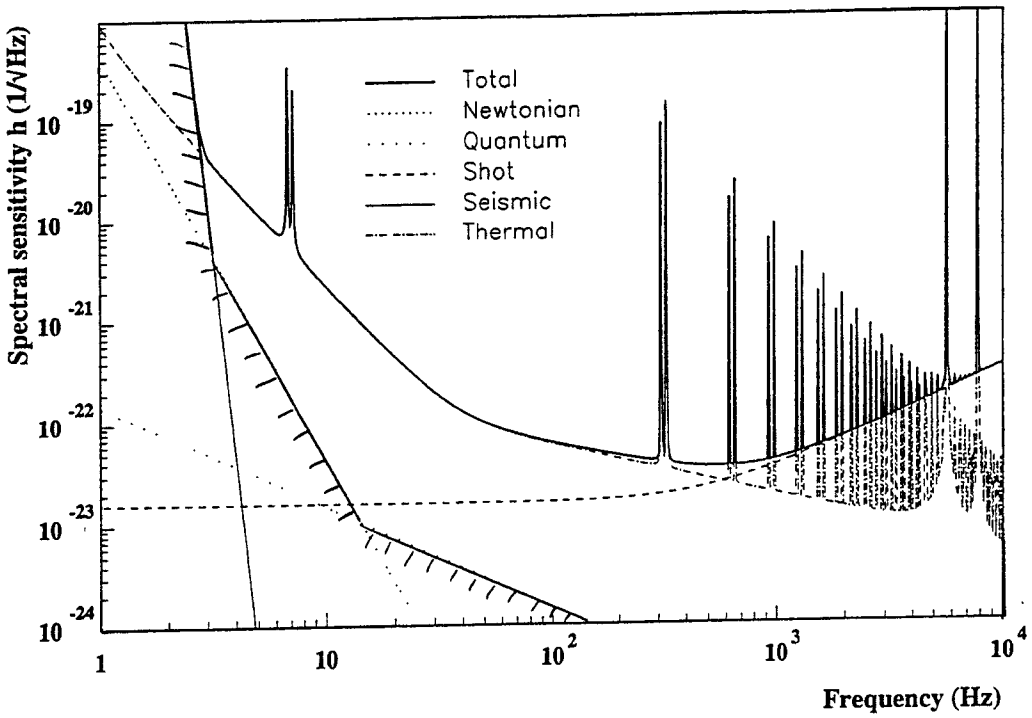

VIRGO sensitivity vs Pulsar upper limits

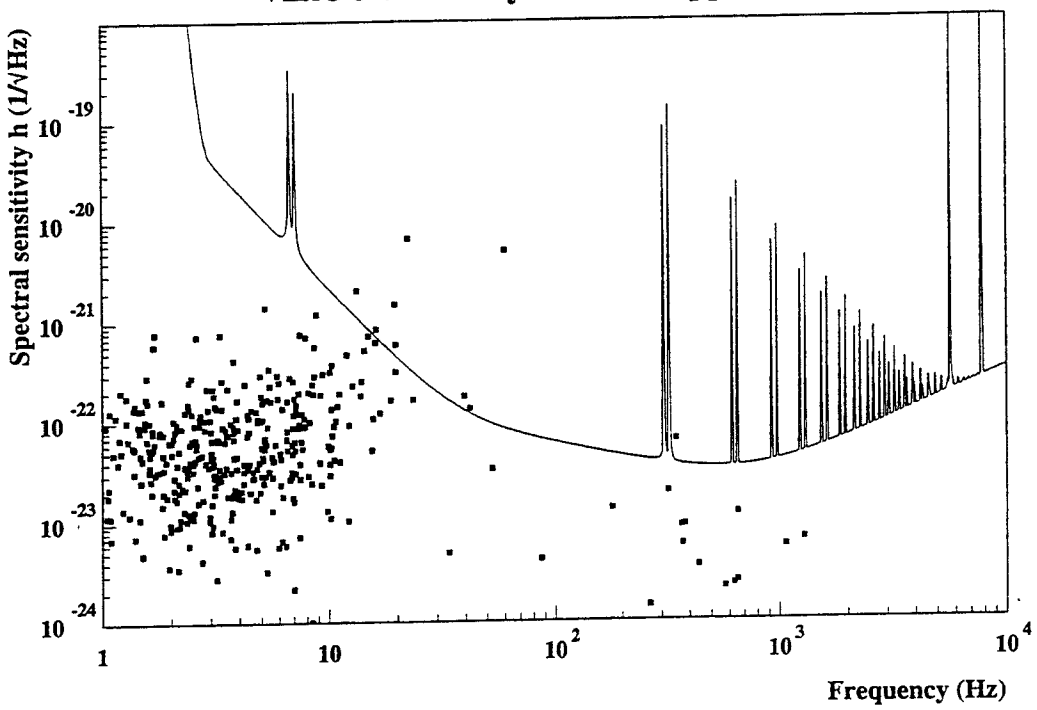

VIRGO sensitivity: improving Thermal Noise

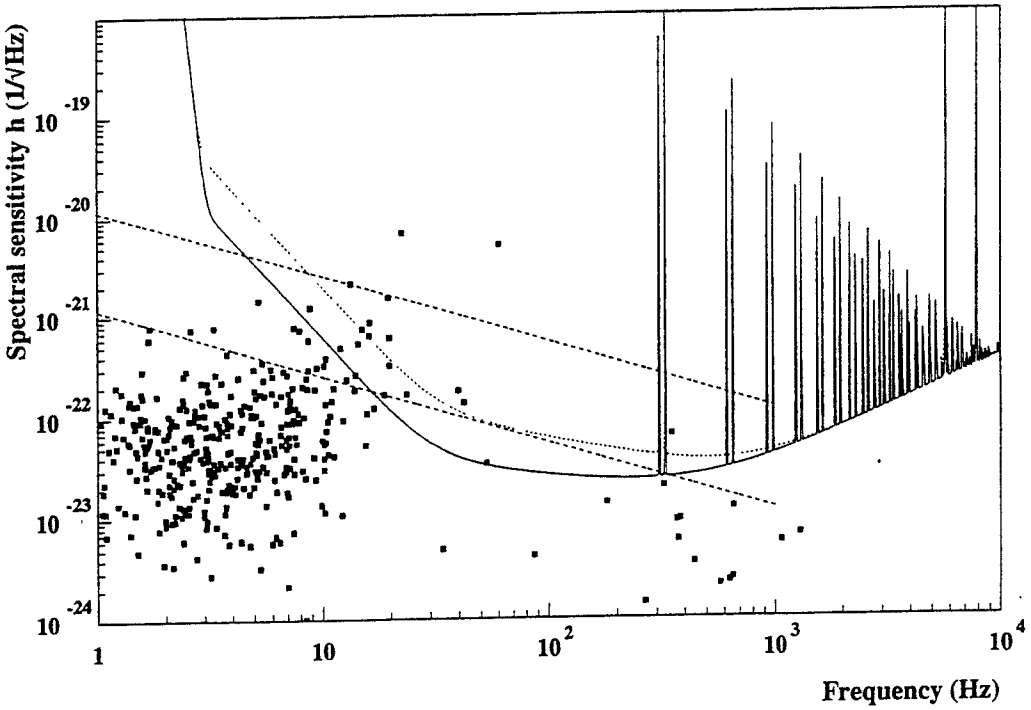

VIRGO sensitivity: improving Shot Noise

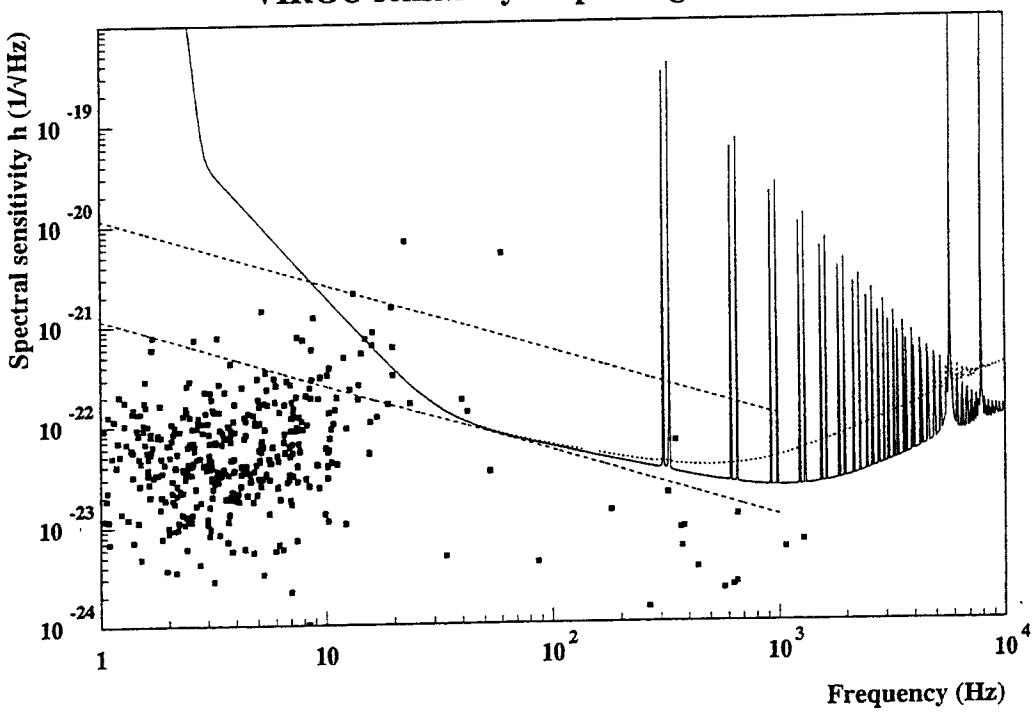

Thermal noise investigations

Mirror thermal noise

- Sapphire test masses (lower losses, larger sound speed, optical quality?)
- Electrostatic actuator (no magnets attached to mirrors)

Pendulum thermal noise

- New wire materials (larger tensile strength, lower losses)
- Monolithic suspensions (no clamps losses)
- Cryogenics

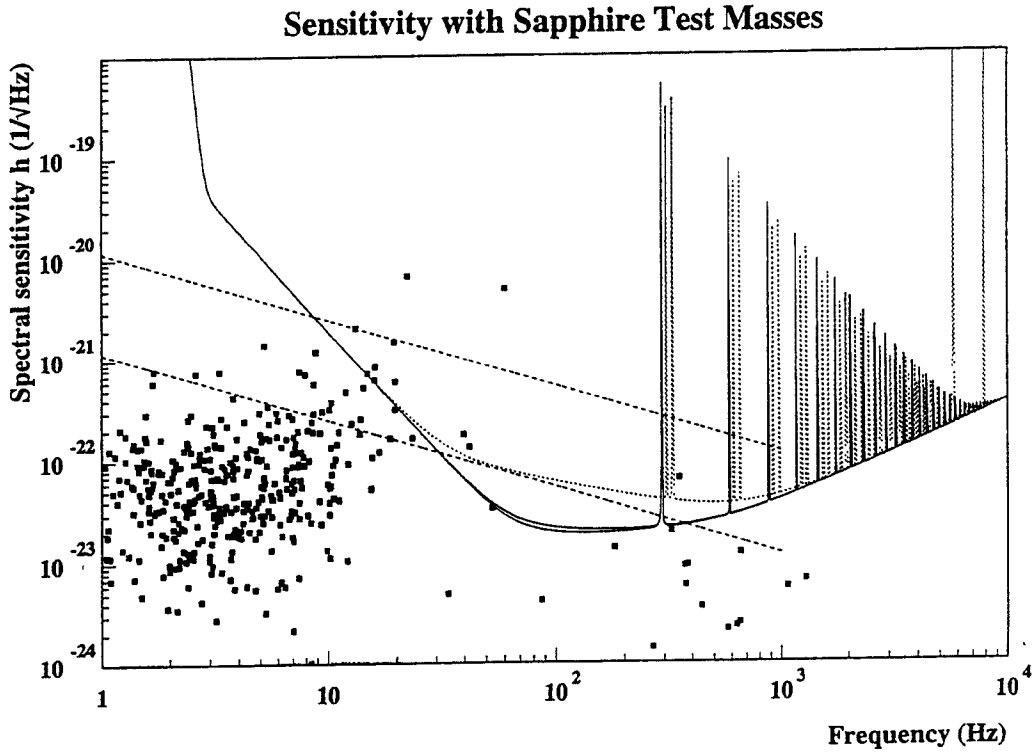

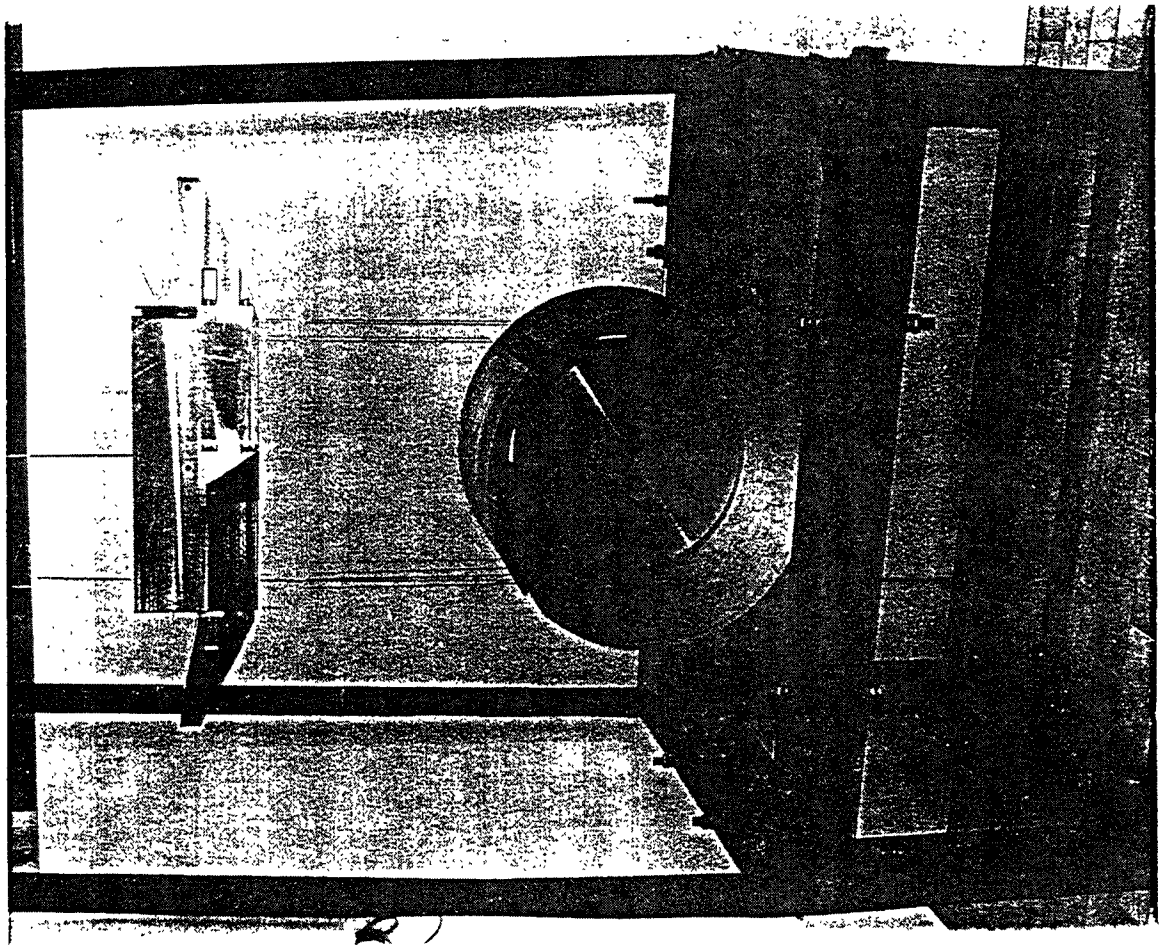

VIRGO Long Term R&D activity

Direct Thermal Noise Measurement

- Q measurements will give indications <u>but</u> ....
- Test of possible solutions need to set-up a special apparatus to measure thermal noise
- This test dedicated apparatus <u>cannot</u> be the interferometers (duty cicle !!)
- Required displacement sensitivity: 10^{-18} to 10^{-20} m/$\sqrt{Hz}$ (10 Hz to 1kHz range)

  use short Fabry-Perot cavity made by two 'real' mirrors

Direct Thermal Noise Measurement

• requirements:

1) good seismic isolation
   (similar to VIRGO)
   ⇒ use Super Attenuator

2) good laser frequency stability
   ($3\ 10^{-1}$ to $3\ 10^{-3}$ Hz/√Hz if L=1mm)
   ⇒ stabilization cavity also suspended

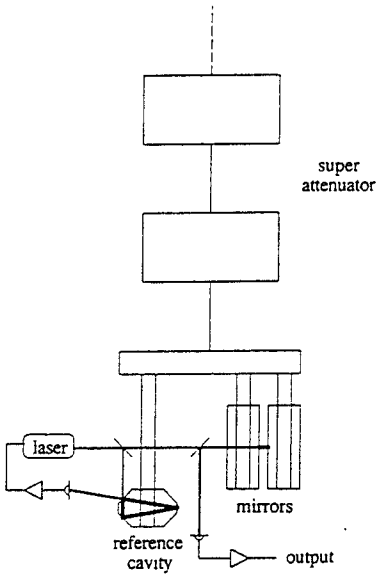

• critical points:

- thermal noise of stabilization cavity ?
  reduced by $L/L_{stab}=1/300$ ($L=1mm$ $L_{stab}=30cm$)
- doppler noise ?
  splitter also seismically isolated
- short cavity geometry ?
  flat-flat: cavity degeneracy .... alignement
  flat-curved: reduce degeneracy .... waist dimension

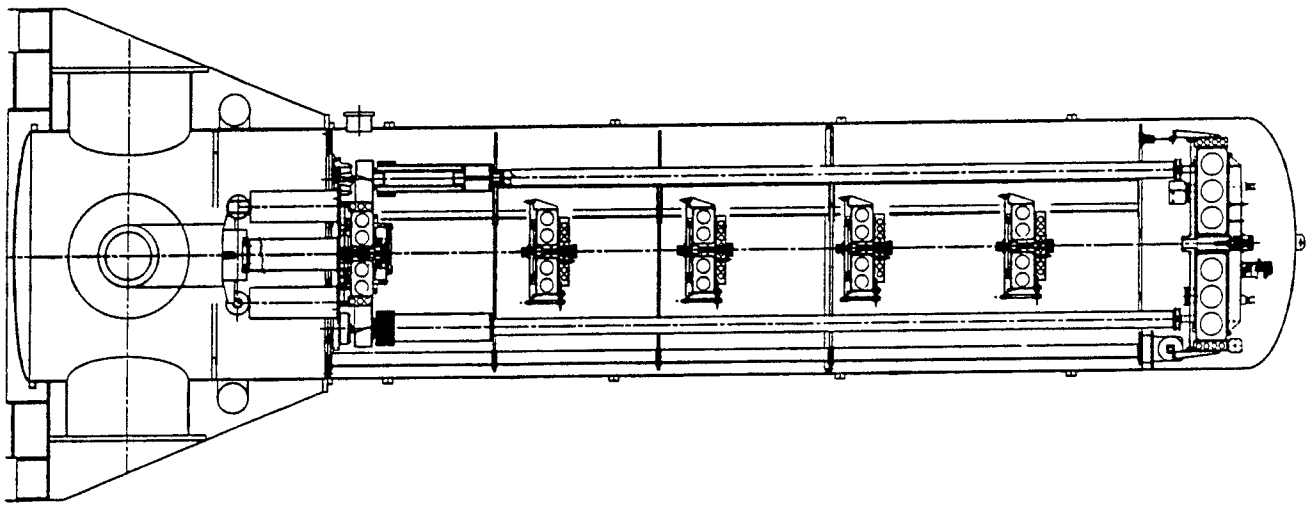

Bruit de frequence et specifications

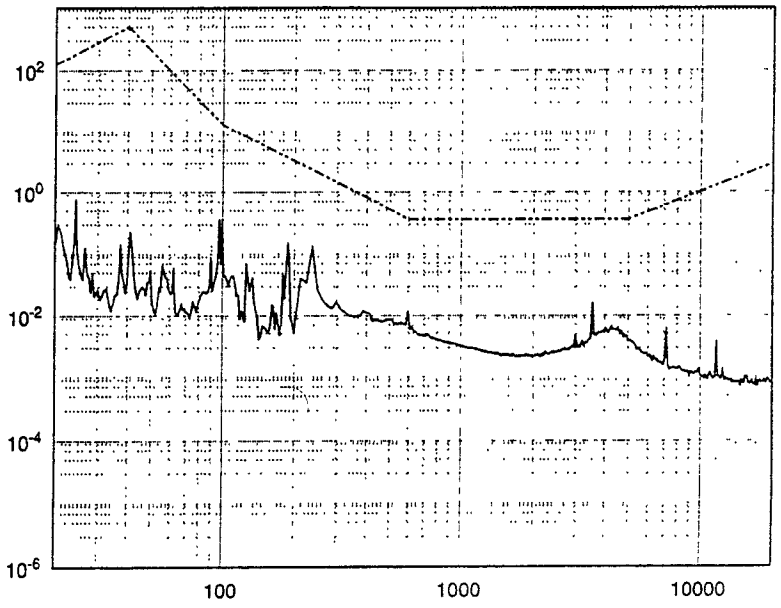

VIRGO Long Term R&D activity

Improving shot noise

- short term:
  - increase laser power
    laser technology rapidly progressing
  - decrease losses
    surface aberrations & corrective coating ($\Rightarrow$ improve metrology)

- mean term:
  - reduce thermal lensing
    sapphire mirrors: better thermal conductivity
  - dual recycling
    VIRGO infrastructure adapted to the use of this technique

- long term:
  - reflecting optics
  - ligth squeezing

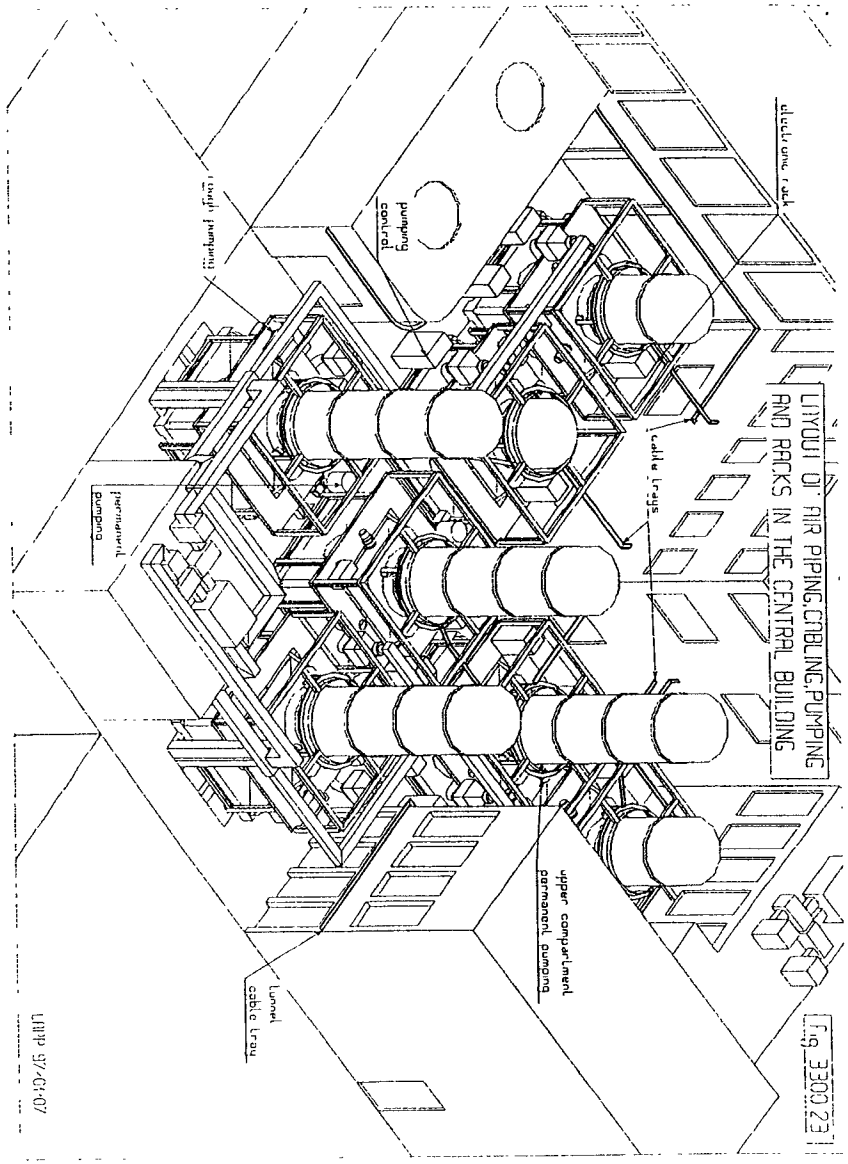

Best result

Diameter : 45mm

PV : 14nm (± 1nm)

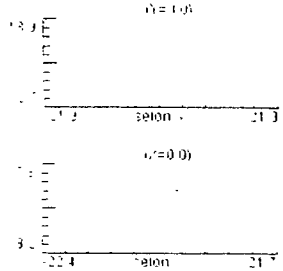

Center of the mirror

Diameter : 25 mm

PV : 9 nm (± 1nm)

As sensitivity improves ....

- review 'technical' noises:
  - laser amplitude noise
  - laser frequency noise (relevant for thermal noise experiment also)
  - actuator noise

- review the dynamic range issue:
  - improve suspended mass damping (ultra-low noise accelerometers)
  - electronics dynamic range (digital and analog)

- don't forget maintenance and diagnostic:
  - Ex. in-situ mirror cleaning techniques

Conclusions

- The construction effort may weaken the R&D acitvity

- A long term R&D program is required to improve sensitivity and detection probability
  - First priority: thermal noise improvement
    $\Rightarrow$ sapphire investigation, thermal noise measurement
  - Then shot noise .... but don't forget 'technical' noises
  - Important: interferometer diagnostic and maintenance (very short term)

- Many activities $\Rightarrow$ organization, coordination and collaboration are required
  - collaboration with LIGO and ACIGA for sapphire investigations
  - collaboration with ACIGA for thermal noise measurement
  - the R&D program should develop the French-Italian comunity around VIRGO
  - it should reinforce the collaboration among the euoropean groups (VIRGO-GEO)

LIGO Advanced Detector R&D Proposal

Gary Sanders

NSF Technical Review

October 22 - 24, 1996

LIGO-G960209-00-M

What We Propose

- A program of research to define advanced subsystems intended to be enhancements to the initial LIGO interferometers
- A program of research to define new advanced detectors
- A five year program in each thrust
  - ›› Some areas of research will enable implementation proposals
  - ›› Some research areas will not be completed and will become part of a following R&D proposal
- A program based upon the benchmark gravitational wave sources, but intended to be flexible if the course of physics research dictates a different evolution of LIGO capabilities

LIGO-G960209-00-M

Collaboration

- Most proposed tasks are highly collaborative, involving institutions outside the LIGO Project
- These institutions will separately propose their required resources

  ››very few subcontracts from LIGO to collaborators

- The proposed program is the LIGO R&D program and collaborators may propose other activities for their institutions
- It is our intention that this collaboration is the "training wheels" for the larger LIGO Collaboration. This is an important development in building this experimental field and it follows the recommendations of the McDaniel Report.

Steps in the Advanced Subsystems Research

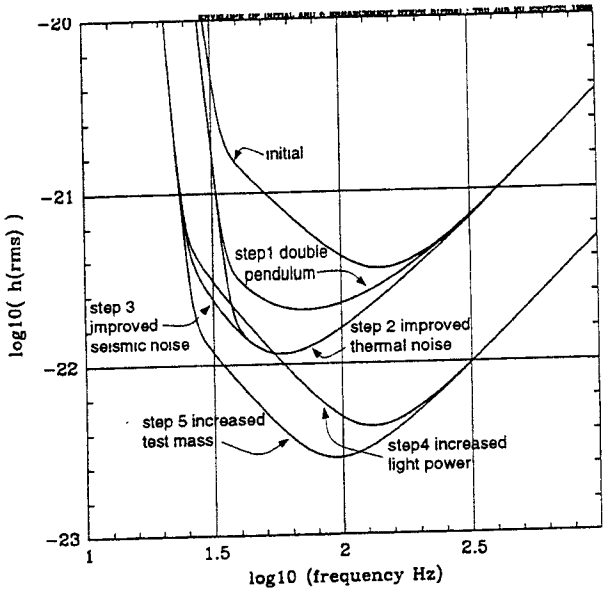

h_{rms} Noise Envelopes for Initial LIGO and Advanced Subsystems/Detectors

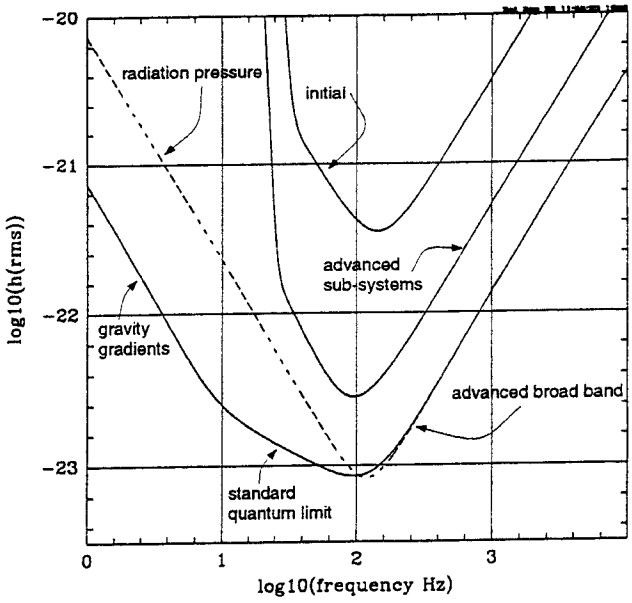

LIGO

Amplitude Spectral Strain Noise Expressed as an Equivalent h(f)

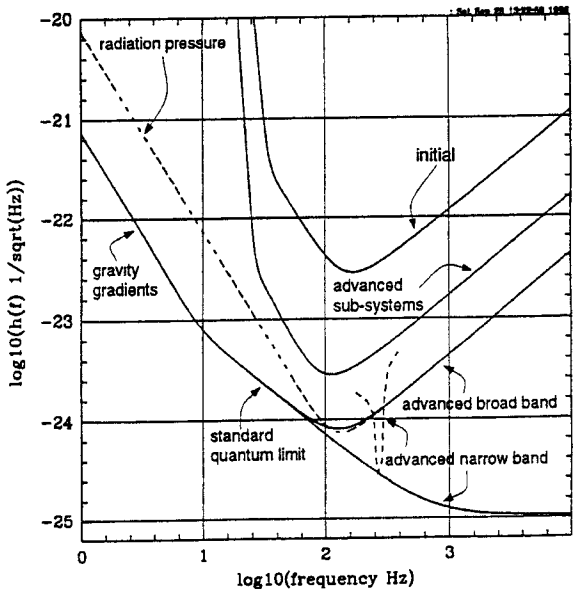

LIGO

Advanced Subsystems R&D

- Double Pendulum Suspension
- Reduced Thermal Noise
- Reduced Internal Test Mass Thermal Noise: Sapphire
- Higher Laser Power and Core Optics for Higher Power
- Increased Mass (Sapphire)

Double Pendulum Suspension

One Concept:

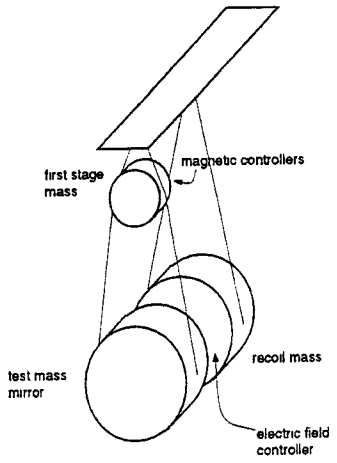

- Added isolation from thermal noise of seismic isolation
- Reduce actuator force dynamic range
- Remove test mass magnets which degrade Q
- Reduce magnetic field and domain jump noise on test mass
- Additional stage of $(f_0/f)^2$ isolation

Reduced Test Mass Internal Noise: Sapphire Development

- Develop the techniques to grow, polish and coat sapphire with all of the required tolerances to enable them to be used as end test masses in LIGO and VIRGO.
- Investigate the absorption, birefringence and optical homogeneity with the goal of demonstrating suitability for the input test masses in LIGO and VIRGO.
- Investigate alternatives to the current wire suspensions which would not degrade the high intrinsic Q of the sapphire and which give higher suspension Q's.

Reduced Test Mass Internal Noise: Sapphire Development

Significant Events	*Responsible*	*Date*
Sample Characterization Complete	LIGO, VIRGO, UWA	July 1997
Test Masses (2) Delivered	LIGO, VIRGO	Jan. 1998
Test Mass Polishing and Figure Characterization Complete	CSIRO	July 1998
Test Mass Q, Absorption Birefringence Characterization Complete	LIGO, VIRGO, UWA	Dec. 1998
First Monolithic Suspension Results	UWA	July 1999

Higher Laser Power

- Continues LIGO development of 10 W 1064 nm for initial LIGO with Stanford and Lightwave
- Lightwave will continue development with rod geometry master oscillator-powered amplifier (MOPA) with an SBIR proposal
- LIGO will work with Stanford to apply LIGO requirements to a slab geometry design

  ››A Lightwave 10 W laser will be used as the master oscillator for the resulting 100 W prototype which will be fully investigated

- This program is planned for three years, leading to an engineering proposal to be carried out with industry

Core Optics for Higher Power

- Goal of 100 W laser is phase sensitivity of 3×10^{-11} rad/$\sqrt{Hz}$
- Achieve this by raising laser power OR by reducing optical losses OR by both
- This program proposes to follow on to LIGO Pathfinder program by extension to more demanding:

  ››optical metrology - principally of mirror polish and coating phase distortions

  ››optimum polishing technique for LIGO requirements

  ››control of coating uniformity and absolute optical characteristics such as reflectivity and loss

Core Optics for Higher Power

Responsibilities	*Collaborators*	*Schedule Initiate--- Complete*
Full precision phase mapping @ 1064 nm of surface figure (upgrade)	LIGO and industry	1998 (mid)--- 1999(late)
Acquire, install, characterize micro-roughness instrument	LIGO and industry	1997(mid)--- 1998(early)
Fully calibrated surface scatter/loss test bed (upgrade)	VIRGO LIGO and industry	1998(early)--- 1998(late)
≤ 1ppm level coating loss measurements. ≤ ± 10% bulk substrate loss mapping	EMU / VIRGO	1999(mid)--- 2001
Design and fabricate developmental silica mirror substrates (quantity ~30)	LIGO and industry	1998 (early)--- 1998(mid)
Surface polishing optimization	LIGO and industry	1998(late)--- 2002(early)
Coating uniformity development	LIGO and industry, VIRGO	1998(late)--- 2002(mid)

Advanced Detector R&D

- Resonant Sideband Extraction and Signal Recycling
- Advanced Seismic Isolation
- Signal Processing
- Measurement and Feedback of Thermal Noise

RSE/SR Research Program

- University of Florida will study dual recycling in a tabletop experiment lasting two years
- LIGO will study resonant sideband extraction in a tabletop experiment lasting two years
- An analytic study will be made by LIGO of suitable future interferometer configurations using the entire range of possibilities promised by these two techniques
  - ››modeling of interferometer sensitivity and response
  - ››modeling of optical sensitivity to distortions using paraxial FFT methods
- Following tabletop experiments, one of the techniques will be studied in a large scale test in a LIGO test interferometer

Advanced Seismic Isolation

- Initial LIGO measurement band limited by seismic noise at 40 Hz
- Goal of research is to:
  - ››push this envelope down to about 1 Hz such that the limiting noise source for the interferometer becomes gravity gradients
  - ››reduce the dynamic range required of the fine control actuators by providing isolation to frequencies as low as the microseismic peak (0.17 Hz).
- Three approaches:
  - ››LIGO MIT Stacis active system from Barry Controls does not meet low frequency requirements
  - ››JILA 3-stage active system promises low frequency performance
  - ››Virgo passive stack is tall and requires additional material qualification

Advanced Seismic Isolation Work Plan

Pgm	Significant Events	Responsible	Date
Near Term	Improved Stacis Isolators: Design, Fab & Unit Test	LIGO, Stanford	Dec 1999
	Improved Stacis Isolators: 2km IFO Tests Completed	LIGO, Stanford	Dec 2000
Long Term	Requirements & Interface Definition	LIGO, JILA, Stanford	Mar 1998
	Preliminary Design	JILA, Stanford, LIGO	Jan 1999
	Final Design	JILA, Stanford, LIGO	Jan 2000
	Fabrication Completed	JILA	Jan 2001
	Unit Test Completed	JILA	Dec 2002

This research is expected to extend into the next five year research period

Collaboration Formation for Advanced Detectors: Introductory Remarks

Gary Sanders

LIGO/Caltech

Aspen Winter Conference on Gravitational Waves and Their Detection

January 26 - Feb. 1, 1997

Steps Leading to Today

- Aspen 1995 Workshop stimulates formation of LIGO Research Community
- LIGO Research Community forms
- NSF forms Panel on the Long Range Use of LIGO
- Report of Panel *(on NSF Web page)* calls for
  - » formation of LIGO Laboratory
  - » formation of LIGO Science Collaboration
  - » formation of strong LIGO Program Advisory Committee
  - » aggressive program of advanced R&D
  - » definition of needs for data analysis
  - » initiation of a Visitor's Program

LIGO Laboratory

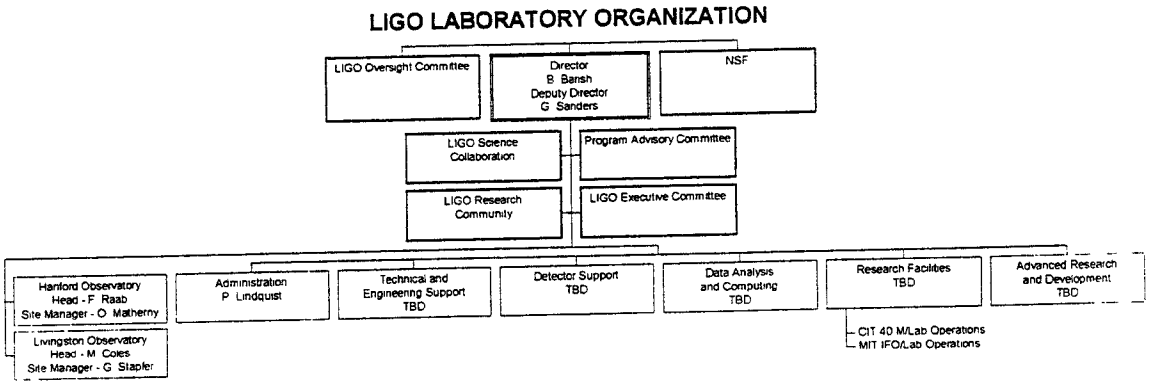

Advanced R&D Program

- LIGO submitted proposal to NSF
  - » goal is improving sensitivity of LIGO
  - » organized very strongly with collaborative emphasis
- Collaborators submitted independent proposals with collaborative activities proposed
- This collaboration organized between August receipt of Panel Report and NSF October 8 deadline
- Much remains to be done in defining collaborative program and refining proposals
- NSF may separate first year support from outyears to allow further time for formation and definition

LIGO Program Advisory Committee

- Principal advisory group to LIGO management
- Will review all aspects of the program
  - » including LIGO-related research by outside groups
- Review requests from LIGO Director or the PAC's own initiation

PAC Charge

The LIGO Program Advisory Committee (PAC) is the principal advisory group to the LIGO management. The committee will meet approximately two times per year and will give advice on policy, management, and scientific and technical issues. The PAC will review all aspects of the program, including LIGO related research by outside groups, as requested by the Director or as initiated by the PAC itself. Some of the work may be done by subcommittees, which can include outside members. The committee will assist LIGO in giving the NSF input on LIGO related issues.

PAC Membership

- W. Frazer - Univ. of California - Chair
- P. Avery - Florida
- A. Brillet - IN2P3/Virgo
- W. Hamilton - LSU
- P. Michelson - Stanford
- V. Sandberg - LANL
- P. Saulson - Syracuse
- A. Seiden - UC Santa Cruz
- R. Vogt - Caltech/LIGO
- LRC Ex Officio - S. Finn (H. Ward sat in this time)

First Meeting Jan 6-7, 1997

- Informational
  - » review project
  - » tour 40 Meter, vacuum chamber models, Drever laboratory
  - » overview of computing/data analysis
- Review and determine PAC Charge
- Review 5 proposals transmitted by NSF
  - » review transmitted in confidence to NSF
- Review and comment on plan to form the LIGO Scientific Collaboration

Results - PAC Transmittal Letter

Dear Barry:

Attached is the report of your Program Advisory Committee on the meeting of January 6 and 7. We found the meeting very informative, and thank you, the LIGO staff, and the spokesmen for the advanced R&D proposals for the excellent presentations.

The principal theme of the meeting was collaboration, a topic of great promise and urgency. We comment below on the plan for creating the LIGO Scientific Collaboration, and then review the specific proposals. Again, an overriding concern in our reviews is the extent to which a true collaboration is evident in the proposals. In many cases, we find this to be indicated only in a very sketchy, preliminary way. We emphasize the urgent need for the proposed researchers to develop, with the help of the LIGO staff and with those making related proposals, better defined plans for productive collaboration.

W. R. Frazer, Chair, LIGO Program Advisory Committee

Draft Plan For LIGO Science Collaboration

- Draft written with input from Stebbins and Michelson/Allen drafts, PAC made aware of these
- LIGO I is h ~ 10^{-21} reached + 2 years
- LIGO Science Collaboration will be formed soon
  - » Collab. Council - 1 member from each institution per 5 participating scientists at the institution
  - » Collab. Spokesman - elected for 3 year term, approved by Director
    - first Spokesman appointed by Director through construction phase
  - » Collab. Deputy Spokesman - chosen by Spokesman
  - » Governance detailed by Collaboration Council
- Membership in Collaboration as LIGO I or II determined in negotiated MOU's

Results - Plan for LIGO Science Collaboration

"The PAC endorses the statement in the Plan that "It is now prudent to form an overall LIGO Science Collaboration ...", and we find the proposed Plan to be generally sound. We recommend, however, that the initial rules for joining the Collaboration be specified in the Plan. Subsequent modifications in these rules could be made by the Collaboration Council, with the concurrence of the Director.

Proposed membership of the LIGO Science Collaboration (LSC):

The members of the LSC are those individuals making major contributions to the project as formalized by MOU's with the LIGO laboratory management. Proposed additional members may be added at the recommendation of the Collaboration Council, with the concurrence of the Director. The criterion for membership should be evidence of intention to contribute significantly to the development, implementation, or data analysis of LIGO. ...

Results - Plan for LIGO Science Collaboration

...Given the plan for an initial two year data run, followed by important enhancements to the project, the collaboration will comprise an initial LIGO I group and an extended LIGO group. The LIGO I group is composed of the members of the LSC who have made major contributions to the design and construction of LIGO and to the initial two year data run and would be the authors of the results coming from these data. The extended LIGO group, based on their contributions to the enhanced experiment, would be authors of the subsequent results.

The LSC should be led by a spokesperson. We endorse the description of the selection process and length of service in the Plan. The spokesperson would represent the collaboration to the laboratory management, be responsible for communication within the collaboration, and have a role in enhancing the coherence and focus of the extended LIGO technology development. Other special areas of responsibility should be either specified or clarified with the LSC Collaboration Council."

LIGO Response to Advice

- We will incorporate PAC advice into Draft LSC Plan
- We will act right after Aspen meeting
  - » Aspen meeting discussions can provide input to Plan
- PAC reviewed LIGO-related Advanced R&D Proposals
  - » reviews are provided to NSF
  - » Fraser cover letter indicates direction of top level advice

Tuesday AM: A. Advanced Interferometry
January 28 Chair: R. Drever

8:00	A. Ruediger(Garching)	The Sagnac Interferometer - Pro and Con
8:25	Discussion	
8:35	D. Schnier(Garching)	Resonance Coincidence Method-A New Locking Scheme for Narrow Band Dual Recycling
9:00	Discussion	
9:10	Coffee Break	
9:25	S. Kawamura(Caltech)	Signal Recycling and Resonant Sideband Extraction
9:40	Discussion	
9:50	V. Braginsky(Moscow)	Recent Results of the MSU Group
10:15	Discussion	
10:25	R. Schilling(Garching)	Transfer Function of Interferometric GW Detectors at Higher Frequencies
10:50	Discussion	

Aspen Winter Conference
on
Gravitational Waves and Their Detection

26 January – 1 February, 1997

Aspen, Colorado, USA

The Sagnac Interferometer – Pro and Con

Albrecht Rüdiger

Max-Planck-Institut für Quantenoptik

D–85748 Garching bei München

27 January 1997

Tel: +49 89 32905-265 e-mail: atr@mpq.mpg.de Fax: +49 89 32905-200

Sagnac Interferometer – Pro and Con

usurp position not due to me

in recent years revived interest in Sagnac:

1987 Rai Weiss first realistic suggestion for GW
1991 T. Kobayashi Proposal, Osaka University
1996 Bob Byer Aspen 1996: showed advantages
1996 Stanford Galileo Proposal, NSF Review
1996 Ke-Xun Sun paper on principle, experiment
1996 Jun Mizuno paper submitted, analysis
1997 Marty Fejer Aspen 1997: shows feasibility
1997 Albrecht Rüdiger Aspen 1997: summarize ?

not presuming to be arbiter, *but*

"no ax to grind":

neither **proposing** nor **opposing** Sagnac
nor having to fear competition for funds

The Sagnac Effect

Historical note:

G.M.M. Sagnac made crucial experiment in 1913

dealt final death blow to ether theory

Sagnac-Versuch [frz. sa'njak; nach dem frz. Physiker G. M. M. Sagnac * 1869, † 1928], eine Abänderung des ↑Michelson-Versuchs darstellender Interferenzversuch, bei dem die interferierenden Lichtstrahlen einer Rotation ausgesetzt werden und der mitrotierende Beobachter eine Verschiebung der Interferenzstreifen feststellt. Der 1913 erstmals ausgeführte S.-V. widerlegte endgültig die Lichtätheritheorie; er ermöglicht das Erkennen rollender Bezugssysteme.

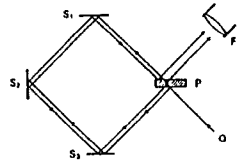

Sagnac-Versuch. Versuchsanordnung mit Strahlengang (Q Lichtquelle, P Trennplatte, S_1, S_2, S_3 Spiegel, F Fernrohr)

Sago (malai.), aus dem Mark von Arten der Sagopalme oder der Urennpalme (*Palm-S.*) bzw. aus Manlokstärke (*Perlsagoka*) gewonnenes, aus verkleisterter und daher bes. quellfähiger Stärke bestehendes, feinkörniges Nährmittel, das zur Herstellung v. a. von Süßspeisen oder Suppen verwendet wird; heute vielfach durch ein entsprechendes Erzeugnis aus Kartoffelstärke (*Kartoffel-S.*) ersetzt.

Weiß, Filme, Schiester, E.: *Kelelogeya (Neuguinea, Normanby-Island). S.gewinnung. 1963. EC (E 529).* – Schuster, M. (Schuster, G.): *Aibam (Neuguinea, Mittlerer Sepik). Zubereiten v. Brei (S. mit Kokos). 1974. EC (E 1377); Zubereiten v. Kuchen (S. mit Kokos u. Banane). 1974. EC (E 1733). Backen v. S.-Fladen u. S.-Brocken. 1974. EC (E 1734).* – ↑auch Sagopalme.

Sagomilz, Milzerkrankung mit an Sagokörner erinnernden Amyloidablagerungen in den Follikeln.

Sagopalme (Metroxylon), Gattung der Palmen mit rund 10 Arten im Malaiischen Archipel, auf Neuguinea und auf den Fi-

counter-propagating beams,

measure rotation in space

application: gyroscopes Ezekiel, MIT

Signal proportional to:

area A

rotation Ω

but here: **zero-area** Sagnac configuration

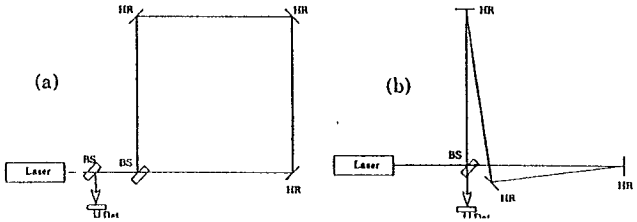

Comparison Michelson / Sagnac

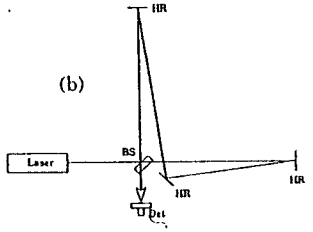

Frequency Responses Michelson vs. Sagnac

assuming:

equal arm lengths ℓ

equal number of passes, $\mathcal{N} = 2$, in the **arms**

i.e. $2\mathcal{N} = 4$ passes in the Sagnac

before recombination

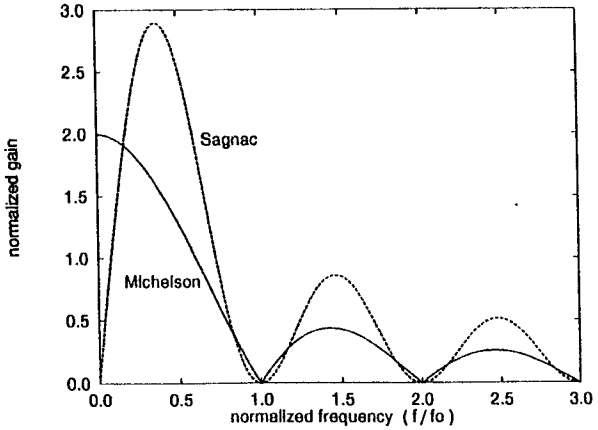

Advantages of Sagnac

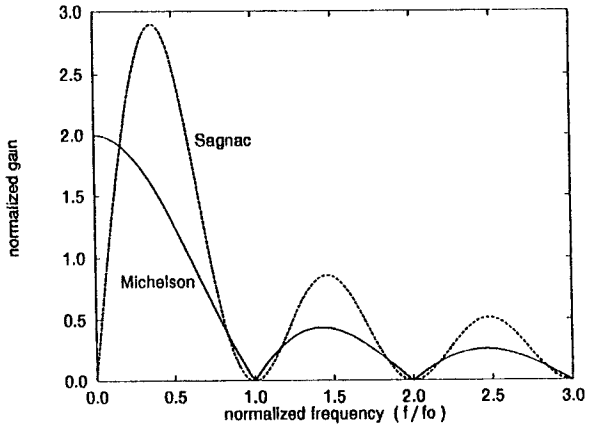

Common Path Interferfometer:

less sensitive to

drifts in **armlength** (*robustness*)

polarization effects

different **losses** in the arms

even with unequal arms

(as are typical for delay line arms)

insensitive to **frequency** fluctuations

sensitivity:

apparently by ≈ 1.4 **higher**

due partly to **double-length path**

(*or, in other words*) **doubled energy**

The Frequency Scale

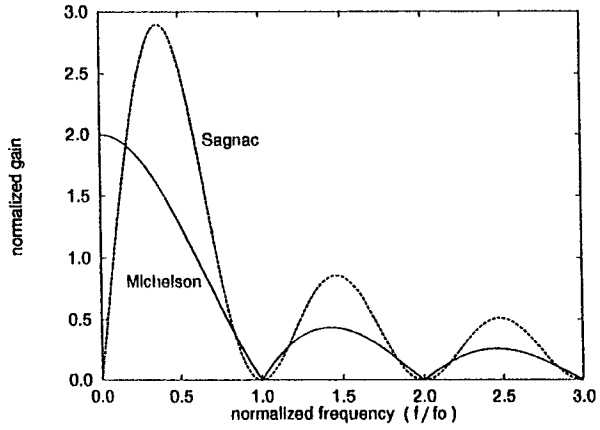

The frequency scale, f_0, is given by

$$f_0 = \frac{c}{2\,\ell}$$

full cancellation at all $f_n = n\,f_0$

for typical (geometrical) arm length of $\ell = 3\,\mathrm{km}$

$$f_0 = \frac{c}{2\,\ell} \;\approx\; 50\,\mathrm{kHz} \times \frac{3\,\mathrm{km}}{\ell}$$

Have to increase **storage time**

either use **delay lines**

or **Fabry-Perot** cavities in the arms

to get into range of **GW frequencies**

Delay Lines

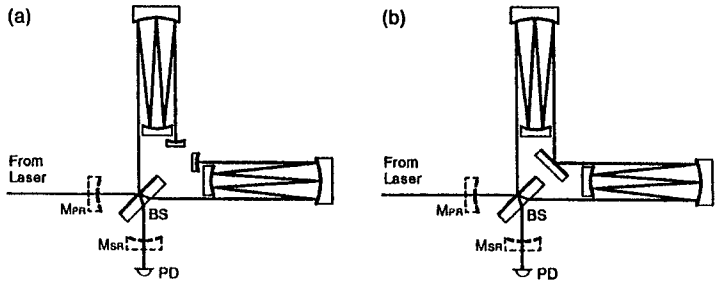

drawings strongly simplified:

show neither true **Herriot** delay line,
nor **zero-area** Sagnac

number of transits (passes) in **one arm**:

for unambiguity: script $\mathcal{N}$,

N in earlier literature: $N = \mathcal{N}$
N in Galileo proposal: $2\,N = \mathcal{N}$

signal response proportional to $\mathcal{N}$,

until optical path $\mathcal{L} = \mathcal{N}\,\ell$

of order $\Lambda/2$, half GW wavelength

Shot Noise Considerations

Gravitational Wave Detection:

at higher detection frequency end:
sensitivity determined by **shot noise**
required: **high light power** (kW)
as long as no such kW lasers in sight: power recycling

attainable power gain
depends on typical **losses** of mirrors
and on number of **bounces,** $\mathcal{N}$, on mirrors

Best condition for comparison (Jun Mizuno):
have identical 'stored energy' $\mathcal{E}_{\rm st}$ in detectors
$\mathcal{E}_{\rm st}$ plays a decisive role in attainable sensitivity

leads to **similar** peak sensitivities

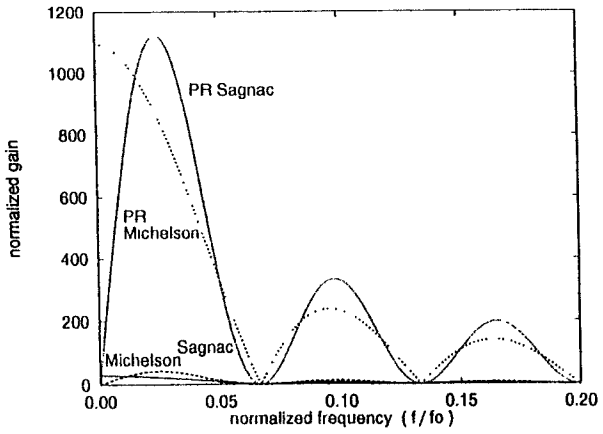

Delay Lines revisited

again: **response** of **power recycled** interferometers:

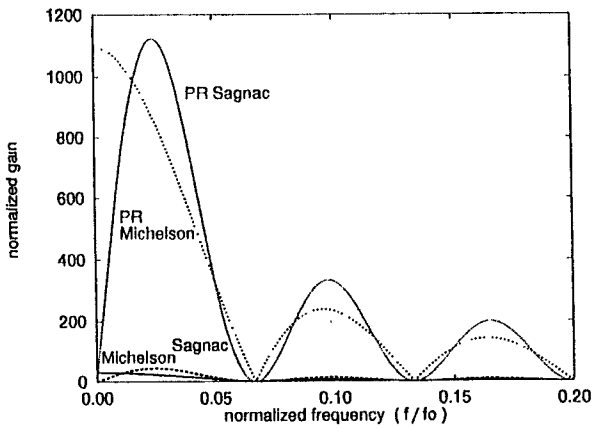

here with rather modest value for
number of bounces: $\mathcal{N} = 30$

and rather optimistic value for
recycling gain $\mathcal{G}_{\mathrm{PR}} = 1000$

each leading to sensitivity enhancement of ≈ 30

first **zero** in response down in **frequency** by $\mathcal{N}/2$
i.e. at $f_z/f_0 = 1/15 = 0.067$
(still $f_z = 3.33$ or 2.5 kHz,
for $\ell = 3$ or 4 km, respectively)

Delay Lines more

Delay Lines (in particular the **Herriot DL**)
have many favorable features:
non-resonant
easy to **align**
insensitive to far-mirror alignment
easy to change **bounces** $\mathcal{N}$

but also have price to pay:
mirror **size**
armlengths determined by radii of curvature
difficulty of **separating** in/out beams

most obvious handicap:
mirror size
typical size (for optimized Herriot scheme):

$$D \approx S \, \frac{2+\sqrt{2}}{\pi} \, \sqrt{\lambda \mathcal{L}}$$

with safety factor of (only) $S \approx 2$
leading to $D \approx 0.71$ m for $\mathcal{L} = 100$ km
so just barely compatible with LIGO tubes

One can relax assumptions,
but **high-tech schemes** required

Stanford Proposal

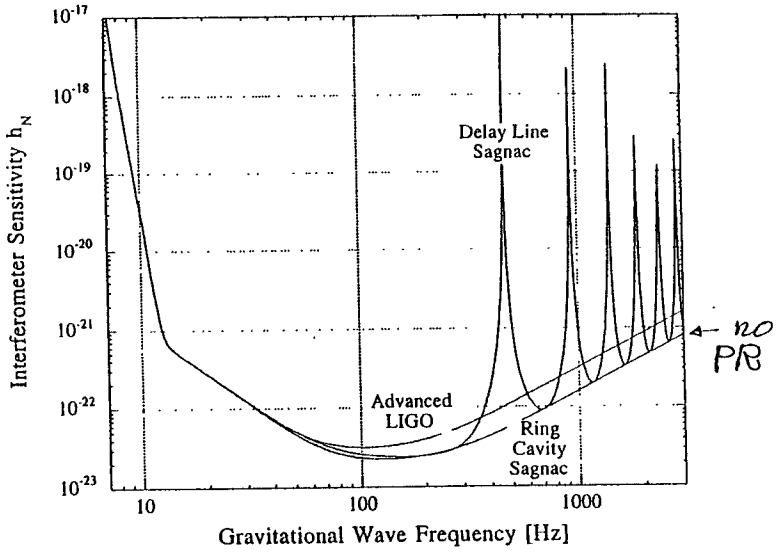

Figure 3.5 A comparison of the sensitivity of the advanced LIGO (upper smooth curve), a delay-line Sagnac (lower curve with several response zeros) and a power-recycled Sagnac with ring-cavity arms (lower smooth curve) like that shown in Figure 3.4. The assumptions on suspension, and test mass Q, vibration isolation and laser power used in these calculations were the same as those used in Figure 1.1 for the advanced LIGO interferometer. We assumed 80 passes in the delay line. Note that in the displacement-noise limited regime at low frequencies, the sensitivity of the Sagnac and Michelson interferometers are similiar despite the lower responsivity of the Sagnac, because the Sagnac response is rolling off to the noise as well as to the signal thus maintaining the signal to noise ratio and hence the sensitivity.

Mirror Size

$$D \sim S \cdot \sqrt{\lambda \cdot \mathcal{L}}$$

$\frac{2+\sqrt{2}}{\pi} \approx 1.09 \Rightarrow 1.0$

case	λ [μm]	$\mathcal{N}$	$\mathcal{L}$ [km]	S	D [m]
"GEO" 3km	1	30	90	3	0.64
"LIGO" 4km	1	160	640	2	1.60
	0.5	160	640	1.7	1.00

Separate Beams In/Out

Herriot:

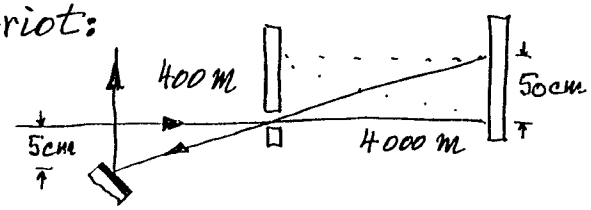

Two-Hole:

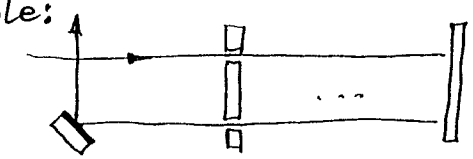

give up many of Herriot DL features,

dense packing?

Retracing

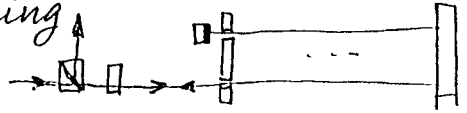

Fabry - Perot

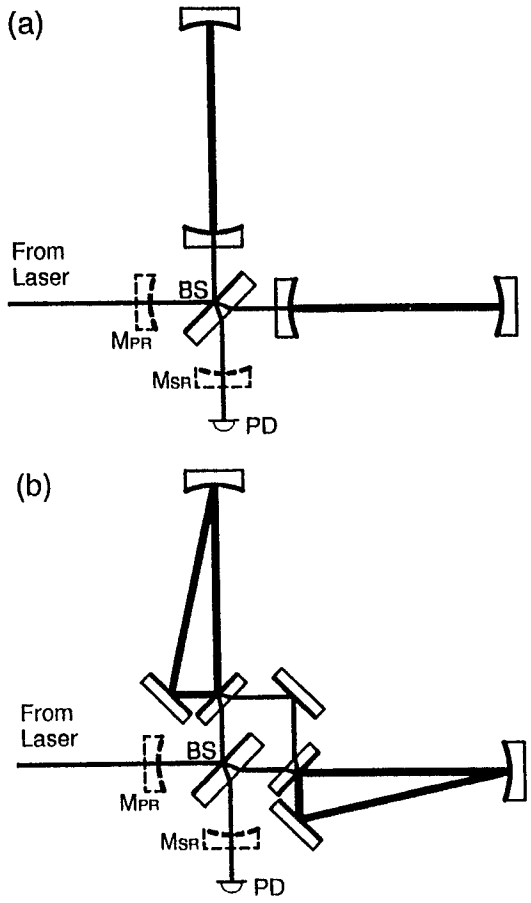

Figure 4: Schematics of (a) Michelson and (b) Sagnac layout using an optical cavity in each arm. Positions for possible power- and signal-recycling (extraction) mirrors (M_{PR}, M_{SR}) are also shown (in dashed lines).

Fabry - Perot

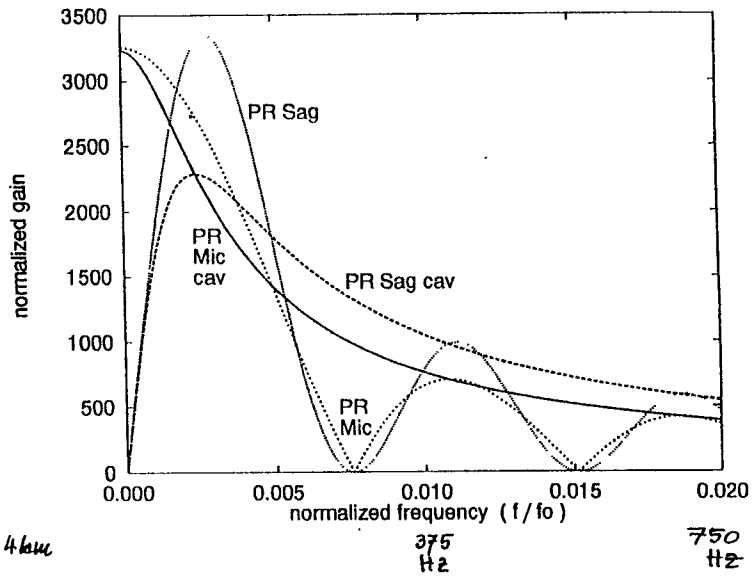

"LIGO" 4km

375 Hz

750 Hz

Figure 5: Response of Michelson and Sagnac interferometers with cavities in the arms ($\mathcal{F} \approx 200$). Power recycling is optimized. Those with multiple-reflection arms ($N \simeq \frac{4}{\pi}\mathcal{F} \approx 254$) are also shown for comparison.

Signal-recycled Michelson
Delay line

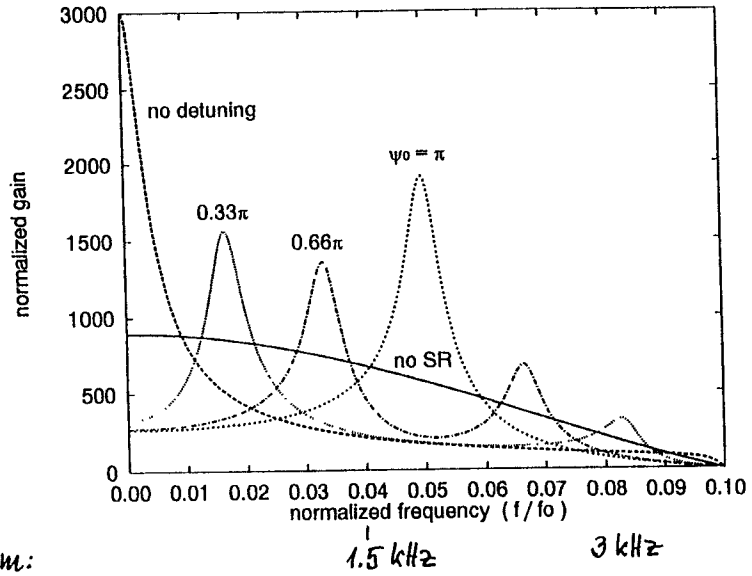

Figure 6: Response of a power-recycled Michelson interferometer with multiple-reflection arms ($N = 20$) and a signal recycling mirror ($|\rho_s|^2 \approx 0.7$). Each curve represents a different tuning condition of the signal recycling mirror. The response without the signal recycling mirror is also shown for comparison.

Signal-recycled Sagnac
Delay line

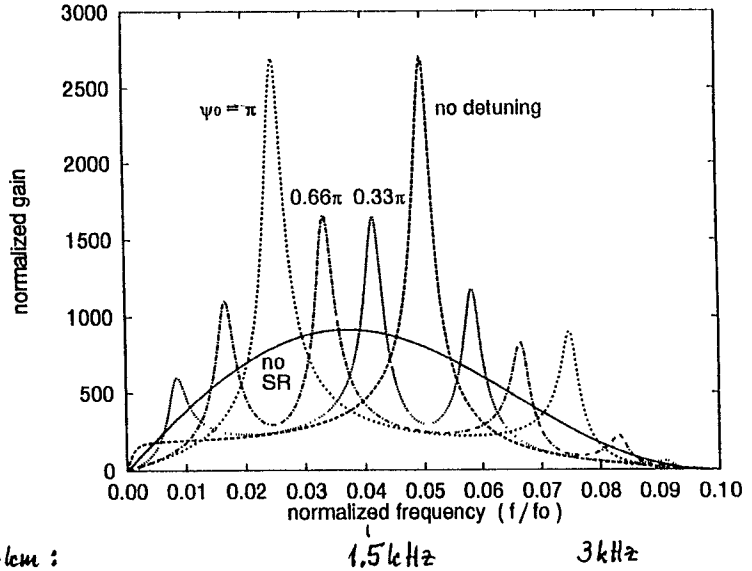

Figure 8: Response of a power-recycled Sagnac interferometer with multiple-reflection arms ($N = 20$) and a signal recycling mirror ($|\rho_s|^2 \approx 0.7$). Each curve represents a different tuning condition of the signal recycling mirror. The response without signal recycling mirror is also shown for comparison.

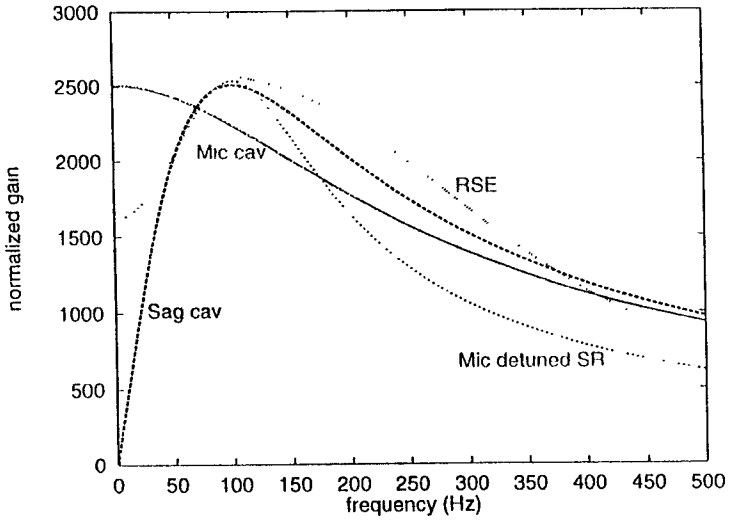

Figure 11: Response optimized for 100 to 200 Hz, assuming 3 km armlength. The curves are: a Michelson with cavity arms ($\mathcal{F} \approx 125$), a Sagnac with cavity arms ($\mathcal{F} \approx 250$), a multi-reflection Michelson with detuned signal recycling ($N = 4$, $\rho_s^2 \approx 0.977$ and $\psi_0 \approx 0.23$ rad), and resonant sideband extraction (arm cavity $\mathcal{F} \approx 5000$ and $\rho_s^2 \approx 0.9$, the signal extraction mirror is placed 3 km away from the beamsplitter and zero detuning) It might worth mentioning that a Michelson with cavity arms shows better sensitivity than others at frequencies higher than those shown here.

Conclusions

Sagnac Interferometer

has many intriguing advantages
particularly
the delay-line type
with direct high-power injection

The question mark:

can we afford the expense in
man power
time invested
technological development
equipment cost ?

the answer
(from GEO's vantage point):
No!

the answer
(for Stanford/LIGO):
Yes, do investigate further

The Resonance Coincidence Method a new locking scheme for narrow band dual recycling

Dietmar Schnier [1],

Max-Planck-Institut für Quantenoptik, Hans-Kopfermann-Str. 1, D-85748 Garching, Germany, Fax: +49(89)32905-200

- Introduction
- The Right Choice of Cavity Lenghts

  Generation of the SR-Mirror Control Signal
- Tuning of the Signal Recycling Cavity

  Sensitivity of PR-Cavity and SR-Cavity Lock

  Decoupled and Coupled Cavities

  MI-Phase Control

  Conclusion

[1] e-mail: dis@mpq.mpg.de
also at: MPQ Aussenstelle Hannover, Appelstr. 2, D-30167 Hannover

Preprint submitted to Physics Letters B

8 January 1997

Set-up for Narrow Band Dual Recycling with Resonance Coincidence Method

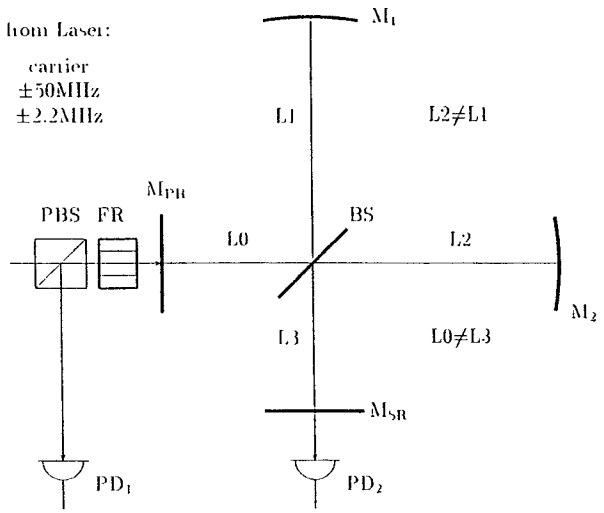

MI is at dark fringe for the carrier

PR-cavity is resonant with the carrier

SR-cavity is resonant with a signal sideband

50 MHz sidebands see MI at bright fringe if L2-L1=1.5m

Cavity between PR- and SR-mirror is resonant with one of these sidebands

All 3 resonance conditions can be fullfilled at the same time for certain choices of the cavity lengths L_{PR} and L_{SR} !!!

The Right Choice of Cavity Lengths

For the Geo600 detector the following relations are valid:

$FSR_{SR} \approx FSR_{PR} \approx 2 \cdot FSR_{DR} \approx 125\text{kHz}$,

$f_{signal} = 1kHz \approx \frac{8}{1000} FSR_{SR}$.

Power recycling cavity: $L_{PR} = L0 + \frac{L1+L2}{2} = n_1 \cdot \frac{1}{2}\lambda_{car}$

Signal recycling cavity: $L_{SR} = L3 + \frac{L1+L2}{2} = (n_2 + \frac{8}{1000}) \cdot \frac{1}{2}\lambda_{car}$

50 MHz sideband cavity: $L_{SB} = L_{SR} + L_{PR} = (n_3 + \frac{1}{2}) \cdot \frac{1}{2}\lambda_{SB}$

$(n_3 + \frac{1}{2})$ because the MI causes an additional phaseshift of π for the transmitted phasors compared to a standard linear cavity. (100MHz sideband will be anti-resonant in the PR-cavity because of a similar phaseshift of π !!)

Reflected and transmitted phasors in a MI:

One posssible choice for cavity lengths

$\Omega_1 = 50MHz$, $\lambda_{CAR} = 1\mu m$)

$L_0 = 1m$

$L_1 = 1198.25m$

$L_2 = 1199.75\text{m}$

$L_3 = 2.476m \pm 4 \cdot 10^{-9}\text{m}$

In this configuration $\Omega_1 = 400 \cdot FSR_{PR}$ is valid!

Reflected and transmitted light intensities

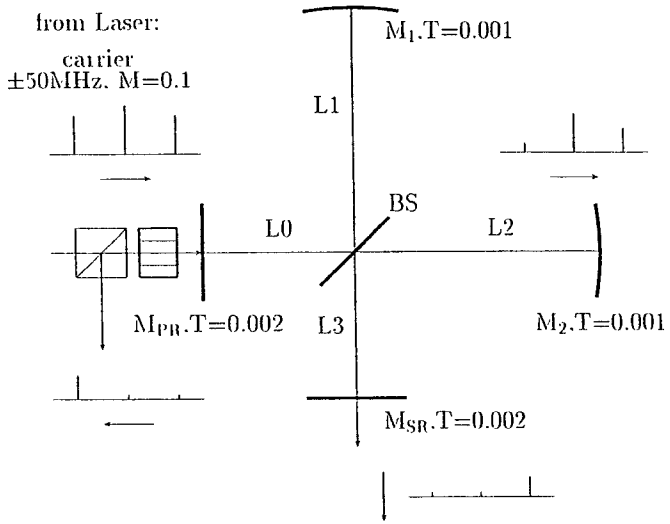

Reflected amplitude and phase of the 50MHz sidebands
as a function of the SR-mirror position L3 + dl3

USB = upper 50MHz sideband

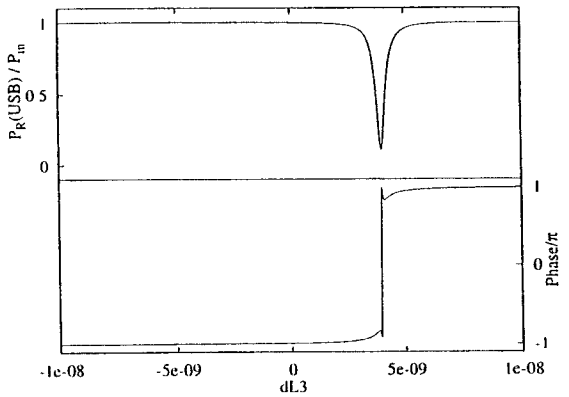

LSB = lower 50MHz sideband

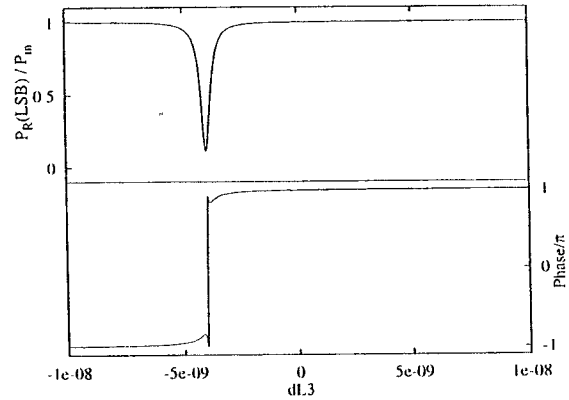

Control Signal for SR-mirror position:

reflected light power demodulated with $\sin(\mathbf{2 \cdot \Omega_1 \cdot t})$
as a function of the SR-mirror position L3 + dl3

Ω_1=50MHz : SR-cavity resonant with 1kHz signal-sideband

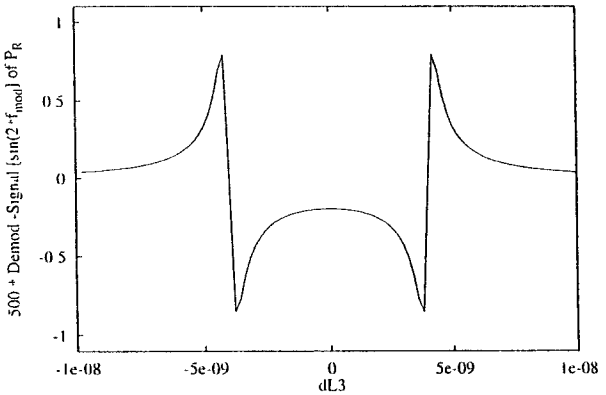

Ω_1=50.0004MHz: SR-cavity detuned to 200Hz sideband

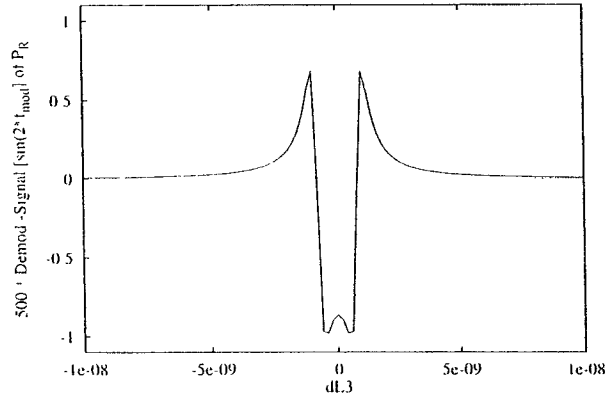

Control Signal for SR-mirror position:

reflected light power demodulated with $\sin(2 \cdot \Omega_1 \cdot t)$

Ω_1=50.0316MHz : SR-cavity antiresonant with carrier

L3=2.476m + $\frac{1}{4}\lambda_{carrier}$ + dL3

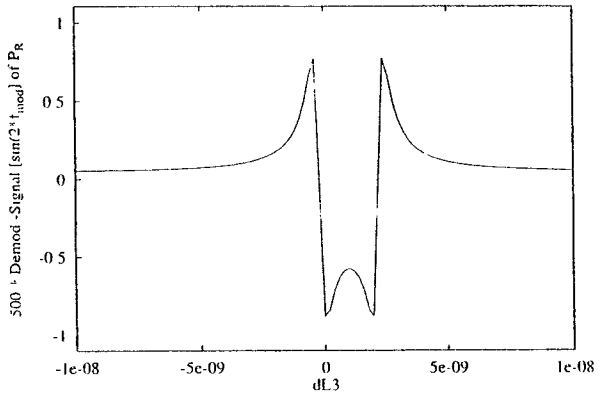

reflected light power demodulated with $\cos(\Omega_1 \cdot t)$

Ω_1=50.00047MHz : SR-cavity resonant with carrier

L3=2.476m + dL3

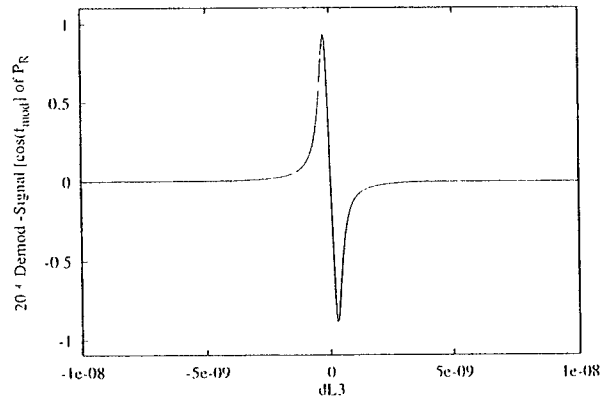

Sensitivity of PR-cavity lock to MI-phase offsets for different positions of the SR-mirror

reflected light power demodulated with $\sin(\Omega_2 \cdot t)$ as a function of the PR-mirror position L0+dL0

L3=2.476+ 1e-9m: SR-cavity close to carrier resonance strong sensitivity to MI-phase offset L2-L1=1.5 + 1e-8m.

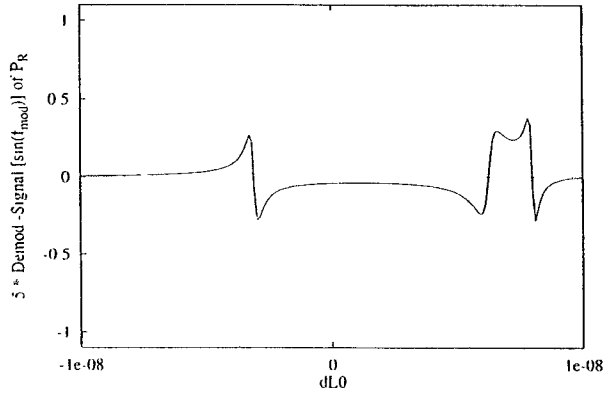

L3=2.476+ .25e-6m: SR-cavity at carrier antiresonance weak sensitivity to MI-phase offset L2-L1=1.5 + 1e-8m.

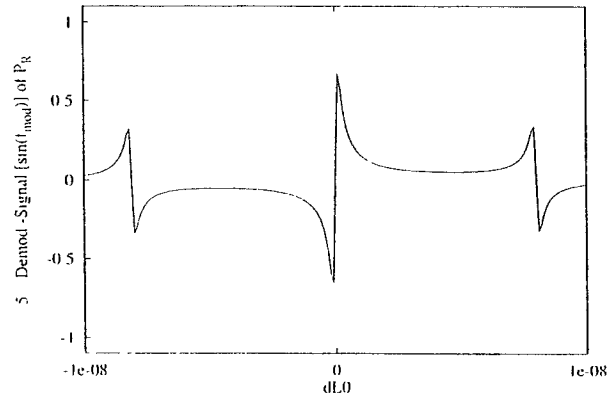

Sensitivity of SR-Cavity lock to MI-Phase and PR-Mirror position offset

reflected light power demodulated with $\sin(2 \cdot \Omega_1 \cdot t)$ as a function of SR-mirror position L3+dL3

SR-mirror follows PR-mirror position offsets
L0 = 1 + 1e-9m

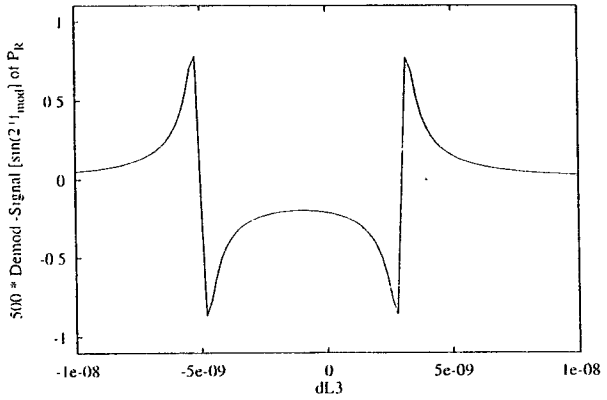

weak sensitivity to MI-phase offset L2-L1 = 1.5 + 3e-8m

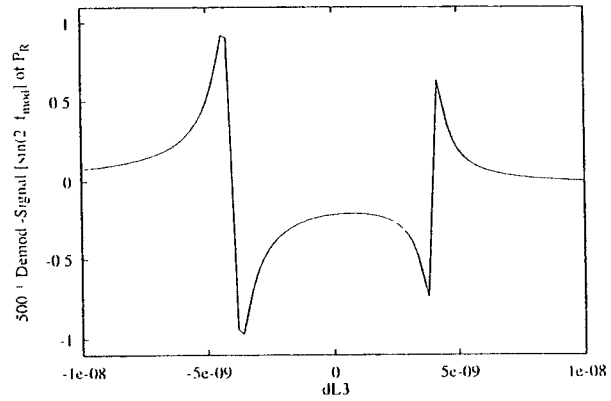

Decoupled → Coupled Cavities

Control Signal for M_{SR} position = P_{refl} demodulated with $\sin(2 \cdot \Omega_1 \cdot t)$ as a function of M_{SR} position

Ω_1 = 50MHz → 15MHz, L3 = 6m : signal broadened

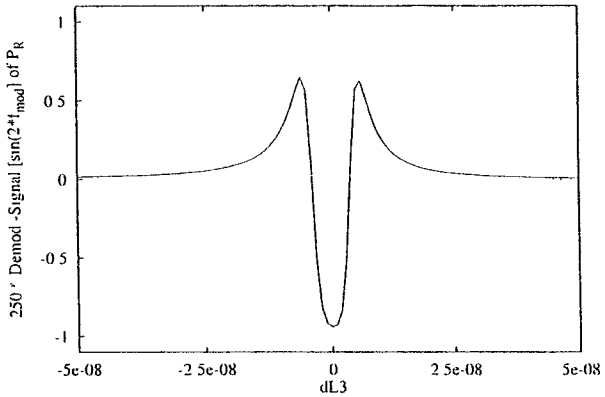

L2-L1 = 1.5m → 0.3m : signal broadened

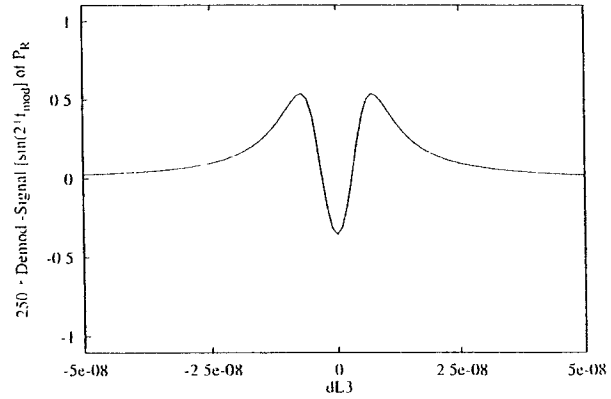

MI-phase control with Resonance Coincidence Method

transmitted carrier and transmitted resonant 50MHz sideband as a function of MI-phase L2-L1 = 1.5m + d(L2-L1)

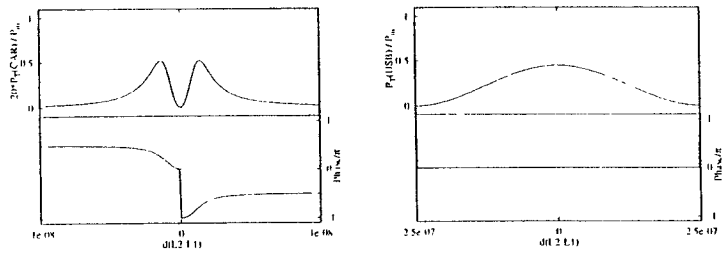

total transmitted light power demodulated with $\cos(\Omega_1 \cdot t)$ as a function of MI-phase L2-L1 = 1.5m + d(L2-L1)

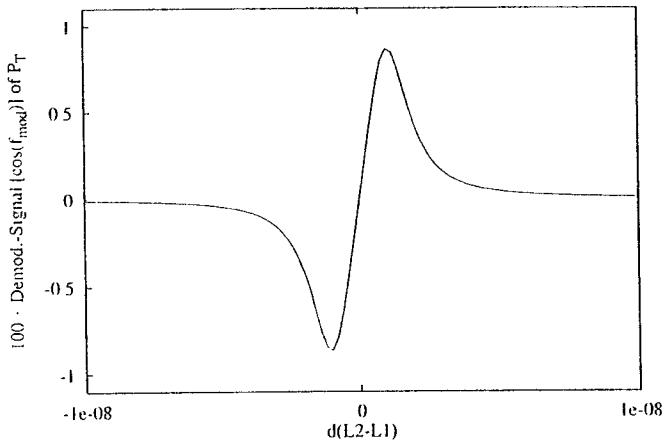

Conclusion

- No modulation of optical components necessary to generate control signals
- The methode is well suited for impeadance matched case and the GEO600 setup
- SR-mirror can be continously tuned with Ω_1 to any signal frequency
- $0.2\text{m} < \text{L2} - \text{L1} < 1.5\text{m}$, $5\text{MHz} < \Omega_1 < 50\text{MHz}$
- Pound- Drever- Signal for PR-cavity lock is sensitive to MI-phase
- For locking aquisition this sensitivity can be reduced if SR-cavity is at anti-resonance for the carrierer
- Beat-Signal between transmitted carrer and transmitted resonant 50MHz sideband gives MI-phase control
- reflected light detected with a quadrant photodetector and demodulated with with sin $(2 \cdot \Omega_1 \cdot t)$ gives tilting control for SR-mirror

Advanced Optical Configuration

- Signal Recycling (Dual Recycling)
  - ››Invented by B. Meers
  - ››Signal is recycled by an additional mirror at an antisymmetric port.
  - ››Narrowband operation is possible.
  - ››Experiment (no arm cavities) done using external modulation
  - ››Adopted for GEO configuration (No arm cavities)
- Resonant Sideband Extraction
  - ››Invented by J. Mizuno
  - ››Signal is extracted by an additional mirror at an antisymmetric port.
  - ››Narrowband operation is possible.
  - ››Power at a beamsplitter can be low, thus less heating effect.
  - ››Experiment done using external modulation.

Research Program

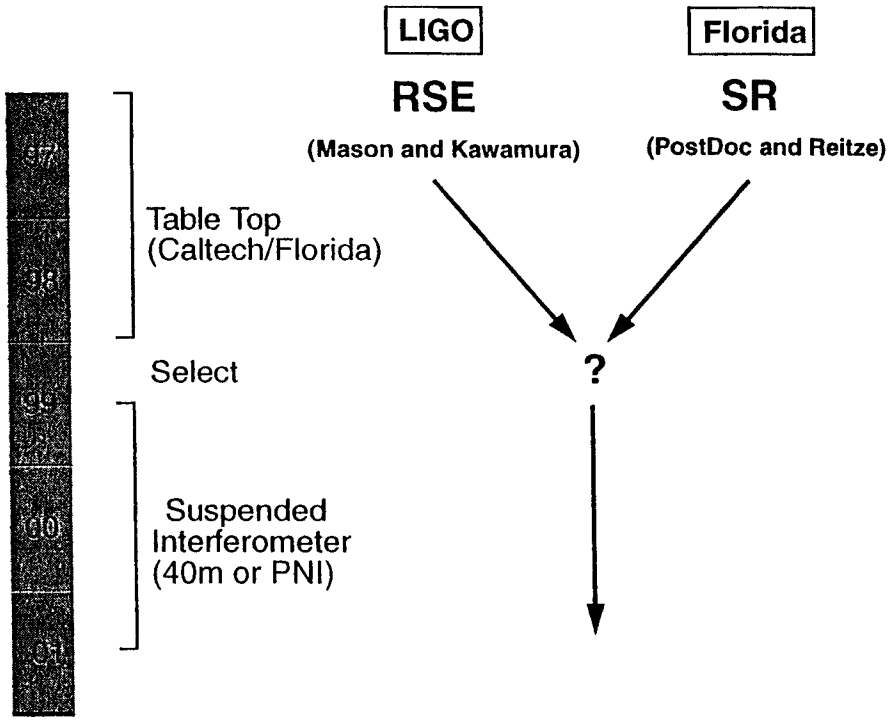

Two Table Top Experiments

- First experiment of DR (with arm cavities) and RSE using the Schnupp modulation
  - ››Sensing and control the length signals
  - ››Switching between broad band mode to narrow band mode
- Comparison
  - ››Practically achievable broad and narrow band sensitivity
  - ››Ease of the band-switching, lock holding, and lock acquisition
  - ››General feasibility and reliability
  - ››Future potentiality
- General experience with each method as a basis for selection for a suspended interferometer experiment

LIGO G970019-00-R

Comparison between SR and RSE

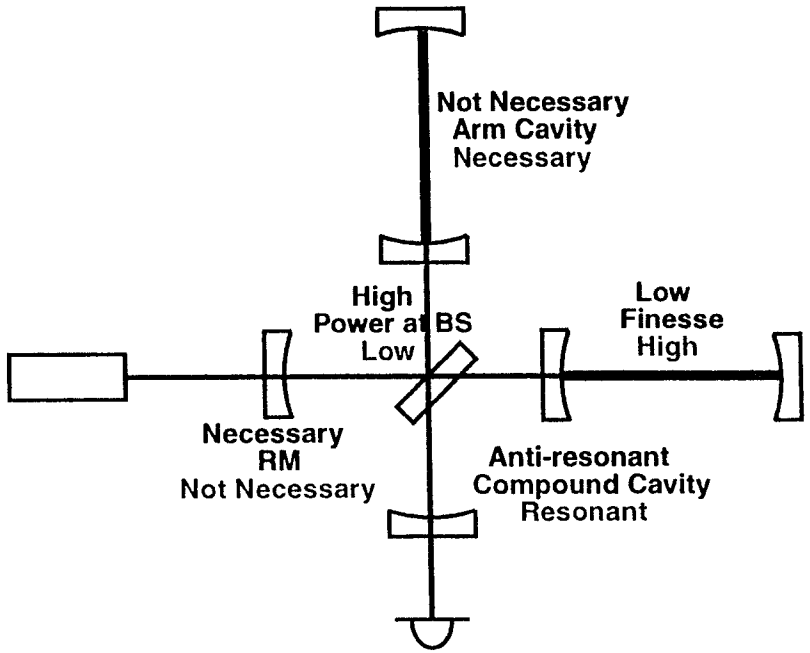

LIGO-G970019-00-R

Experiment on a Suspended Interferometer

- To investigate issues associated with scaling to a suspended interferometer
- To learn the way to operate the interferometer (including control issues such as lock acquisition and hold) with the scheme in more realistic condition
- To achieve the shot noise limited sensitivity predicted by the model
- To assess the feasibility of implementing at the level of a full scale enhanced LIGO

The recents results of MSU group

(1995-1996)

V. BRAGINSKY

1) Q values in SiO_2 suspension

2) The excess noise in metal wires and in other „places"

3) Considerations about the readout system.

Ia The thermal noise

Trivial classical condition for the simpliest model:

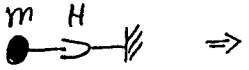

⇒ very close to the pend. mode

$$F_{sz} = \frac{1}{2} h L m \omega_{gravv}^2 \geq \sqrt{4 k_B T H(\omega) \frac{1}{\tau_{avez}}}$$

The signal — depends on the confidence limit — Boltzmann constant

$$\tau_{avez} \geq \frac{2\pi}{\omega_{gravv}}$$

$$h_{SQL} = \frac{2 \Delta x_{SQL}}{L} \simeq \frac{1}{\pi L} \sqrt{\frac{\hbar \tau_{avez}}{m}}$$

$$h_{SQL} \simeq \frac{1}{3 \times 4 \cdot 10^5} \times \sqrt{\frac{10^{-27} \cdot 10^{-2}}{10^4}} \simeq 2{,}5 \cdot 10^{-23}$$

$$F_{gravv} \simeq 10^{-8}\ dyn = 10^{-13}\ NEWTON$$

$$H \lesssim 4 \times 10^{-5}\ \frac{sec}{sec}$$

$$\tau^*_{PEND} \gtrsim 2 \times 10^{+5}\ sec$$

$H(\omega) = ?$

The big "mess":

1) $H = \text{const}$ (viscous friction → → used in the Nyquist model)

2) $Q^{-1} = A \dfrac{\omega\tau_{relax}}{1+(\omega\tau_{relax})^2}$ (Debye model) $(Q\omega \simeq \text{const})$

3) $Q^{-1} = \sum A^{(i)} \dfrac{\omega\tau^{(i)}_{relax}}{1+(\omega\tau^{(i)}_{relax})^2}$ ("multi Debye")

$\Downarrow$

$Q \simeq \text{const}$

In real measurement:

$$1 = H_{viscouse} + H_{Debye} + H_{surf} + H_{elastz} + H_{magn} + \ldots$$

the cracks — the layers of H_2O, N_2... — the dust

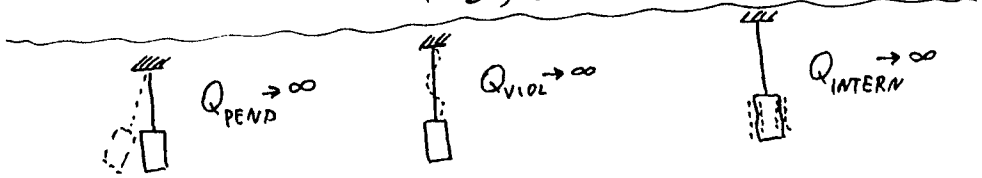

PHYS. LETTS A 218, (1996) 164.

sional mode being $\omega_{sup} \simeq 4 \times 10^3$ rad/s) as a support and to use the torsional-pendulum mode of the cylinder oscillation which had $\omega_{tors\ pend} \simeq 2$ rad/s for the distance $2a \simeq 2.5$ cm. Relatively simple calculations which we omit gave an estimate of the limit of $Q_{tors\ pend}$ to the recoil losses at a level of 10^9 due for the above values of $\omega_{tors\ pend}$ and ω_{sup} and with the mass of the cage $m_{cage} = 25$ kg.

All accumulated experience [3,4,6] of losses in fused silica fiber permits one to assume that a substantial part of the material losses may be described by the structural dissipation model [7]. According to this the Young's modulus Y and the shear modulus G of the material have imaginary parts which are independent of the frequency,

$$Y = Y_0(1 + i\phi_Y), \quad G = G_0(1 + i\phi_G),$$

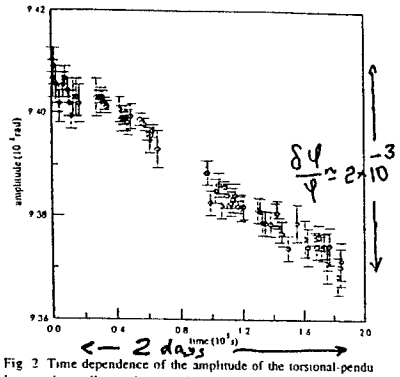

Fig. 2. Time dependence of the amplitude of the torsional-pendulum mode oscillation during a free decay.

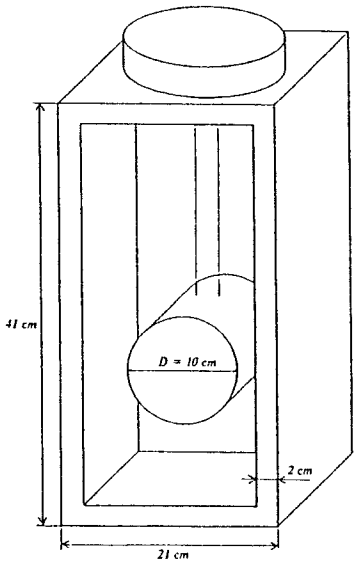

Fig. 1. Design of the pendulum and the suspension support structure.

where ϕ_Y and ϕ_G are the angles of losses in the material. These two values define $Q_{tors\ pend}$:

$$Q^{-1}_{tors\ pend} \simeq \frac{\pi G r^4}{Mga^2}\phi_G + \frac{1}{2l}\sqrt{\frac{\pi Y r^4}{2Mg}}\,\phi_Y,$$

where g is the gravitational acceleration, r the radius of the fibers. Substituting in this formula $\phi_Y = \phi_G = 1.4 \times 10^{-7}$ (see Ref. [5]), $a = 1.25$ cm, $r = 1 \times 10^{-2}$ cm, we can expect $Q^{-1}_{tors\ pend} \simeq 10^{-9}$ to be reached. EXPECTED

In the described experiments four pendulum suspensions were tested, and the values obtained were $Q_{tors\text{-}pend} \simeq (0.5\text{–}1) \times 10^9$. These values are more than one order smaller than the expected $Q = 10^9$. Additional losses could be explained as due to several small dust particles on the fiber's surface and due to the sedimentation of silica vapour on the surface of the fiber near the welding area.

Fig. 2 presents the measured time dependence of the amplitude of torsional-pendulum mode free oscillations in one of our tests. The recorded relative decrease of the amplitude 2×10^{-3} during two days corresponds to the relaxation time $\tau_m = 4.8 \times 10^7$ s ($\pm 10\%$). The gas pressure in the vacuum chamber was 2×10^{-6} Torr. Correcting for this pressure we obtain the excellent value $\tau_m \simeq 1 \times 10^8$ s $\simeq 3$ years, which corresponds to $Q_{tors\text{-}pend} \simeq 1 \times 10^9$ ($\pm 25\%$) OBTAINED

Physics – Doklady, Vol. 40, No. 11, 1995, pp. 564 - 566. Translated from Doklady Akademii Nauk, Vol. 345, No. 3, 1995, pp. 324 - 326.
Original Russian text Copyright © 1995 by Braginskii, Mitrofanov, Tokmakov.

DOKLADY, 345, (1995), 324

PHYSICS

Energy Dissipation in Violin Modes of the Test Mass Suspensions of Gravitational-Wave Antennas

Corresponding Member of the RAS V. B. Braginskii, V. P. Mitrofanov, and K. V. Tokmakov

Received May 17, 1995

One of the basic problems concerning the LIGO, VIRGO, and GEO-600 laser gravitational-wave antennas, which are currently being constructed (see, for example, [1]) is a suppression of the thermal motion of the centers of test masses (interferometer mirrors). The only method for solving this problem is to increase the quality factors Q of all the mechanical vibration modes that influence the motion of the test masses. According to the fluctuation-dissipation theorem, an increase in Q leads to a decrease in the spectral densities of the displacements of the centroid of a test mass away from the resonance frequencies of the mechanical vibration modes of the suspension and, consequently, to the possibility of detecting a broadband burst of gravitational radiation. The most important modes are those of the pendulum and violin vibrations in the suspension and the normal (internal) modes of a test mass (mirror) (see, for example, [2, 3]). This work reports the results of measurements of Q_{viol} for the violin vibration modes of the suspension of the test mass m that is close in value to the mass of the mirrors in the LIGO and VIRGO antennas. The development of a technique for the suspension of masses was aimed at the possibility of reaching and exceeding the so-called standard quantum limit (SQL) of sensitivity.

It is known that, at a sufficiently low level of dissipation (see, for example, [4]), the retroaction of the instrumental fluctuations (an inevitable consequence of the quantum theory) determines the sensitivity limit for the measurements of a force action on a test mass. If an instrument is continuously recording the coordinate of a mass during the time interval τ, and the acting force has the shape of a single period τ of a sinusoidal wave, then the SQL for the displacement amplitude of the test mass is

$$\Delta L_{SQL} = \frac{1}{2\pi}\sqrt{\frac{\hbar\tau}{m}}, \qquad (1)$$

where $\hbar$ is Planck's constant.

If the test mass is suspended by a thin filament of length l and total mass μ, then the rms displacement of the mass ΔL_{viol}, induced only by thermal vibrations in the violin modes of the filament, is

$$\Delta L_{viol} = \frac{1}{\pi^2 n^2}\frac{\mu}{m}\sqrt{\frac{2\pi kTl}{mgQ_{viol}}}, \qquad (2)$$

where k is the Boltzmann constant, T is the thermostat temperature, g is the free-fall acceleration, and n is the number of the violin mode ($n = 1, 2, 3, \ldots$).

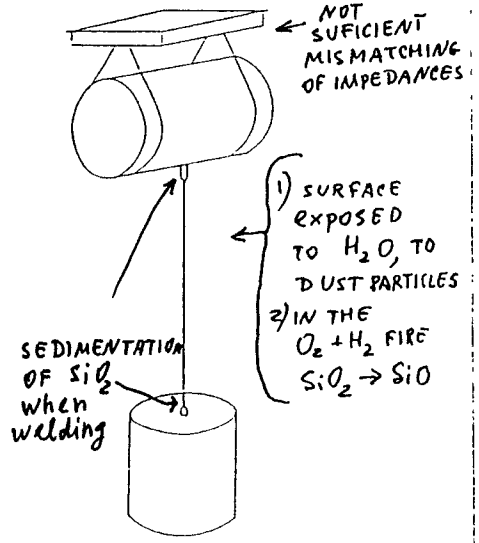

Fig. 1. Schematic of the test-mass suspension.

Moscow State University, Vorob'evy Gory, Moscow, 119899 Russia

Thus, to achieve a high sensitivity of the antenna and, for instance, to satisfy the condition $\Delta L_{SQL} > \Delta L_{viol}$, we need the smallest possible value of μ and large values of Q_{viol}. In the measurements described below, we mainly applied the same technique as was used in the preliminary experiments [5]: the test mass and the suspension filament, including the upper part of its attachment, were made from fused silica. The filament was made from high-purity fused silica and, as a result, had low characteristic losses. It was welded to the test mass and to the upper part of the filament attachment.

In contrast with the preliminary experiments [5], where the values of Q_{viol} were measured in filaments with a small suspended mass ($m = 30$ g), in our experiments, we suspended a mass $m = 1.6$ kg, which is close to the mass of the mirror planned for the final version of the LIGO program. This significant increase in the mass made it necessary to use an intermediate element with a mass of approximately 2 kg in the suspension (Fig. 1.). This allowed us to suppress the leakage of the energy of the violin vibrations to the support. The calculations of the insertion loss Q_{viol}^{-1} introduced by this leakage (they are not presented here) give an estimate of $Q_{viol}^{-1} \le 10^{-11}$.

The second significant difference in our experiments from the preliminary ones is that the fused-silica filaments used were more heavily stressed. This made it possible for filaments with the diameter $D = 150$ μm and length $l = 0.2$ m to have a rather small value of $\mu = 8 \times 10^{-3}$ g. The suspended mass induced the stress

$$\sigma = 4mg/\pi D^2 = 10^9\ \mathrm{N/m^2},$$

in these fibers, i.e., approximately 2% of the Young's modulus.

The Q-factor for the violin vibration modes Q_{viol} of strained filaments depends on their tension, which is determined by the suspended mass M and intrinsic losses in the filament material characterized by the loss angle φ_q.

$$Q_{viol}^{-1} = \frac{2}{l}\sqrt{\frac{YI}{Mg}}\left(1 - \frac{(\pi n)^2}{2l}\sqrt{\frac{YI}{Mg}}\right)\varphi_q. \qquad (3)$$

where $I = \pi D^4/64$ is the moment of inertia for the cross section of the fused-silica filament, Y is the Young's modulus, and g is the free-fall acceleration.

The losses in the material were determined from the measured value of Q_{pend}, the Q-factor for the bending vibration modes of unloaded filament segments approximately 10 mm long with one end welded to a massive support. They were made from KS-4V analytical-purity fused silica with the lowest impurity concentration. In this case, $Q_{pend}^{-1} = \varphi_q$. Figure 2 shows the experimental values of Q-factors for lower modes of bending vibrations of the filaments. The curve is calculated for the case when the energy losses are determined only by the thermoelastic mechanism [6].

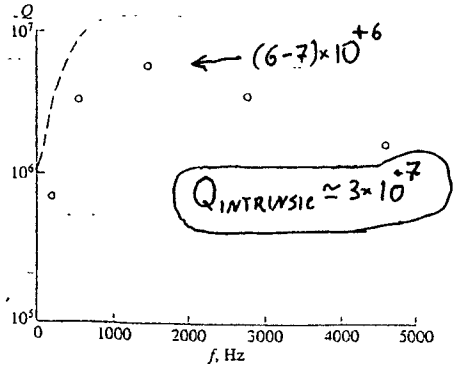

Fig. 2. Q-factors for lower modes of the bending vibrations of a fused-silica filament.

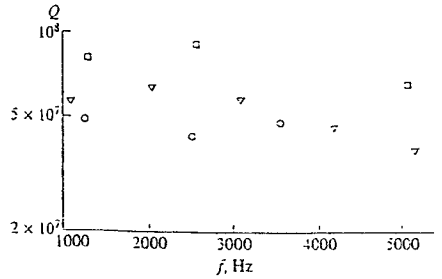

Fig. 3. Q-factors for violin vibration modes of the suspension filaments for three fused-silica pendulums.

The maximum of thermoelastic losses for the filaments under study was located near the characteristic frequency $f = 40$ Hz, so that, at frequencies above 1 kHz, thermoelastic losses made an insignificant contribution to the damping of bending vibrations of the filaments.

Substituting numerical values of the parameters into (3), we obtain the expected value of the Q-factor for violin vibration modes of the suspension filaments, $Q_{viol} = 2 \times 10^9$.

Figure 3 presents the values of the Q-factors for lower harmonics of the violin vibration modes of the suspension filaments, measured for the several pendulums that were studied. The statistical errors of the measurements were about 5%. The damping introduced by the energy transfer to the molecules of the residual gas in the vacuum chamber was

$$(Q_{viol}^{-1})_{gas} = (3 \pm 2) \times 10^{-9}$$

FROM THE BOOK "SYSTEMS WITH SMALL DISSIPATION" Kip S. THORNE ED.

; Made from Sapphire Monocrystals

~~Caltech Community~~

~~January 6, 1997~~

FROM: David Goodstein

SUBJECT: The Michelin Lecture

~~Movie Director Oliver Stone, will~~ give this year's James Michelin Distinguished lecture at 8:00 p.m., Tuesday, January ~~28th~~, in Beckman Auditorium. The title is "Film, Chaos and Mass Delusion." Admission is free and tickets are not required, but we anticipate a good crowd, so free tickets (valid until 7:45 p.m.) may be useful. If you wish to have one or two free tickets, ~~please~~ call (ext. 4652), write or e-mail the Ticket Office (Tickets@caltech.edu).

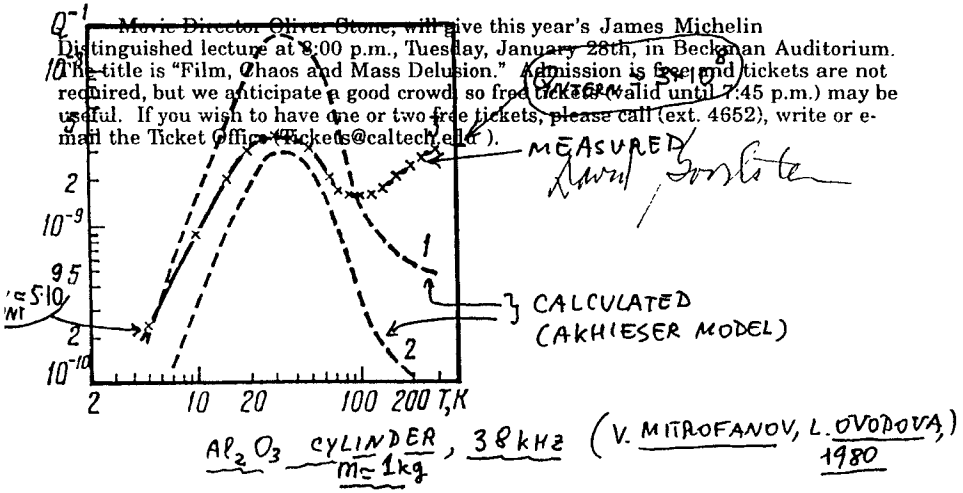

Al_2O_3 CYLINDER, 38 kHz (V. MITROFANOV, L. OVODOVA, 1980) $m \simeq 1$ kg

curves 1 and 2) and experimental (curve 3) temperature
$^{-1}$ for a sapphire resonator with vibration frequency of

re of less than 10^{-5} Torr.

factor was determined by measuring the damping

Conclusion of Ia part:

1) $(Q_{pend})_{SiO_2} \simeq 1\times10^8$

$(Q_{VIOL})_{SiO_2} \simeq 1\times10^8$

$(Q_{INTERN})_{SiO_2} \simeq 3\times10^7$

$(Q_{INTERN})_{Al_2O_3} \simeq 3\times10^8$

these values are neither ultimate ones nor final ones.

2) $H(\omega)$ may not be accurately derived from the values of Q;
Only the floor of the noise from the antenna may provide correct(?) values of $H(\omega)$?
The high Q give only a hope but not a guarantee.

II.6 The excess noise

The thermal equilibrium is a grand illusion: the always existing free energy wants to "leak" → to redistribute itself in other forms. This process is always acompanied with the decrease of the total amount of free energy and with the rise of entropy

Thus FD theorem is a correct one in the ultimate approximation only.

The simpliest examples:

1) the acoustic emission from stressed solids
2) the random change of the size (of the dimensions) of solid bodies

For LIGO probably the most important are

(1) The excess noise in the violin modes of the suspension fiber.
(2) The random change of the mirrors diameter and length.
(3) The creem noise from the last element of the antiseismic filter.

(1) The sketch of the setup for the measurements of the Brownian motion of the suspension fiber (MSU group)

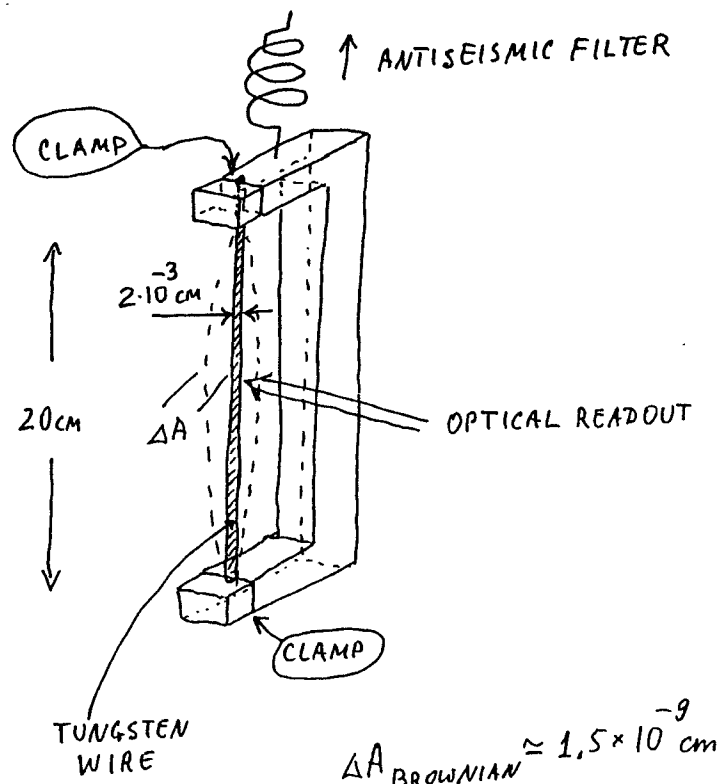

$\Delta A_{BROWNIAN} \simeq 1,5 \times 10^{-9}$ cm

$\Delta A_{READOUT} \simeq 2 \times 10^{-10} \frac{cm}{\sqrt{Hz}}$

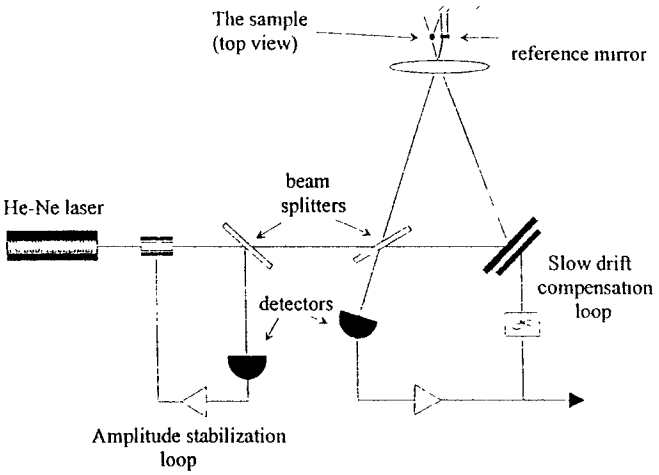

Figure 1.
The sketch of the measurement system
(optical readout)

	Theory prediction (averagin time 30 s)	Well stressed samples			Intermediate stressed samples		Low stressed samples		
Sample number		1	2	3	4	5	6	7	8
Stress value, S/S_b		0.84	0.85	0.83	0.48	0 63	0 18	0 25	0.27
total data length, hrs		2	1 5	4	2 5	4	4.5	2	1
Number of the amplitude bursts overcoming the levels									
$>3\,\bar{A}$	115±15	343	306	217	236	155	112	126	72
$>4\,\bar{A}$	25±2	59	116	77	82	32	44	48	22
$>5\,\bar{A}$	4±4	12	36	16	20	4	15	16	4
$>6\,\bar{A}$	0	9	13	3	4	0	2	4	0
$>7\,\bar{A}$	0	6	2.5	0	0	0	0	1	0
$>8\,\bar{A}$	0	6	0	0	0	0	0	0	0
$>9\bar{A}$	0	6	0	0	0	0	0	0	0
$>10\bar{A}$	0	6	0	0	0	0	0	0	0

Table 1 The results of the violin mode noise measurements on the tungsten wires The S_b is a break point stress value for the samples, $\bar{A}$ is the mean amplutude of oscillation

Two types of noise:

1. Relatively long ($\simeq$ 1 min) and rare rise of the noise floor (above Brownian level)
2. Big bursts (peaks) which rate depends on the value of the stress.

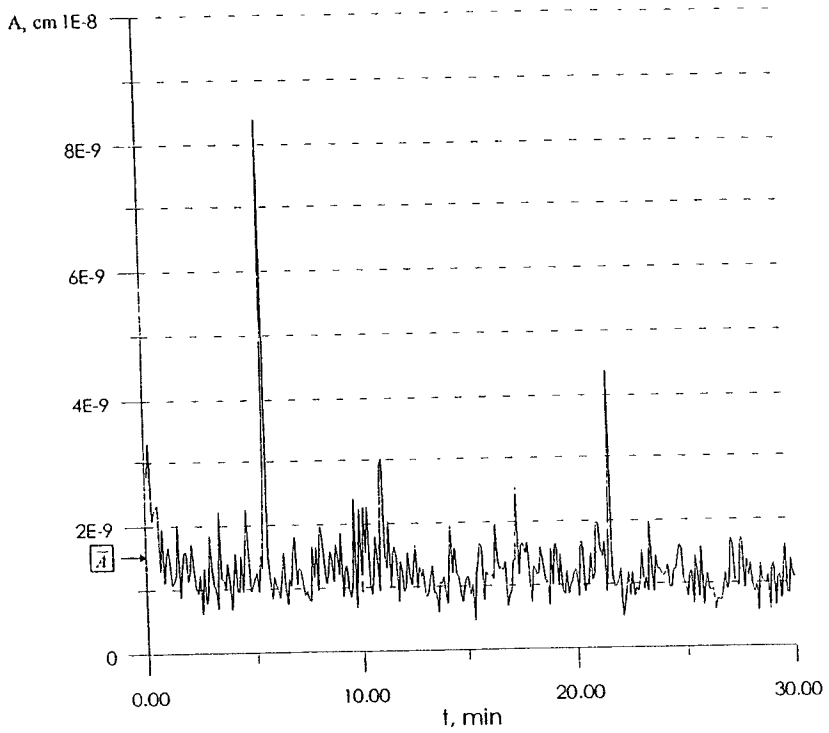

Figure 2
The time dependence of the oscillation amplitude for the well stressed sample of tungsten wire. Strain is 0 85 of break point value The averaging time is 30 second
$\overline{A}$ is a theoretical prediction for the thermal noise mean amplitude

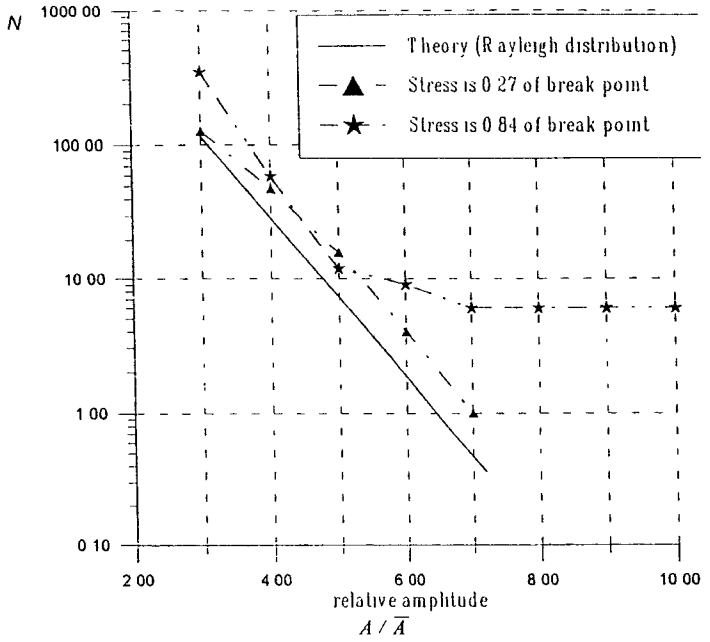

Figure 3
The peak intensity hystogram N is the number of peaks per hour with the amlitude larger than A.

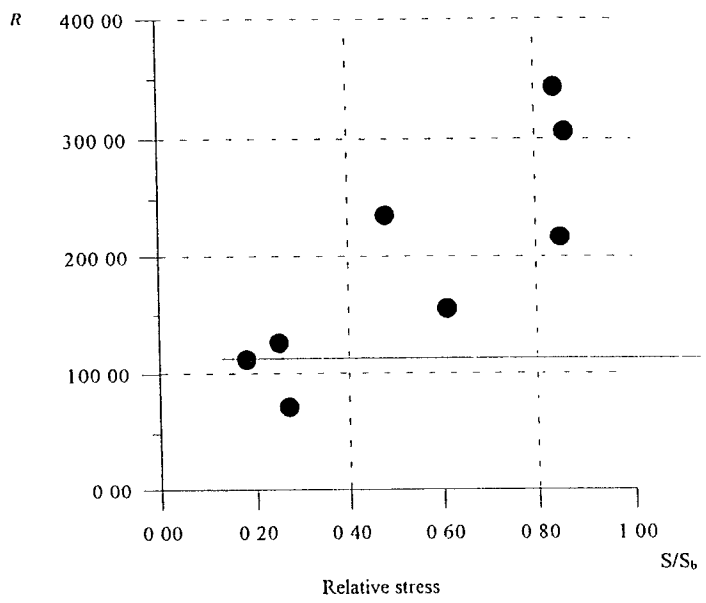

Figure 4
The dependence of excess peak rate R on the stress value The peaks with the amplitude 3 times higher then the *rms* value are counted Solid line is theoretical prediction for the thermal noise

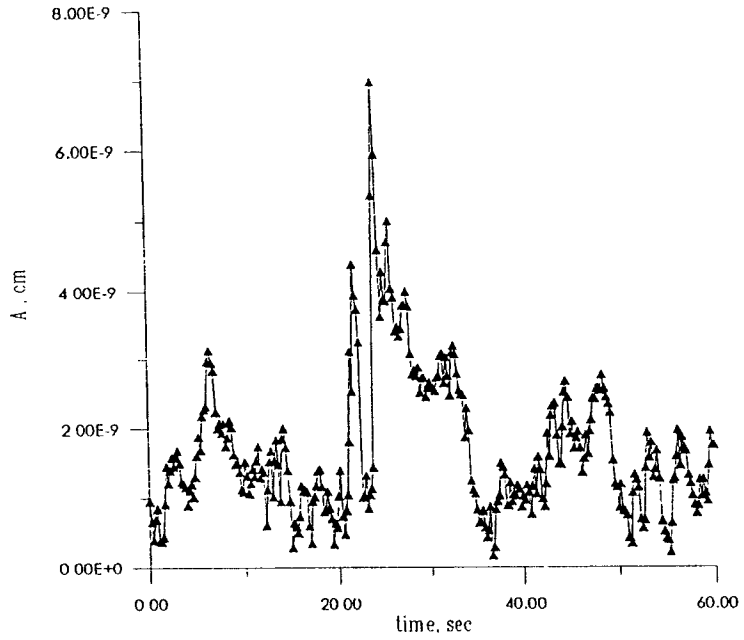

Figure 5
Typical shape of the excess noise event

In 1997 the steel wires noise will be tested.
In 1997/1998 the fused silica fiber's noise will be tested.

(2.)(3.) Several numerical cosiderations

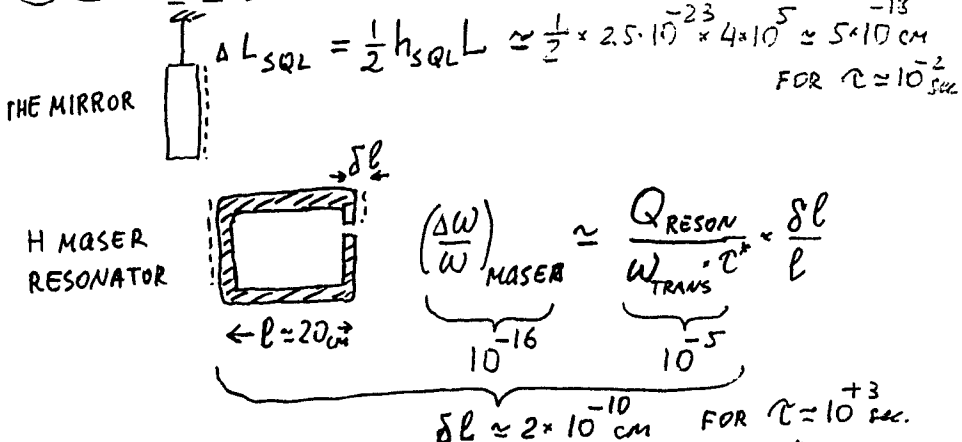

$\Delta L_{SQL} = \frac{1}{2} h_{SQL} L \simeq \frac{1}{2} \times 2.5 \cdot 10^{-23} \times 4 \times 10^{5} \simeq 5 \times 10^{-18}$ cm FOR $\tau \simeq 10^{-2}$ sec

$\left(\frac{\Delta\omega}{\omega}\right)_{MASER} \simeq \frac{Q_{RESON}}{\omega_{TRANS} \cdot \tau^*} \simeq \frac{\delta l}{l}$

$\left(\frac{\Delta\omega}{\omega}\right)_{MASER} \simeq 10^{-16}$, $\frac{Q_{RESON}}{\omega_{TRANS} \cdot \tau^*} \simeq 10^{-5}$

$\delta l \simeq 2 \times 10^{-10}$ cm FOR $\tau \simeq 10^{+3}$ sec.

$\Delta L_{SQL} \simeq 5 \times 10^{-18}$ cm, $\tau \simeq 10^{-2}$ sec } compare WITH $\delta l \simeq 2 \times 10^{-10}$ cm, $\tau \simeq 10^{+3}$ sec

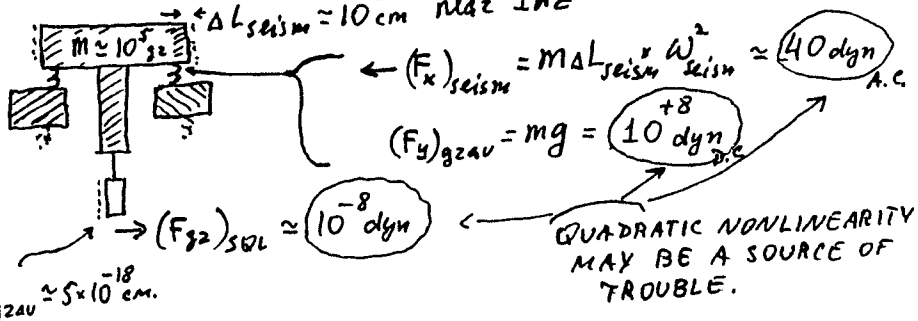

It is likely that the output will demonstrate a polymodal, and nonstationary noise. Thus it will be a problem to establish the level of confidence when the signal is recorded.

III The problem of a new readout system

Nonlinear meter for the grav. wave antenna
Phys. LETTS. A 218 (1996), 167

for $h_{SQL} \simeq 2.5 \cdot 10^{-23}$, $\tau \simeq 10^{-2}$ sec, $W_{OPTIM} \simeq 10^{10}$ $\frac{ergs}{sec}$

$h_{SQL} \simeq 1 \times 10^{-23}$, $\tau \simeq 10^{-3}$ sec, $W_{OPTIM} \simeq 2 \times 10^{+13}$ $\frac{ergs}{sec}$

This power may cause nonlinear effects in the resonator.

To explor the use of long relaxation time

$\tau^*_l = \frac{L}{C(1-R)}$ → $\frac{4 \cdot 10^{5}}{3 \cdot 10^{10} \cdot 10^{-5}} \simeq 1$ sec

→ $\frac{4 \times 10^{5}}{3 \times 10^{10} \cdot 10^{-6}} \simeq 10$ sec.

$\frac{\tau_{grav} \simeq \tau_{aver.}}{\tau^*_l} \ll 1$!

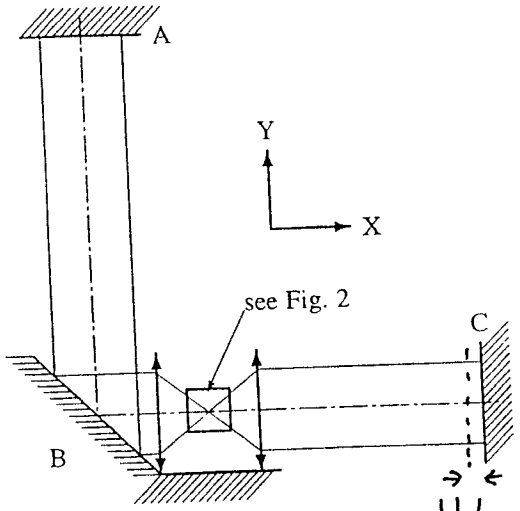

Fig. 1.

optical wave, which has to be exited by an external source (e.g. by a laser). The amplitude of this shift in the area near mirror B is equal to

$$\delta x = \frac{\delta L_{AB} - \delta L_{BC}}{2}, \tag{3}$$

where δL_{AB} and δL_{AB} are the variations of the distances between the mirrors A, B and B, C, respectively. In the case of an optimal direction and polarization of the gravitational wave the value of δx is equal to

$$\delta x = \frac{hL}{2},$$

where L is the unperturbed value of the distances.

The spatial shift of the wave may be measured by a special device mounted on mirror B. This device has to consist of two optical lenses separated by a double focal length (see Fig. 1) and a thin dielectrical plate with cubic nonlinear dielectrical susceptibility $\chi^{(3)}$. This plate has to be situated inside a capacitor part of a microwave resonator. If the plate is located on the

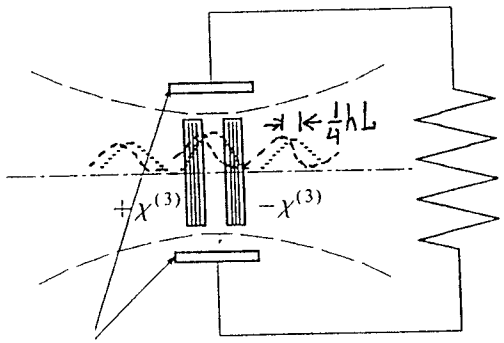

Fig. 2

where

$$K = \frac{\pi\chi^{(3)} E_{opt}^2 \omega_e L}{\epsilon c} \frac{\sin(\omega_{opt} l\sqrt{\epsilon}/c)}{\omega_{opt} l\sqrt{\epsilon}/c},$$

E_{opt} is the amplitude of the electric field of the optical wave, c is the speed of light, ϵ is the linear term of the dielectrical susceptibility and l is the thickness of the plate with nonzero $\chi^{(3)}$.

This change of frequency may be registered by the measurement of the phase shift in the microwave resonator (see Fig. 2),

$$\delta\phi_e = \delta\omega_e \tau = K\frac{h\omega_{opt}\tau}{2}. \tag{5}$$

The device described above evidently has to be a monolithic dielectrical structure with the nonlinear plate created by doping in the way it is done in superlattices.

It is necessary to note that the fluctuations of the optical energy in the resonator will randomly change

Comparir
clude that tl
efficiency o:
1×10^{-14} C
(the optical
10^{11} s^{-1}, ϵ
Thus the
phase shift
the phase sh
in the traditi
be necessary
10^{20} in the
power W_e w

$$W_e = \frac{\hbar\omega_e N_c}{\tau}$$

To realize a
resonator of
is necessary
cm. This m
the focal ar
10^{-1} cm $\simeq$
of the light
of two sphe
optical ener

$$\mathcal{E}_{opt} = \frac{LS_{opt}}{l}$$

and the pun
be

$$W_{opt} = \frac{\mathcal{E}_{opt}}{\tau^*_{opt}}$$

Thus the no
to obtain a
tical power
microwave

Aspen Winter Conference on Gravitational Waves and Their Detection

26 January – 1 February, 1997

Aspen, Colorado, USA

Transfer Function of Interferometric GW Detectors at Higher Frequencies

Roland Schilling

Max-Planck-Institut für Quantenoptik

D – 85748 Garching bei München

26 January 1997

Will appear as *"Angular and Frequency Response of LISA"* in a special issue of *Classical and Quatum Gravity.*

Preprint available under *ftp://ftp.rzg.de/pub/grav/lisa/angfres-paper.ps.gz*

Tel: +49 89 32905-264 e-mail: ros@mpq.mpg.de Fax: +49 89 32905-200

Sensitivity limitations: temperature fluctuations shot noise antenna transfer function

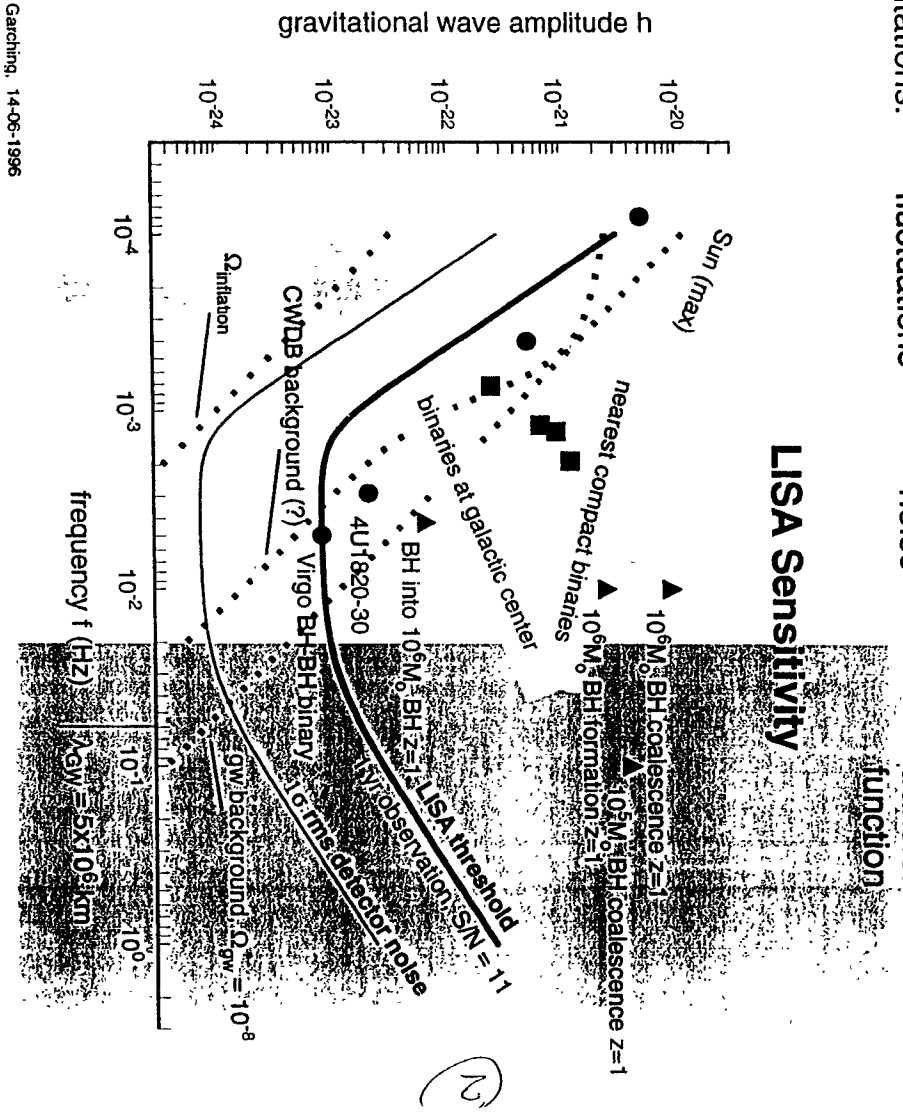

Single round trip in a single arm of length ℓ_0

$$\ell(t) = \ell_0 + \frac{1}{2}\, c \cos^2\vartheta \int_{t_0-\ell_0/c}^{t_0} h\left[t + t'(1-\sin\vartheta)\right]\, \mathrm{d}t'$$

For $h(t) = \hat{h}\exp(\mathrm{i}\,\omega t)$ and $t_0 = 0$ this becomes

$$\ell(t) = \ell_0 + \frac{1}{2}\,\hat{h}\ell_0 \cos^2\vartheta\ \mathrm{sinc}\left[\frac{\omega\ell_0}{2\,c}\,(1-\sin\vartheta)\right] \times \exp\left[\mathrm{i}\,\omega t - \mathrm{i}\,\frac{\omega\ell_0}{2\,c}\,(1-\sin\vartheta)\right]$$

or, expressed as normalized transfer function $\mathcal{T}$,

$$\mathcal{T} = \cos^2\vartheta\Big\{\ \mathrm{sinc}\left[\pi\Omega\,(1-\sin\vartheta)\right]\exp\left[-\mathrm{i}\,\pi\Omega\,(3+\sin\vartheta)\right] \quad (\text{red}) + \mathrm{sinc}\left[\pi\Omega\,(1+\sin\vartheta)\right]\exp\left[-\mathrm{i}\,\pi\Omega\,(1+\sin\vartheta)\right]\Big\} \quad (\text{green})$$

with the red term representing the forward pass
and the green term representing the return pass.

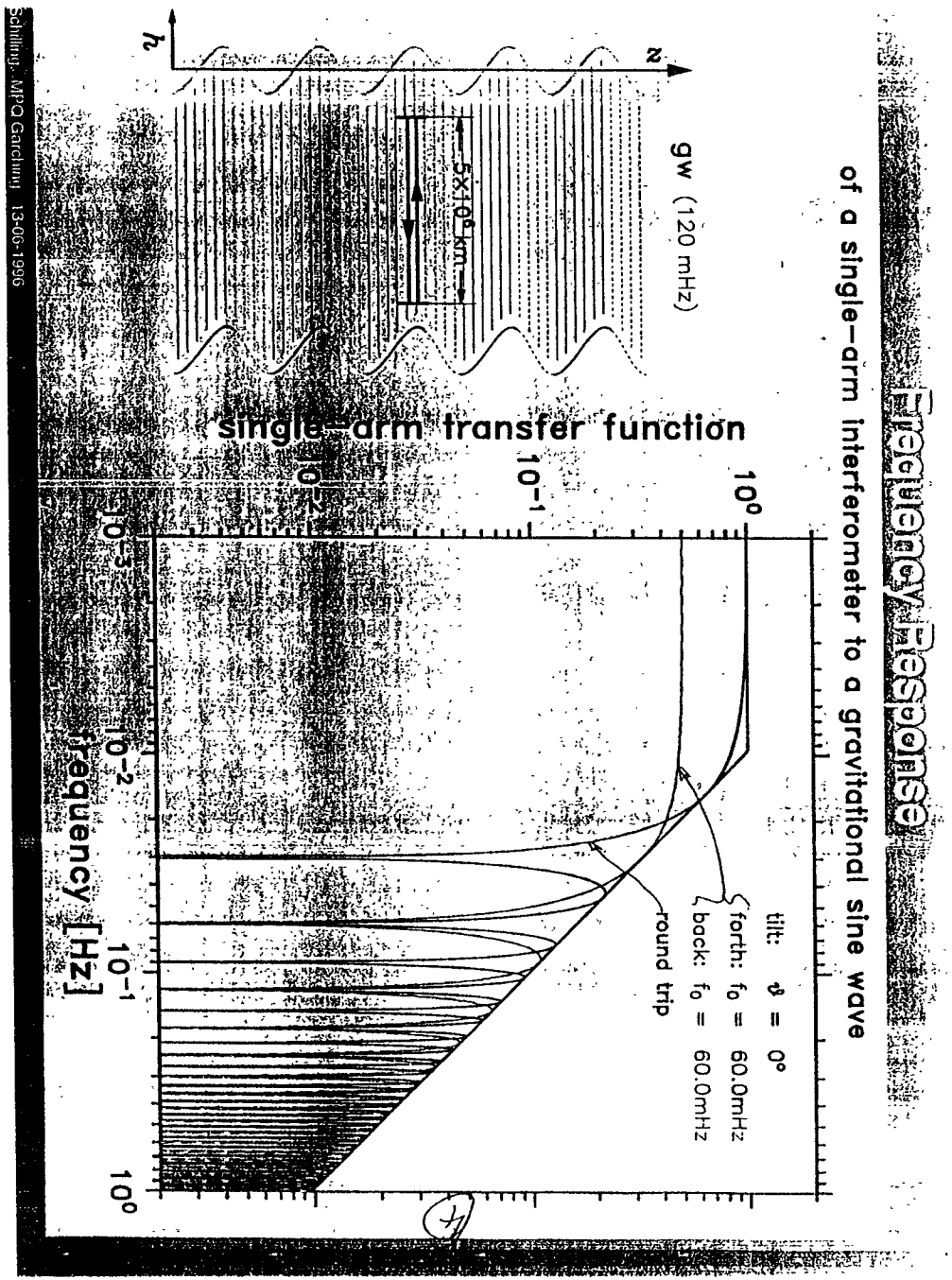

Frequency Response

of a single-arm interferometer to a gravitational sine wave

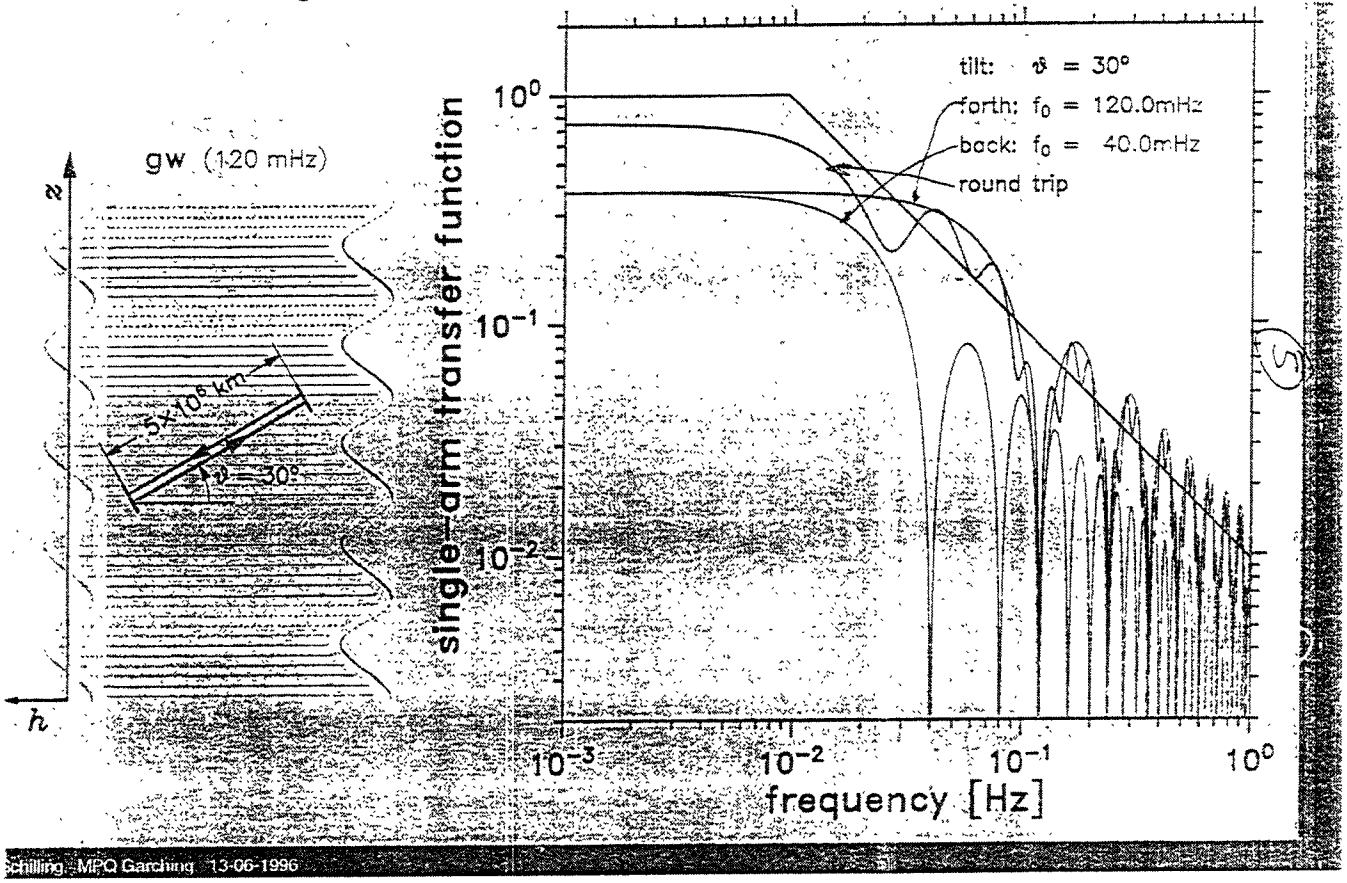

Frequency Response

of a single-arm interferometer to a gravitational sine wave

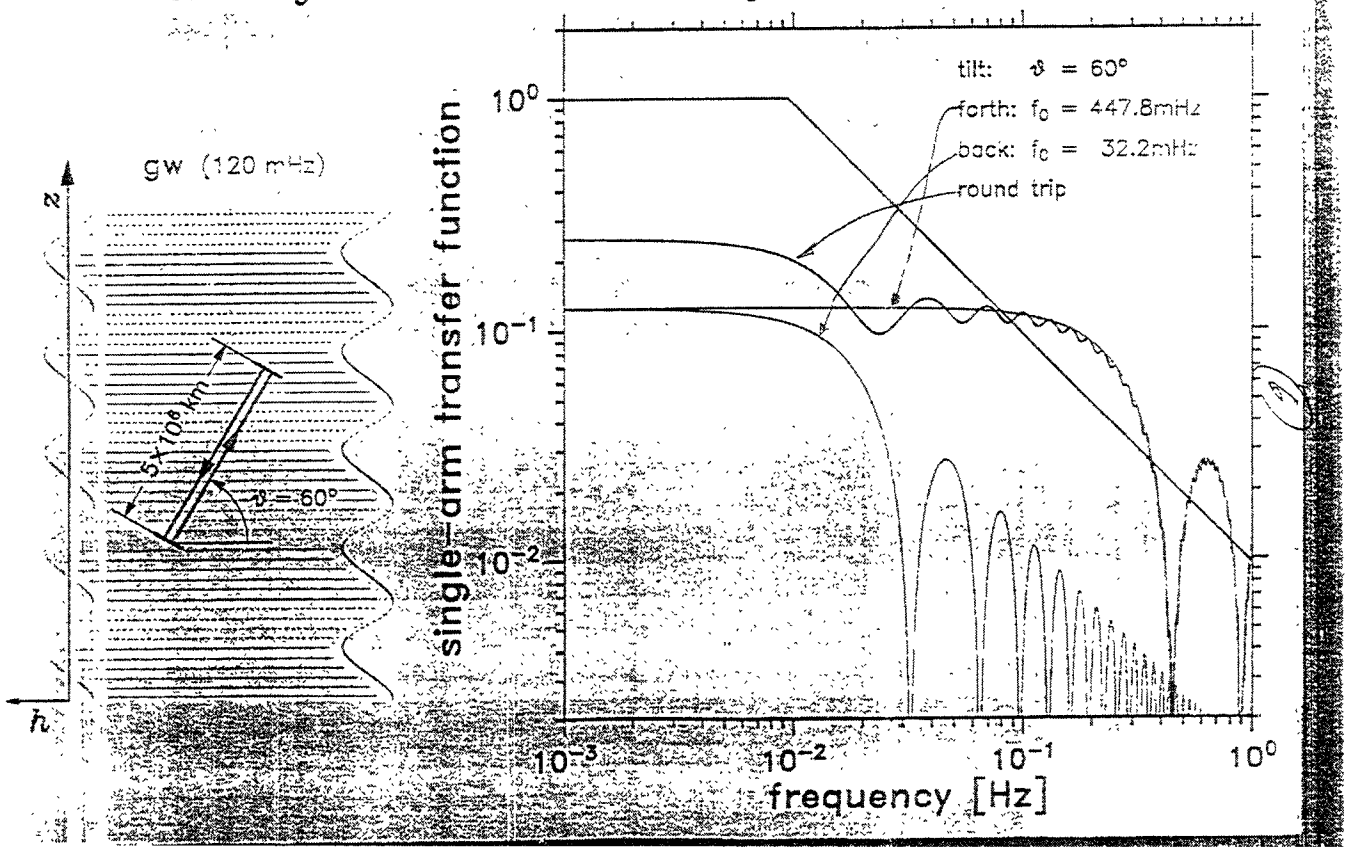

Multiple round trips in a single arm of length ℓ_0

Normalized transfer function $\mathcal{T}_n$ for n round trips:

$$\mathcal{T}_n = \cos^2\vartheta \Big\{ \operatorname{sinc}\big[\pi\Omega\,(1-\sin\vartheta)\big]\,\exp(-\mathrm{i}\,\pi\Omega) \quad (\text{red}) + \operatorname{sinc}\big[\pi\Omega\,(1+\sin\vartheta)\big]\,\exp(\mathrm{i}\,\pi\Omega)\Big\} \quad (\text{green}) \times \frac{\sin(2n\pi\Omega)}{n\sin(2\pi\Omega)}\,\exp\big[-\mathrm{i}\,\pi\Omega\,(2n+\sin\vartheta)\big] \quad (\text{brown})$$

with the red term representing a single forward pass, the green term representing a single return pass and the brown term describing the effect of multiple round trips.

$\Omega = \ell_0 \cdot f/c$

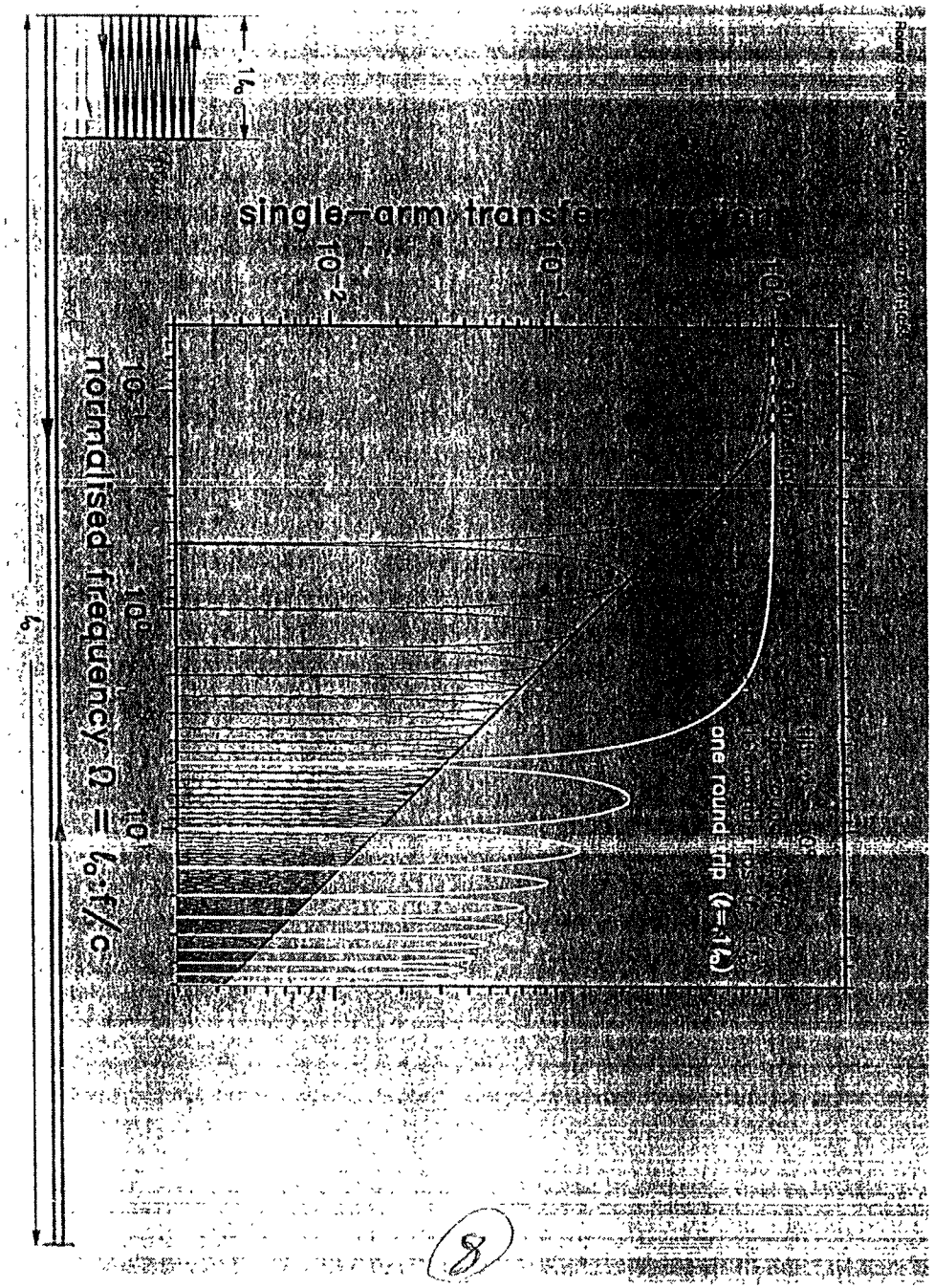

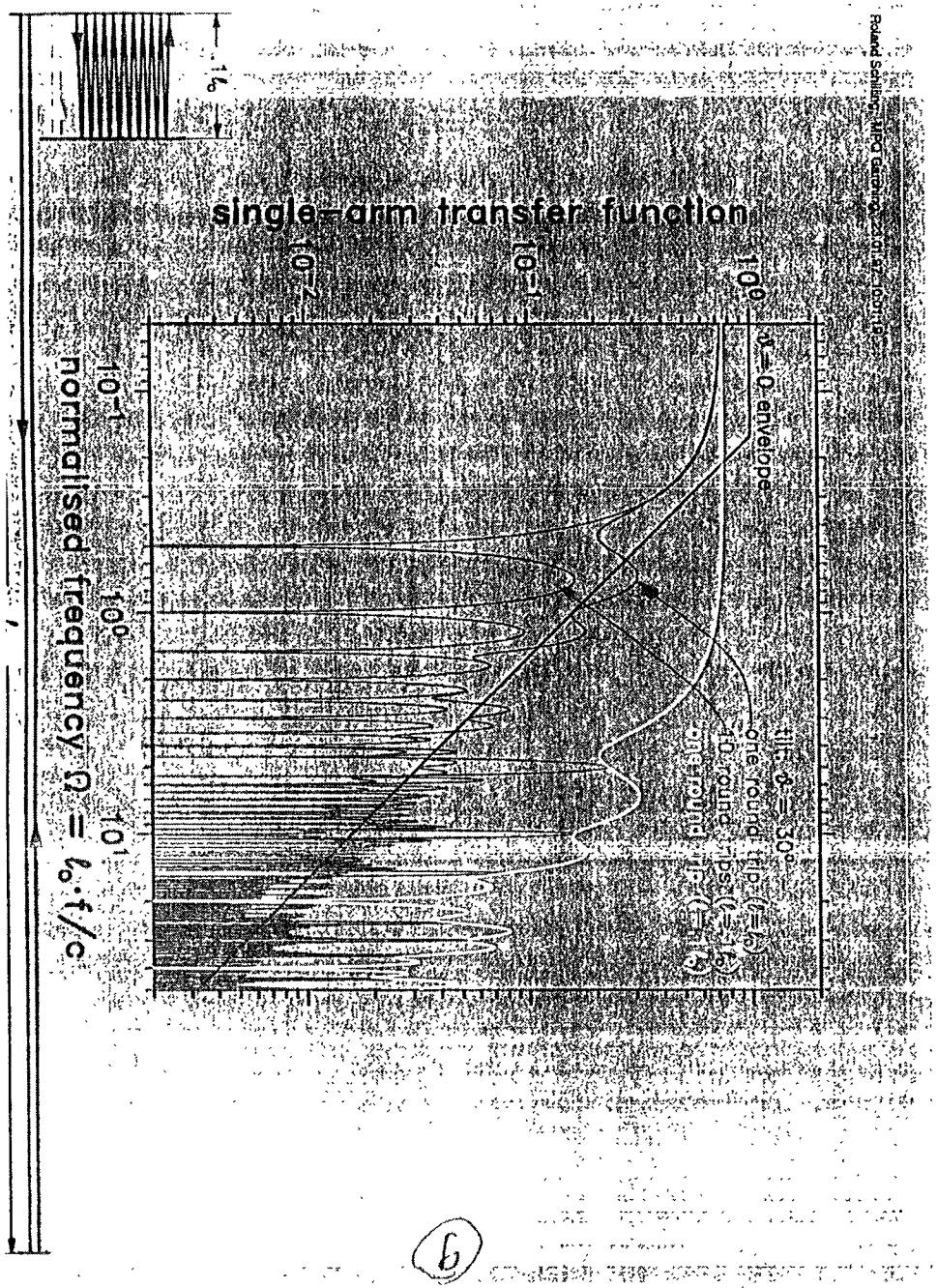

A single Fabry-Perot cavity of length ℓ_0

Corresponds to multiple round trips with $n \to \infty$ and an amplitude attenuation factor per round trip of $\varrho < 1$.

$$\mathcal{T}_C = \cos^2\vartheta \Big\{ \operatorname{sinc}\big[\pi\Omega\,(1-\sin\vartheta)\big]\,\exp(-\mathrm{i}\,\pi\Omega) + \operatorname{sinc}\big[\pi\Omega\,(1+\sin\vartheta)\big]\,\exp(\mathrm{i}\,\pi\Omega)\Big\} \times \frac{\exp\big[-\mathrm{i}\,\pi\Omega\,(2+\sin\vartheta)\big]}{1-\exp(-4\,\mathrm{i}\,\pi\Omega)}\,\frac{1-\varrho}{\varrho} \times \sum_{n=1}^{\infty} \varrho^n\big[1-\exp(-4n\,\mathrm{i}\,\pi\Omega)\big]$$

with the violet term decribing the infinite number of round trips.

This is equivalent to

$$\mathcal{T}_C = \frac{\mathcal{T}_1}{\sqrt{(1-\varrho)^2 + 4\sin^2 2\pi\Omega}}$$

Here the violet term decribes the resonance of the cavity.

$\Omega \;\; \ell_0 \cdot f/c$

Roland Schilling, MPQ Garching, 23.01.97 11:09:21

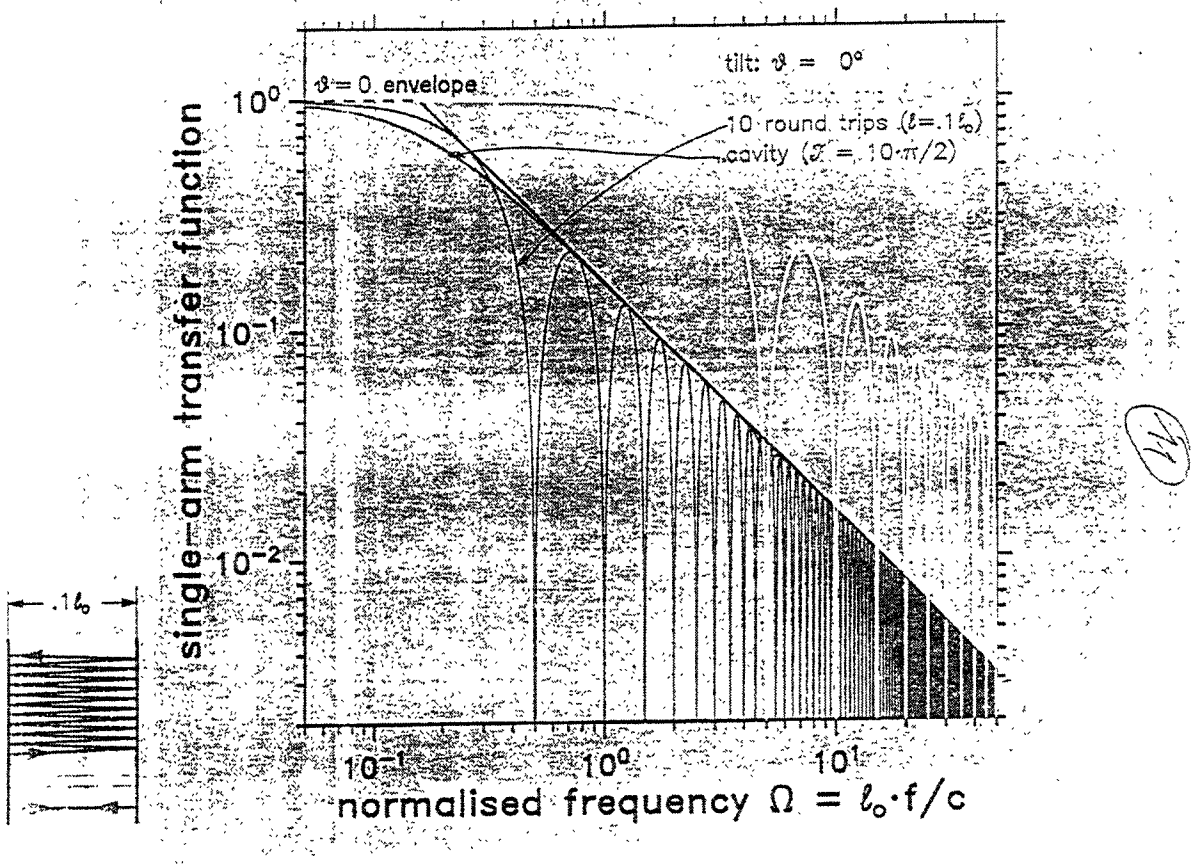

(11)

Roland Schilling, MPQ Garching, 23.01.97 11:05:00

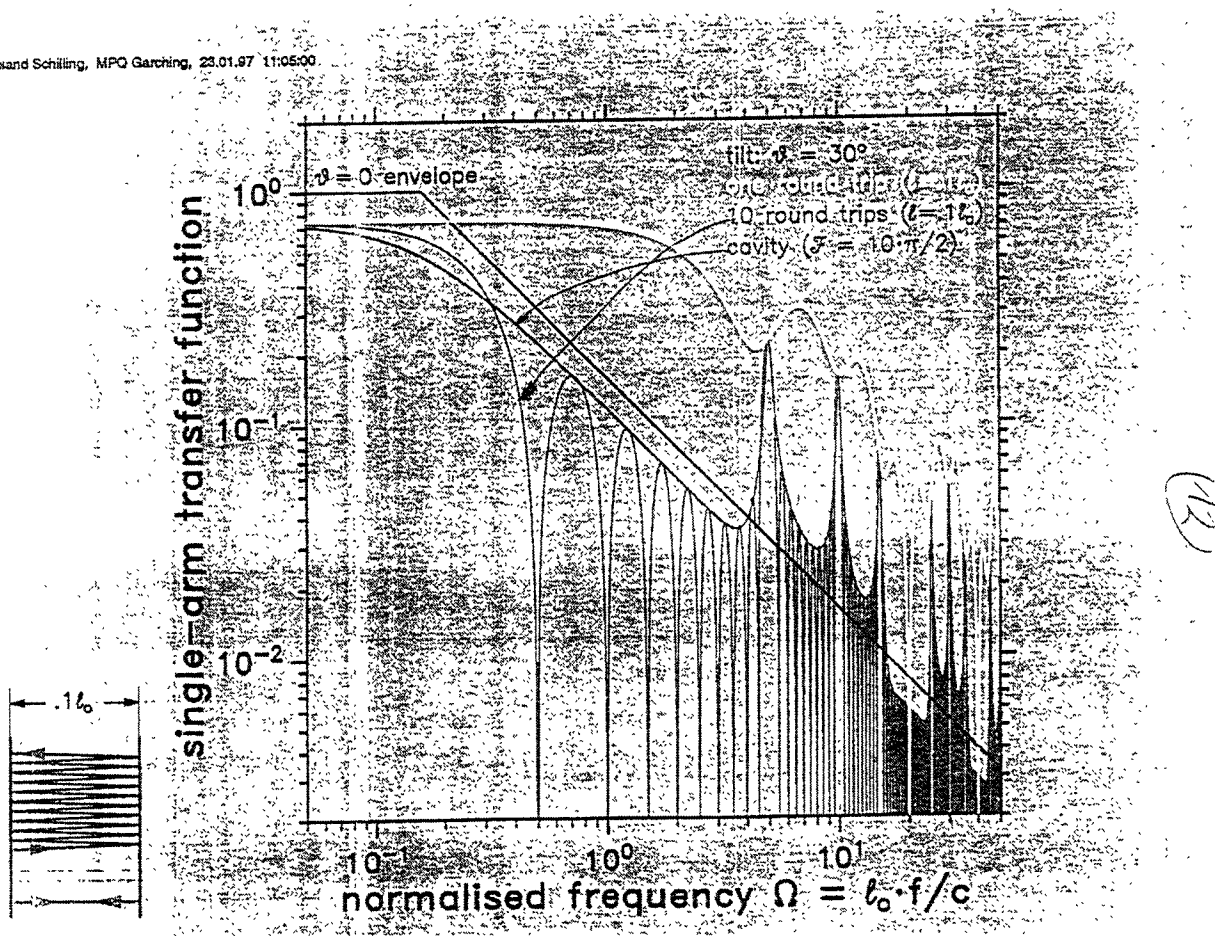

(12)

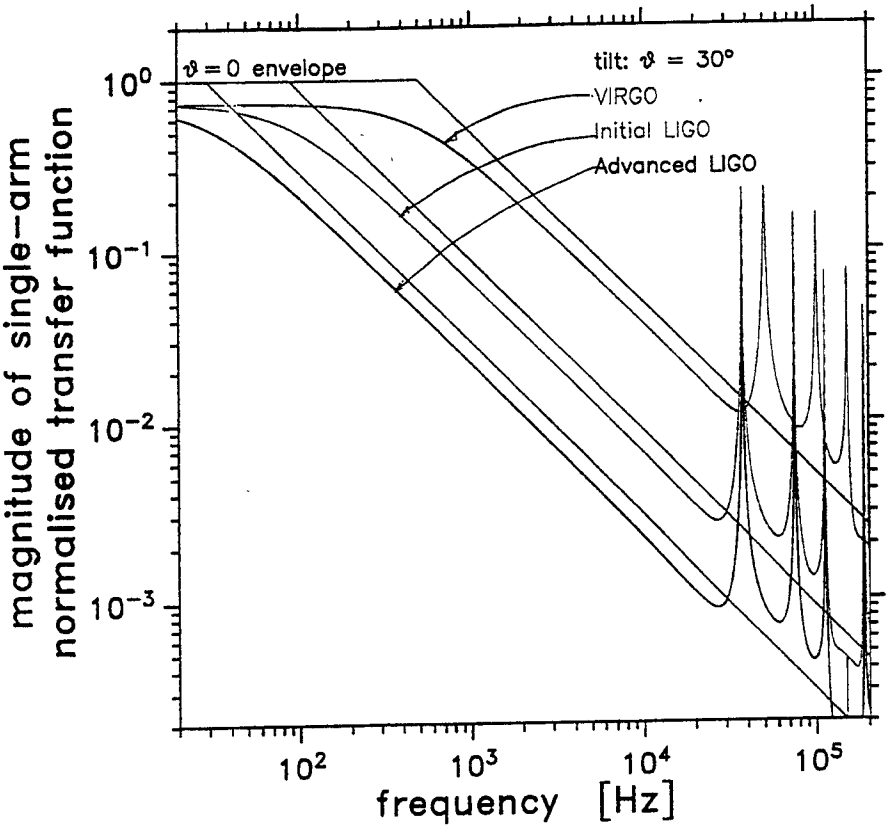
magnitude of single-arm
normalised transfer function
10^0
10^{-1}
10^{-2}
10^{-3}
$\vartheta = 0$ envelope
tilt: ϑ = 30°
VIRGO
Initial LIGO
Advanced LIGO
10^2
10^3
10^4
10^5
frequency [Hz]

(13)

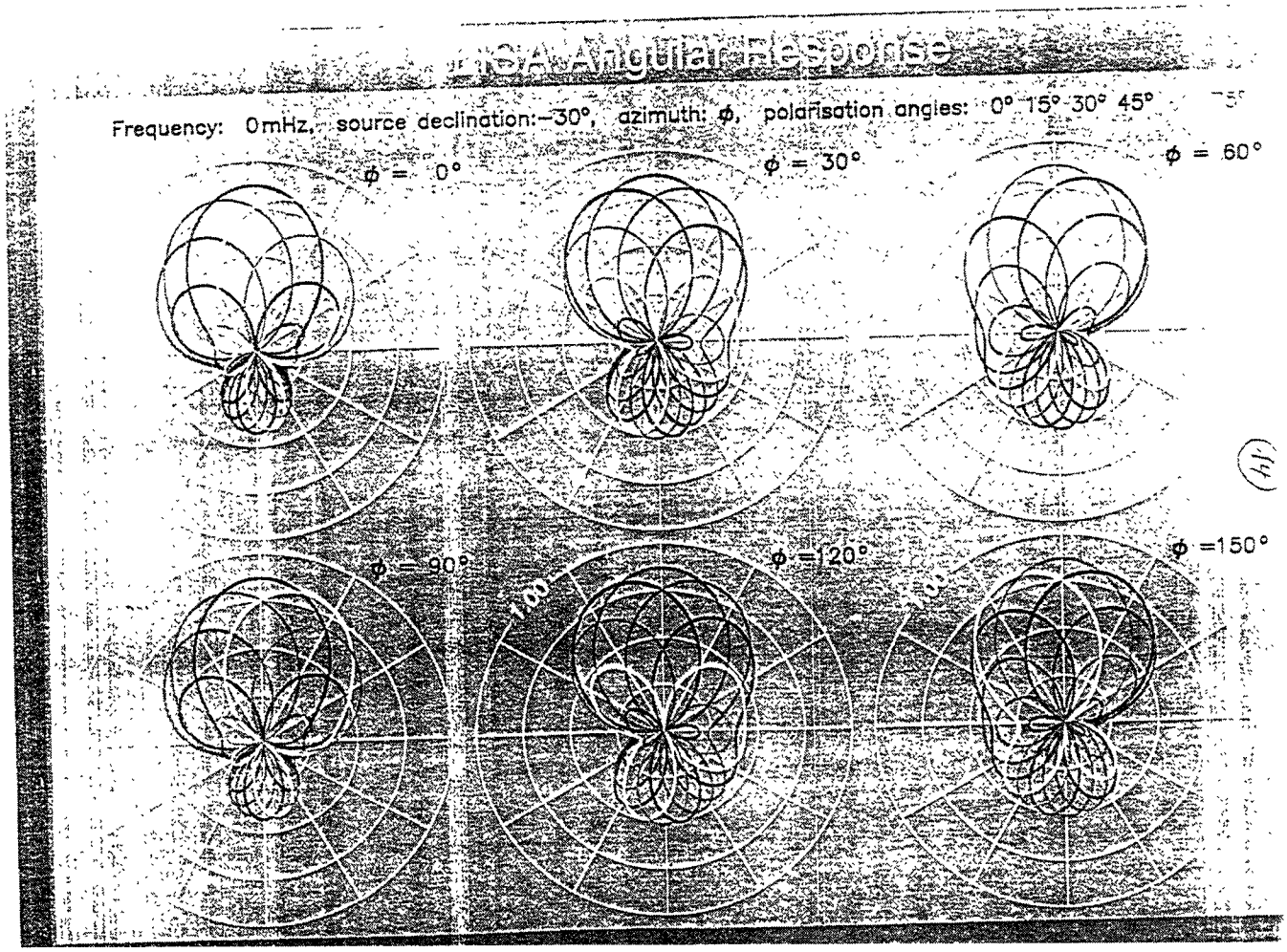
LISA Angular Response
Frequency: 0mHz, source declination:−30°, azimuth: ϕ, polarisation angles: 0° 15° 30° 45°
ϕ = 0°
ϕ = 30°
ϕ = 60°
ϕ = 90°
ϕ =120°
ϕ =150°

(14)

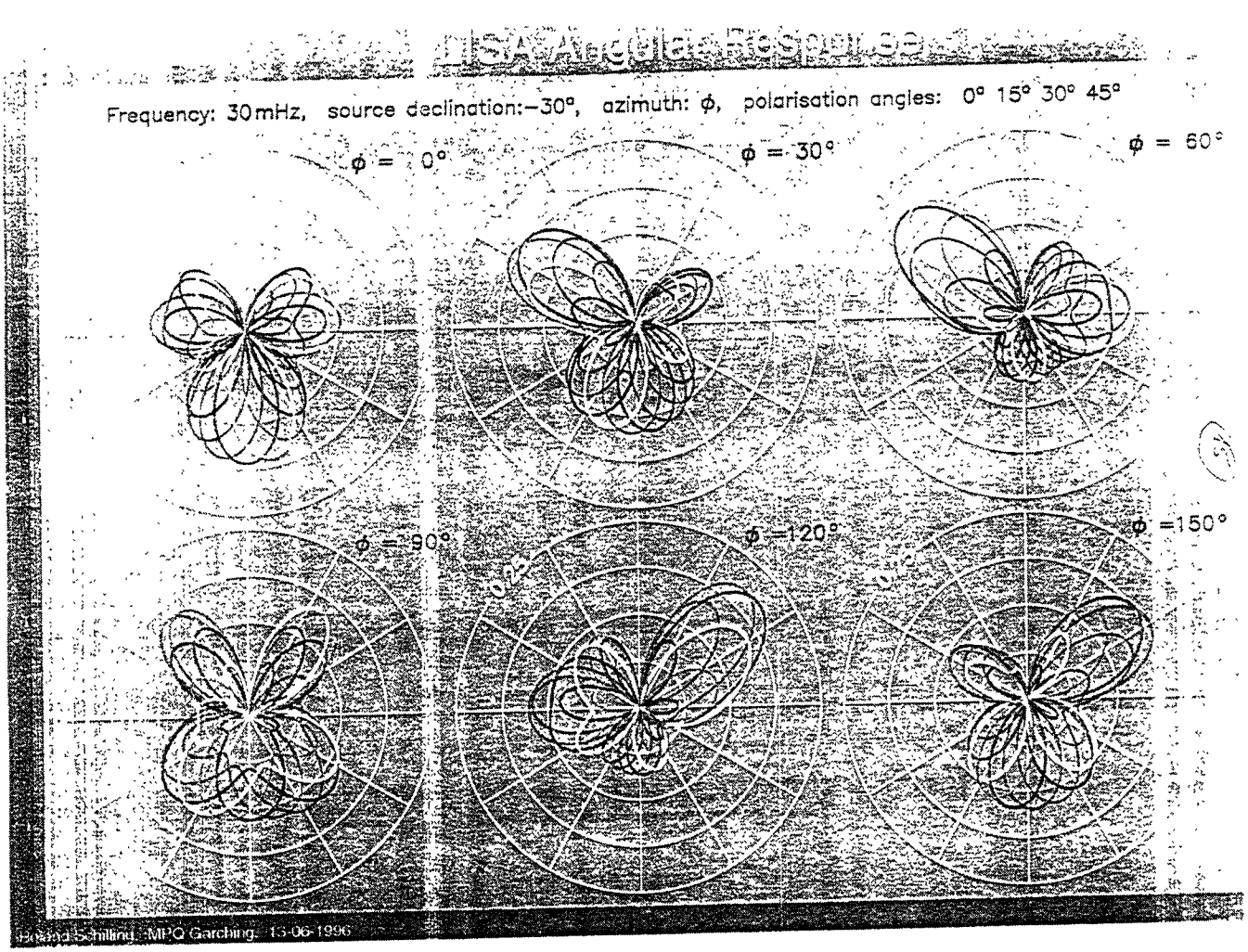
LISA Angular Response
Frequency: 30 mHz, source declination: −30°, azimuth: ϕ, polarisation angles: 0° 15° 30° 45°
ϕ = 0°
ϕ = 30°
ϕ = 60°
ϕ = 90°
ϕ =120°
ϕ =150°
0.25
Roland Schilling, MPQ Garching, 13-06-1996

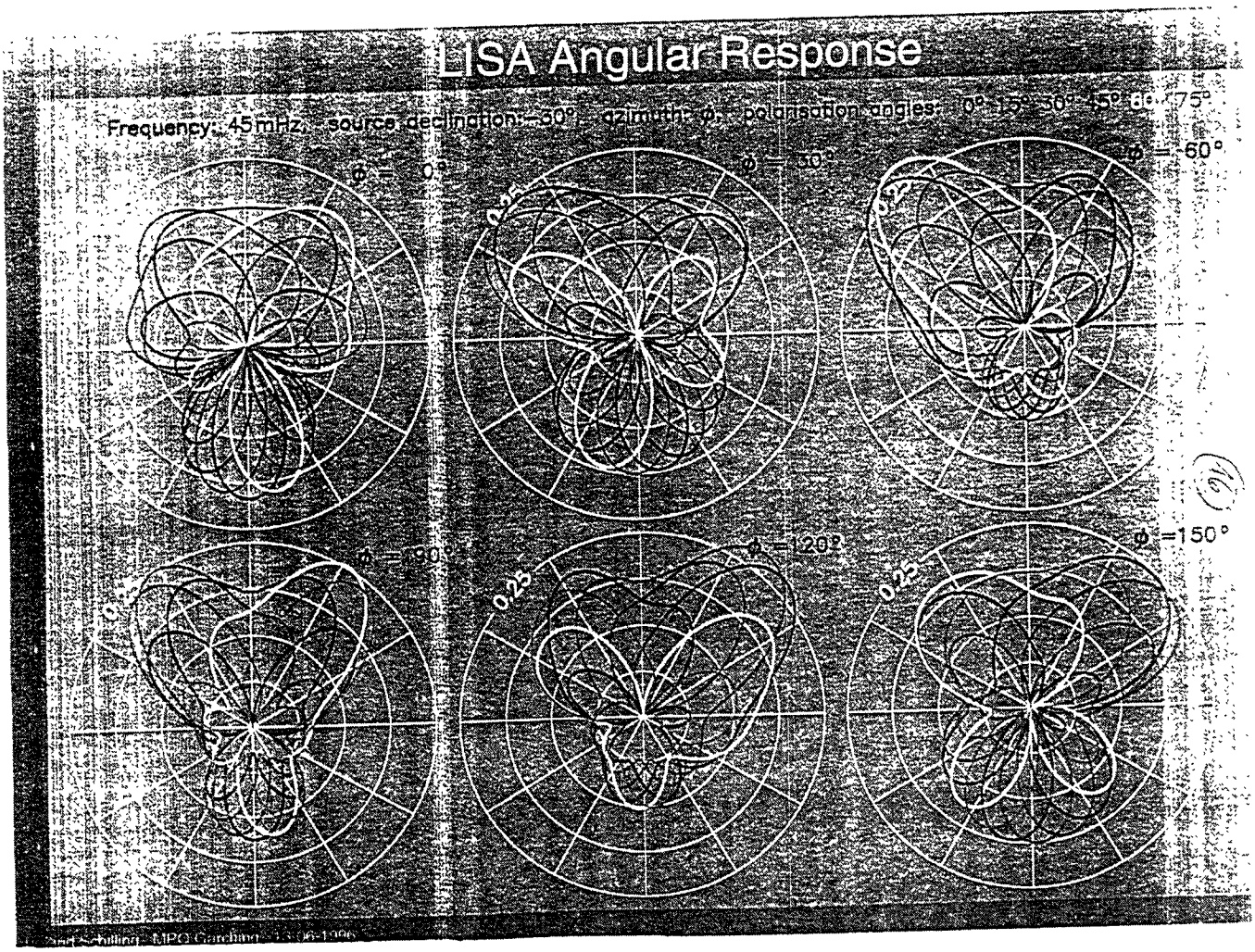
LISA Angular Response
Frequency: 45 mHz, source declination: −30°, azimuth: ϕ, polarisation angles: 0° 15° 30° 45° 60° 75°
ϕ = 0°
ϕ = 30°
ϕ = 60°
ϕ = 90°
ϕ =120°
ϕ =150°
0.25
Roland Schilling, MPQ Garching, 13-06-1996

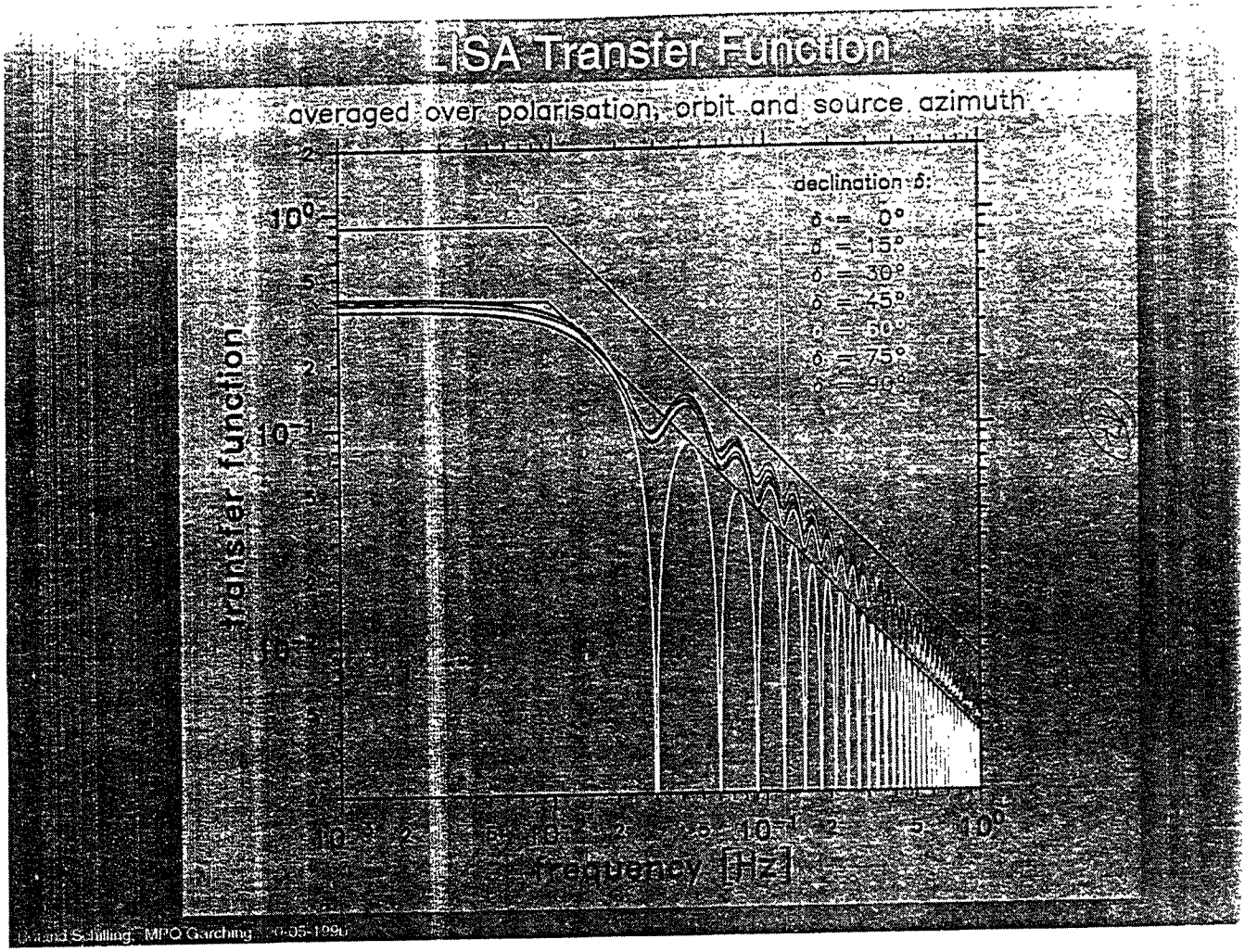
LISA Transfer Function
averaged over polarisation, orbit and source azimuth
declination δ:
δ = 0°
δ = 15°
δ = 30°
δ = 45°
δ = 60°
δ = 75°
δ = 90°
transfer function
frequency [Hz]

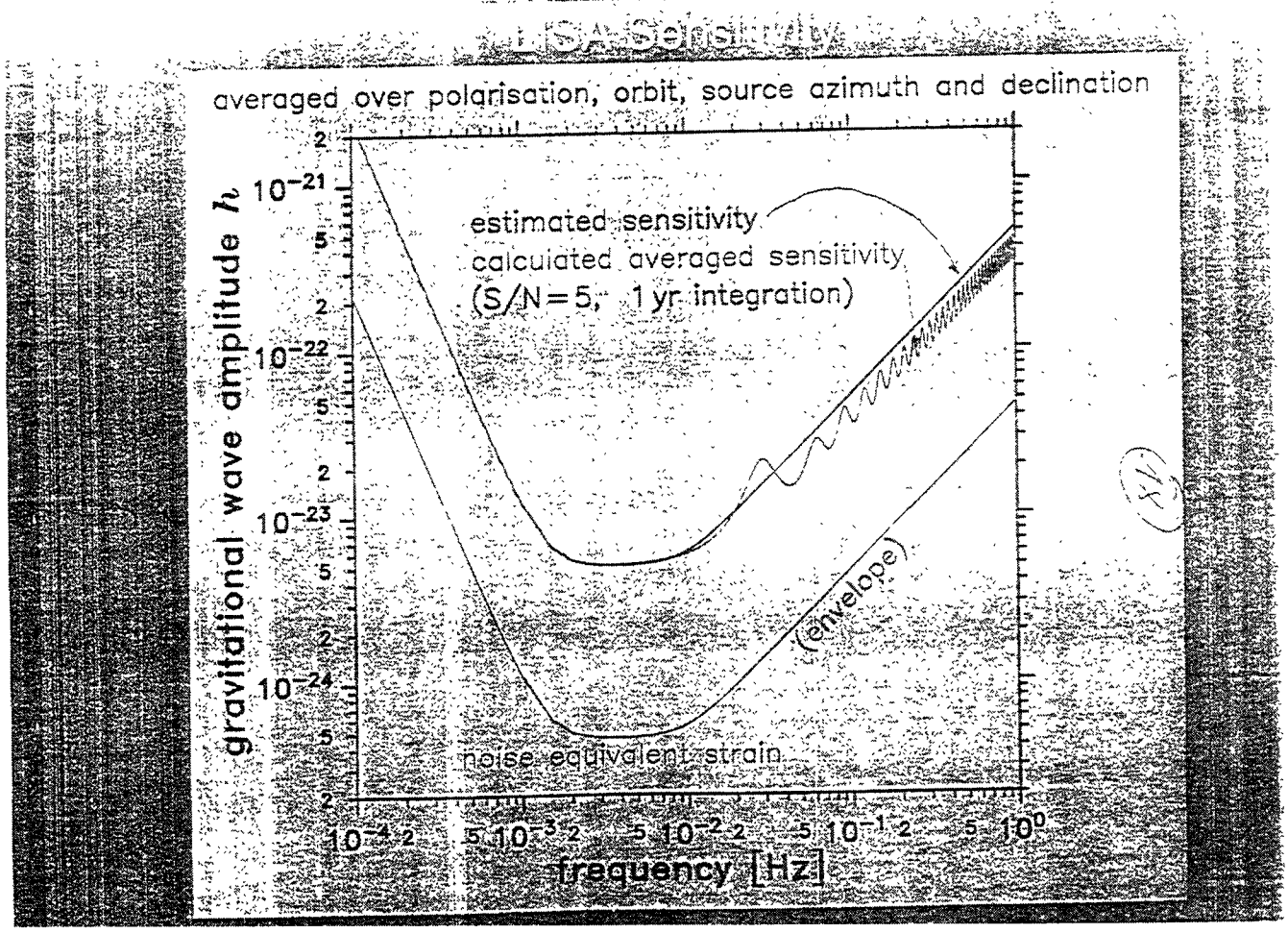
LISA Sensitivity
averaged over polarisation, orbit, source azimuth and declination
estimated sensitivity
calcuiated averaged sensitivity
(S/N=5, 1 yr integration)
(envelope)
noise equivalent strain
gravitational wave amplitude h
frequency [Hz]

Tuesday PM Suspensions and Seismic Isolation I
January 28 Chair: R. Stebbins

4:30	S. Richman(JILA)	Progress on Low-Frequency Active Seismic Isolation
4:55	Discussion	
5:05	J. Giaime(JILA)	Improvements to the JILA Isolation Platform
5:30	Discussion	
5:40	D. DeBra(Stanford)	Strategies for Vibration Isolation and Alignment
6:05	Discussion	
6:15	Coffee Break	
6:30	S. Kawamura(Caltech)	The Initial LIGO Suspension and Isolation
6:45	Discussion	
6:55	G. Gonzales(MIT)	Advanced LIGO Suspensions and Seismic Isolation
7:10	Discussion	
7:20	Round Table Discussion	Braccini, DeBra, DeSalvo, Drever, Kawamura, Robertson, Stebbins

Progress on Low-Frequency Active Seismic Isolation

S. J. Richman, J. A. Giaime, R. T. Stebbins,
P. L. Bender, J. E. Faller

JILA

Aspen Winter Conference on Gravitational Waves and their Detection

January 28, 1997

Project Outline

- Demonstrate technology for reduction of seismic noise below other noise sources at 1 Hz and above in an advanced, low-frequency gravitational wave interferometer
- $\left[1\times10^{-13}\left(\frac{1Hz}{f}\right)^{2.5}+3\times10^{-15}\right]m/\sqrt{Hz}$
  noise floor for both vertical and horizontal motion
- Combination of soft suspensions (passive isolation) and feedback (active isolation)
- 3 stages, each providing ~40 dB attenuation

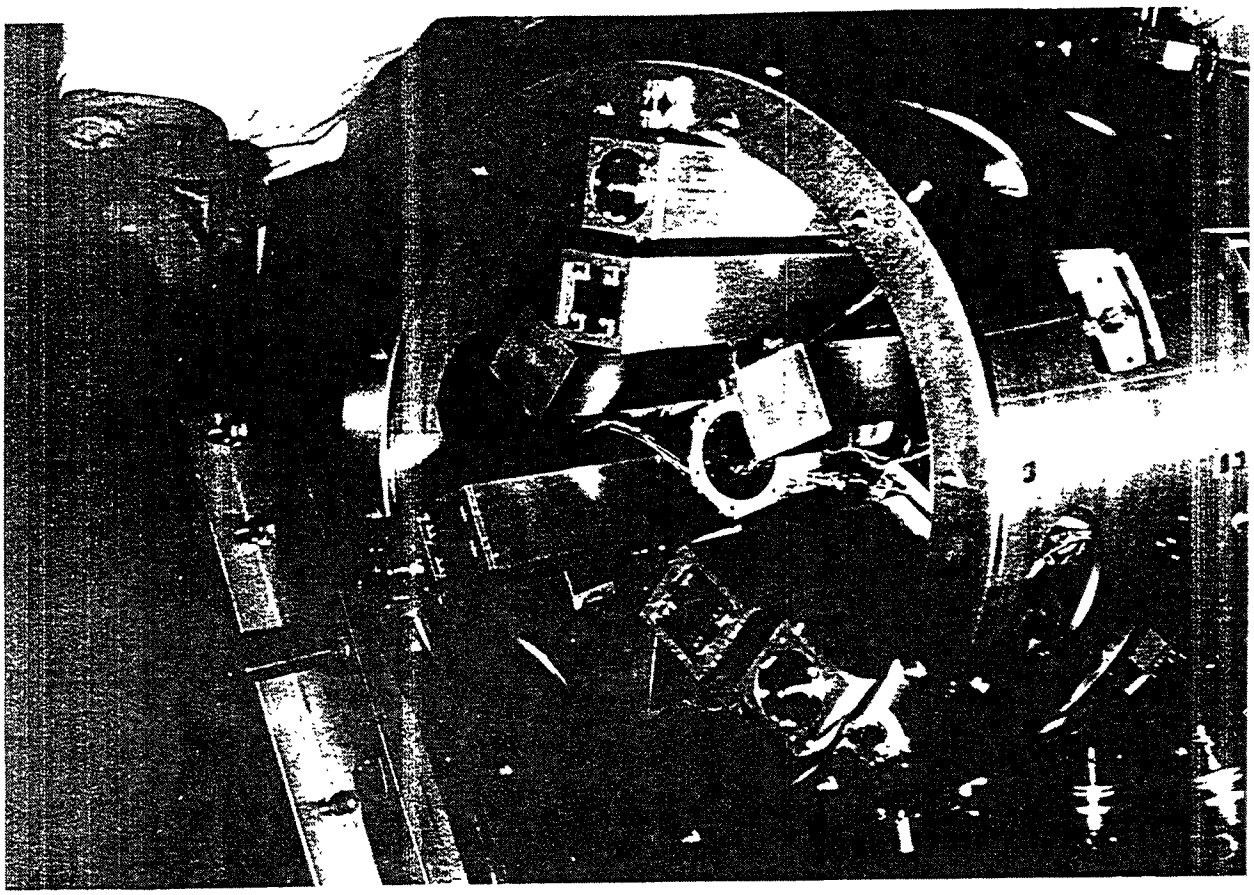

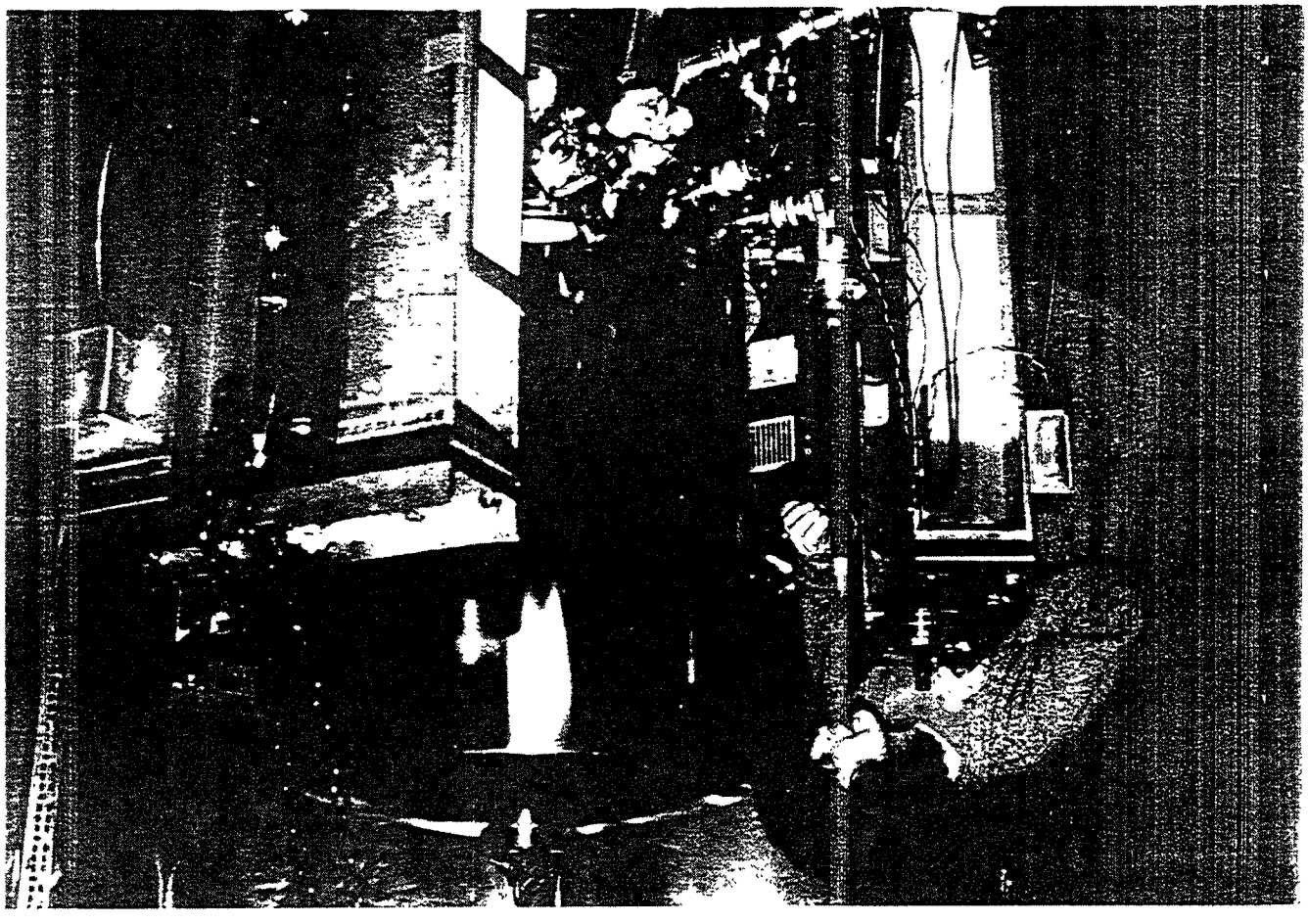

1ST MAIN VERTICAL SEISMOMETER

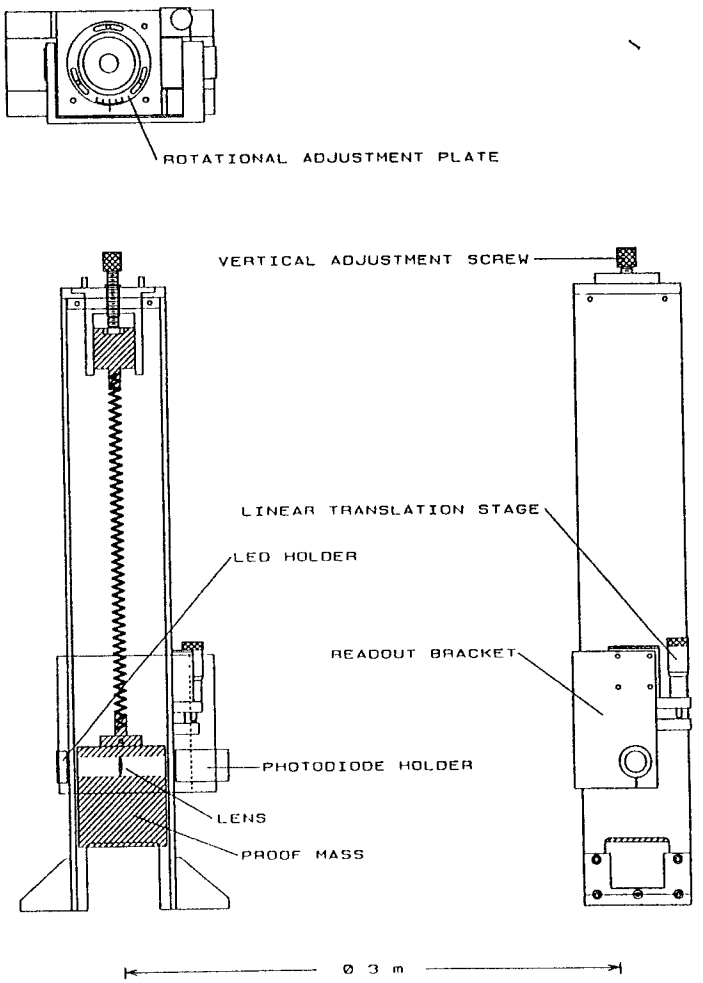

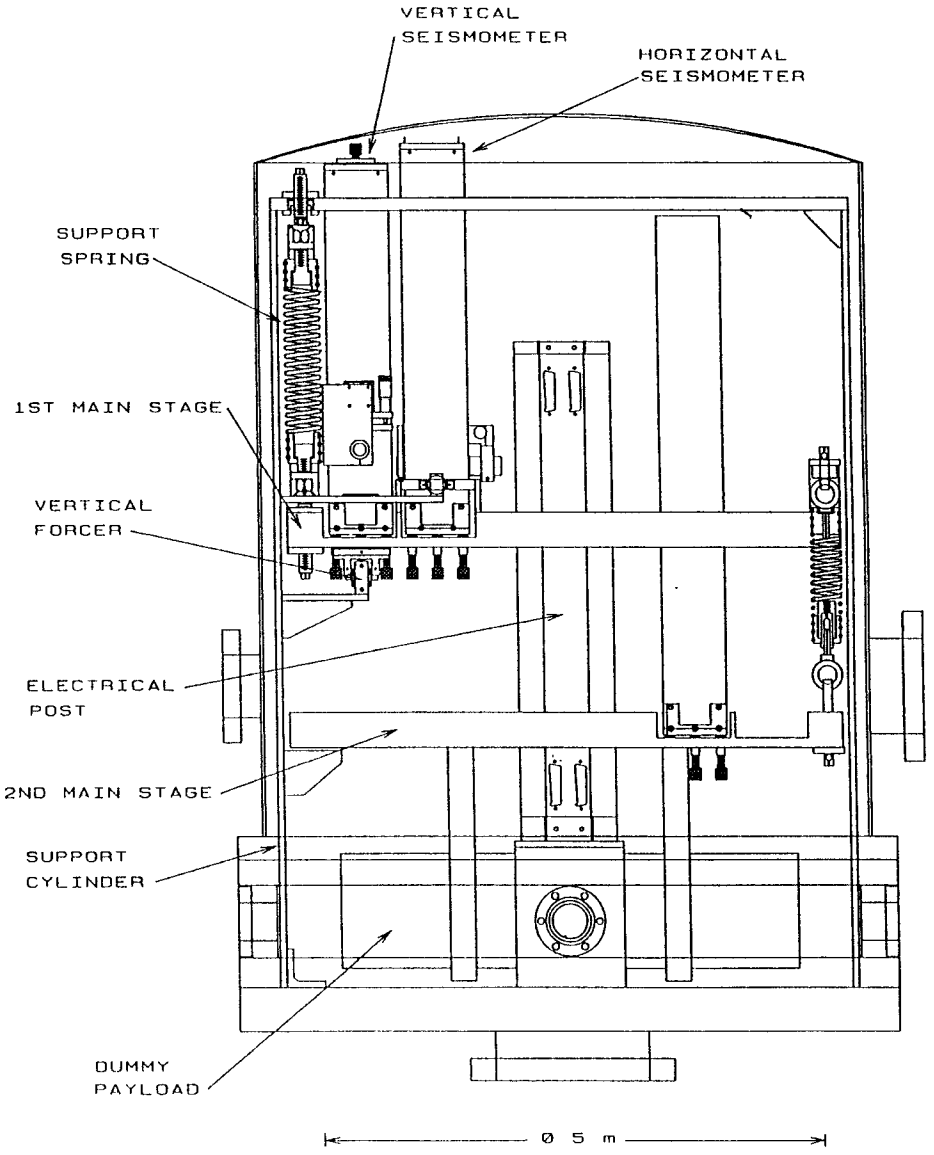

1ST MAIN HORIZONTAL SEISMOMETER

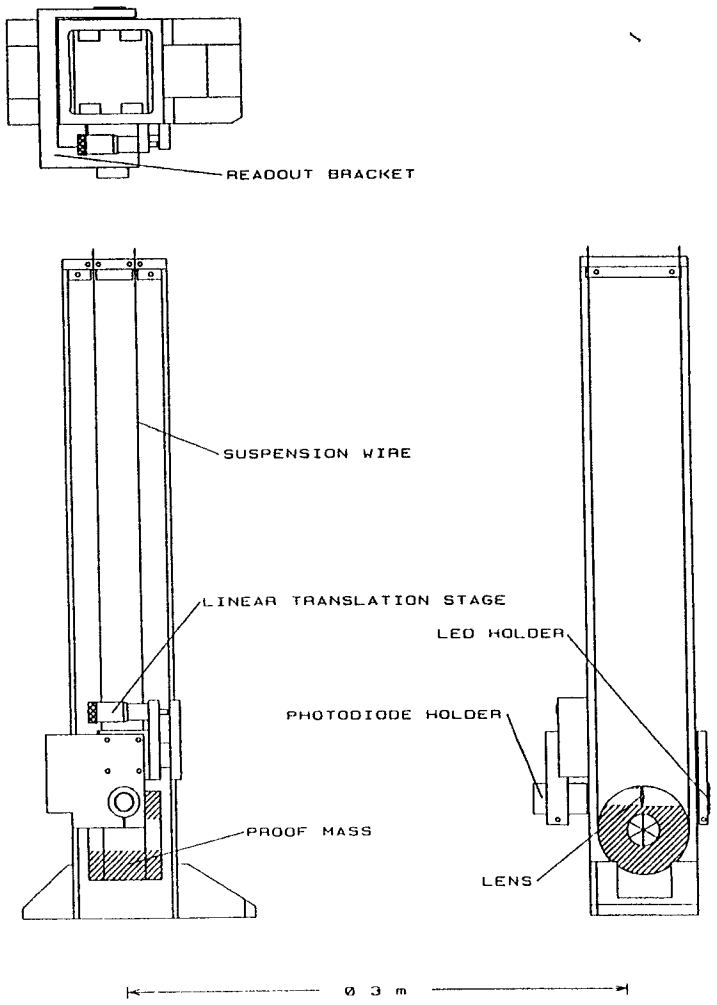

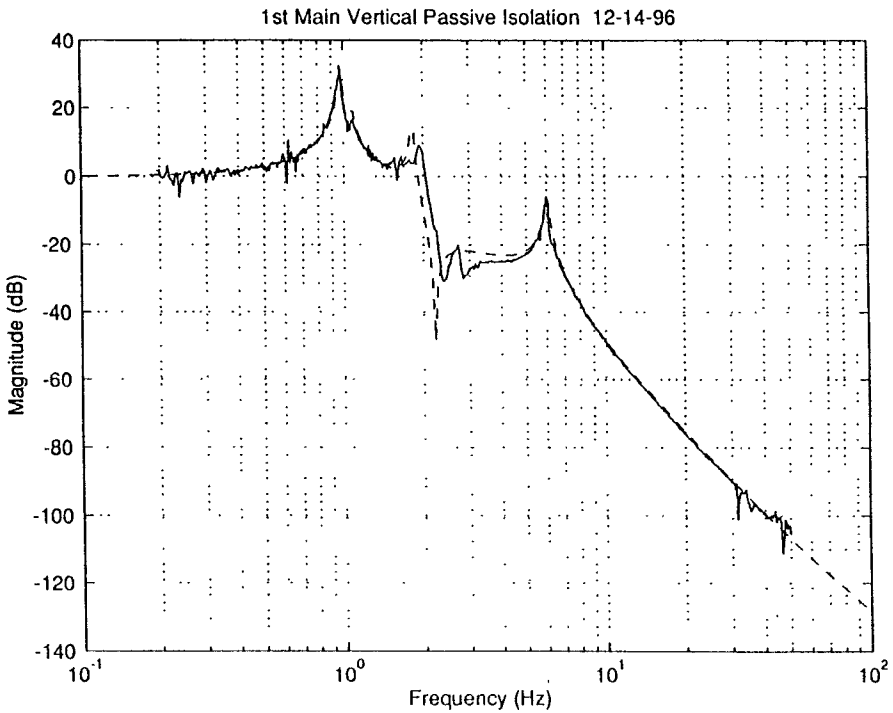

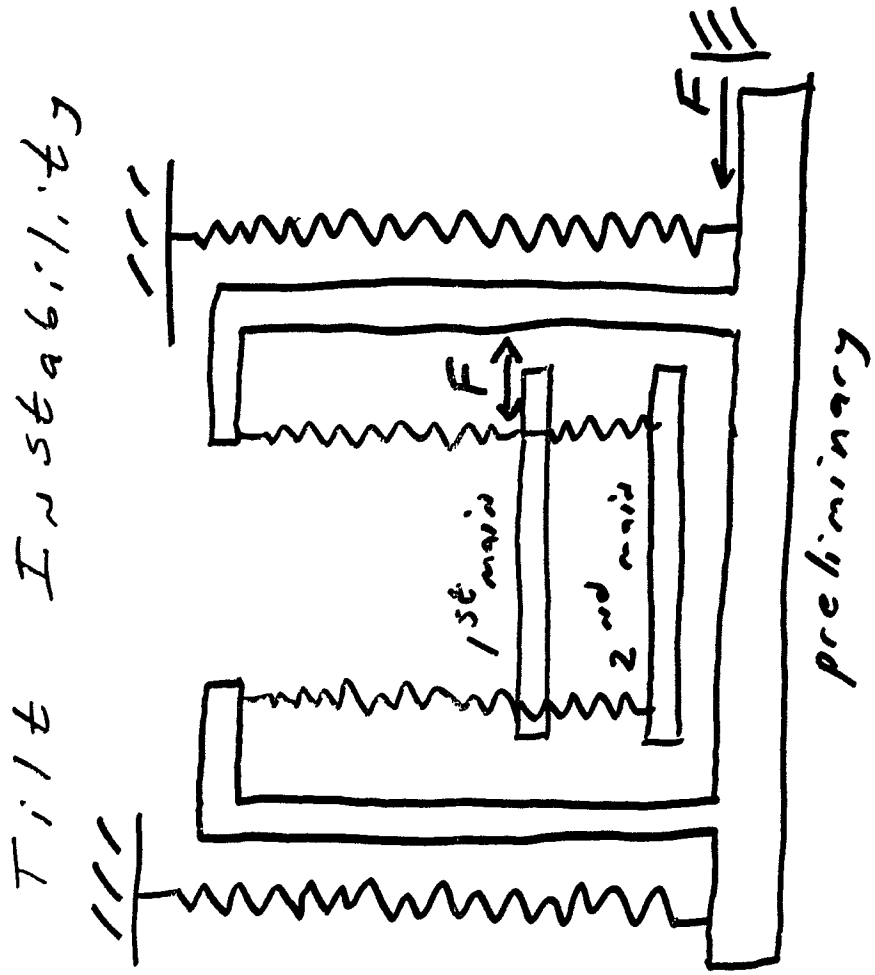
Tilt Insteag, ing
F
1st main
2nd main
preliminary

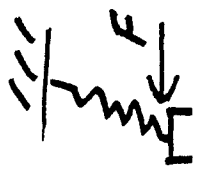
F


F

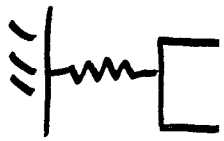

At low f...

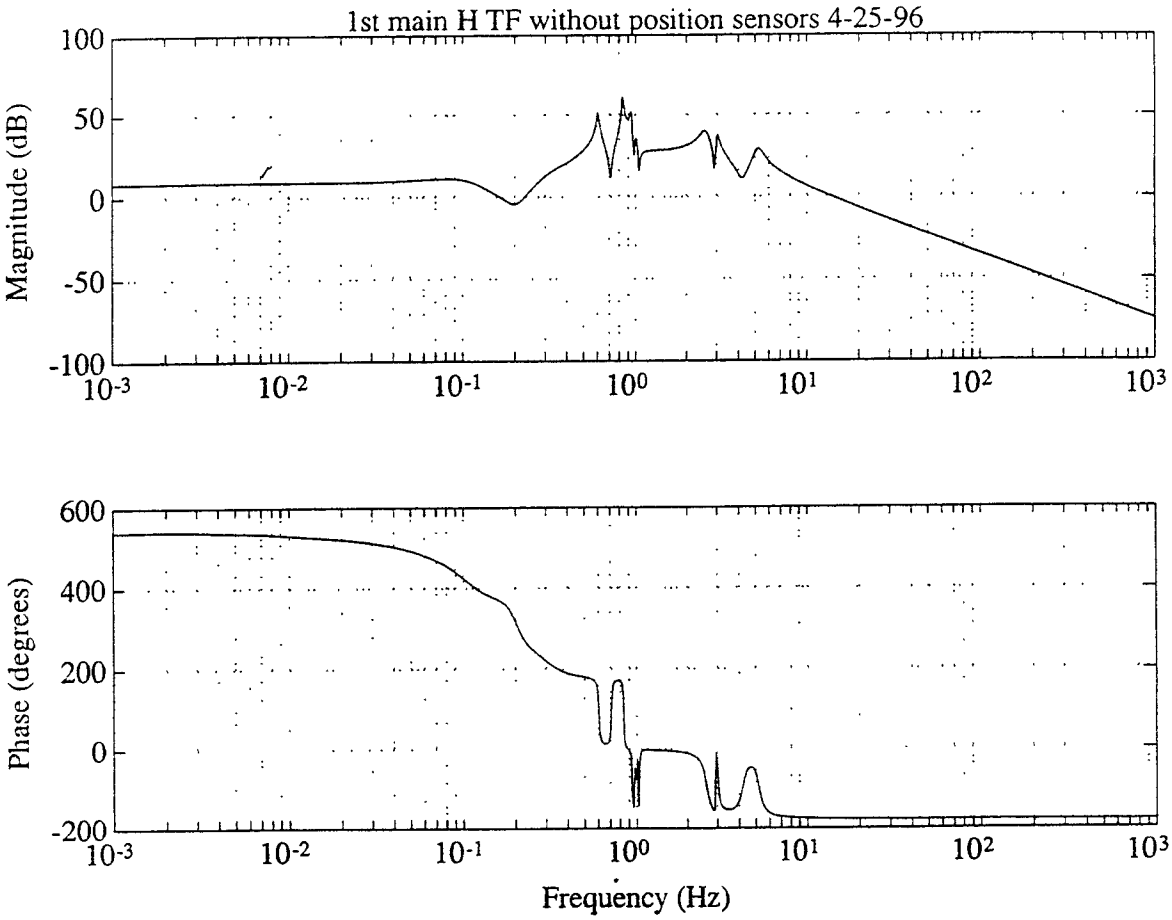
1st main H TF without position sensors 4-25-96
Magnitude (dB)
100
50
0
-50
-100
10-3
10-2
10-1
100
101
102
103
Phase (degrees)
600
400
200
0
-200
Frequency (Hz)

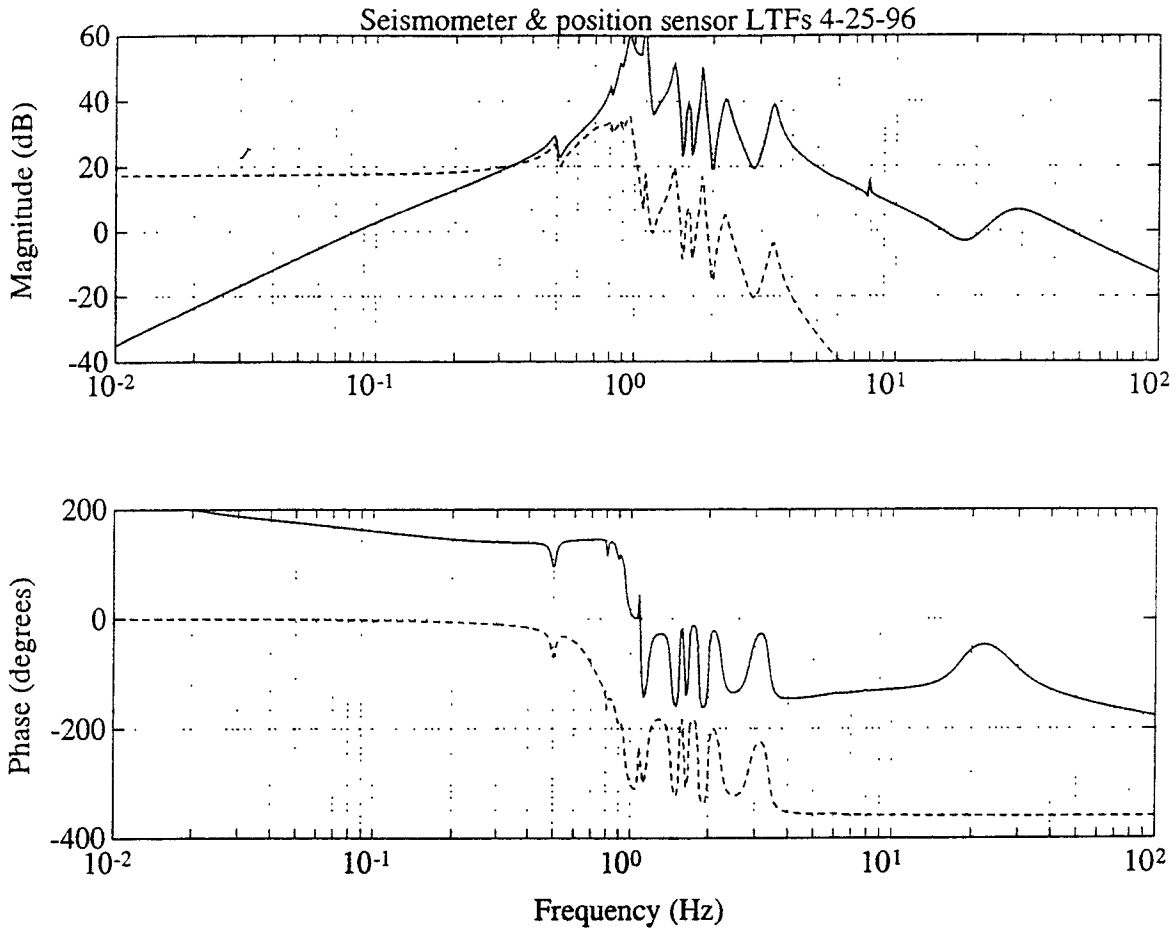
Seismometer & position sensor LTFs 4-25-96
Magnitude (dB)
60
40
20
0
-20
-40
10-2
10-1
100
101
102
Phase (degrees)
200
0
-200
-400
10-2
10-1
100
101
102
Frequency (Hz)

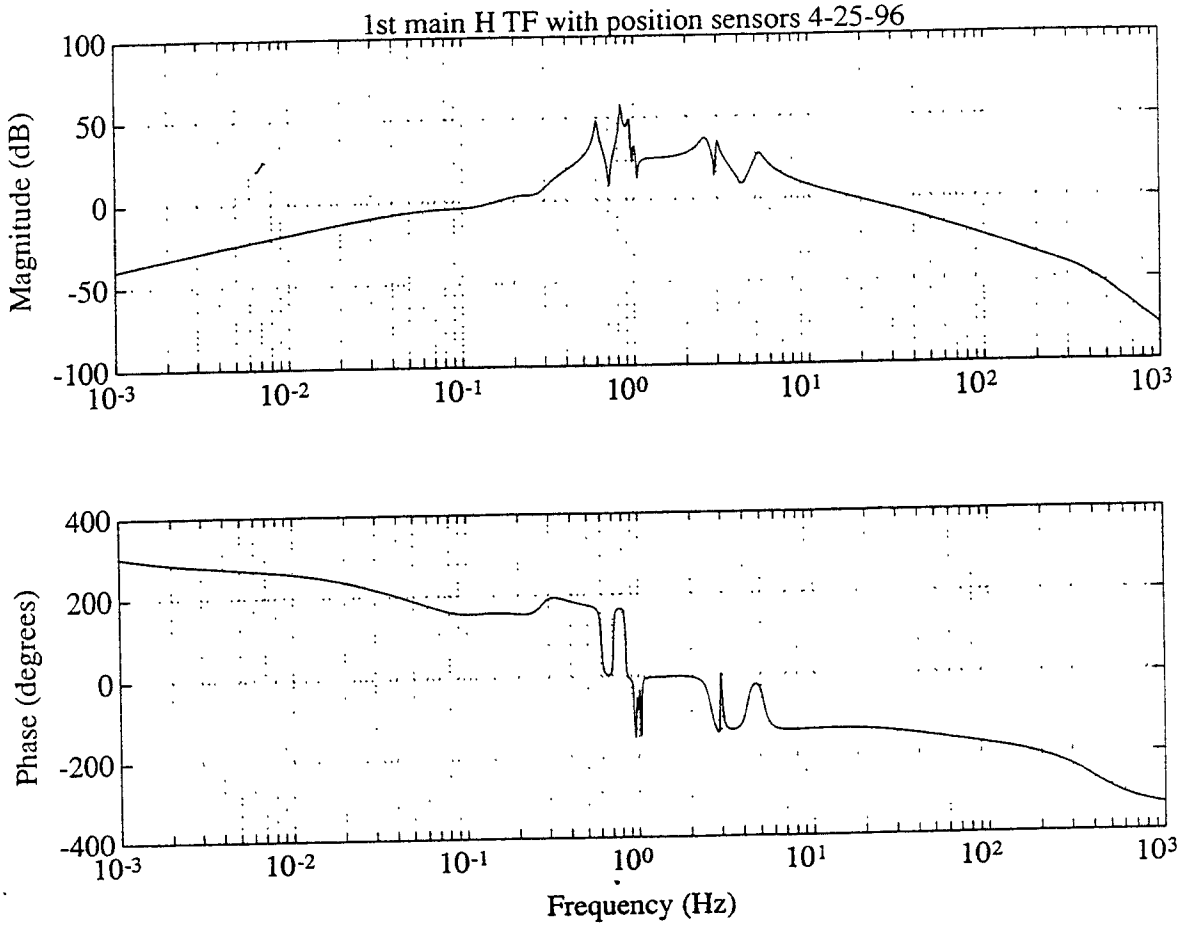
1st main H TF with position sensors 4-25-96
Magnitude (dB)
100
50
0
-50
-100
10-3
10-2
10-1
100
101
102
103
Phase (degrees)
400
200
0
-200
-400
10-3
10-2
10-1
100
101
102
103
Frequency (Hz)

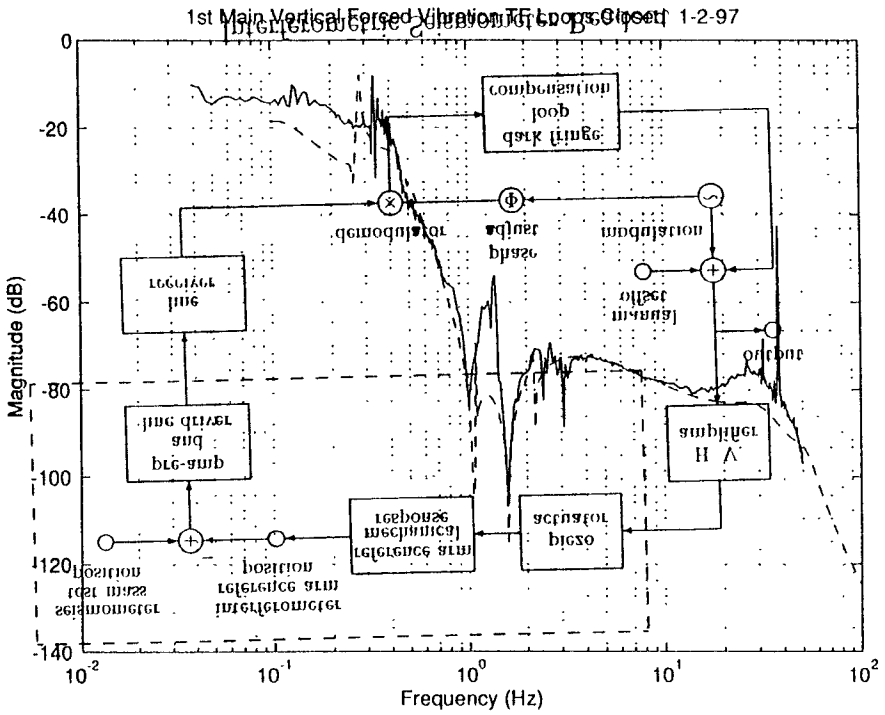
1st Main Vertical Forced Vibration TF Loops Closed 1-2-97
Magnitude (dB)
Frequency (Hz)
0
-20
-40
-60
-80
-100
-120
-140
10^{-2}
10^{-1}
10^{0}
10^{1}
10^{2}

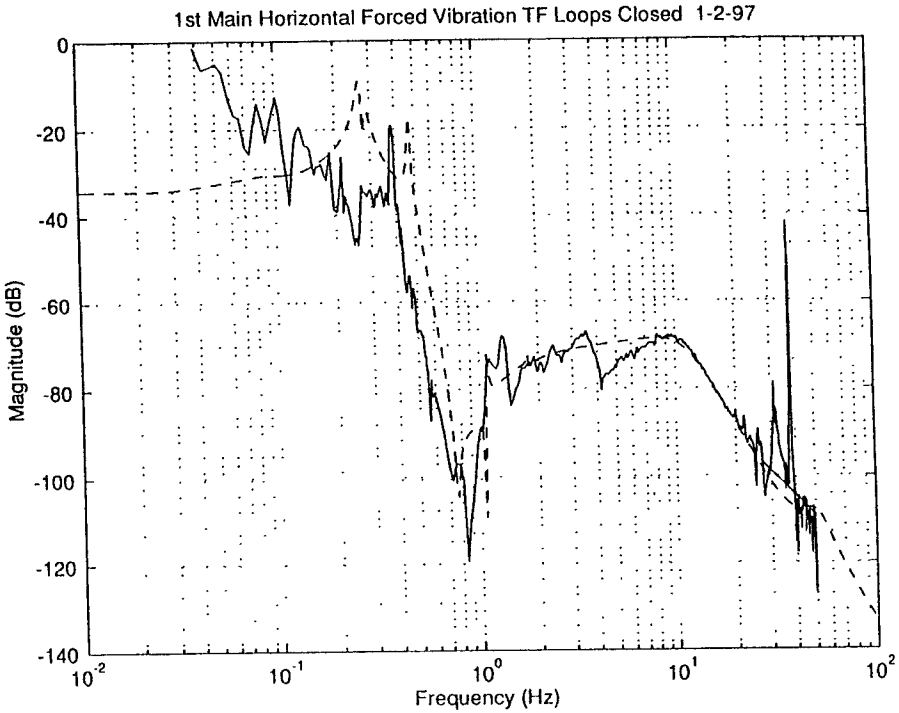
1st Main Horizontal Forced Vibration TF Loops Closed 1-2-97
Magnitude (dB)
Frequency (Hz)
0
-20
-40
-60
-80
-100
-120
-140
10^{-2}
10^{-1}
10^{0}
10^{1}
10^{2}

Improvements to the JILA isolation platform

J. Giaime, P. Bender, J. Faller, S. Richman,
R. Stebbins

JILA Gravity Group, University of Colorado

`http://onehertz.colorado.edu`
`(username & password: JILA)`

Present state of the JILA active seismic isolation platform

Intentions:

- proof-of-principle test bed
- show concept feasibility
- show performance goals could be met
- function as quiet site for suspension thermal noise experiment.

Concept: Three cascaded stages, each stage instrumented with 6 seismometers. Each measures an error signal, which is the displacement away from a test mass along one of 6 non-orthogonal axes. Servo loops minimize the error signals by applying forces along the 6 axes with non-contacting forcers.

Realization: design focus was on simplicity and symmetry, both to reduce risk of complicated extra noise sources and to allow easier computer modelling. (Complete details as described by Sam Richman)

If "proof-of-principle," principles proven so far:

- cascaded active stages with similar modal frequencies can give cascaded isolation, both vertically and horizontally.

- Servo stability up to desired gains (two stages at least) can be obtained without MIMO.

- Operation of control loop using interferometer readout seismometer is possible, although necessary seismometer noise floor not yet demonstrated.

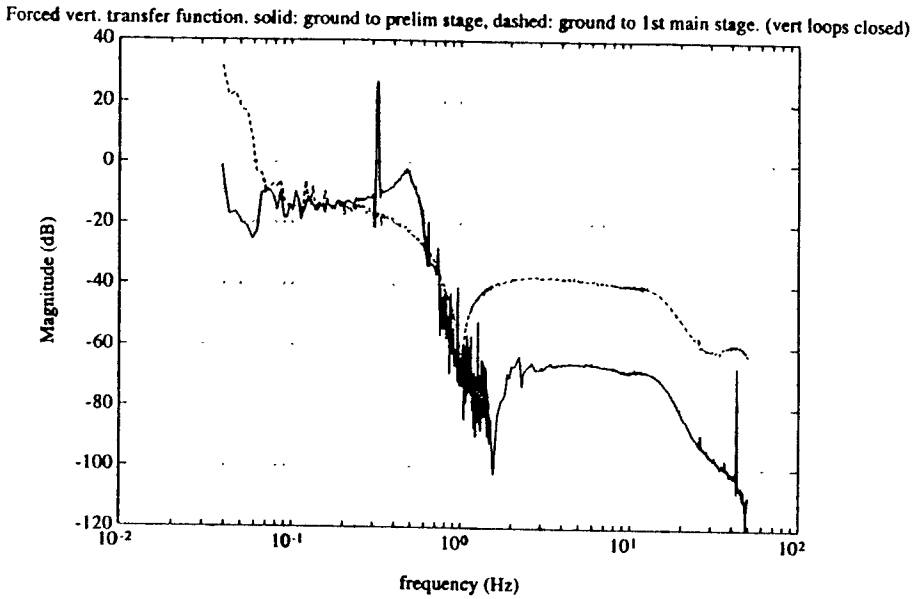

Refining the initial design:

In Progress/ near term planned for proof-of-principle apparatus:

- redesigned universal joint for platform suspension.
- Installation of interferometric seismometer readouts.
- Elimination of quadrupole mass distribution in test masses.
- Damping or elimination of "uncontrollable" or "unobservable" DOFs.
- Preliminary tests of feed-forward (with Stanford: DeBra, How, etc.)

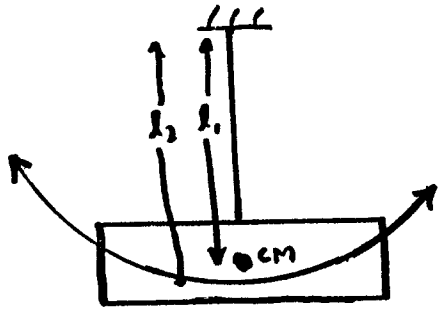

test mass quadrupole moment
⇒ two pendulum periods, perhaps weakly coupled.

so horizontal motion can torque test mass, coupling to spin.

JILA 1st main stage seismometer.

bored hole for imaging readout ⇒ quad moment
⇒ slight coupling to spin

⇒ 0.3 Hz excess noise closed-loop

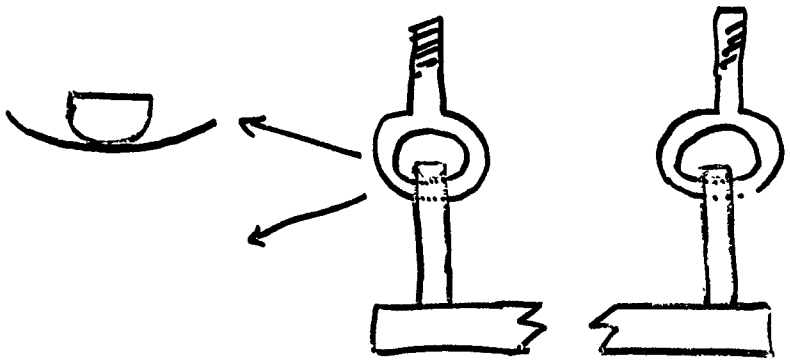

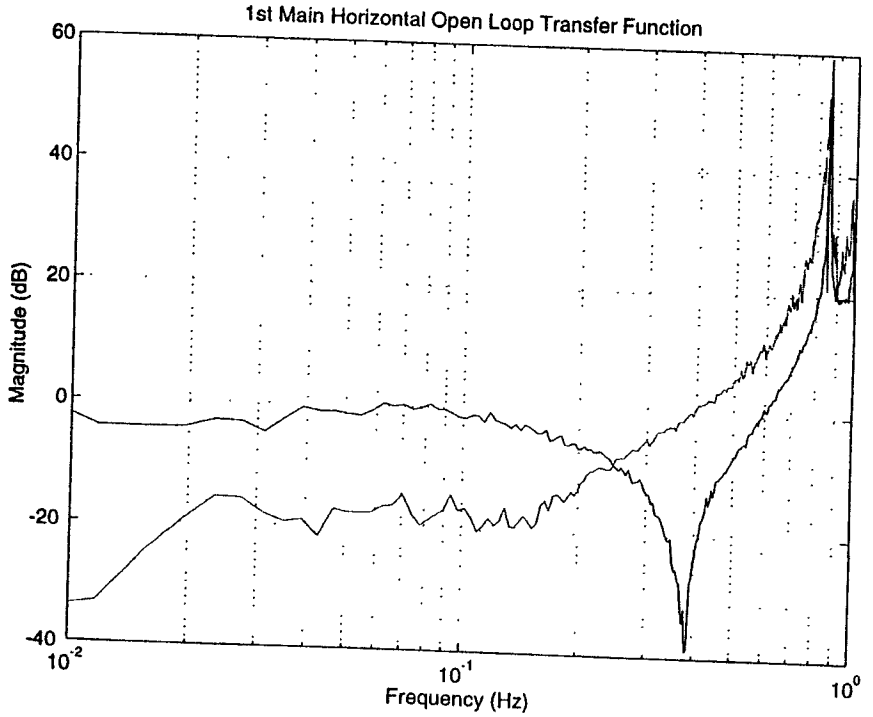
1st Main Horizontal Open Loop Transfer Function
Magnitude (dB)
60
40
20
0
-20
-40
10^{-2}
10^{-1}
10^{0}
Frequency (Hz)

Research leading to the prototype design:

- possible seismometer improvements: constrained suspensions, variable dampers on all test mass DOFs ?

- Imaging position sensors on upper stages:
  - Measure position w.r.t. preliminary stage
  - used to quiet system for interferometer readout seismometer lock.
  - used to monitor exact platform position in case of interferometer re-lock, and for system alignment

- Computer/DSP servo implementation.
  - computer control of lock acquisition
  - dynamic range monitoring
  - make possible more complex servo design to tailor impulse responses to common local noises.

- MIMO study (with Stanford: DeBra, How, etc.) MIMO servos might allow servo stability greater range of misalignment of sensors and forcers than is possible with SISO.

- Automatic Alignment/system identification study. This will allow automated setting of feedforward system functions after initial alignment.

Interferometric readout for JILA Seismometers

Sensitivity goal

$$x(f) = 10^{-13}\left(\frac{1\,\mathrm{Hz}}{f}\right)^{2.5} + 3\times 10^{-15}\ \mathrm{m}/\sqrt{\mathrm{Hz}}$$

Interferometer design

- Light source: 1.3μ Lightwave miser, coupled to single-mode PM fiber.
- Light delivery: Light split 12 ways in fiber, fed into vacuum, and terminated in connectorized GRIN lenses.
- Topology: equal-arm-length one-bounce Michelson.
- Control/Readout: reference arm dithered and output held at dark fringe using PZT stack; dynamic range 2μm.

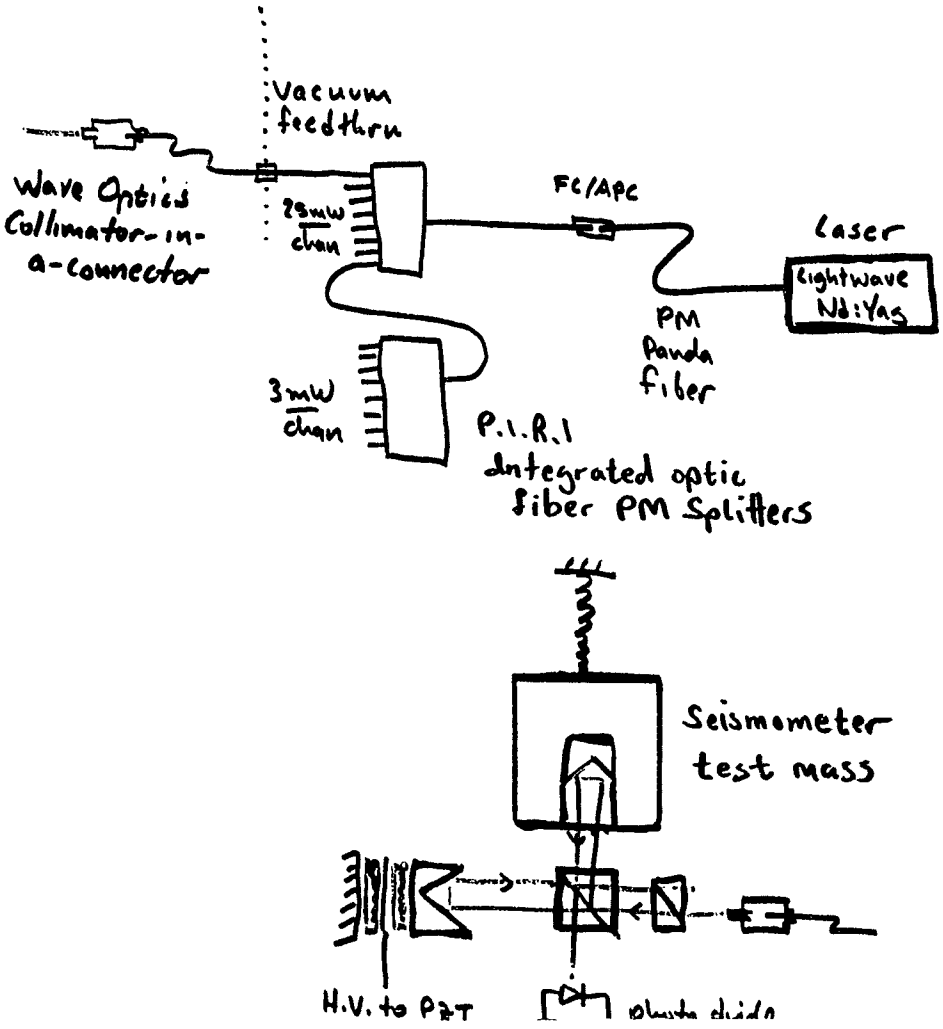

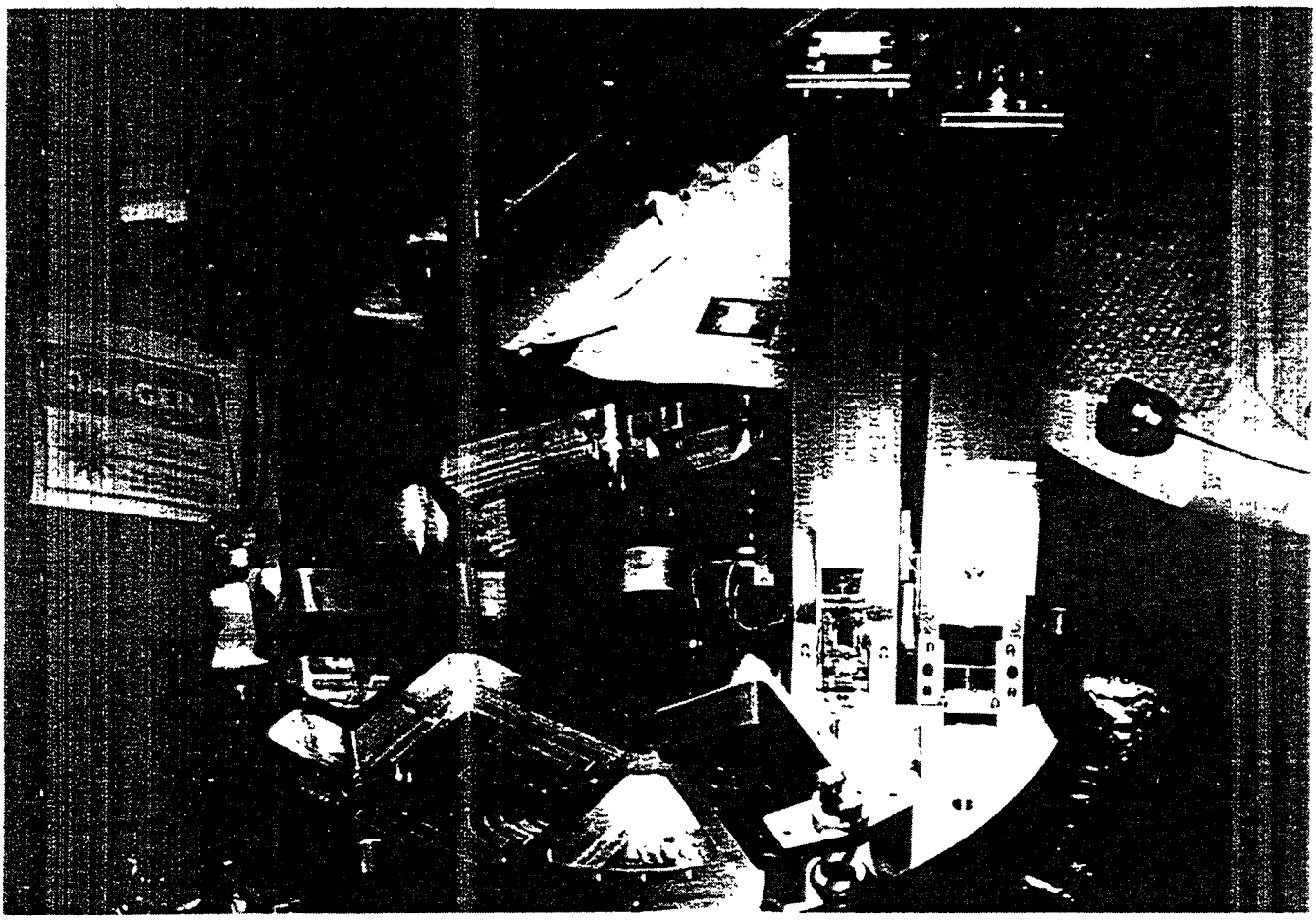

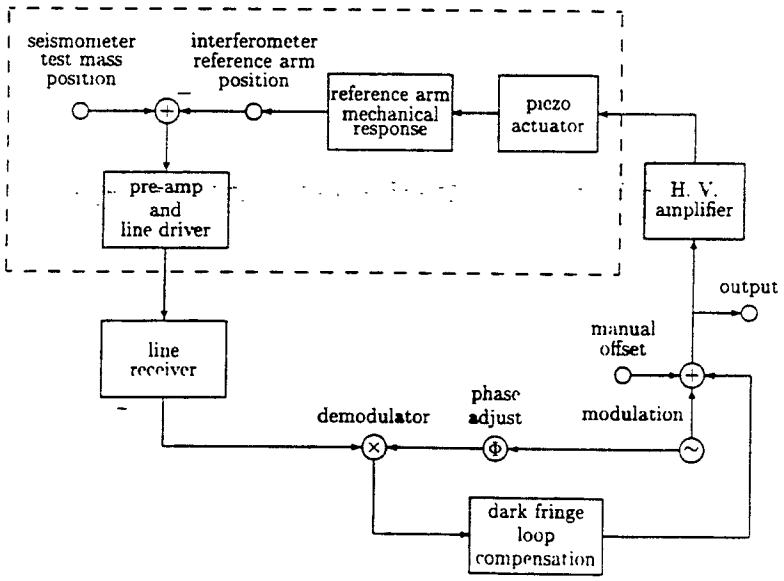

Interferometric Seismometer Readout

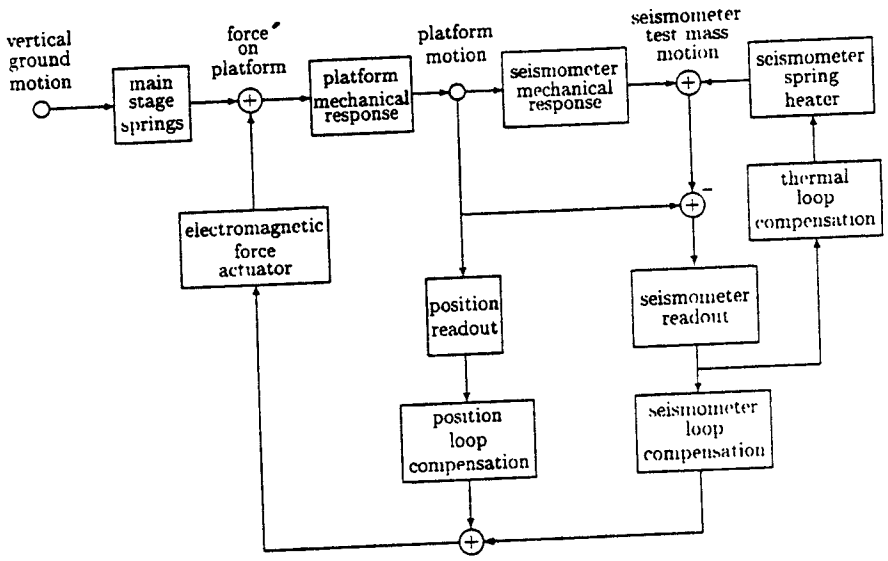

Preliminary Stage Vertical Servo

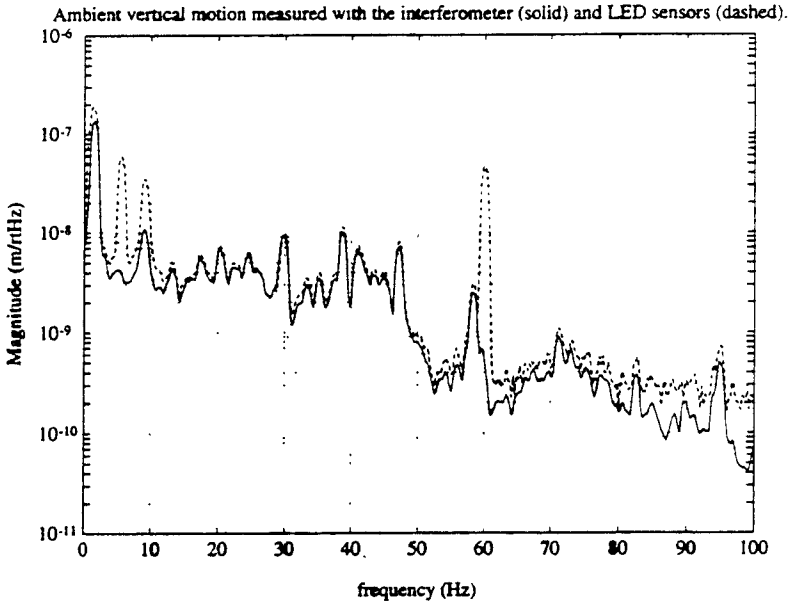

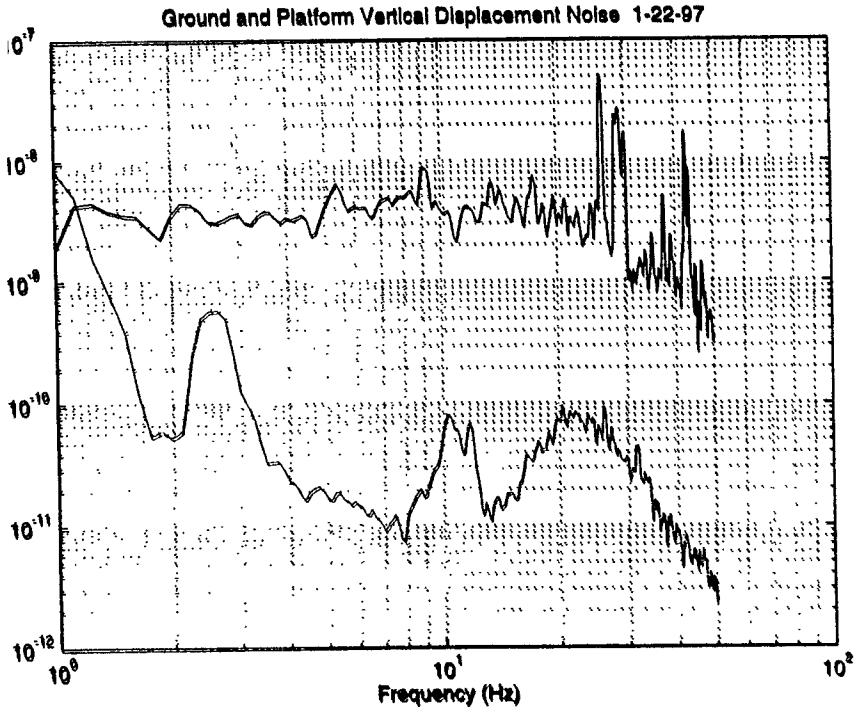

Noise sources:

Frequency noise from laser

$$\frac{d\phi}{d\nu} = \frac{2\pi\,\Delta x}{c} \Rightarrow \Delta x = \frac{\phi(f)}{\nu(f)}\frac{c}{2\pi}.$$

$$x(f) = 3\times10^{-15}\mathrm{m}/\sqrt{\mathrm{Hz}} \Rightarrow \phi(f) = 1.5\times10^{-8}/\sqrt{\mathrm{Hz}}$$

For the Miser:

$$\nu(f = 1\,\mathrm{Hz}) = 10^{3}\mathrm{Hz}/\sqrt{\mathrm{Hz}} \Rightarrow \Delta\, x \leq 0.7\mathrm{mm}$$

Amplitude noise

$$\frac{\phi(f)}{\phi_{\mathrm{RMS}}} = \frac{\delta I(f)}{I}$$

For the Miser:

$$\frac{\delta I(f)}{I} = 10^{-4}$$

$$\phi_{\mathrm{RMS}} \leq 1.5 \times 10^{-4}.$$

For the Preliminary stage,

$$x(f) < 10^{-9}\mathrm{m}/\sqrt{\mathrm{Hz}} \Rightarrow \phi(f) < 7 \times 10^{-4}.$$

FIBER PENDULA — PUSHING LIMITS

violin make

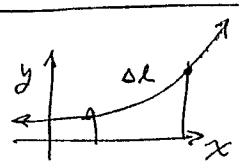

$F = Mg$

$F = Sa$

$(\rho a\, ds)\ddot{y} = F\, y''\, dx$

$y = XT \rightarrow \frac{\ddot{T}}{T} = \frac{F}{a\rho}\frac{X''}{X} = -\omega^2$

$\ddot{T} + \omega^2 T = 0 \rightarrow \omega$ is natural frequency

$X'' + \frac{\omega^2 \rho a}{S a} X \rightarrow X = A\cos\lambda x + B\sin\lambda x$

$\lambda^2 = \frac{\omega^2 \rho}{S}$

$X = 0 \quad x = 0,\ x = L$

$\downarrow \quad \downarrow$

$A = 0 \quad \lambda L = n\pi$

$n = 1 \quad \omega\sqrt{\frac{\rho}{S}}L = \sqrt{\pi}$ $\quad \boxed{\omega_0 = \frac{1}{L}\sqrt{\frac{\pi S}{\rho}}} \Rightarrow S = \frac{\omega_0^2 L^2 \rho}{\pi}$

Pendulum $\omega_p^2 = g/L \rightarrow L = g/\omega_p^2$

STRESS $\boxed{S = \frac{\rho g^2}{\pi}\frac{\omega_0^2}{\omega_p^4}} \Rightarrow \left[\frac{M}{L^3}\ \frac{L^2}{T^4}\ T^2\right] = \left[\frac{ML}{T^2}\right]\frac{T^2}{L^2} = \left[\frac{F}{L^2}\right] = Pa$

example $\rho = 3000\ kg/m^3$

$g = 10\ m/sec^2$

$\omega_0 = 3\ kHz = 2^{14}\ r/s$

$\omega_p = 1\ Hz = 6^{10}\ r/s$

$S = \frac{3^3}{3}\frac{1^2}{1^3}\frac{4^{18}}{1^3} = 4^{10}\ Pa$

$S = 4^{10}\ Pa = 4^{15}\ at = 6^{16}\ psi \rightarrow$ beyond realization

change $\omega_p \rightarrow 3\ Hz \rightarrow \frac{g}{100} = 60{,}000\ psi$

S/E as driver for minimum ω_n

All mechanical springs, low ω_n → large size → high stress here are two examples

Ex1 Compression spring.

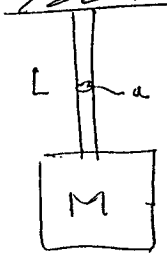

$k = \frac{Ea}{L}$

$Mg = F = Sa$

$k/M = \frac{Ea}{L}\frac{g}{Sa} = \left(\frac{E}{S}\right)\left(\frac{g}{L}\right)$

$\boxed{\omega_n^2 = \left(\frac{E}{S}\right)\left(\frac{g}{L}\right)}$ $\quad \boxed{\left(\frac{S}{E}\right) = \frac{g/L}{\omega_n^2}}$

BENDING SPRING

Ex2

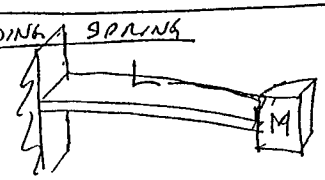

$k = \frac{P}{\frac{PL^3}{3EI}} = \frac{3EI}{L^3}$

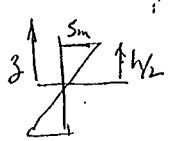

$S = \frac{2S_m z}{h}$ $\quad T = MgL = \int (S\, b\, dz\, z)$

$= \frac{2bS_m}{h}\int_{-h/2}^{h/2} dz\, z^2 = \frac{2bS_m}{3h}\left(\frac{h^3}{8}\right) = \frac{bh^2 S}{6}$

$S_m = \frac{6MgL}{bh^2}$ $\quad M = \frac{bh^2 S_m}{6gL}$

$\frac{k}{M} = \frac{3E\, bh^3}{2\, L^3\, bh^2 S_m}\frac{gh}{2} = \frac{3}{2}\left(\frac{E}{S_m}\right)\frac{gh}{L^2}$ $\quad \boxed{\left(\frac{S}{E}\right) = \frac{3}{2}\left(\frac{gh}{L^2}\right)\frac{1}{\omega_n^2}}$

LOW ω_n RESULTS IN HIGH STRESS

SISO — EFFECT OF SEIS. MAT. FIXED.

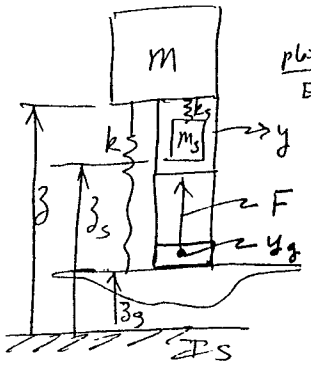

sensor $y = z - z_s + v$ for feedback

platform EOM

(also can use y_g for feedforward $y_g = (z_g - z_{sg}) + v_g$)

$$m\ddot{z} = -k(z - z_g) + F - k_s(z - z_s)$$

seismmass EOM $m\ddot{z}_s = -k_s(z_s - z)$

$$\begin{bmatrix} (ms^2 + k + k_s) & -k_s \\ -k_s & (m_s s^2 + k_s) \end{bmatrix} \begin{bmatrix} z \\ z_s \end{bmatrix} = \begin{bmatrix} k z_g + F \\ \end{bmatrix}$$

$F = -C(s)\, y$ for feedback (add $F = -(k_{model}) y_g$ for feed forward)

$$\frac{y}{F} = \frac{z - z_s}{F} = \frac{m_s s^2 + k_s - k_s}{m_s m \left(s^4 + \left[\frac{k_s}{m_s} + \frac{k}{m} + \frac{k_s}{m} \right] s^2 + \frac{k}{m} \frac{k_s}{m_s} \right)}$$

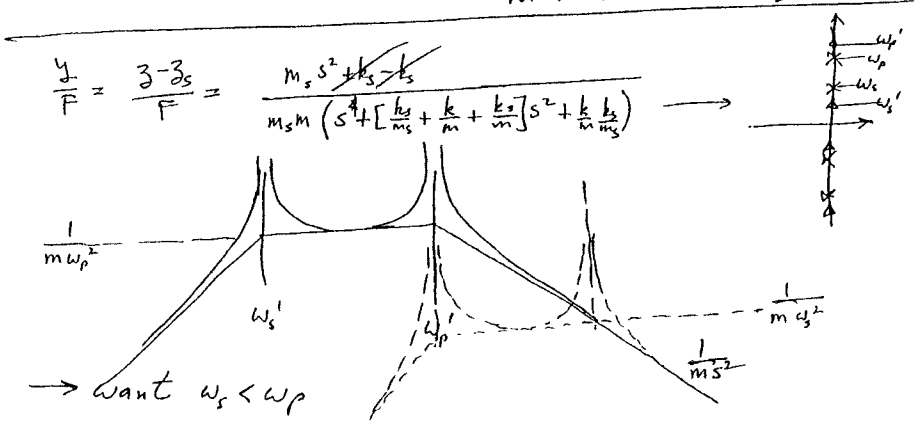

→ want $\omega_s < \omega_p$

FEEDBACK DESIGN EXAMPLE FOR 1 D.O.F. MODEL USING LQR Design

$(z - z_s)$ weight

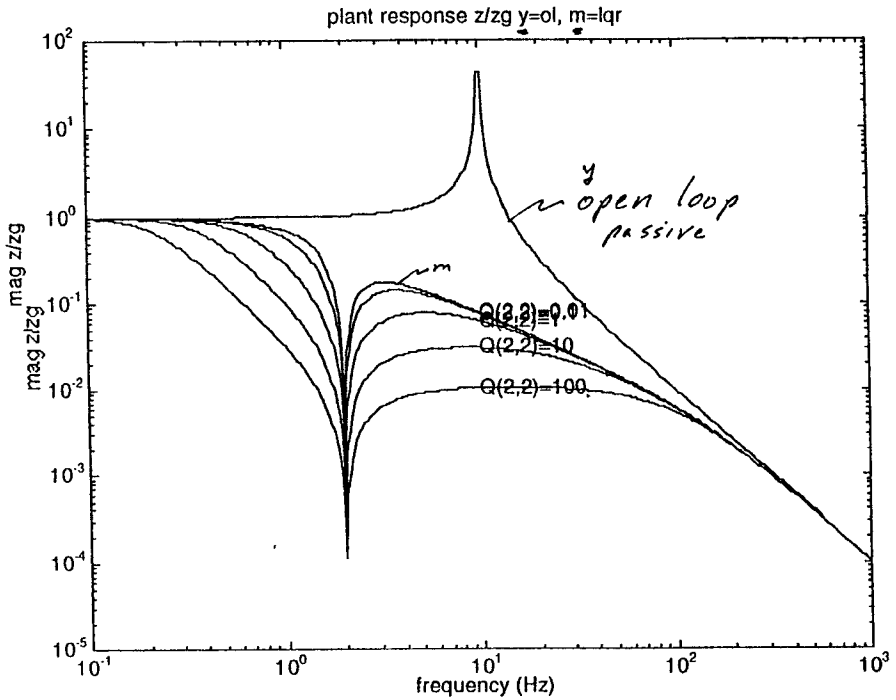

→ attenuation "shaping" can be done in the design process without extending the bandwidth.

→ maximum attenuation is below ω_p

→ "pleasant" choice of attenuation at 10 Hz = 30.

→ additional attenuation due to feedforward ~ 10.

STACK HIERARCHY

Vibration Isolation and Alignment

STAGE	Wp (Hz)	Atten	sag (m)	Actu. Auth (m)	Q	Vib@10 (m/rtHz)	BW (Hz)
outside	-	-	-	0.1	-	1e-8	-
1	20	30*10	6e-4	1e-8/3e-3	1	3e-11	200
2	15	30*10	1e-3	3e-11/1e-5	1	1e-13	150
3	10	30*?10	3e-3	1e-13/3e-8	10	3e-15,16	100
other	2 (seis)	100	8e-2?	-	4e3	3e-17	
pend1	5	4	?	3e-17/1e-9	4e5	1e-17	
pend2	3	10	?	1e-17/1e-9	2e6	3e-18	
pend3	2	25	?	3e-18/1e-9	1e8	1e-19	

14

STACK HIERARCHY

Combining needs for Isolation, Alignment & Damping.

Use active stages from ground in until limited by seismometer noise.

Use pendula from suspended optics outward. If violin mode frequency is a constraint (e.g. keep above 2 kHz) and keep stress low → minimum pendulum frequency ≳ 2 Hz.

Spread natural frequencies for robust identification and estimation.

Increase natural frequencies away from optics to allow large authority actuation at the stages near ground to provide inner damping and alignment

Point design at 10 Hz → 100 for pendula so vertical coupling not a design driver for the pendula.

Minimise control authority near optic - minimize dynamic range and potential for disturbance. Larger authority in active stages must provide damping and alignment.

"other" supplied by - improved seismometer performance
- selection of seismometer resonance zeros.
- lower pendula ω_n separation will require
  - more sensors on pendula for damping
  - anisoelastic vertical coupling reduction

13

The Initial LIGO Suspension and Isolation

Seiji Kawamura
(LIGO, Caltech)

Aspen Winter Conference

Jan. 26 - Feb. 2, 1997

Mechanical System of LIGO Suspension

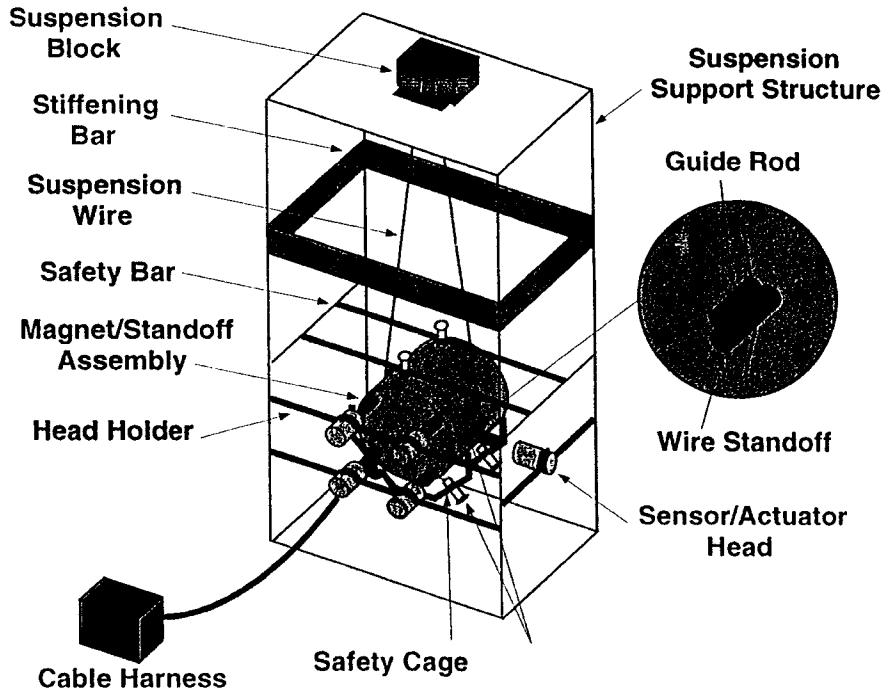

Balancing Test Mass with Single Loop Wire

- Test Mass: balanced within 0.3 mrad.
- Q: OK with attachments

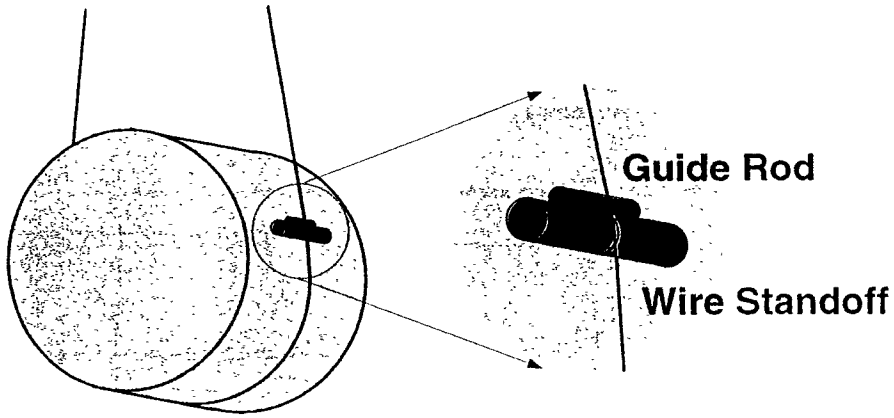

Screening of Wire Material

Wire[a]	Clamp[b]	Tension (N)	Measured Q	Yield Tension (N)	Extrapolated Q for LIGO Suspension[c]
Steel Music Wire	H, S	10 - 34	17,000 - 40,000	90	200,000
Invar	H, S	3.5 - 11	28,000 - 91,000	21	140,000
Tungsten	H, S, T	13 - 32	10,000 - 40,000	100	130,000
Niobium	S	3.6	25,000 - 31,000	10	65,000
Molybdenum	S	6 - 14	14,000 - 14,500	30	59,000
	A	1	900 - 1,600	N/A	N/A
Tantalum	S	1.3	15,000	8	46,000
Titanium	H, T	4 - 10	20,000 - 43,000	8	22,000
Beryllium Copper	S	4 - 5	1,000 - 11,000	12	20,000
Aluminum	Too weak to test			3	N/A

a.l = 10 cm, ϕ = 0.25 mm except steel music wire (ϕ = 0.30 mm)
b.H: Hardened steel, S: Stainless steel, T: Titanium, A: Aluminum
c.Diameter of wire is chosen to give half yield tension for the LIGO test mass (10.7 kg).

Sensor and Actuator

- Resonant frequency of the magnet/standoff assembly: ~8 kHz
- Q: OK with attachments

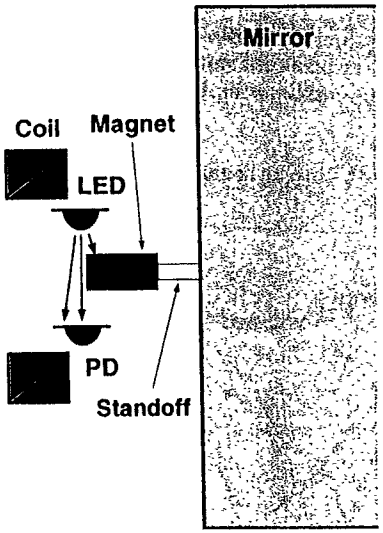

Requirements (Large Optics Suspension)

Item		*Requirements*
Actuator Range	Displacement	> 40 μm_{pp} (f < 0.15 Hz)
	Orientation	> 2 $mrad_{pp}$ (f < 0.15 Hz)
Actuator Noise		$> 5 \times 10^{-20} \times \left(\frac{40\text{Hz}}{f}\right) \text{m}/\sqrt{\text{Hz}}$
Mechanical Loss	Internal Mode	$< 4 \times 10^{-7}$
	Pendulum	$< 7 \times 10^{-6}$
	Eddy Current	$< 6 \times 10^{-9}$ at 0.74 Hz
Resonance of Support Structure	Frequency	160 Hz
	Q	< 300

FIBER PENDULA — PUSHING LIMITS

violin works

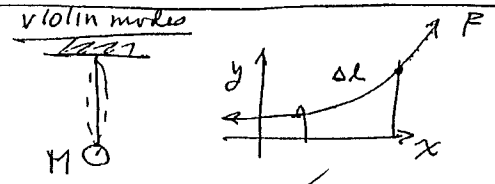

$F = Mg$

$F = Sa$

$(\cancel{A}\, a\rho)\ddot{y} = F y'' \cancel{\Delta x}$

$y = XT \rightarrow \frac{\ddot{T}}{T} = \frac{F}{a\rho}\frac{X''}{X} = -\omega^2$

$\ddot{T} + \omega^2 T = 0 \rightarrow \omega$ is natural frequency

$X'' + \frac{\omega^2 \rho A}{S A} X \rightarrow X = A\cos\lambda x + B\sin\lambda x$

$\lambda^2 = \frac{\omega^2 \rho}{S}$ $\quad X = 0$ $\quad x = 0,\ x = L$

$\downarrow \quad A = 0 \quad \downarrow$

$\lambda L = n\pi$

$n = 1 \quad \omega\sqrt{\frac{\rho}{S}}L = \sqrt{\pi}$ $\quad \boxed{\omega_v = \frac{1}{L}\sqrt{\frac{\pi S}{\rho}}} \Rightarrow S = \frac{\omega_v^2 L^2 \rho}{\pi}$

Pendulum $\quad \omega_p^2 = g/L \rightarrow L = g/\omega_p^2$

STRESS $\quad \boxed{S = \frac{\rho g^2}{\pi}\frac{\omega_v^2}{\omega_p^4}} \Rightarrow \left[\frac{M}{L^3}\ \frac{L^2}{T^4}\ T^2\right] = \left[\left(\frac{ML}{T^2}\right)\frac{T^2}{L^2}\right] = \left[\frac{F}{L^2}\right]$ OK

example $\quad \rho = 3000\ kg/m^3$

$g = 10\ m/sec^2$

$\omega_v = 3\ kHz = 2^{14}\ r/s$

$\omega_p = 1\ Hz = 6^{10}\ r/s$

$S = \frac{3^3 1^3}{3}\frac{4^{18}}{1^3} = 4^{10}\ Pa$

$S = 4^{10}\ Pa = 4^{15} At = 6^{16}\ psi \rightarrow$ beyond realization

change $\omega_p \rightarrow 3\ Hz \rightarrow \frac{g}{\omega^2} = 60{,}000\ psi$

S/E as driver for minimum ω_n

All mechanical springs, low ω_n → large size → high stress here are two examples

Ex1 Compression spring

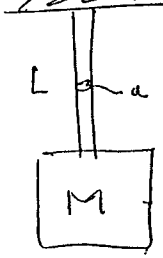

$k = \frac{Ea}{L}$

$Mg = F = Sa$

$k/M = \frac{E a g}{L S a} = \left(\frac{E}{S}\right)\left(\frac{g}{L}\right)$

$\boxed{\omega_n^2 = \left(\frac{E}{S}\right)\left(\frac{g}{L}\right)}$ $\quad \boxed{\left(\frac{S}{E}\right) = \frac{g/L}{\omega_n^2}}$

BENDING SPRING

Ex2

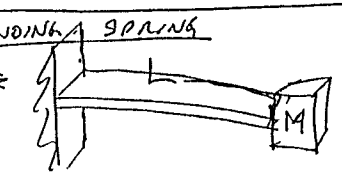

$k = \frac{P}{\frac{PL^3}{3EI}} = \frac{3EI}{L^3}$

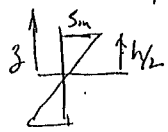

$S = \frac{2 S_m z}{h}$ $\quad T = MgL = \int (S b\, dz\, z)$

$= \frac{2bS_m}{h}\int_{-h/2}^{h/2} dz\, z^2 = \frac{4bS_m}{3h}\left(\frac{h^3}{8}\right) = \frac{bh^2 S_m}{6}$

$\cancel{S_m = \frac{6Mgl}{6h^2}}$ $\quad M = \frac{bh^2 S_m}{6gL}$

$\frac{k}{M} = \frac{3E\,\cancel{b}\,\cancel{h^3}\,\cancel{g}\,\cancel{L}}{\cancel{2}\,L^{\cancel{2}}\,\cancel{b}\,\cancel{h^2}\,S_m}\ \frac{3}{2}\left(\frac{E}{S_m}\right)\frac{gh}{L^2} \rightarrow \boxed{\left(\frac{S}{E}\right) = \frac{3}{2}\left(\frac{gh}{L^2}\right)\frac{1}{\omega_n^2}}$

LOW ω_n RESULTS IN HIGH STRESS

Design 1996 Oct 3rd

DISSIPATION → POWER OUT

$$m\ddot{x} = -b\dot{x} - kx + F$$

$$\text{Power} = F \cdot v = F \cdot \dot{x}$$

$$\underbrace{m\ddot{x}\dot{x}}_{\approx 0} = \underbrace{-b\dot{x}^2}_{\text{POWER OUT}} \underbrace{-kx\dot{x}}_{\approx 0} + [(F\dot{x}) = \text{Power IN}]$$

Power Released when a structure CREEPS

CAN BE THE SOURCE OF EXCITATION OF DISTURBING MOTION

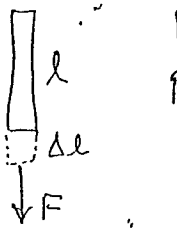

$$F = mg$$

$$\text{Power} = F\dot{\Delta l} = F\frac{\Delta l}{\Delta t} = F\left(\frac{\Delta l/l}{\Delta t}\right)l$$

$$= Fl\left(\frac{\Delta l/l}{\Delta t}\right)$$

STRAIN RATE

COUPLING = C

$$\frac{b}{m} = 2\zeta\omega_n \Rightarrow \qquad b\dot{x}^2 = c(mg)l\left(\frac{\Delta l/l}{\Delta t}\right)$$

$$\left(\frac{\Delta l/l}{\Delta t}\right) < \frac{\left(\frac{b}{m}\langle\dot{x}^2\rangle\right)BW}{cgl}$$

Numerically

$$\frac{b}{m} = 2(0.1)(6\text{ r/sec}) \sim 1\text{ r/sec}, \quad \langle\dot{x}^2\rangle < (\omega_h L)^2 = (2\pi\cdot 10^{-8})^2 = 6^{-34}\ \text{m}^2/\text{sec}^2\text{Hz}$$

$$c = 10^{-6}, \quad gl \sim 1\ \text{m}^2/\text{sec}^2, \quad BW = 10^3\text{Hz}.$$

$$\left(\frac{\Delta l/l}{\Delta t}\right) < \frac{1}{10^{-6}}6^{-34}10^3 = 6^{-25}\ \frac{\text{strain}}{\text{sec}} = 6^{-25}\pi^{17} = 18^{-18} = 2^{-17}\ \frac{\text{strain}}{\text{year}}$$

To: ddebra@sun-valley.Stanford.EDU
From: "Robert S. Polvani" <Robert.Polvani@nist.gov>
Subject: CREEP NOISE
Cc: cjevans@enh.nist.gov

Dan,

If you are serious about strain resistance below 1e-17 per year, I think you have a problem.

Yes, years ago we and Draper were working together to measure microcreep, ONR supported us. To me the definitive result was that the stock, itself, was dimensionally instable at the > 1 e-6 strain per year level, despite best fabrication practice. Dimensional instability is the part strain that occurs without an external applied loading. Notably, we focused on I400 grade, the highest strength Be. Draper continued making measurements, but using a method that involved unloading and reloading the specimen each time a strain reading was taken. This made the task very practical, but introduces a serious error from the load cycling. Even they were divided about the utility of their results.

At NIST we are still making dimensional instability measurements on a small assortment of engineering construction materials ranging from 6061 aluminum onto Reaction Bonded and CVD silicon carbides. The "parts" were fabricated to recognized "best stability" specifications. We are fully confident of our practice, but here again we see monotonic strains that are more than 1 e-7 per year even in the ceramics. The experiment has run for 4-5 years now. The problem seems to be an instability of the "bulk" material itself. Some steadily grow and others shrink. We independently tried to filter out a surface fabrication contribution to the instability, but could find none. Steel gauge block have this same problem, which is traceable to very small retained austenite concentrations.

If necessary, I could dig out some of that old Be work, but if you really mean strains of 1 e-17 per year, I question the utility. Could we talk about your problem, especially your choices of construction material, beforehand? Where does thermal instability fit into this situation?

You clearly have an interesting situation, but I would hope you could work with far more strain instability. You can reach me here or at (301) 975-3487 on the telephone.

Bob

→ BASED ON - NIST Experience with creep - The DeSalvo work - The Braginsky group results on excess noise - creep and its implied driver of acceptably low stress must be considered in the choice of natural frequency of spring-mass systems.

THERMAL NOISE

$$\langle v \rangle^2 = 4 k_B T \, \mathrm{Re}(A(j\omega))$$

example $m\ddot{x} + b\dot{x} + kx = F$

$$\frac{x}{F} = \frac{1}{ms^2+bs+k} \quad A = \frac{\dot{x}}{F} = \frac{s}{ms^2+bs+k}$$

$$\mathrm{Re}\left(A(j\omega)\right) = \frac{b\omega^2}{(k-m\omega^2)^2 + (b\omega)^2} \qquad \omega_n^2 = k/m$$

limiting cases $\omega \longrightarrow 0 \Rightarrow \dfrac{b\omega^2}{k^2}$

$\omega \longrightarrow \infty \Rightarrow \dfrac{b\omega^2}{m^2\omega^4}$

$v = \omega x \;\therefore\; \langle x \rangle^2 = \dfrac{\langle v \rangle^2}{\omega^2} = \dfrac{4 k_B T \, \mathrm{Re}(A(j\omega))}{\omega^2}$

limits

$\dfrac{\omega \to 0}{\omega_n} \quad \langle x \rangle^2 = 4 k_B T \, b / k^2$ ← MIRROR

$\dfrac{\omega \to \infty}{\omega_n} \quad \langle x \rangle^2 = 4 k_B T \, b / m^2 \omega^4$ ← PEND $\times (\omega_n^2/\omega^2)$ .... MIRROR BAR MODES

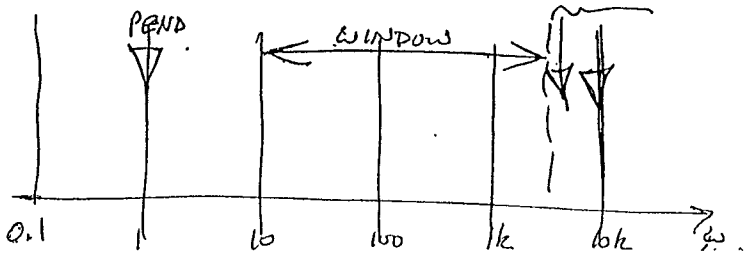

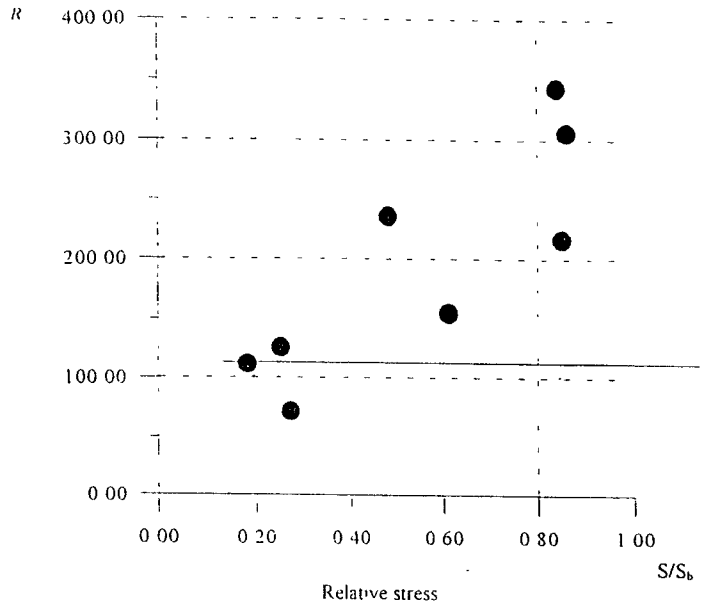

Figure 4
The dependence of excess peak rate R on the stress value The peaks with the amplitude 3 times higher then the *rms* value are counted Solid line is theoretical prediction for the thermal noise

Ageev et al 1997 Ph Letters A

LIGO Science h Requirement• 4000 m = Displacement Noise Requirement

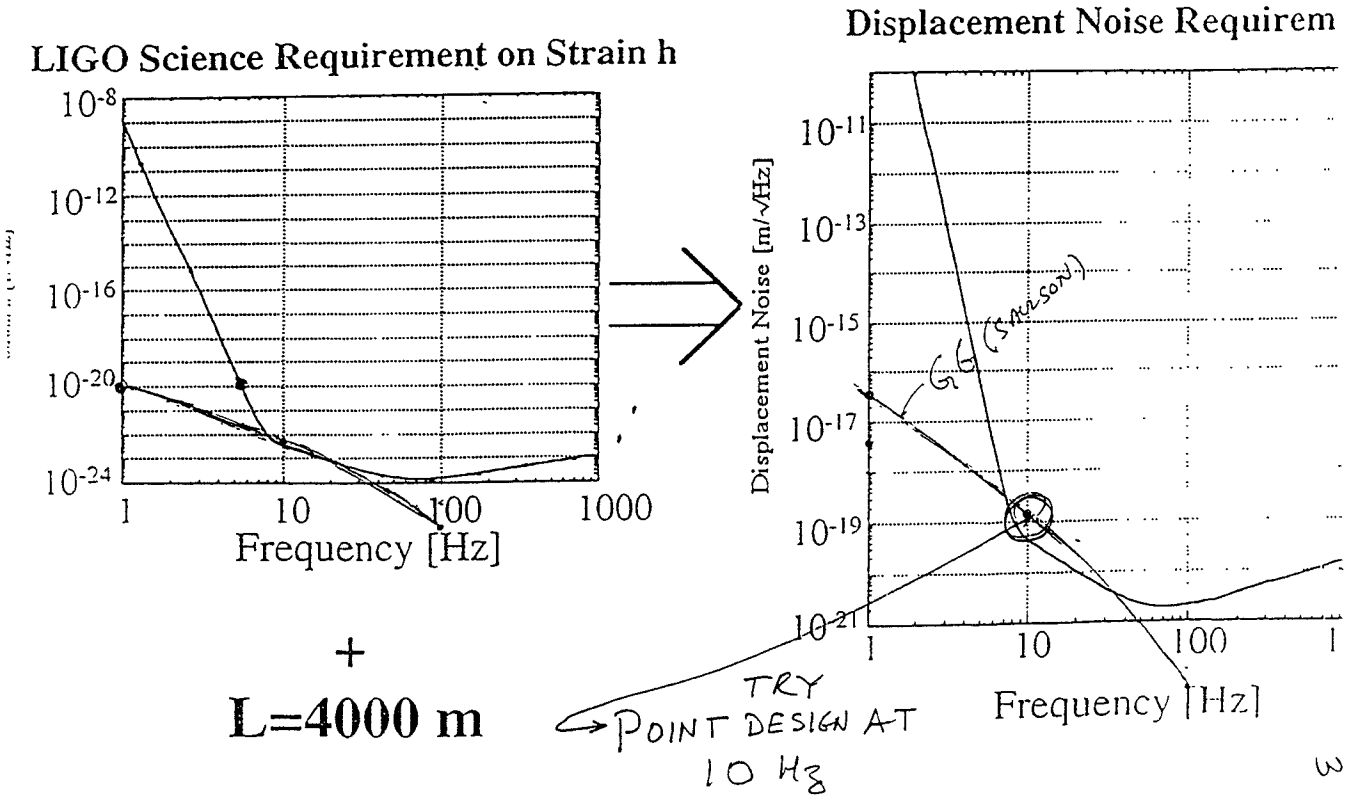

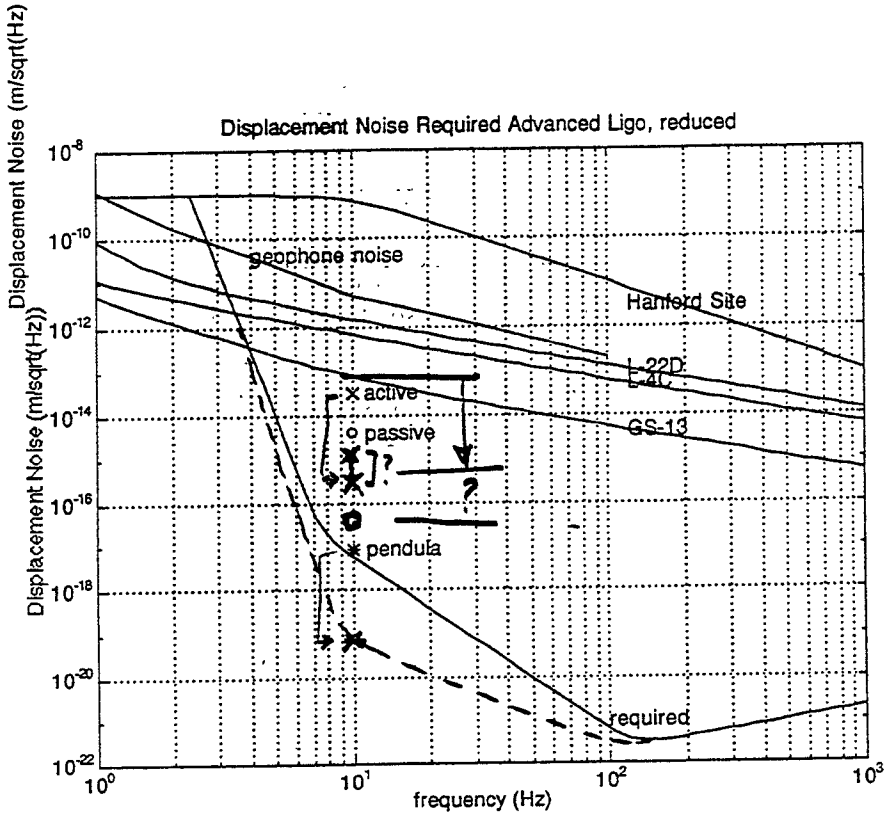

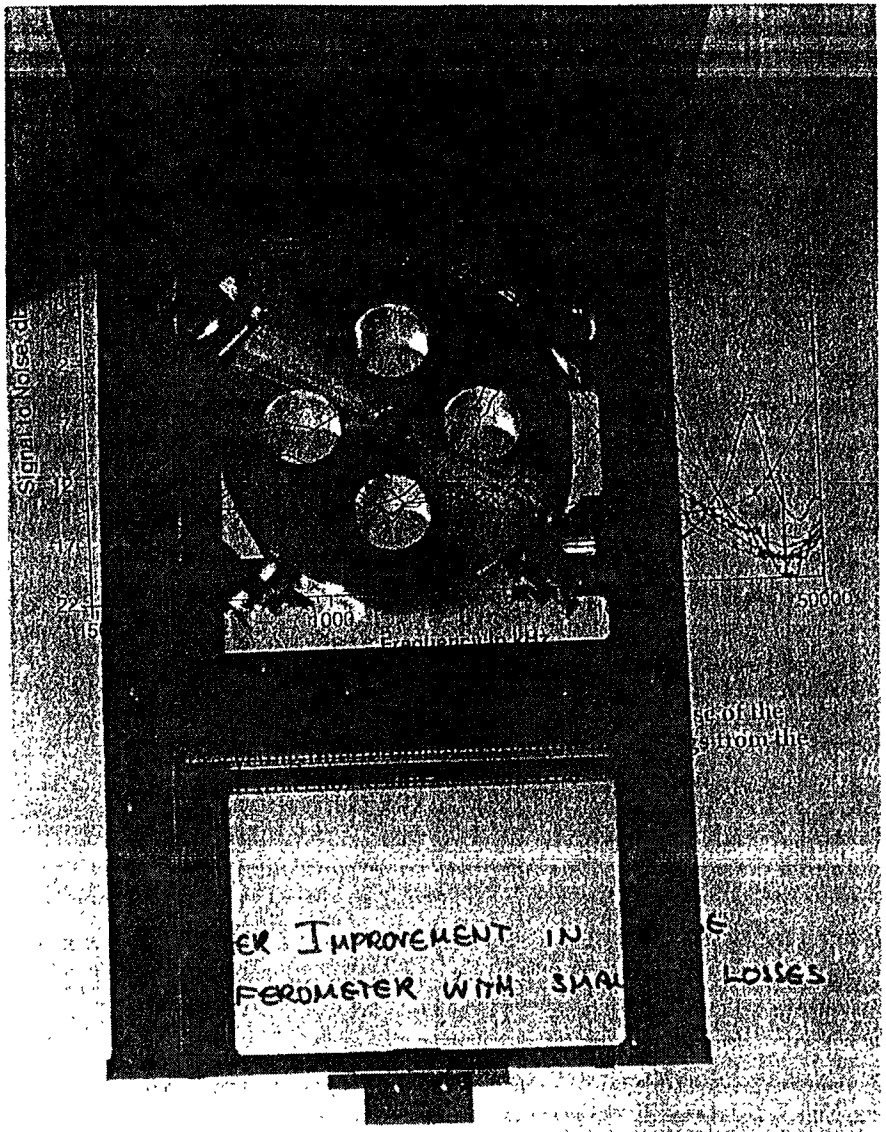
ER IMPROVEMENT IN
FERROMETER WITH SHA
LOSSES

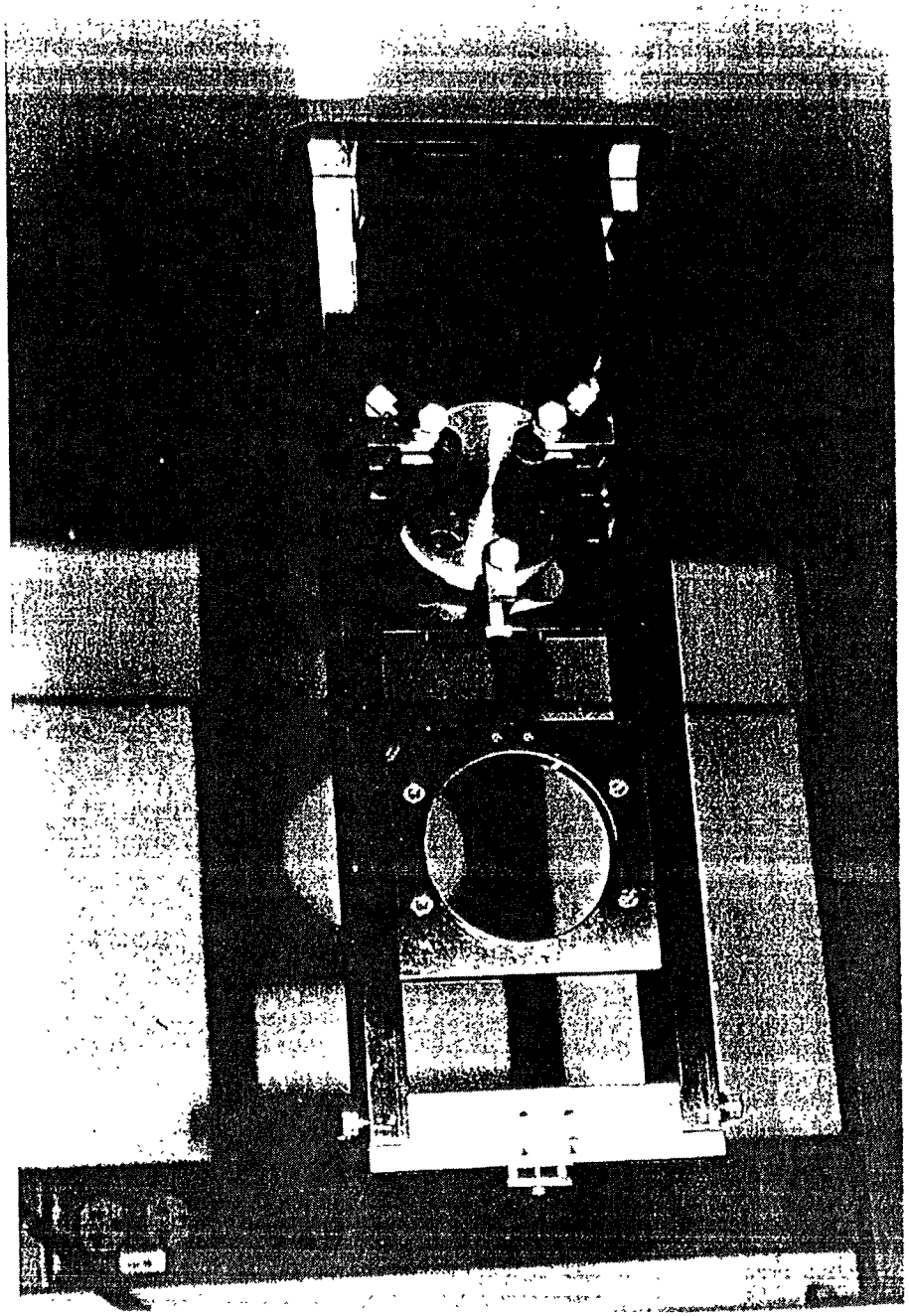

IMPROVEMENT WITH RESPECT TO A SIMPLE MICHELSON

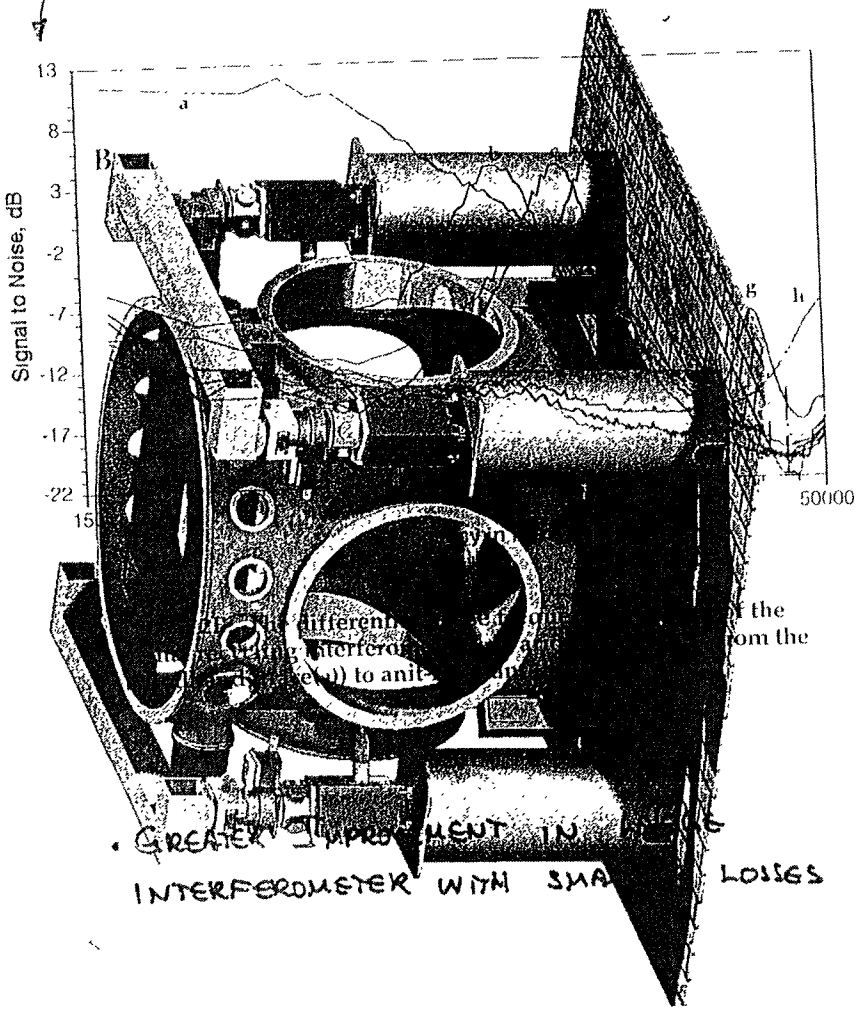

• GREATER IMPROVEMENT IN
INTERFEROMETER WITH SMA LOSSES

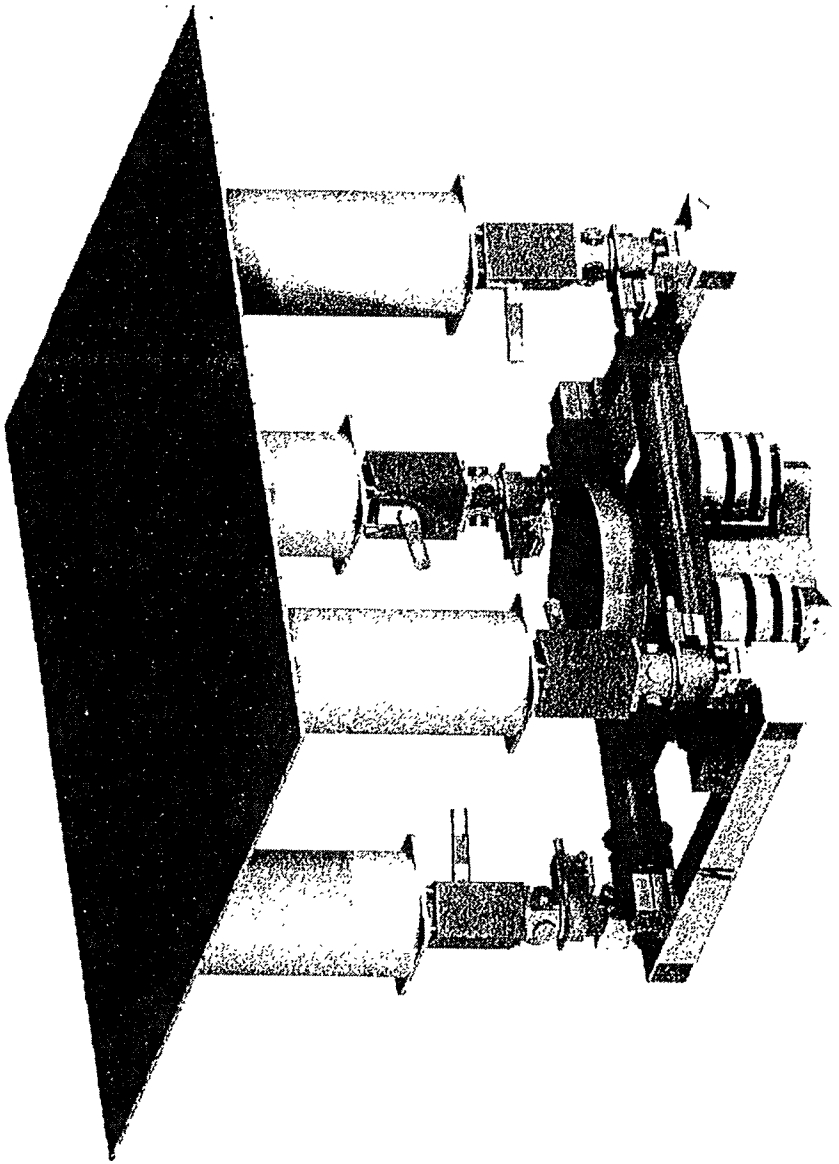

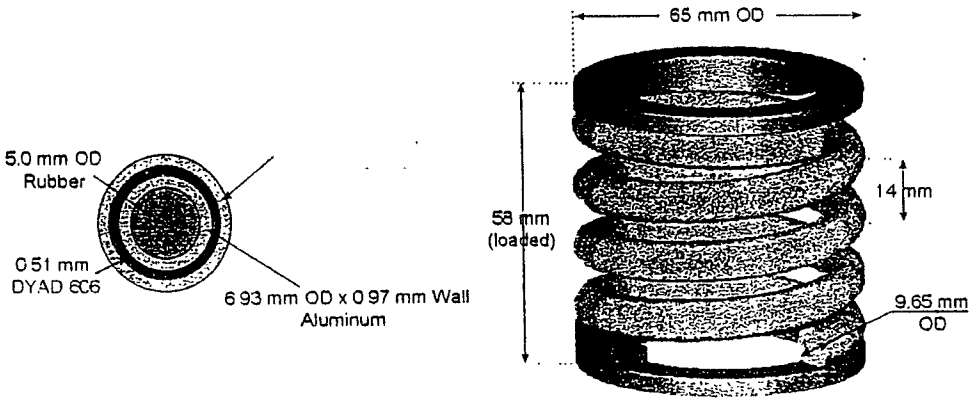
65 mm OD
5.0 mm OD
Rubber
0.51 mm
DYAD 606
6.93 mm OD x 0.97 mm Wall
Aluminum
58 mm
(loaded)
14 mm
9.65 mm
OD

Advanced LIGO detector:

Suspensions and seismic isolation

Gabriela Gonzalez
LIGO - MIT
January 28, 1997

Initial and Advanced ("Enhanced") Detectors

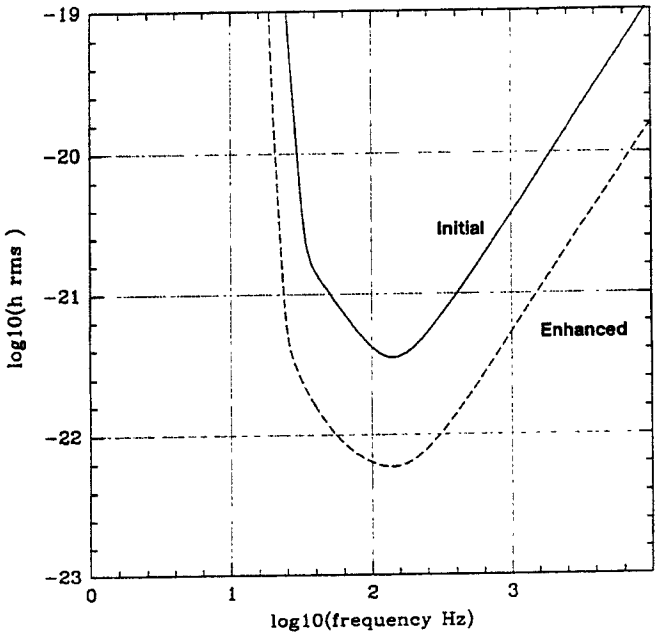

Initial LIGO Detector

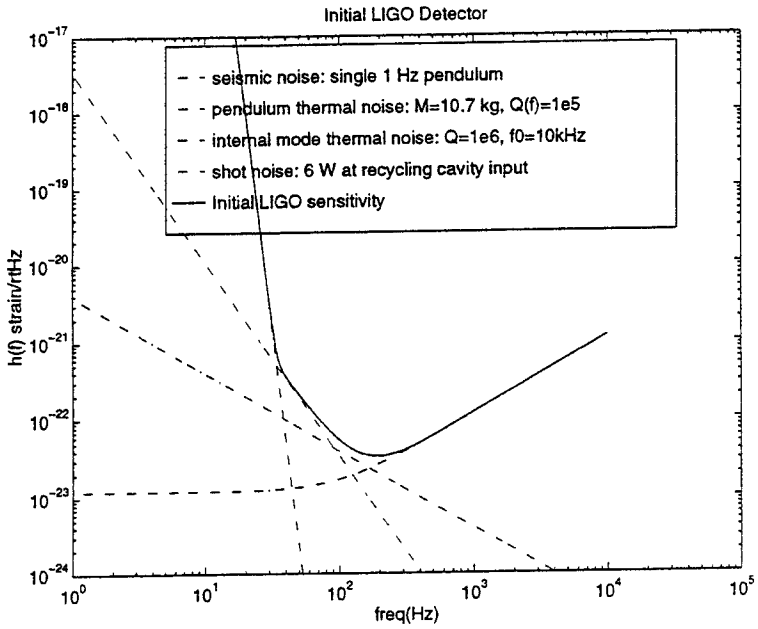

Seismic Noise at the Sites

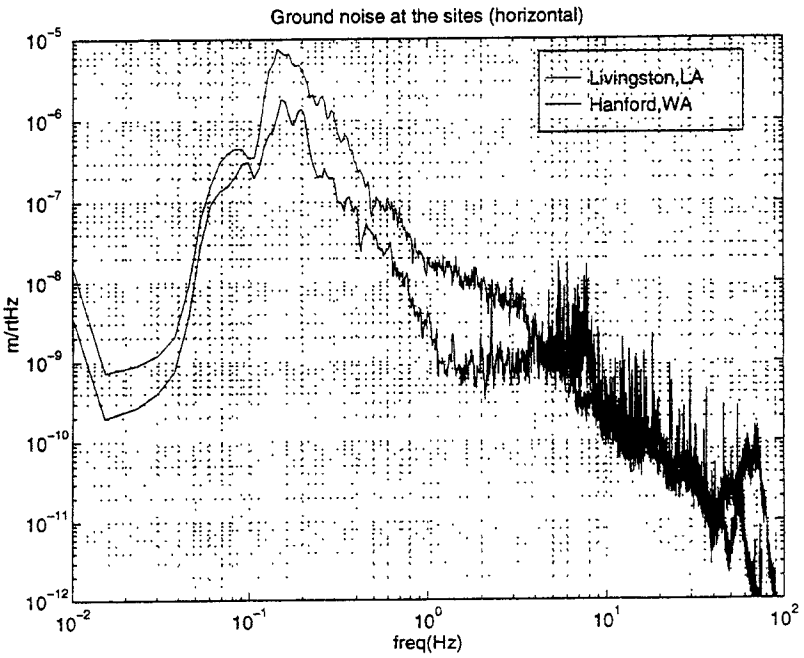

Seismic Noise at the Sites

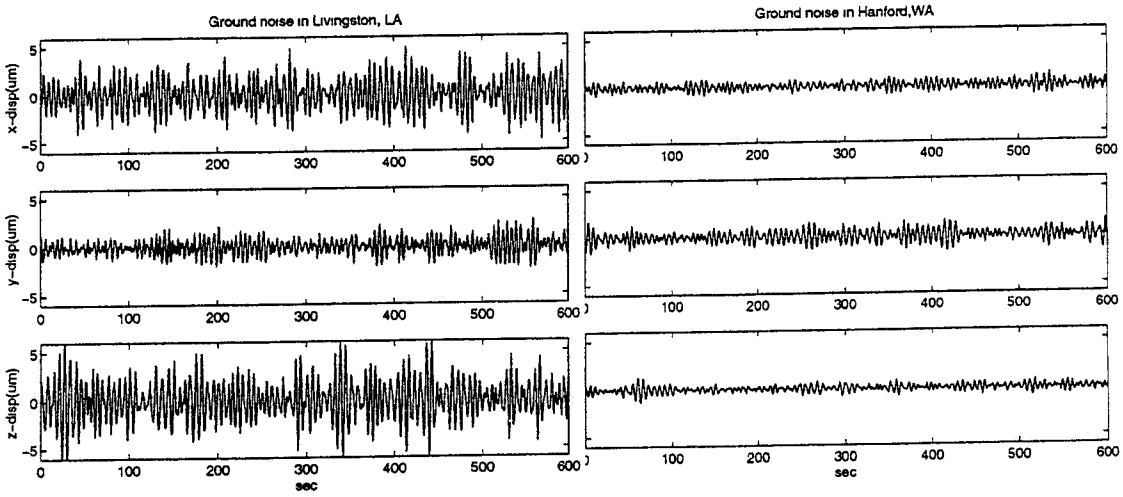

Initial LIGO Goal vs. Seismic Noise

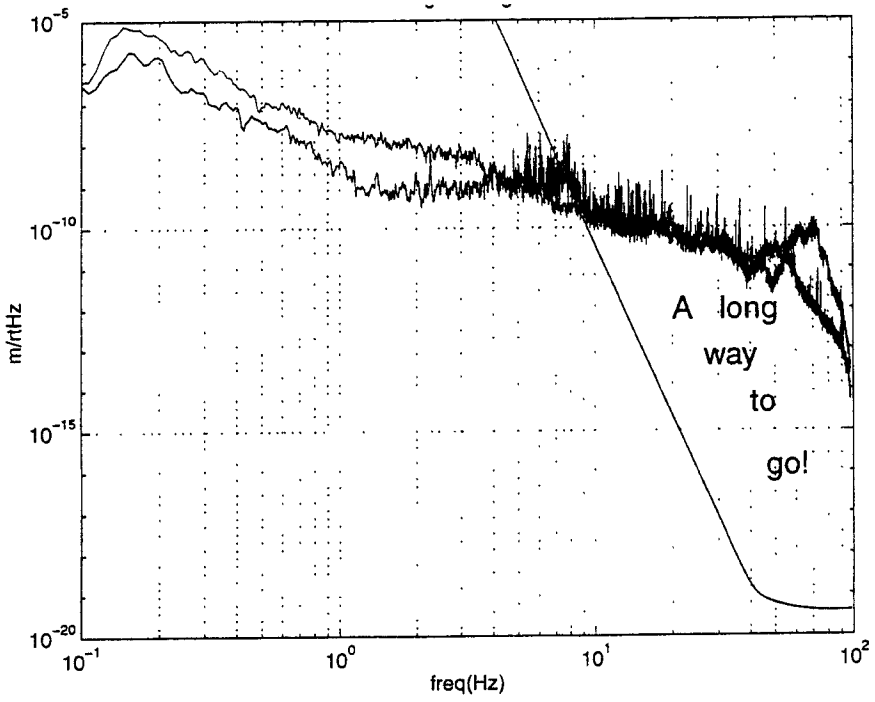

Use a single pendulum...

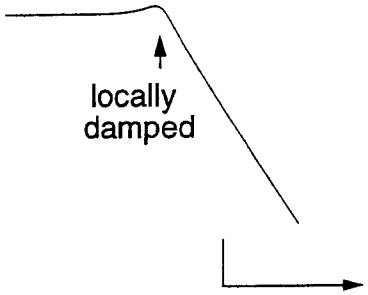

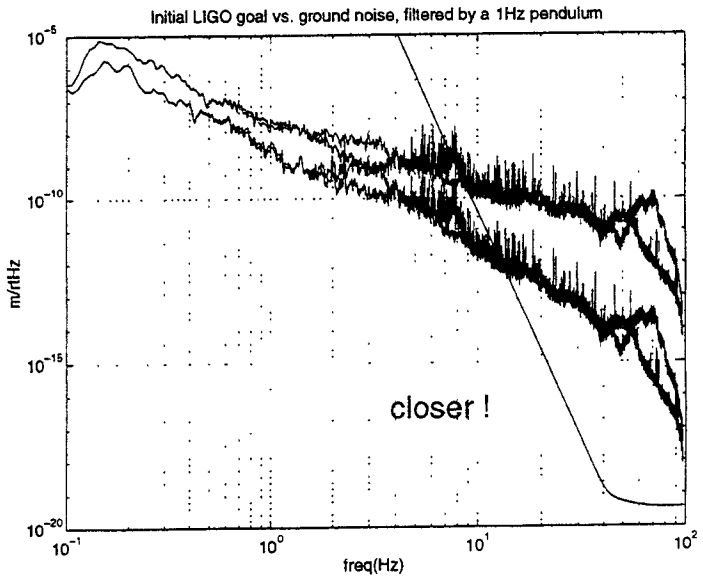

Add (a lot of) seismic isolation:

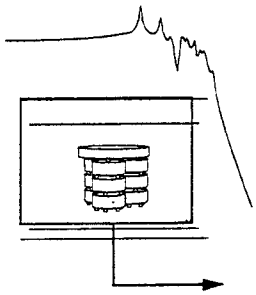

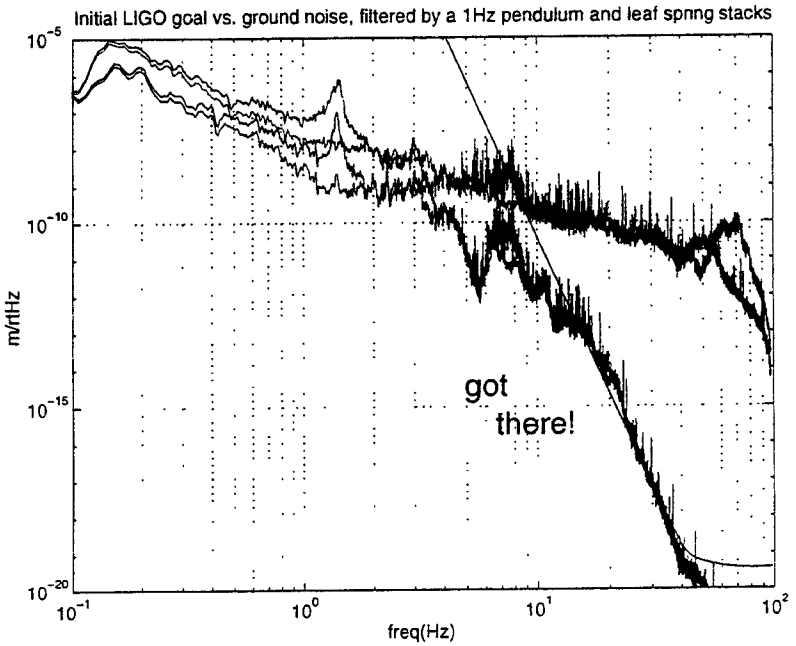

BUT...

The free mirrors still move too much: the interferometer needs to be locked, and the residual rms motion has to be controlled by the "length sensing servos".

a whole fringe! →

desired residual rms →

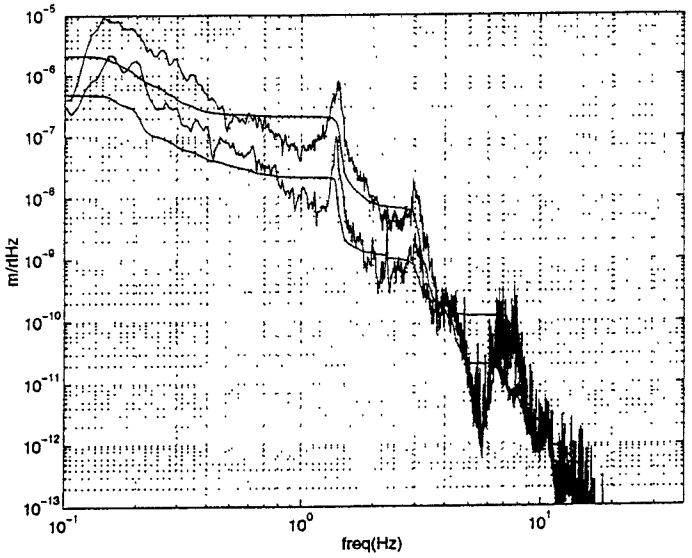

Advanced Detector: how to do better

with more power

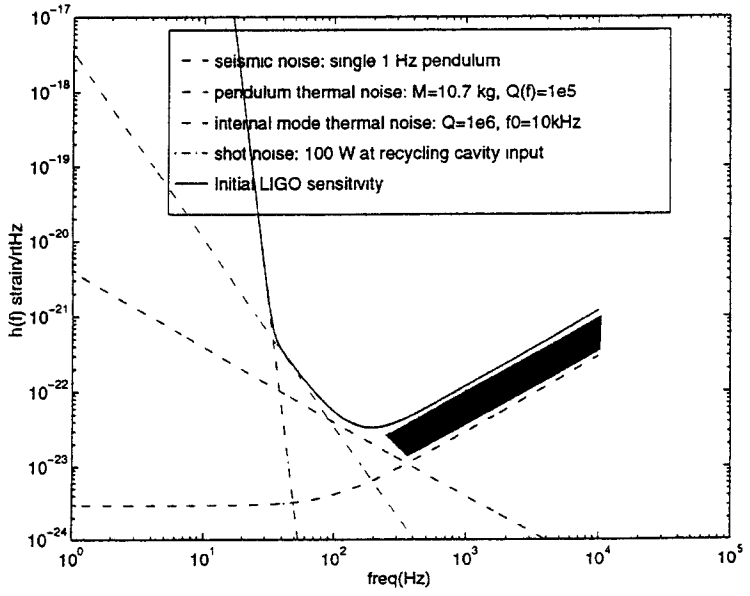

Advanced Detector: how to do even better

better Qs,
improved isolation
(double pendulum)

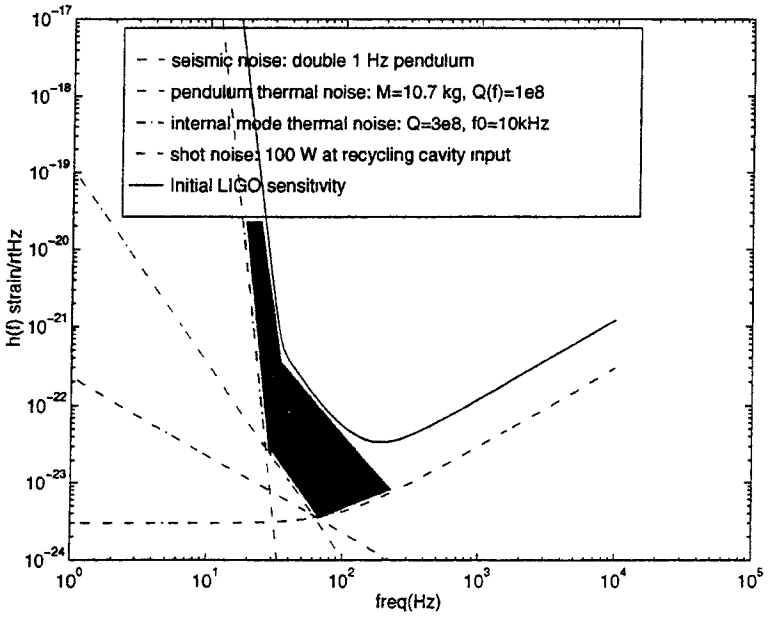

Double Pendulum

>>A double pendulum provides

—more seismic isolation=>a broader detection band

—easier requirements on the servos => servos with less noise

—no magnets on the mass => makes it easier to achieve high Qs, masses less sensitive to magnetic fields.

>>We require on the suspensions

—the ability to be used with length and alignment servos that guarantee lock stability and small residual motion

—local damping servos that guarantee lock acquisition

—violin modes resonances?

—angular thermal noise?

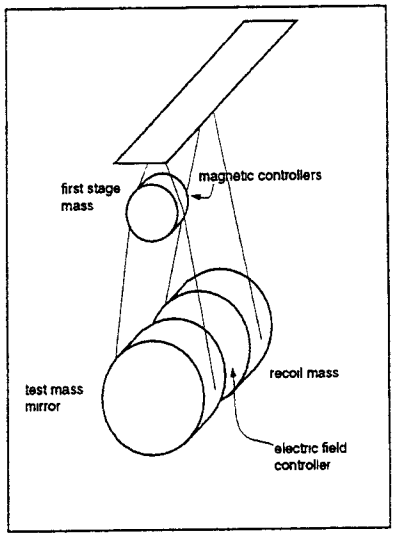

Improved Seismic isolation

An "improved" seismic isolation means

—better (more) isolation => broadens the detection band

AND/OR

—better isolation at low frequencies=> makes lock acquisition, stability easier to get: highly desired!.

The first can probably be done with different springs.

The latter can be achieved with ACTIVE seismic isolation.

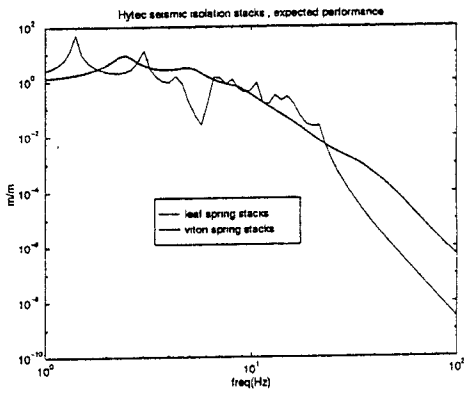

Conclusions

Advanced R&D in LIGO focuses on

- ››vibration noise:
  - —passive isolators;
  - —active feedback control isolation;
  - —multiple suspensions systems.
- ››thermal noise:
  - —high-Q materials and fixtures
  - —electrostatic test mass control
- ››Shot noise, other interferometer configurations.

The program starts in 1997, and it is expected to be done in collaboration with other groups.

Wednesday AM LIGO Research Community(LRC)
January 29 Chair: S. Finn

8:00	J. Munch(Adelaide)	ACIGA Prototype and Activities
8:30	Discussion	
8:45	D. Berley(NSF)	The View From NSF
9:15	Discussion	
9:30	Coffee Break	
9:45	Meeting of LIGO Research Community and Discussion	
1:30	Meeting of LIGO Research Community(continued)	

AUSTRALIAN CONSORTIUM FOR INTERFEROMETRIC GRAVITATIONAL ASTRONOMY (ACIGA)

J. SANDEMAN, ANU
DIRECTOR

D. BLAIR, UWA	J. MUNCH, UA	D. McCLELLAND, ANU
SUSPENSION SAPPHIRE	LASERS DIFFRACTIVE OPTICS	RECYCLING INJECTION LOCKING NOISE

IN COLLABORATION WITH CSIRO, INDUSTRY

ACIGA PARTICIPANTS

- J. SANDEMAN, DIRECTOR
- ANU
  McClelland, Gray, Harb, Huntington, Ralph, Bachor, Sandeman
- UA
  Munch, Veitch, Hamilton, Mudge, OHaway, Tikhomirov
- UWA
  Blair, Nottcut, Ju Li, Tobar, Yang, Eng, Taylor, Winterflood, Liu, Taniwaki, Zhao

Contents

1. ACIGA Plans

2. Recent Results

ANU
UWA
UA

ACIGA Aims, 1997

Australian Participation in Grav. Wave Interferometry

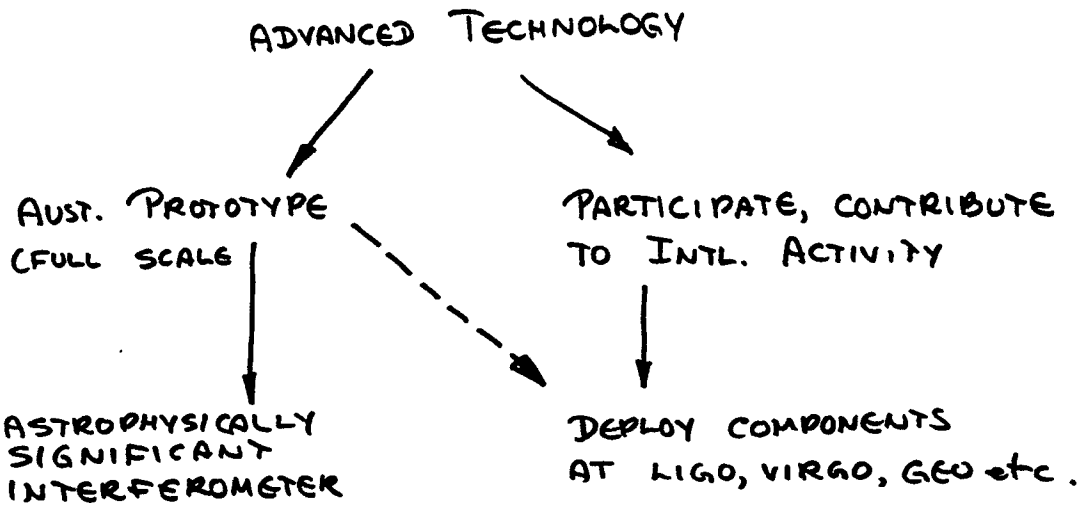

ACIGA PLANS

- CONTINUING ADVANCED TECHNOLOGY DEVELOPMENT WITH STRONG INTERNAL COLLABORATIONS
- DEVELOP STRONG COLLABORATIONS WITH WORLD COMMUNITY

  eg: SAPPHIRE TECHNOLOGY

  THERMAL NOISE ACIGA/VIRGO COLLABORATIONS

  LIGO TECHNOLOGY
- PROTOTYPE INTERFEROMETER IN AUSTRALIA

  eg. 10 m EXTENDABLE

ACIGA / VIRGO
COLLABORATION ON THERMAL NOISE

PROBLEM

- THERMAL NOISE AT LOW FREQUENCIES LIMIT SENSITIVITY OF PRESENT INTERFEROMETERS
- THERMAL NOISE PRESENTLY INFERRED BY

  – MEASURE Q

  ↓

  FLUCTUATION DISSIPATION THEOREM

  +

  ASSUMED KNOWLEDGE OF DISSIPATION MECHANISMS

  ↓

  [illegible] BELOW RESONANCE

ACIGA / VIRGO
COLLABORATION ON THERMAL NOISE
(VIRGO NOTE OCT 1996)

AIM : DIRECT MEASUREMENT OF RESIDUAL THERMAL NOISE IN SUPER ATTENUATOR AS FUNCTION OF FREQUENCY.

- PERMIT DIRECT COMPARISONS OF VARIOUS SUSPENSION CONFIGURATIONS AND TEST MASS MATERIALS
- LASER FREQUENCY LIMITED BY NOISE IN REFERENCE F.P.

$$\delta\nu = \frac{\nu_0}{L_0}\,\delta x_{thermal}$$

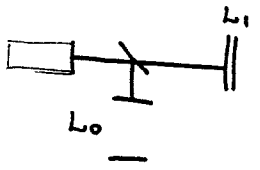

- $\therefore \frac{\delta l_1}{L_1} = \frac{\delta\nu}{\nu_0} = \frac{\delta x_{th}}{L_0}$

$$\therefore \boxed{\delta l_1 = \frac{L_1}{L_0}\,\delta x_{th}}$$

EXPERIMENT PARAMETERS

- $\Delta L_1(\text{SHOT}) = L_1\frac{\Delta\nu}{\nu} = \frac{L_1}{L_0}\frac{c}{2F_0}\frac{1}{J_0(\beta)}\sqrt{\frac{h}{8\eta\nu P_{in}}} = \frac{10^{-16}L_1}{L_0F_0}$

  ($\lambda = 1\mu m$, $f = 4Hz$, $P_{in} = 1W$, $M = 10kg$)
- DOPPLER EFFECT OF CAVITY 1 → FREQUENCY CHANGE REMOVED BY LOCK
- RAD PRESSURE $\Delta L_{rp} = \frac{F}{k(Mf^2)}\sqrt{h\nu P_{in}} = 3\times10^{-22}F$

  INDEPENDENT OF L
- SHOT NOISE IN READ OUT: $\Delta L_{read} = \frac{c}{2F}\cdot\frac{1}{J_0\beta}\cdot\sqrt{\quad}$

  $= 1\times10^{-16}/F$

FOR $\Delta L_{TOT} < 10^{-18}\,m/\sqrt{Hz}$

$$\boxed{100 < F < 3400\,,\quad \frac{L_0F_0}{L} > 100}$$

Experiment Design

- Develop Diagnostic Experiment to be used both on Virgo Super Attenuator and equilalent ACIGA design
- Short cavity formed by two suspended test masses, coated for specified Finesse
- Control system of SA to control F.P.
- Laser stabilized to long, suspended F.P.
- Length ratio & Finesse chosen for $(\text{Noise Level})_{\text{STABL F.P.}} \ll (\text{Noise Level})_{\text{TEST F.P}}$

Strong Collaboration

ACIGA

- Expertise in
  - Isolation
  - Laser stabilization
  - Interferometry
- Develop Expt. Technique
- Prove on ACIGA SA
- Provide copy for Virgo

Virgo

- Concept
- Expert Consultation
- SA in Pisa
- Reference Cavities

Collaborate at Virgo and Australia on

- Mirror matls
- Test masses
- Suspension systems ...

ACIGA / VIRGO COLLABORATION

- READY TO BEGIN

TABLE TOP EXPTS.

EXPT. CHARACTERIZATION IN ADELAIDE VAC.

COMPLETE UWA SA CONTROL SYSTEM

FULLY SUSPENDED EXPT, UWA

EXPTS IN DISA

ACIGA / VIRGO R&D ON MATLS, SUSPENSION

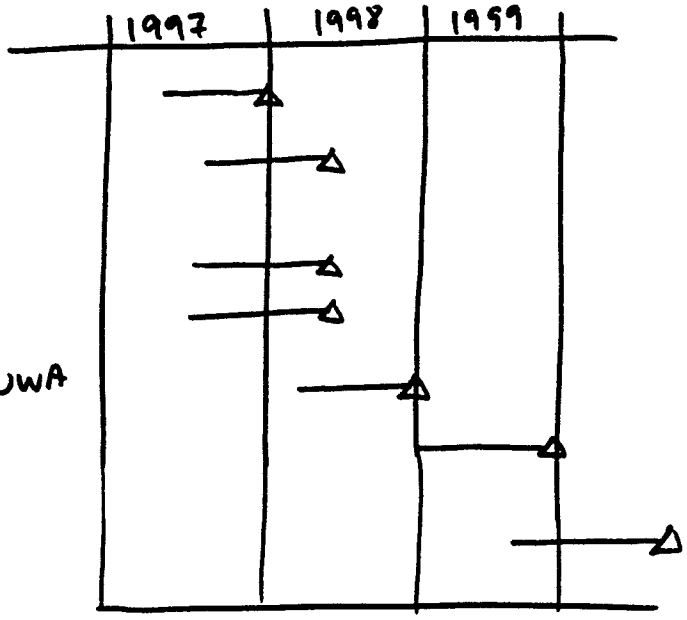

PROTOTYPE INTERFEROMETER

- FULL SIZE SUSPENSION, VACUUM TANKS
- AS LONG AS POSSIBLE (AFFORDABLE) ≥ 10m
- BUILT ON SITE WITH ROOM TO EXPAND (0.6km - 1km OR BEYOND)
  (WA, SA OR PERHAPS ELSEWHERE)
- CREATIVE FINANCING PACKAGE

ARC INFRASTRUCTURE
ARC RESEARCH GRANTS —
UNIVERSITY CONTRIBUTIONS
STATE "
CONTRIBUTIONS FROM OVERSEAS LABS

- UA : LASER, INJECTION OPTICS
- ANU : OUTPUT BENCH, RECYCLING
- UWA : SUSPENSION, TEST MASS, CONTROL

CURRENT RESULTS FROM ACIGA

- SUSPENSION, SAPPHIRE TECHNOLOGY
- LASERS
- "TABLE-TOP" EXPERIMENTS ON
  - injection locking
  - noise suppression
  - recycling

⇓

NEXT STEP : PROTOTYPE INTERFEROMETER

ANU

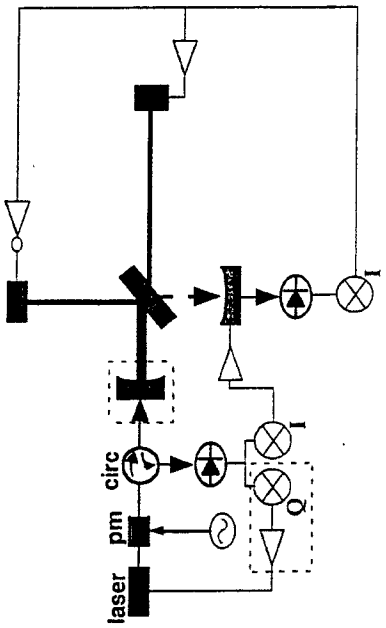

TABLE-TOP DUAL RECYCLED MICHELSON INTERFEROMETER

- SIMPLE (no 3-mirror coupled FPs)
- EASY TO CHANGE FREQUENCY RESPONSE:
  - BROADBAND
  - NARROW BAND

IMPROVEMENT WITH RESPECT TO A SIMPLE MICHELSON

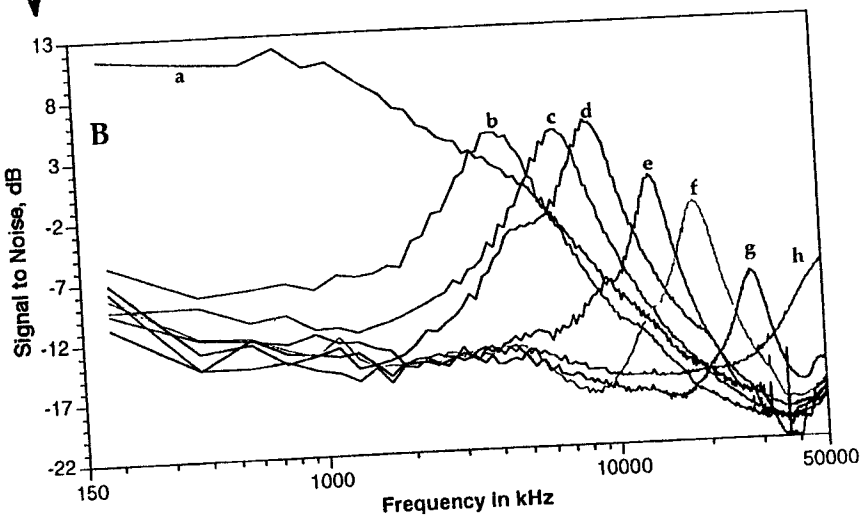

Figure 2B: The differential phase frequency response of the signal recycling interferometer for various detunings from the broadband (trace(a)) to anit-resonant (trace(h)).

- GREATER IMPROVEMENT IN LARGE INTERFEROMETER WITH SMALLER LOSSES

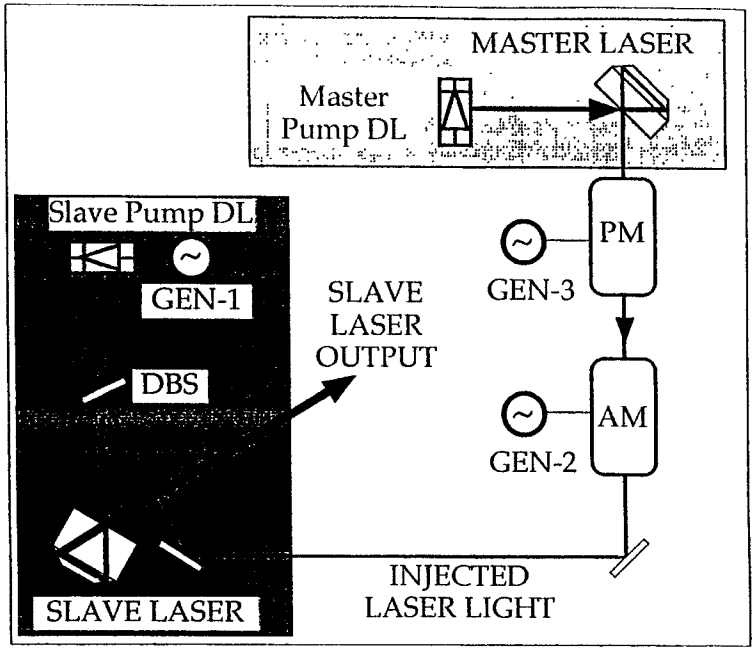

- Schematic diagram showing the basic elements of the injection locking system.
- The abbreviations are:
  - DL := diode laser;
  - AM := amplitude modulator;
  - PM := phase modulator;
  - GEN := sinusoidal signal generator; and
  - DBS := dichroic beamsplitter.

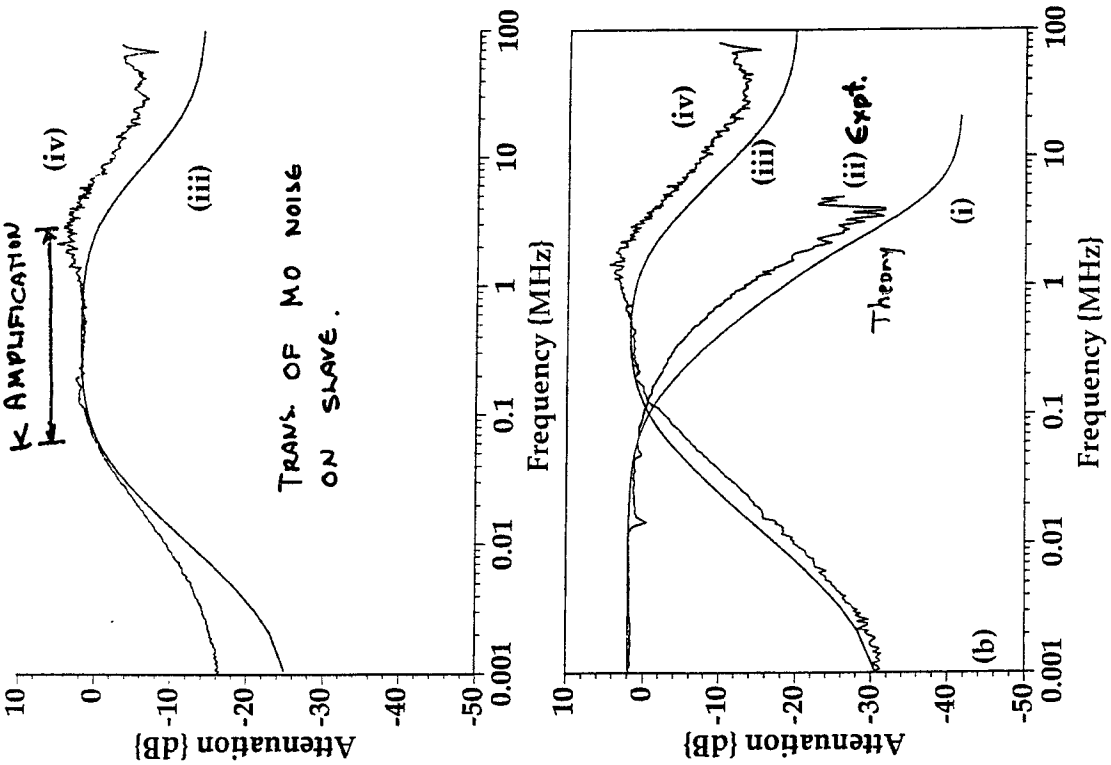

ANU STUDY OF TRANSFER OF NOISE THRU INJECTION LOCKED SYSTEMS

Ralph et. al. Phys Rev A, 1996, p. 4359

Harb et al. " " 1996, p. 4370

SLAVE LASER: LOW PASS FILTER FOR OWN PUMP NOISE

REGION OF AMPLIFICATION OF NOISE FROM MO

UW A Results
Summary

- Sapphire Optics and Test Masses
  - $Q \rightarrow 10^8$ in progress
  - Opt. Abs $\alpha \sim$ 3.5 ppm/cm at 1 μm
    ∴ small thermal lensing
    ($\sim \frac{1}{30}$ silica)
  - Virgo coils: Fabry Perot
    $F \sim 10^5$
  - Niobium cantilever wheel susp.
  - Optical Frqq. Reference
    $\frac{\Delta\nu}{\nu} \sim 10^{-15}$
- Super-Attenuator Research
  - Inverted Pendulum
  - X-Pendulum
  - Conical Pendulum (Scott-Russel Linkage)
  - Folded Pendulum Preisolator
    resonance at 29 mHz
    40db at 7 Hz

THREE-STAGE INJECTION LOCKED LASER

MASTER LASER: 100mW DIODE-PUMPED, Nd:YAG NPRO

$S_v^{1/2}(1\text{kHz}) \sim 20\ \text{Hz}/\sqrt{\text{Hz}}$

$S_{RIN}^{1/2}(1\text{kHz}) \sim 10^{-7}\ /\sqrt{\text{Hz}}$

MEDIUM POWER SLAVE LASER

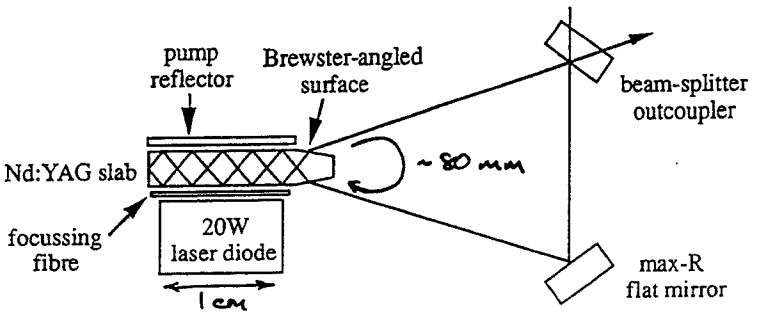

- CONDUCTION COOOLED THROUGH TOP AND BOTTOM FACES

- FREE-RUNNING (20W PUMP):
  THERMAL LENSES: 2.0m (horizontal), 200-250mm (vertical)
  WAISTS: 240μm (horizontal), 190μm (vertical)
  2.6W OF TEM_{00} IN EACH DIRECTION
  $M^2 = 1.1$ (horizontal), $M^2 = 1.15$ (vertical)

Slab Laser Pumping Scheme

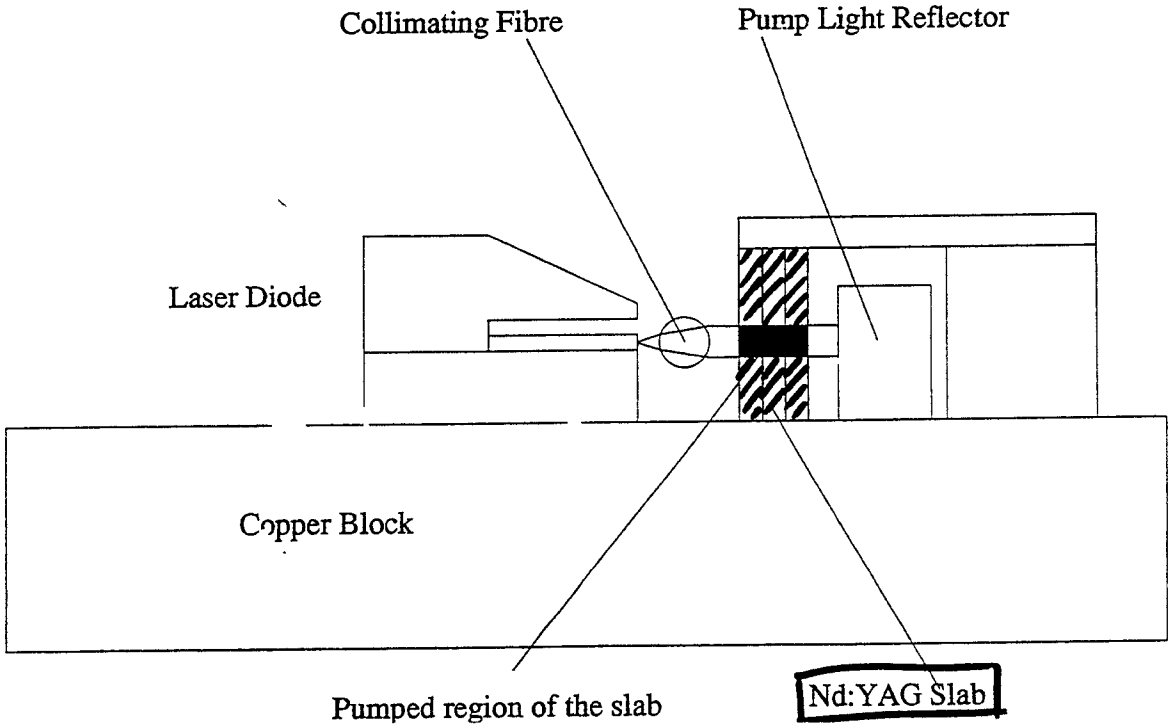

Medium Power Laser Frequency Stability

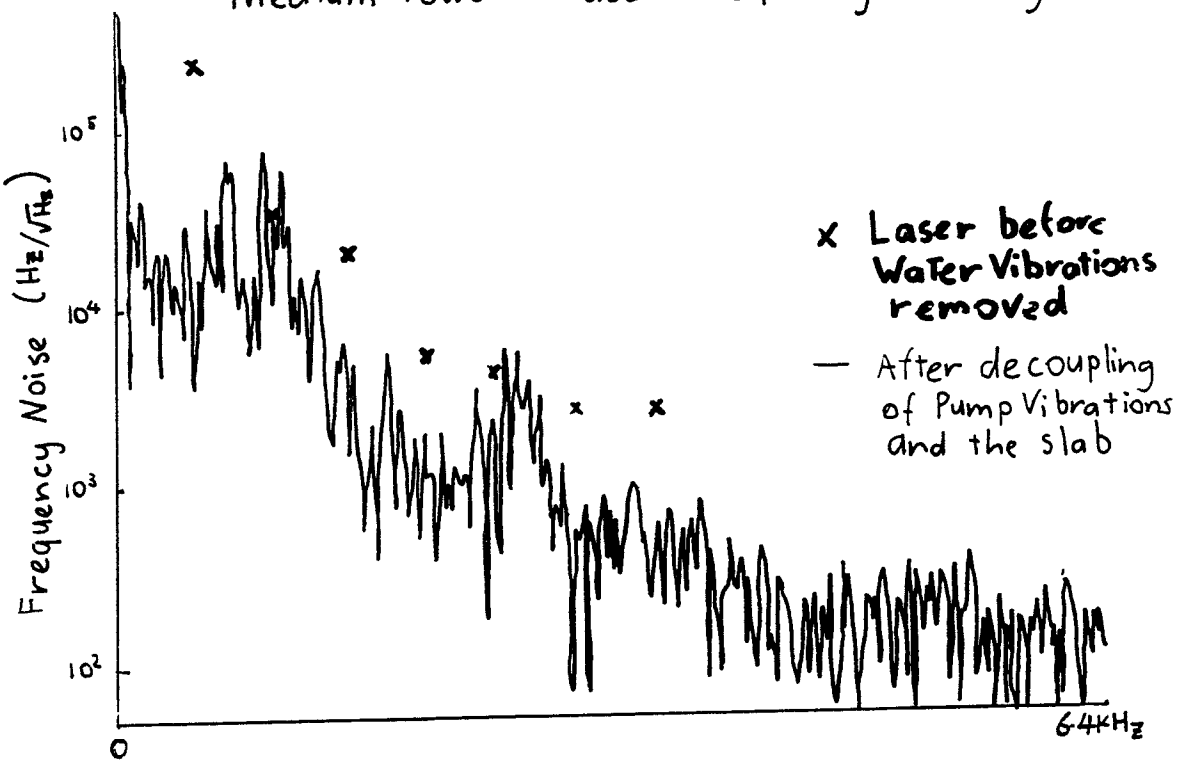

Optical Spectrum – Injection-Locked Slave

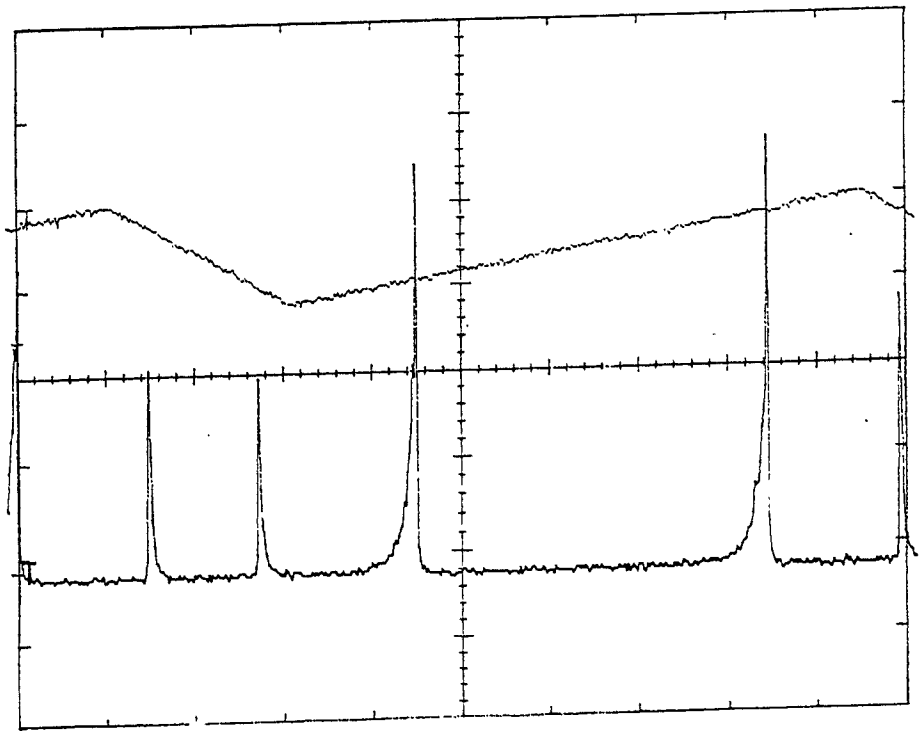

LASER HAS ACHIEVED
REQUIRED INTENSITY NOISE, INJECTION LOCKED

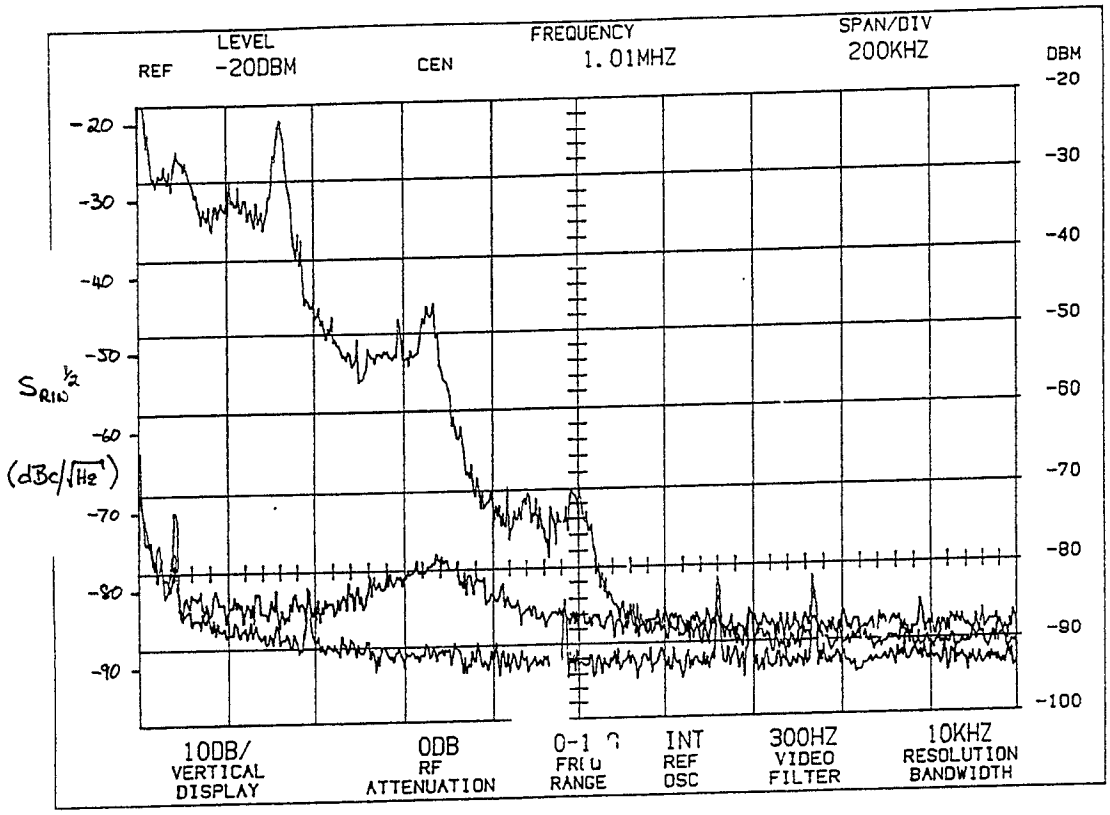

POWER LIMITING FACTORS IN SOLID STATE LASERS

- THERMAL GRADIENTS
- STRESSES
- POTENTIAL TO SCALE TO HI POWER
- LIMITS DUE TO FRACTURE
  - THERMAL BROADENING (?)
  - BIREFRINGENCE
  - THERMAL LENSING
  - STRESS-INDUCED BIAXIAL FOCUSSING
  - ⋮

HIGH POWER LASER APPROACH

- STABLE RESONATOR DESIGNS ARE REACHING ACHIEVABLE LIMITS (~100W)

  side pump, side cooled : 62W
  end " " " 60W

- UNSTABLE RESONATORS ARE INHERENTLY FOR HIGH POWER, HIGH GAIN DEVICES

↓

FIBER COUPLING AND VARIABLE REFLECTIVITY MIRRORS

↓

LARGE MAGNIFICATION NOT REQUIRED

∴ SUITABLE FOR HIGH POWER SOLID STATE LASERS

UNSTABLE RESONATOR APPROACH

- CYLINDRICAL RESONATOR
- STABLE IN NARROW WIDTH, (DETERMINED BY PUMP ABSORPTION)
- COOLED THRU PUMP FACE
- POWER SCALED IN VERTICAL DIRECTION WITH UNSTABLE RESONATOR.
- SMALL VERTICAL THERMAL GRADIENT
- ZIG-ZAG IN HORIZ. DIRECTION

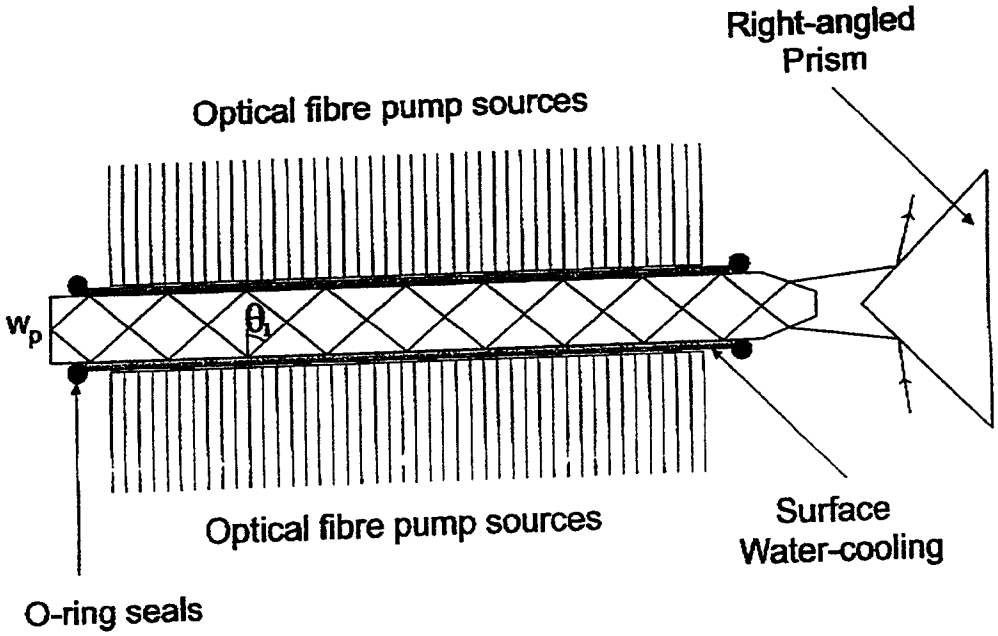
Right-angled
Prism
Optical fibre pump sources
w_p
θ_i
Optical fibre pump sources
Surface
Water-cooling
O-ring seals

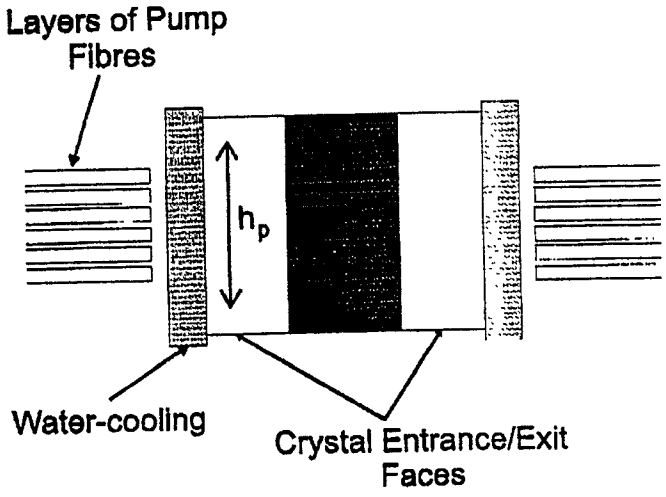
Layers of Pump
Fibres
h_p
Water-cooling
Crystal Entrance/Exit
Faces

CALCULATED NEAR FIELD

INTENSITY

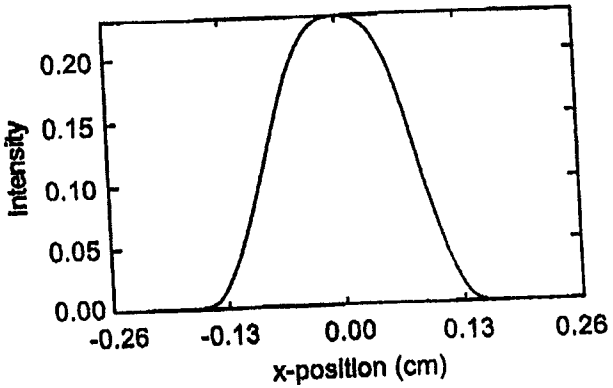

PHASE

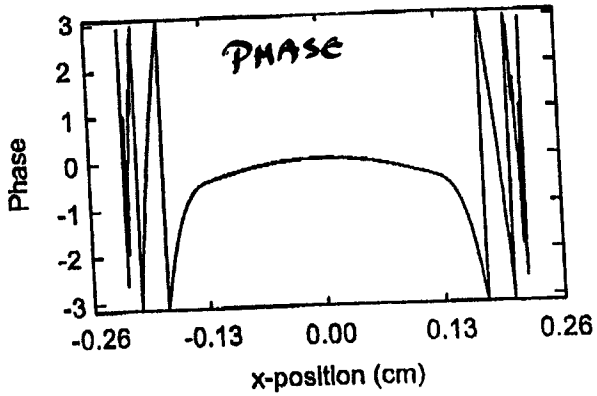

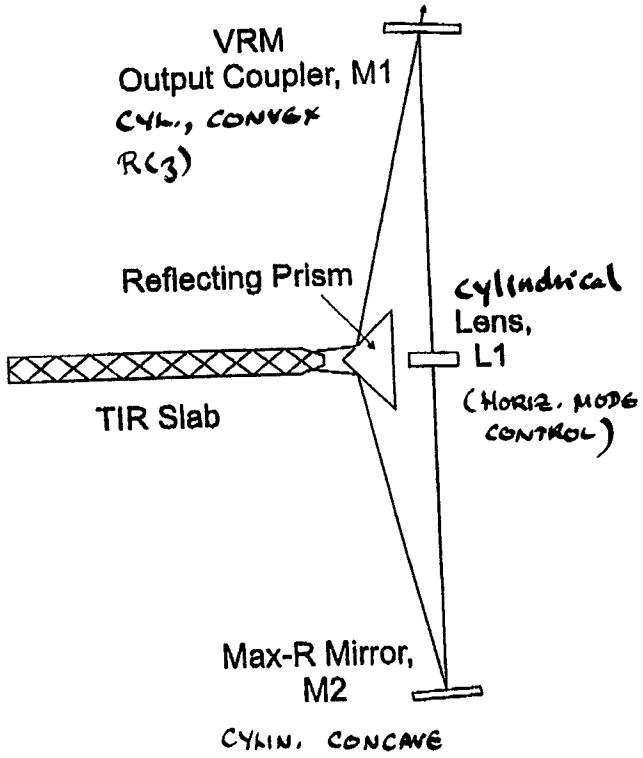

$M_1 - M_2$ TELESCOPE, MAG. 1.3

CALCULATED FAR FIELD

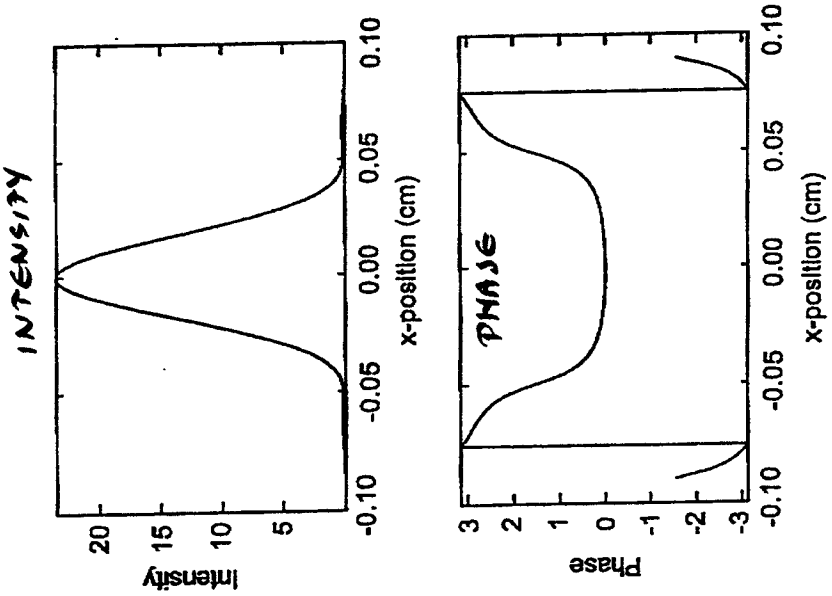

PROBLEM: VISIBILITY OF INTERFERENCE FRINGES LIMITED BY

- QUALITY OF OPTICS
- LASER HEATING AND DEFORMATION OF TRANSMISSIVE COMPONENTS

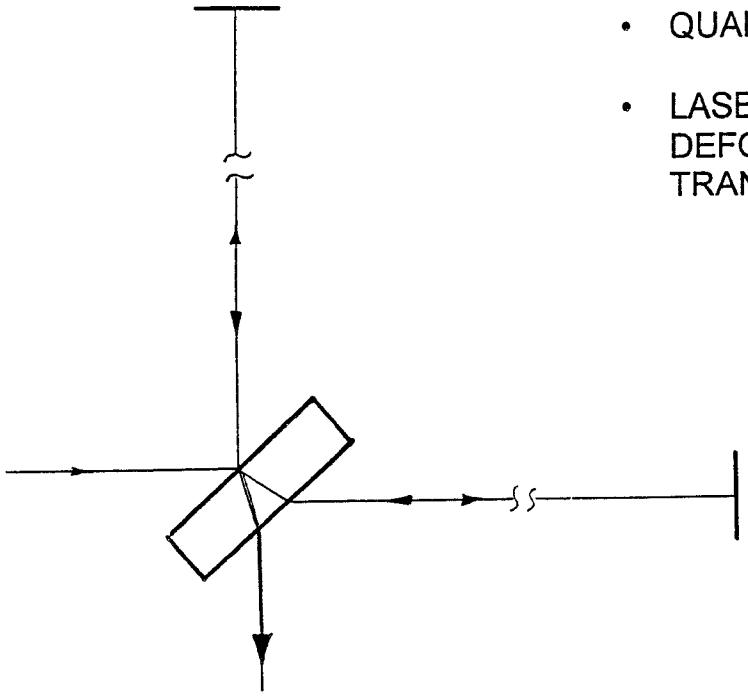

USE HOLOGRAPHIC / DIFFRACTIVE OPTICAL COMPONENTS

1. CORRECTION OF OPTICAL ABERRATIONS

2. SPATIAL MODE MATCHING

3. BEAM SPLITTERS WITHOUT TRANSMISSION

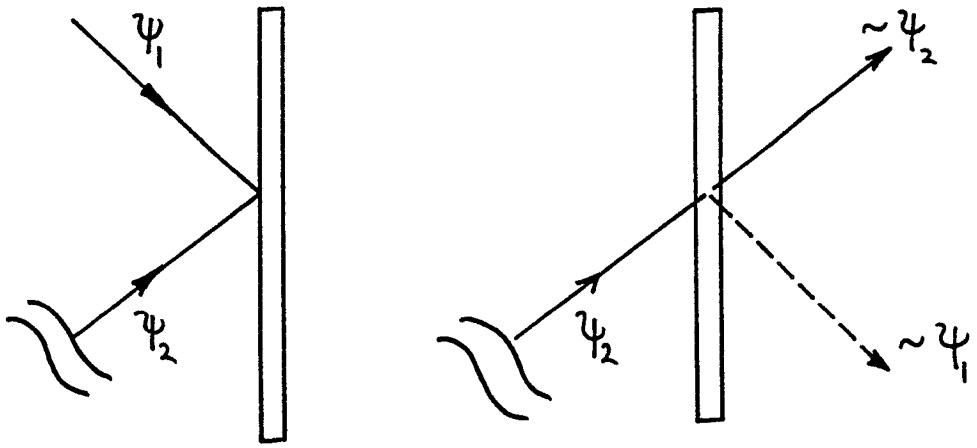

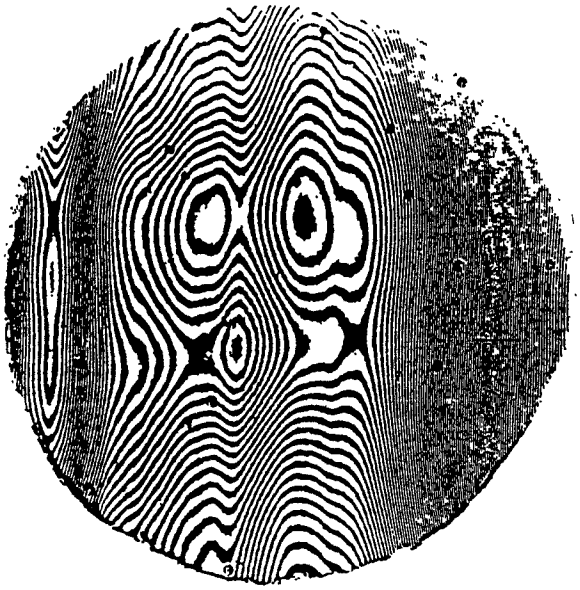

EXPERIMENTAL DEMONSTRATION OF POWER RECYCLING WITH HOLOGRAPHIC BEAM SPLITTER

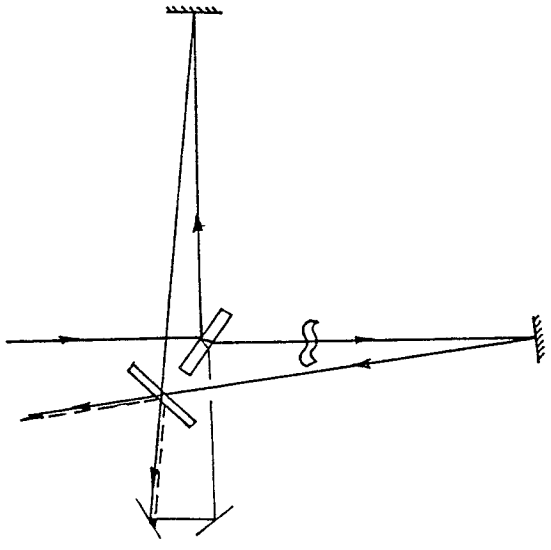

ABERRATION CORRECTION WITH RECYCLING

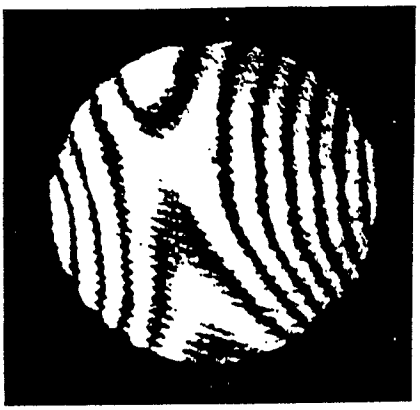

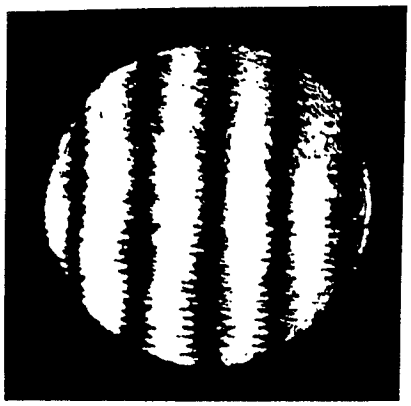

- VISIBILITY OF SIGNAL > 0.97
- ABERRATIONS → POWER LOSS

3 BEAM HOLOGRAPHIC MIRROR

RECORDING WITH 3 BEAMS

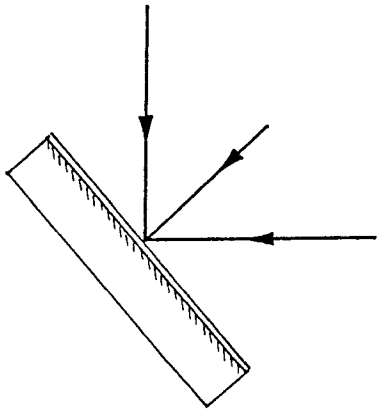

RECONSTRUCTING WITH 2 BEAMS

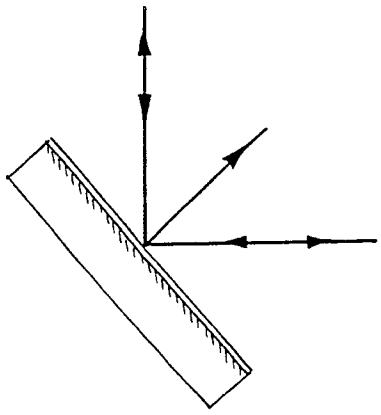

HOLOGRAPHIC MATERIALS

VISIBLE WAVELENGTHS:

- SILVER HALIDE NOT SUITABLE
- DICHROMATED GELATIN WORKS VERY WELL

  $\eta_{DIFF} \rightarrow 100\%$

  50/50 HAS ALSO BEEN ACHIEVED

  SCATTER $< 10^{-3}$
- PHOTOPOLYMERS ALSO EXCELLENT

  $\eta_{DIFF} \sim 50\%$

INFRA-RED :

NO SUITABLE MATERIAL AVAILABLE

AOS XI

AUSTRALIAN OPTICAL SOCIETY

AT

THE UNIVERSITY OF ADELAIDE

see: www: bragg.physics.adelaide.edu.au

10 - 12 DEC. 1997

PRECEEDED BY WORKSHOPS IN

- QUANTUM OPTICS
- GRAVITATIONAL WAVE INTERFEROMETRY
- ATMOSPHERIC PROPAGATION (?)

LIGO
THE VIEW FROM NSF

WINTER CONFERENCE ON GRAVITATIONAL WAVES

January 29, 1997

David Berley

LIGO Project Funding

Panel on the Use of LIGO

NSF Review of Proposals

Funding Projections

LIGO STATUS

- SITES
  - Hanford, Washington
  - Livingston, Louisiana
- COST/%AWARDED
  - Construction $272M (90%)
  - Supporting R&D 24M (97%)
  - Operations to 2001 69M (0.4%)
- COMPLETION
  - Construction 2000
  - Commissioning 2001
    - $h = 10^{-21}$ at 200Hz

PANEL ON THE USE OF LIGO CHARGE

- ADVISE
  - on the development of a users community
  - on procedures, NSF policies, and resources required
    - on the respective roles of the LIGO Project and the NSF in the organization, review and funding of the scientific observations and the detector R&D
- ESTIMATE
  - the size of the likely users community

PANEL ON THE USE OF LIGO

Web Address

http://www.nsf.gov:80/mps/phy/ligorpt.htm

PANEL ON THE USE OF LIGO

Members

William Frazer
Edwin L. Goldwasser
Russel Hulse
Boyce McDaniel (Chair)
Piermaria Oddone
Peter Saulson
Sydney C. Wolff

PANEL ON THE USE OF LIGO

COMMUNITY REPRESENTATIVES

- Barry Barish
- Alain Brillet
- Robert Byer
- Karsten Danzmann
- Ronald Drever
- Sam Finn
- William Hamilton
- Albert Lazzarini
- Gena Mitselmakher
- Robin Stebbins
- David Tanner
- Rai Weiss
- Bernard Whiting

PANEL ON THE USE OF LIGO

- Priorities
  - Near Term
    - LIGO Construction & Commissioning
  - Mid-Term
    - Definitive Detection of GW
  - Long Term
    - Inauguration of GW Astronomy

PANEL ON THE USE OF LIGO Recommendations

- Incorporate Outside Community
  - National
  - International
- Establish Two Entities
  - Laboratory
  - Collaboration
- Institute Aggressive R&D Program
  - Open to Groups Inside and Outside LIGO
  - Coordinated by LIGO Project

PANEL ON THE USE OF LIGO Recommendation

- Program Advisory Committee
  - Provide Advice
    - Formation of The Collaboration
    - Acceptance of other collaborations
    - Assignment of priorities
  - Review Proposals Relevant to LIGO
    - Part of NSF review process

REVIEW OF PENDING NSF PROPOSALS

- NSF Request to LIGO Project
  - Provide a Scientific and Technical Evaluation
- Process within LIGO
  - Internal Staff Review
  - PAC Review
- NSF Peer Review
  - NSF Criteria

LIGO COLLABORATIVE ACTIVITIES

- Contributions to Initial Detector
- R&D for Detector Upgrades
  - Collaboratie with
    - LIGO Project
    - Later with the Collaboration
  - Define Collaboration Tasks through Substantive Memoranda of Understanding
- Development of Advanced Detectors
  - Requires a Coherent Effort

PANEL ON THE USE OF LIGO Recommendation

- Data Handling
  - Take measures to avoid false signals
- Data Processing
  - Initially by collaboration
  - Possible later distribution of data products
- Analysis
  - Technical scope of the task to be defined

PANEL ON THE USE OF LIGO
Recommendation

- Form an International Coordinating Group
  - exchange information
  - coordinate facility utilization
  - coordinate research activities
  - minimize redundant efforts
- Be Open to Foreign Participation in the Collaboration

PANEL ON THE USE OF LIGO
Funding Projection

- Uncertainties
  - Size of the community
  - Little understanding of the computing requirements
- Anticipated Requirements

– Operations	$20M/yr....
– Equipment	6
– R&D	5+1
– LIGO & Collaborators	
– Collaborator base	3 to 5
– Computing Net	1.5
– Computing	?
TOTAL	36 to 39

Wednesday PM A. Lasers
January 29 Chair: R. Byer

4:30	S. Rowan(Glasgow)	Excess Intensity Noise at High Frequencies in Nd:YAG Laser Amplifiers
4:50	Discussion	
5:00	W. Tulloch(Stanford)	Conceptual Design of a 100W Diode Laser Pumped Nd:YAG Laser for GW Interferometry
5:20	Discussion	
5:30	Coffee Break	

B. Optical Elements
Chair: P. Saulson

5:45	D. Reitze(Florida)	Design Considerations for LIGO Input Optics
6:10	Discussion	
6:20	W. Kells(Caltech)	LIGO Optic Quality and Improvement R&D
6:45	Discussion	

C. Advanced Concepts
Chair: J. Hall

6:55	R. Drever(Caltech)	Coupled Suspensions, Magnetic Levitation, and Other Ideas
7:20	Discussion	
7:30	J. Wilson(Livermore)	General Relativistic Numerical Hydrodynamics for Neutron Star Binaries
7:50	Discussion	

Preliminary Measurements on Excess Intensity Noise at high frequencies in Nd:YAG Laser Amplifiers

R.Ewart, W.Tulloch, S.Rowan,
KeXun Sun, E.Gustafson, J. Hough,
M.Fejer, R.Byer

Plans for current generation gravitational wave detectors require ~10W of very stable Nd:YAG light

One way to get this - use a laser amplifier

- Relatively simple
- Scalable to high (100W+) powers

In this context - important to understand the noise associated with amplified light

In particular would like intensity noise to be shot noise limited at modulation frequencies (in the amount of light detected at the interferometer output)

Consider simple amplifier, with gain G.

Let : power at output = P_o

power at input = P_o/G, shot noise limited

Naively,

noise in power out = G x shot noise at input

Then

$$\frac{\text{noise observed}}{\text{shot noise in power out}} = G$$

- In fact this estimate of the noise is too low.
- It can be shown (Harris et al 1992) that

$$\frac{\text{noise observed}}{\text{shot noise in power out}} = 1 + 2(G-1)\eta_{\text{eff}} X = R$$

Results from beating of amplified laser mode with amplified spontaneous emission

- where η_{eff} = effective quantum efficiency of the optical chain including detector

X = possible excess noise factor

- Want to measure intensity noise of amplified light as a function of Gain, G and compare with photoelectron shot noise

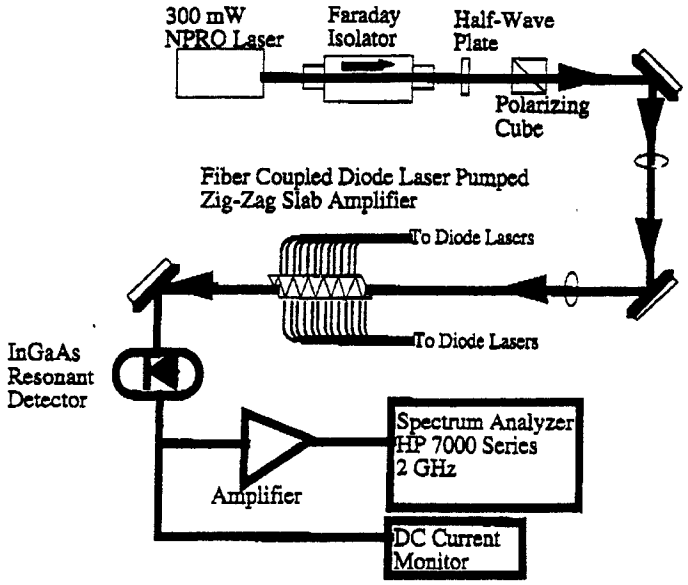

Figure 1: Schematic of the single pass amplifier intensity noise measurement.

Experimental check

Measurements made at 15MHz over 1MHz bandwidth (typical modulation frequency)

All noise measurements - photocurrent = 1mA

- NPRO input beam attenuated appropriately for different pump powers
- Amplifier output was photoelectron shot noise limited for G = 1

As pump power varied between 10 and 100%, following quantities measured:

- ASE power : G : η_{eff} and output intensity noise

Measured amplified spontaneous emission as a function of (Gain -1)

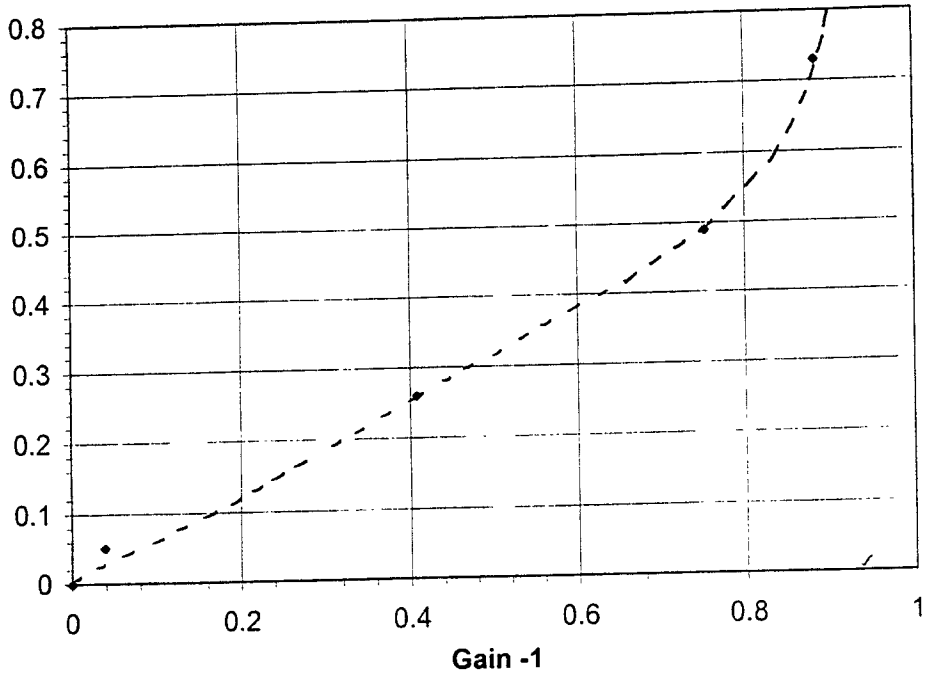

Measured intensity noise of amplified light, along with expected noise level if no excess noise, plotted as a function of (Gain -1)

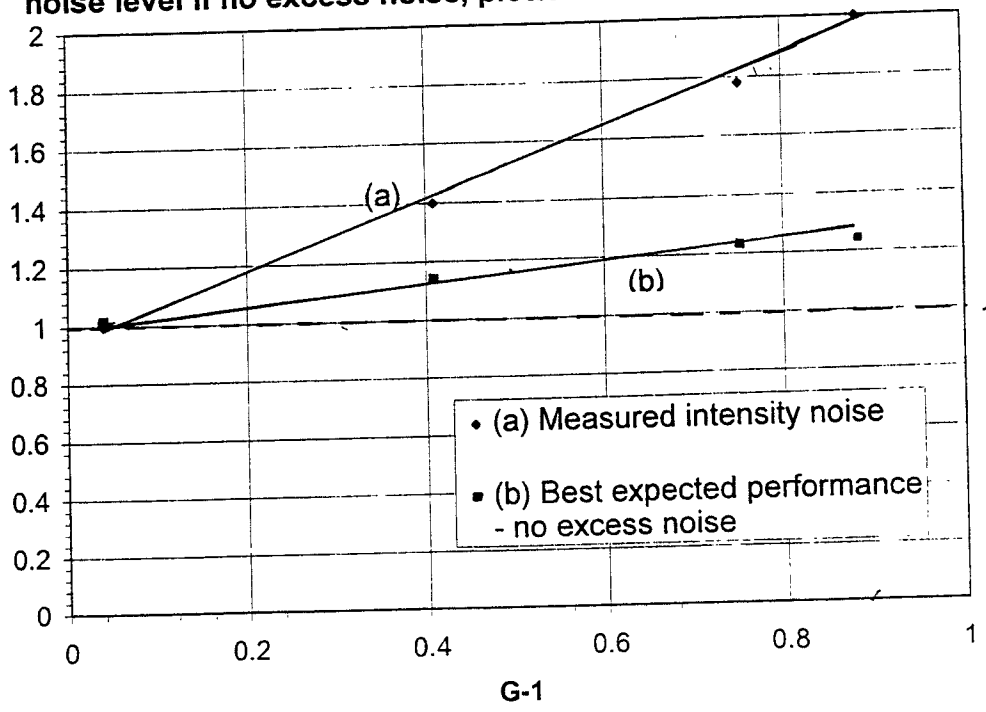

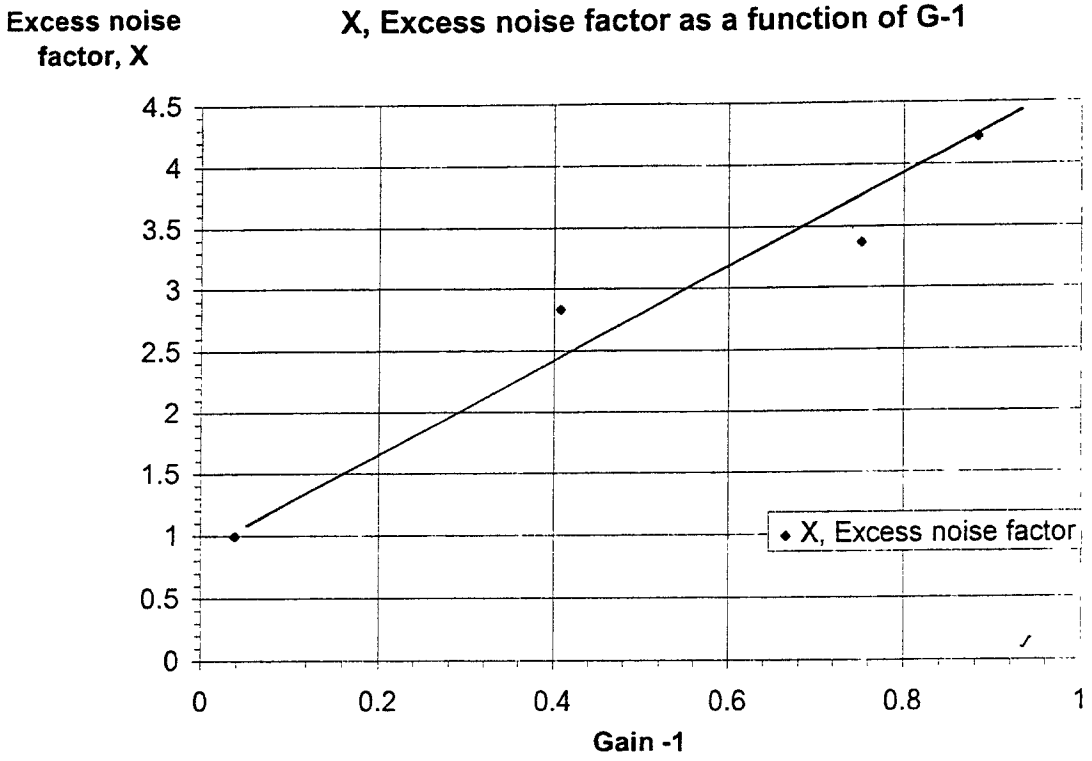

Interpretation of results

Excess noise clearly present.

Excess noise approximately $\propto$ (G-1)

Excess noise approximately $\propto$ $ASE^{1/2}$

Excess noise due to inclusion in measurement of ASE not in the mode of the amplified beam?

- Thus these measurements are a worst case situation
- Noise may be improved by placing by putting single mode fibre or modecleaner in front of detection diode.

Assuming worst case :

Consider 700mW NPRO amplified by diode pumped slab to give output power of 10W.

- Thus (G - 1) ~ 11
- $\eta_{eff} \sim 0.1$
- $X_{\text{worst case}} \sim 40$ (at 15MHz)

Thus R = 89, or noise power is 89 times photo-electron shot noise in the detected photocurrent

Passive filtering

Single optical cavity - 6db/octave filtering of intensity fluctuations above corner frequency

$\Rightarrow$ Cavity corner frequency ~1.5MHz for photoelectron shot noise limited performance

Easily provided by modecleaner for example

1997 ASPEN WINTER CONFERENCE ON GRAVITATIONAL WAVES AND THEIR DETECTION,

DESIGN CONSIDERATIONS FOR INPUT OPTICS FOR LIGO INTERFEROMETERS

Dave Reitze
Physics Department
University of Florida
Gainesville, FL 32611

UF LIGO Group

Faculty (Physics Department):

Guenakh Mitselmakher - IFO simulations
Paul Avery - Data Handling
Bob Coldwell - Signal Extraction from Noise
Dave Reitze - Lasers, Optics, Materials
David Tanner - Optics, Interferometry, Materials
Bernard Whiting - Gravitational Astrophysics

Research Scientist:

Qi-Ze Shu - Cavity optics, RF modulation, prototyping, simulations

Graduate Students:

Tom Delker - Optics Design; prototyping

UFLIGO

UF's Road to Participation in LIGO Research

- DEC '95 : "AWARENESS" - OPPORTUNITIES FOR PARTICIPATION IN LIGO
- JAN '96 : TANNER, REITZE ATTEND ASPEN; MEET W/ C. SANDERS & D. SHOEMAKER
- FEB '96 : UF GROUP VISITS CALTECH TO DISCUSS FRAMEWORK FOR PARTICIPATION, IDENTIFIES I00 SUBSYSTEM
- MARCH '96 : 1) UF GROUP MEETS WITH DEANS, VP FOR RESEARCH AT UF; SECURES SEED MONEY FOR EFFORTS
  2) UF LOOKS AT LIGO-RELATED ISSUES W/ PHOTO DIODES; LASERS
- APRIL '96 : 1) RAI WEISS & STAN WHITCOMB VISIT UF
  2) UF SUBMITS I00 PROPOSAL TO LIGO
- MAY '96 : TANNER VISITS CALTECH FOR ~1 MONTH
- JUNE '96 : UF ATTENDS NSF MEETING ON "PANEL FOR USE OF LIGO"
- AUGUST '96 : REITZE VISITS CALTECH FOR 6 WKS; DISCUSSES I00 & ADVANCED R&D
- OCTOBER '96 : UF SUBMITS PROPOSAL TO NSF
- NOVEMBER '96 : UF PRESENTS "I00 DESIGN REQUIREMENTS / CONCEPTUAL DESIGN" TO LIGO
- NOVEMBER '96 (CON'T) :
  I00 DESIGN ACCEPTED; UF AWARDED SUBCONTRACT TO DESIGN & FAB I00 FOR LIGO
- JAN '96 : UF PRESENTS NSF PROPOSAL TO LIGO P.A.C.

Input Optics

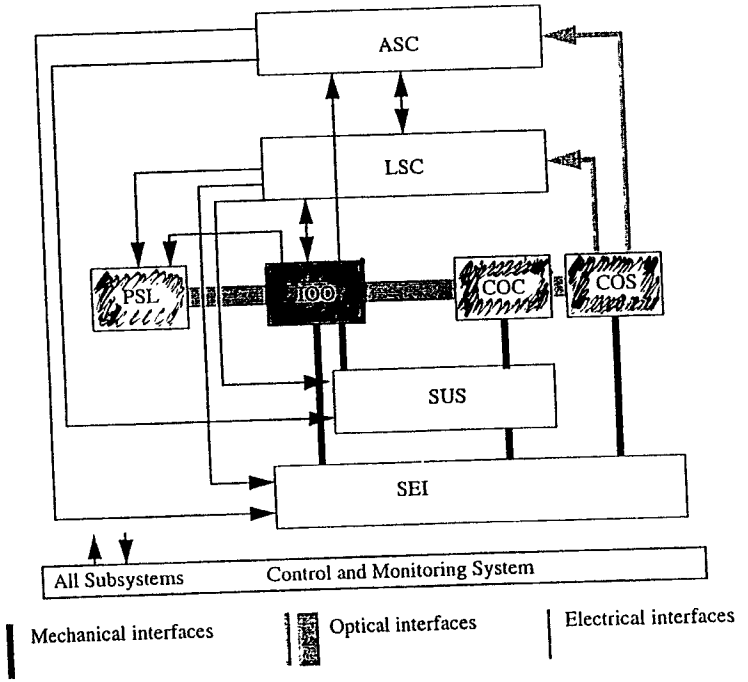

Figure 1: Relationship of IOO to the rest of the detector subsystem. IOO is shaded.

Conceptual layout

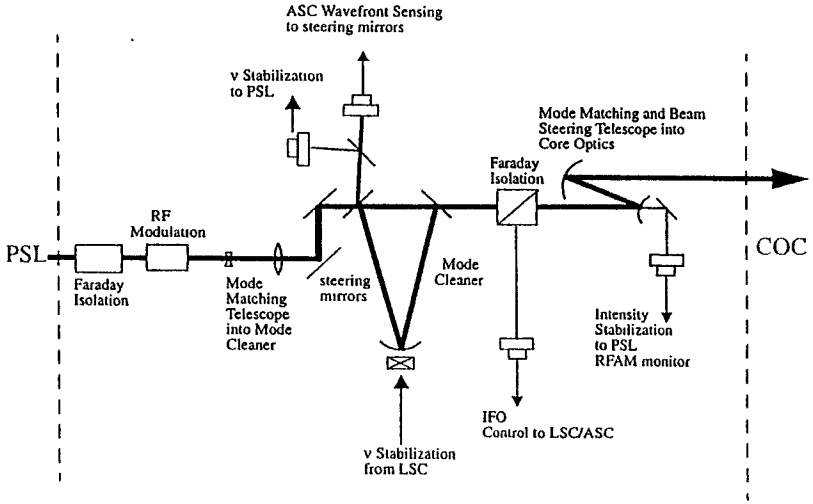

Figure 2: Conceptual layout of IOO optical components

Overall IOO Layout

- In-air IOO components mounted on PSL platform; enclosed and HEPA filtered

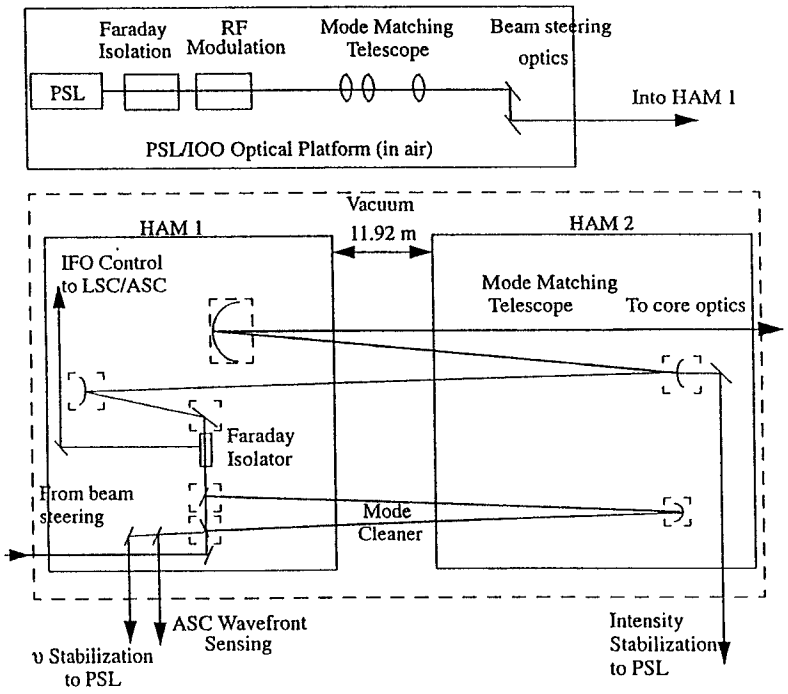

Functions of the Input Optics

- RF Modulation
  - Pound-Drever locking of FP arms
  - " " " of recycling cavity
  - " " " of mode cleaner
- Mode Cleaning
  - pure TEM 00 mode for the IFO
  - in-band suppression of beam pointing fluctuations
  - additional frequency/intensity stabilization in GW band
- Mode Matching
  - good coupling efficiency
  - no added frequency noise in GW band

Vacuum chamber dimensions

- Fix mode-cleaner and recycling cavity lengths.
  - Relevant dimensions are given in the following table.
  - HAM1 and HAM2 are part of the IOO system; hold mode cleaner.
  - HAM3 holds the recycling mirror.
  - BSC3 (4 km IFO) or BSC8 (2km IFO) hold the input test masses.
  - Assume the separation may be adjusted over a total range of 3 m for the mode cleaner and 2.4 m for the recycling cavity.

(See M. Zucker and P. Fritschel, LIGO-T960122-00-I)

	4km IFO	*2km IFO*
HAM1 -- HAM2 spacing (center - center, m)	13.72	13.72
HAM1 -- HAM2 adjustment (m)	+/- 1.5	+/- 1.5
HAM3 -- BSC3/8 (cntr-cntr, m)	8.41	13.05
HAM3 -- BSC3/8 adjustment (m)	+/- 1.2	+/- 1.2

RF modulation design requirements

›› Length and alignment control require sidebands for cavity locking.

- Modulation frequencies
  - Sideband 1 resonant in the recycling cavity for locking FP arms.
  - Sideband 2 which is not resonant in the interferometer for locking recycling cavity.
  - Sideband 3 for locking mode cleaner.
  - Sidebands 1,2 resonant in mode cleaner. Sideband 3 antiresonant in mode cleaner.
- Modulation depths
  - Sideband 1 set by GW shot noise considerations: $\Gamma \sim 0.5$
  - Sideband 2 set by reflected light shot noise: $\Gamma \sim 0.05$
  - Sideband 3 set by " " " " : $\Gamma \sim 0.005$
  - The IOO must provide for a range of modulations about the specified depths to accommodate diagnostic functions and changes in interferometer controls configuration.

RF modulation design requirements

- Modulation cross products
  - Modulation cross products, far from IFO resonance and anti-resonance, can mix to give in-band signals.
  - Eliminate cross products by:
    1) parallel modulation
    2) phase+amplitude modulation
- Free spectral range stability
  - Variation of the modulation frequency from the mode cleaner FSR couples with oscillator phase noise to produce AM of the transmitted sidebands.
  - to limit AM to 10% of shot noise on 6 W laser light requires the RF modulation frequency and the mode cleaner free spectral range to be held equal within < 2 Hz

Modulation frequencies

- Two modulation frequencies:

  ›› f_1: Resonant in the recycling cavity but not resonant in the interferometer arm cavities; used to lock the arm cavity mirrors and the beam splitter.

  ›› f_2: Not resonant in the recycling cavity, used to lock the recycling mirror.

- f_1 set by the lengths of vacuum chambers,

$$f_{mc} = n\, c / 2L_{mc}$$

$$f_{res} = (k + 1/2)\, c / 2L_{rc}$$

here, n is an integer (1,2,3 ...), L_{mc} the mode cleaner length, $k = 0,1,2 \ldots$, and L_{rc} the recycling cavity length.

- $f_1 = f_{mc} = f_{res}$

Modulation frequencies (2)

- f_2 set to a mode-cleaner resonance with a *different* n; not resonant in recycling cavity. (fails to satisfy eqn for f_{res})
- It is not possible to make f_2 maximally antiresonant (unless it is $2f_1$).
- Nominal values given in the table:

	4k IFO	*2k IFO*
Mode cleaner length (m)	12.55	14.75
Free spectral range (MHz)	11.95	10.17
f_1 Resonant modulation frequency (MHz)	23.90	30.51
Recycling cavity length (m)	9.41	12.29
Indices n, k	2,1	3,2
f_2 Non-resonant modulation frequency (MHz)	35.86	20.34
Index n	3	2
Offset from closest RC resonance (MHz)	3.99	2.03

RF modulation I

- Produces both resonant and non-resonant sidebands.
- Modulation is applied so cross products of the two frequencies do not occur.
- Length control either of beam combiner or PM2.

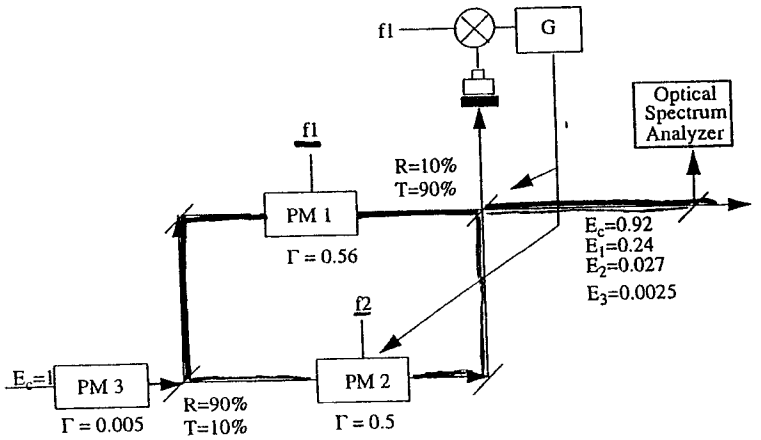

DISADVANTAGE: ADDITION CONTROL SYSTEM

Complex Optical Modulation

FILTER: $\hat{M}(\omega) = \frac{\hat{E}_{out}(\omega)}{\hat{E}_{in}(\omega)}$

$$E = e^{-i(\omega t + f(t))}$$

$$f(t) = \phi(t) + i\alpha(t)$$

Phase Modulator Amplitude Modulator

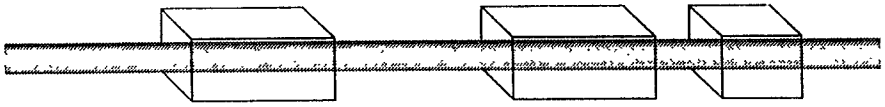

$\phi_1(t)$ $\phi_2(t) + i\alpha(t)$

$$\phi(t) = \phi_1(t) + \phi_2(t)$$

DISADVANTAGE : ENERGY LOSS

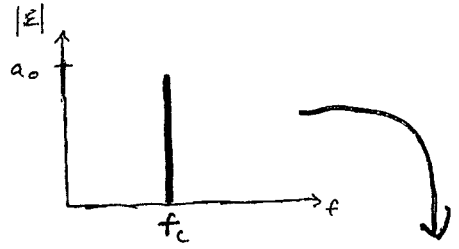

Single Frequency Sidebands

Waveforms of the phase and amplitude modulation

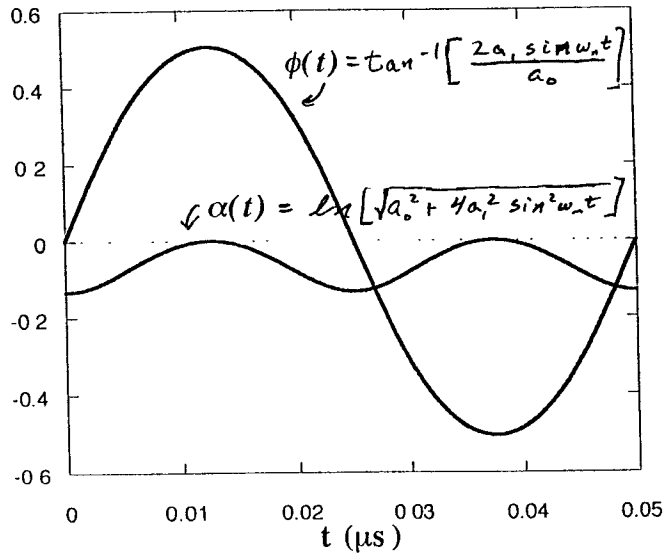

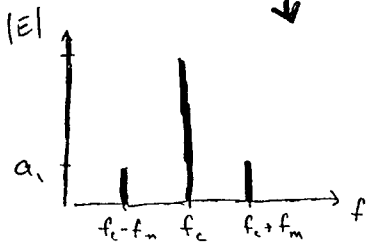

BUT

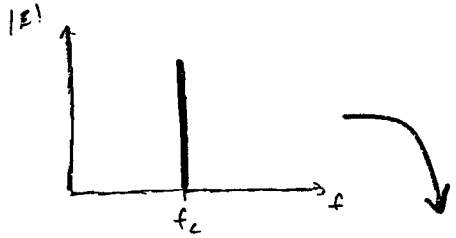

Single Frequency Sidebands

$\Gamma = 0.5$

Power Loss and Signal Loss

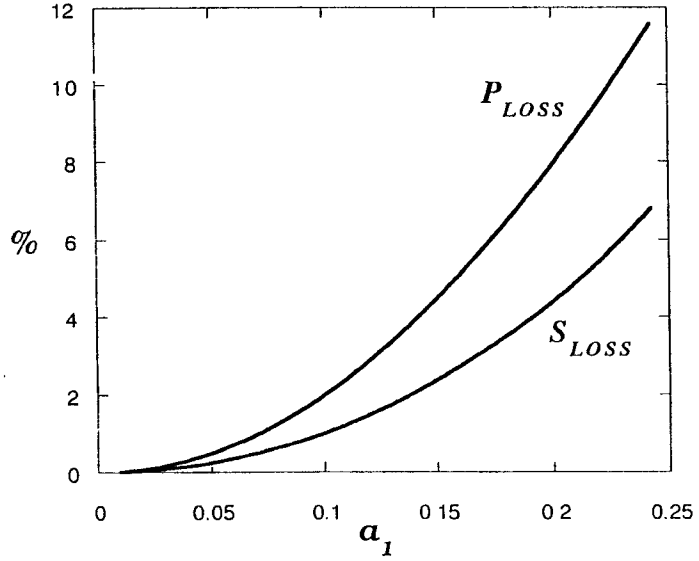

(relative to input field amplitude)

Double Frequency Sidebands

Waveforms of the phase and amplitude modulation

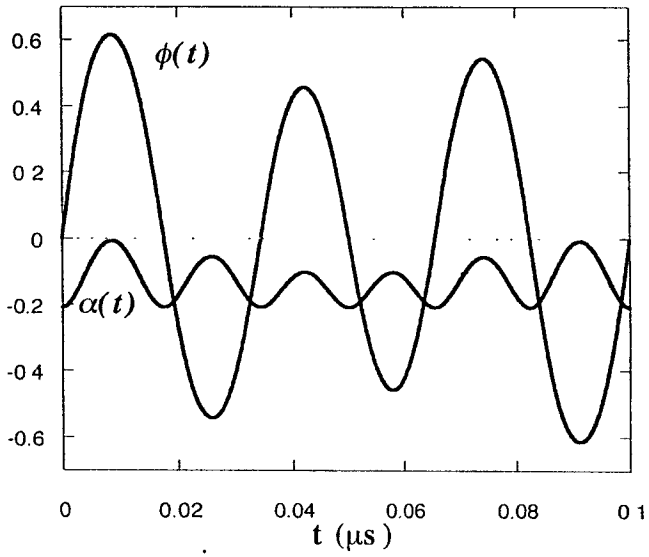

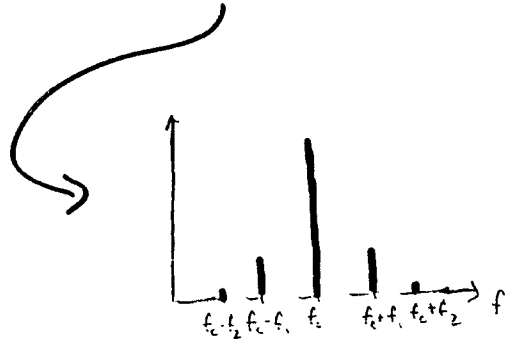

NO CROSS PRODUCTS!

Mode cleaner design requirements

Mode Cleaner - provide frequency and spatial stabilization

- *Frequency Stabilization*

  ›› Frequency noise < 1 x 10^{-7} Hz / $Hz^{1/2}$ at IFO input

  —> mode cleaner stability; frequency noise: $\delta\nu(f) < 10^{-4}$ Hz / $Hz^{1/2}$

- *Intensity Stabilization*

  ›› Intensity stabilization feedback to the PSL from the IOO;

  $\frac{\delta I}{I} < 10^{-8} / \sqrt{Hz}$

- *Mode Cleaner Spatial Stabilization*

  – Attenuation of 01, 10 modes and higher modes at the PSL output to a level consistent with ASC beam jitter requirements: $\varepsilon_1 < 3.5 \times 10^{-9}$ / $Hz^{1/2}$

  – No frequency degeneracy of high-order modes with fundamental up to mode 15

Mode cleaner Conceptual Design

- suspended triangular ring cavity for isolatiòn of laser/suppression of back-reflected light

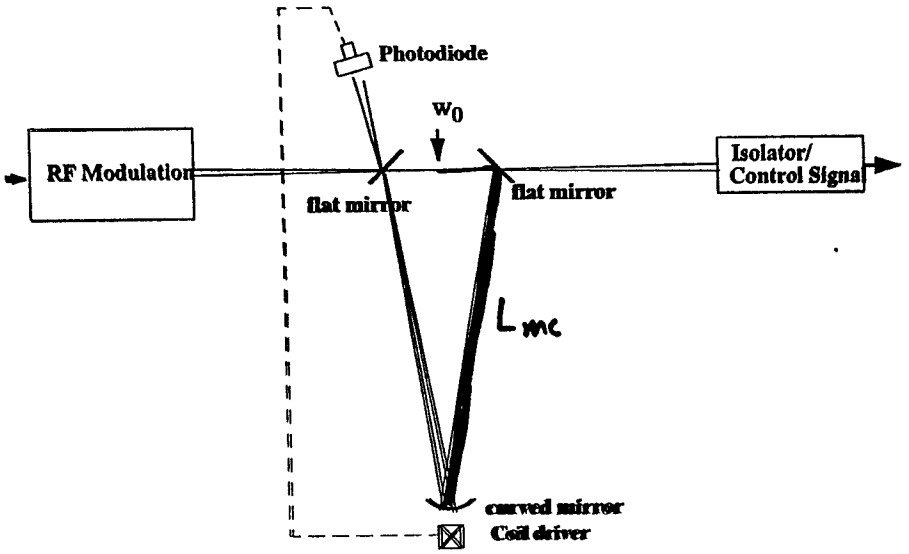

Mode cleaner Conceptual Design

- Optical parameters:

	4k IFO	*2k IFO*
Optics diameter (mm)	75	75
Optics thickness (mm)	25	25
Cavity length (m)	12.55	14.75
Free spectral range (MHz)	11.95	10.17
Finesse	1550	1550
Radius of curvature of converging mirror (m)	18.15	21.34
waist size (mm)	1.685	1.827
Rayleigh range (m)	8.38	9.86
Cavity stability product g	0.309	0.309
Beam radius at curved mirror (mm)	3.03	3.29
Beam radius at flat mirrors (mm)	1.68	1.83
Flat mirror transmittance (%)	0.2	0.2
Mirror absorption/scattering loss (ppm)	30	30
Intensity at curved mirror (kW/cm^2)	14	12
Intensity at flat mirror (kW/cm^2)	45	38
Circulating power (kW)	4.0	4.0

Transmission of mode cleaner

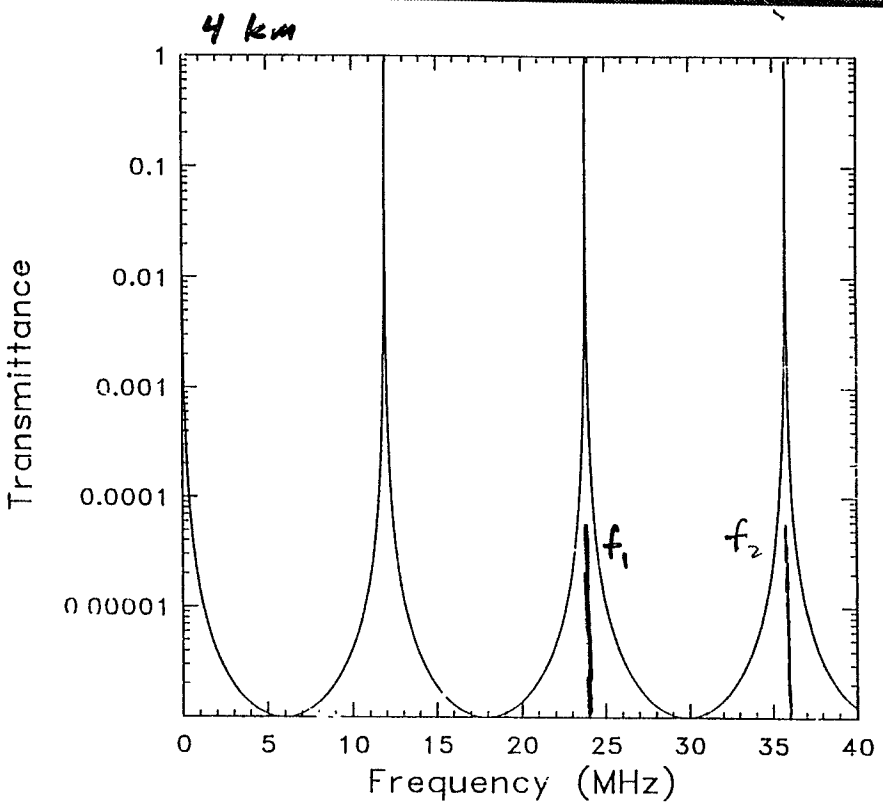

Higher-order mode suppression

- The TEM_{qmn} mode is resonant when

$$f_{qmn} = \left[q + (m+n+1) \cdot \left(\frac{\operatorname{acos}(\sqrt{g_1 g_2})}{\pi} \right) \right] \cdot \frac{c}{2L}$$

- Choose R_i such that only TEM_{q00} resonates at a given L.
- Avoid confocal ($R_i = L$) cavity.
- Best rejection of modes up to $m+n=15$ when $g_i = 0.309$.

Mode N=n+m	*4k IFO MC Suppression*	*2k IFO MC Suppression*
1	0.0014	0.0014
2	0.0012	0.0012
3	0.0058	0.0058
4	0.0016	0.0016
5	0.0011	0.0011
6	0.0029	0.0029
7	0.0020	0.0020
8	0.0011	0.0011
9	0.0020	0.0020
10	0.0029	0.0029

Mode Cleaner Length Control

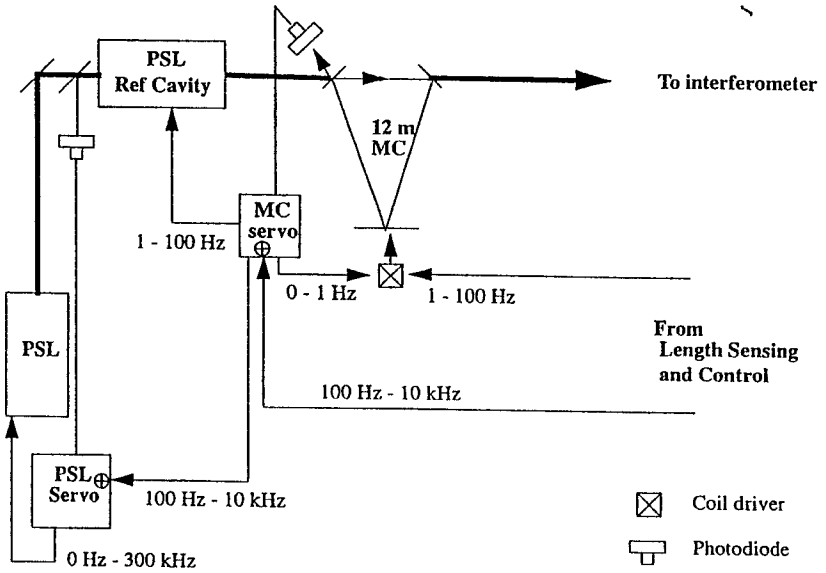

Figure 3: Mode Cleaner ν Stabilization Topology

Mode Cleaner Alignment Requirement

- DC: Preserve ν noise performance
  - ››Beam drift -> ν noise
    - $\Delta\theta_{rms} \sim 3 \times 10^{-7}$ rad REQUIRED
    - verify with modal model
    - $\Delta\theta_{rms}$ (open loop) < 10 μrad (NPRO YAG laser)
    - feedback to steering mirrors (in air)
  - ››other requirements satisfied
    - power throughput (10^{-5} rad)
- In-Band: Preserve pointing fluctuation rejection
  - ›› $\Delta\theta \sim 10^{-12}$ rad / $Hz^{1/2}$ (achieved with suspended optic)

IFO Mode-Matching Telescope (cont.)

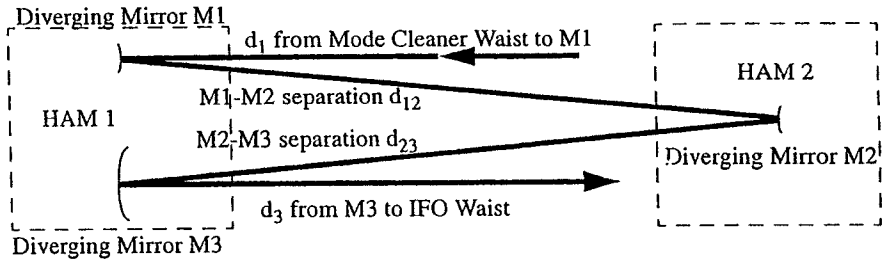

- Radii of Curvature Selection
  - ›› waist magnification: $\omega_{o,IFO} / \omega_{o,MC}$ = 20.9 (4 km)
    = 17.1 (2 km)
  - ›› d_1, d_{12}, d_{23} constrained by HAM dimensions and separation

IFO Mode-Matching Telescope (cont.)

Table 1: Input to Telescope Design Parameters

Parameter	*4 km*	*2 km*
MC waist (cm)	0.168	0.183
IFO FP cavity waist (cm)	3.51	3.13
d_1 = MC waist - M1 distance (m)	1.5	13.1
M3 - IFO waist distance (m)	960.0	628.2
recycling mirror radius of curvature (m)	9998.0	9934.0
ITM radius of curvature (m)	14558.0	14558.0
M1 radius of curvature (m)	-7.00	TBD
M2 radius of curvature (m)	-13.41	TBD
M3 radius of curvature (m)	35.27	TBD
M1 - M2 separation (m)	13.0	TBD
M2 - M3 separation (m)	13.0	TBD
M1 Incident Angle (mrad)	10.0	10.0
M2 Incident Angle (mrad)	10.0	10.0

Mode Matching Adjustment

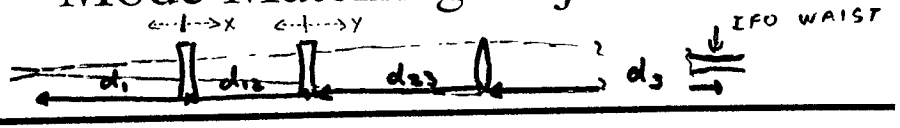

- Possible solution for independent adjustment of waist size and position by moving M1 and M2

Moving M1 and M2 such that the Waist Size and Position can be independently adjusted.

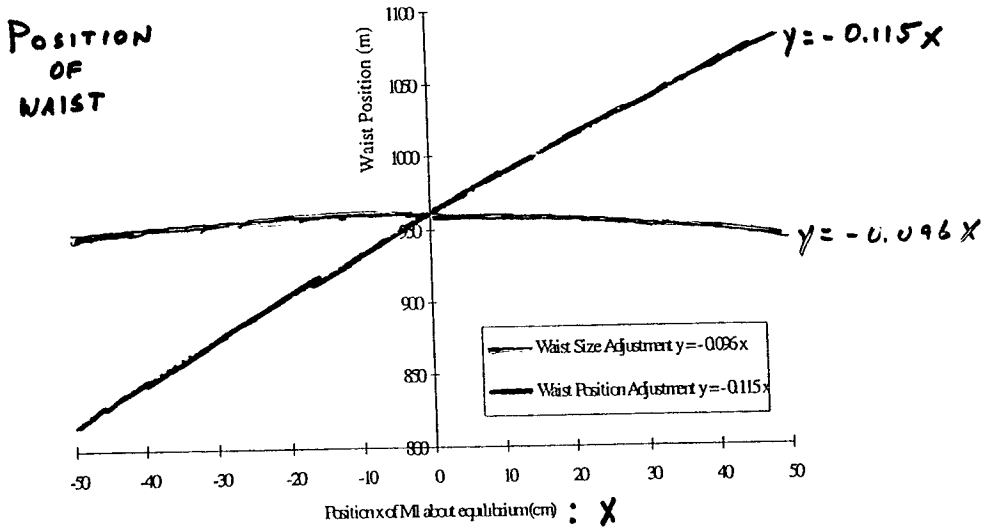

Mode Matching Adjustment

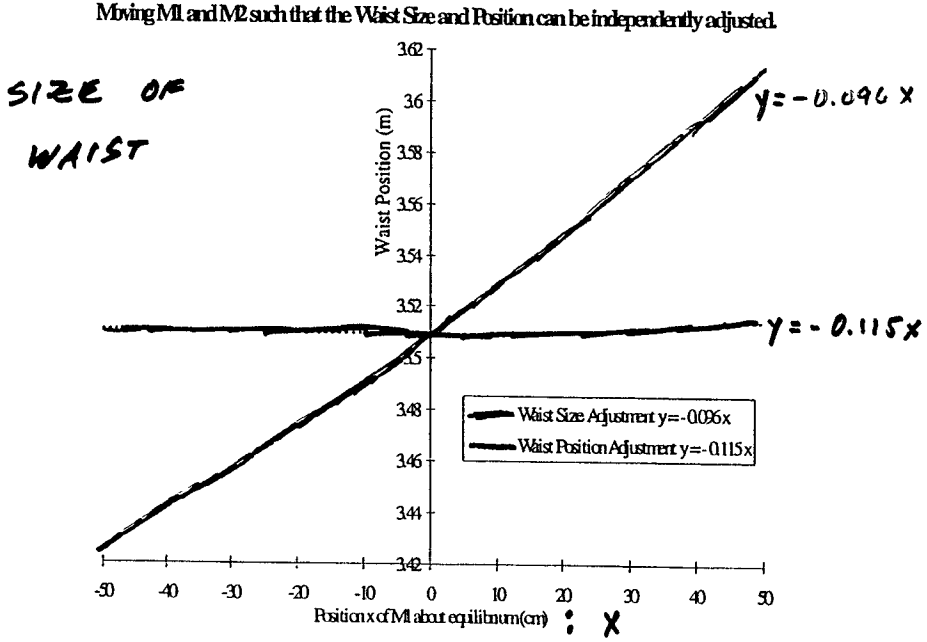

Telescope Beam Steering: Modal Modeling

- Beam pointing influence on modal fidelity

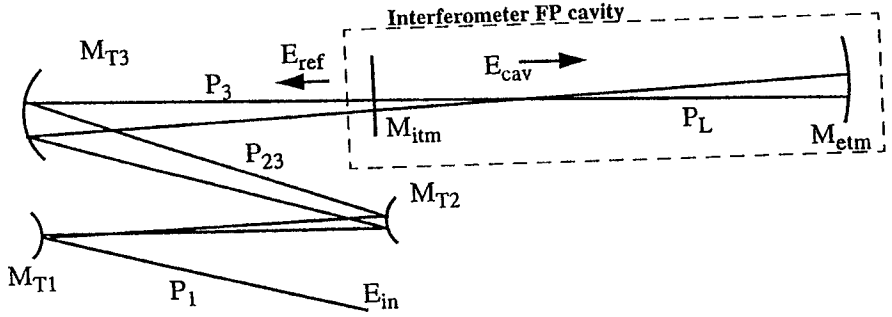

- 1D modal analysis[1] for misaligned telescope coupling into 4 km cavity (include effects of spherical optics)

$$E_{ref} = r_1 M_{itm}^{H}\left(I - \frac{r_1^2 + t_1^2}{t_1^2} P_{cav}\right)(I - P_{cav})^{-1} P_3 M_{T3} P_{23} M_{T2} P_{12} M_{T1} P_1 E_{in}$$

$$E = [TEM_0, TEM_1, \ldots]^T; \; P_{nm} = \delta_{nm} e^{-ikd} e^{i(n+m+1)\eta}; \; P_{cav} = (-r_1)(-r_2) M_1 P_L M_2 P_L$$

1. Y. Hefetz, et al., see Principles of Calculating Alignment Signals in Complex Resonant Optical Interferometers, LIGO-T960005-00-R

Telescope Beam Steering: Modal Modeling

Misalignments

$$M_{m,n}(z_1, z_2) = \iint_{-\infty}^{\infty} U_m{}^H(x, z_1) M(x) U_n(x, z_2) dx$$

$$M_\theta(x) = e^{-2ik\left(x\theta + \frac{x^2\theta^2}{r}\right)}$$

FINITE RADII OF CURVATURE

$$M_\Delta(x) = e^{-2ik\left(\frac{x\Delta}{r} + \frac{\Delta^2}{2r}\right)}$$

where θ = angular deviation from aligned configuration

Δ= transverse displacement deviation " "

r = mirror radius of curvature

Tilt misaligmnent of M_{T2}

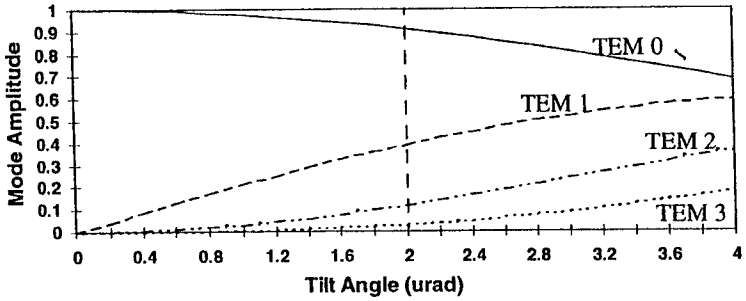

Compensating Tilt by M_{T3}

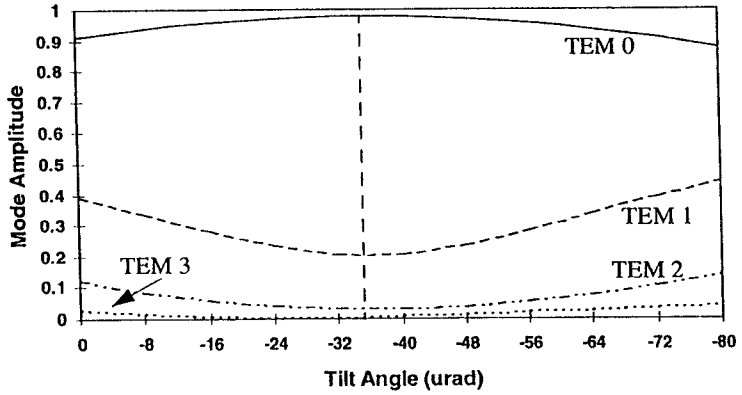

IOO Optical Efficiency Design Requirements

- Shot noise limited requirement for TEM_{00} circulating IFO power (carrier + resonant sidebands) to detect strains of $h \sim 10^{-21}$
  - ›› $P_{IFO} > 6.0$ W
- Expected PSL output power in TEM_{00}: $P_{PSL} \sim 8.0$ W (HOPEFULLY BETTER)

  Required IOO Optical throughput: $> 75\%$!
- Model: $P_{out} = T_1 T_2 \ldots\ldots T_n P_{in}$
  - ›› T_i is the optical efficiency of each element or subsystem
  - ›› AR coatings, max transmittances, reflectances taken from standard optics vendor specifications.

IOO Optical Efficiency (cont.)

Expected IOO Throughput - Ideal Optics

Item	*Loss(%)*	*Transmittance*	*Accumulated*
Faraday isolator 1	5	0.95	0.95
RF modulation unit	3.5	0.965	0.917
3 mode matching lenses	0.6	0.994	0.911
HAM1 window	0.2	0.998	0.910
3 beam steering mirrors	0.06	0.999	0.909
Mode cleaner	5	0.95	0.864
Faraday isolator 2	5	0.95	0.820
Steering mirror	0.02	0.998	0.820
Telescope negative mirror	1	0.999	0.812
Telescope positive mirror	0.2	0.998	0.810

- "Dirty" optics: 1000 ppm scattering losses, 37 surfaces (ALSO OPTICS ABERRATION)
- Efficiency reduced to 0.96 of ideal --->>>

Overall IOO efficiency: 0.781 ; BUT ...

*UF*LIGO

Conclusions

- Design issues for the LIGO input optics
- RF modulation
  - ›› requirements, selection of frequencies
  - ›› alternative methods for producing clean sidebands
- Mode cleaner
  - ›› requirement and functions
  - ›› ring cavity optical layout
  - ›› controls
- Mode matching
  - ›› reflective three element telescope design
  - ›› waist size and position adjustment
  - ›› beam steering
- Layout and optical efficiency

Bill Kells
Caltech

Status of LIGO Optic Quality and Improvement R&D

- Absorption (heating --> thermal lensing)
  - ››Substrate Bulk : ITM and Splitter
  - ››Coatings and surface (contamination)
- Scattering loss from cavity mirrors
  - ››Micro-roughness of polish process
  - ››Imperfections
  - ››Rayleigh
- Polishing ("Figure") accuracy
  - ››Shperical shape deviations
  - ››Absolute R_{curv} and matching
- Coating uniformity
  - ››coating layer deposition flattening
  - ››Matching and reproducibility (ITM pairing, BS split, $R_{recycle}$)

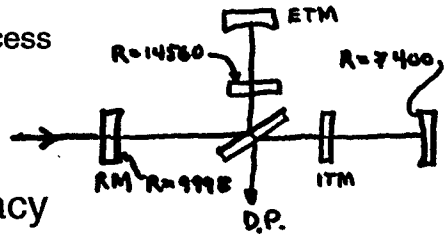

LIGO-G960000-00-M

Aborption (heating)

- Low "OH" silica (~5ppm/cm) for ITM and split.
  - ››Loss and surface distortion insignificant.
  - ››Heating=> thermal lensing OPD ~25% that of mirror (ITM)
  - ››Degenerate recycling cavity properties altered.
    - —Resonant carrier power is unaffected.
    - —Resonant SB power in TEM_{00} is markedly reduced.
    - —Arm matching of lensing not critical (5±1ppm/cm OK)
  - ››Reduction of $\tilde{h}$(100Hz) ~10-20% if uncompensated.
    - —Study compensation assuming predictable lensing
    - —Lower OH silica: special process Heraeus. Possible "Drying" ?
    - —On going photo thermal characterization of sample material.
    - —Can advanced materials do at least as well (e.g. Sapphire)?

SAG ~.5μm
R_{curv}=14560m

LIGO-G960000-00-M

Absorption (heating)

- COATING ABSORPTION : EVIDENCE FOR SiO_2/Ta_2O_5 LIGO DESIGN:
  - ≤ 1 ppm - VIRGO photo THERMAL (1064nm)
  - ≤ 2 ppm - R.E.O. RINGDOWN (514)
  - 6-10 ppm - CALTECH RING DOWN (514) TOTAL LOSS
  - 1.6 ppm - J. Kimble - CAVITY (850) TOTAL LOSS
  - < 1 ppm — STANFORD - CAVITY MODES (1064)
- WHAT MEAN ABSORPTION FOR LARGE AREA ?
  - APPARATUS TO SCAN LIGO MIRRORS IN DESIGN.
  - R.L.G. EXPERIENCE & PHOTOTHERMAL MAPPING INDICATE LARGE VARIATIONS POSSIBLE.
- LIGO ARMS : P ≥ 12 K Watt ⇒ 1.6ppm ABSORPTION WILL CAUSE LENSING ≈ THAT OF BULK ABSORPTION (ITM)
  - COMPENSATION POSSIBLE ONLY IF COATING ABSORPTION REPRODUCIBLE TO << ppm AND NEGLEGIBLE CONTAMINATION

Scattering loss

- NON SPECULAR, UNCORRELATED SCATTER LOSS = $\frac{P_{INC}\left(4\pi \sigma_s/\lambda\right)^2}{P_{LASER}}$ (σ_s roughness) ~ 2% ($\sigma_s \sim 1\text{Å}$), IR ADVANTAGE
  - $\sigma_s = \langle \sigma_{PATCH}(2\text{-}3\,mm^2) \rangle_{SURFACE}$ CORRESPONDS TO RESONANT FIELD SIMULATION GRANULARITY.
  - ASSUME INTRINSIC COATING SCATTER NEGLIGIBLE (R.L.G. FACT)
  - PROPORTIONAL (=?) TO SUBSTRATE μROUGHNESS (VIA MIFO OR AFM
- BLEMISH SCATTER (SUBSTRATE POLISH OR COATING SURFACE)
  - 1μm * 1μm "POINT DEFECT" ON LIGO ITM ⇒ .5ppm Loss
  - Specify < $2.5 \times 10^{4}\,\mu m^2$ POLISH BLEMISH (CENTRAL AREA) ⇒ 1.3% Loss
  - CONTAMINATION : DUST @ $10/cm^2$ ⇒ few 1/10% Loss
- COMBINED UNCERTAINTY IS LARGE: ~ 2 → 20% / MIRROR DOMINATES POWER BUDGET
  - will BLEMISH OR μROUGHNESS Loss DOMINATE ?
  - FIELD SIMULATION EFFECTIVENESS REDUCED ⇒ $R_{RECYCLE}$?

Scattering loss

- FUTURE R & D
  - SYSTEMATIC DIRECT MEASUREMENT PROGRAM.
    + SCANNING INSTRUMENT FOR LARGE AREAS : $\langle \sigma_s \rangle_{surf}$
    + FINGER PRINT MIRRORS : DOCUMENT DEGREDATION.
  - POLISH PROCESS DEVELOPMENT
    + ESTABLISH ~0 BLEMISH AS SPECIFICATION
    + ESTABLISH $\lesssim$ 1 Å rms σ_s ("SUPER POLISH") WITH NO SURFACE FIGURE COMPROMISE.
    + EXPECT LIGO IFO FABRICATION PHASE TO INDICATE EXPEDIENT IMPROVEMENTS
  - IN SITU CLEANING & MEASUREMENT OF LOSSES

REO micro-map surface roughness measurements
(633 nm light)

Table 1: rms (Angstroms) of micromap frames

PATHFINDER Optic	Surface	2.5x resolution (at optic axis)	20x resolution (average of 5 locations)	PSD area analysis (R. Weiss)	
004 (HDOS)	Curved	4.08	5.04	5	
004	Flat	1.65	4.07	3.8	
001 (HDOS)	Curved	4.58	5.33	3	
001	Flat	2.59	3.47	5	
005 (GO)	Curved	0.89	0.85	0.6 - 1.4	
005	Flat	0.90	0.88	0.7 - 1.2	
006 (CSIRO)	Curved	4.33	3.62	3.7	
006	Flat	3.33	2.82	2.7	
002 (CSIRO)	Curved	3 48	2.66	3	
002	Flat	3.39	3.10	3	
0.5 A calibration flats (REO) FULL SUPER POLISH			0.52	cavity ring-down 1064nm loss (ppm)	CALC.
				1	.4
1.0 A calibration flats (REO)			1.02	3	1.5
2.0 A calibration flats (REO)			2.0	16	6
4.0 A calibration flats (REO)			3.77	53	24

MICRO ROUGHNESS

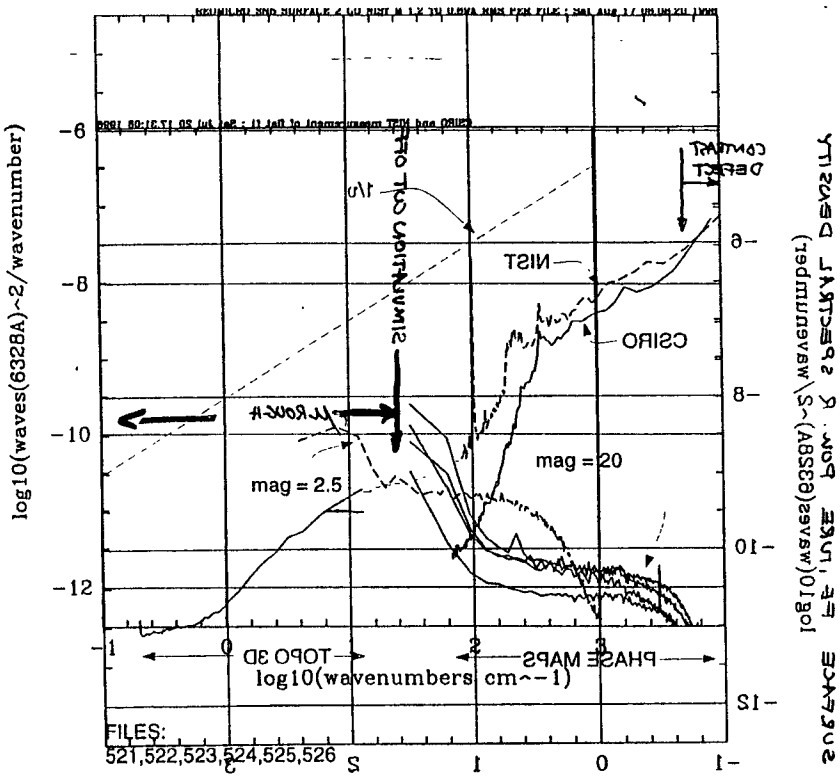

GO

sn5 surface 2 NIST M cm~-1)
1.2 to 0.7 A rms

VG 17 REO Micro

MICRO ROUGHNESS

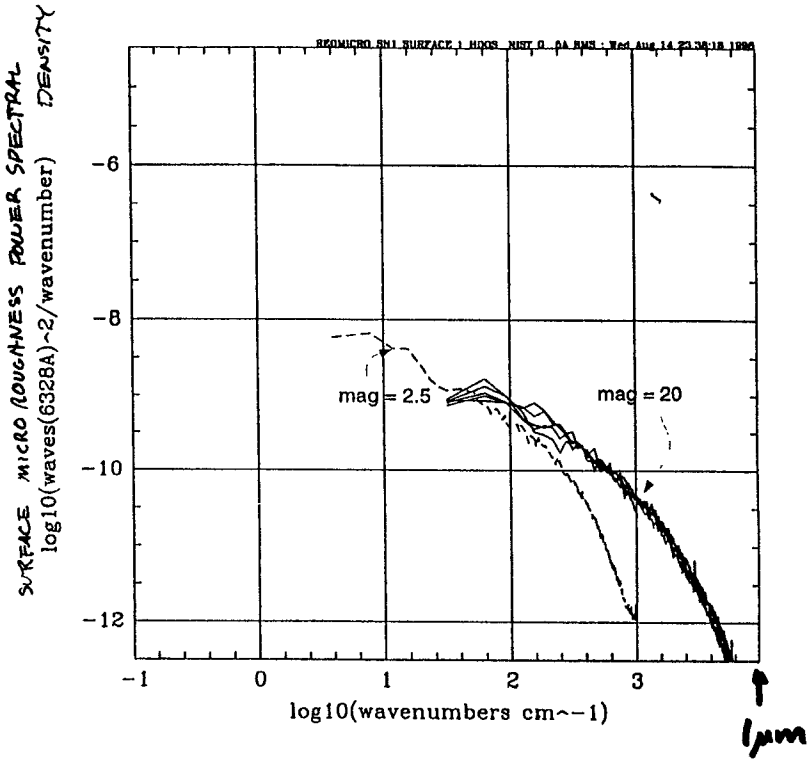

FILES:
111,112,113,114,115,116

sn1 surface 1 HDOS NIST G 3A rms

VG 14 Reo micro

Polishing Accuracy

- **STRATEGY**: – MEASURE REFLECTION PHASE MAPS, All OPTICS ($\phi_{optic} \rightarrow \lambda_{laser}$)
  - USE PHASE MAPS IN FOII IFO SIMULATION:
    - CONTRAST DEFECT
    - R_{rm}
    - DIFFRACTIVE LOSSES
    - DARK PORT FIELD COMPONENTS ⇒ S/N
  - DEDUCE POLISHING/COATING SPECIFICATIONS.
- **GENERAL FEATURES**
  - CD. FROM ONLY LOWEST ORDER ABERRATIONS: MISMATCH ($R_{curve}^{\neq NOR}$ ASTIGMATISM COMA.
  - HIGHER ORDER ABERRATIONS ⇒ DIFF. LOSS (ARMS CAN'T SUPPORT HTN COMPETES WITH μROUGH LOSS TO DOMINATE P_{LASER} BUDGET)
- **PROBLEMS**: METROLOGY LIMITED DATA:
  - R_{curve} AN ABSOLUTE DETERMINATION (7400.00 m FOR ETM)
    - REQUIRES STRINGENT FIZEAU CHARACTERIZATION.
    - LIMITED MATCHING REQUIREMENTS (RELATIVE R_{curv})
  - Good PATHFINDER MIRRORS: RESIDUAL RMS ≤ 0.5 Å
  - 633 nm FIZEAU TEST BEDS SO FAR: NEED 1064 nm FOR FULL MIRROR PHASE MAPS.

LIGO-G960000-00-M

INTERFEROMETRIC MEASUREMENT of POLISHED SUBSTRATE TOPOGRAPHY

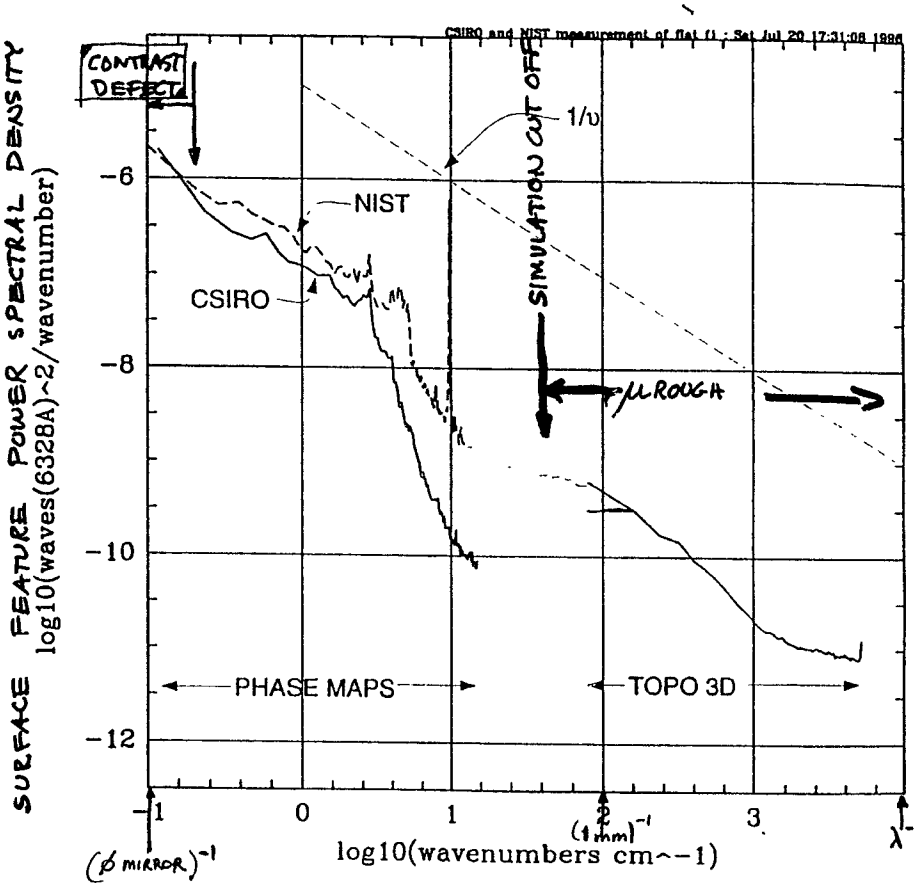

CSIRO phase map f1avwr
NIST phase mao kvyp_d
CSIRO topo 3d maps f6

} PATHFINDER OPTIC

yÎjê íã £ £ £

GO "m" CURVED SURFACE

CURVATURE, COMA, SPHERE REMOVED

$\sigma = .27$ nm

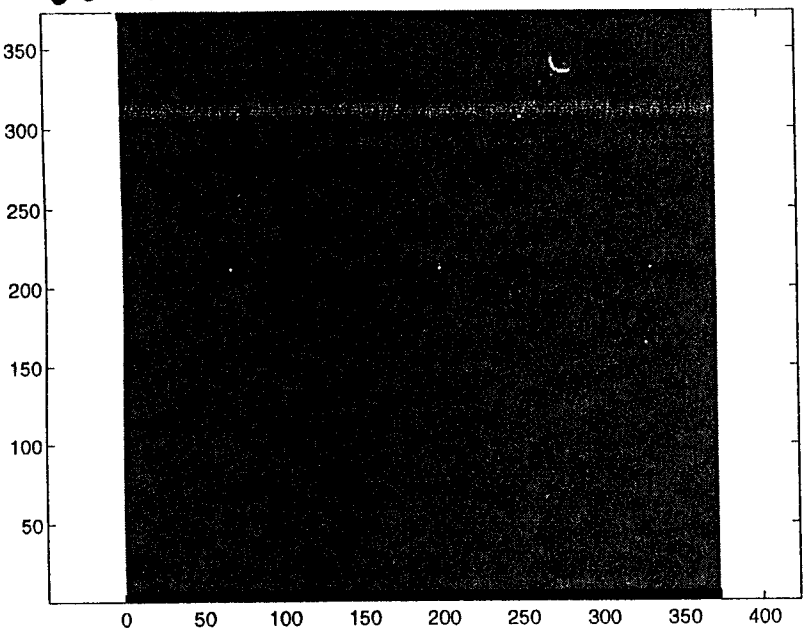

flat GO m

flat GO m

GO "n" CURVED SURFACE

CURVATURE (6000 m R)
& COMA & SPHERICAL ABR.
REMOVED

$\sigma_{pic} = 1.15$ nm

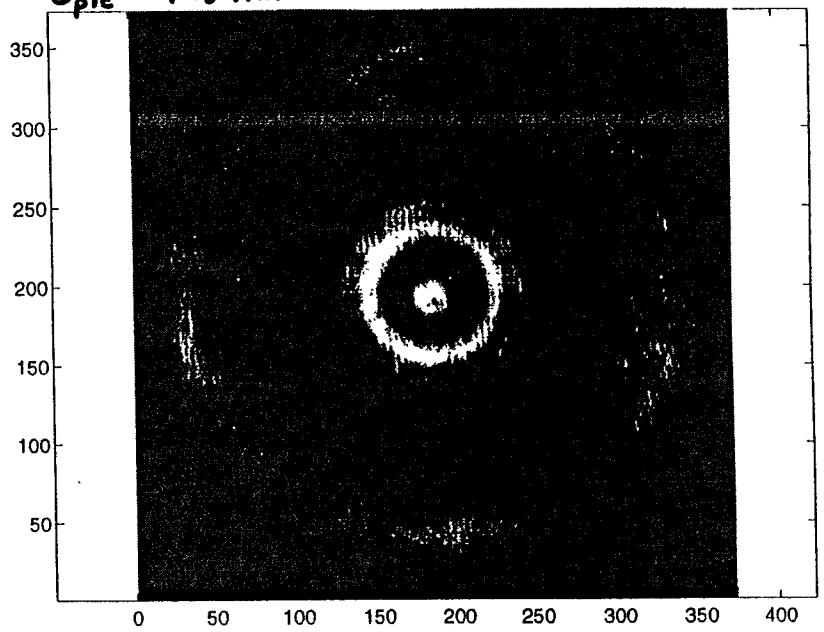

OBVERSE [FLAT] $\sigma = .371$ nm !

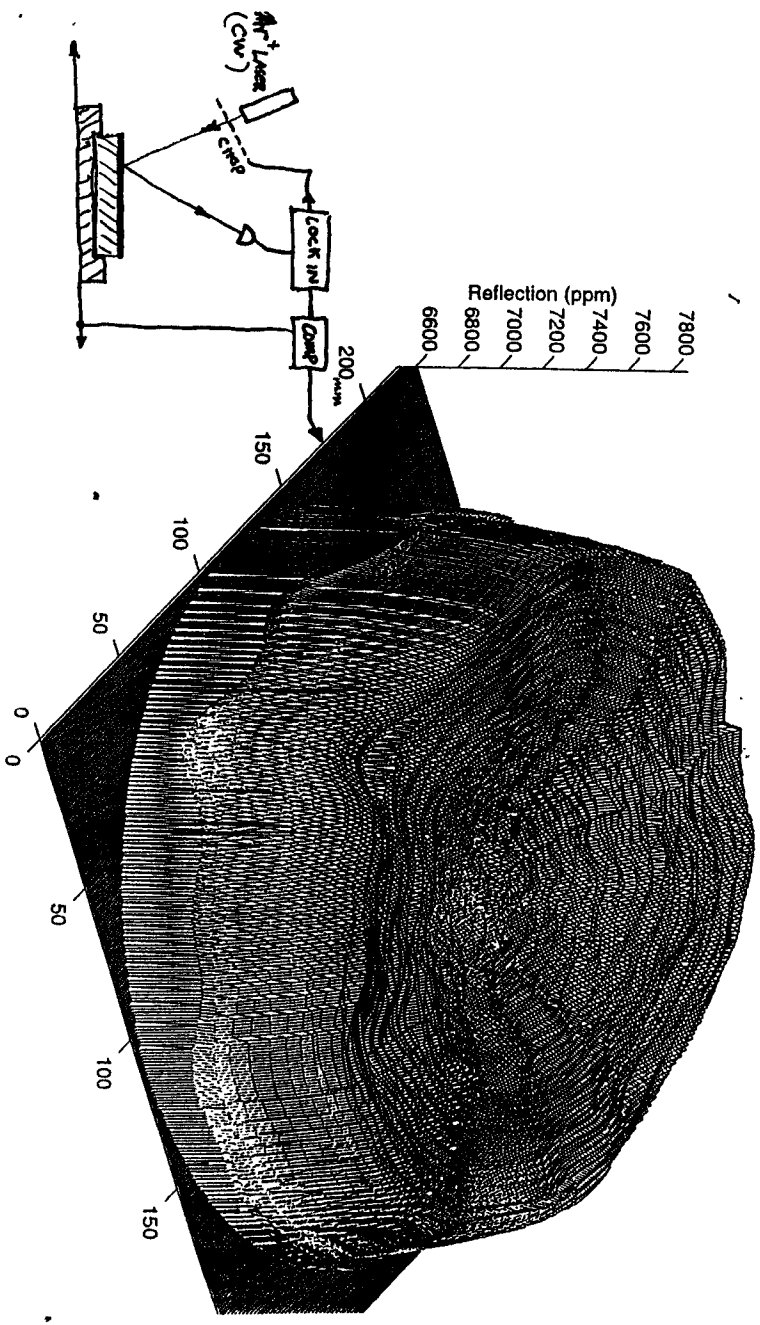

Interpolated, normalized map of substrate C7572 (Ta2O5 sensitive side); at 15 degrees, S-polariz.

REFLECTIVITY DATA FOR Ta_2O_5 + SiO_2 "AR" TEST COATING

Coating Uniformity

- HR MIRRORS @ 1064nm REQUIRE ~40 SiO_2 + Ta_2O_5 $\lambda/4$ LAYERS
- MODEL: - LAYERS EXACTLY CONFORM TO SUBSTRATE TOPOGRAPHY
  - BUT ADD VARIABLE THICKNESS
  - AVERAGE DEVIATION FROM $\lambda/4$ - MINOR EFFECT.
  - UNIFORMITY VARIATION OF 0.01% RMS ⇔ 0.5 Å POLISH
- STARTING POINT: COATING "GUN" FWHM ~15cm!
  HOW TO FLATTEN & MEASURE PROGRESS?
- METHOD: - FULL Ø TEST COATINGS WITH 2 LAYER "AR" DESIGN
  - SCAN THESE FOR SCALAR REFLECTIVITY.
  - INSENSITIVE TO SUBSTRATE POLISH: LOW QUALITY "DISPOSIBLE"
  - BACK OUT LAYER THICKNESS MAPS.
  - SYNTHESIZE ~40 LAYER MIRROR PHASE MAPS
  - RUN SIMULATION CODE WITH THESE PHASE MAPS + POLISH MAPS
- STATUS: METHOD PROVEN WITH SHORT TERM REPRO. <.05%
  - MIRROR COATING MAPS NOW DOMINATE PERFORMANCE (ETM)
  - SIMULATIONS INDICATE JUST ACCEPTABLE.
  - PLENTY OF SENSITIVITY TO FURTHER ITERATE PROCESS
  - NOW AT LEVEL THAT "MATCHED PAIR" DIFFERENCES SEEN.

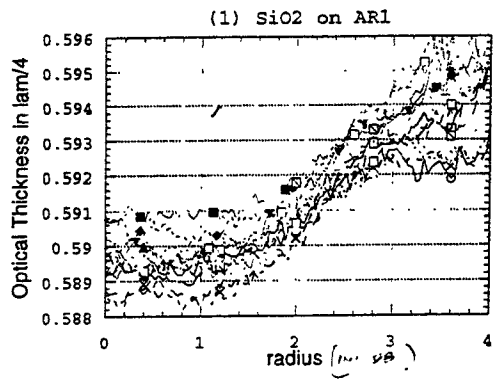
(1) SiO2 on AR1
Optical Thickness in lam/4
0.596
0.595
0.594
0.593
0.592
0.591
0.59
0.589
0.588
0
1
2
3
4
radius (inches)

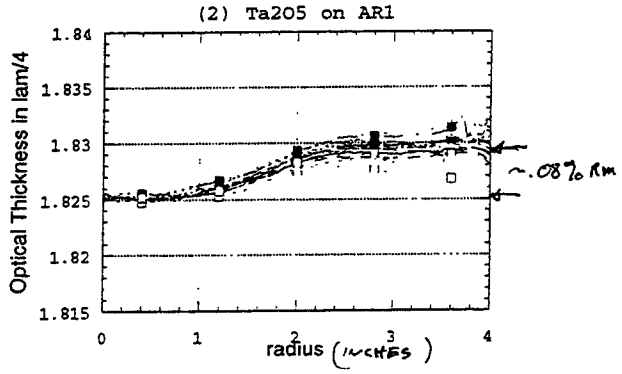
(2) Ta2O5 on AR1
Optical Thickness in lam/4
1.84
1.835
1.83
1.825
1.82
1.815
0
1
2
3
4
radius (inches)
~.08% Rm

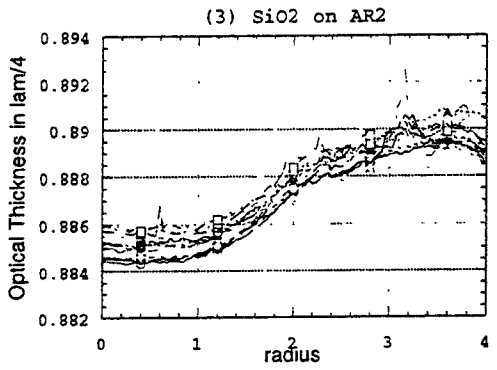
(3) SiO2 on AR2
Optical Thickness in lam/4
0.894
0.892
0.89
0.888
0.886
0.884
0.882
0
1
2
3
4
radius

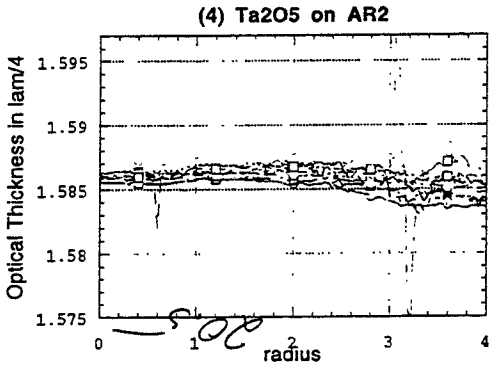
(4) Ta2O5 on AR2
Optical Thickness in lam/4
1.595
1.59
1.585
1.58
1.575
0
1
2
3
4
radius

COUPLED SUSPENSIONS, MAGNETIC LEVITATION, — AND OTHER IDEAS.

R. DREVER.
(ASPEN JAN. 1997.)

NEW RESEARCH EFFORT ON "ADVANCED" CONCEPTS

1) Extending Low Frequency Performance

   - Coupled isolation systems
     - Coupled in position and tilt.
     - Use of magnetic levitation. ← LARGELY PASSIVE

2) Extending High Frequency Performance

   Use of diffractive optics – can allow higher light power –> reduce shot noise

   - Reduces internal test mass thermal noise.

We concentrate on (1) initially, since in our situation this seems likely to give important results earlier.

THE MAIN SOURCES OF NOISE WHICH LIMIT SENSITIVITY.

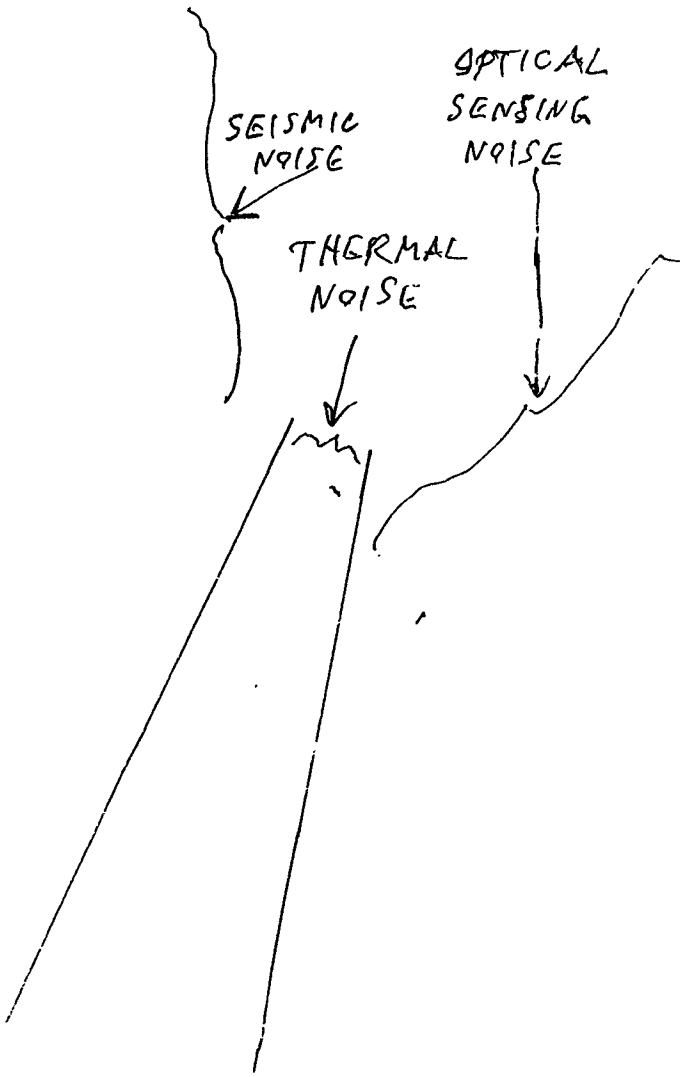

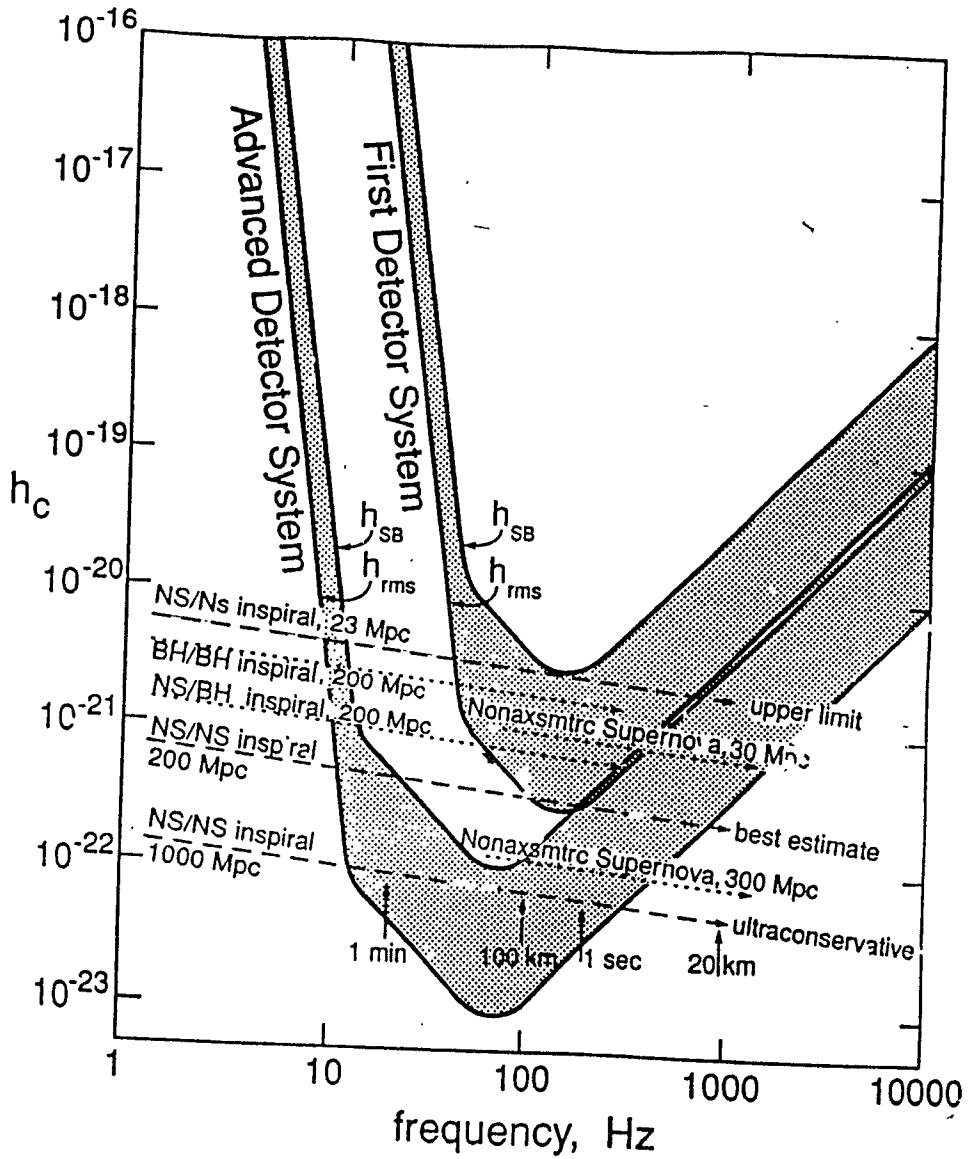

PENDULUM

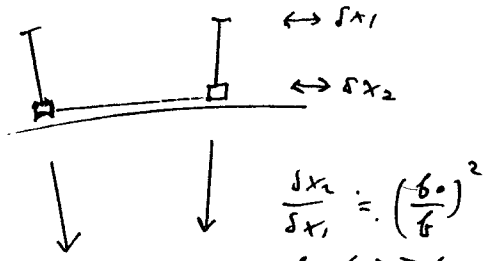

$$\frac{\delta x_2}{\delta x_1} \simeq \left(\frac{f_0}{f}\right)^2$$

for $f >> f_0$.

LONG-PERIOD
WEIGHTLESS, FRICTIONLESS WHEELS

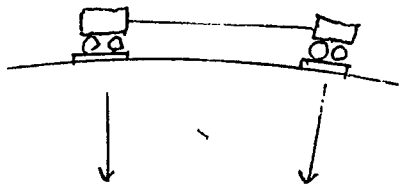

MONITOR SUSPENSION POINTS

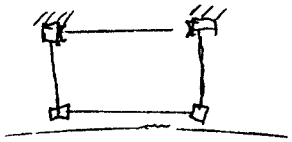

MONITOR RELATIVE TILTS

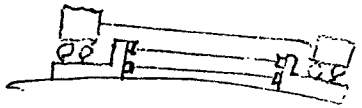

ALMOST ANY PASSIVE LONG-PERIOD SUSPENSION IS EQUIVALENT TO THIS.

(INCLUDES GATE-TYPE SUSPENSION, X-PENDULUM MAGNETIC SYSTEMS TO BE DESCRIBED)

MAGNETIC SUSPENSIONS PROPOSED CAN GIVE PRACTICAL WAY TO IMPLEMENT THIS

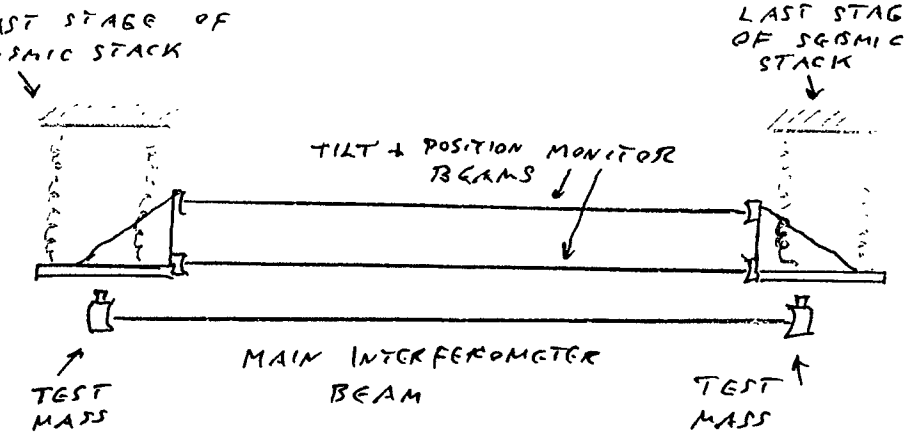

TILT-COUPLED SUSPENSIONS — MAGNETIC LEVITATION EXAMPLE.

→ ALSO APPLICABLE TO OTHER SUSPENSIONS

STANDARD SEISMIC ISOLATION – SPRING-MASS STAGES OF LOWEST CONVENIENT RESONANT FREQUENCY

ADVANTAGES of Using Magnetic Fields Instead of Metal or Rubber "Springs":

a) Avoid high-frequency paths through springs, etc.

b) Low resonant frequency obtainable in passive systems.

(Servo is only a stabilizer.)

c) Relatively simple – essentially passive.

d) Easy damping by eddy currents.

e) High vacuum compatible.

OBVIOUS DISADVANTAGES

a) Superconductors require reduced temp – inconvenient.

Plan to avoid them.

b) Permanent magnets unstable alone (Earnshaw's theorem).

- But can make stable by servo sytem

c) Must avoid response to outside field noise.

SOME MAGNET ARRANGEMENTS PROPOSED

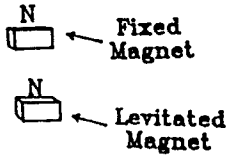

(A) SIMPLE

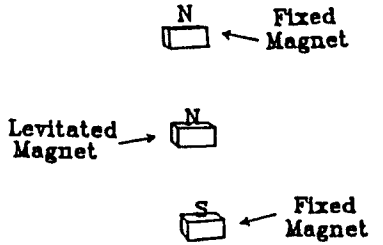

(B) LONGER PERIODS THAN (A).
TRANSLATION – ROTATION COUPLING CAN GIVE INSTABILITY.

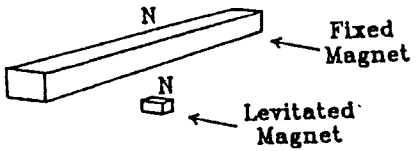

(C) [illegible] LONG PERIODS IN [illegible] DIRECTION.

Magnetically Levitated Test Mass

"QUADRUPOLE" VERSION – 2 MAGNETS ON MASS

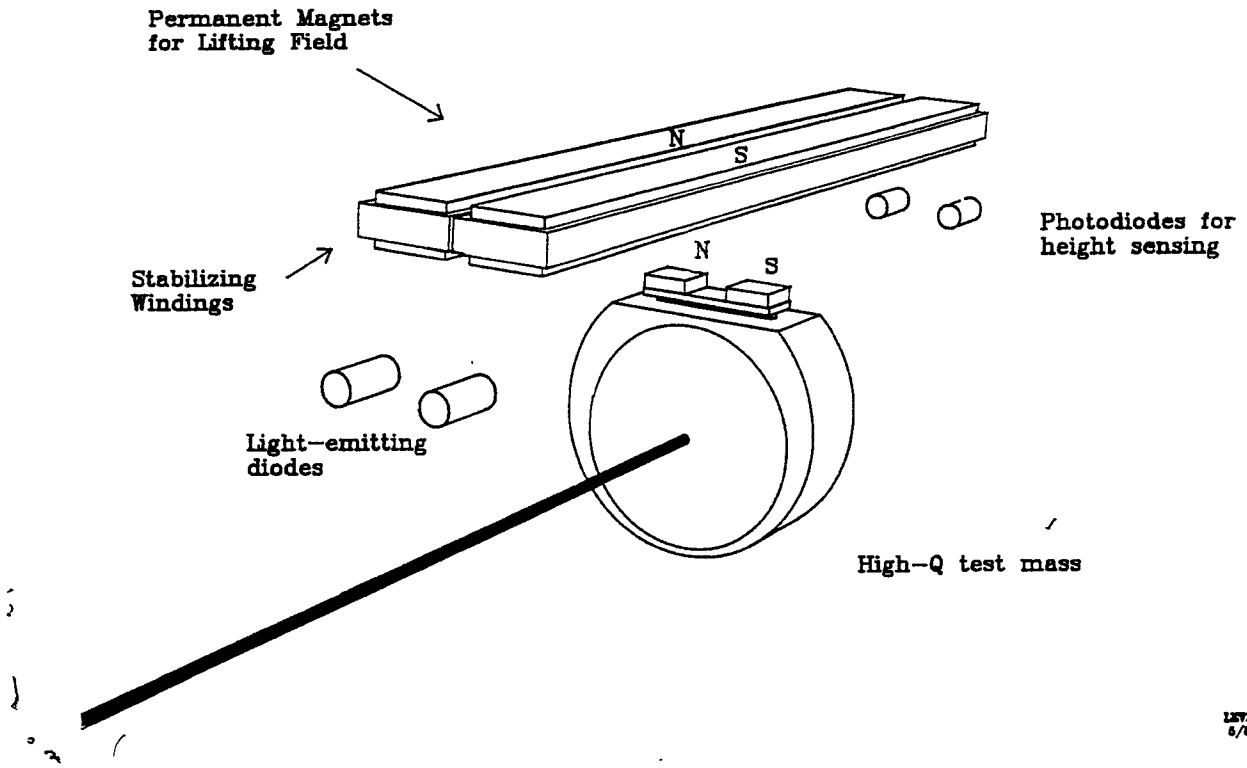

LSTMAPS 5/8/90

ONE STAGE FOR A SEISMIC ISOLATION SYSTEM.

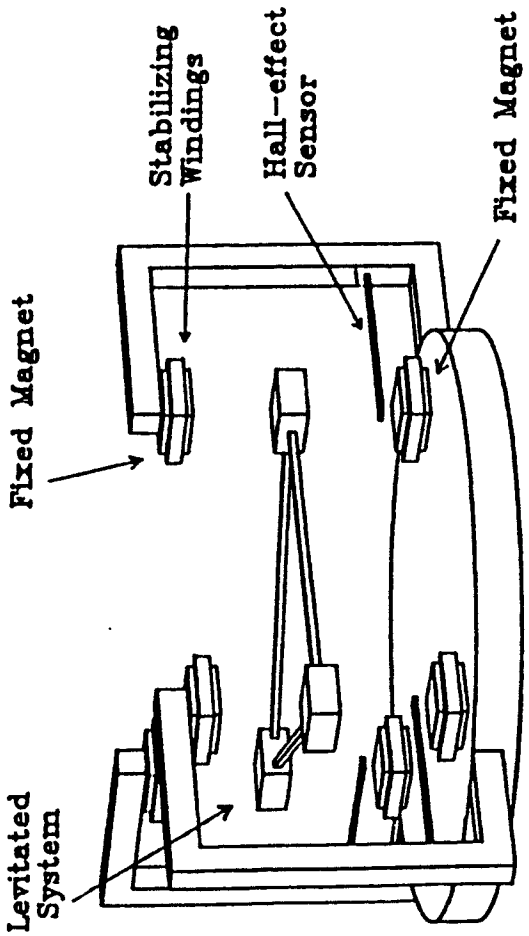

Fig. 8.

SMALL TEST SYSTEM :–
PAYLOAD 1 KG
NATURAL PERIODS :– HORIZONTAL 2 – 4 SEC.
VERTICAL 0.5 SEC
(CAN BE MADE LONGER BY TRIMMING FIELDS AND SERVO RESPONSE)

BUILT AND TESTED BY S. ALGERT.

A8

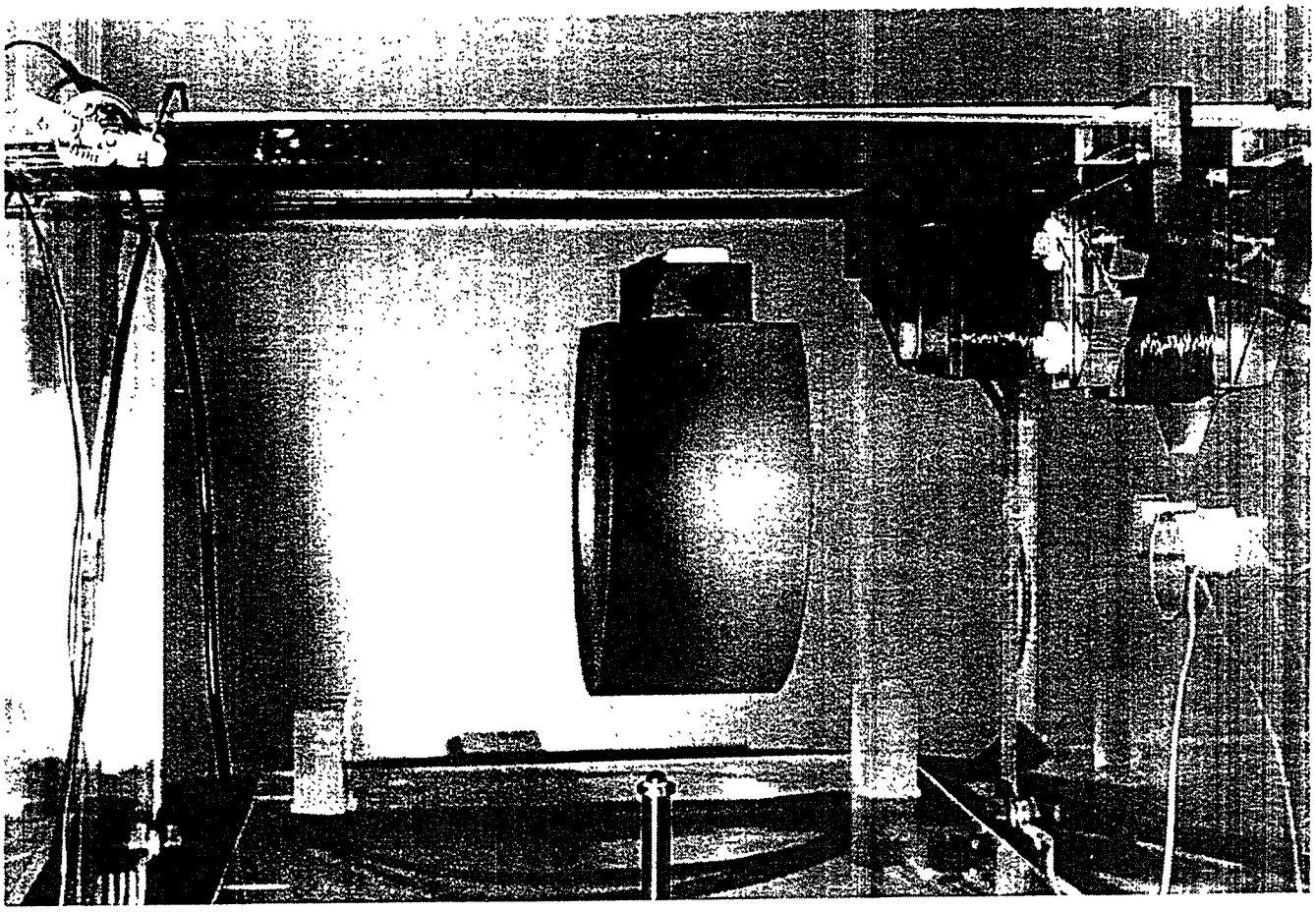

TEST MASS LEVITATION SYSTEM :— FINE CONTROL OF MIRROR ROTATION, TILT, AND LONGITUDINAL POSITION, BY AUXILIARY COILS A, B, C, D.

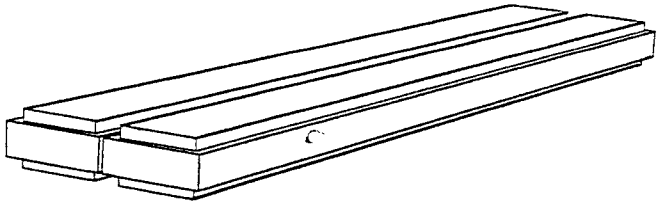

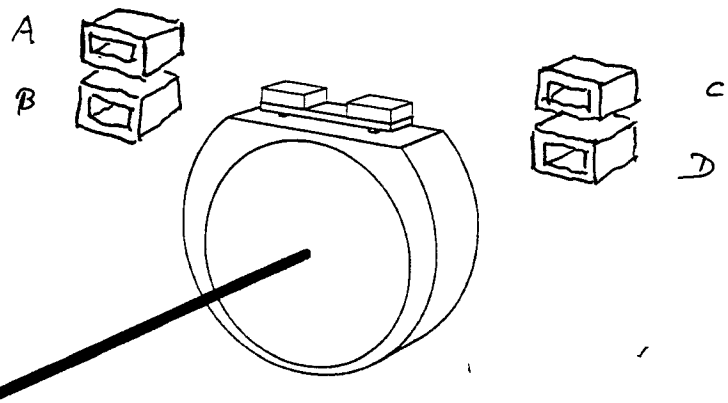

EXPERIMENTAL FINDINGS
with 1-magnet and 2-magnet versions test mass systems

1) Natural period depends on non-uniformity of support magnet(s).

   Typical period 8 seconds –> 12 seconds

   with simple trim –> 20 seconds

2) Relaxation Time (Horizontal mode)

   Typical in range 8 to 18 hours

   (under investigation – preliminary only)

   Typically longer with insulating magnets on mass (ceramic) than conducting (rare-earth) (by factor <2).

3) Stabilizing Power << 1 mw

   Typical ~50 microwatts

4) Permanent magnets have temp coefficient.

   Equilibrium height function of room temperature.

   Now using servo to control field via temperature.

5) Thermal Noise Plans

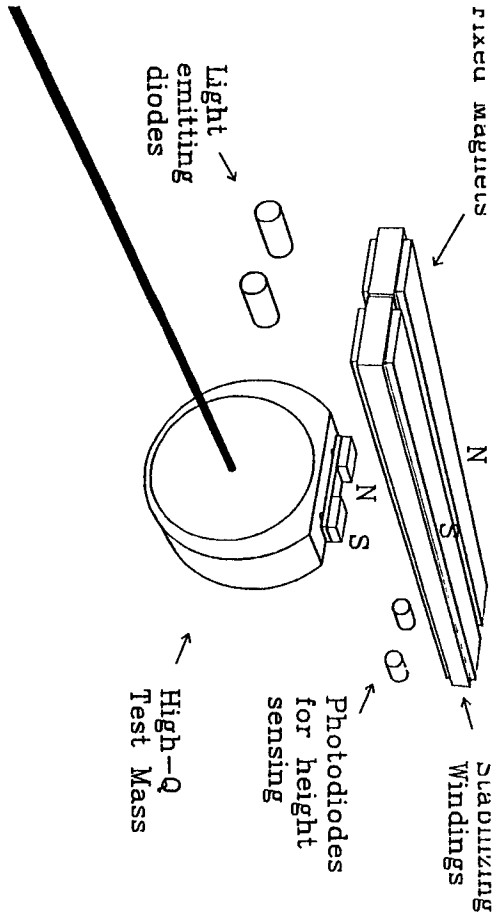

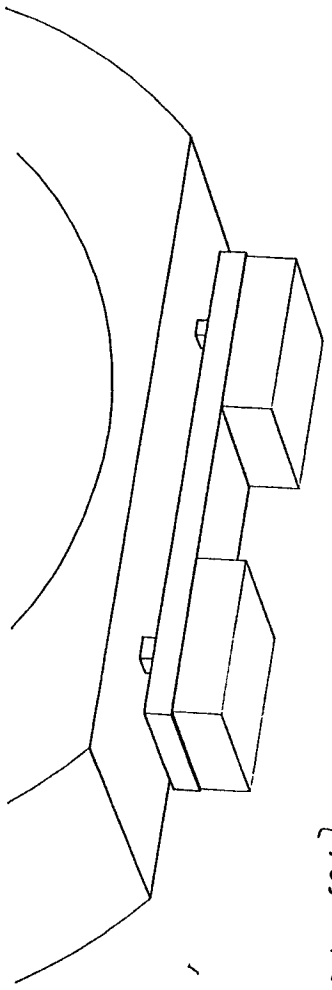

Enlarged view of top of Test Mass

(POST FLEXURE VERSION)

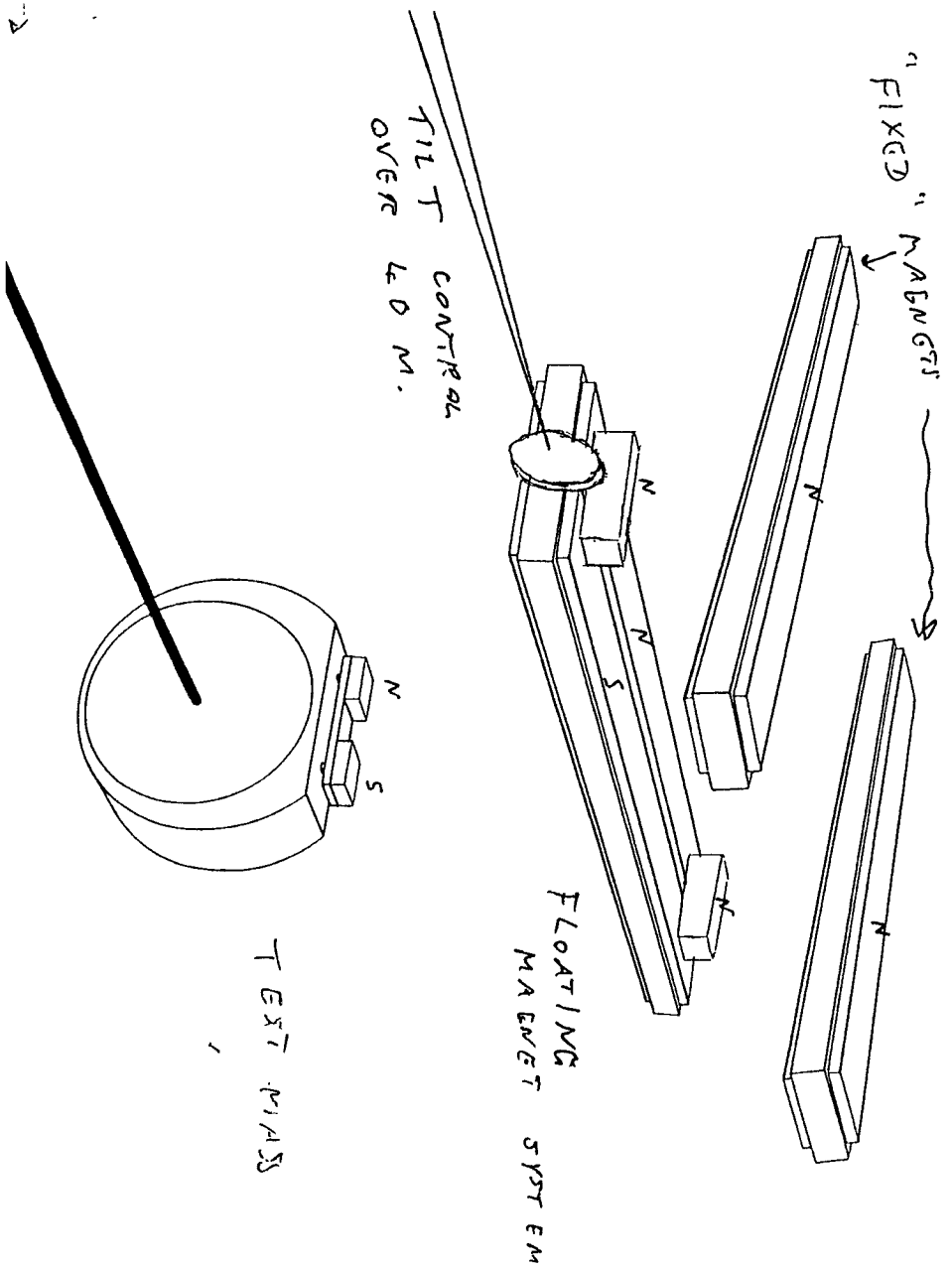

CONTROL OF MAGNETIC FIELD VIA MAGNET TEMPERATURE.

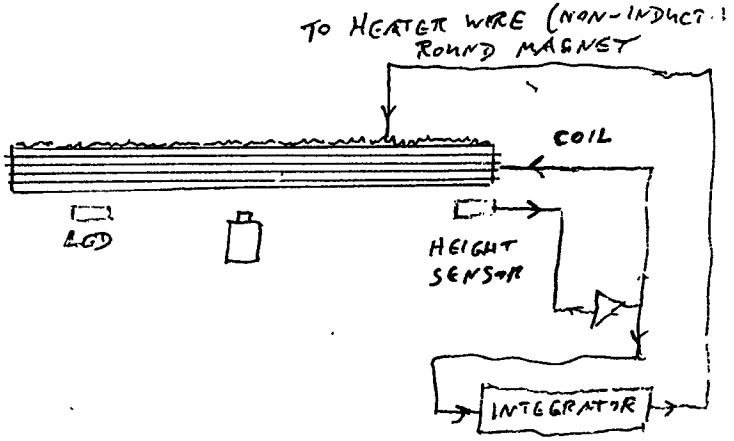

(INTEGRATE CO. VOLTAGE OVER MINUTES → TO DRIVE MEAN VAL. TO ZERO)

2 EFFECTS:-

① KEEPS COIL POWER $<< 1\,mW$

② KEEPS HEIGHT OF TEST MASS CONSTANT INDEPENDANT OF AMBIENT TEMPERATURE

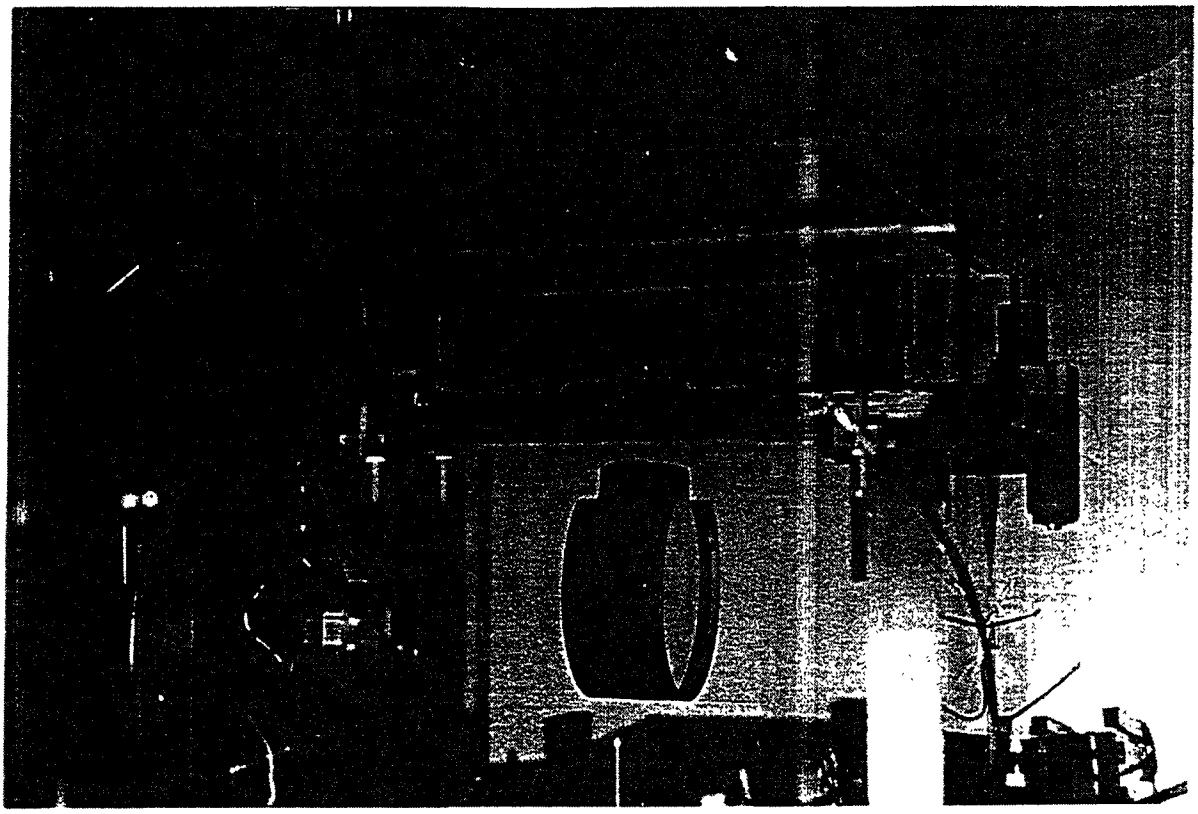

Fig. 3. View of initial assembly of 2-stage levitation system, incorporating tilt control by optical lever.

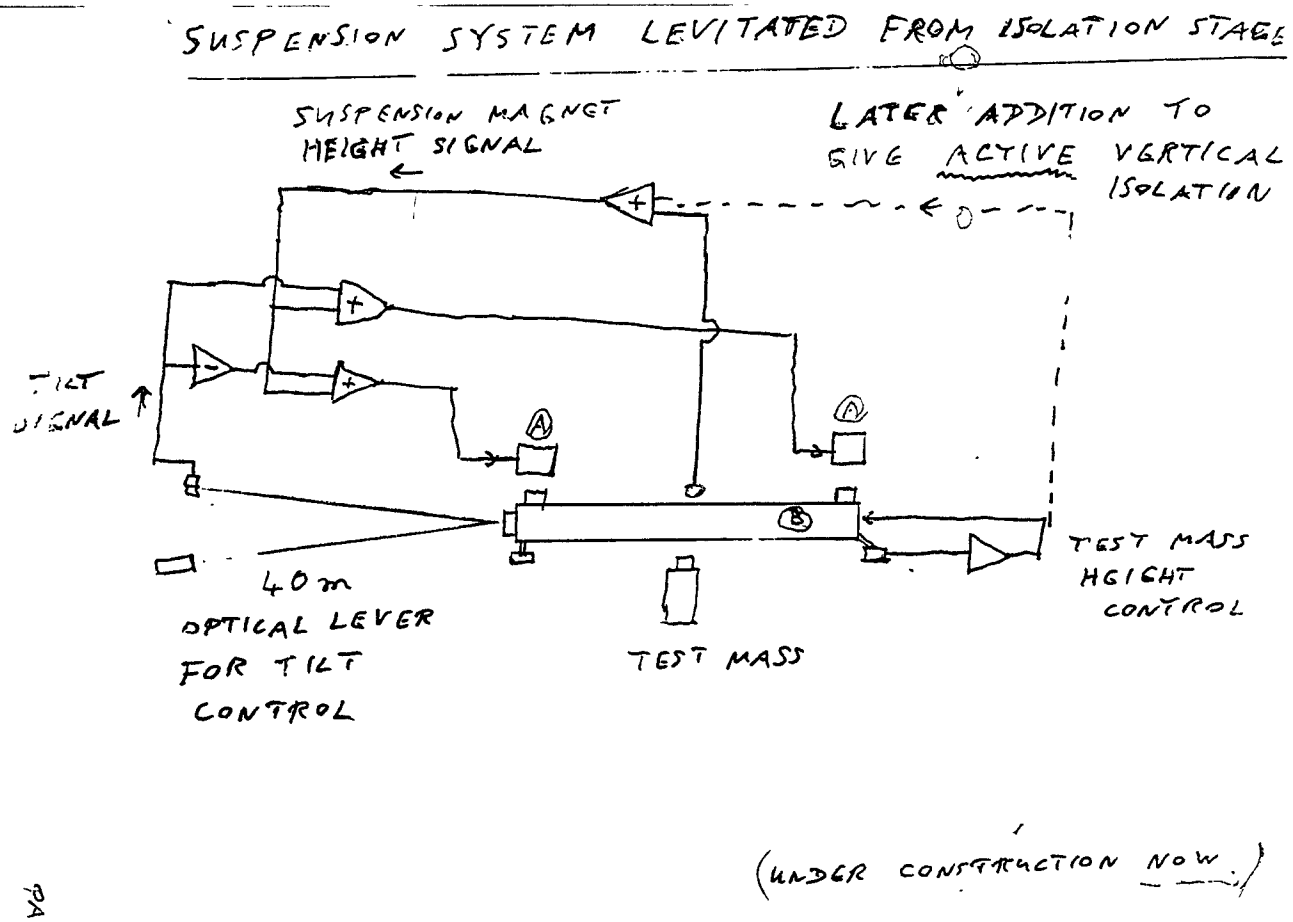

ANNED ENHANCEMENTS TO 2-STAGE SYSTEM.

TICAL

NEGATIVE FEEDBACK TO SUPPORT MAGNETS (A) FROM TEST MASS ACTING AS VERTICAL ACCELEROMETER - FORM ACTIVE SYSTEM

- ADDITION OF VERTICAL CORRECTION SIGNAL TO MAGNETS (A) TO LENGTHEN VERTICAL PERIOD OF UPPER STAGE.
- FEED FORWARD OF SIGNAL FROM UPPER STAGE TO MAGNET (B)
- ADDITION OF VERTICAL CORRECTION SIGNAL TO MAGNET (B) TO LENGTHEN VERTICAL PERIOD OF LOWER STAGE.

HORIZONTAL - ALONG BEAM DIRECTION

1. CONTROL TILT DIFFERENCE BETWEEN ENDS OF EACH ARM FROM MAIN INTERFEROMETER OUTPUT,
   i.e. FEEDBACK TO MASSES BY TILT ALONG.

2. ADD LOCAL SENSOR OF TEST MASS POSITION RELATIVE TO MAGNET (B).
   USE SIGNAL TO CAUSE MAGNET TO TRACK TEST MASS. (VIA ADDITIONAL PUSHER COIL)

SIDEWAYS

1. ADD SIDEWAYS SENSORS AND FEEDBACK SIDEWAYS SIGNALS FROM TEST MASS TO (B)

ETC., ETC. ....

OVERALL EFFECT.

TEST MASS ACTS AS ACCELEROMETER FOR ADDITIONAL ACTIVE ISOLATION IN ALL DIRECTIONS.

Diffractive-Coupled Interferometers

- proposed new technique aimed at improved power-handling capability and thermal noise.

Basic Concept: Couple light into and out of cavities and interferometer arms by diffraction grating pattern on mirrors of test masses or beamsplitters

- to divide wavefront by diffraction instead of transmission

Possible Advantages: No need to pass light through test masses or beamsplitters, so -

1. Can select materials for high Q , and if needed good thermal conductivity / expansion properties
   - without any transparancy constraint

2 Thermal lensing eliminated , leaving thermal expansion as the only thermal effect - so higher light power is practicable

3 Power dissipation reduced, as transmission losses eliminated
   - reduces thermal distortions further

4. Reduction in power dissipation makes cryogenic test masses more practicable
   - improving possibility of getting higher Q than at room temperature, and possibility of further reduction in thermal noise.

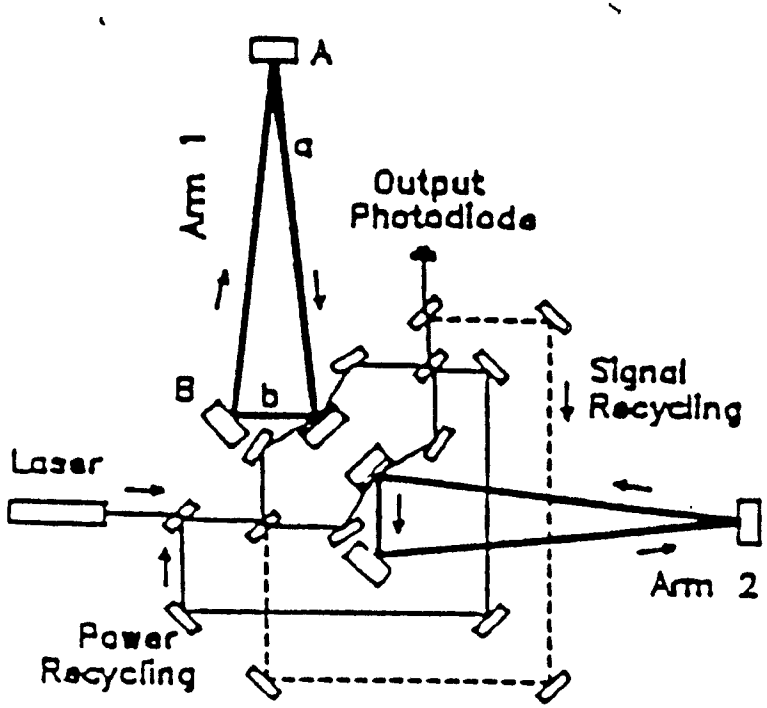

Fig.13.

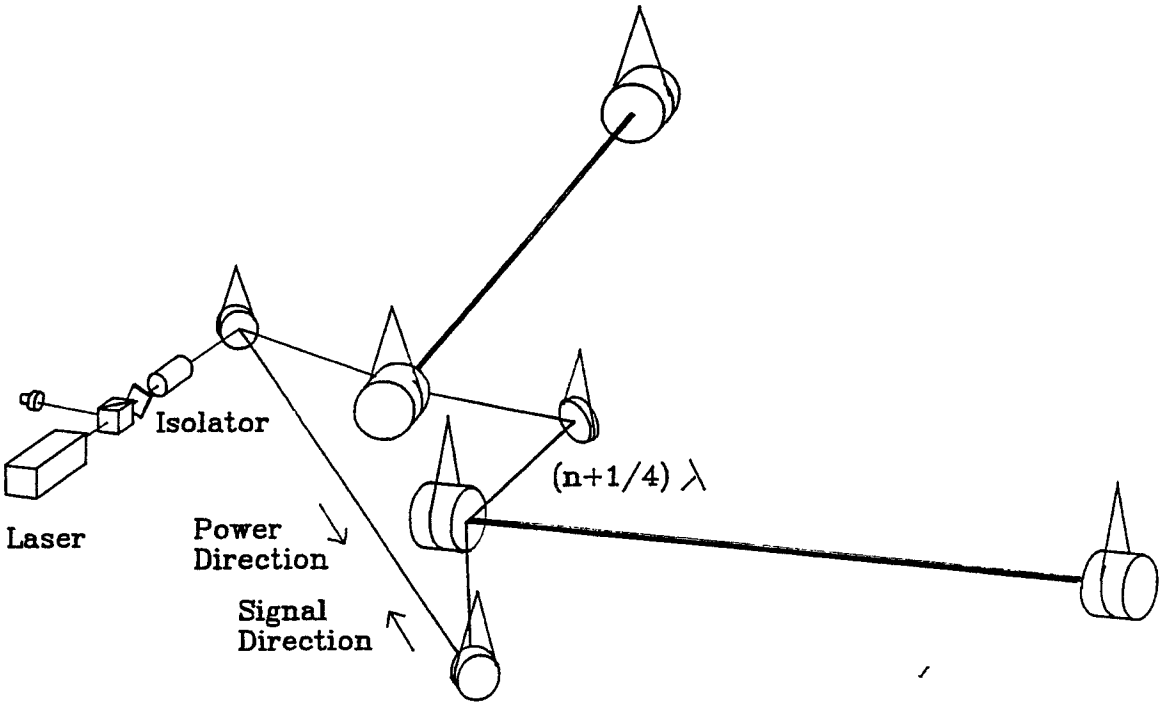

(Diagram shows main beams only)

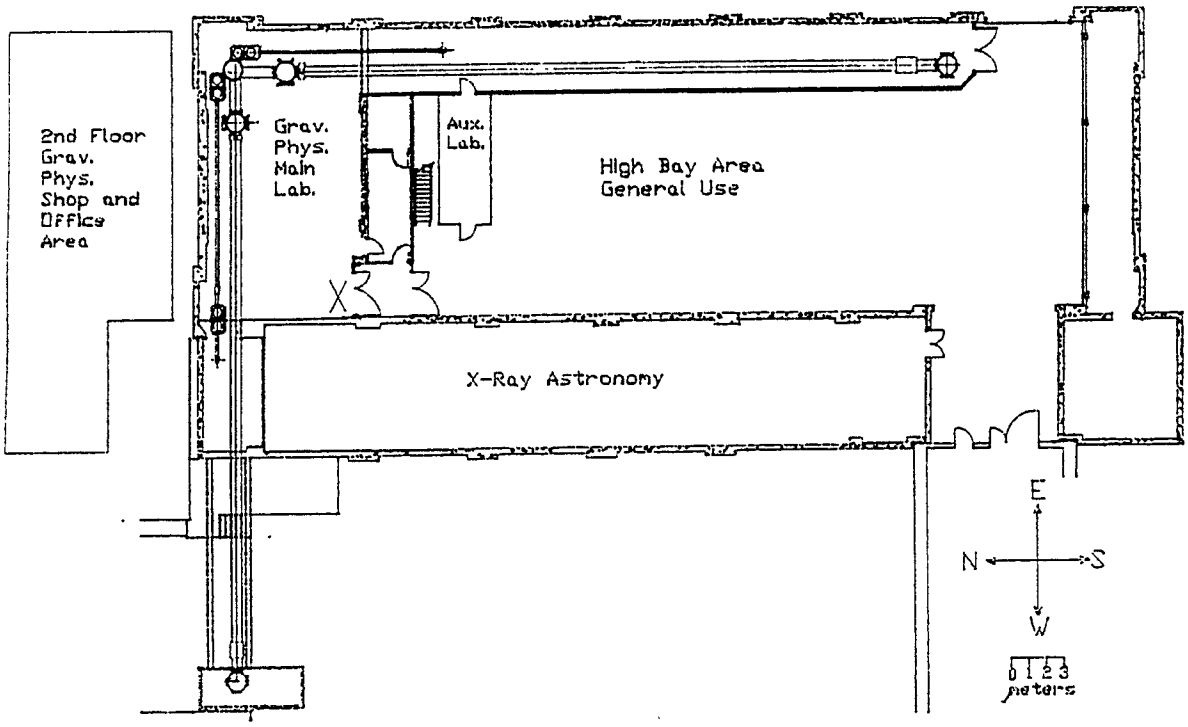

Fig. 16. Simplified layout of new laboratories and facilities planned for this project.

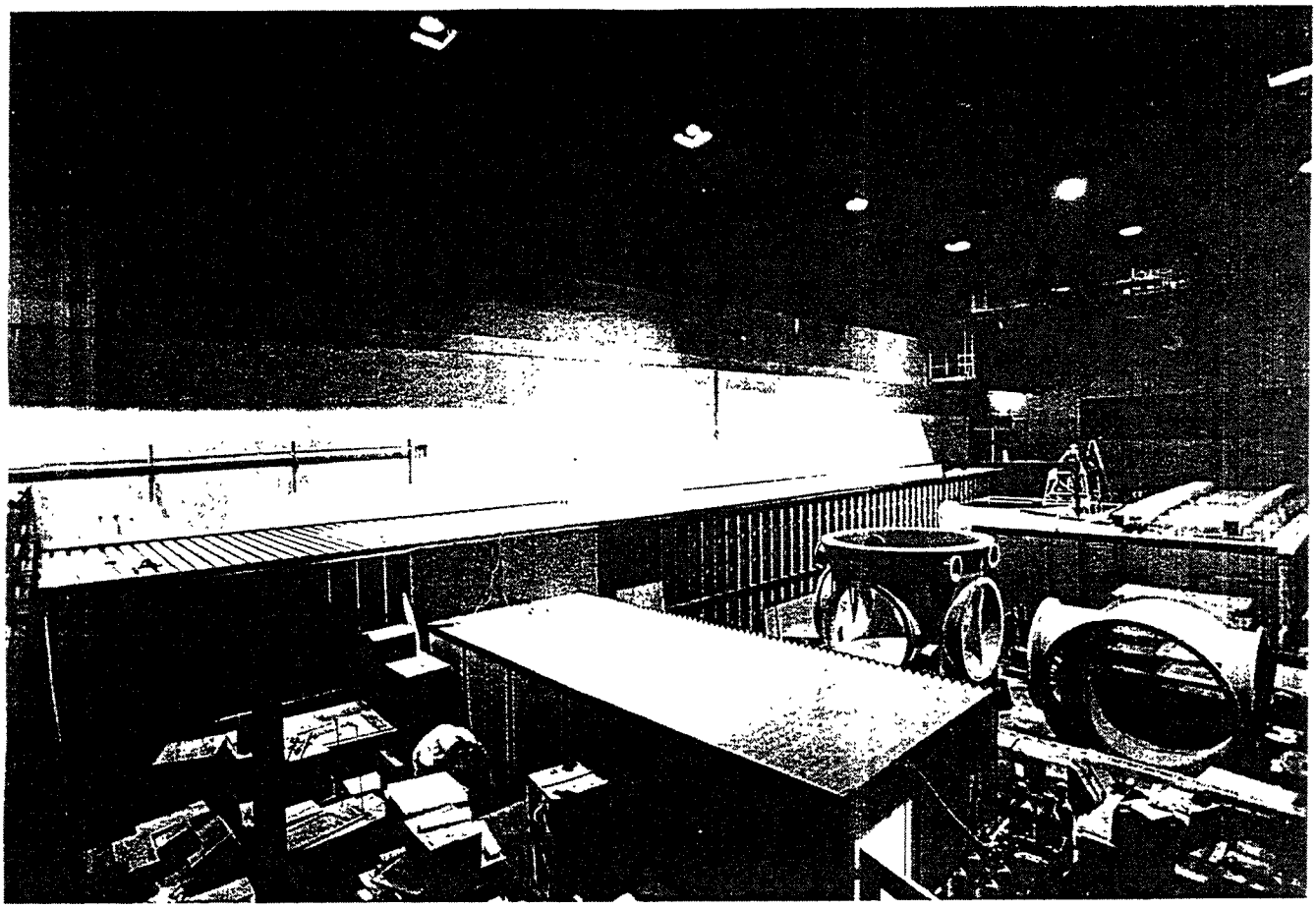

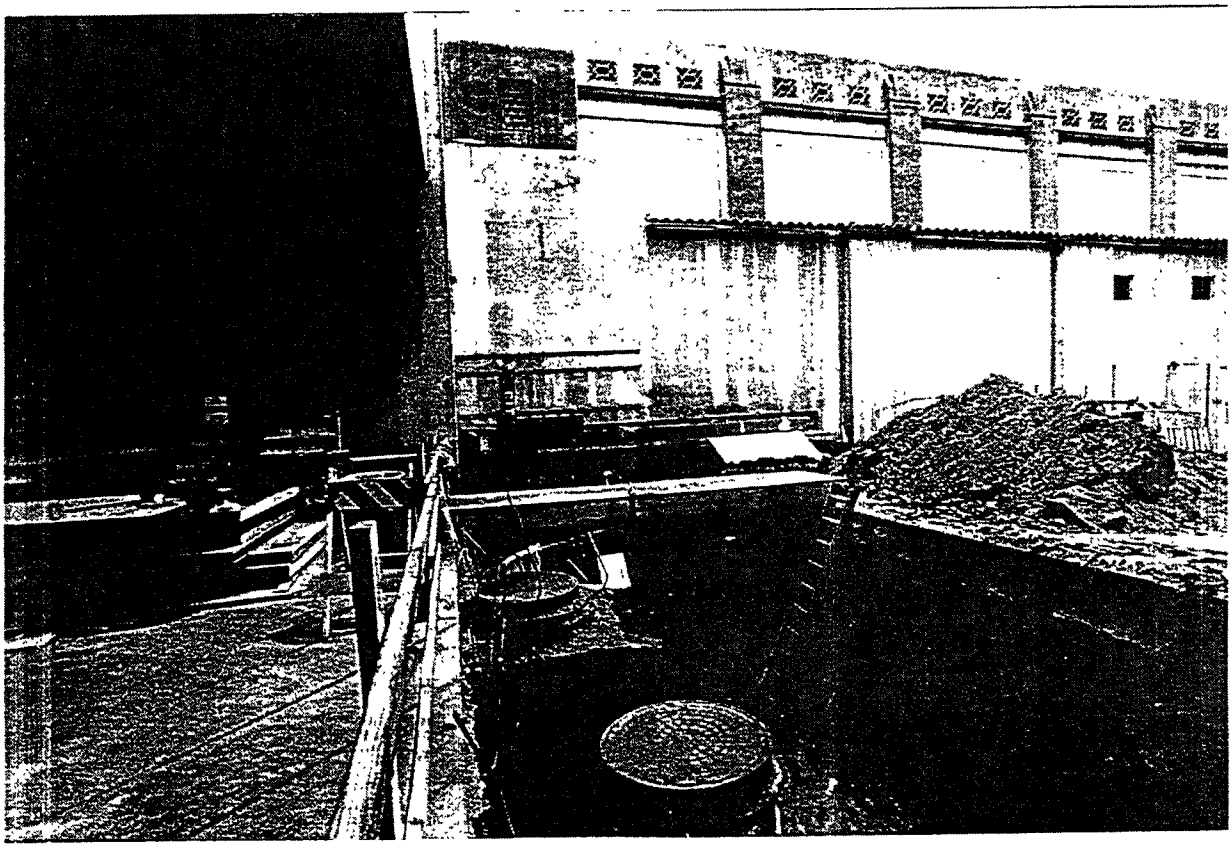

Fig. 1. View of excavations for the west tunnel extension of the laboratory, looking eastwards at the west wall of the main building housing the lab. (Photo taken January 16, 1997.)

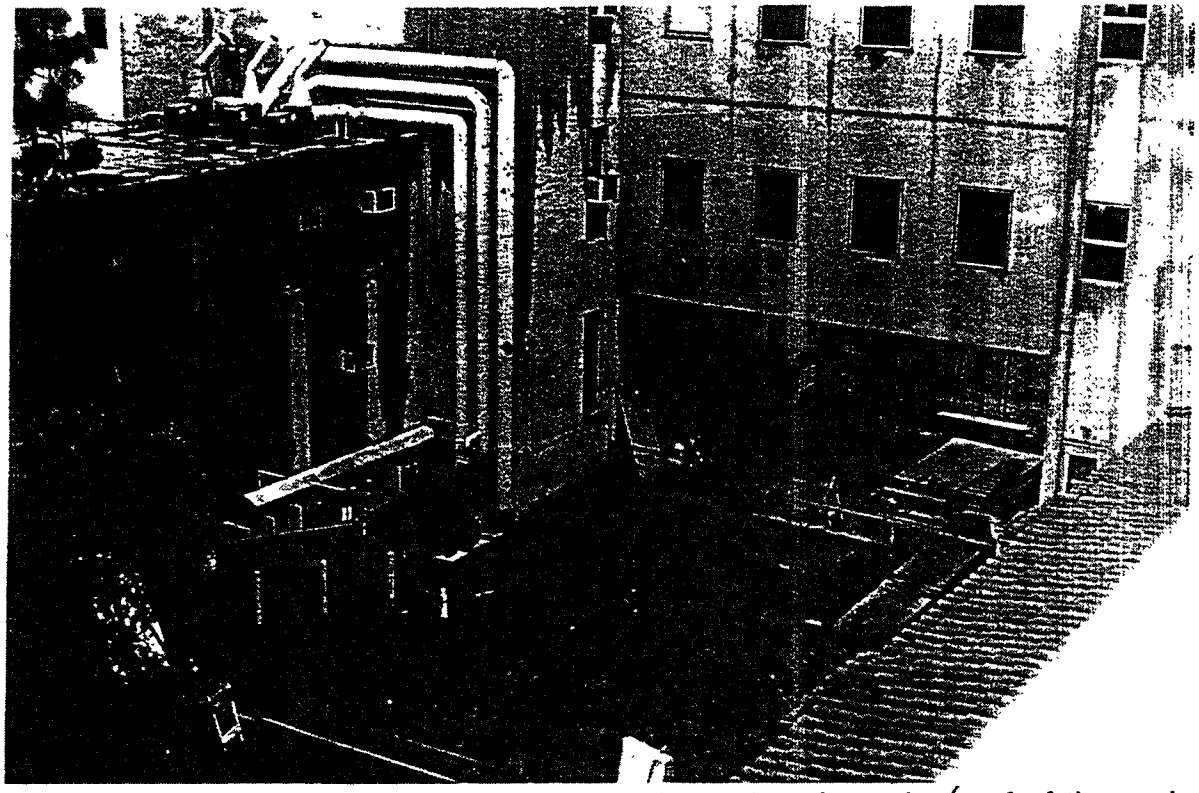

Fig. 2. View of west laboratory extension, taken from the roof of the main building looking northwest, showing the excavation for the end housing. (Photo taken January 16, 1997.)

A 26

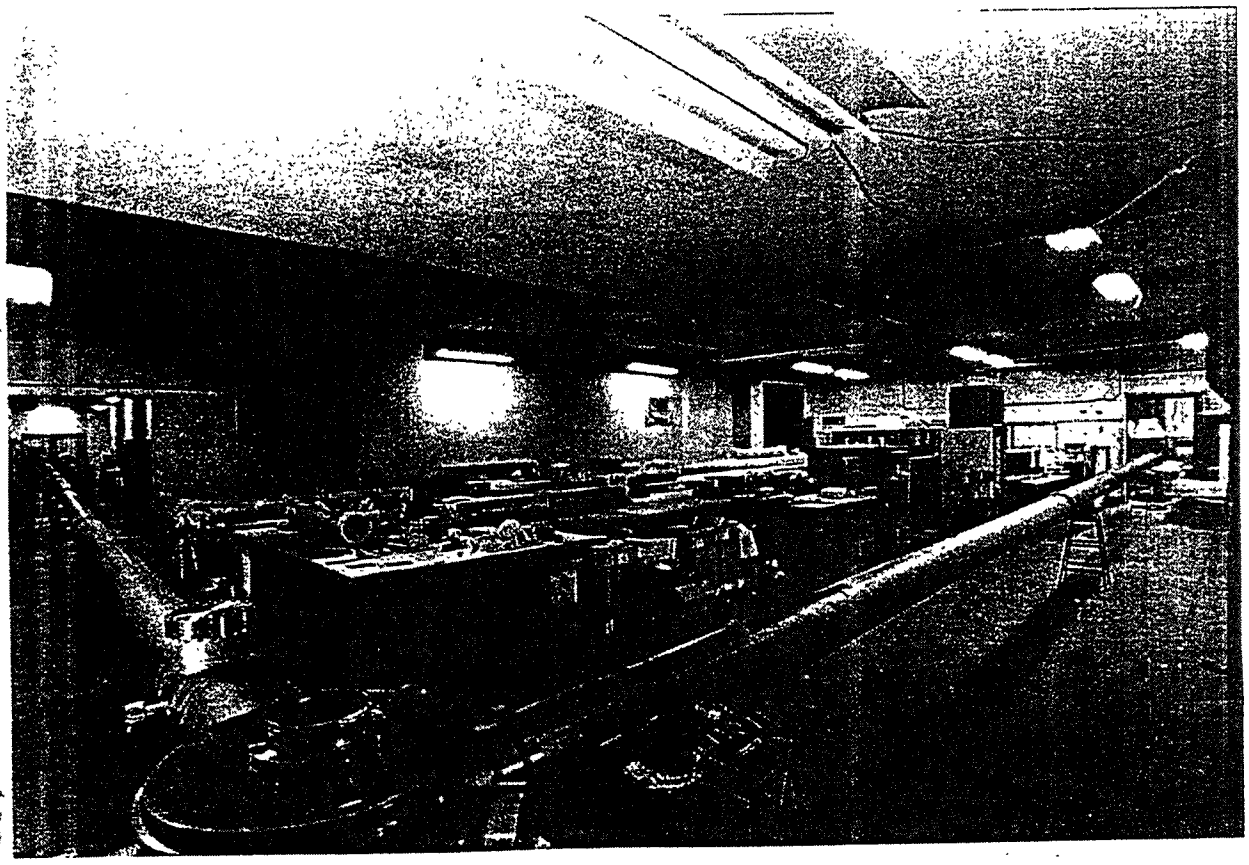

A 27

General Relativistic Numerical Hydrodynamics for Neutron Star Binaries

J. R. Wilson[1,2] and G. J. Mathews[1]

[1]University of Notre Dame
[2]Lawrence Livermore National Laboratory

METHOD

- Solve general relativity equations for neutron star binaries taking three space to be conformally flat

- These are exact solutions of general relativity but:

  No gravitational radiation is accounted for

Except at quadrupole approximation

Physical Processes in Close Neutron Star Binaries

- **Orbit Instability**
- **Collapse Instability**
- **Compression/Heating/Neutrino Emission**
- **Internal Stellar Fluid Circulation**

The Metric:

$$ds^2 = -(\alpha^2 - \beta_i\beta^i)dt^2 + 2\beta_i dx^i dt + \phi^4 \delta_{ij} dx^i dx^j$$

Hamiltonian Constraint

$$R = 16\pi\rho_H + K_{ij}K^{ij} - K^2$$

- **Conformal Factor**

$$\nabla^2\phi = -4\pi\rho_1$$

$$\rho_1 = \frac{\phi^5}{2}\left[\rho W^2 + \epsilon\rho\Big(\Gamma W^2 - \Gamma + 1\Big) + \frac{1}{16\pi}K_{ij}K^{ij}\right]$$

- **Lapse function**

$$\nabla^2(\alpha\phi) = 4\pi\rho_2$$

$$\rho_2 = \frac{\alpha\phi^5}{2}\left[\rho(3W^2 - 2) + \epsilon\rho[3\Gamma(W^2 + 1) - 5] + \frac{7}{16\pi}K_{ij}K^{ij}\right]$$

Momentum Constraint

$$D_j K^{ij} = 8\pi S^i$$

- **Shift Vector**

$$\nabla^2 \beta^i = 4\pi \rho_3^i$$

$$\rho_3^i = 4\left(\alpha\phi^4 S_i - \beta^i \rho W^2(1+\Gamma\epsilon)\right) + \frac{1}{4\pi}\left[\frac{\alpha}{\phi^6}\frac{\partial(\alpha/\phi^6)}{\partial x^j}\left(\frac{\partial\beta^i}{\partial x^j} + \frac{\partial\beta^j}{\partial x^i} - \frac{2}{3}\delta_{ij}\frac{\partial\beta^k}{\partial x^k}\right)\right]$$

Relativistic Hydrodynamics

Perfect Fluid Stress-Energy Tensor: $T_{\mu\nu} = (\rho + \rho\epsilon + P)U_\mu U_\nu + P g_{\mu\nu}$

Hydrodynamic Variables:

- Coordinate covariant matter density, $D = W\rho \quad ; W = \alpha U^t = \left[1 + \frac{\sum_{i=j}^{3} U_i^2}{\phi^4}\right]^{1/2}$
- Internal energy density, $E = W\rho\epsilon$
- Three velocity, $V^i = \frac{\alpha U_i}{\phi^4 W} - \beta^i$
- Pressure, $P = (\Gamma - 1)\rho\epsilon$
- Momentum density, $S_i = (D + \Gamma E)U_i$

- **Conservation of baryon number**

$$\frac{\partial D}{\partial t} = -6D\frac{\partial \log\phi}{\partial t} - \frac{1}{\phi^6}\frac{\partial}{\partial x^j}(\phi^6 D V^j)$$

- **Internal energy conservation**

$$\frac{\partial E}{\partial t} = -6\Gamma E\frac{\partial \log\phi}{\partial t} - \frac{1}{\phi^6}\frac{\partial}{\partial x^j}(\phi^6 E V^j) - P\left[\frac{\partial W}{\partial t} + \frac{1}{\phi^6}\frac{\partial}{\partial x^j}(\phi^6 V^j)\right]$$

- **Momentum conservation**

$$\frac{\partial S_i}{\partial t} = -6S_i\frac{\partial \log\phi}{\partial t} - \frac{1}{\phi^6}\frac{\partial}{\partial x^j}(\phi^6 S_i V^j) - \alpha\frac{\partial P}{\partial x^i} + 2\alpha(D+\Gamma E)(W - \frac{1}{W})\frac{\partial \log\phi}{\partial x^i} + S_j\frac{\partial\beta^j}{\partial x^i}$$

$$-W(D+\Gamma E)\frac{\partial\alpha}{\partial x^i} - \alpha W(D+\Gamma E)\frac{\partial\chi}{\partial x^i}$$

SUMMARY OF RESULTS

1 We find that as the orbit shrinks, the increased gravitational forces compress and heat the stars

$$E_{thermal} \sim 10^{53} \text{ ergs}$$

2 Interior temperatures as high as 70 MeV are possible

3 Neutrino luminosities as high as 0.5×10^{53} ergs sec^{-1} per star are possible before the stars collapse to black holes.

4 The neutrinos escaping the surface will cause the blow off of an $e^+ - e^-$ plasma.

5 Relativistically induced fluid vorticities in the stars may cause intense magnetic fields $\sim 10^{17}$ gauss to form around the stars

Stellar Compression in Neutron Star Binaries

- There exists terms in the relativistic hydrodynamics equations which increase the effective self gravity of the stars

The Metric:

$$ds^2 = -(\alpha^2 - \beta_i\beta^i)dt^2 + 2\beta_i dx^i dt + \phi^4 \delta_{ij} dx^i dx^j$$

- Sources for lapse function (α) and conformal factor (ϕ) are enhanced

$$\nabla^2\phi = 2\pi\phi^5 \left[\rho(1+\epsilon) + \epsilon\Gamma(W^2-1)\right]$$

$$\nabla^2(\alpha\phi) = 2\pi\phi^5 \left[\rho(1+\epsilon) + 6(\Gamma-1)\rho\epsilon + 3\rho(1+\epsilon\Gamma)(W^2-1)\right]$$

where $W = \sqrt{1 + \sum U_i^2/\phi^4}$ and $\Gamma = 1 + P/\rho\epsilon$.

- Acceleration terms in equilibrium configuration

$$\frac{\partial P}{\partial x^i} = -(\rho + \rho\epsilon\Gamma)\left(\frac{\partial \log\alpha}{\partial x^i} - \frac{U_j}{\alpha}\frac{\partial \beta^j}{\partial x^i} + \left[\frac{\partial \log\alpha}{\partial x^i} - 2\frac{\partial \log\phi}{\partial x^i}\right](W^2-1)\right)$$

Note: $\alpha \sim 1/\phi^2$

Compression effect $\sim (v/c)^2$ should be apparent in post Newtonian approximation

- In post-Newtonian approximation

$$g_{tt} = -1 - 2\Phi - 2\Phi^2 - 2\Psi$$

Φ *is the Newtonian potential*
$2(\Phi^2 + \Psi)$ *is the* $(v/c)^4$ *correction*

- In our rotating coordinates

$$\nabla^2\Psi = 4\pi G\Big[2(W^2-1)[\rho(1+\epsilon)+P] + 3P\Big]$$

- As in GR, fields are enhanced by factors $\sim (W^2 - 1)$.
- The acceleration terms are also similarly enhanced.

Indicators that our method is satisfactory for neutron-star binaries

- Estimated relative rate of change of the orbit angular momentum from the quadrupole formula is small:

$$\frac{\dot{J}}{\omega J} \lesssim 10^{-3}$$

Our solution is exact but must contain hidden radiation components

---

- **Estimate hidden gravitational wave energy using York's extrinsic curvature decomposition**

$$K^{ij} = K^{ij}_L + K^{ij}_T$$

where

$$D_i K^{ij}_L = 8\pi S^i$$

$$D_i K^{ij}_T = 0$$

where K^{ij}_T is traceless.

- We find

$$\int K^{ij}_T K_{Tij} \frac{dV}{8\pi} \approx 2 \times 10^{-5}\ \mathrm{M_G}$$

Note: $K^{ij}_T K_{Tij}$ is a measure of the radiation energy density.

- **Cook, Shapiro. & Teukolski (1996) calculated the structure of extremely rapidly rotating neutron stars both in their exact formalism and in a conformally flat "approximation."**
  They found differences to be very small ($\lesssim 1\%$)

But they assumed constant angular velocity and four velocity,

$$\vec{U} = U^t \left(\frac{\partial}{\partial t} + \Omega \frac{\partial}{\partial \varphi} \right)$$

Reith & Schäfer (1996 preprint) calculated the properties of neutron star binaries to order $(v/c)^4$ in the post-Newtonian approximation in both an unconstrained and conformally flat metric.

POINT PARTICLE P.N.

$$k = 1+\frac{1}{2}(5-2\nu)\frac{E}{c^2}+\frac{5}{4}(7-2\nu)\frac{1}{h^2c^2}$$ Fractional Perastron advance per orbit.

$$k_{mat} = 1+\frac{1}{2}(5-\frac{3}{2}\nu-\frac{41}{12}\nu^2)\frac{E}{c^2}+\frac{1}{4}(35-\frac{27}{2}\nu-\frac{31}{4}\nu^2)\frac{1}{h^2c^2}$$

$$P = 1-\frac{1}{4}(15-\nu)\frac{E}{c^2}-\frac{3}{32}(35+30\nu+3\nu^2)\frac{E^2}{c^4}+\frac{3}{2}(5-2\nu)\frac{\sqrt{-2E^3}}{hc^4}$$ P = Period

$$P_{mat} = 1-\frac{1}{4}(15-\nu)\frac{E}{c^2}-\frac{15}{32}(7+6\nu-25\nu^2)\frac{E^2}{c^4}+\frac{1}{2}(15-\frac{9}{2}\nu-\frac{41}{4}\nu^2)\frac{\sqrt{-2E^3}}{hc^4}$$

$$h = 1+\frac{1}{2}(3+\frac{1}{3}\nu)\frac{\omega^{2/3}}{c^2}+\frac{1}{8}(27-19\nu+\frac{1}{3}\nu^2)\frac{\omega^{4/3}}{c^4}$$ $h = \frac{J}{GM\mu}$

$$h_{mat} = 1+\frac{1}{2}(3+\frac{1}{3}\nu)\frac{\omega^{2/3}}{c^2}+\frac{1}{8}(27-39\nu-\frac{17}{3}\nu^2)\frac{\omega^{4/3}}{c^4}$$

$\nu = \frac{m_1 m_2}{(m_1+m_2)^2}$ $E = -\frac{1}{2}k^2$ ω = frequency

$\nu = \frac{1}{4}$ $A \approx 6$

$k - k_{mat} = \frac{\nu(24+67\nu)}{24A^2} \Rightarrow .012$

$P - P_{mat} = \frac{\nu(-6+65\nu)}{8A^4} \Rightarrow .00025$

$k - k_{mat} = \frac{\nu(10+3\nu)}{4A^4} \Rightarrow .0005$

} SMALL

Likelyhood stars will collapse before fir
infall depends on:

A) Equation of State
B) Neutron Star Masses

For B) 1.15<M<1.50 Solar Mass
See S. FINN
For A) We have the results:
If max M=1.55 then
M*=1.35 is unstable
If max M=1.70 then
M*=1.35 is unstable to collapse&inspiral
at same J
If max M=1.84 then
M*=1.45 is unstable to collapse&inspiral
at same J
Hence if EOS max Mass> 1.70 few collapses

Arguments for low max. Mass EOS
1) SN1987a Stiff EOS cools too quickly
2) Bethe, Brown argue from nucleosynthesis
M<1.56
3) Lattimer argues EOS soft for neutron
star cooling Iffy
4) Statistical Mechanics arguement
5) Weinberg G and C.

"It follows that in general

$$0 \le p \le \frac{\rho c^2}{3}$$

EQUATION OF STATE

T = 0. Parametrization

Symmetry Energy-related

$$P_S = (1-2t_0)^2\left(11.6 + \frac{72.1}{(1+4.4y)^2}\right) F_0 y^2$$

$$\mu_e = \frac{dE_S}{dY_e} \quad \text{e.g. in } V_0 \qquad y = \rho/\rho_0$$

B.C.K

$$P_{BCK} = \frac{K}{q\Gamma}\left(y^\Gamma - 1\right) F_0$$

$$P = P_S + P_{BCK} + P_{electron}$$

IF $\frac{dP}{d(\rho+\epsilon)} > \frac{c^2}{3}$ at $\frac{dP}{d(\rho+\epsilon)} = \frac{c^2}{3}$

stronger restriction than

$$\frac{dP}{d(\rho+\epsilon)} \leq c^2 \; !$$

EOS → M_G^{MAX}

K MeV	Γ	$M_{G\,M_\odot}^{MAX}$	y	ρ_{MAX}	
*200	2.75	1.60	7.7	19.7	
200	3.00	1.68	7.6	19.5	
200	3.25	1.61	6.9	17.7	
300	2.75	1.70	7.1	18.1	$\frac{dP}{P_{TOT}} \leq \frac{1}{3}$
300	3.00	1.75	6.6	17.0	
300	3.25	1.77	6.2	15.9	
400	4.0	1.78			
140	2.75	1.48	8.5	21.8	
140	3.00	1.56	9.6	24.8	
140	3.25	1.62	8.1	20.8	
140	3.50	1.66	7.8	19.9	
200	3.00	1.95			$\frac{dP}{dP_{TOT}} \leq 1$
300	3.00	2.30			
400	4.00	2.75			

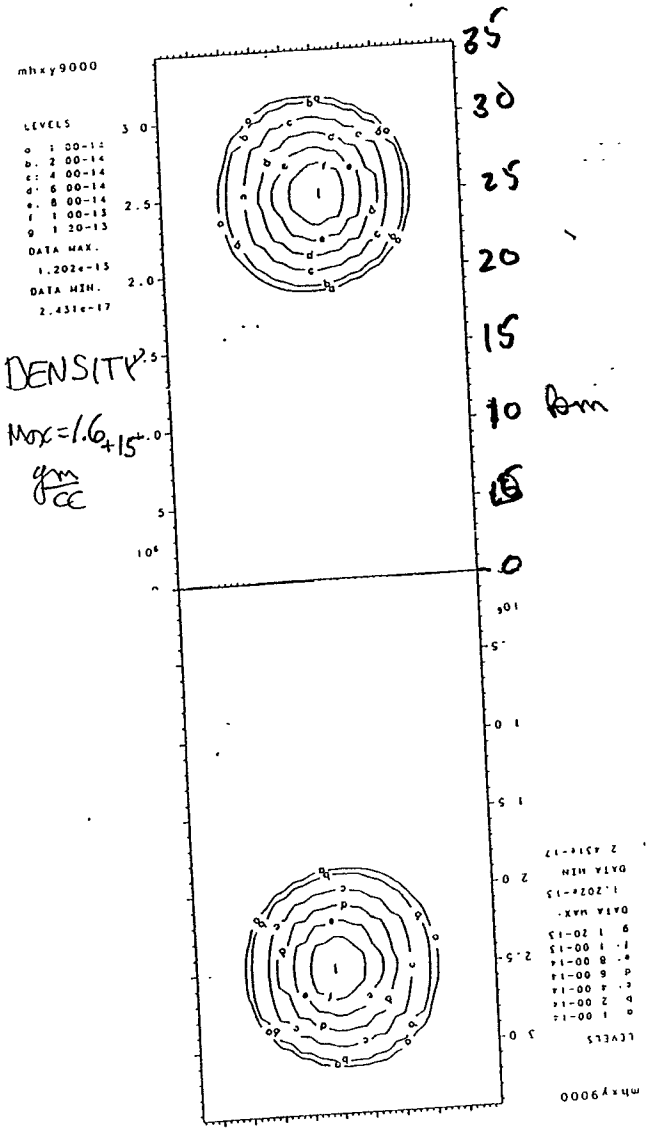

150 ∝ CONTOURS

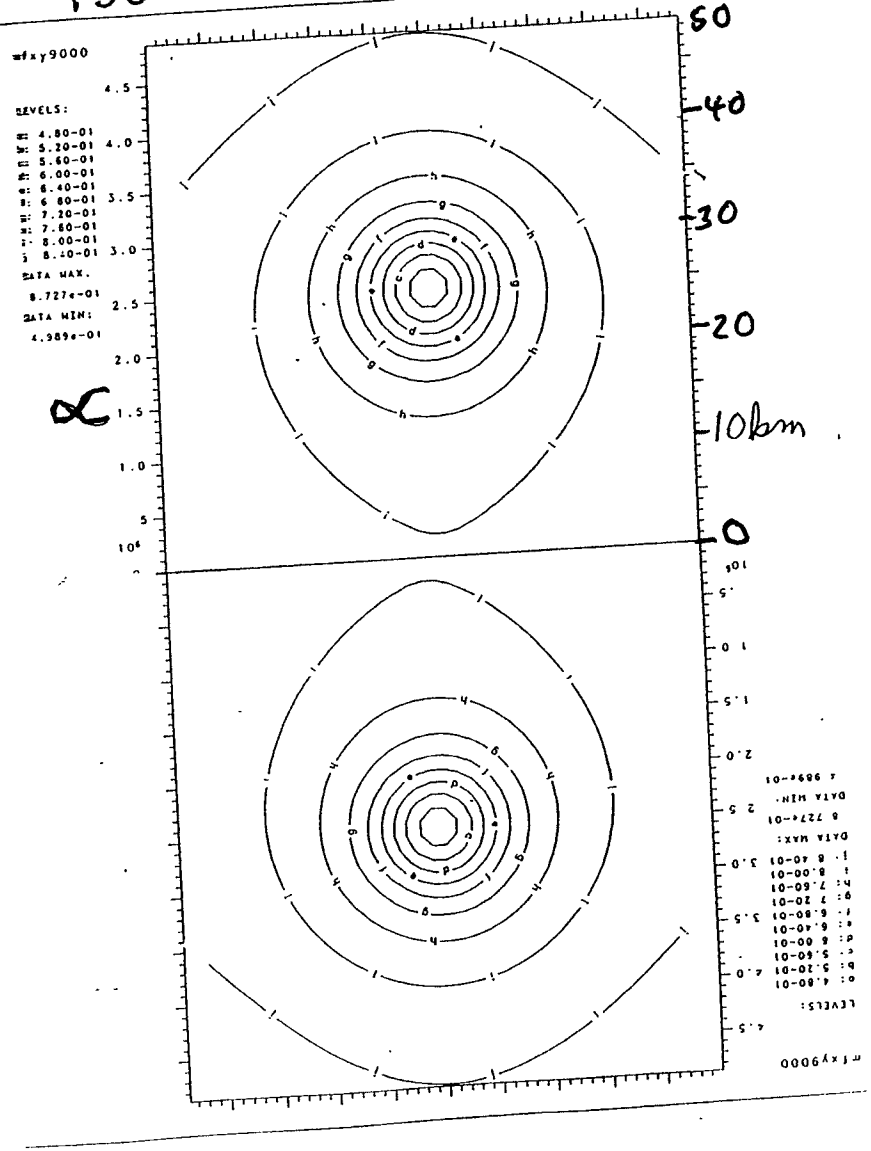

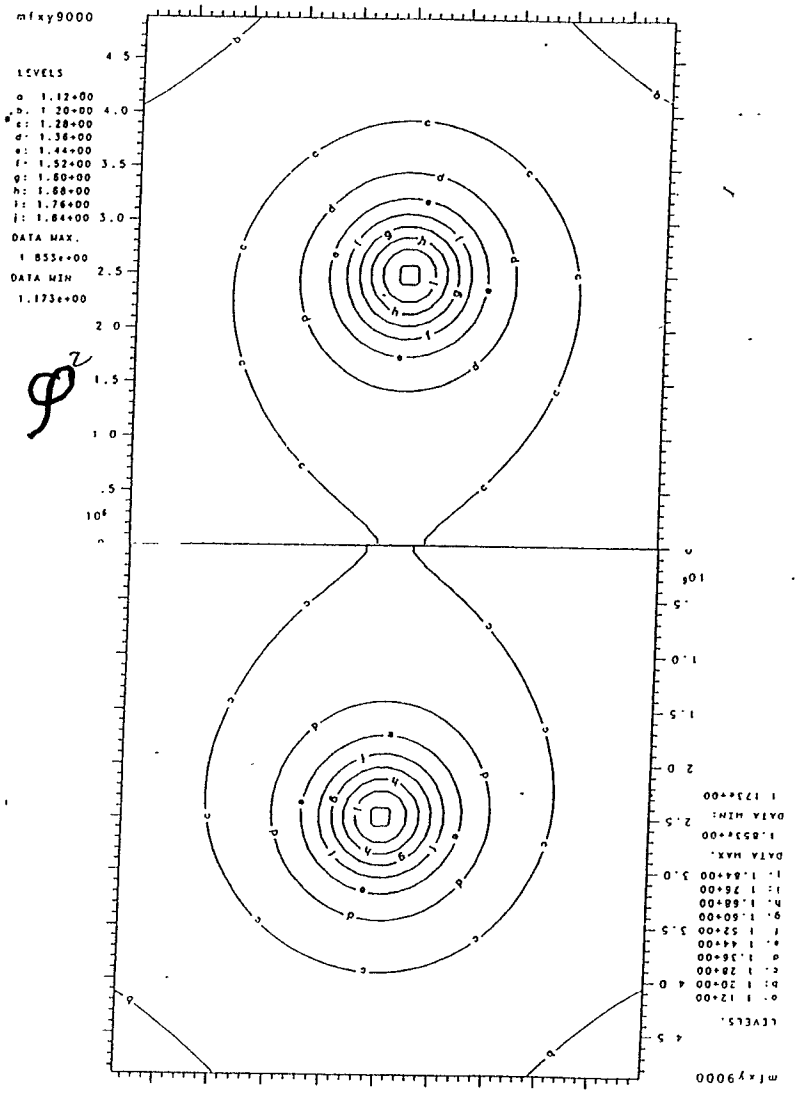

SHIFT VECTOR $-(\vec{\omega}\times\vec{R})$

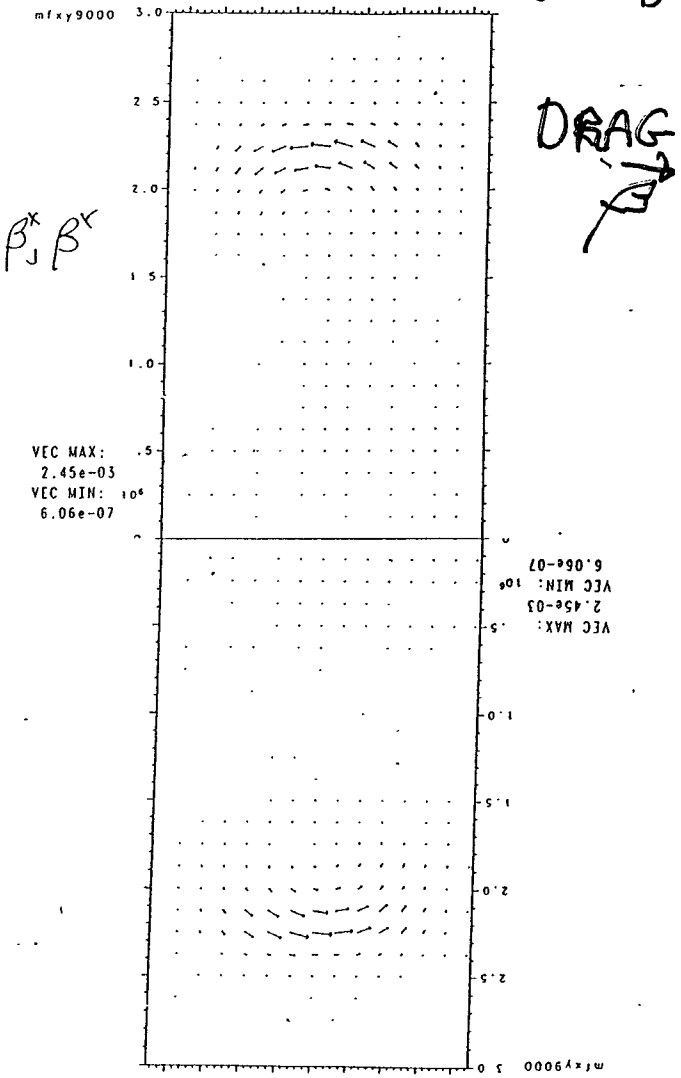

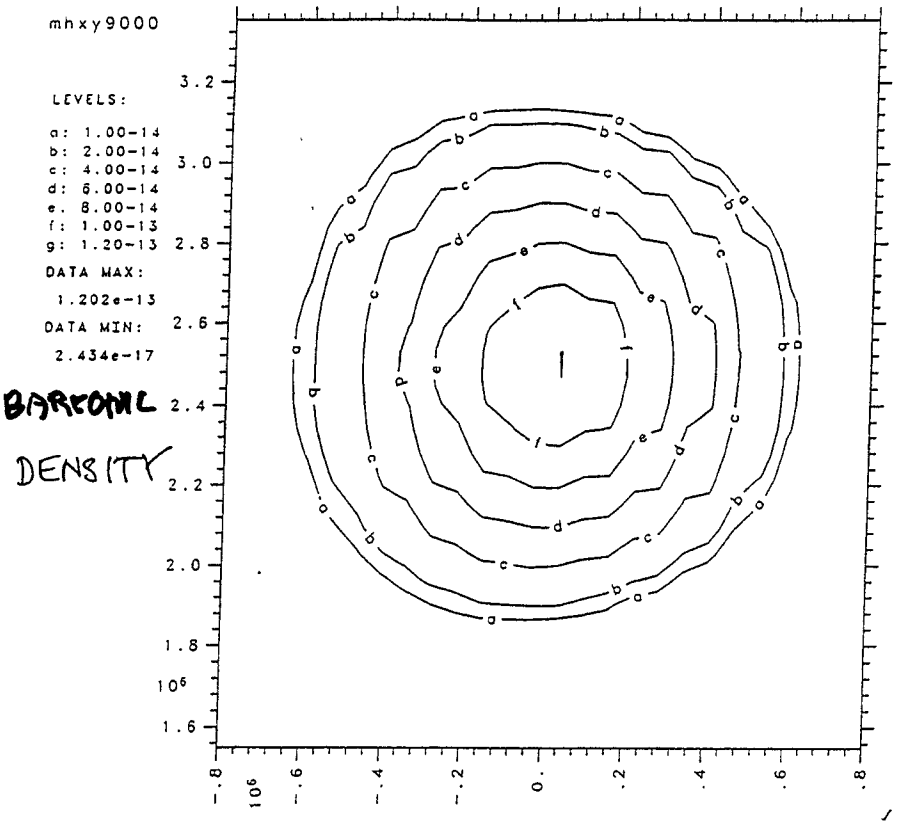

BARYONIC DENSITY

00000 iso d

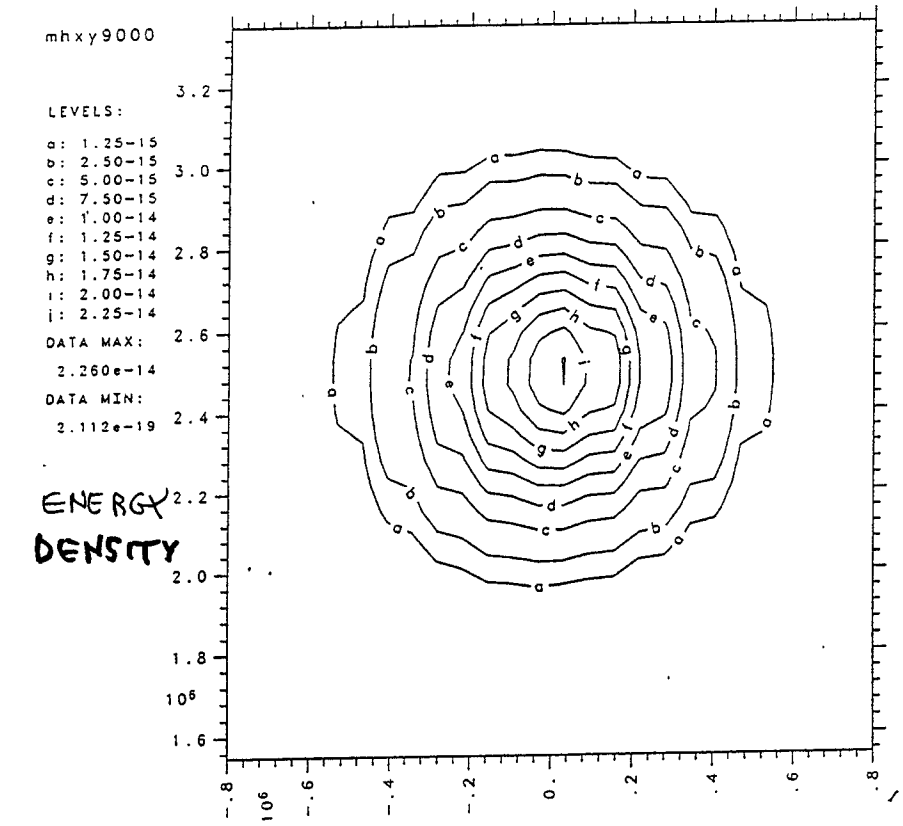

ENERGY DENSITY

00000 iso e

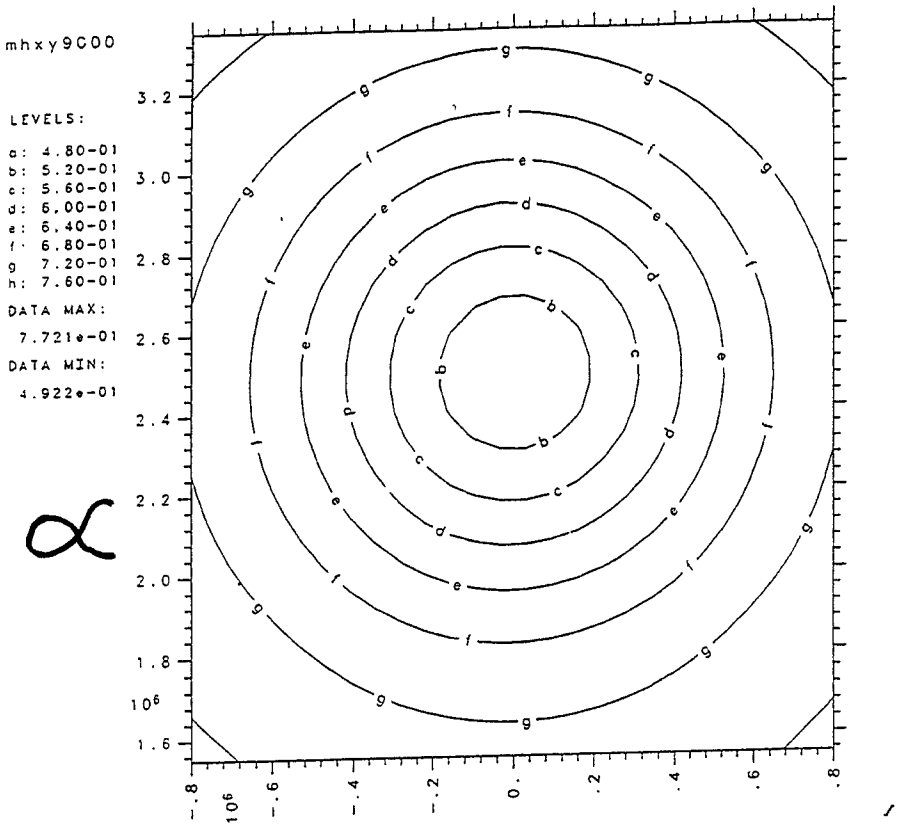

00000 iso al

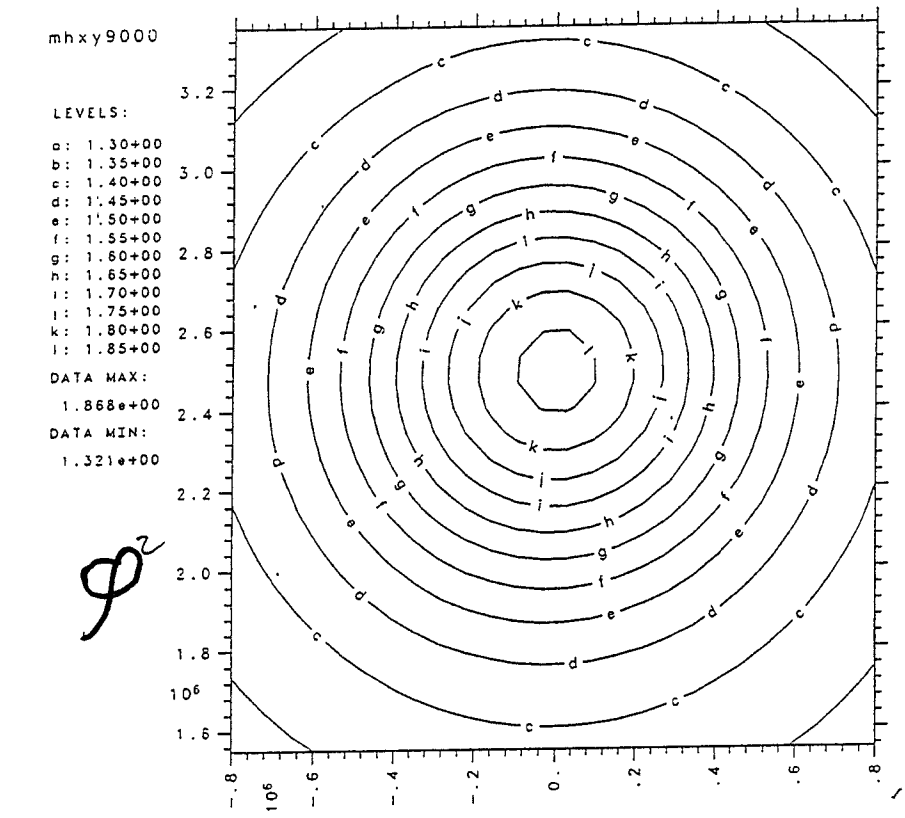

00000 iso phisq

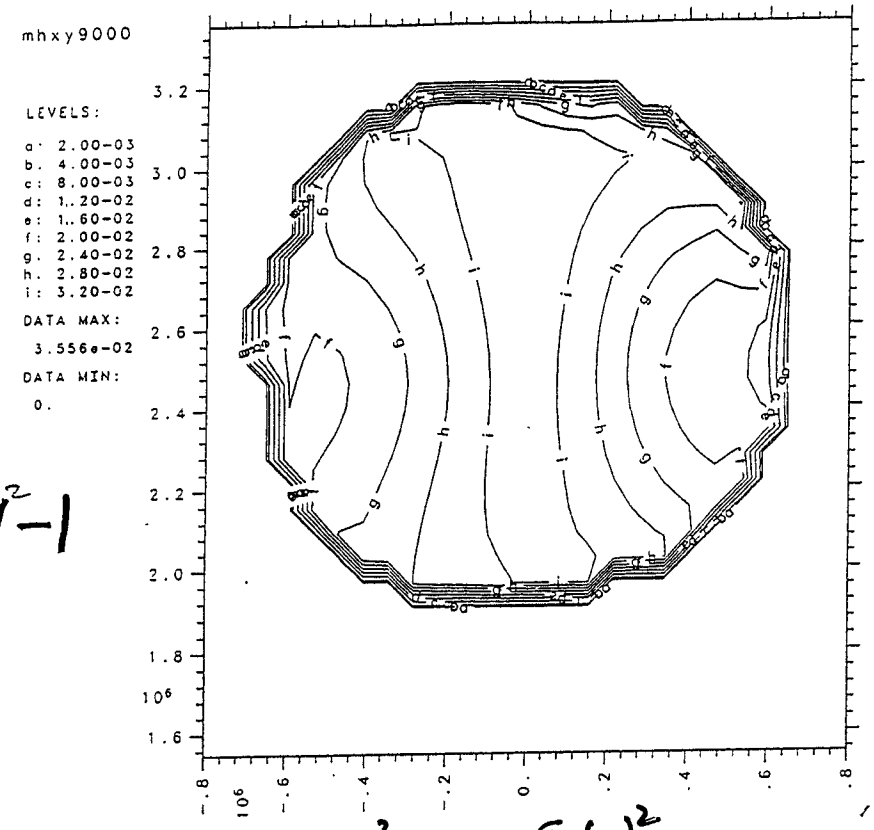

W^2-1

$$W^2-1=\xi_i\frac{U_{\infty}^2}{\varphi^4}$$

00000 iso wsq

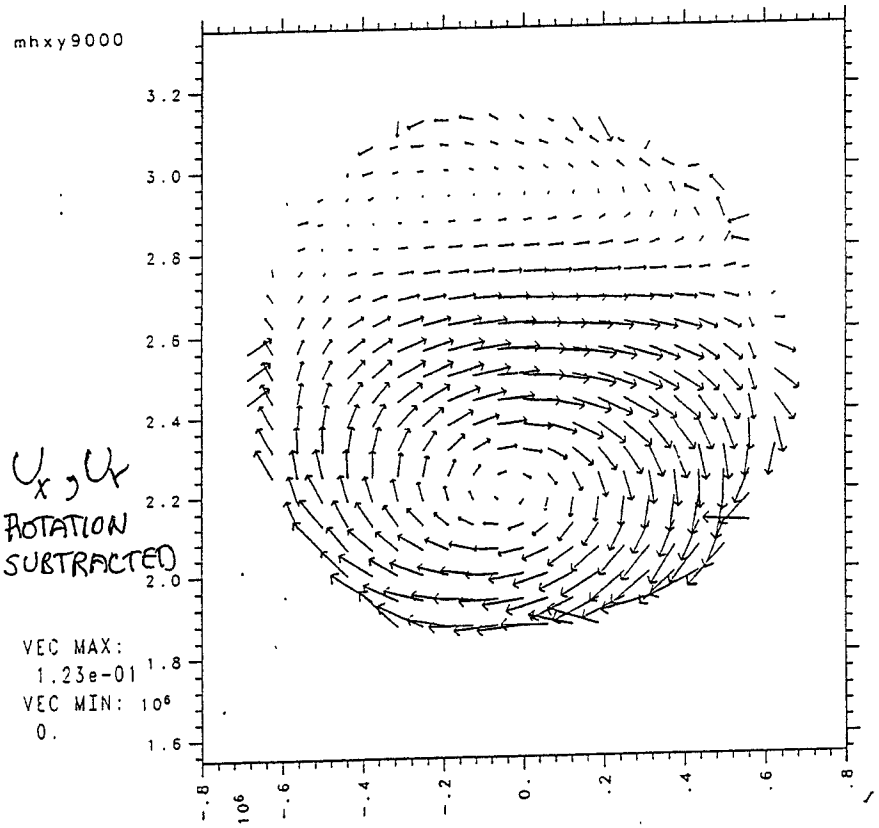

U_x, U_y
ROTATION SUBTRACTED

00000 vector sx sy

Why is K=200

CONCLUSION

There exists a wealth of physical effects in Neutron star binaries that is not seen is PN calculations.

Matthews talk will give details of calculations.

Thursday AM Suspensions and Seismic Isolation II
January 30 Chair: J. Hough

8:00	S. Braccini(Pisa)	Virgo Superattenuator System
8:25	Discussion	
8:35	L. Holloway(Illinois)	A Pre-Isolation Stage for the Virgo Superattenuator
9:00	Discussion	
9:10	R. DeSalvo(INFN-Pisa)	Noise in the Virgo Superattenuators
9:35	Discussion	
9:55	S. Rowan(Glasgow)	Measurements on Fused Quartz Pendulums for Gravitational Wave Detectors
10:20	Discussion	
10:30	N. Robertson(Glasgow)	Suspension Design for GEO 600
10:55	Discussion	
11:05	P. Saulson(Syracuse)	A Few Advances in Understanding Thermal Noise
11:30	Discussion	

VIRGO Superattenuator System

by S.Braccini

I.N.F.N. PISA

Required attenuation performances

The input seismic noise is approximated by

$$\tilde{X}(f) = A / f^2 \qquad A \approx 10^{-8} - 10^{-6}\,\mathrm{m \cdot Hz^{3/2}}$$

@ 10 Hz this means

$$\tilde{X} \approx 10^{-8} - 10^{-10}\,\mathrm{m}/\sqrt{\mathrm{Hz}}$$

@ 10 Hz VIRGO needs

$$\tilde{X} \approx 10^{-18}\,\mathrm{m}/\sqrt{\mathrm{Hz}}$$

A VERY STRONG ATTENUATION IS NECESSARY !!!

Horizontal attenuation

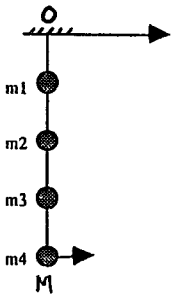

$$\frac{\tilde{X}_M(f)}{\tilde{X}_0(f)} \approx \frac{C}{f^{2N}}$$ Above the resonant frequencies

$$\left(C = f_1^2 \cdot f_2^2 \cdots f_N^2 \right)$$

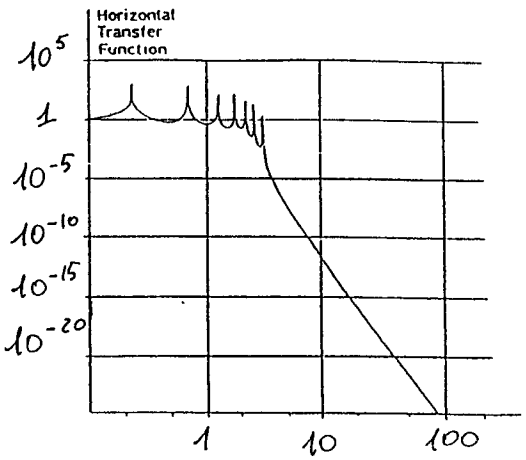

A good horizontal attenuation at few Hz can be obtained if the chain's resonant frequencies are at very low frequency

Long pendula are desired !!!

Vertical attenuation

The coupling between different degrees of freedom forces to attenuate seismic noise also in the vertical direction

The same attenuation scheme: a chain of vertical pendula

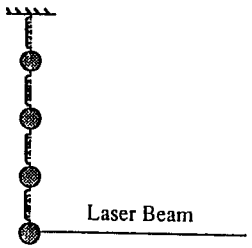

Low resonant frequencies, i.e. soft springs !

⇓

On this principle relies the design of the VIRGO Superattenuators

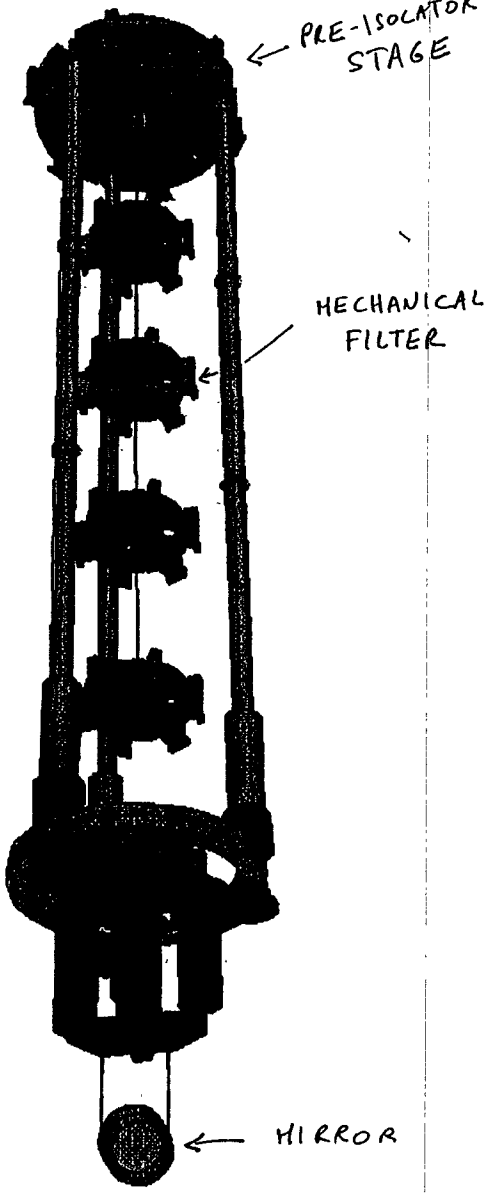

$h \sim 9\ m$

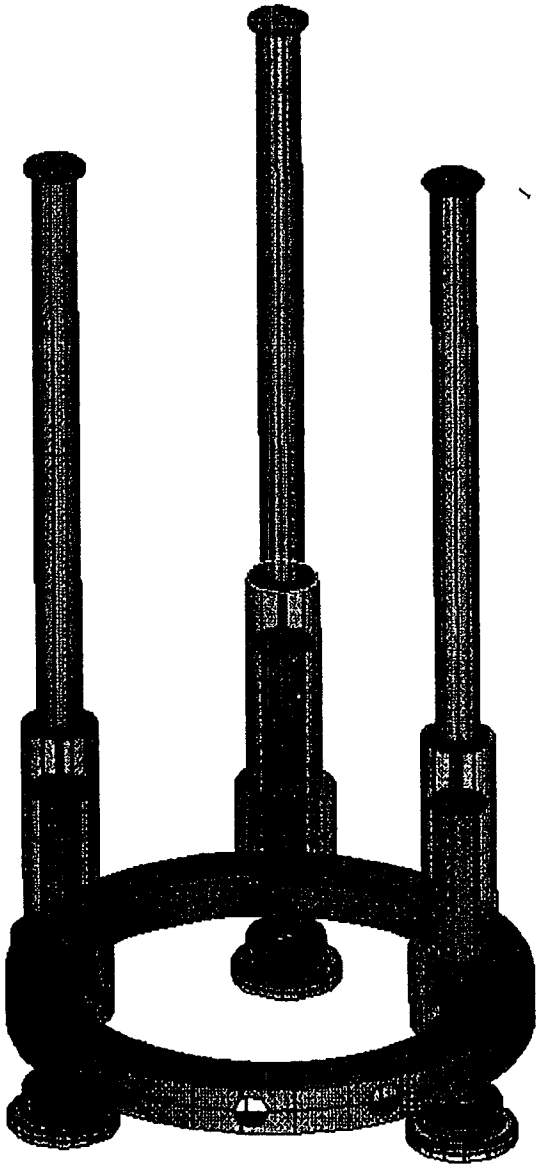

VIRGO mechanical filters

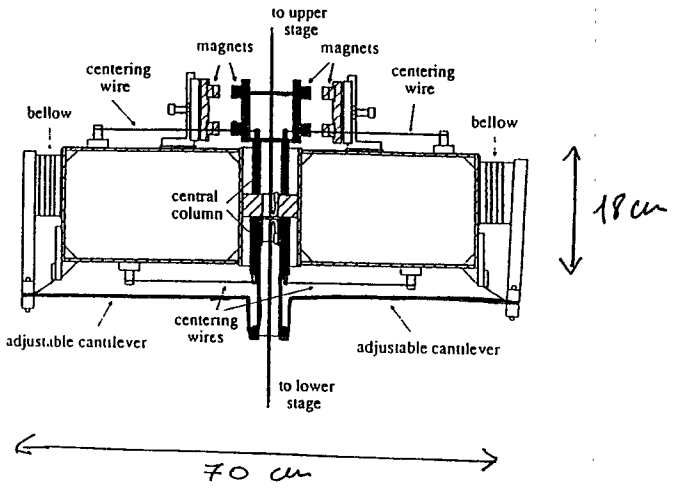

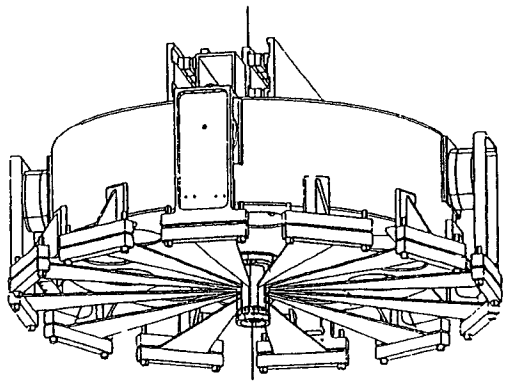

Filter Blades

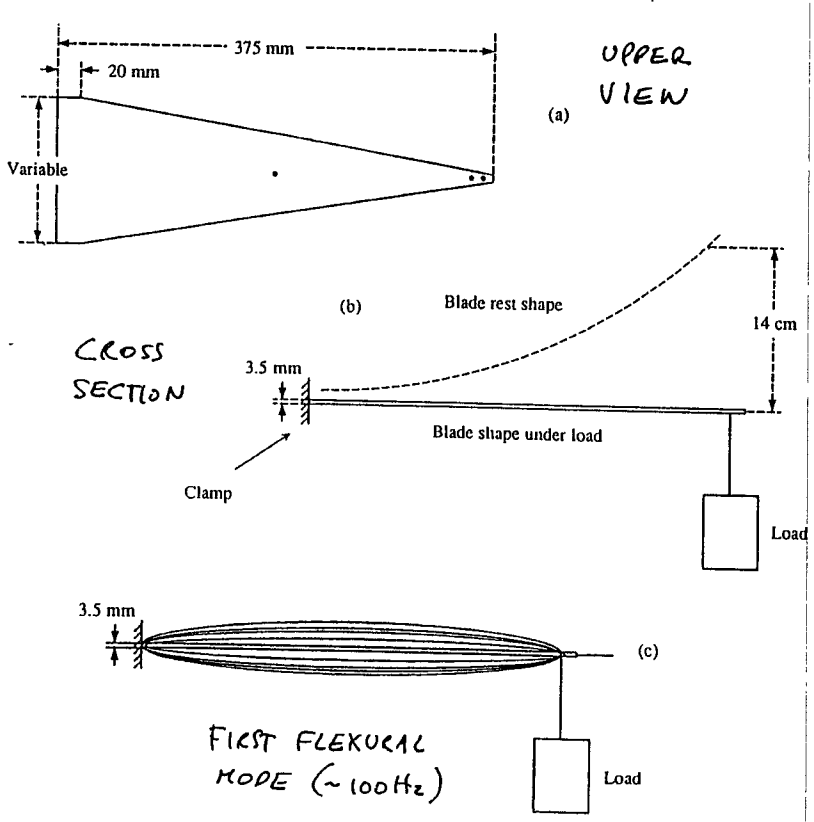

Bare filter attenuation performances

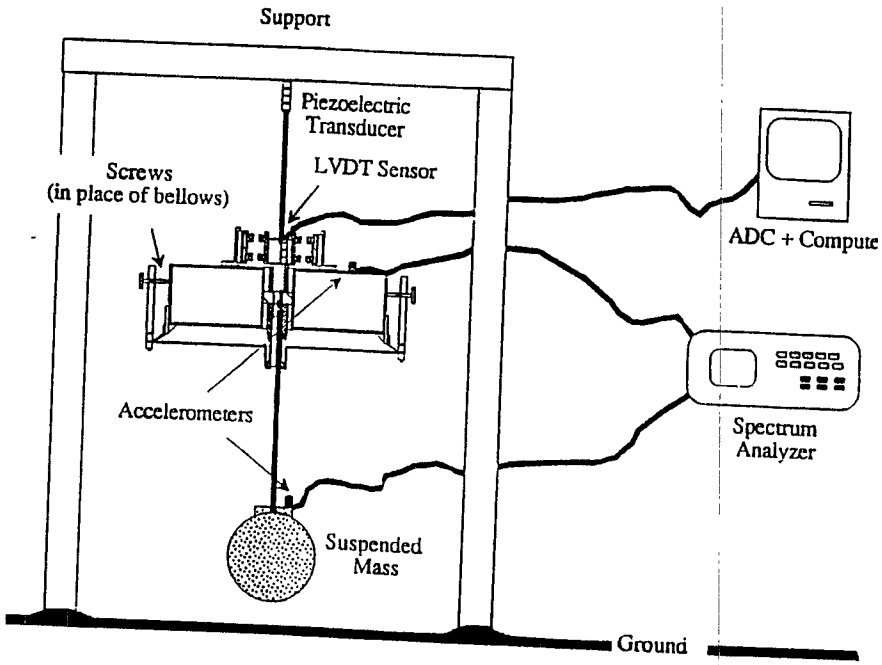

HORIZONTAL TRANSFER FUNCTION

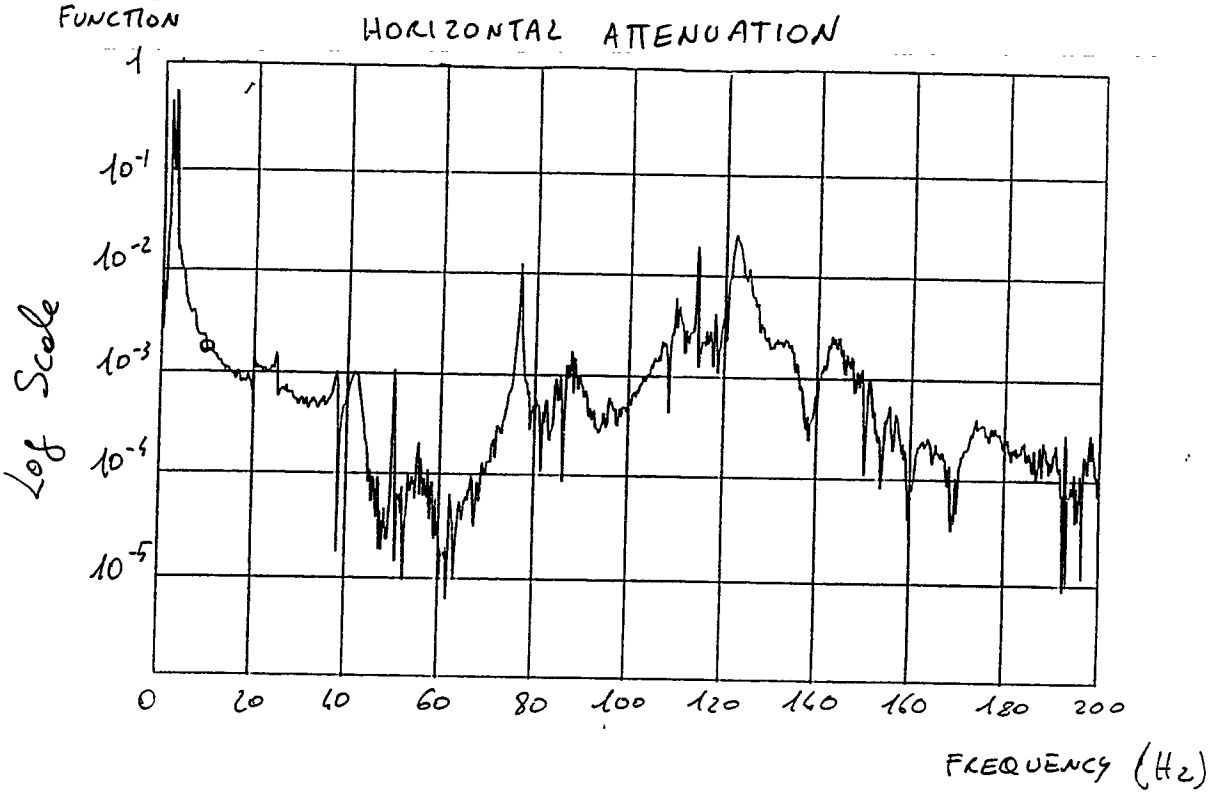

VERTICAL TRANSFER FUNCTION

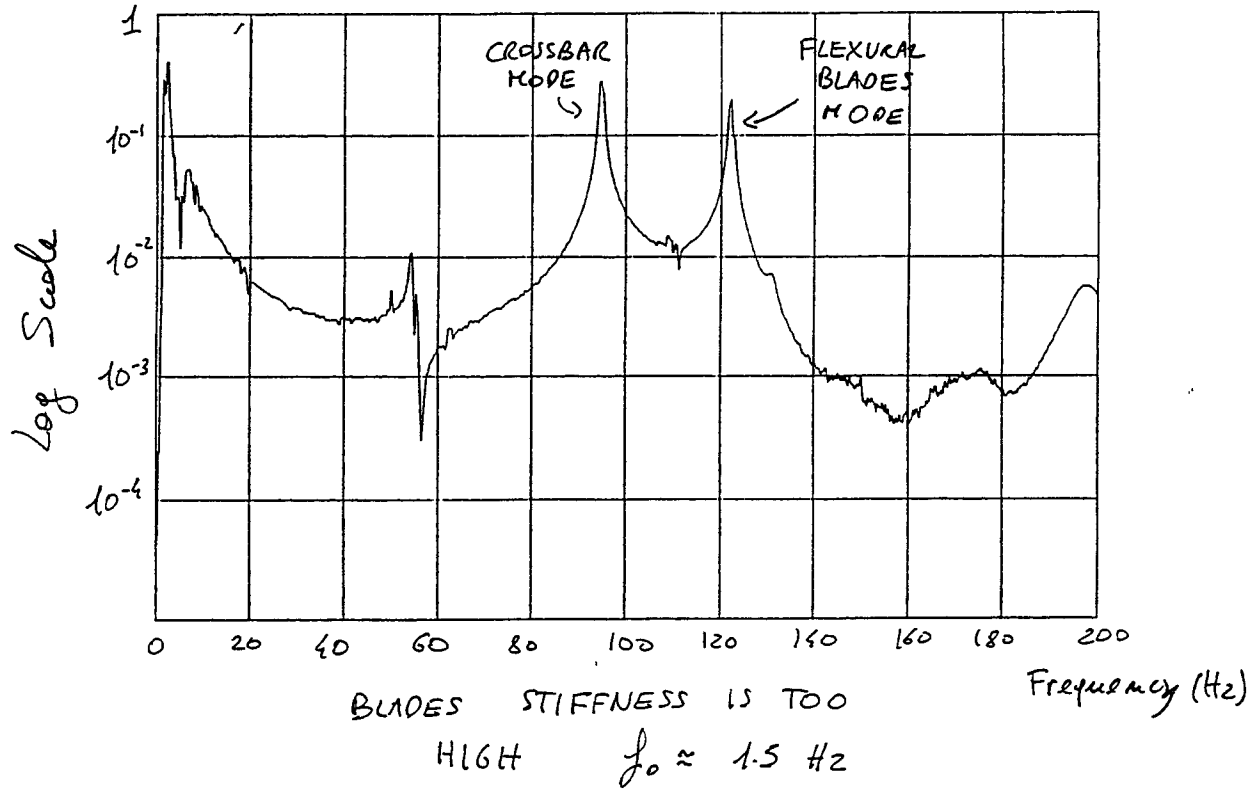

BLADES STIFFNESS IS TOO HIGH $f_0 \approx 1.5$ Hz

Antispring system

Vertical transfer function is a crucial point (high blade stiffness and less stages in the vertical direction)

Reduction of the blades stiffness by magnetic antisprings

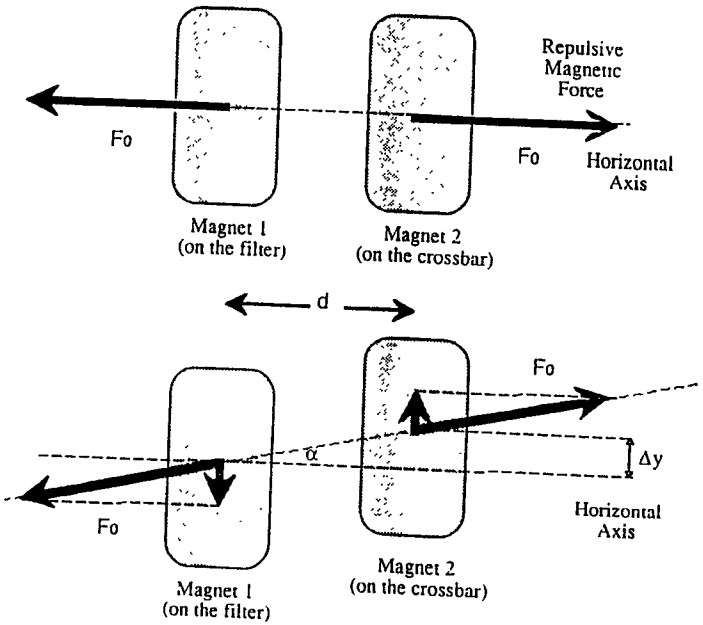

$$Fy \approx Fo\alpha = Fo(\Delta y/d)$$

MOUNTING OF THE ANTISPRINGS ON THE MECHANICAL FILTERS

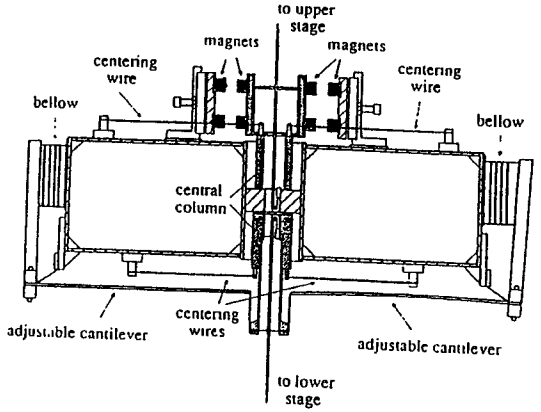

$$K_{TOT} = K_{blades} - K_{A.spring}$$

GOAL ====> f vertical $= \frac{1}{2\pi}\sqrt{\frac{K_{tot}}{M}} < 0.5$ Hz

In this way all the vertical resonances are below the highest horizontal resonance (2.5 Hz)

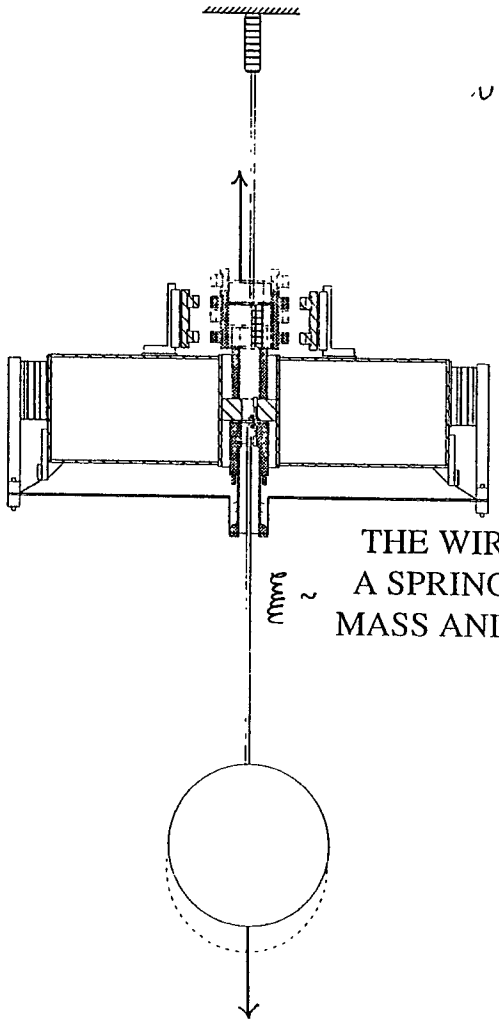

~ 78 Hz

THE WIRE ACTS AS
A SPRING BETWEEN
MASS AND CROSSBAR

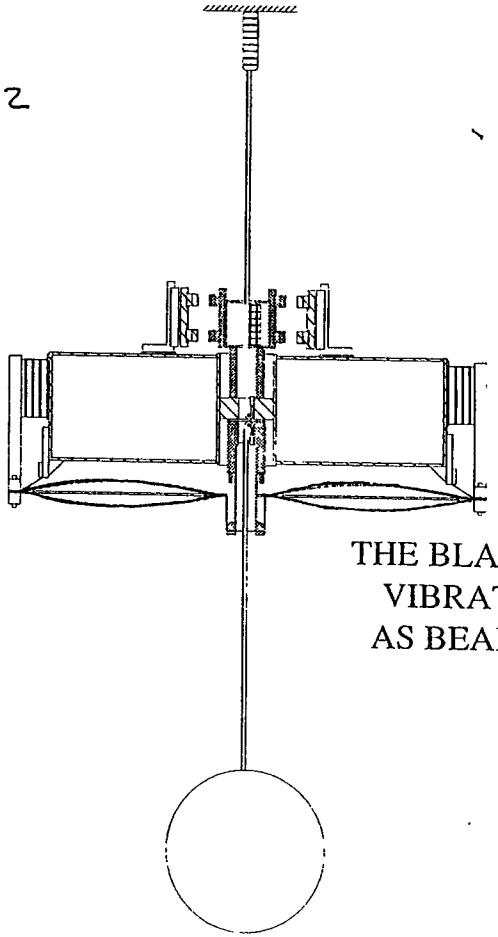

~ 115 Hz

THE BLADES
VIBRATE
AS BEAMS

CROSS BAR DAMPER

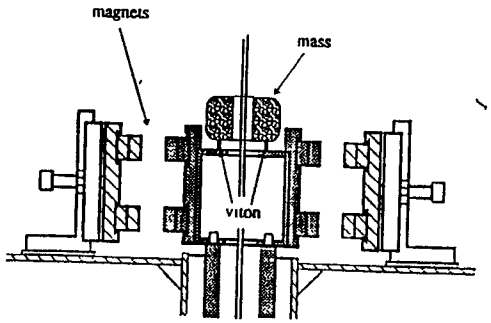

BLADE DAMPER

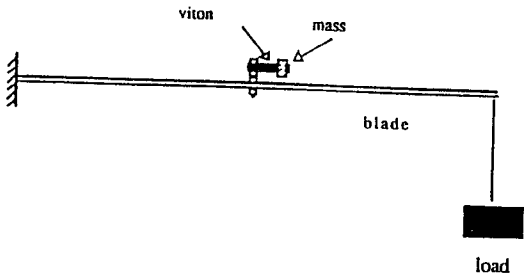

Systematic characterization of the antispring system

Measurement of the performances as a function

- of the temperature

- of the relative position between the magnetic matrices

Conclusion

The goal ($f < 0.5$ Hz) is obtained within large tolerances in the setting of the magnetic matrices

THE SYSTEM IS NOT CRITICAL !!

On the stability of the superattenuator

Stability requirements

1) stable mechanical response (to lock the interferometer)

2) to avoid large swings of the chain position

Experimental evidence

The vertical direction is much more sensitive to thermal changes because of the presence of the antispring magnets

Main trouble

Magnetic field thermal dependence

$$K_{TOT} = K_{BLADES} - K_{A.SPRING}$$

$$\left(\frac{\partial f}{\partial T}\right)_{y=0} = \frac{15\text{mHz}}{^0\text{C}}$$

TEMPERATURE CONTROL ∇_0

Thermal vertical swing of the filter

$$\Delta y/\Delta T = 200\mu\text{m}/^0\text{C}$$

Small enough to make the remote control of the vertical position of the blades superfluous

Conclusions on the superattenuator stability

- Temperature control of the tower is indispensable (0.1 ^{0}C pk/pk)

- Passive chain: No active resetting during the data taking

VERTICAL TRANSFER FUNCTION

EFFECT OF THE ANTISPRING ON THE VERTICAL ATTENUATION $f_0 = 0.4$ Hz

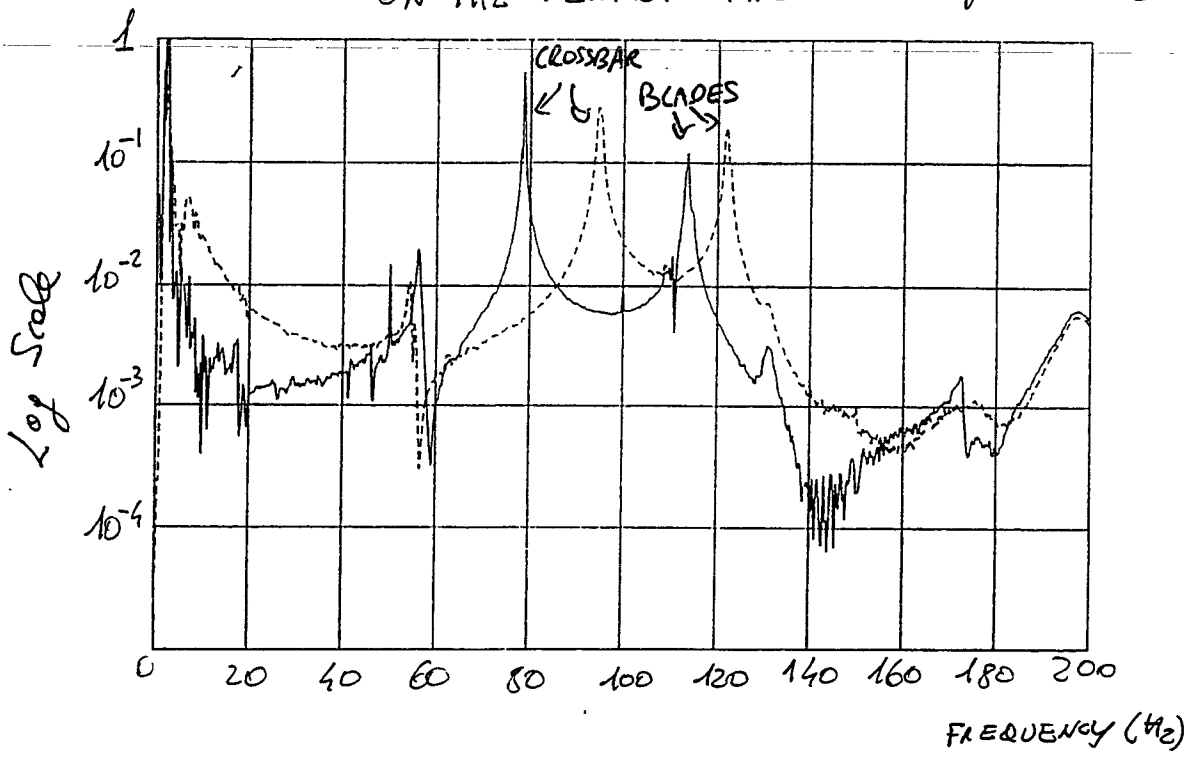

VERTICAL TRANSFER FUNCTION

EFFECT OF THE DAMPERS ON THE VERTICAL ATTENUATION $f_0 \approx 0.4$ Hz

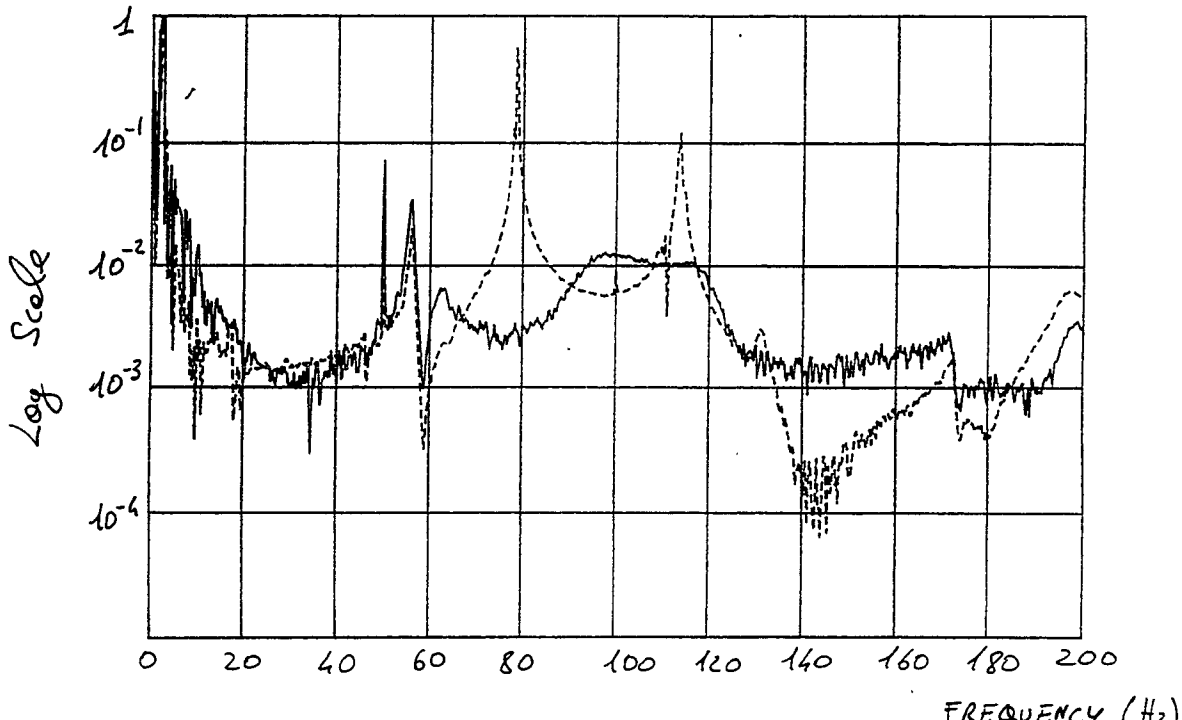

GOOD ATTENUATION !

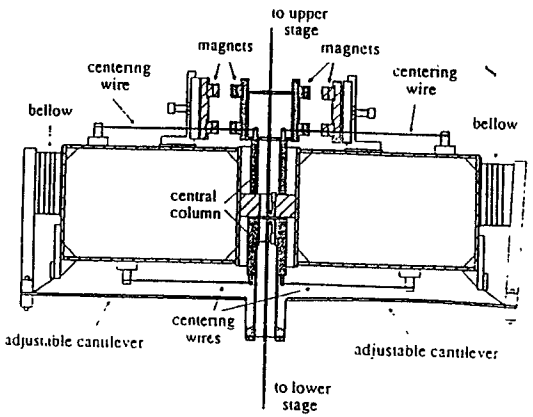

BELLOW HYDRAULIC SYSTEM TO TUNE THE VERTICAL POSITION OF THE FILTER

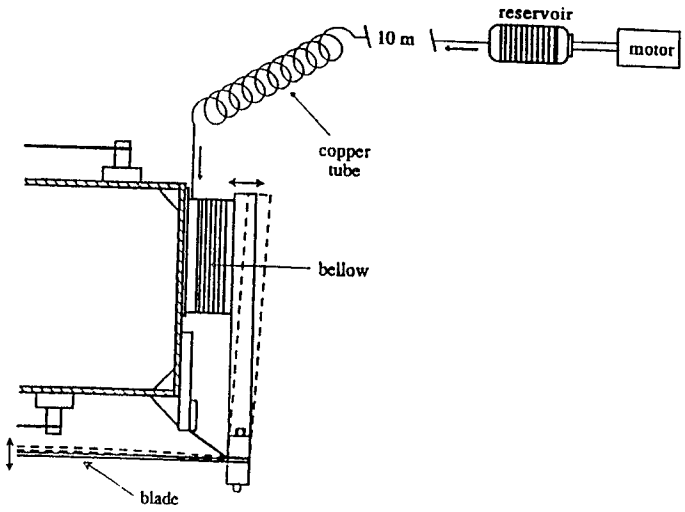

The creep problem

Materials under stress, as the filter blades, are subject to creep processes

Experimental evidence

At 35 ^{0}C (VIRGO designed temperature) the creep rate was measured to be too high

30 μm/Day

Consequences for VIRGO

1 - The creep leads in few weeks the antispring system out of the working position (few tenths of mm)

2 - It could generate mechanical vibrations in the detection band (required stability < 10 nm per day)

Exponential dependence on temperature

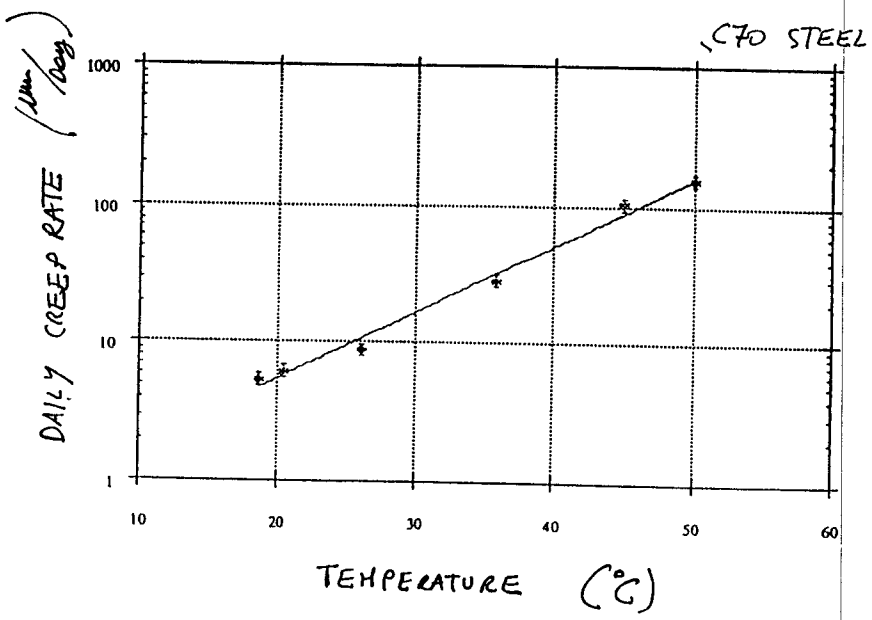

SOLUTION ==> Maraging steel

(R. DE SALVO)

MAIN CONCLUSIONS ON SUPERATTENUATOR MECHANICAL FILTERS

1 - Good attenuation performances

2 - Good tolerances in the mounting

3 - Full characterization of the antispring system

4 - Stability on long period obtained only by controlling the temperature of the vacuum towers

5 - Remote control for the vertical positioning can be eliminated (Passive Chain)

6 - Creep problem has been discovered

NEXT TALKS

Pre-isolator stage for the Superattenuator (L.Holloway)

Solution of the creep problem (R.De Salvo)

SA TRANSFER FUNCTION

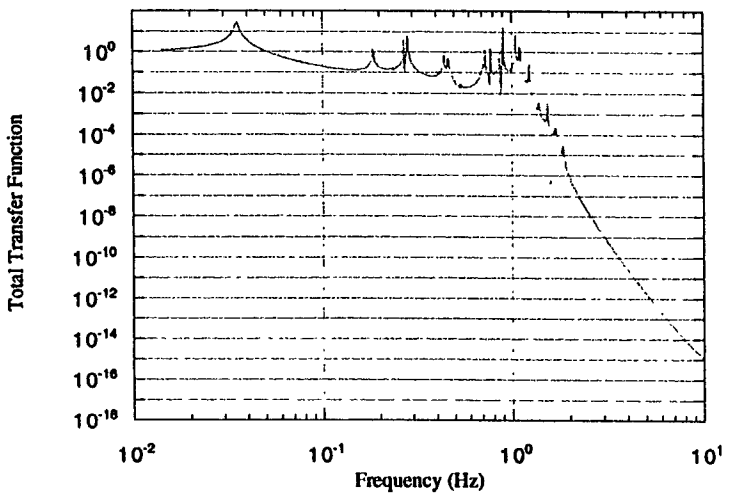

NOISE IN THE VIRGO SUPERATTENUATORS

RICCARDO DESALVO

INFN - PISA

VIRGO

INFN - CNRS

ASPEN Co

30 - JANUARY 1997

How crazy is Virgo ?

VIRGO Design Sensitivity

Sensitivity;

1 nnm/$\sqrt{\text{Hz}}$ over **3 + 3 Km** arm length

nano-nano

h = 3 $10^{-22}/\sqrt{\text{Hz}}$

1 Wavelength	10-6 m	1000 nm
1 Atom	10-10 m	10-1 nm
1 proton	10-15 m	1000 nnm

seismic motion 10-6 m/$\sqrt{\text{Hz}}$ = 1012 nnm/$\sqrt{\text{Hz}}$

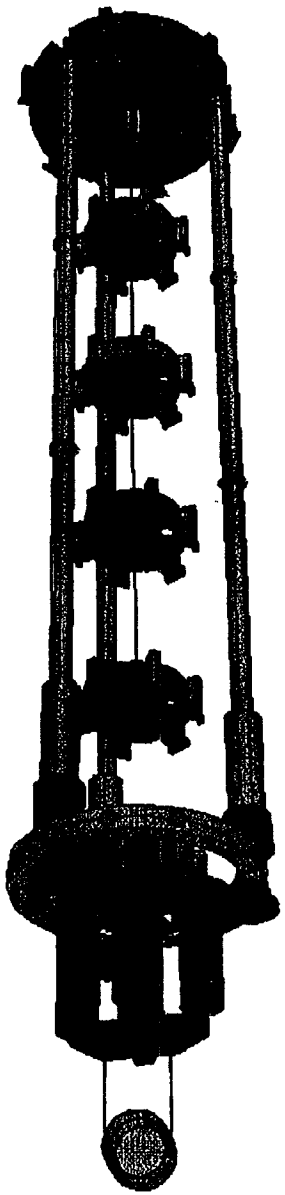

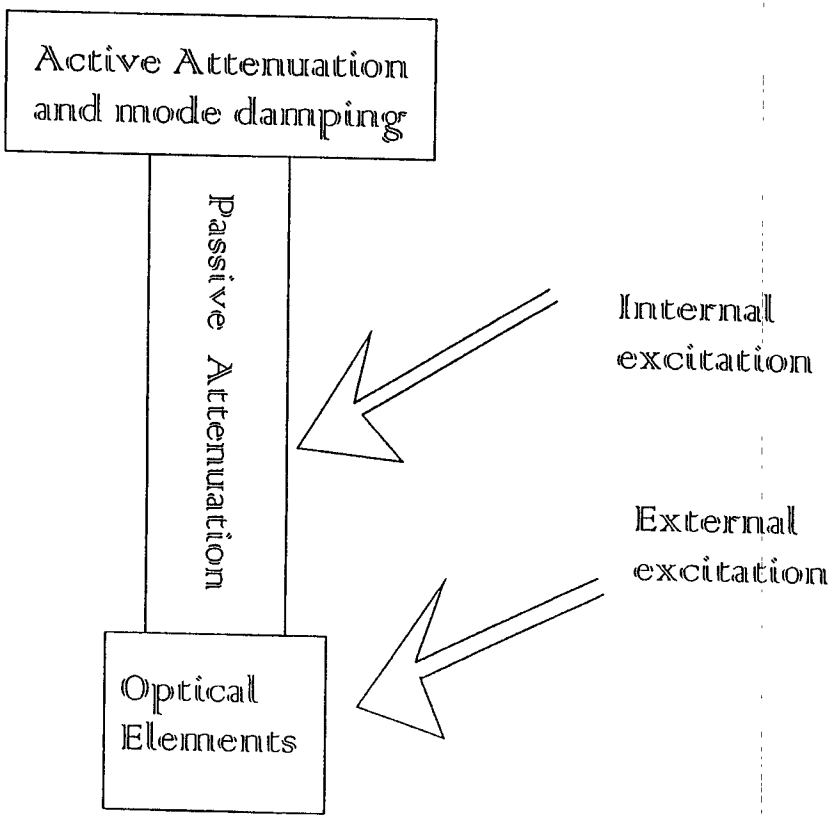
Active Attenuation
and mode damping
Passive Attenuation
Internal
excitation
External
excitation
Optical
Elements

Attenuation Scheme

A 1 Hz pendulum at 10 Hz attenuates x 10^{-2}

A 6 pendula chain at 10 Hz attenuates x 10^{-12}

If you add x 10^{-3} active damping at level 0

the x 10^{-14} attenuation can be achieved

Believe me,
mathematically it can work !

Let's look at the problems we encountered!
(and solved)

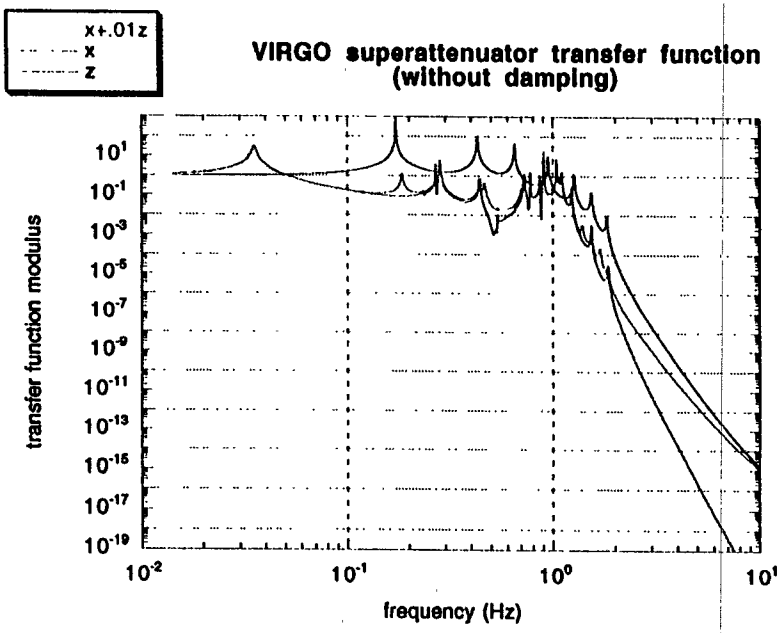

a)

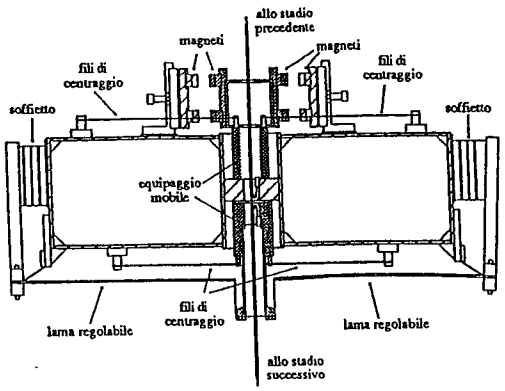
allo stadio precedente
magneti
magneti
fili di centraggio
fili di centraggio
soffietto
soffietto
equipaggio mobile
fili di centraggio
lama regolabile
lama regolabile
allo stadio successivo

b)

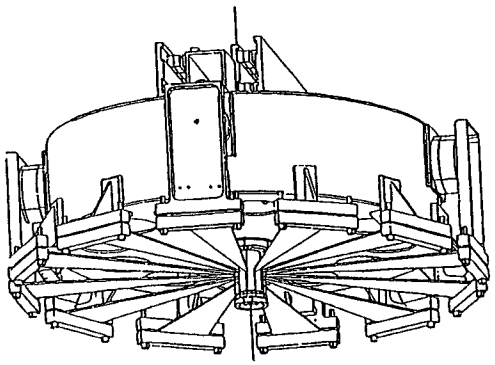

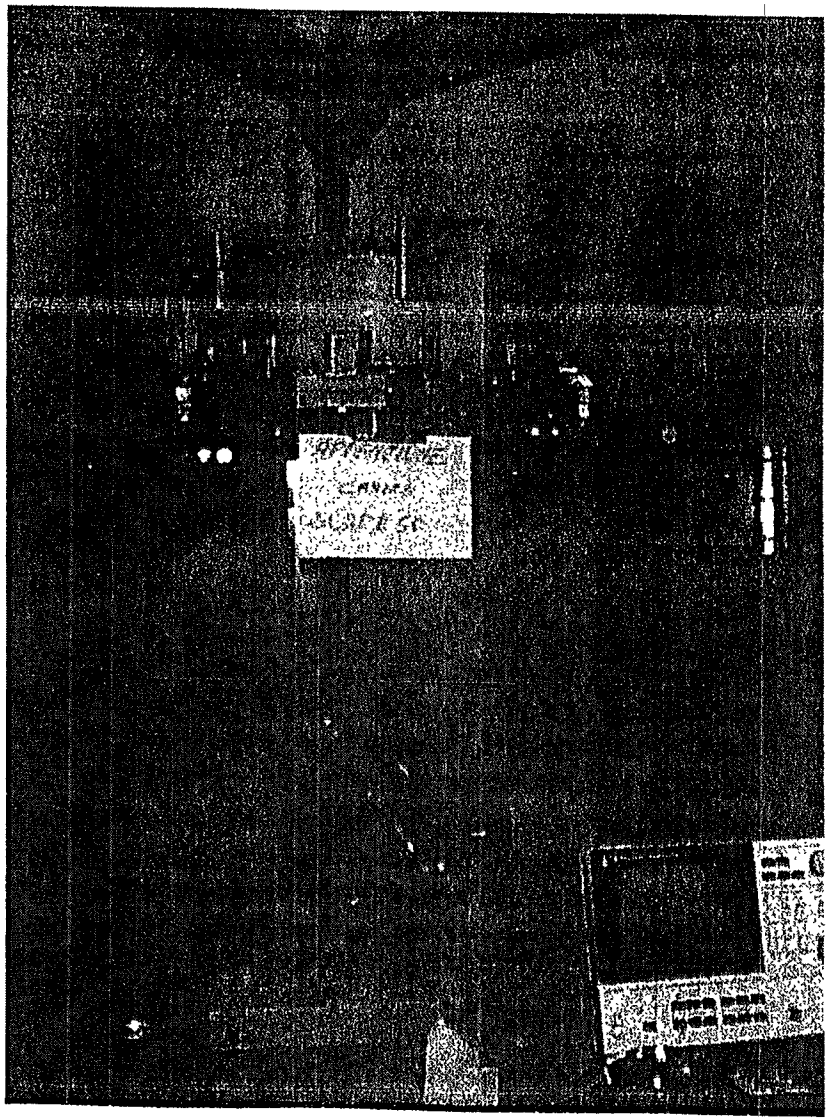

Passive Attenuation

Need:

long lever springs and

high stress on spring material

to reach low vertical oscillation frequency

1.5 Hz Mechanical filter oscillation frequency

0.5 Hz freq. reduction by magnetic antisprings

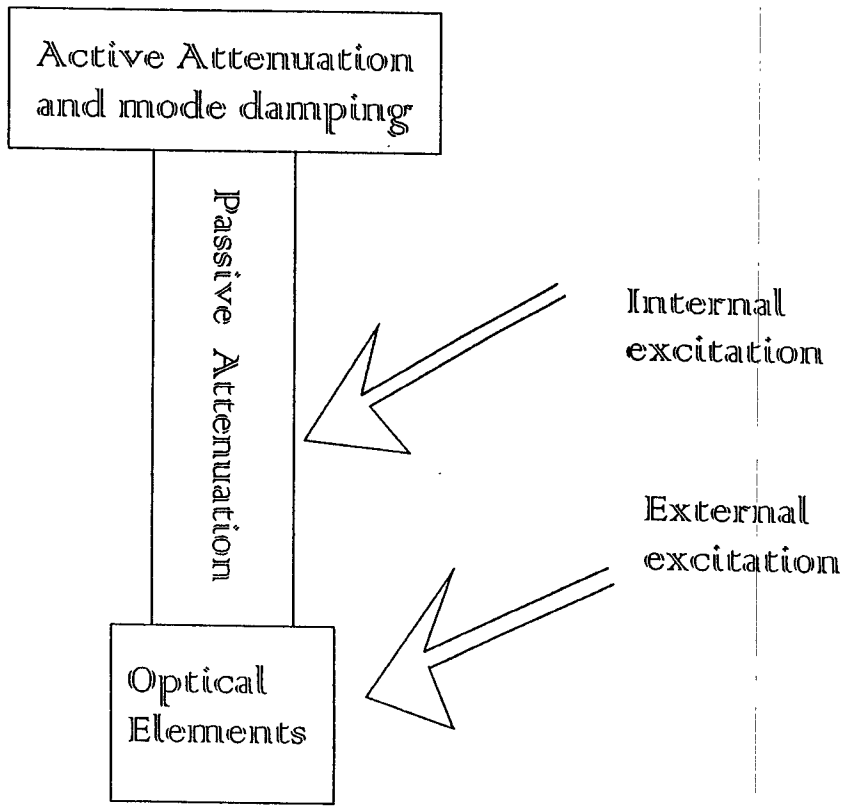

Internal Excitations

Energy releases in the S.A. chain

can generate nano-seisms

Suspended masses are inexhaustible reserve of energy

Consider Crystal slippage

one single Crystal stressed near the metal yield point of the metal contains (and releases at slippage) energy equivalent to the dropping of the suspended optical component by **several pm**

A pico-meter is a **Mega-nano-nano-meter**

It's the **"big one"**

Internal Excitations

1 µm/day = 10 **"big ones"** per second ! ! !

This is independent from where in the system creep happens

(+)The creep step energy spreads over all modes

(-)The attenuators above may bottle down the internal excitation noise

creep figure old blades, figure creep vs temperature

WE WILL INSIDE OF THREE 5 μm CRYSTALS

Sources of Internal Excitations

Dislocations inside single crystals

accumulate stress on

Crystal border **impurities**

Eventually will exceed stress yield point

all crystals **will** slip

Integrated continuous motion.

Sources of Internal Excitations

Dislocations have activation energies

of few Kcal/mole

$$\text{Freq.}_{\text{slippage}} = n\, e^{\frac{\Delta E}{KT}} \text{ (Bq)}$$

Creep Speed **x 10** for $\Delta T = 5 - 20^{\circ}C$

Creep speed is controlled by the temperature

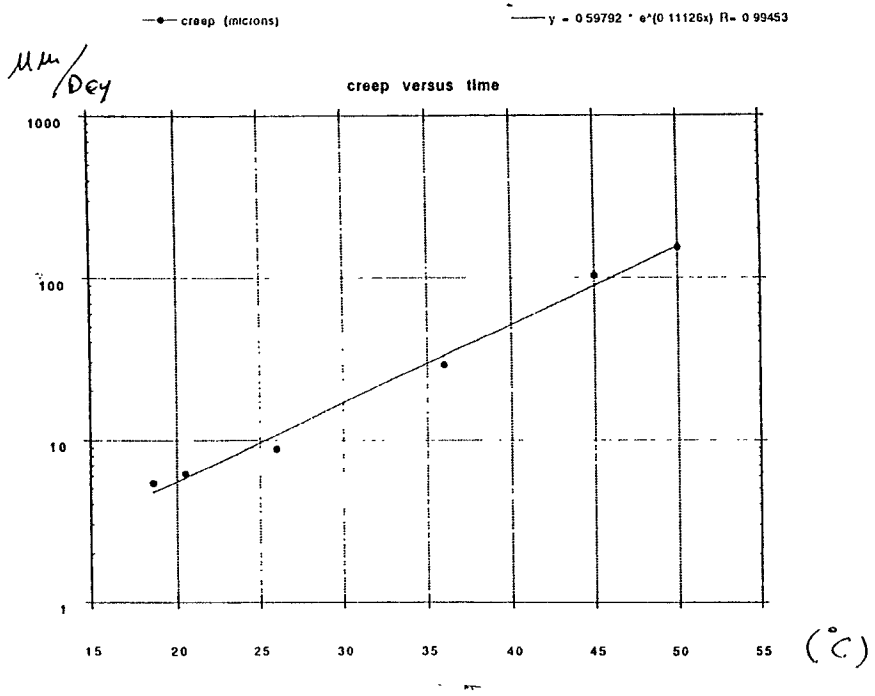

→ CREEP $\left(\frac{\mu m}{Day}\right)$ VS. TEMPERATURE

Sources of Internal Excitations

The only ways out are:

a) Infinitely small crystals

(gain with d^3 but unfeasible)

b) frozen crystals

b1) freeze by cooling

b2) chemical freezing

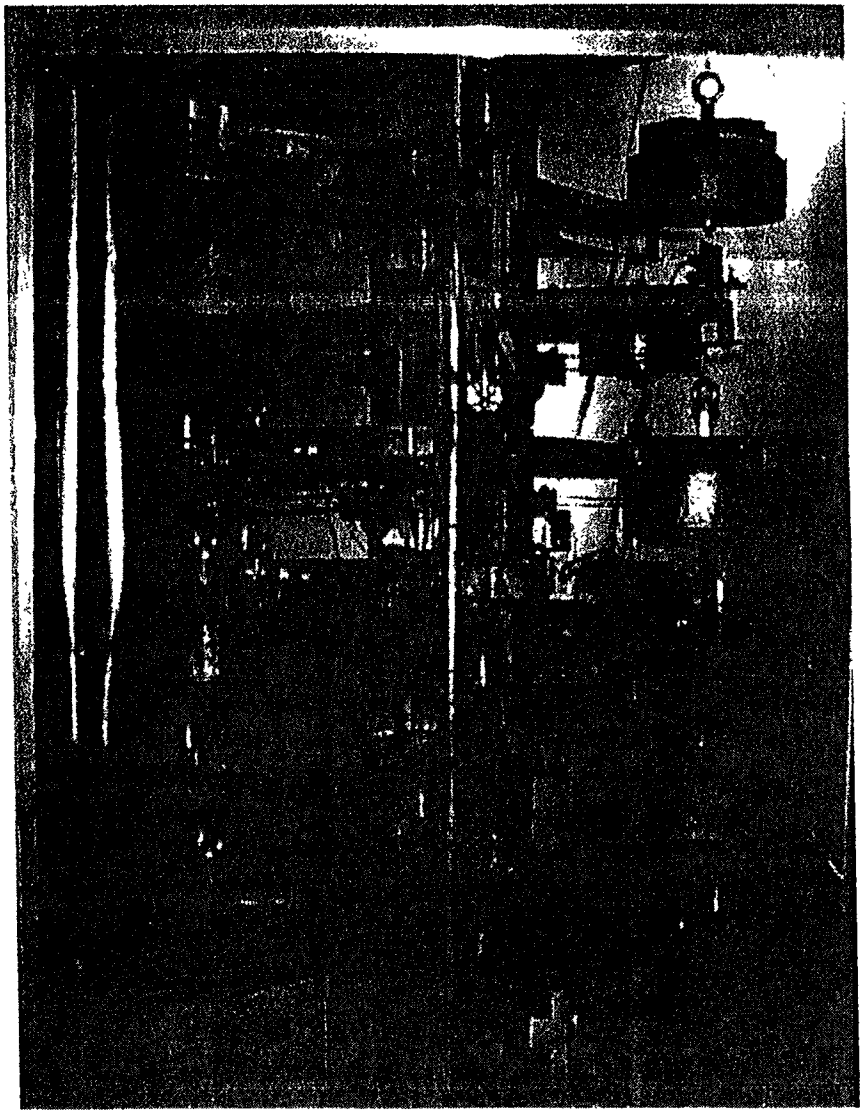

Sources of Internal Excitations

Freezing crystals by cooling

Metal brittleness

Spontaneous fracture

freeze only high ΔE dislocations

low ΔE dislocations can still move and generate catastrophes

Sources of Internal Excitations

Chemical freezing of crystals

Precipitation hardened steel

Maraging

Fe + Co + Ni + Ti

High purity (no precipitation centers)

- Solution stable in Fusion

- Solid solution stable at > 850°C

-Solid solution thermodynamically unstable <450°C

in 10^{many} years would precipitate

Ti-Co nano-crystals inside Fe crystals

Risolubilised State

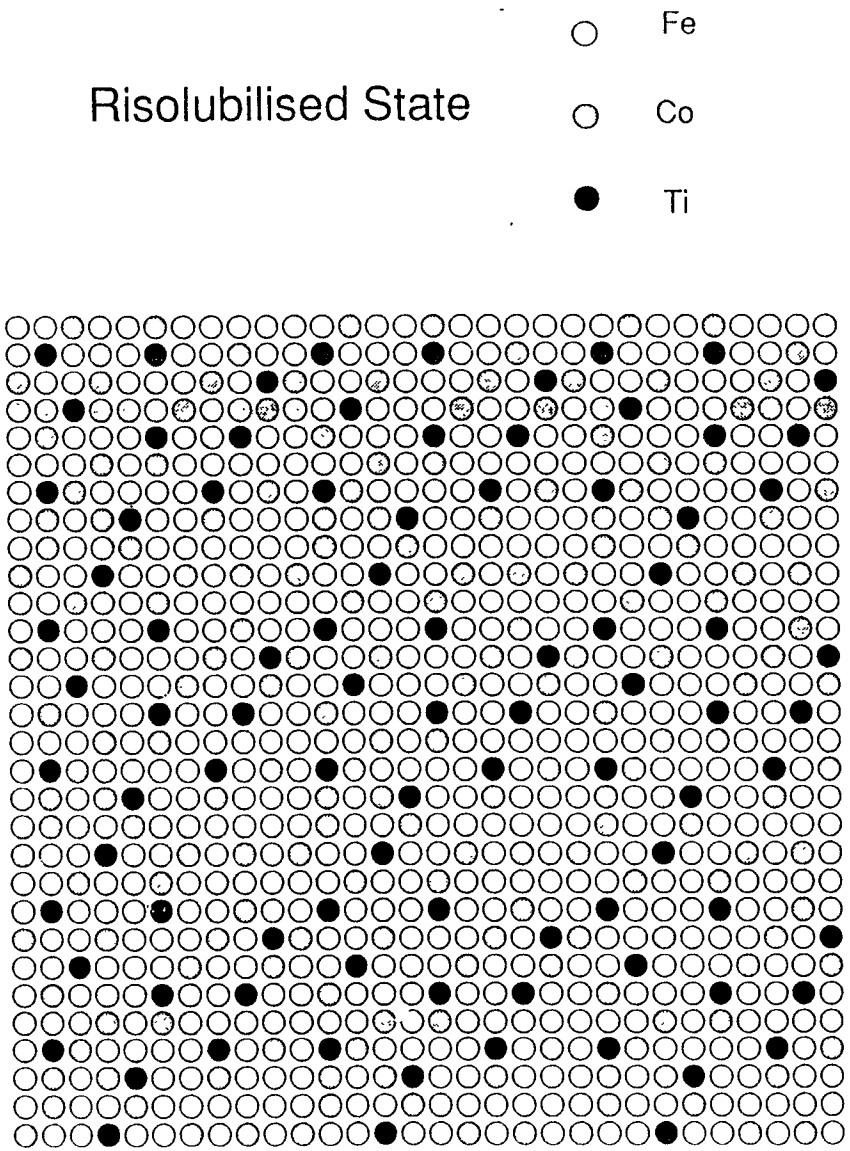

Precipitation hardened steel

Precipitation process is impeded

at room temperature

by lack of Co and Ni diffusion

inside Fe crystals

Solubilised form metastable at 20°C

At 450°C FE Crystal are still stable but

Co, Ti, Ni atoms can diffuse

typical diffusion distance 30 nm

Every 30 nm a nano-crystal forms inside the otherwise un-perturbed Fe Crystal

about 10^6 nano-crystals/Crystal

Precipitated State

○ Fe

○ Co

● Ti

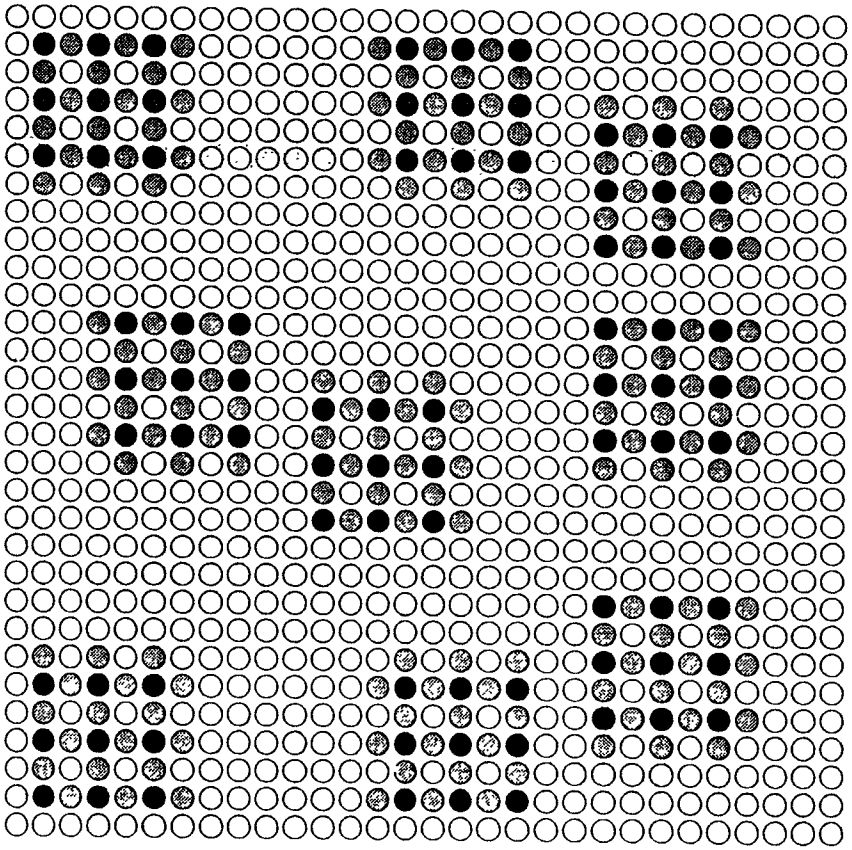

Risolubilised State

○ Fe

○ Co

● Ti

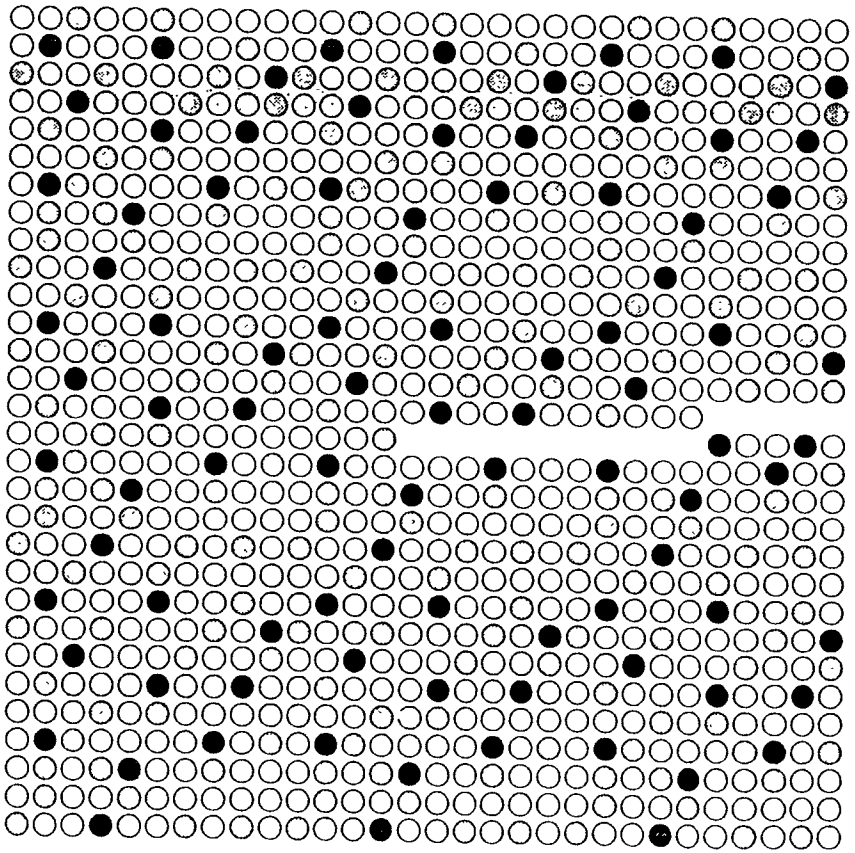

Precipitation hardened steel

Nano-crystals inside crystals

form dislocation drift barriers

Dislocations are trapped throughout the Crystal

Dislocations impeded to reach the Crystal border

cannot trigger Crystal slippage

creep stops ! ! !

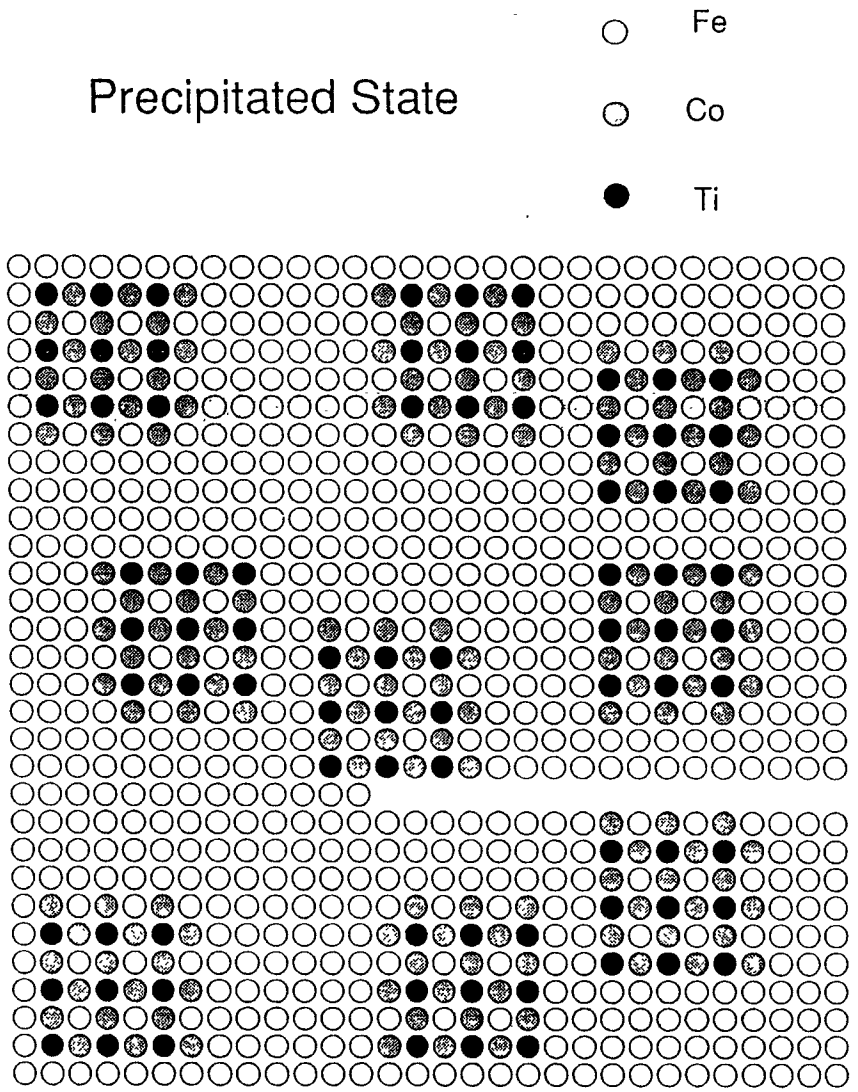

C 70 AT 50 C
MARAGING AT 80°C

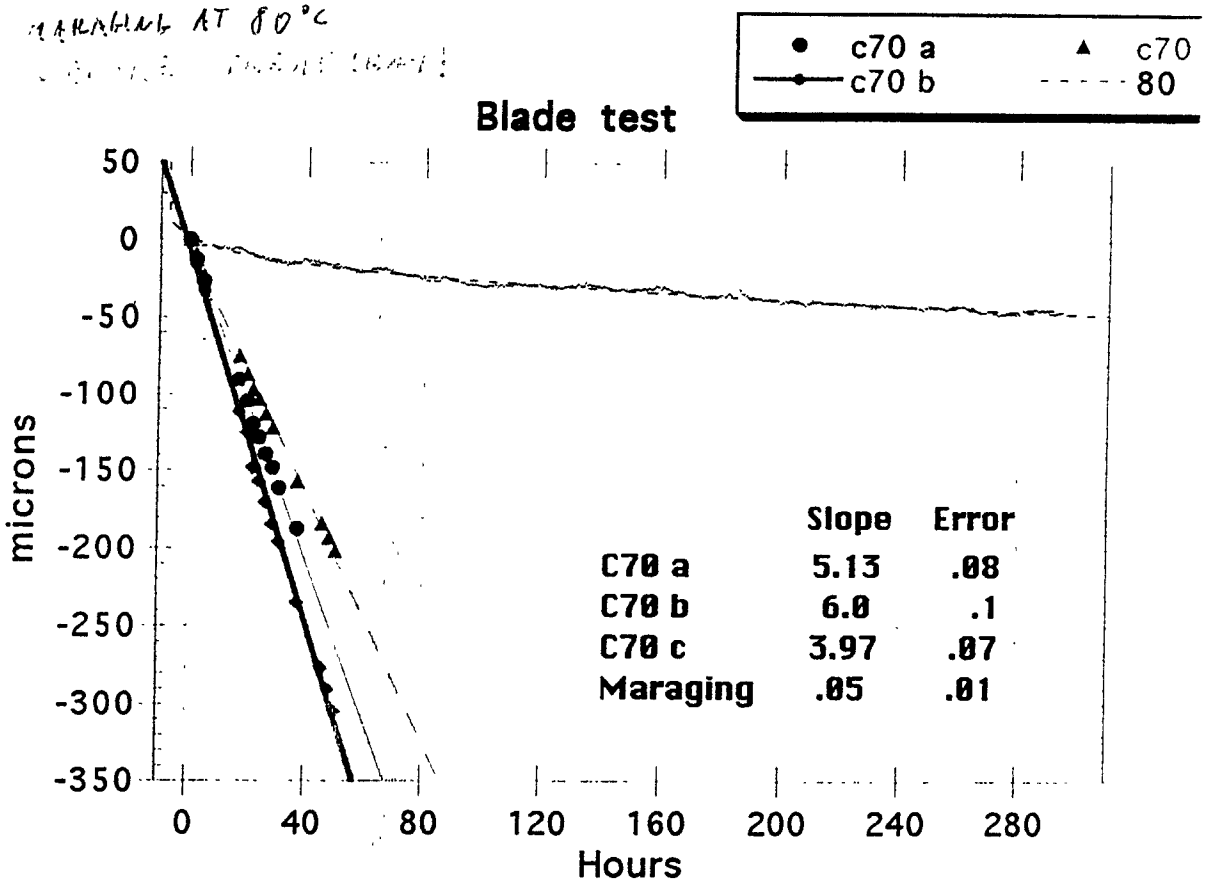

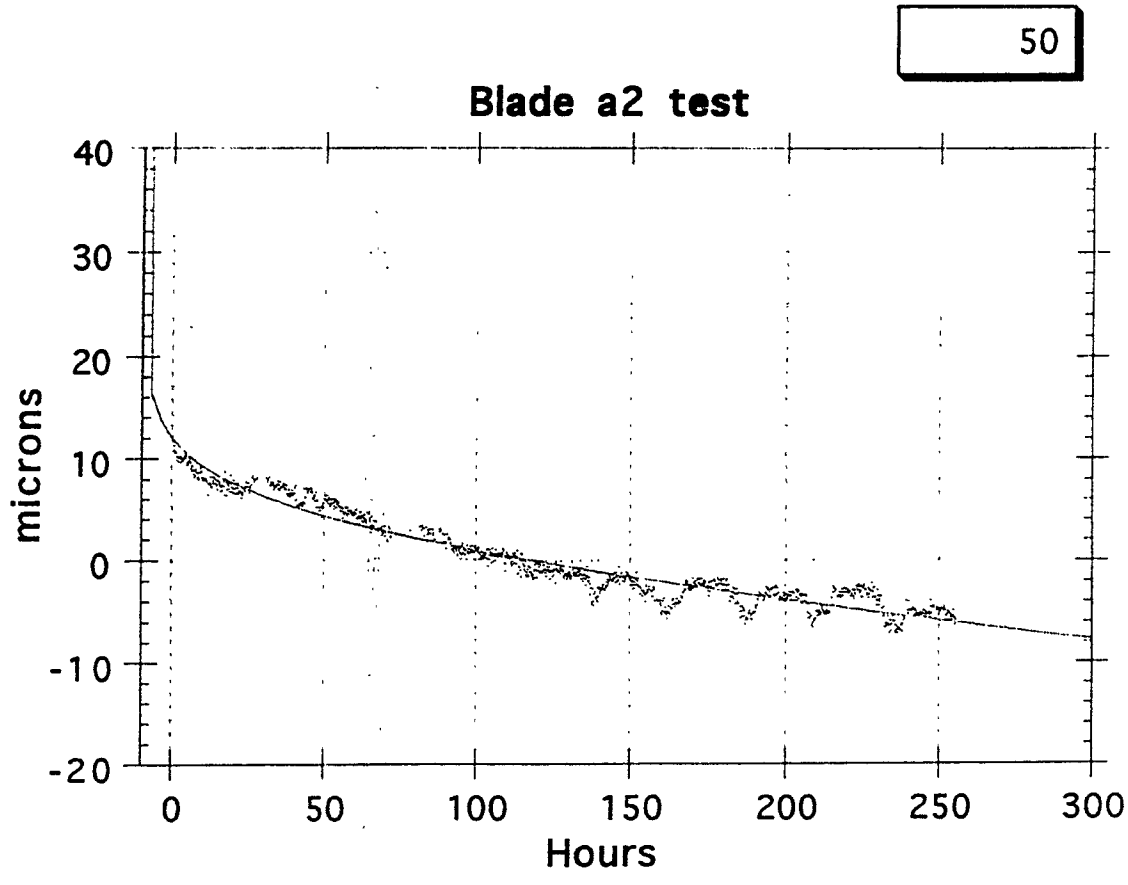

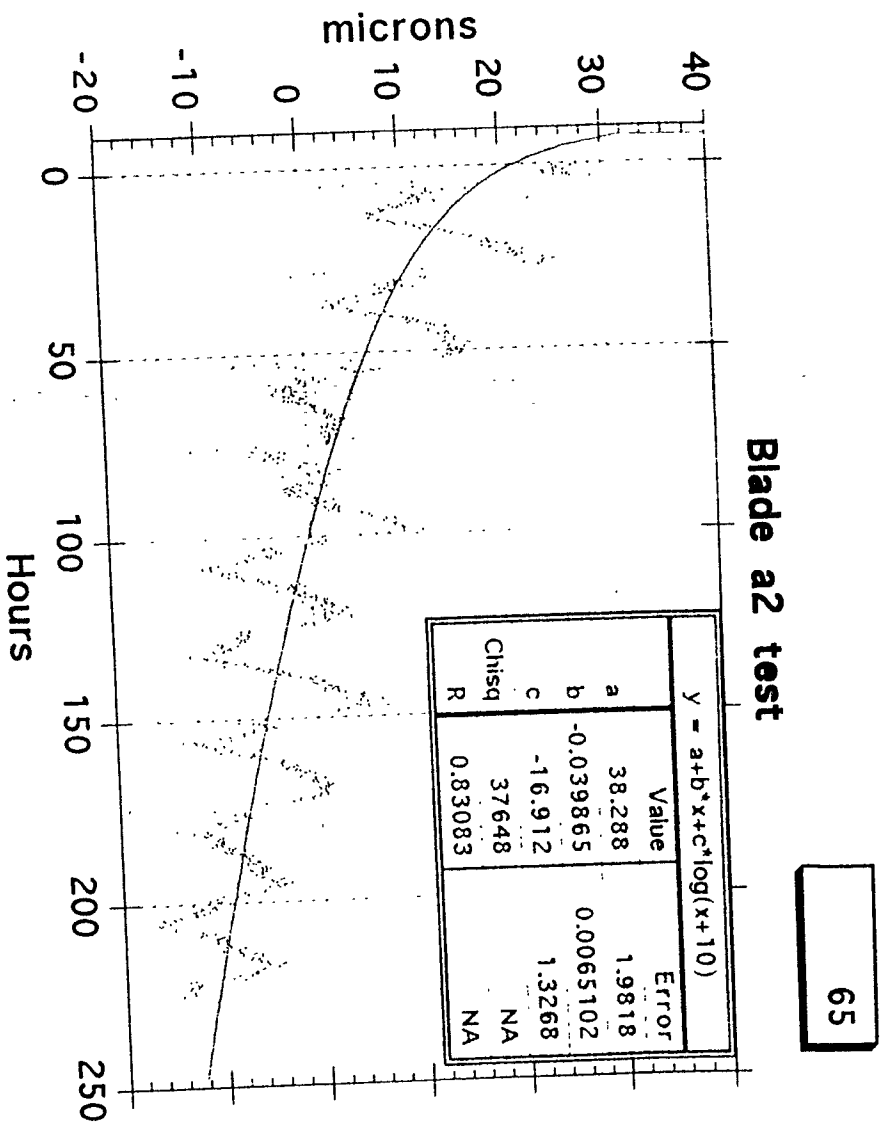

Precipitation hardened steel

After precipitation hardening,

creep shows logarithmic behavior

Given our measurement errors creep

can be directly measured at < 50-100 nm/day

Need an indirect measurement.

Need to guarantee much lower

creep level

80

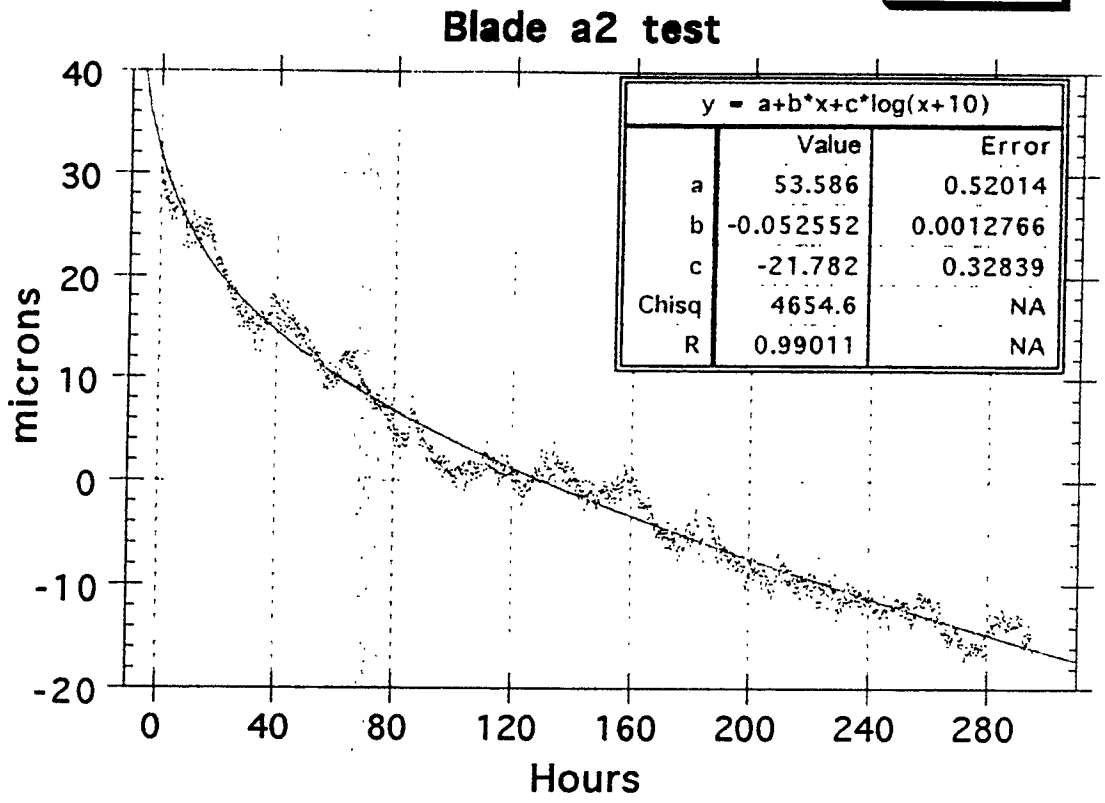
Blade a2 test
y = a+b*x+c*log(x+10)
Value Error
a 53.586 0.52014
b -0.052552 0.0012766
c -21.782 0.32839
Chisq 4654.6 NA
R 0.99011 NA
microns
Hours
40
30
20
10
0
-10
-20
0
40
80
120
160
200
240
280

65 II

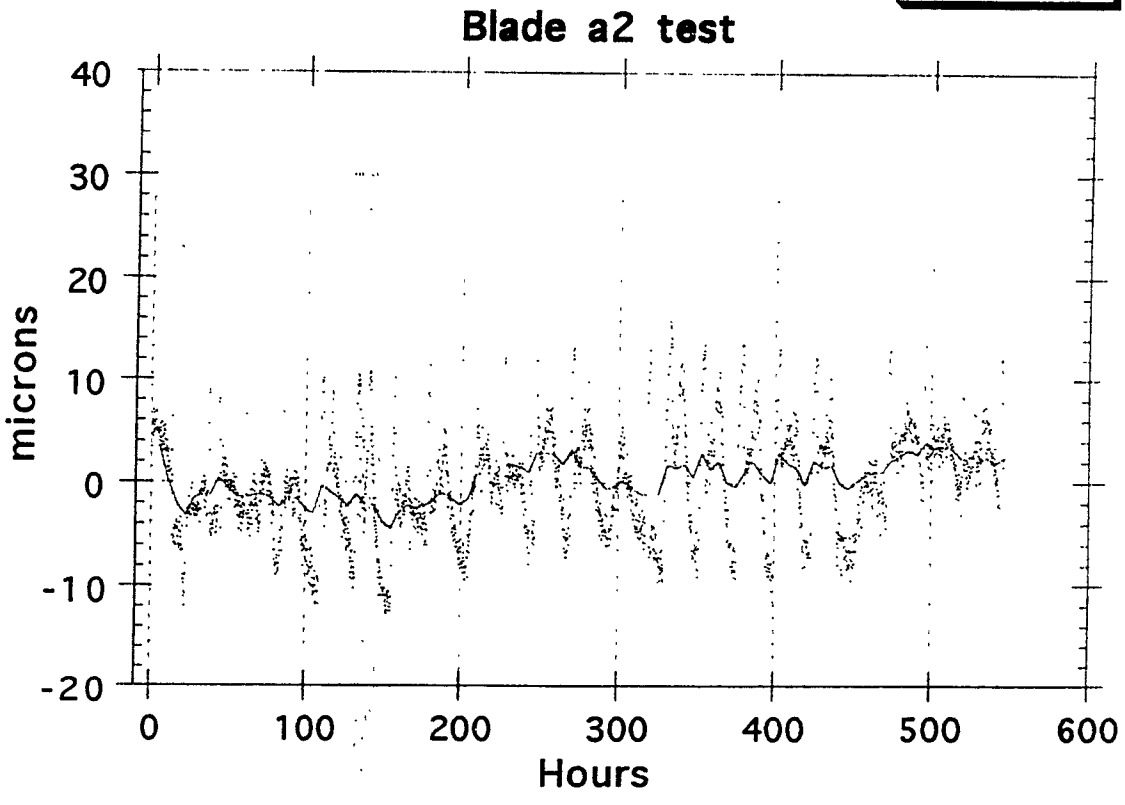
Blade a2 test
microns
Hours
40
30
20
10
0
-10
-20
0
100
200
300
400
500
600

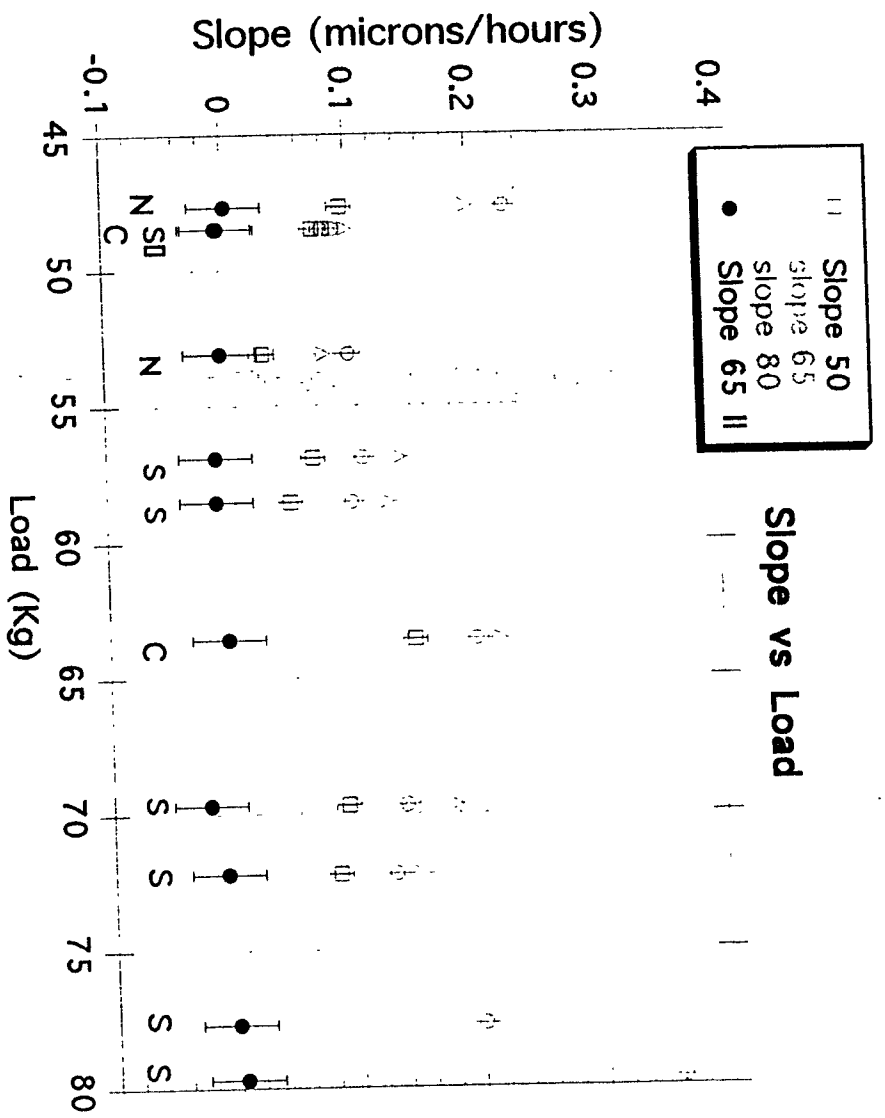

Precipitation hardened steel

With Maraging observe the creep speed

to increase x 30 for 10°C rises

Bake blades under stress at >= 80°C for a week

Observe creep at < 1 µm / day @ 80°C

Observe creep at < 50-100 nm / day @ 65°C

Estimate residual creep at < 1 µm / day @ 20°C

1 Crystal slippage / day

Most residual creep may be due

to pure dislocations

(slippage under threshold)

Thermal noise requirements for GEO 600:

- Require h sensitivity of $2\times10^{-22}/\sqrt{\text{Hz}}$ at 50Hz
- Set by expected thermal noise from internal modes of test mass: Typically, for fused silica:-

  $Q_{internal} \sim 5 \times 10^6$ - difficult to improve on this
- Sets limits on thermal noise from pendulum modes, violin modes suspension such that require

  $Q_{pendulum} > 2 \times 10^6$ (assumes structural damping)

  $Q_{violin} > 1 \times 10^6$
- Would like $Q_{pendulum} > 10^7$ - all fused quartz suspension ?

Relationship between $Q_{pendulum}$ and $Q_{material}$:

$$Q_{pendulum} = Q_{material} \frac{mgl}{4\sqrt{TEI}}$$ for a 2-loop suspension

where:

m = mass E = Youngs modulus

l = length I = moment of mass = $\frac{\pi r^4}{4}$

T = tension r = radius of wire

n = number of wires

Typical dimensions :

length ~ 12.5cm

width ~ 0.3cm

thickness ~ 54μm

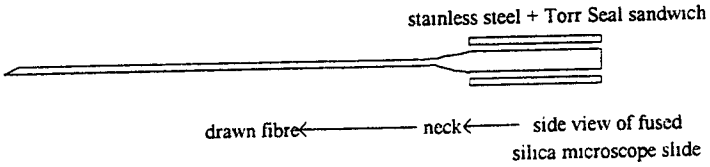

Fused Silica Ribbon Fibre

Q_{mat} measurements for fused quartz ribbons

- Fused quartz ribbon - drawn from fused quartz slide using RF oven
- Use positive feedback and electrostatic drive to excite resonances of quartz fibre
- Measure decay of amplitude of resonances to find Q_{mat}

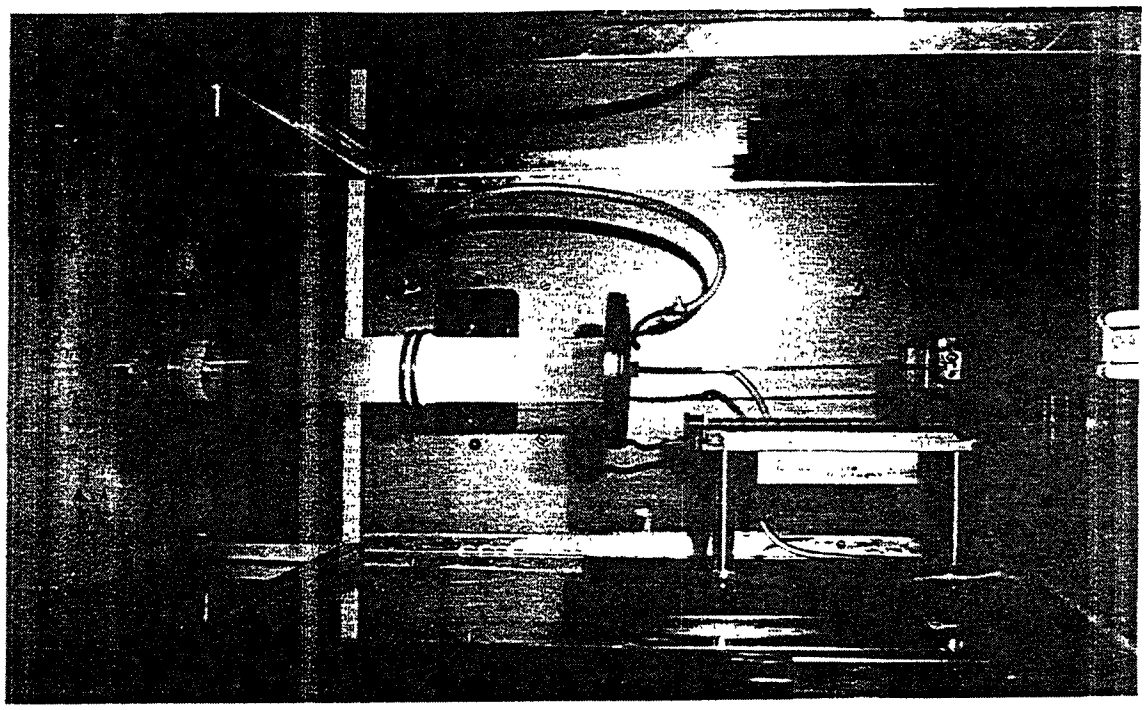

Plot showing measured material Q of fused quartz ribbon as a function of frequency

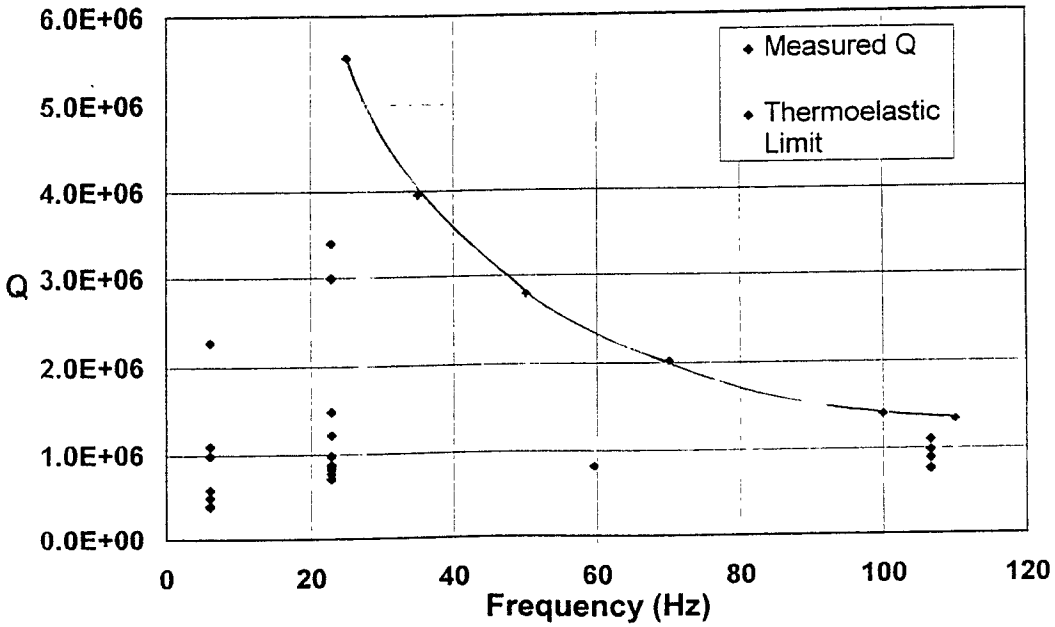

Conclusions

- Q_{mat} of the order of few x 10^6
- Q_{mat} of welded fibre of similar order
- Q_{mat} of replacement fibre of similar order

$\Rightarrow$ Limiting Q_{pend} = few x 10^8 - more than good enough

Experiments with pendulums suspended on fused quartz fibres

- Measure Q of pendulum mode for pendulums suspended on 2 fused quartz fibres
- Measure effect of different fibre attachment methods for joining fused quartz fibres to mass
- Initial experiments used:

  Mass: 200g

  Length: ~ 26cm
- Fibres attached to mass and plate from which pendulum is suspended by mixture of clamping/glueing

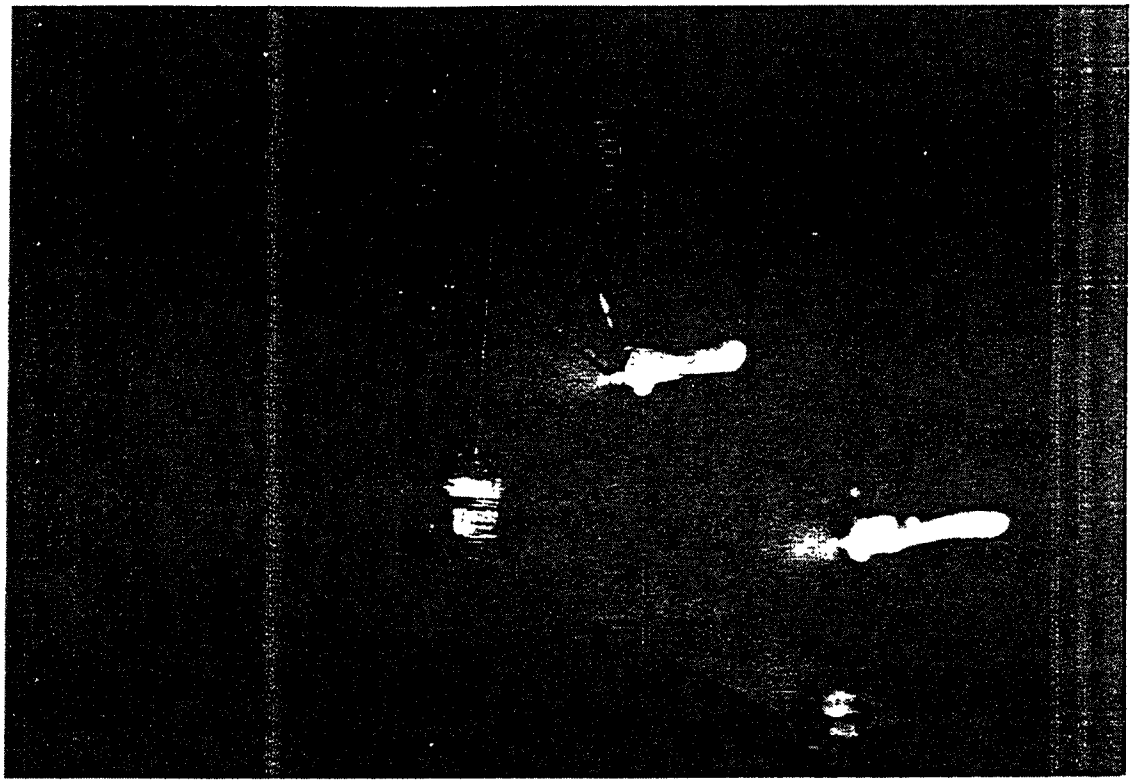

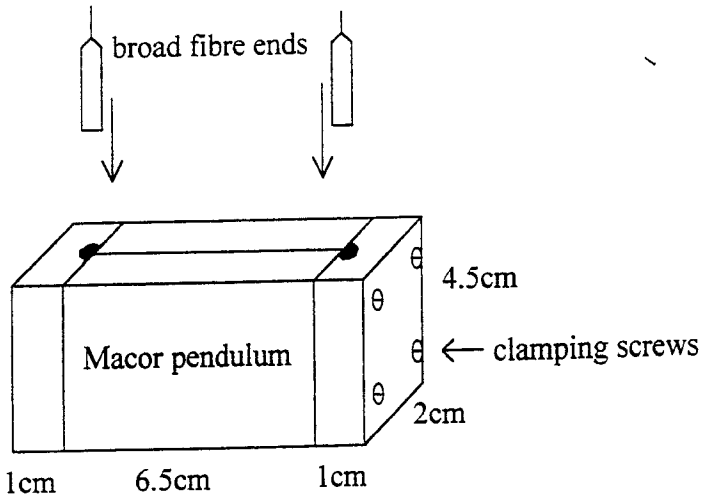

"Macor" machinable ceramic pendulum

$\rho_{Macor} = 2.52 g/cm^3$

$m_{pend} \cong 200g$

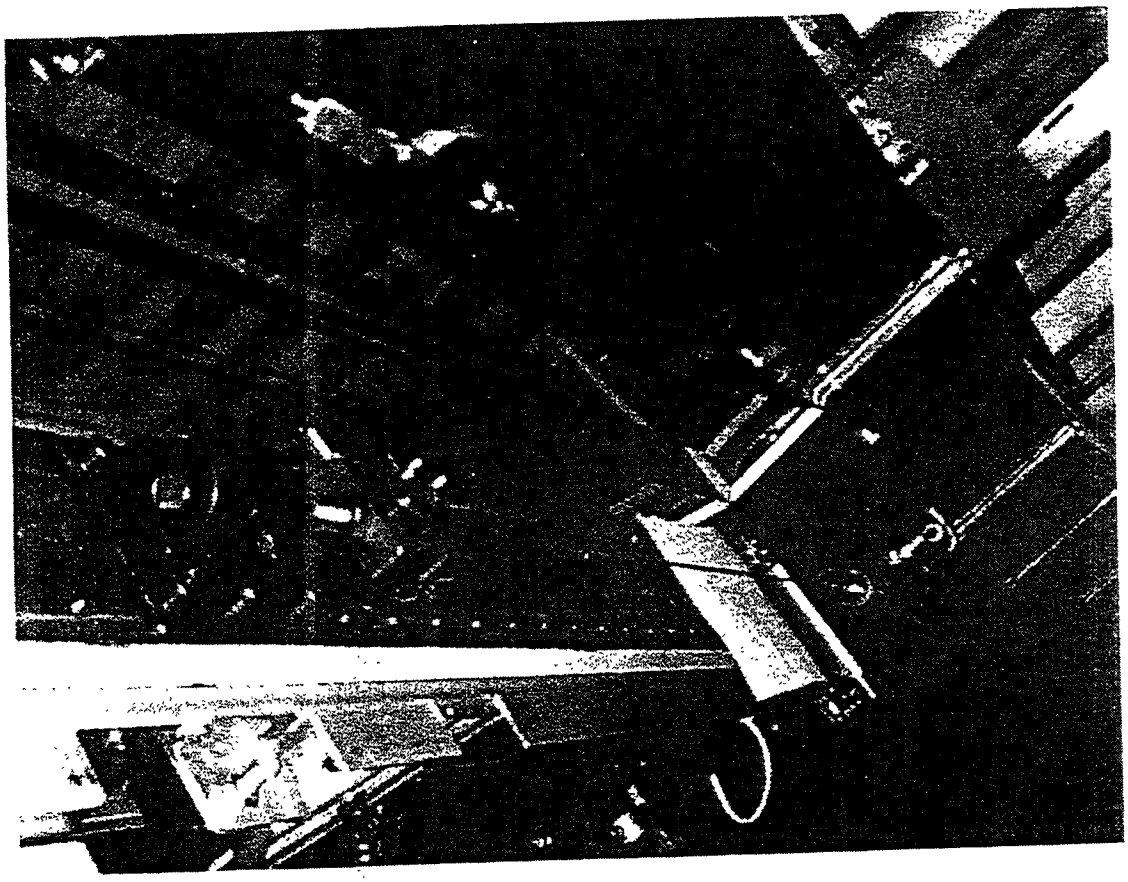

observed after this initial cycle.

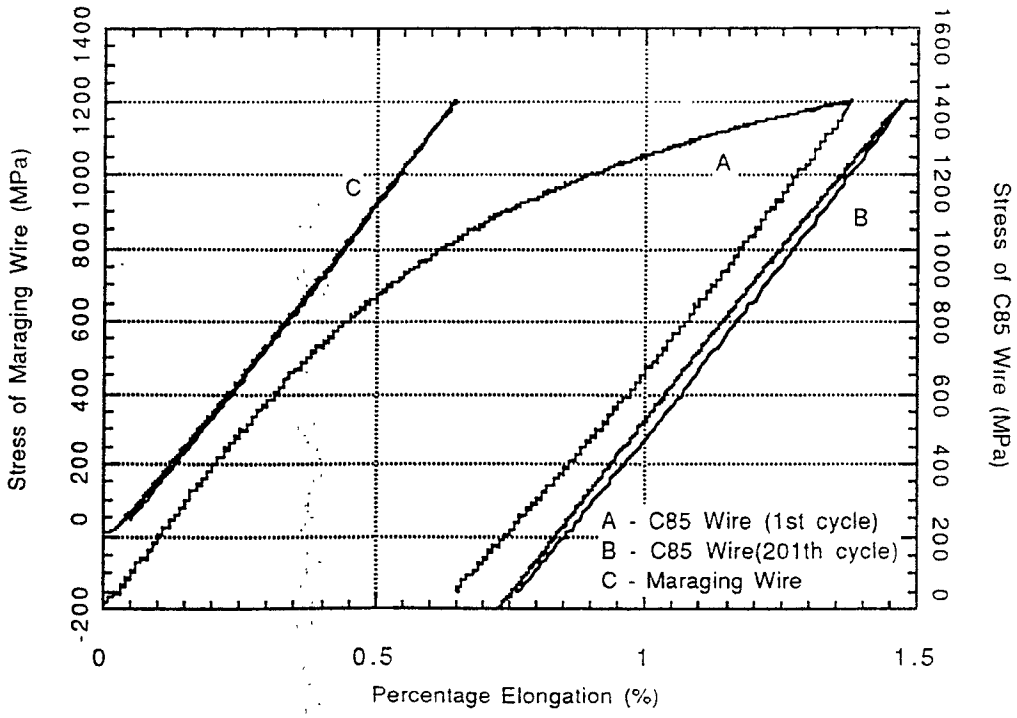

Fig.2 Behavior of Strain and Stress of the Piano and Maraging Wires

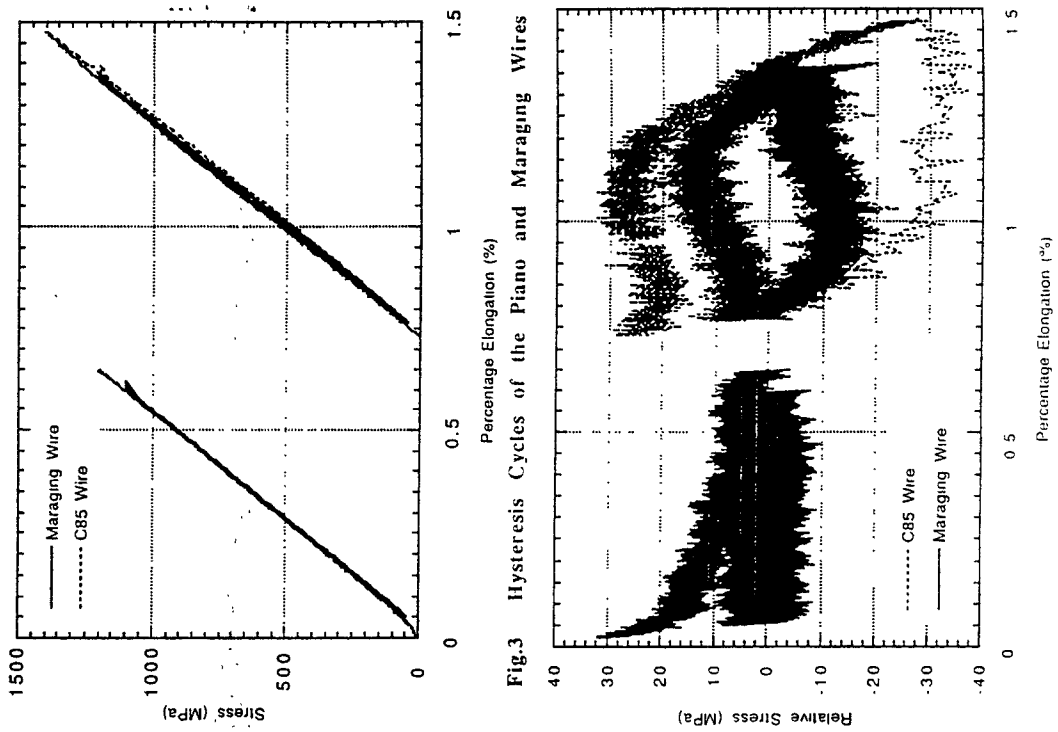

Fig.3 Hysteresis Cycles of the Piano and Maraging Wires

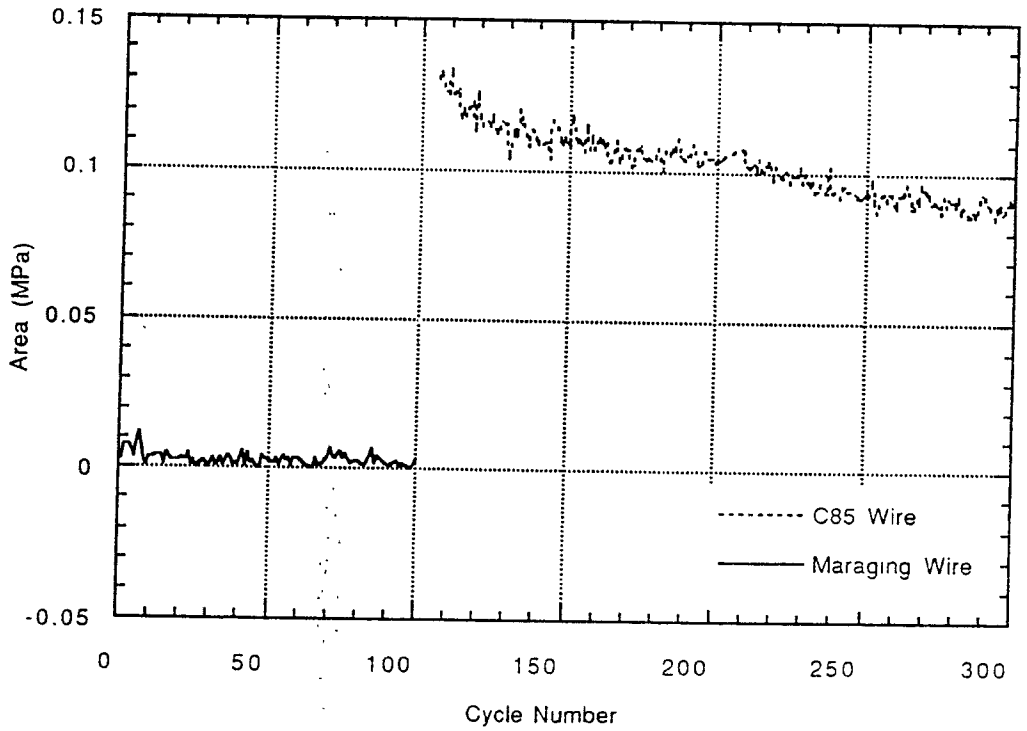

Fig.5 Hysteresis Area of the Piano and Maraging Wires

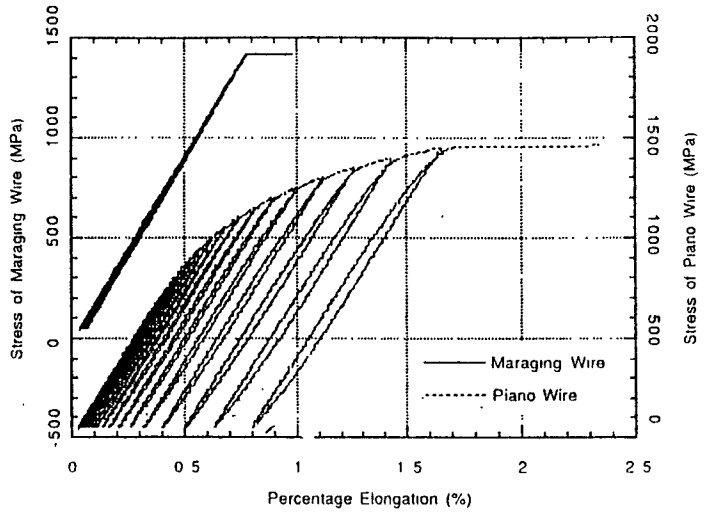

Fig.7 Hysteresis Cycles of the Broken Wires

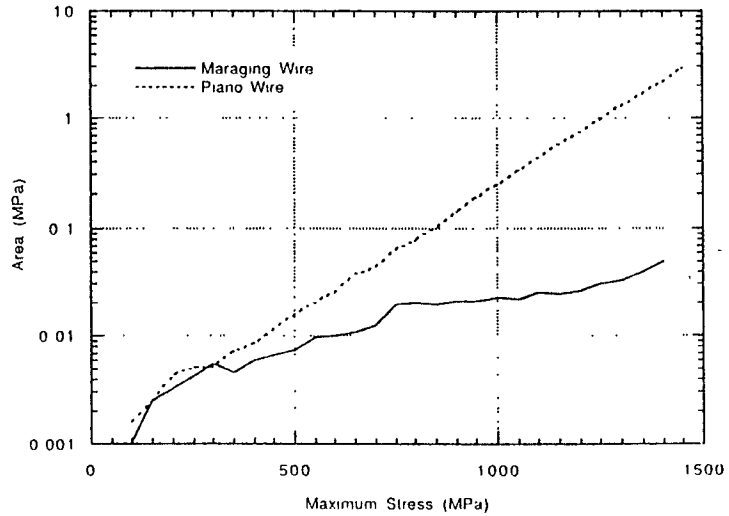

Fig.8 Hysteresis Area of the Broken Wires

Elimination of Internal Excitations

A)

Maraging steel used in all stressed components

B)

>100°C baking of assembles attenuators

relieves excess stresses and

consumes all possible slippage

C)

If will detect problems with Virgo operation

further safety factor by chilling

No low temperature brittleness with Maraging

Thermal noise requirements for GEO 600:

- Require h sensitivity of $2\times10^{-22}/\sqrt{\text{Hz}}$ at 50Hz
- Set by expected thermal noise from internal modes of test mass: Typically, for fused silica:-

  $Q_{internal} \sim 5 \times 10^6$ - difficult to improve on this
- Sets limits on thermal noise from pendulum modes, violin modes suspension such that require

  $Q_{pendulum} > 2 \times 10^6$ (assumes structural damping)

  $Q_{violin} > 1 \times 10^6$
- Would like $Q_{pendulum} > 10^7$ - all fused quartz suspension ?

Relationship between $Q_{pendulum}$ and $Q_{material}$:

$$Q_{pendulum} = Q_{material} \frac{mgl}{4\sqrt{TEI}}$$ for a 2-loop suspension

where:

m = mass E = Youngs modulus

l = length I = moment of mass = $\frac{\pi r^4}{4}$

T = tension r = radius of wire

n = number of wires

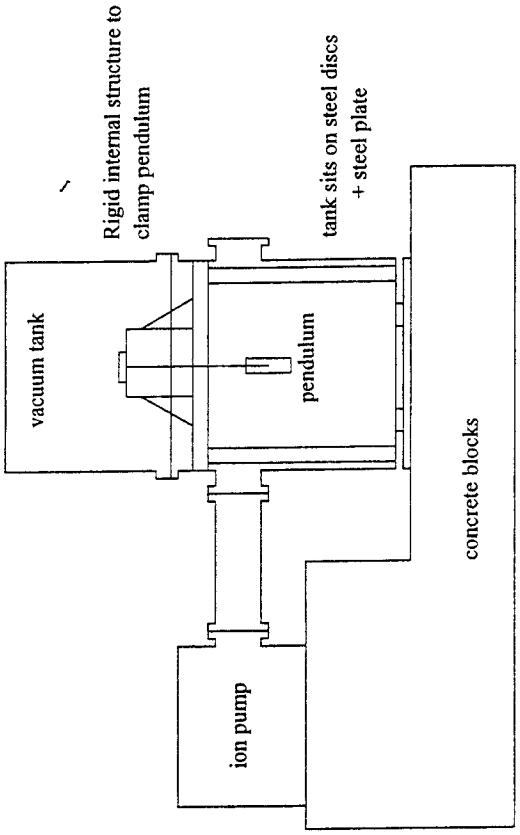

Limit to measurable Q as set by recoil damping:

$$Q_{limit} = \frac{1}{m\omega_0^2}\frac{k}{\phi}$$

m = pendulum mass = 0.21kg

ω_0 = resonant frequency = 1Hz

k = stiffness of structure = $5.5 \times 10^6 \pm 0.7 \times 10^6$ Nm^{-1}

ϕ = phase angle between the recoil displacement and the drive force = $-1.61° \pm 0.05°$

$$Q_{limit} = 2.4 \times 10^7 \pm 0.3 \times 10^7$$

Amplitude decay as a function of time for glass pendulum suspended by silica fibres

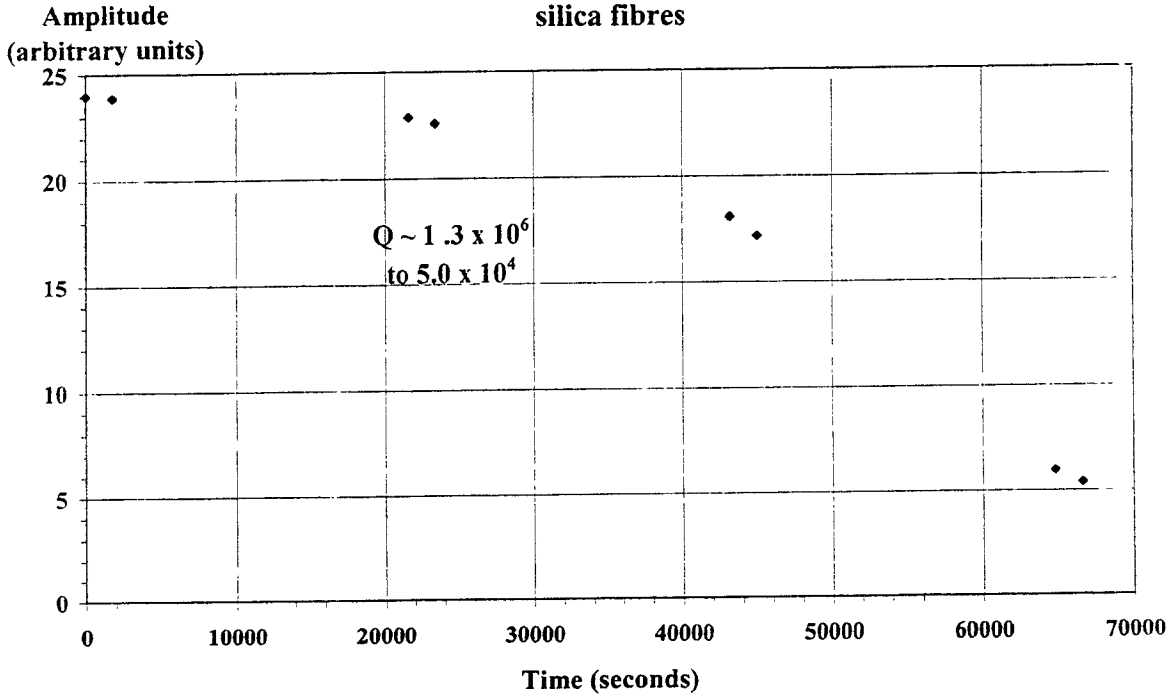

S. Rowan et al
Class. Quant. Grav
In Press

Investigations:

- Noted that bare wire inside tank acting as an aerial - picking up signal at pendulum frequency
- Suggests pendulum is charged - moving charge is inducing currents in surroundings

Experiments suggest pendulum is negatively charged and that:

Ion pump is producing UV

UV is liberating electrons from walls/structure inside tank

Electrons are collecting on pendulum resulting in an overall negative charge

Initial experiments

- Found measured Q_{pend} changed over course of a decay - decreased from few x 10^6 to few x 10^4
- Experiments revealed Q_{pend} sensitive to electrostatic charging of pendulum by UV from ion pump
- Problem overcome by suitable shielding, but, Q_{pend} still only 3 x 10^6, ~ 6 times too low

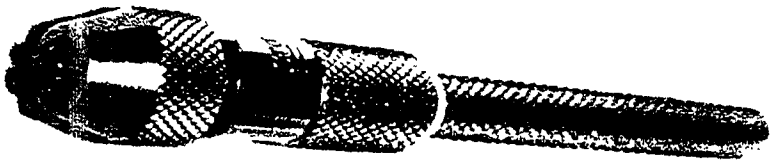

~9cm

Further experiments

- Made a series of measurements to try and determine source of excess loss
- Consider:

$$\frac{1}{Q_{measured}} = \frac{1}{Q_{pend}} + \frac{1}{Q_{recoil}} + \frac{1}{Q_{excess}}$$

$$= \frac{1}{Q_{expected}} + \frac{1}{Q_{excess}}$$

Possible sources of excess loss

- Recoil loss of structure greater than expected
- $(1/Q_{mat})_{excess} \propto$ stress
- Losses at points where fibres are clamped to top plate and mass

Summary of results from measurements of pendulum Q of a selection of pendulums suspended on fused quartz fibres - assuming Q_{mat} ~1 x 10^6

		Pendulum mass (g)	Fibre diameter (μm) (+/- 10%)	$1/Q_{pend}$ (meas) (+/- 5%)	$1/Q_{rotation}$ (meas) (+/- 5%)	$1/Q_{expected}$ (+/- 25%)*	$1/Q_{excess}$
Original clamps	1	200	290	3.3×10^{-7}		5×10^{-8}	(2.8 +/- 0.2) x 10
	2	32	60	1.0×10^{-7}		8×10^{-9}	(9.2 +/- 0.5) x 10
	3	96	60	2.2×10^{-7}		2×10^{-8}	(2.0 +/- 0.1) x 10
	4	96	60		3.3×10^{-7}		
New clamps	5	12	290	6.9×10^{-8}		4×10^{-8}	$(3+/-1) \times 10^{-8}$
	6	28	290	6.1×10^{-8}		3×10^{-8}	$(3+/-1) \times 10^{-8}$
Clamps tightened	7	28	290	3.2×10^{-8}		3×10^{-8}	$(0 +/-1) \times 10^{-8}$
	8	96	290	3.1×10^{-8}		3×10^{-8}	$(0 +/-1) \times 10^{-8}$

*The uncertainty in this number is a combination of uncertainties from
(a) the recoil of the system
(b) the exact point of bending of the fibre and thus the exact fibre diameter and length of the pendulum

(a) Excess loss - due to recoil?

- For this case expect

$$\frac{1}{Q_{excess}} \propto m$$ Results 5 and 7 suggest not

$$\frac{1}{Q_{pend}} > \frac{1}{Q_{rot}}$$ Results 3 and 4 suggest not

$\Rightarrow$ Excess loss NOT due to extra recoil

(b) Excess loss - stress dependent?

- For this case

$$\frac{1}{Q_{excess}} \propto \sqrt{m}$$ for constant fibre radius — Results 5 and 7 suggest not

$$\frac{1}{Q_{excess}} = \text{const.}$$ for: m const, r varying — Results 3 and 8 suggest not

$\Rightarrow$ Excess loss NOT due to any stress dependence of material loss of fused quartz

(c) Excess loss - loss at clamps?

- For this case expect clamp changes to improve measured Q

- Comparing : Results: 2 with 7
  6 with 7

  consistent with this

  $\Rightarrow$ Excess losses are related to clamping technique

Measurements of Pendulum Q

- Using fused quartz as suspension material allows possibility of monolithic suspensions - minimising losses at fibre/mass joints
- Possible approaches:

  (a) welding of fibres to test mass

  (b) optical contacting of fibres with rod ends to mass

Current Progress

- Using an all fused quartz, welded pendulum of mass ~100g, $Q_{pend} \sim 3 \times 10^7$ achieved
- In agreement with measured suspension fibre and recoil losses
- Same pendulum with efforts made to reduce recoil losses - evidence of $Q_{pend} \sim 1 \times 10^8$

Pendulum excitation by seismic noise

- Want to check that measured Q_{pend} is not significantly affected by seismic noise
- Assume seismic noise = white noise spectrum
- Relation between pendulum motion, x_1, and seismic motion, x_o, can be expressed as:

$$\frac{x_1}{x_0} = \sqrt{\frac{\pi f_0 Q}{2}}$$

- Measured ground motion

$$x_0 \approx 10^{-8}\,\mathrm{m}/\sqrt{\mathrm{Hz}}\ @\ 1\mathrm{Hz}$$

- Say $Q_{pend} \approx 3\times10^7$

$$\Rightarrow x_1 \approx 68\,\mu\mathrm{m_{rms}}$$
$$\Rightarrow x_1 \approx 192\,\mu\mathrm{m_{pk\text{-}pk}}$$

- Initial pk-pk amplitude of pendulum swing

$$= 3\text{-}4\mathrm{mm}$$

$\Rightarrow$ factor of 15-20 times larger than seismic excitation

- This suggests that measured Q_{pend} should be unaffected by ground motion

Current plans

- Continue pendulum Q measurements on
  (a) welded pendulums of greater mass *
  (b) pendulums with suspension fibres attached by optical contacting
- Make measurements of internal Q of masses with welded/optically contacted fibres attached

* Larger mass pendulums to be tested in Perugia
Initial results (with Kovalik et al) show $Q_{pend} \sim 10^7$ for $m \doteq 2$kg

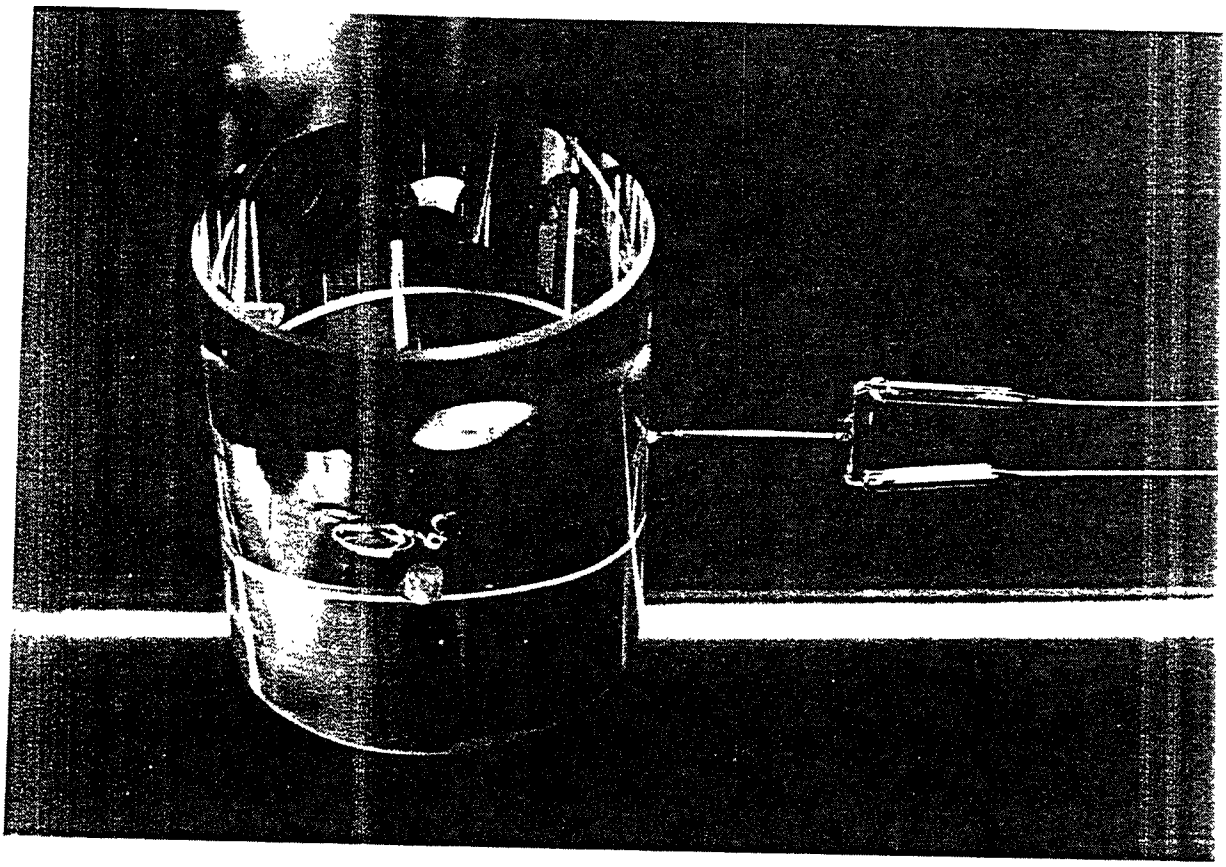

SUSPENSION DESIGN FOR

GEO 600

Norna A Robertson

University of Glasgow

Aspen

Jan 1997

TEST MASS SUSPENSIONS

Reminder of design considerations

- good seismic isolation
  (horizontal, vertical and tilt)
- good thermal noise properties
  (pendulum, violin and internal modes)
- implementation of control
  (orientation, damping, longitudinal)
- UHV compatibility

SUSPENSION DEVELOPMENTS FOR GEO 600

(Glasgow commitment)

- **stacks/double pendulum**

  N Robertson, M Plissi, K Strain, C Torrie,

  S Killbourn, J Hough + P Aufmuth (Hannover)

- **thermal noise developments**

  S Rowan, S Twyford, S Killbourn, J Hough

- **control/electronics**

  H Ward, D Robertson, K Strain, K Skeldon,

  G P Newton, M Casey

N Robertson	head of working group on suspensions
H Ward	head of working group on control

GEO 600 Revised Specification:

$h \sim 2\times 10^{-22}/\sqrt{Hz}$ at 50 Hz

	→	$\Delta x_{mass} < (7 \times 10^{-20}\ m/\sqrt{Hz})_{50\ Hz}$
So design goal		$\Delta x_{seismic} < (7 \times 10^{-21}\ m/\sqrt{Hz})_{50\ Hz}$
	Assuming	$\Delta x_{ground} \sim 10^{-7}/f^2\ m/\sqrt{Hz}$
→	Isolation	$\sim 6 \times 10^{9}$ at 50 Hz in horizontal
		$\sim 6 \times 10^{6}$ at 50 Hz in vertical
		(assuming 0.1% coupling)

Should be achievable with

- 2 layer isolation stack
- 2 vertical spring stages
- double pendulum

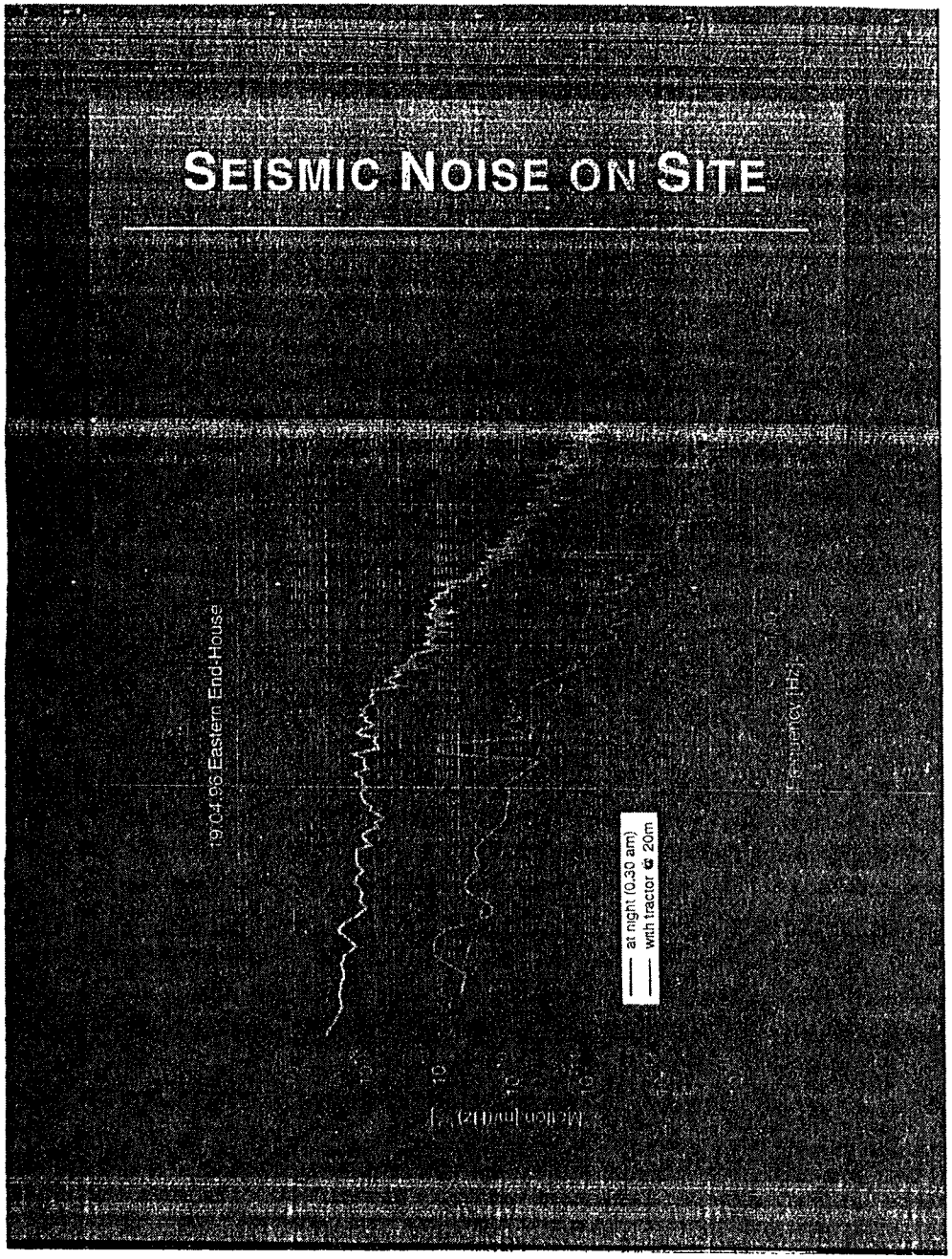

GEO 600 Main Suspension

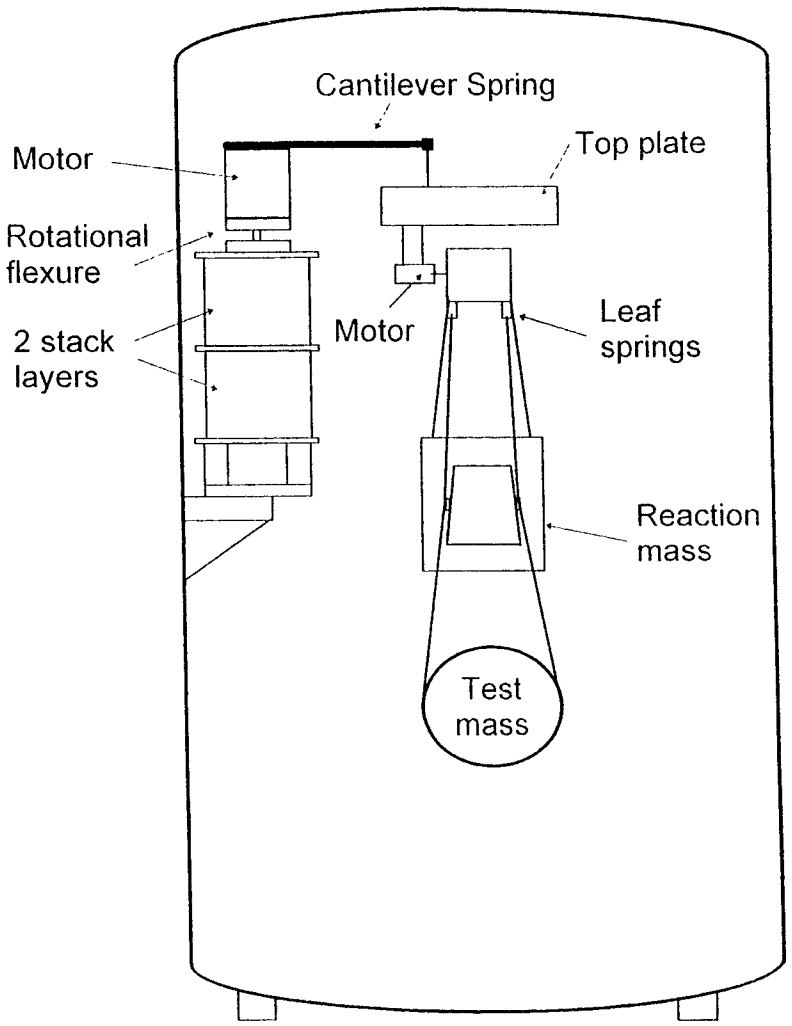

10 m

GEO 600 STACK DESIGN

3 legs, each consisting of

- **graphite loaded RTV cylinders**
- **stainless steel masses**
- **encapsulated in bellows, and differentially pumped**

vertical section through stack

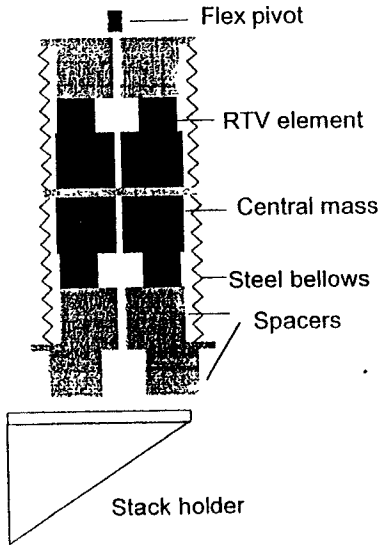

SOME DETAILS OF STACK DESIGN

1. Use of RTV

- advantages — low spring constant; can be molded
- disadvantages — stiffens with load; high Q (~20)
- solution — load RTV with graphite filler

Damping tests

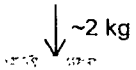

RTV CYLINDER
(diameter=30 mm; height=40 mm)

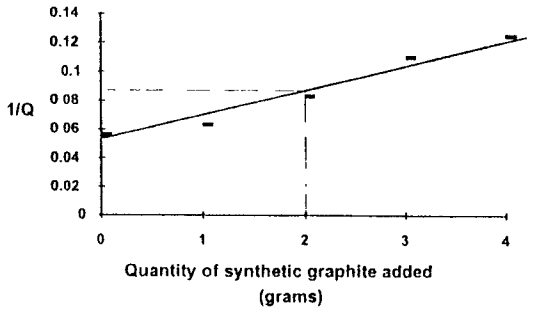

SOME DETAILS OF STACK DESIGN

1. Use of RTV continued

RTV stiffness tests:

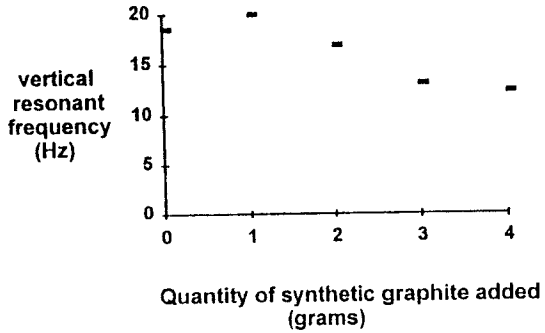

Conclusions

Can achieve Q<10 by loading with graphite, with no change in stiffness.

SOME DETAILS OF STACK DESIGN

2. Use of Bellows

- **advantage** — **remove potential contamination from rubber**
- **disadvantage** — **high Q resonances**
- **solution** — **line inside of convolutions with mixture of Q-compound and silicone grease**

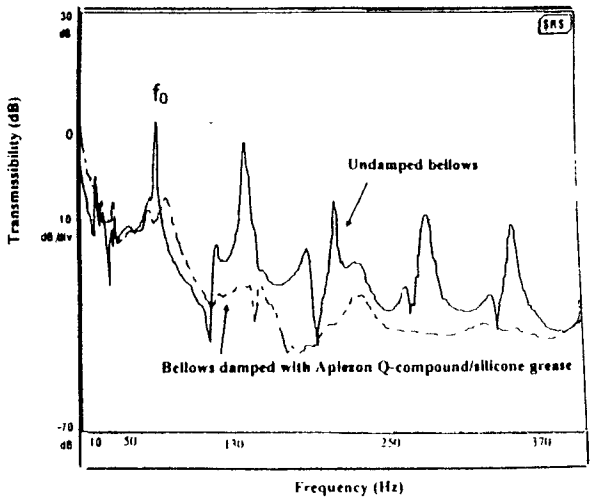

SOME DETAILS OF STACK DESIGN

3. Use of Flex Pivot

Bellows are very rigid in rotation about their cylindrical axis

=> use flex pivot to reduce coupling of rotational motion to top of stacks

=> with loads envisaged (~30 kg per leg) rotational resonance around 1-2 Hz

---

Vertical Transmissibility of Stack System (3 legs) with Loaded Top Plate

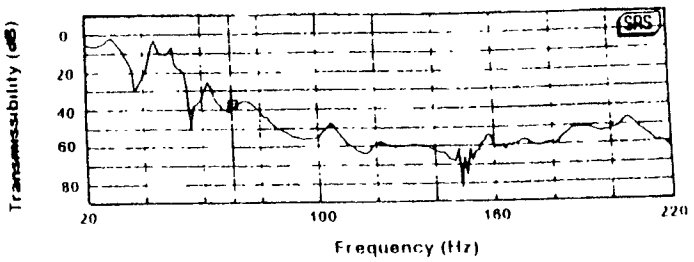

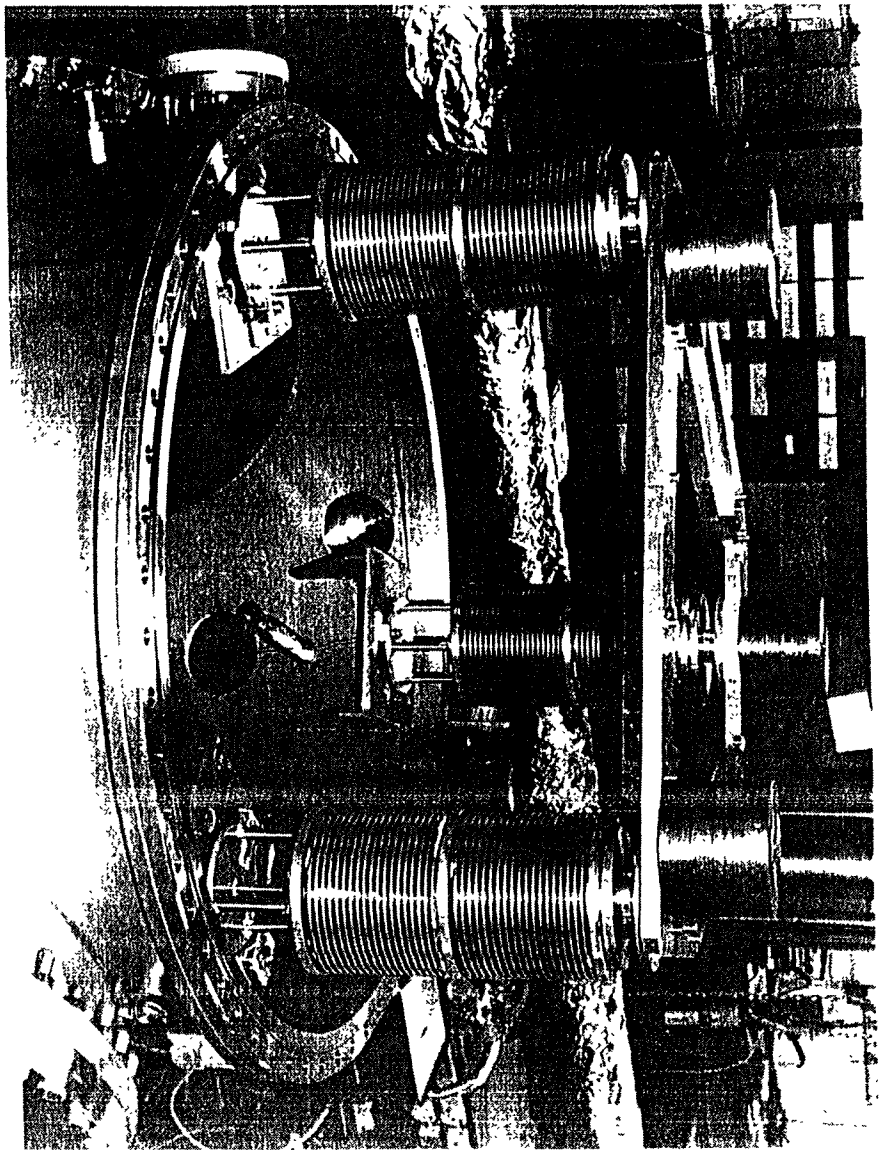

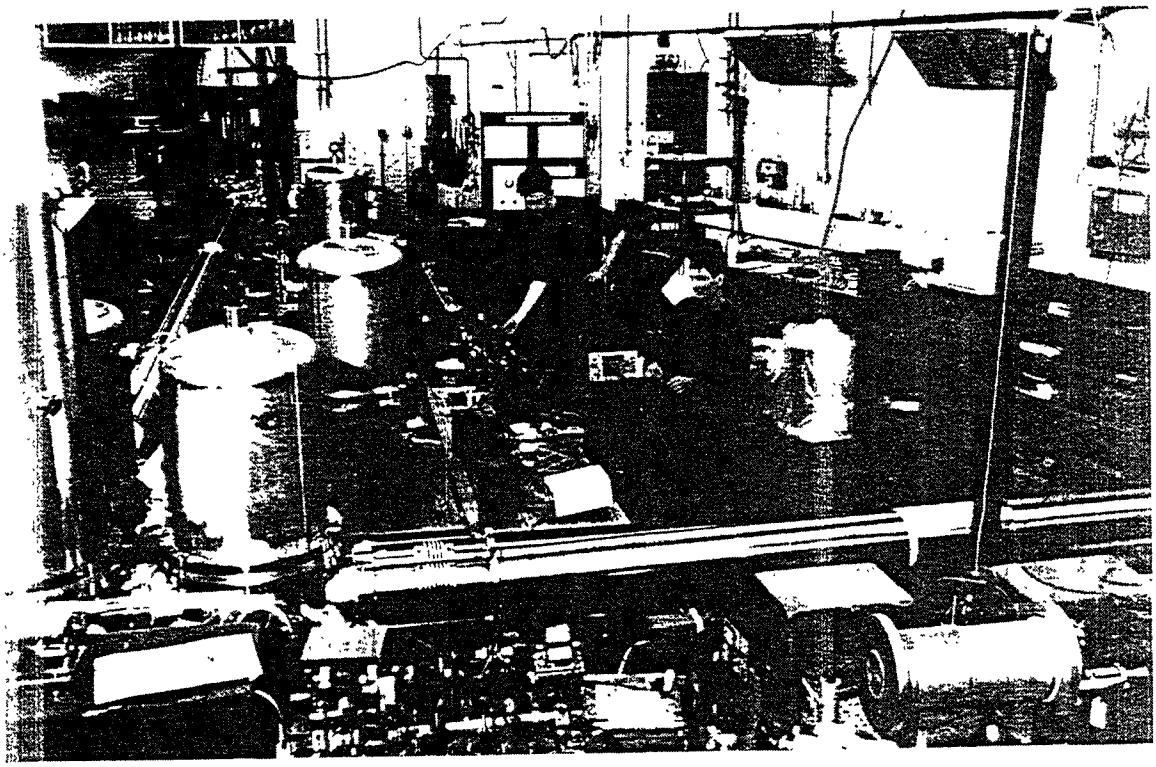

GLASGOW 10 m PROTOTYPE DETECTOR

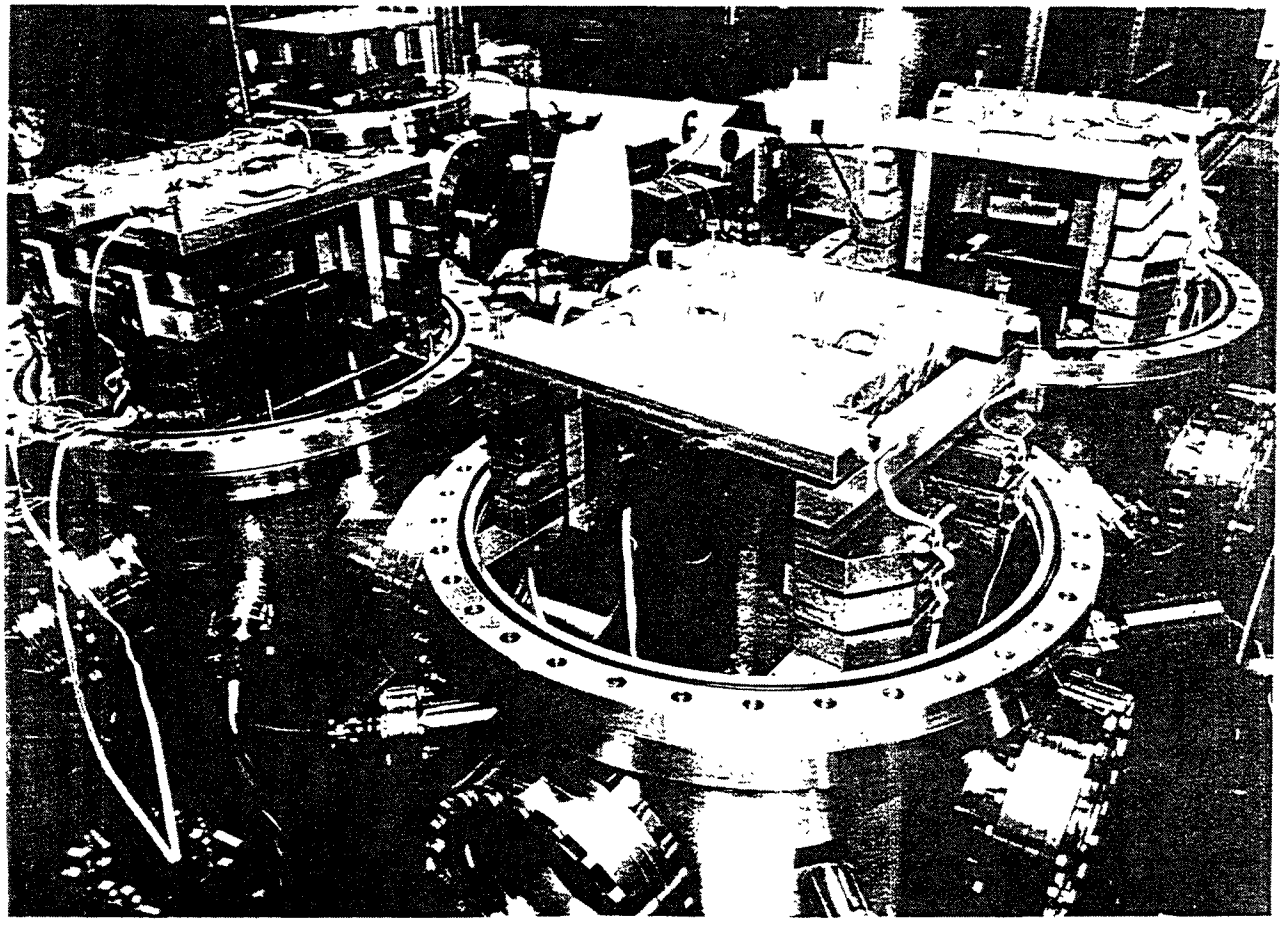

Double Pendulum Suspension

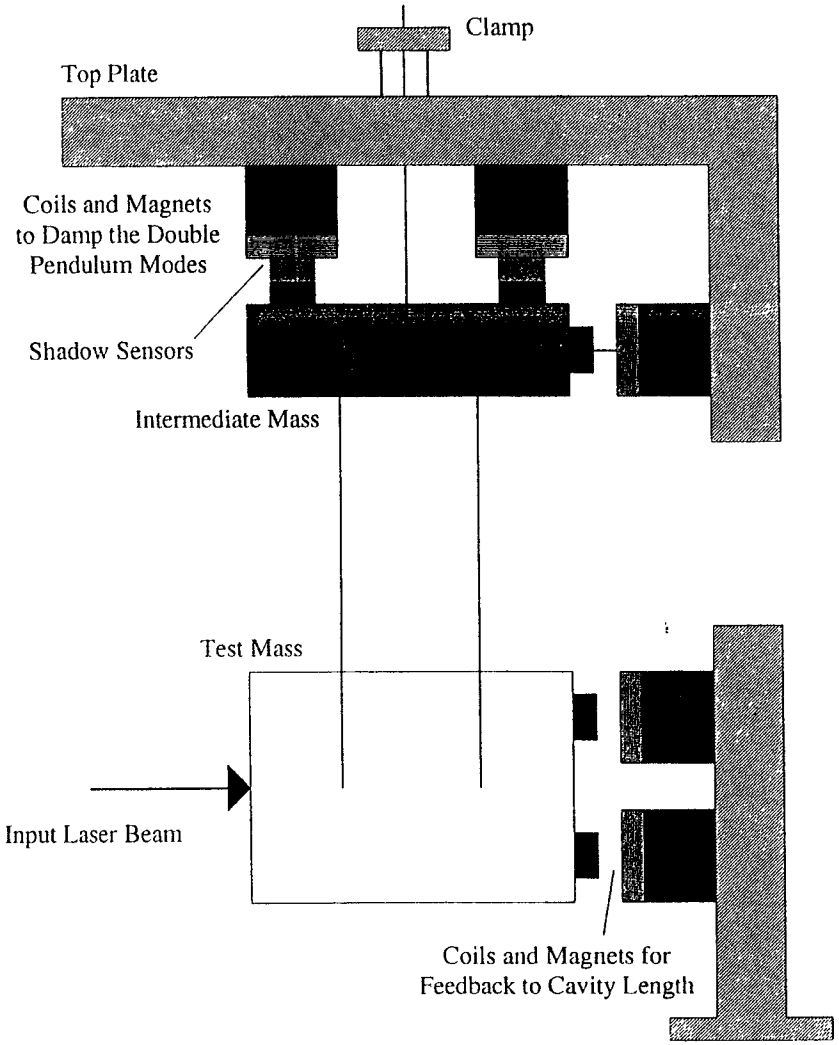

Fig. 1

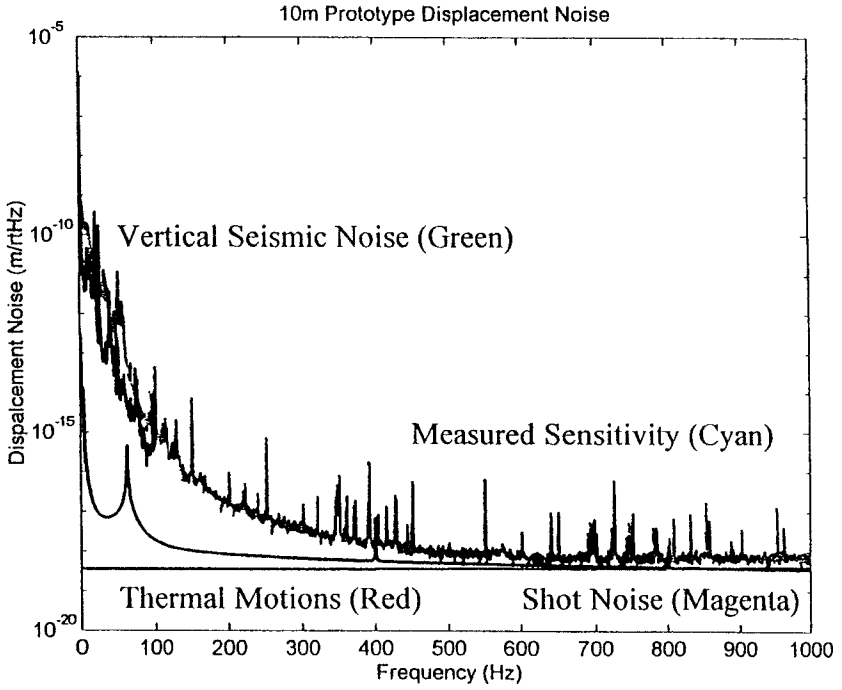

DOUBLE PENDULUM SUSPENSION
IN GLASGOW PROTOTYPE DETECTOR.

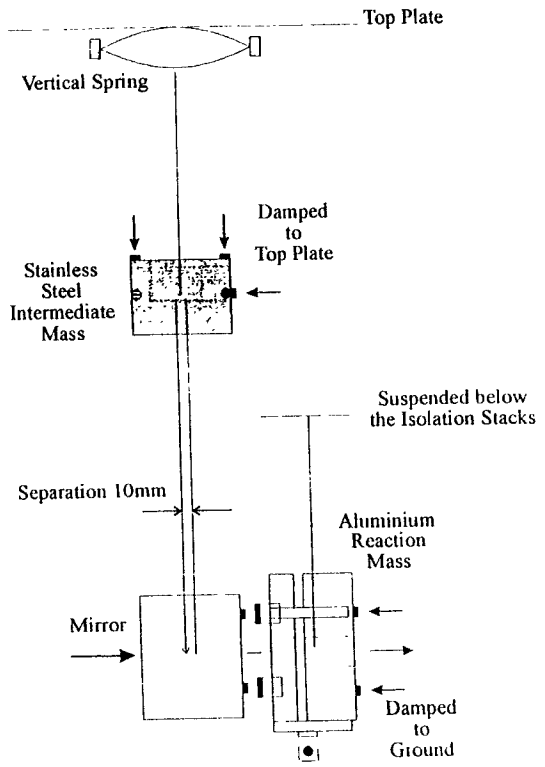

(S KILLBOURN)

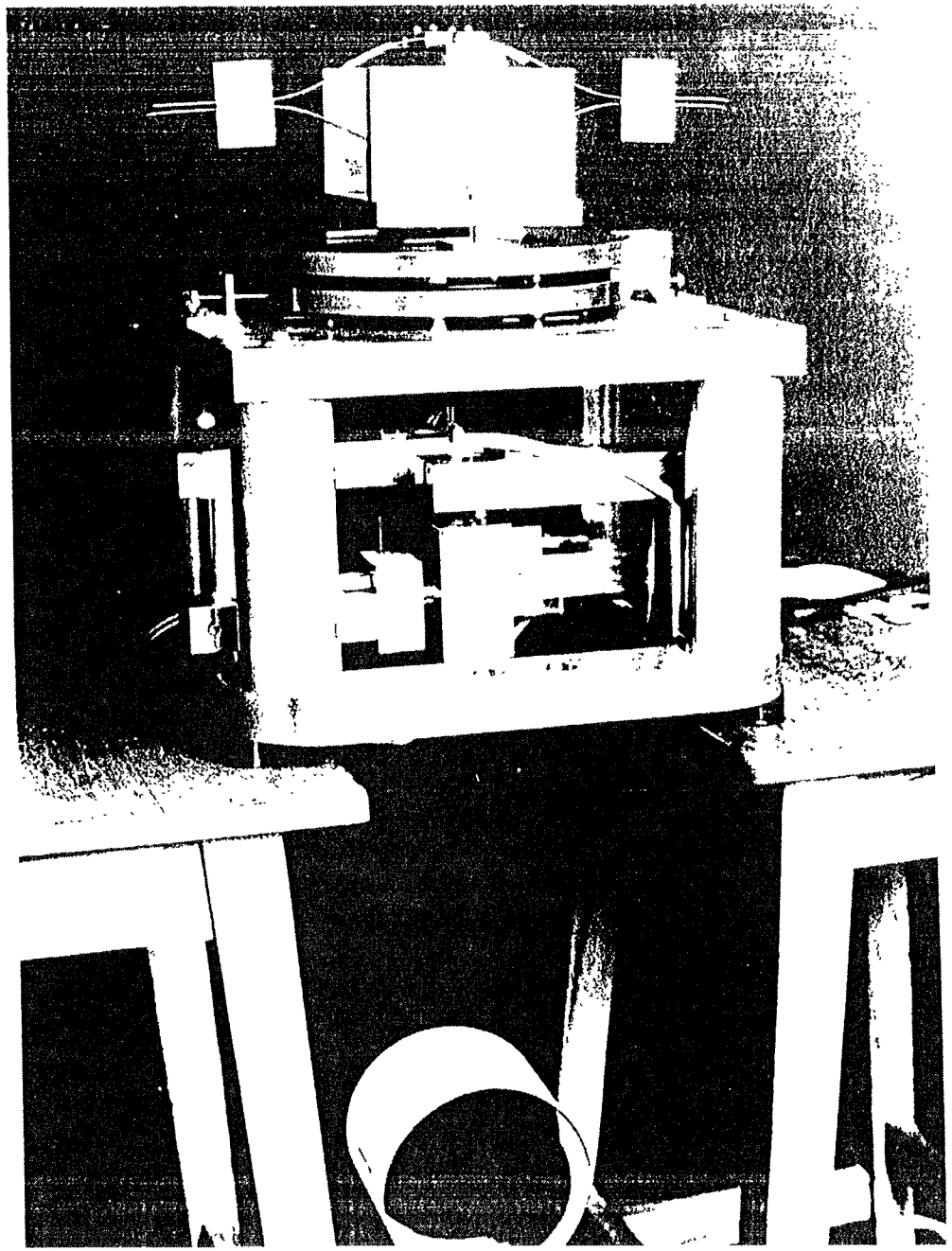

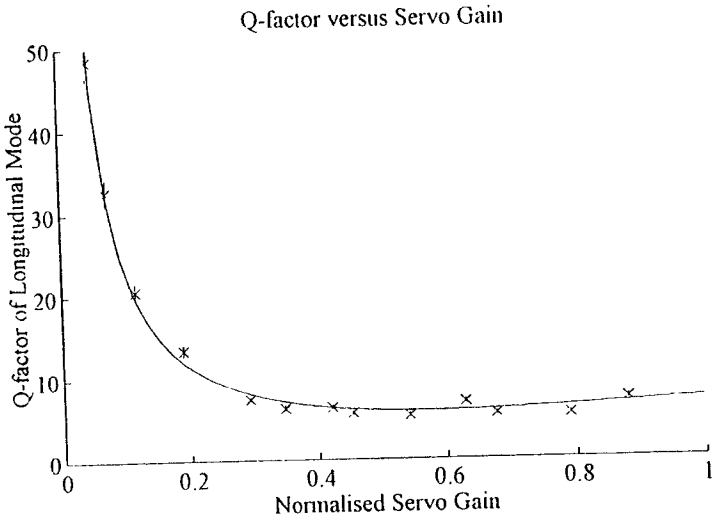

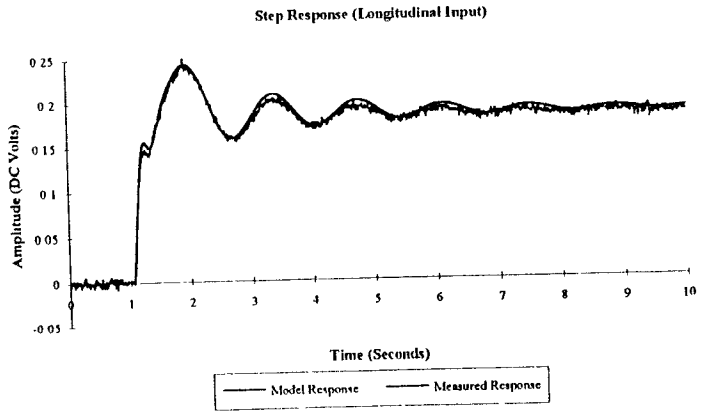

IMPLEMENTATION OF CONTROL

Design philosophy : to reduce coupling of electronic and seismic noise to test mass

- **Orientation** (tilt and rotation) and **damping** of modes applied at **upper mass** using **suspended reaction mass** with shadow sensors and coil and magnet actuators

  (modecleaner masses - coils mounted on rigid supports extended from top plate)

- **Longitudinal control - split feedback** (except modecleaners) applied at

  - **upper mass** at **low frequencies**
    (shadow sensors and coil and magnet actuators)
    and
  - **lower (mirror) mass** at **high frequencies**
    (possibly electrostatic drive)

  using upper and lower suspended reaction masses.

Some experience already gained at Glasgow of using split feedback and of orientation and longitudinal control of masses from a suspended mass (e.g. P Veitch et al, Rev Sci Inst **64** 1330, and current work on 10 metre prototype)

SUSPENSION DEVELOPMENTS - TIMESCALES

- **modecleaner suspension**
  - test — March '97
  - deliverable prototype — Summer '97
- **main suspension**
  - design — May '97
  - test* — late '97
  - deliverable prototype — Jan '98
- **further research to allow operation at high sensitivity to lower frequencies (~ 20 Hz)**
  - use of ultra-low loss materials (collaboration with Stanford +) — start early '98
  - development of active isolation and low noise control systems, and test in 10 m system (collaboration with JILA +) — start late '98

* in GEO size tank on one end of 10 metre prototype

A Few Advances in Understanding Thermal Noise

Peter R. Saulson
Syracuse University

OUTLINE

1) Test of "dissipation dilution" in pendulums - Y. Huang

2) Measurement of $\phi(f)$ in test masses via the anelastic aftereffect - M. Beilby

Fluctuation-Dissipation Thm.

$$x^2(f) = \frac{4k_B T}{(2\pi f)^2}\,\mathrm{Re}\left[-Y(f)\right]$$

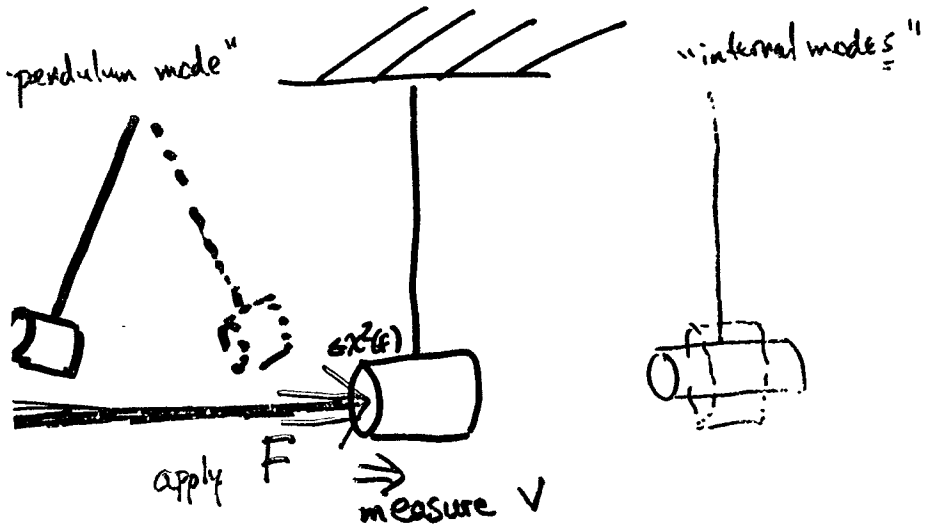

$$Y(f) \equiv \frac{v(f)}{F(f)}$$

$$x^2(f) = \frac{2}{\pi}\frac{k_B T}{k}\,\frac{1}{f\left[(1-f^2/f_0^2)^2+\phi^2\right]}\,\phi(f)$$

Pendulum Thermal Noise

Pendulum is good because $Q \gg \phi_{wire}^{-1}$

$$Q_{\substack{pend,\\violin}} = \phi_{wire}^{-1} \times \underbrace{\frac{L}{2}\sqrt{\frac{T}{ET}}}$$

"dissipation dilution" $\approx 10^3$

Test Q's of violin modes
(recoil damping small)

Look for agreement with theory
or else for excess losses due to

- Change in ϕ at high stress
- rubbing friction at contacts
- ?

Ph.D. Thesis of Yinglei Huang (1996)

Huang's Method

1 Measure $\phi_{wire}(f)$ by Kovalik's technique

.) Predict $Q_{violin}(f) = \phi_{wire}^{-1}(f) \times \frac{L}{2}\sqrt{\frac{T}{EI}}$

3) Measure $Q_{violin}(f_i)$

4) Compare results of steps 2 and 3

5) Declare victory

OR

Search for excess loss $\delta\phi \equiv Q_{violin}^{-1} - Q_{pred}^{-1}$

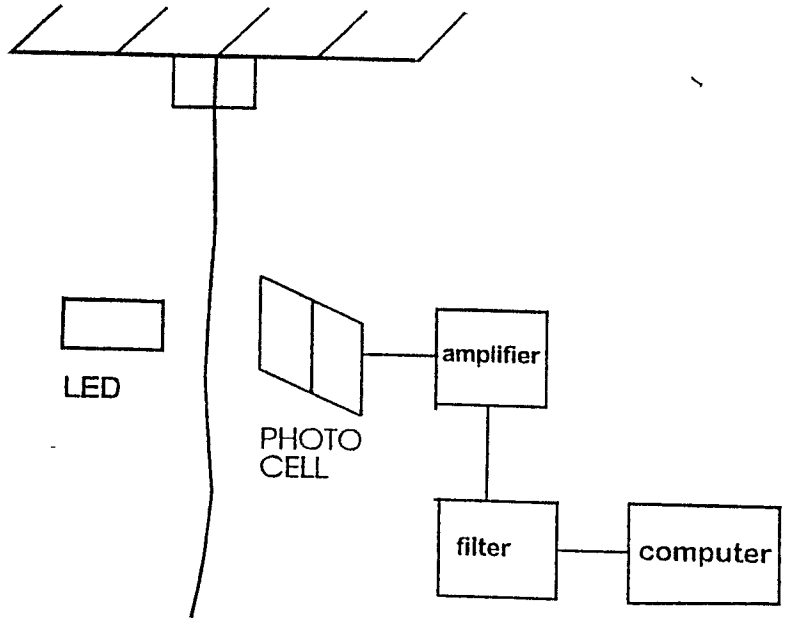

* $Q(\omega_n)$ measurement (under Tension)

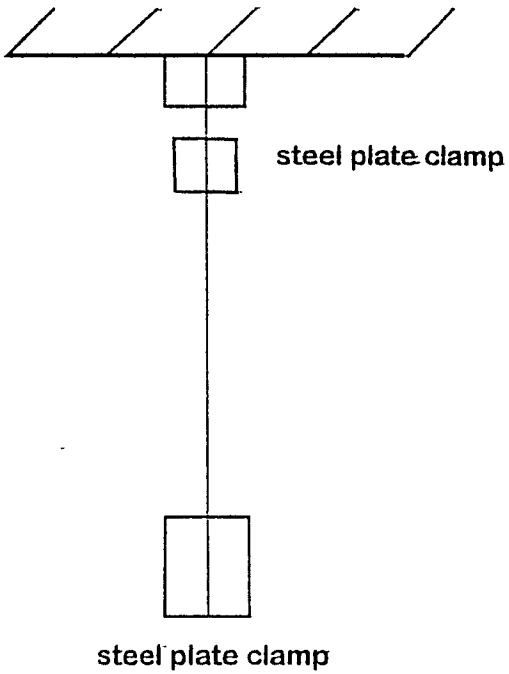

Summary of results

* *Did the most precise test of "dissipation dilution" effect,*

* *"Dissipation dilution" works*

  At stress comparable to the breaking stress in wires;

  With statistical error <10%;

  Agreement excellent for Q's up to 500,000;

  Some discrepancies exist for Q_{theory}>500,000, (a factor of 2 ~ 4);

* *Developed clear diagnosis for sliding friction (partial slip) at contact;*

* *Discovered breakdown of classical model of thermoelastic damping; Developed a new theory of the damping in beam under large tension ;*

*Studied sources of excess loss at $\delta\Phi \sim 10^{-6}$ level :

Not due to residual gas damping (~10^{-6} torr);

Not due to eddy current damping (~ 1Gauss);

Not due to recoil in support structure (double pendulum);

Not due to excitation of test mass internal motion;

Not due to coupling with other modes (bouncing, swing, rocking);

Not due to wire damage at clamping;

Not due to nonlinear (hysteresis) sliding friction at contact;

Single Wire double pendulum

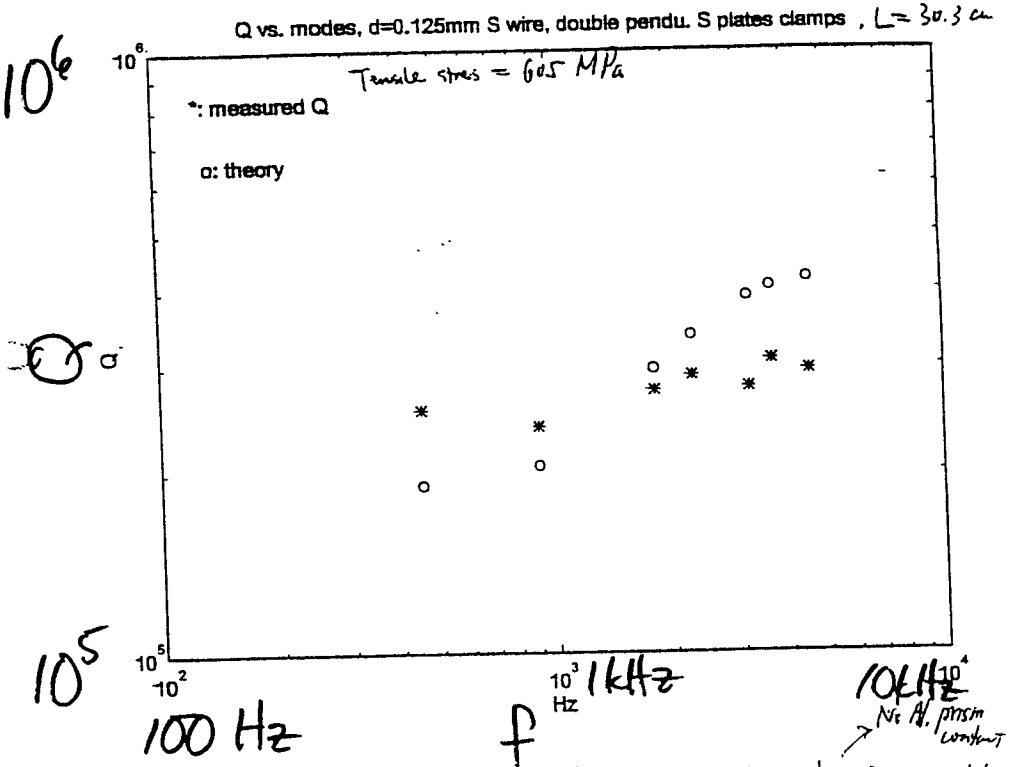

Fig. (5.13)

- Better Clamping, Simple → Double pendulum and recoil diagram
- $Q_m > Q_{th}$ (n=1, 2), still flat
- Steel wire anomaly

Thermoelastic damping under tension (Steel wire)

* Heat flow into clamp, & cross wire
* Most dissipation occur in $\Delta L = \sqrt{\frac{EI}{T}}$

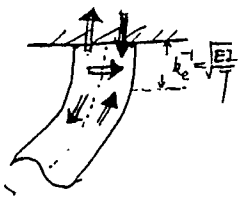

* Pictures of bending distribution
* 2-D Zener theory

$$\begin{cases} i\omega\tau = D\left(\frac{\partial^2}{\partial x^2} + \frac{\partial^2}{\partial y^2}\right)\tau - \left(i\omega \frac{E\alpha T_0}{C_\sigma}\right) y''(z)\, x \\ \left.\frac{\partial \tau}{\partial x}\right|_{x=\pm\frac{a}{2}} = 0, \quad \tau|_{y=\pm\frac{L}{2}} = 0 \end{cases}$$

Given by the mode shape

$$\Rightarrow \Phi_{th} = 2\sqrt{\frac{EI}{TL^2}}\, \frac{E\alpha^2 T_0}{C_\sigma}\left[\frac{f/f_d}{1+(f/f_d)^2} + \frac{(n\pi)^2}{2}\sqrt{\frac{EI}{TL^2}}\, \frac{f/f_d}{1+(f/f_d)^2}\right.$$

$$\left. -\left(2\frac{k_e}{|\Omega_0|}\cos\gamma_0\right)\frac{f/f_d}{1+(f/f_d)^2} + \left(2\frac{k_e}{|\Omega_0|}\sin\gamma_0\right)\frac{(f/f_d)^2}{1+(f/f_d)^2}\right]$$

less transverse flow

flow into the clamp

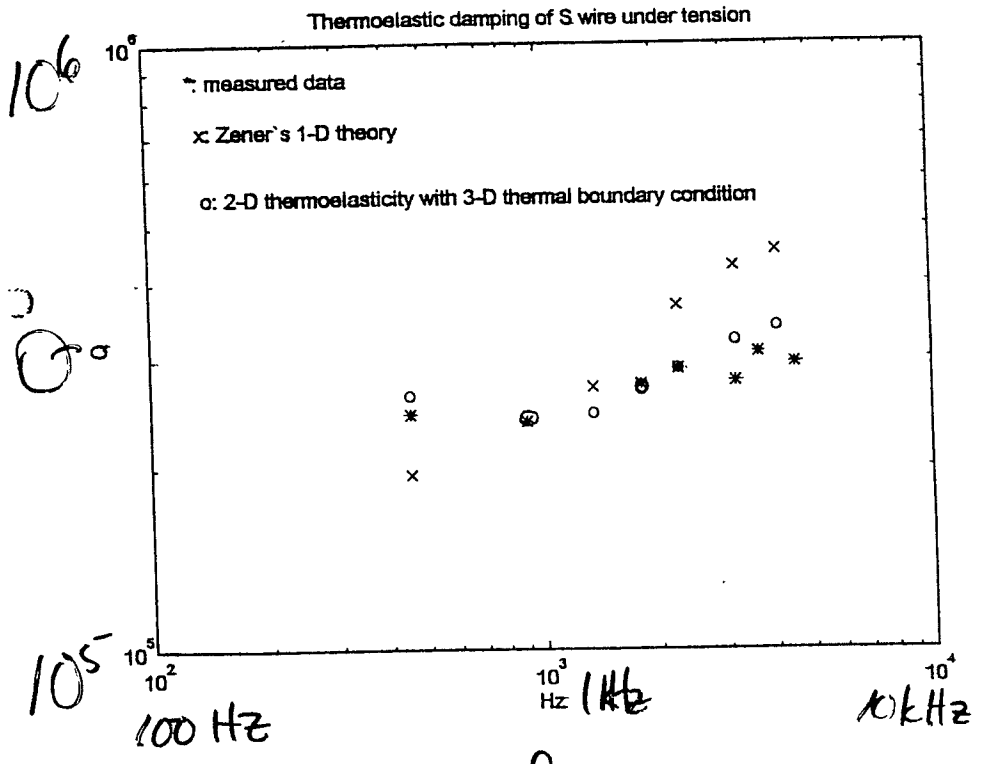

Fig (7.5)

Mirror Thermal Noise

+ frequency f, thermal noise depends on dissipation $\phi(f)$

rdinary method: $\phi(f_i) = Q^{-1}_{\text{resonance}}(f_i)$

Mirror resonances $f_i \gtrsim 10$ kHz,

but we want $\phi(f)$ in the range

$$10\,\text{Hz} \lesssim f \lesssim 10\,\text{kHz}$$

NEW METHOD:

Anelastic aftereffect $J(t)$ gives $\phi(f)$ at frequencies below lowest resonance

Work of postdoc Mark Beilby

CREEP AND THE ANELASTIC AFTEREFFECT

Hooke's Law:

$\epsilon = J\,\sigma$

ϵ: strain; J: compliance; σ: stress

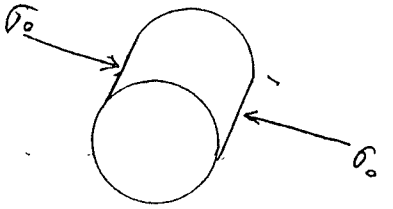

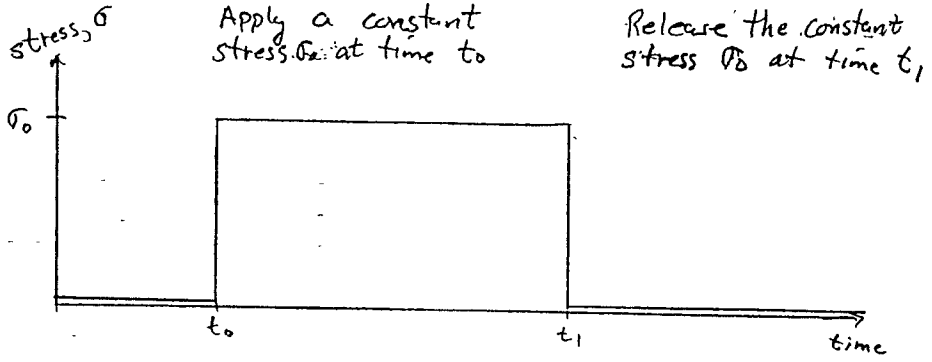

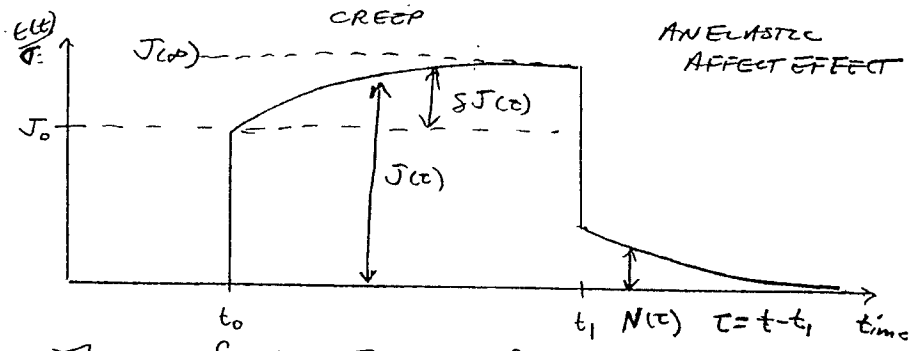

The creep function $J(t)$ is defined:

$$J(t) \equiv \frac{\epsilon(t)}{\sigma_0} \qquad t = t - t_0 \qquad J(t) = J(\infty) - N(t)$$

Calculating $\phi(f)$ from $J(t)$

$$\phi(f) \approx \frac{\pi}{2} \left. \frac{d \ln J(\tau)}{d \ln \tau} \right|_{\tau = \frac{1}{2\pi f}}$$

(see Nowick and Berry's book)

EXPERIMENTAL SET-UP

MEASURE $\epsilon(t)$ BY USE OF PHOTOELASTIC EFFECT (STRESS-DEPENDENT BIREFRINGENCE)

$$\Delta n_x = C \Delta \epsilon_x$$

(Δn_x: index of refraction; C: constant)

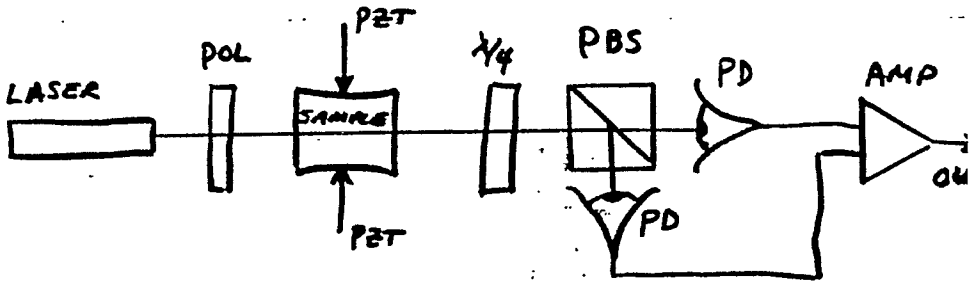

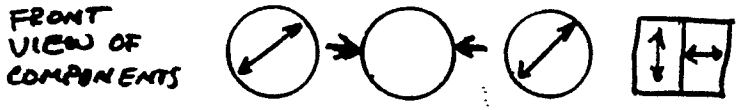

null output when birefrigence = 0
first order sensitive to birefringence

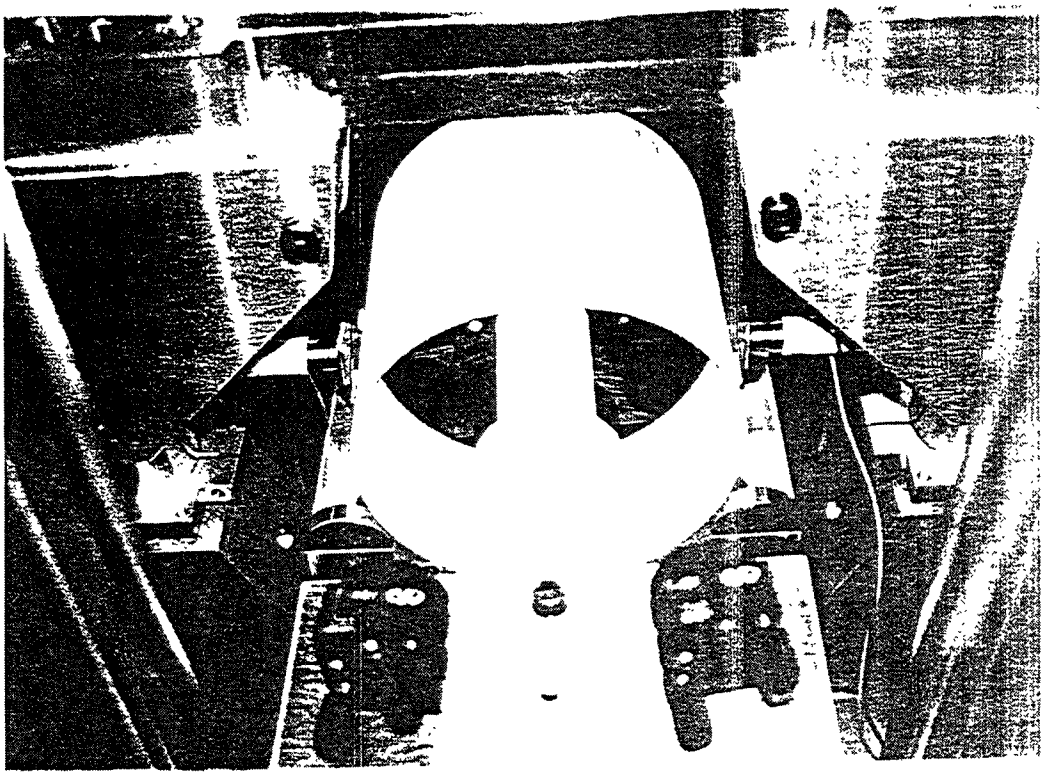

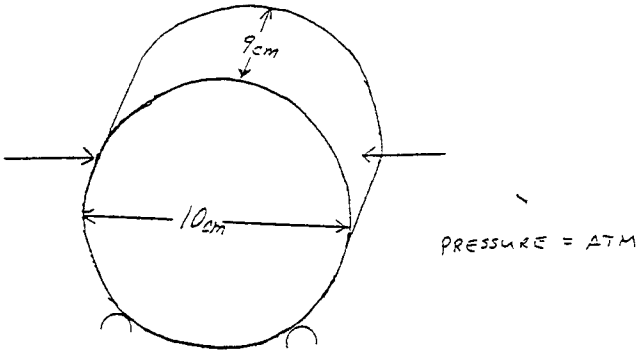

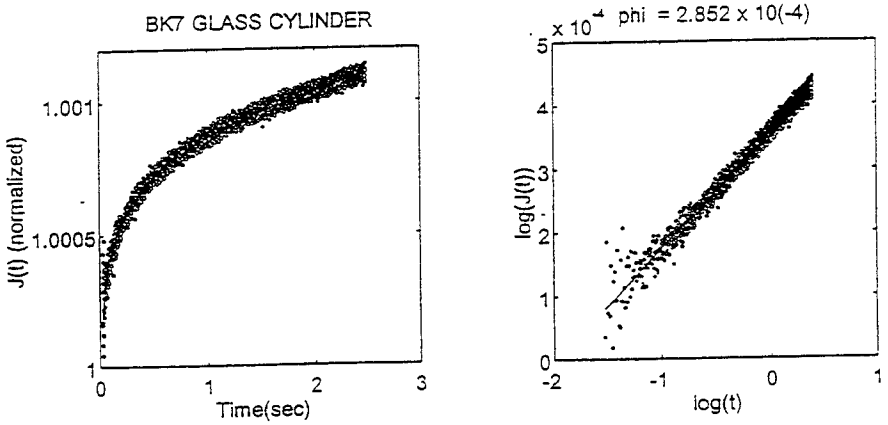

$\phi = (2.94 \pm 0.16) \times 10^{-4}$ $\quad 5\,H_2 \rightarrow 0.06\,H_2$

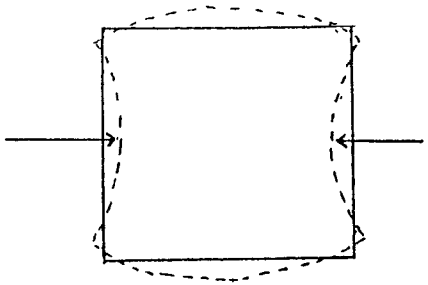

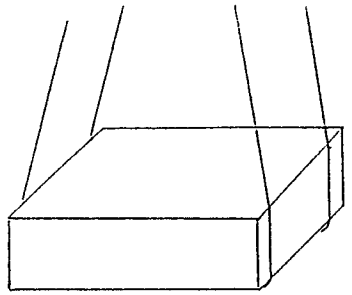

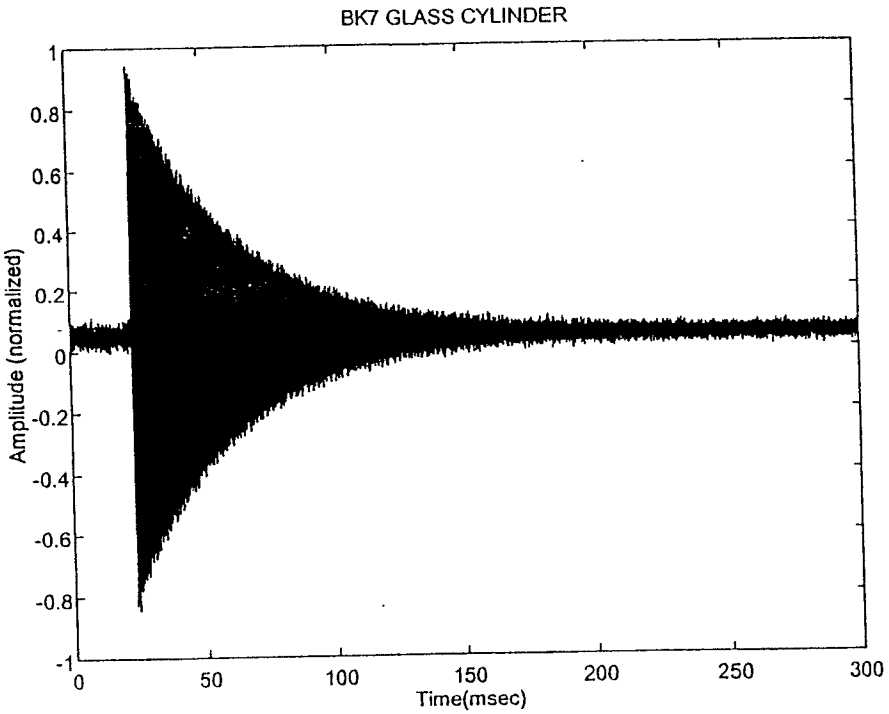

$\tau_{damp} \approx 0.040$ sec

$f_{resonance} = 26,900$ Hz

$Q = 3.4 \times 10^3$

$\frac{1}{Q} = \phi = 2.9 \times 10^{-4}$

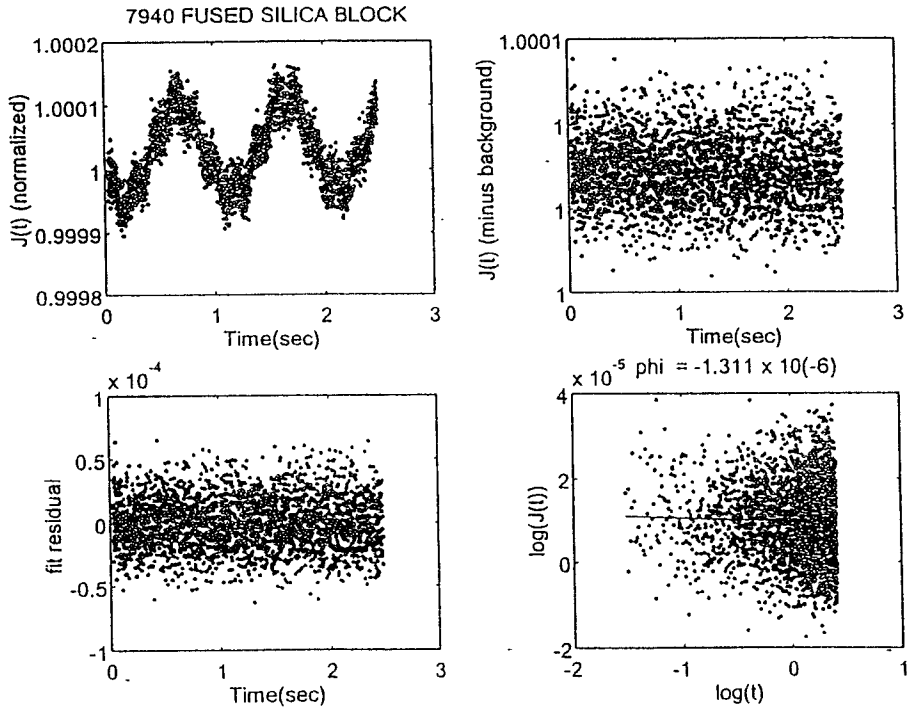

$\phi = (-0.6 \pm 36) \times 10^{-6}$ (wire suspension in ATM)

$5 Hz \rightarrow 0.06$ Hz

$Q @ f_0 \approx 2 \times 10^4$ (wire suspension in ATM)

$Q @ f_0 \gtrsim 5 \times 10^5$ (wire suspension @ 10^{-4} torr)

$f_0 \simeq 3 \times 10^4$ Hz

MODULATING SCHEME
with Photoelastic-Modulator (PEM)

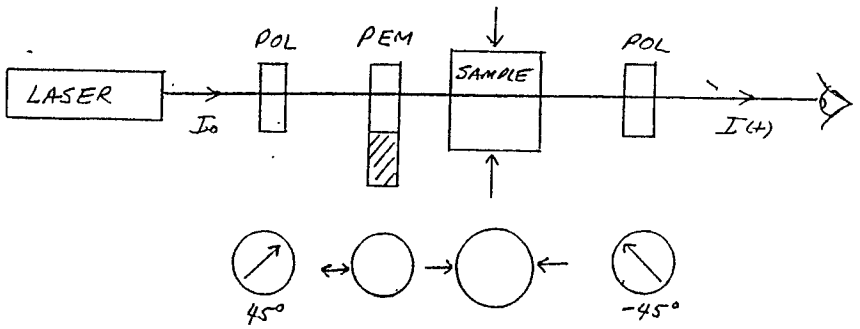

$$I(t) = \frac{I_0}{2}\left[1 - \cos\left(B + A_0 \cos(2\pi f)\right)\right]$$

I_0 = intensity of laser
A_0 = PEM retardation amplitude in radians
f = frequency of PEM (typically ~ 50 kHz)
B = net retardation of the sample

Thursday PM — Status of Present Detectors II
January 30 — Chair: R. Flaminio

4:30	M. Barton (ICRR-Tokyo)	A 2D X-Pendulum Vibration Isolation System
4:55	Discussion	
5:05	G. Mathews (Notre Dame)	GR Numerical Results Relevant to Gravity Wave Detectors
5:30	Discussion	

Thursday Evening: Public Lecture, Wheeler Opera House
Chair: S. Meshkov

8:00	G. Sanders (Caltech)	Listening to Einstein's Universe

Aspen Winter Conference

January 1997

A 2D X-Pendulum Vibration Isolation System

Mark A. Barton[A], Takashi Uchiyama[A],
Kazuaki Kuroda[A] and Masa-Kazu Fujimoto[B]

A: Institute for Cosmic Ray Research, University of Tokyo,
3-2-1 Midori-cho, Tanashi-shi, Tokyo 188 JAPAN
mbarton@icrr.u-tokyo.ac.jp
uchiyama@icrr.u-tokyo.ac.jp
kuroda@icrr.u-tokyo.ac.jp

B: National Astronomical Observatory,
Mitaka-shi, Tokyo 181 JAPAN,
fujimoto@gravity.mtk.nao.ac.jp

TAMA300
(多摩300)

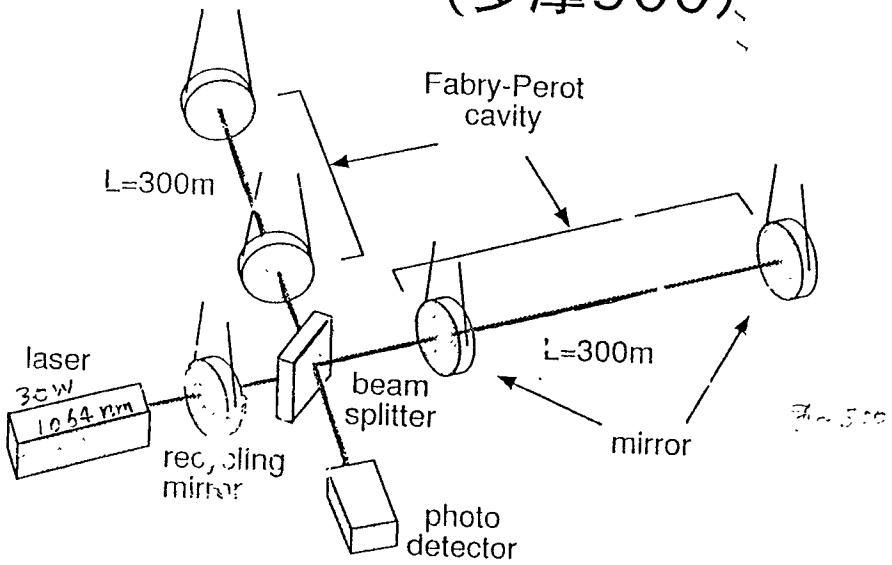

purpose:

1) to establish techniques necessary for future km-class detectors

2) to operate the detector to catch possible gravitational wave events in the nearby galaxies such as Andromeda

phase I (1998) $h_{rms}=3\times10^{-20}$
phase II (1999) $h_{rms}=3\times10^{-21}$
($f\sim300$Hz, $\Delta f\sim300$Hz)

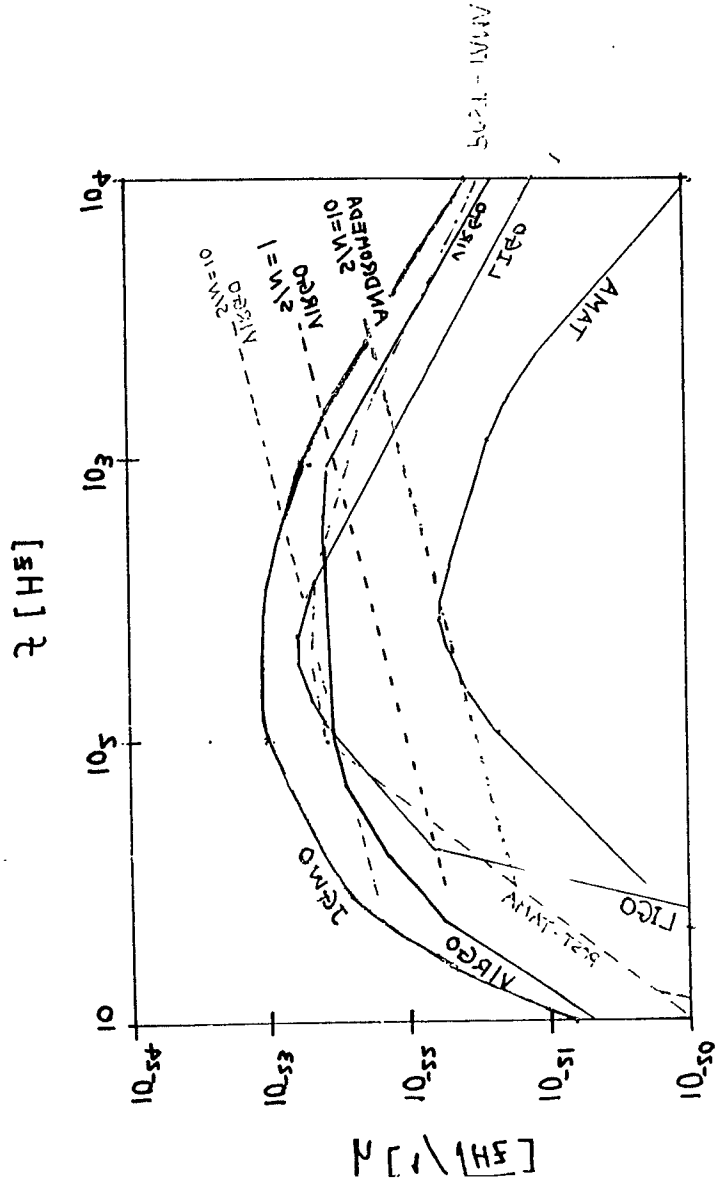

300-m laser interferometer fundamental parameters

target sensitivity

$h=3\times10^{-21}$
@300Hz

arm-length

300m

detector type

recombined Fabry-Perot
type with power recycling

cavity finesse

520

laser

LD pumped Nd:YAG
effective power 30W
wavelength 1064nm

vacuum

10^{-6}Pa

Laser interferometer GW detectors

country	project	base-line
USA	LIGO	4km(×2)
Italy France	VIRGO	3km
Germany UK	GEO	600m
Japan	TAMA	300m

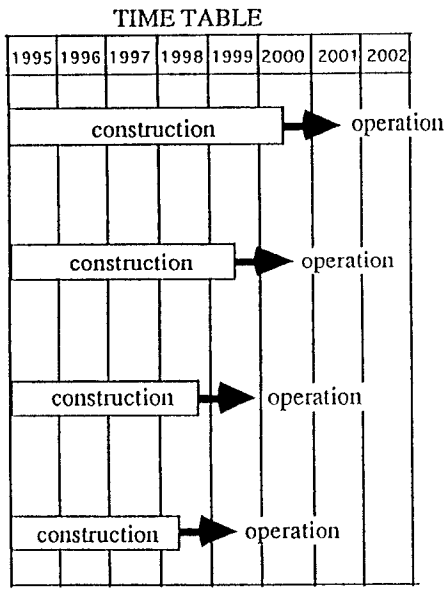

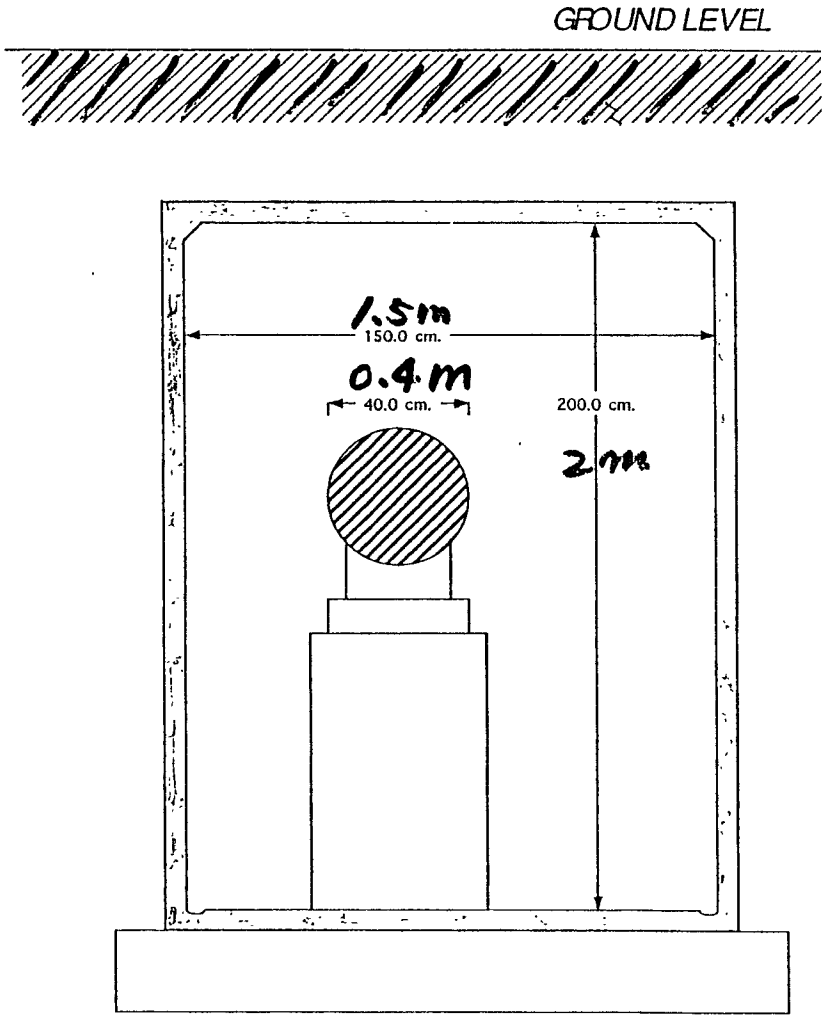

TAMA Progress

- Building finished (March 96)
- Mode cleaner tanks installed and vacuum tested
- Stack (and bellows) tested in vacuum
- Mode cleaner installed (but no data taken yet)
- Double pendulum design near final - being drawn by Nikon.
- 10 W Nd YAG Laser delivered. Slightly fiddly - only Sony people can adjust to 10W routinely (yet)
- Laser amplitude stabilization being worked on (no freq. stab yet)
- 22 m prototype exceeds target - will be reconfigured for recycling from March 97

Basic 1D X-Pendulum

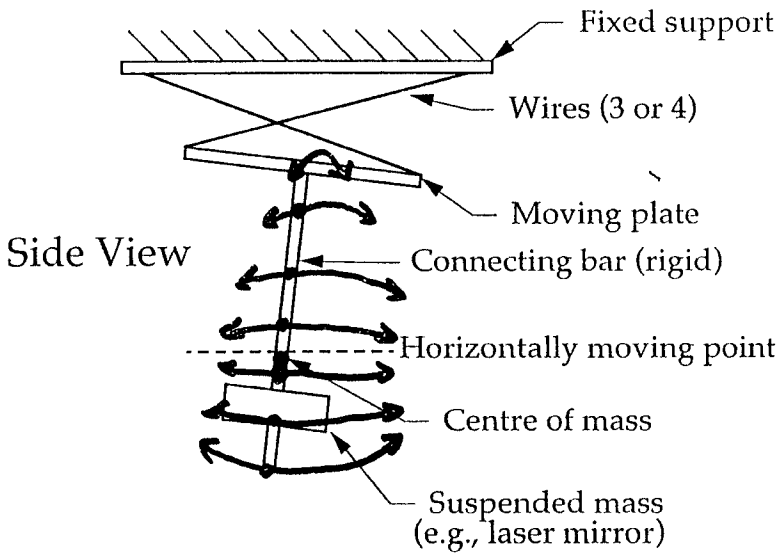

Advantages

- Low frequency
- Small size, especially vertically
- Good stability

Disadvantages

- Rotation of suspended mass
- Poor high-frequency performance
- Mass position is critical

Advanced 1D X-Pendulum

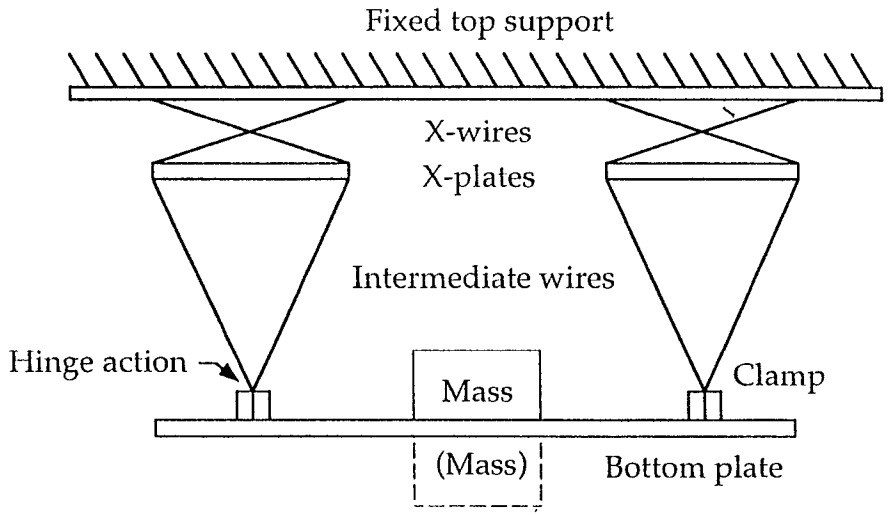

Use of wires

- saves weight
- decouples rotation of X-plate

Advantages

- Good high frequency performance
- Non-rotating lower table
- Mass position is not important

Centre of Percussion Tuning

The transfer function will not fall indefinitely as $1/f^2$ unless tuning is done:

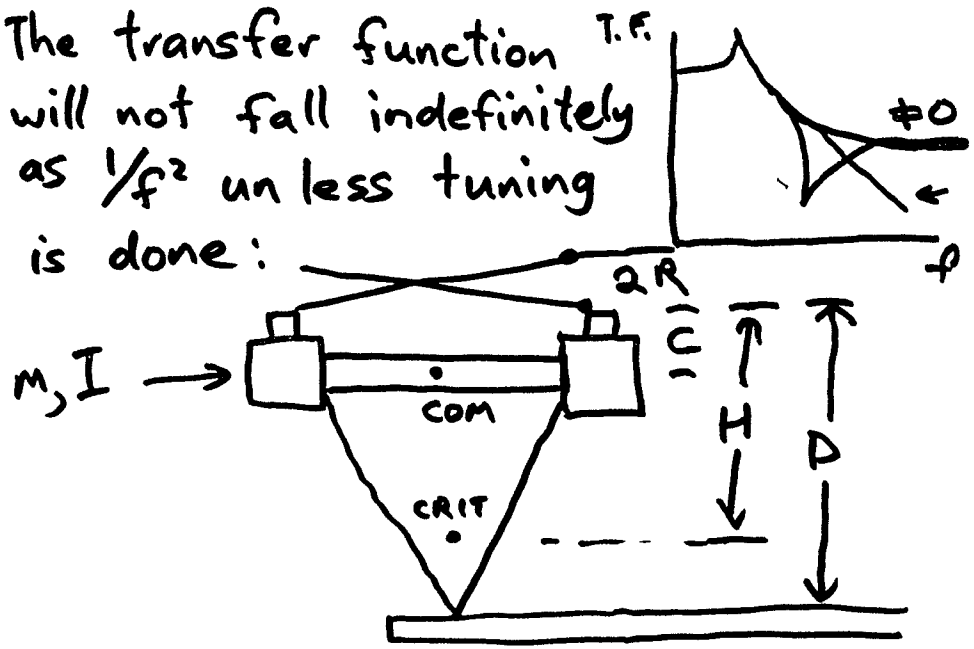

Optimization Condition

$$I = m(D-C)(C+R)$$

Note: independent of M

Typically requires more mass at the edges than for a uniform

Results

No Spacers

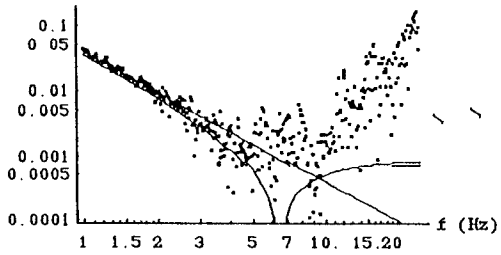

Optimum Spacers

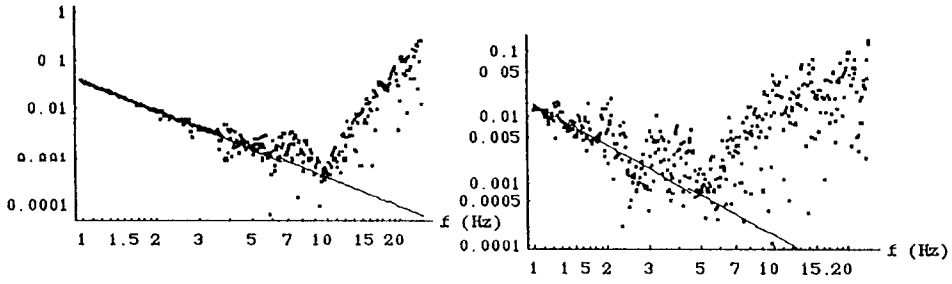

Long Spacers

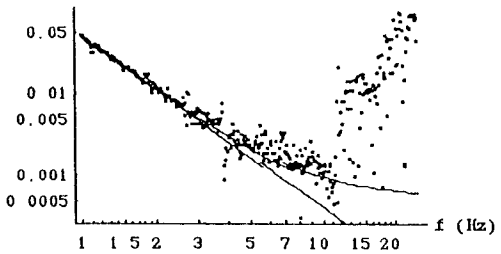

Inverted X-Pendulum

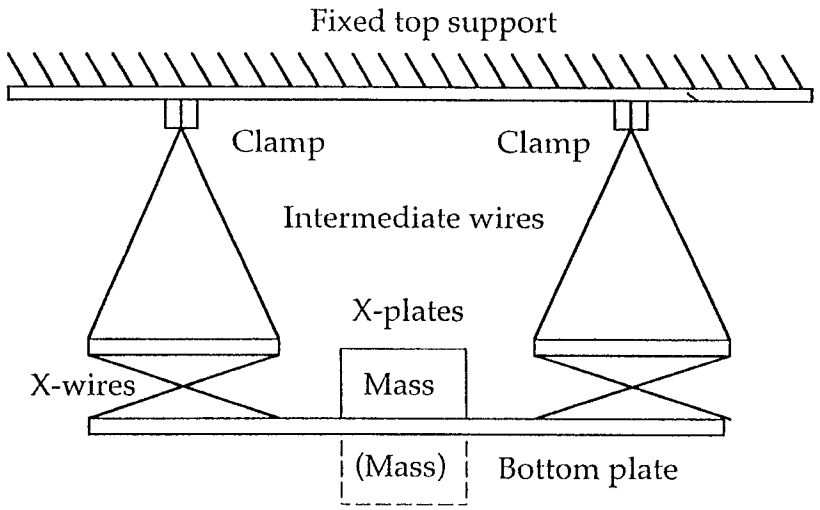

- Neither half is stable alone, due to the lack of a horizontal reference.
- Each half supplies the horizontal reference for the other.
- No particular advantages used alone, but allows a very simple 2D version.

2D X-Pendulum Mechanism

One of four identical corner mechanisms:

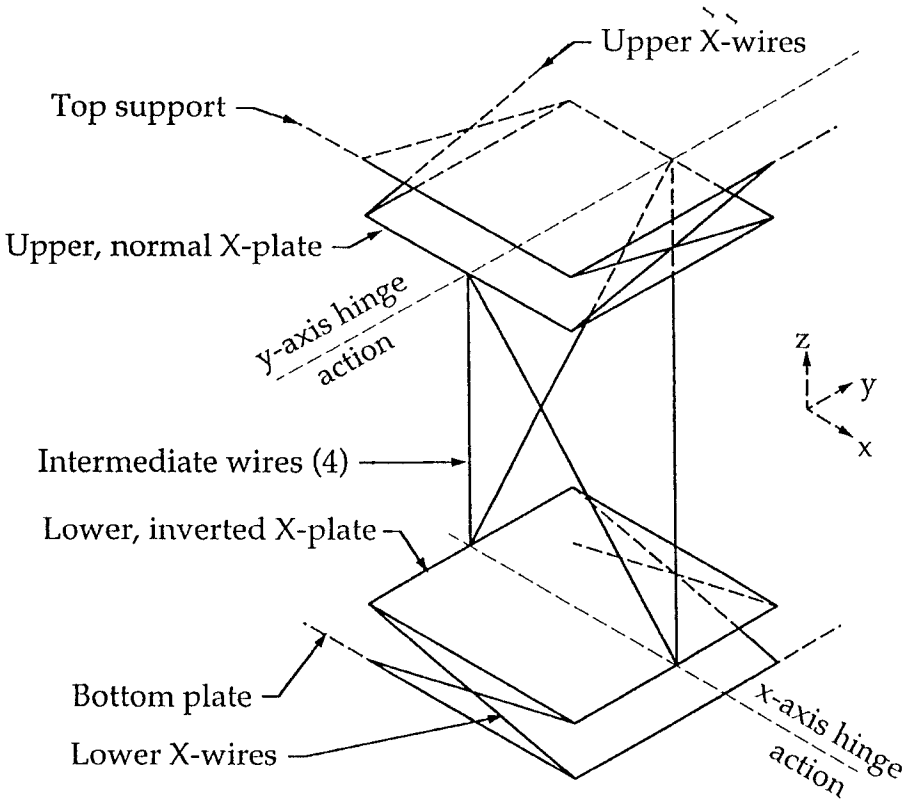

- Special arrangement of intermediate wires combines normal and inverted X-mechanisms at 90°.

2D X-Pendulum Side Views

Side View

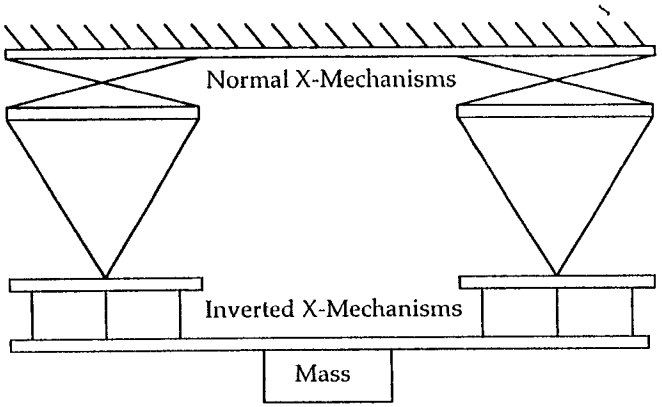

End View

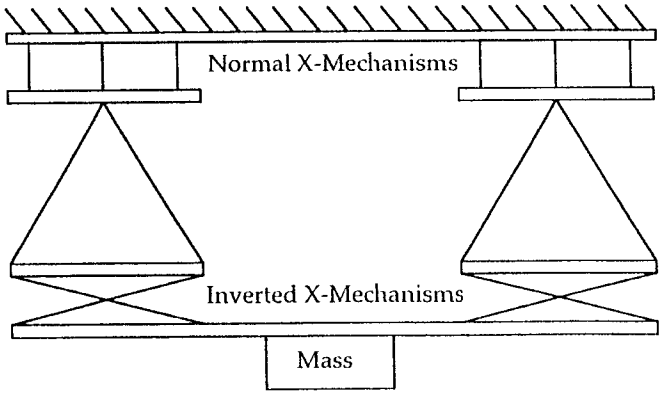

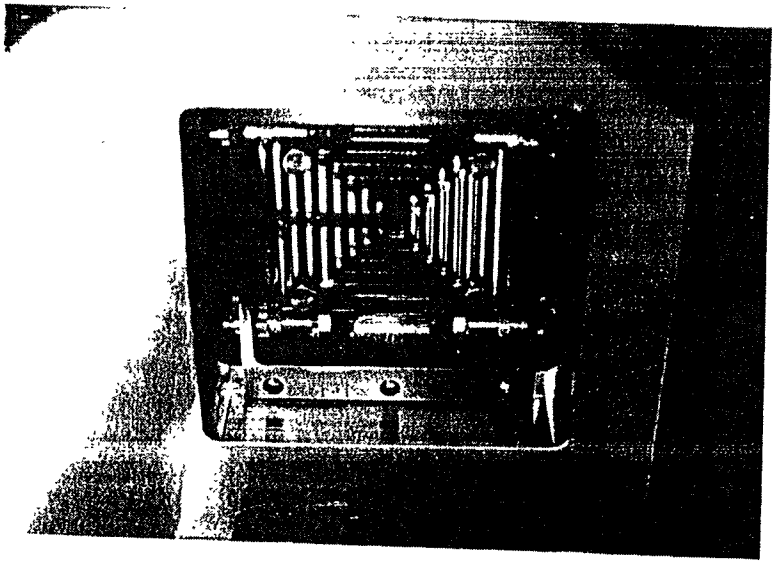

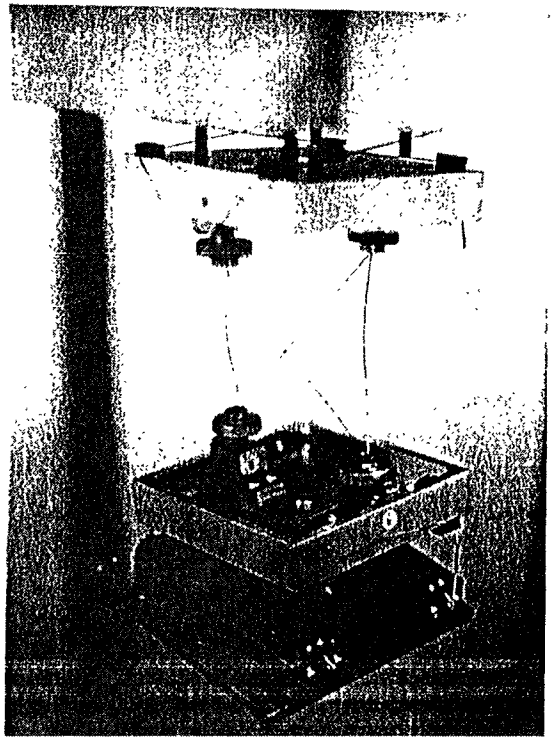

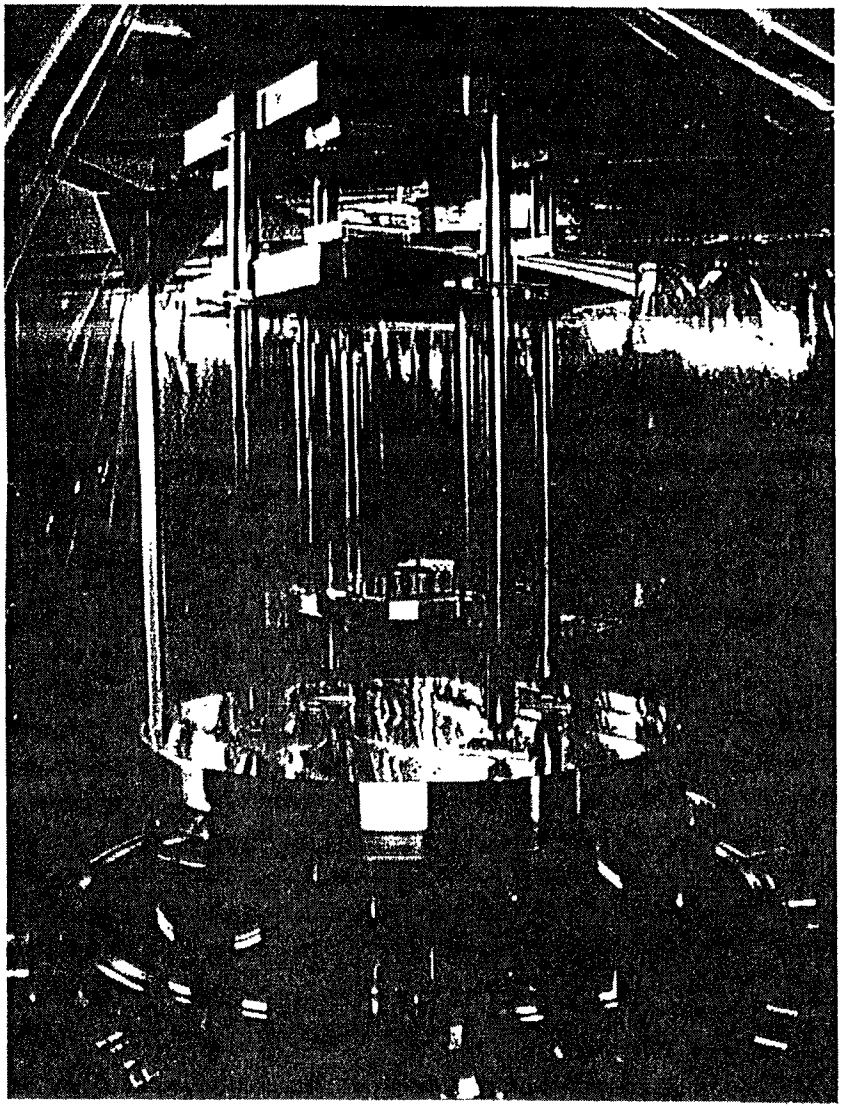

X-mechanism Features

- High quality clamps for good Q factor

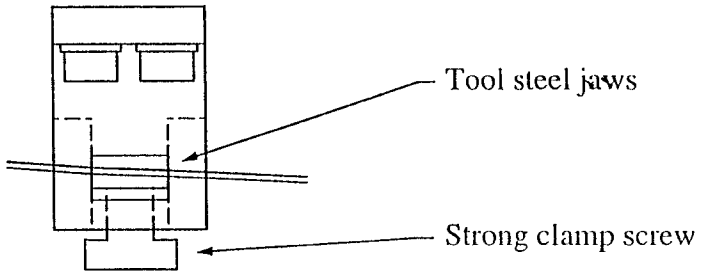

- Fine adjustment by bodily motion of X-wire clamps using double-screw actuated lever

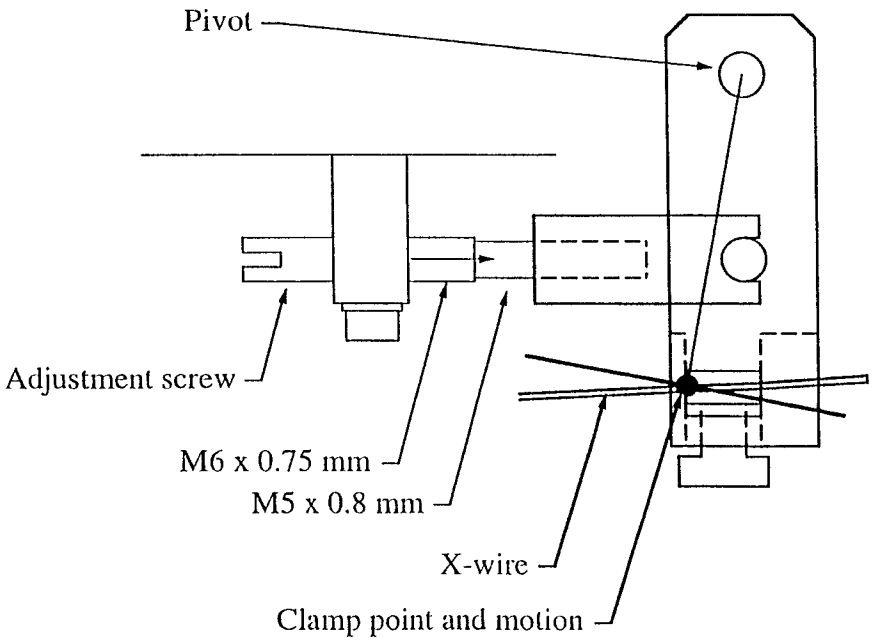

Complete Design

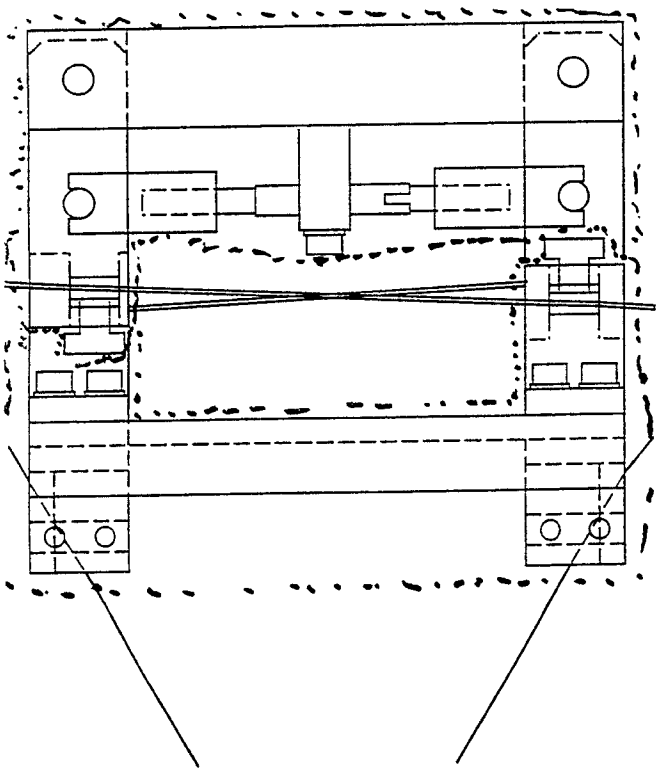

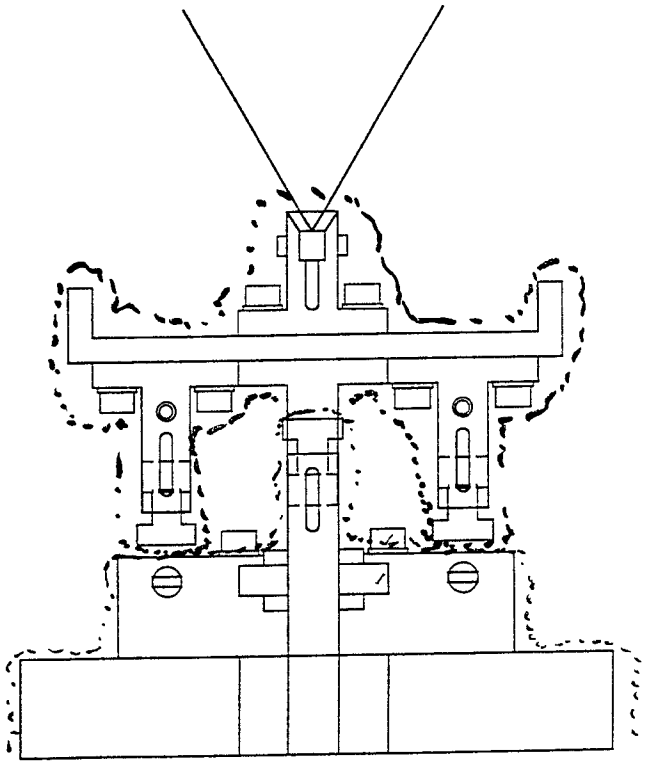

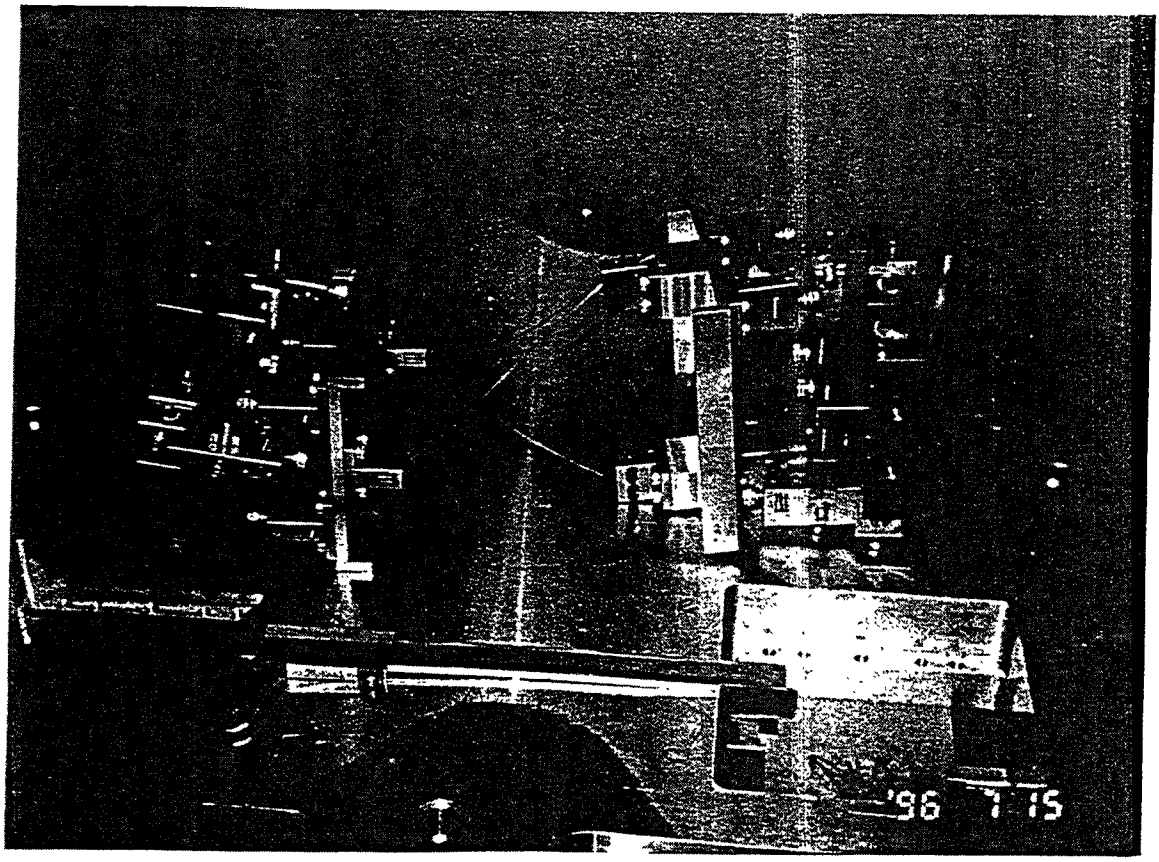

Transfer Function Measurements

- x->x, z->z and z->x successfully measured
- x->z contaminated by z motion of vibration table - data useless
- Large displacement far from the centre of mass, as in Mr Uchiyama's experiment
- Much smaller displacement near centre of mass of load table.
- Performance is not especially good since the second prototype was not optimised for good high frequency performance
- Required improvements are straightforward.

Transfer functions: z->z and z->x
PZT sensors on "kotatsu"

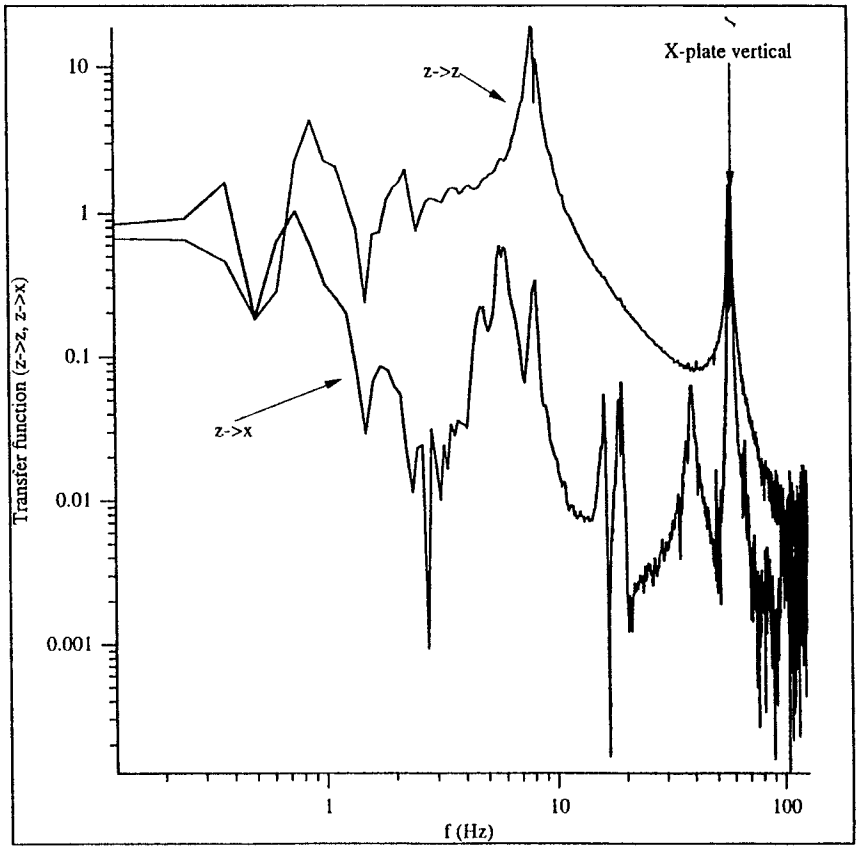

X-Pendulum Final Design (iii)

• Support table should *probably* be much more rigid horizontally. This is still to be determined.

• Design should allow for the possibility of adding PZT actuators for active vertical isolation later if necessary.

• Design should incorporate an automatic levelling mechanism to remove long term tilt due to vibration isolation stack.

• Normal mode analysis program has been optimized for speed and some minor errors have been eliminated.

• Agreement with measured mode frequencies is improved but a slight discrepancy in some of the tipping modes needs to be hunted down.

• Requirements for new design are nearly finalised.

• Drawing up is to be done by Nikon Technologies, who will also make the double pendulum.

Significance of Normal Modes

• The x and y pendulum modes are the useful modes and involve mainly gravitational restoring force.

• The moving parts are held together by relatively thin wires.

• Thus there will be many low to medium frequency elastic modes as well.

• The elastic modes may amplify seismic and thermal noise by resonance.

• Thus we would like to know the mode spectrum

Number of Normal Modes

• The load table and the 8 X-plates can move in 6 degrees of freedom (x, y, z, roll, pitch, yaw).

-> 54 degrees of freedom

• The support table is very stiff vertically due to the legs, but can move horizontally (x, y, yaw).

-> 3 degrees of freedom

• Ignore internal degrees of freedom of the parts and violin modes of the wires which are all very high frequency (>1000 Hz).

-> 57 degrees of freedom

Summary of Normal Modes

Group No.	Count of Modes	Calc. Freq. (Hz)	Meas. Freq. (Hz)	Description
1	8	557	490(?)	X-plate tipping
2	8	362	375(?)	X-plate tipping
3	4	339	344(?)	X-plate tipping
4	4	233	239(?)	X-plate tipping
5	4	155	180(?)	X-plate tipping
6	2	59	57	X-plate vertical
7	4	32	36	X-plate tipping
8	2	17.5	21	X-plate tipping
9	1	17.5	17	support plate yaw
10	7	9-12	?	X-plate horizontal
11	1	10	7.5	load plate vertical
12	2	9.0	5.6	load plate tipping
13	1	8.6	8.0	support plate yaw
14	2	5.6	8.0, 8.25	support plate horizontal
15	1	2.7	2.7	load plate yaw
16	2	adjust-able	adjust-able	support plate horizontal

17

(2) Working modes

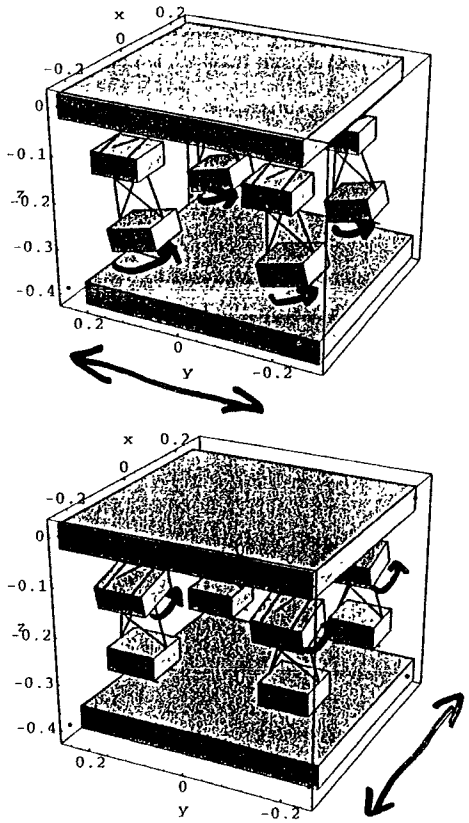

Frequency is adjustable

$f < 0.2\,Hz$

$T > 5s$

$Q \approx 150 @ 0.2\,Hz$

16: (1: 55) Yawing mode of the load plate

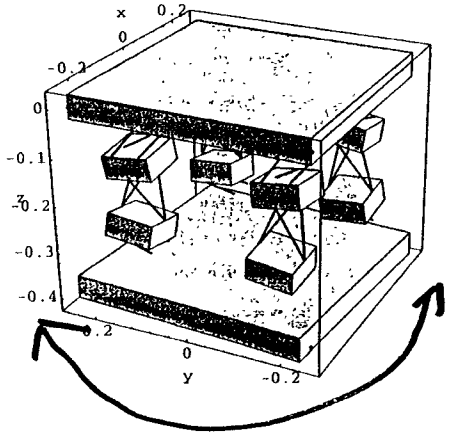

Theory: 2.7 Hz

Measured: 2.7 Hz

Q ≈ 1000

13: (2, 50-51) Tipping modes of the load plate

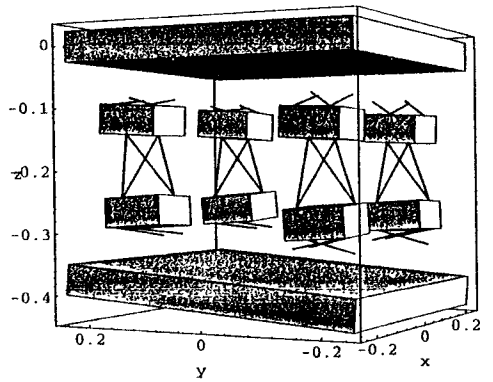

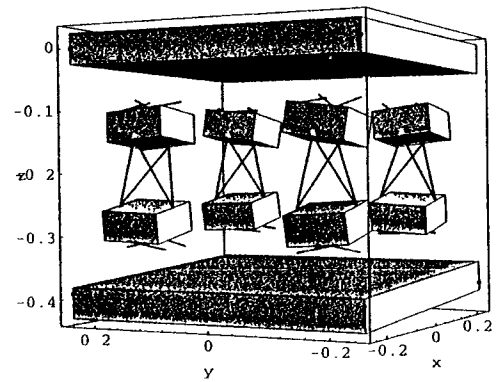

Theory: 9 Hz

Measured: 5.6 Hz

X-Pendulum Final Design (i)

• X-wires and intermediate wires should attach to the X-plates at the same vertical level.

• X-plates should be as light as possible.

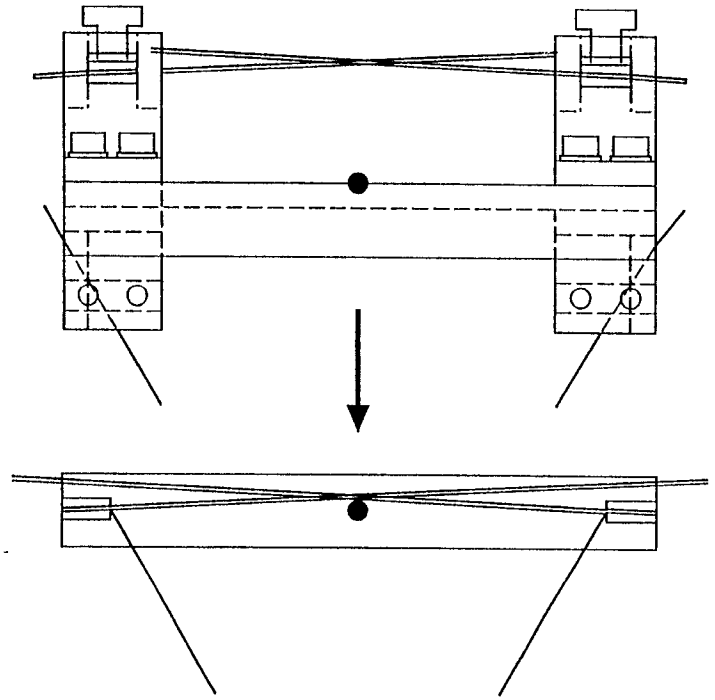

• *Probably* the centre of mass should also be at the same height but this is still to be determined. There is a trade-off with optimising the basic X-pendulum operation.

15: (2, 53-54) Horizontal modes of the support plate.

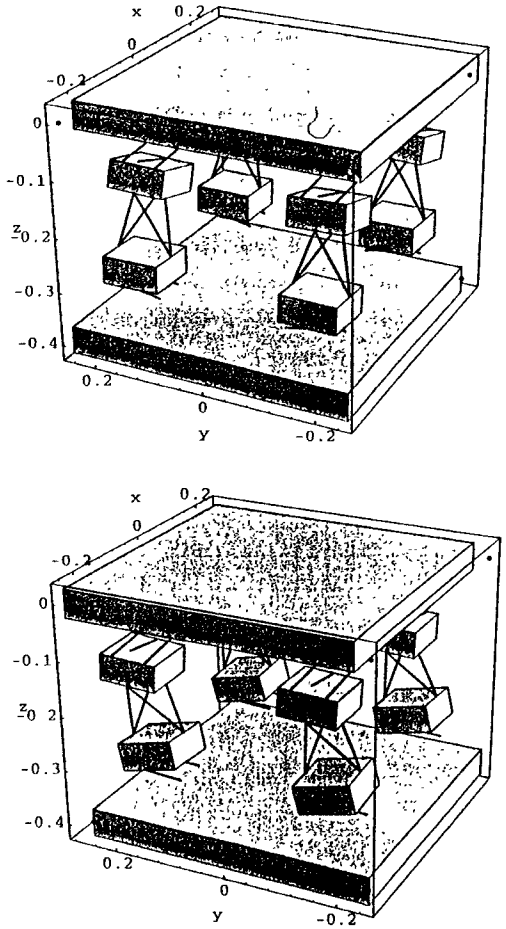

Theory: 5.6 Hz

Measured: 8.0, 8.25 Hz

9: (2, 37-40) More non-descript tipping modes involving all the X-plates.

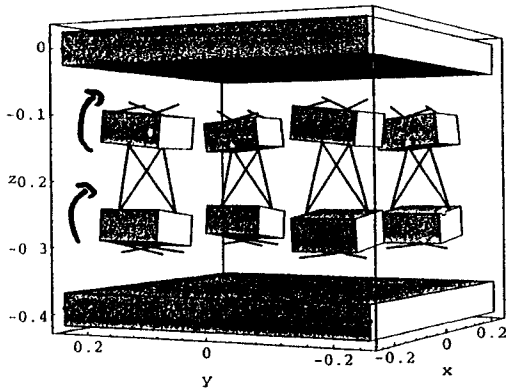

Theory: 17.5 Hz

Measured: 20.75 Hz

6: (2, 29-30) Vertical motions of the X-plates with top/bottom pairs in phase

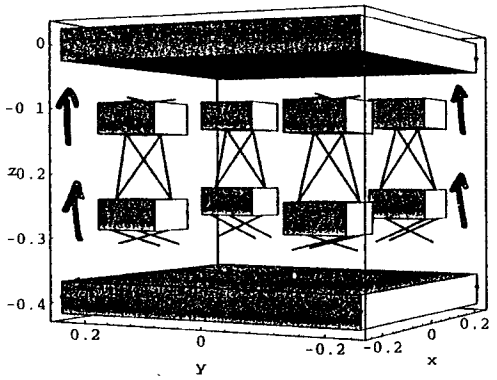

Theory: 59 Hz

Measured: 57 Hz

Transfer function: x->x at different vertical positions

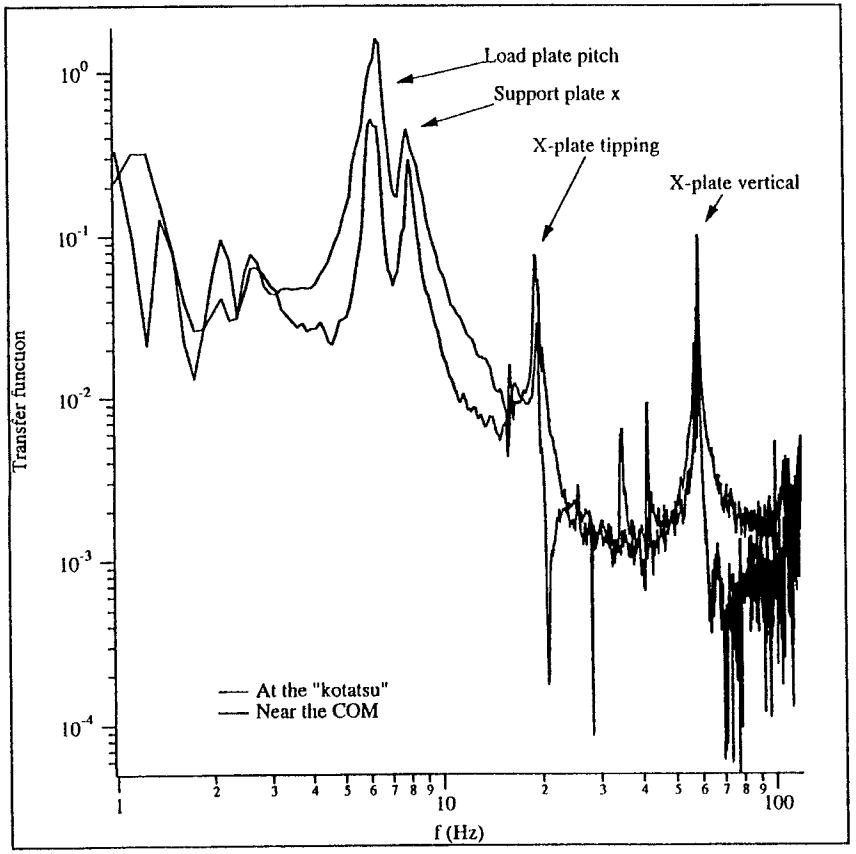

X-Pendulum Final Design (ii)

• There should be 4 X-wires (for greater rigidity) but only 2 adjustment mechanisms (for lower cost).

• The X-wires should attach to the load plate at the same vertical level as the centre of mass.

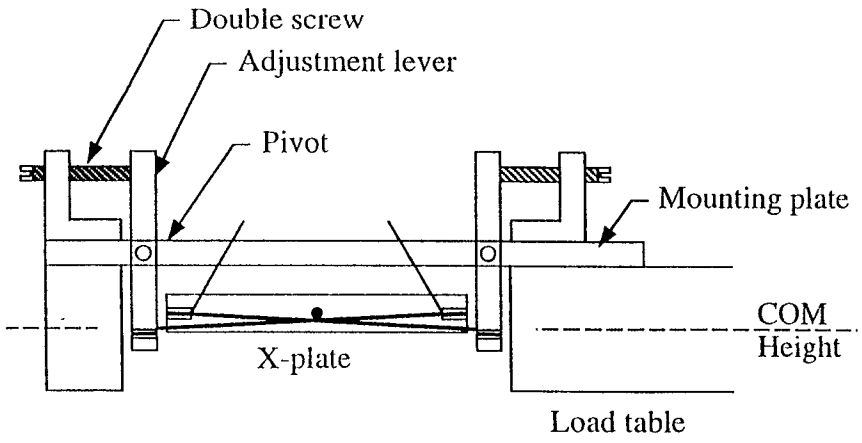

• The suspension point of the double pendulum wires should also be at the COM height

Anticipated Improvements from Optimization of Dynamics

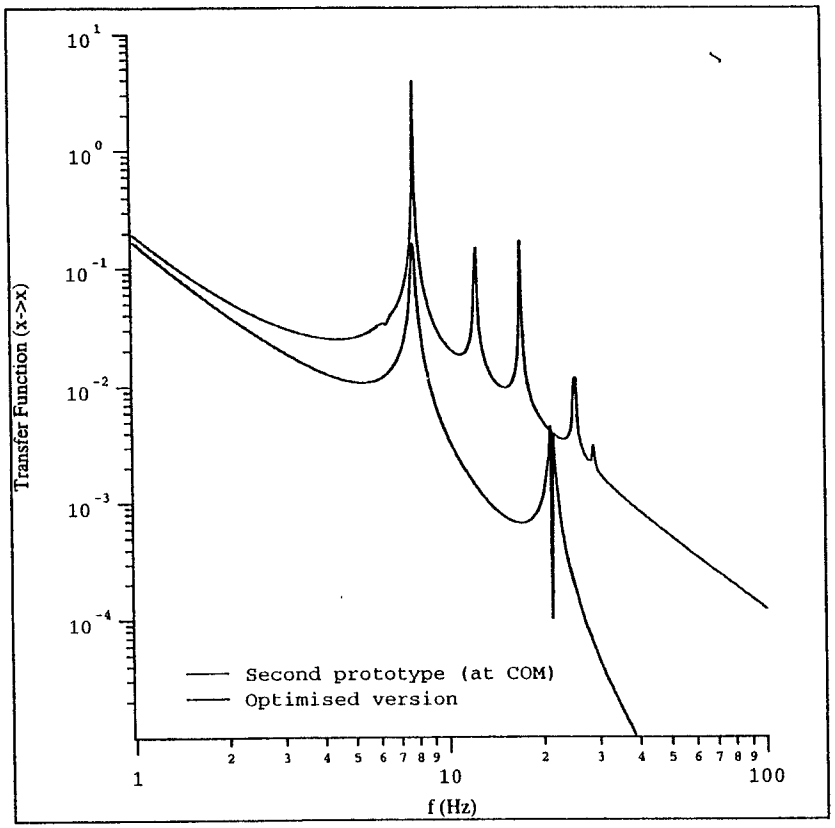

The upper curve is based on a normal mode analysis of the second prototype.

The lower curve is for a system with identical masses and moments of inertia, but with X-plate and load table clamps aligned vertically with the respective centres of mass.

General Relativistic Numerical Hydrodynamics for Neutron Star Binaries

Results Relevant to Gravity Wave Detectors

G. J. Mathews
P. Marronetti - University of Notre Dame

J. R. Wilson - Lawrence Livermore National Laboratory

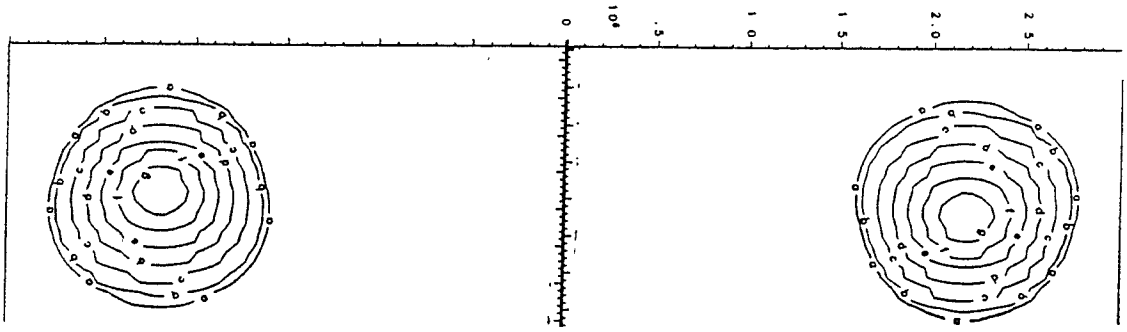

Physical Processes in Close Neutron Star Binaries

In LIGO Window

- Orbit Instability
- Collapse Instability
- Compression/Heating/Neutrino Emission
- Internal Stellar Fluid Circulation

Maxwell's Eq's

$$\dot{E} = \nabla \times H - J$$

$$\dot{H} = \nabla \times E$$

$$\nabla \cdot E = \rho$$

$$\nabla \cdot H = 0$$

General Relativity

$$\dot{\gamma}_{ij} = -2\alpha K_{ij} + D_a \beta_b + D_b \beta_a \quad \text{(metric)}$$

$$\dot{K}^i_j = -D_i D^i \alpha + \alpha S^i_j + \alpha R^i_j - \frac{1}{2}\alpha \gamma^i_j (S - \rho) + \beta_k K^i_{j,k}$$

(Extrinsic Curvature)

$$R = 16\pi\rho + K^{ij} K_{ij} - K^2$$

Hamiltonian Constraint

$$D_i \left(K^{ij} - \gamma^{ij} K \right) = 8\pi S^j$$

Momentum Constraint

Relativistic Hydrodynamics

$$T^{\mu\nu} = (\rho + \rho\varepsilon + P) U^\mu U^\nu + P g^{\mu\nu}$$

$$T^{\mu\nu}{}_{;\nu} = 0 = \frac{1}{\sqrt{-g}} \frac{\partial}{\partial x^\nu} \left(\sqrt{-g}\, T^{\mu\nu} \right) + \Gamma^\mu_{\nu\lambda} T^{\nu\lambda}$$

Momentum Conservation

$$\dot{S}_i + S_i \frac{\dot{\gamma}}{\gamma} + \frac{1}{\gamma} \frac{\partial}{\partial x^i} (S_i V^i \gamma) + \alpha \frac{\partial P}{\partial x^i} - \text{Resist.}$$

adiabatic

$$+ (D + \Gamma\varepsilon) \left(W \frac{\partial \alpha}{\partial x^i} + \frac{U_k U_l}{W} \frac{\partial \gamma^{kl}}{\partial x^i} - U_i \frac{\partial B^i}{\partial x^i} \right) = 0$$

acceleration

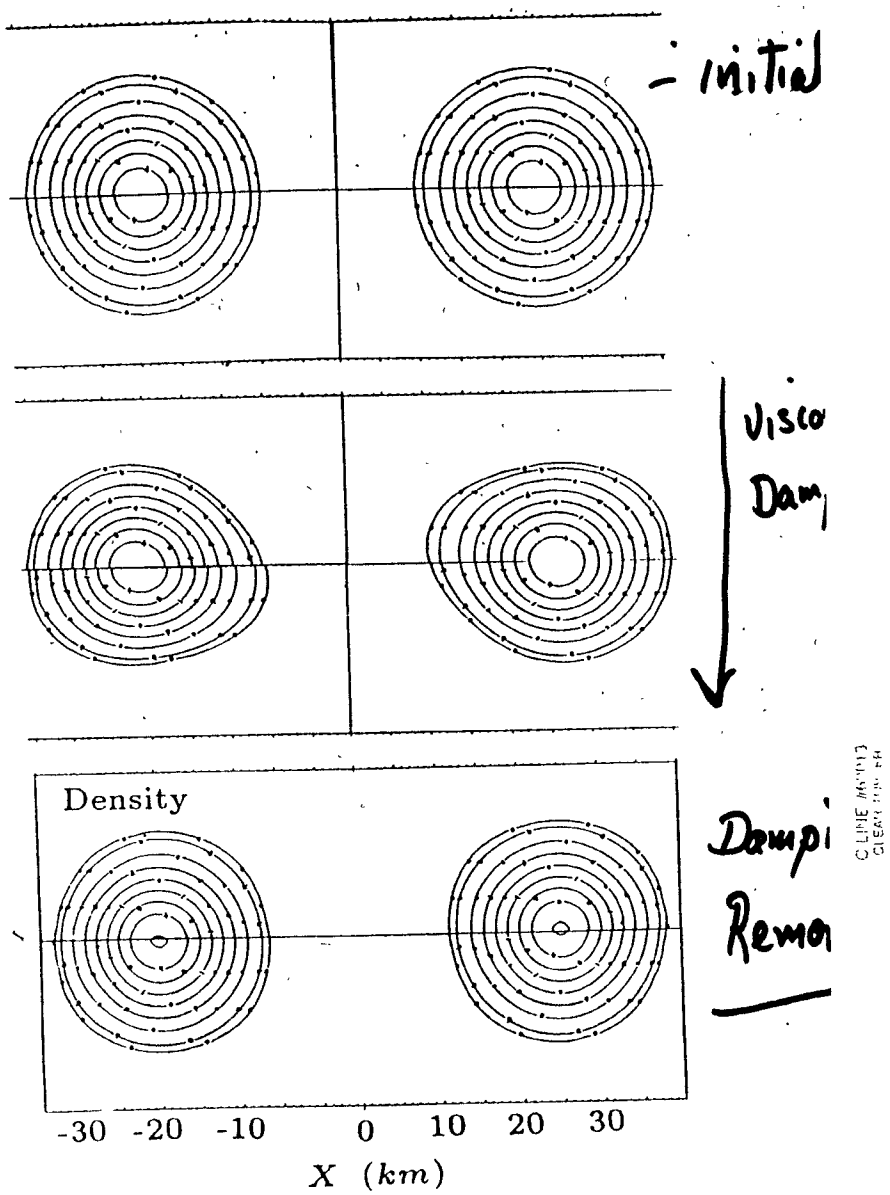

- initial

Visco
Dam

Dampi
Remo

Initial Conditions

2 equal mass stars

$\sim 10^6$ zone resolution

no radiation

⇒ look for stable orbit

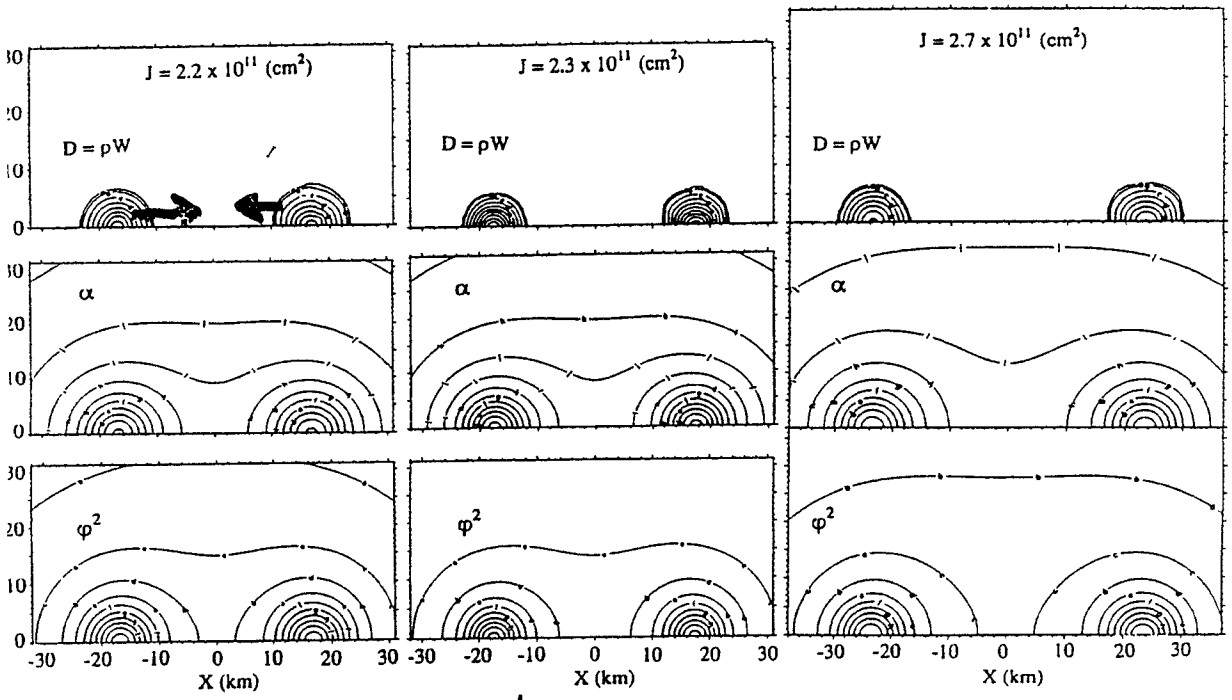

Unstable Orbit

Stable Orbit

Stable Orbit

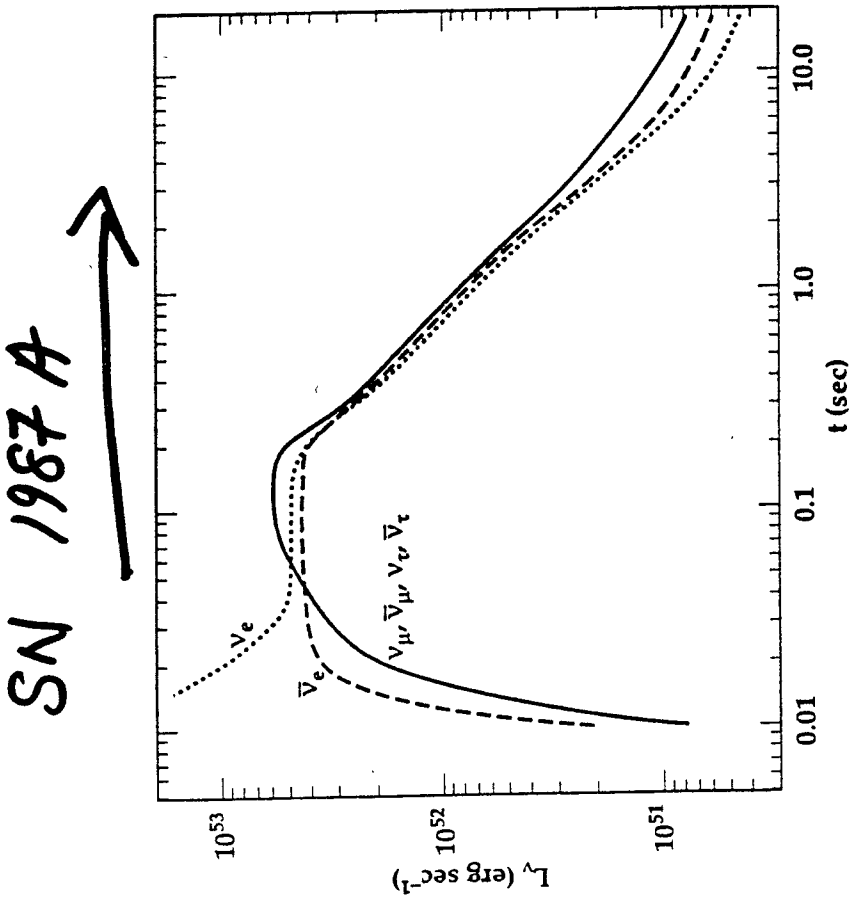

Processes which may occur in the LIGO Window

Conclusions/Implications

- Orbit instability may occur at low frequency
- Collapse instability may occur ~ sec to hrs before merger
- Compression heating may produce observable signatures
  - Gravity Wave
  - Neutrino Burst
  - Baryon Wind
  - Gamma-Ray Burst?
  - Radio Burst?
- Power loss from neutrinos and (electromagnetic?) radiation may dominate late evolution

---

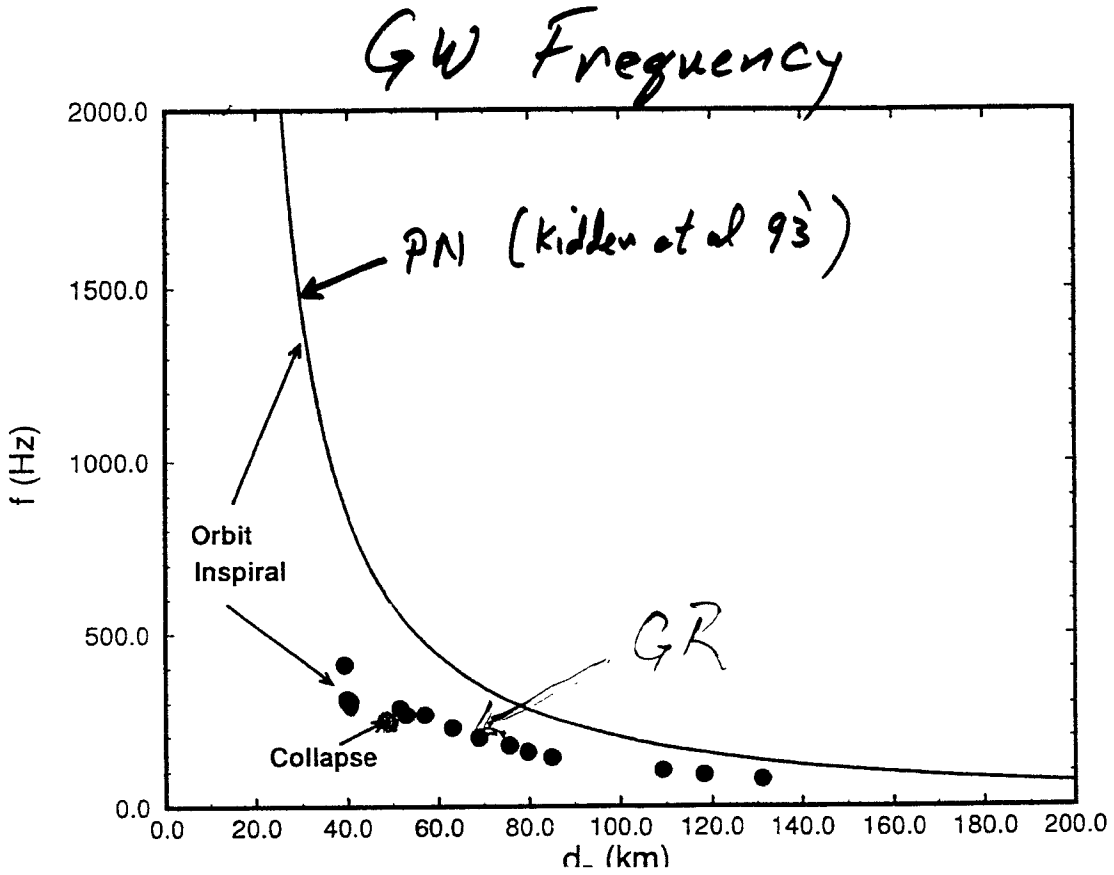

Why is the Frequency Lower?

Circular Orbit Condition

(Post)$^{5/2}$- Newtonian (Kidder at al. 1993)

$$\omega^2 = \frac{M}{r^3} A_0$$

$$A_0 = 1 - \frac{3}{2}\frac{m}{d_h}\left[3 - \frac{77}{8}\frac{m}{d_h} + (\omega_0 d_h)^2\right] + \frac{9}{4}(\omega_0 d_h)^2$$

Relativistic Hydrodynamics

$$W(D+\Gamma E)\frac{\partial \alpha}{\partial x^i} = S_j \frac{\partial \beta^j}{\partial x^i}$$

$\beta^y \approx \omega r$ and $S_y = (D+\Gamma E)U_y$, $\alpha \to 1 - M/r$ implies

$$W\frac{M}{r^2} = \omega U_y \quad , \quad U_y = \omega r \frac{\phi^4 W}{\alpha}$$

Hence,

$$\omega^2 = \frac{M}{r^3}\left(\frac{\alpha}{\phi^4}\right) \sim 1/4$$

Gravity Waves (Thorne 1980)

$$h^{TT}_{jk} = \sum_{l=2}^{\infty}\sum_{m=-l}^{l}\left[r^{-1}\,{}^{(1)}I^{lm}(t-r)T^{E2,lm}_{jk} + r^{-1}\,{}^{(1)}S^{lm}(t-r)T^{B2,lm}_{jk}\right].$$

Sum to $l=4$

$$\frac{dE}{dt} = \frac{1}{32\pi}\sum_{l=2}^{\infty}\sum_{m=-l}^{l}\left\langle \left|{}^{(l+1)}I^{lm}\right|^2 + \left|{}^{(l+1)}S^{lm}\right|^2\right\rangle.$$

Slow motion ~ 10% Correction

$$I^{lm} = \frac{16\pi}{(2l+1)!!}\left(\frac{(l+1)(l+2)}{2(l-1)}\right)^{1/2}\int \tau_{00}x^l Y^{lm*}_l d^3x$$

$$+\sum_{k=0}^{\infty}\frac{16\pi}{2^k k!(2l+2k+1)!!}(\theta_l)^{1/2}\int \tau_{Nl}r^{l+2k}\left[\frac{(2l+2k+1)}{2(k+1)}\frac{(l+1)(l+2)}{2(2l-1)(2l+1)}\right]^{1/2} T^{2,lm*}_{Nl}$$

$$+\left(\frac{3(l-1)(l+2)}{(2l-1)(2l+3)}\right)^{1/2} T^{2,lm*}_{Nl} + \frac{2k}{2l+2k+3}\left(\frac{l(l-1)}{2(2l+1)(2l+3)}\right)^{1/2} T^{2,lm*}_{Nl}\Big]d^3x,$$

$$c^{lm} = -32\pi\,/(l+2)(2l+1)\,\Big)^{1/2}\int \ldots \sim \ldots r^{l+1}, lm*_{-1} d^3x$$

$m = 1.45\ M_\odot$

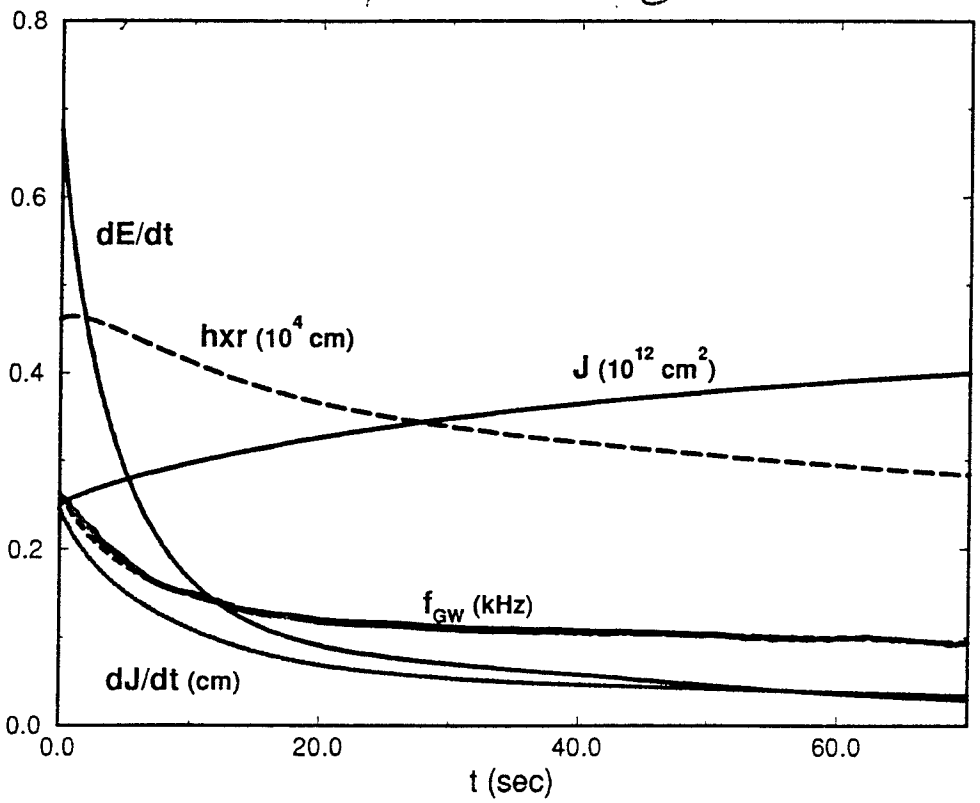

C-LINE #62013

$m = 1.45\ M_\odot$

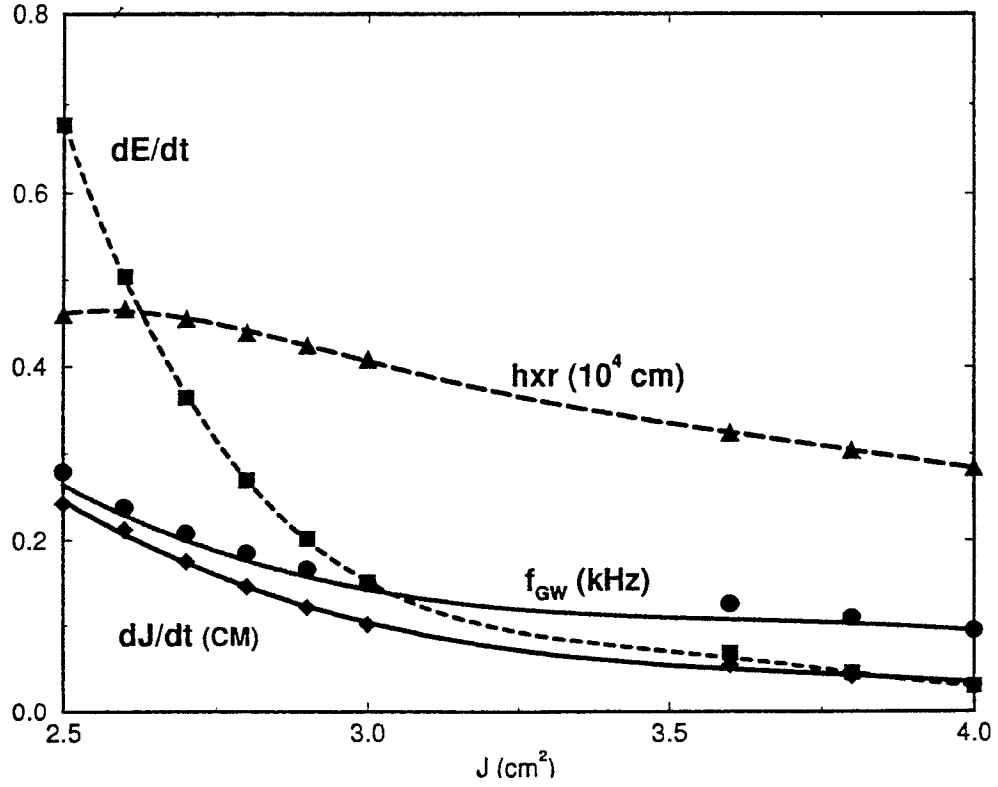

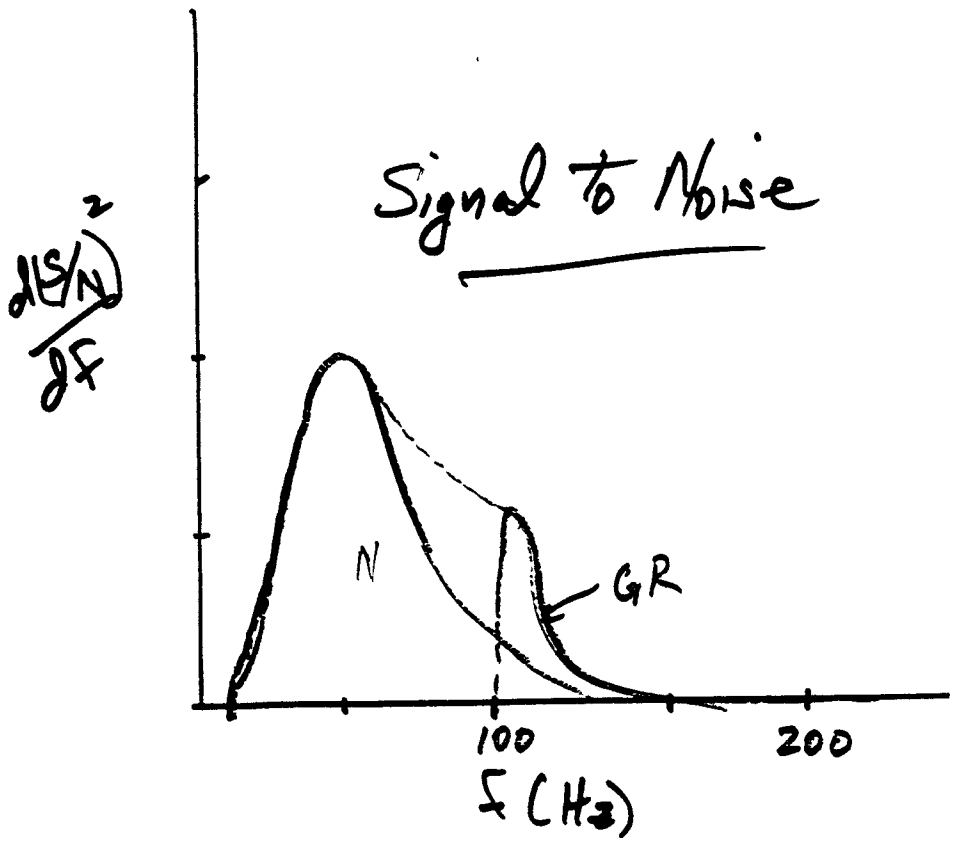

C-LINE #62013

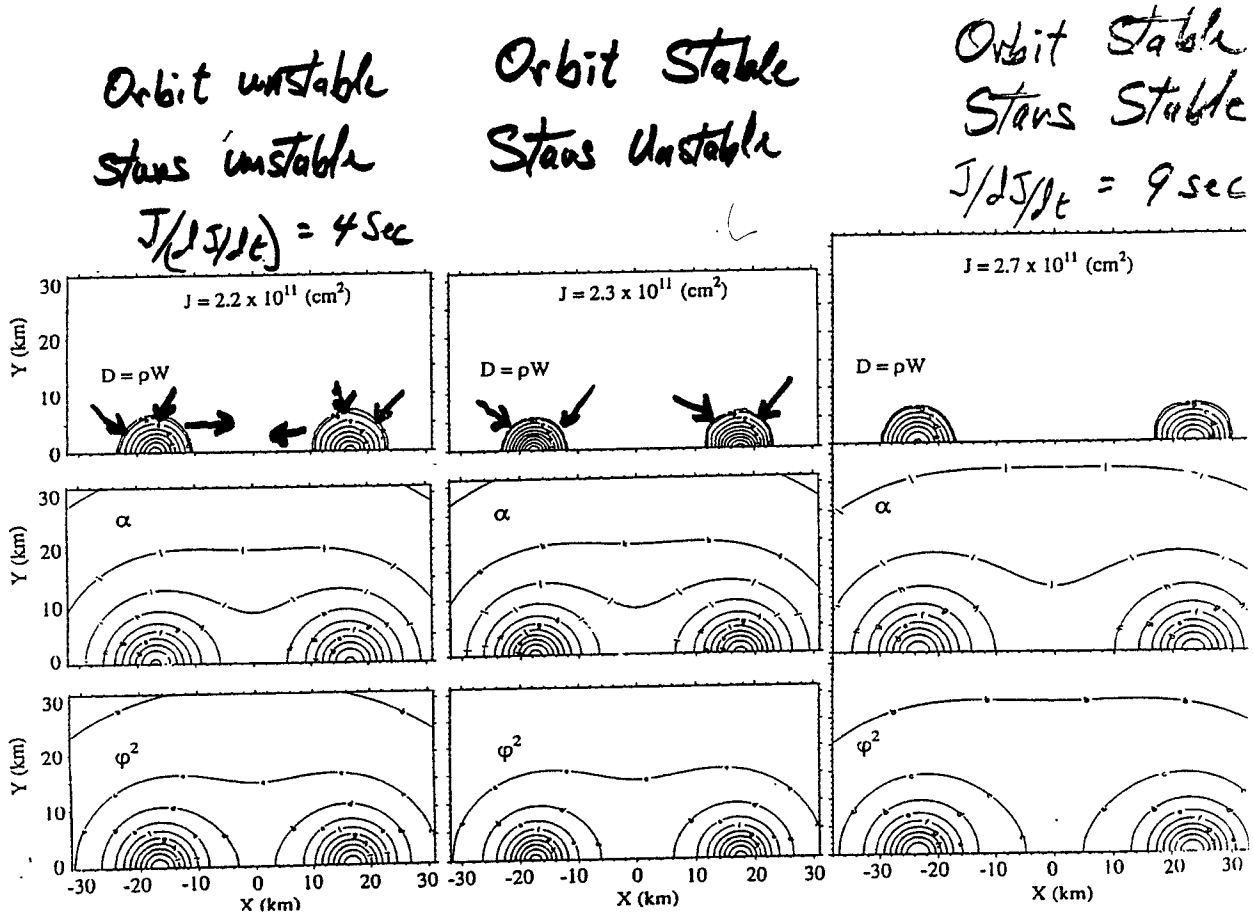

Why do the stars collapse?

Hydrostatic Equilibrium

Newtonian

$$\frac{dP}{dr} = -\rho\frac{GM_r}{r^2}$$

Momentum Equation

$$0 = \frac{\partial S_i}{\partial t} = -6S_i\frac{\partial \log\phi}{\partial t} - \frac{1}{\phi^6}\frac{\partial}{\partial x^j}(\phi^6 S_i V^j) - \alpha\frac{\partial P}{\partial x^i} + 2\alpha(D+\Gamma E)(W-\frac{1}{W})\frac{\partial \log\phi}{\partial x^i}$$

$$+S\frac{\partial \phi^j}{\partial x^i} - W(D+\Gamma E)\frac{\partial \alpha}{\partial x^i}$$

Isotropic Coordinates

$$\frac{\partial P}{\partial x^i} = -(\rho+\rho\epsilon\Gamma)\left(\frac{\partial \log\alpha}{\partial x^i} + \left[\frac{\partial \log\alpha}{\partial x^i} - 2\frac{\partial \log\phi}{\partial x^i}\right](W^2-1)\right)$$

$$(W^2-1) = \frac{\sum U_i^2}{\phi^4} \approx \frac{1}{(\alpha^2/\phi^2 R^2\phi^4) - 1)}$$

When does the collapse occur?

$$(W^2-1) = \frac{\sum U_i^2}{\phi^4} \propto \frac{m}{r}$$

Post Newtonian

$$(W^2-1) \approx \frac{m}{r} = \frac{(m\omega_0)^{3/2}}{(1-(64/5)m^{5/3}\omega_0^{8/3}t)^{1/4}} \approx \frac{(W^2-1)_0}{(1+kt)^{1/4}}$$

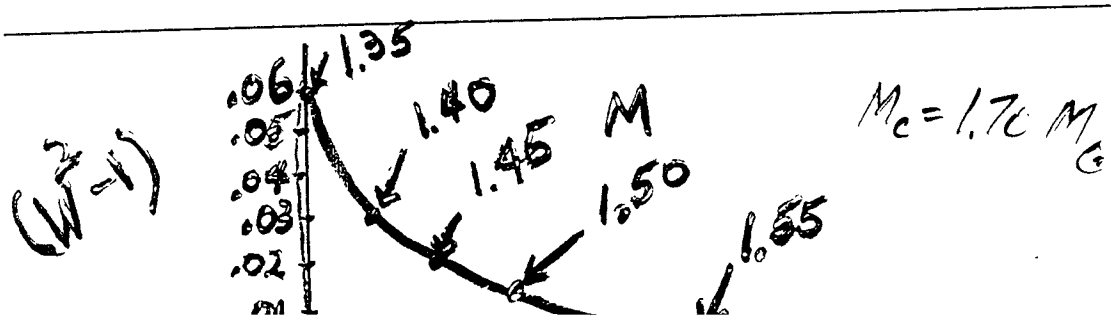

$M_c = 1.70\ M_\odot$

Can Newtonian Tidal Energy Stabilize the Stars?

Lai 9

$$\Delta E_{Tidal} \sim \lambda \frac{GM^2}{R}\left(\frac{R}{r}\right)^6$$

$$\Delta E_{GR} \simeq 2(W^2-1)\frac{GM^2}{R}$$

$$\Rightarrow \frac{\Delta E_{Tidal}}{\Delta E_{GR}} = \frac{\lambda}{2(W^2-1)}\left(\frac{R}{r}\right)^6 \approx 10^{-1}$$

$\frac{R}{r} \sim 0.2$, $W^2-1 \sim 0.05$, $\lambda \sim 0.1$

No! Can not stabilize

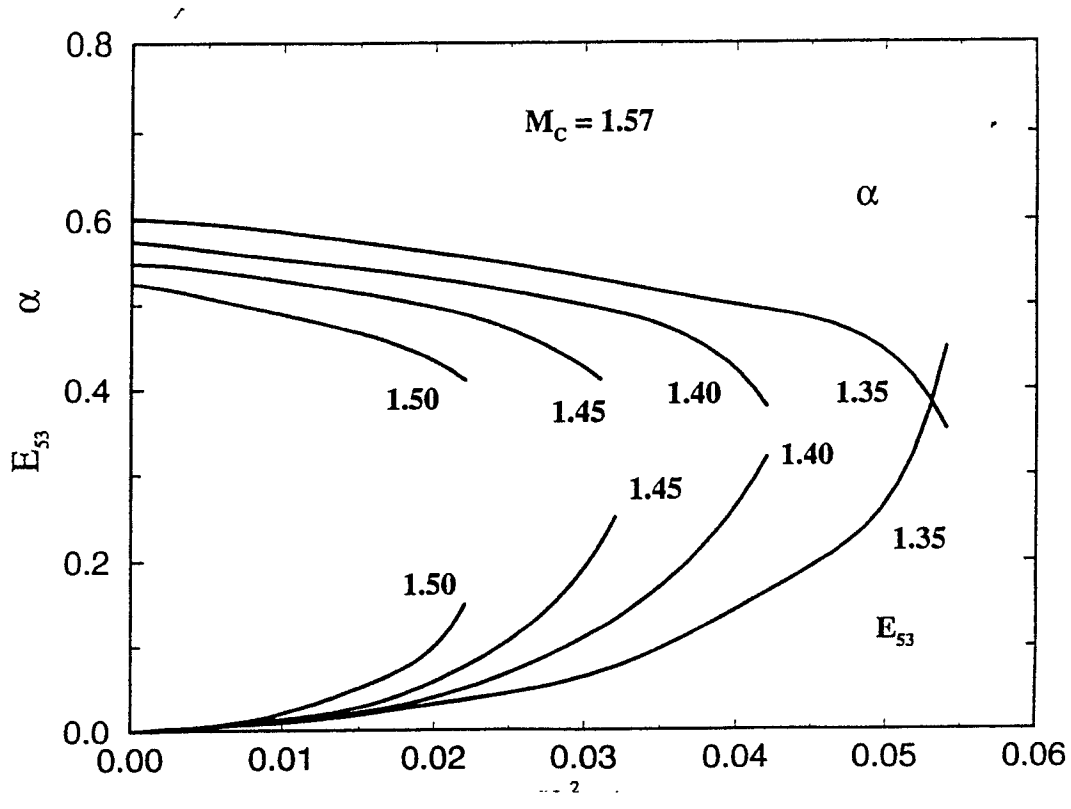

Compression Heating

$$\dot{E}_{th} = \dot{E}_{in} - L_\nu$$

Input thermal energy

$$E_{in} \propto (W_0^2 - 1)^2$$

$$\dot{E}_{in} = \frac{dE_{in}}{d(W_0^2 - 1)} \frac{d(W_0^2 - 1)}{dt}$$

Neutrino flux

$$F_\nu(r,T) \propto \left(\frac{r^2 T_0^2}{\rho \kappa_0 T^2}\right) \frac{d(T^4)}{dr} \propto \frac{r^2}{\rho} T \frac{dT}{dr}$$

Assume proportional to interior mass

$$F_\nu(r) \propto 4\pi \int_0^r \rho r'^2 dr$$

$$T(r) = A\left[\left(\frac{\int_0^r m(r')dr'}{r'^2}\right) - \left(\frac{\int_0^R m(r')dr'}{r'^2}\right)\right]^{1/2}$$

$$\int_0^R \epsilon(T) 4\pi r^2 \rho dr = E_{th}$$

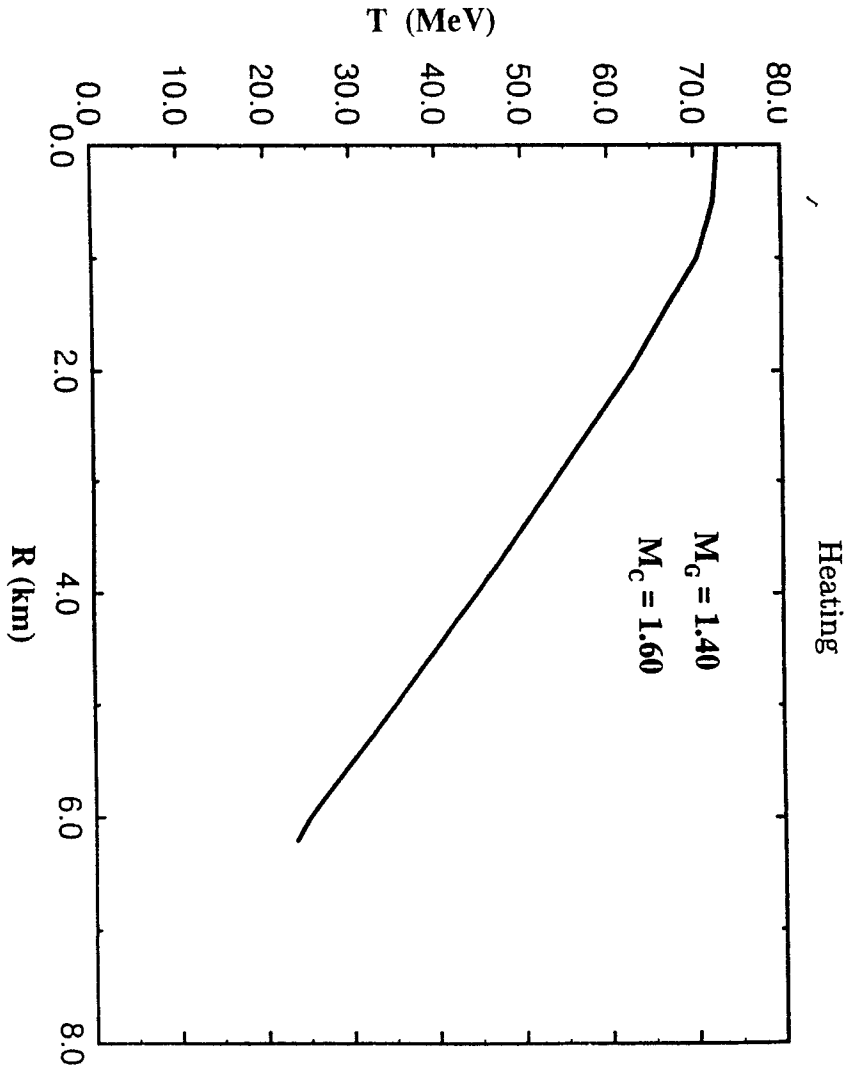

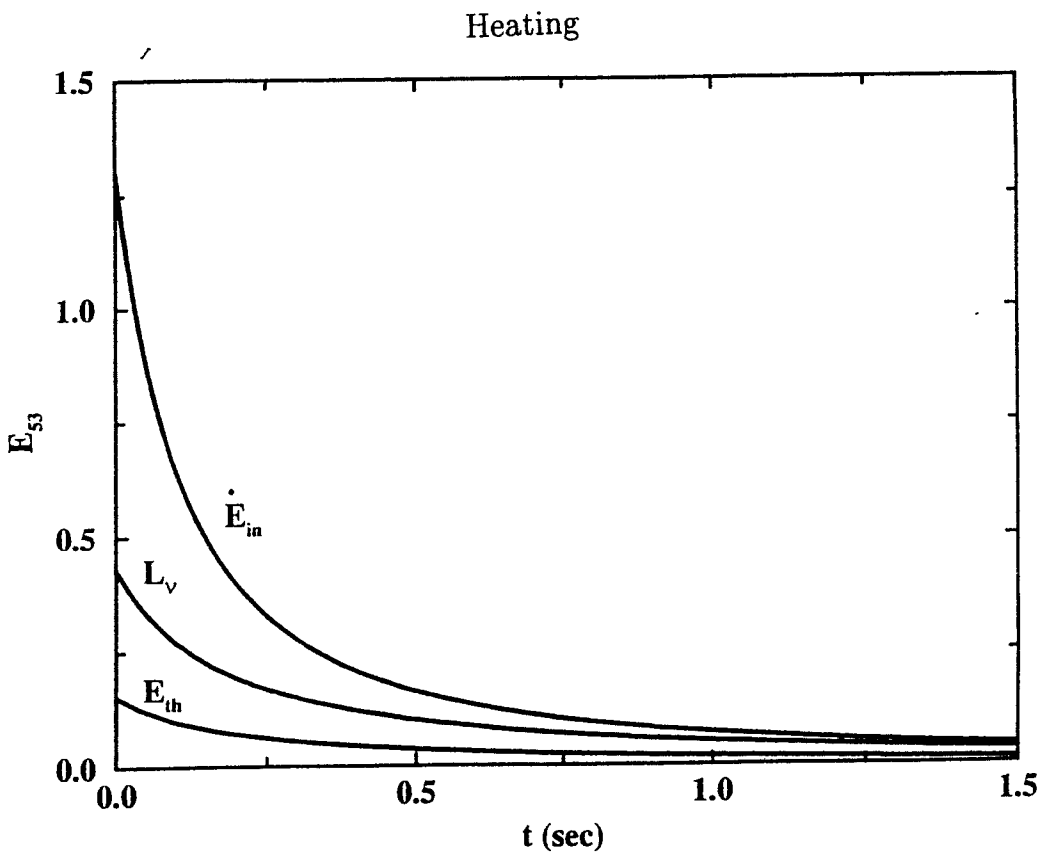

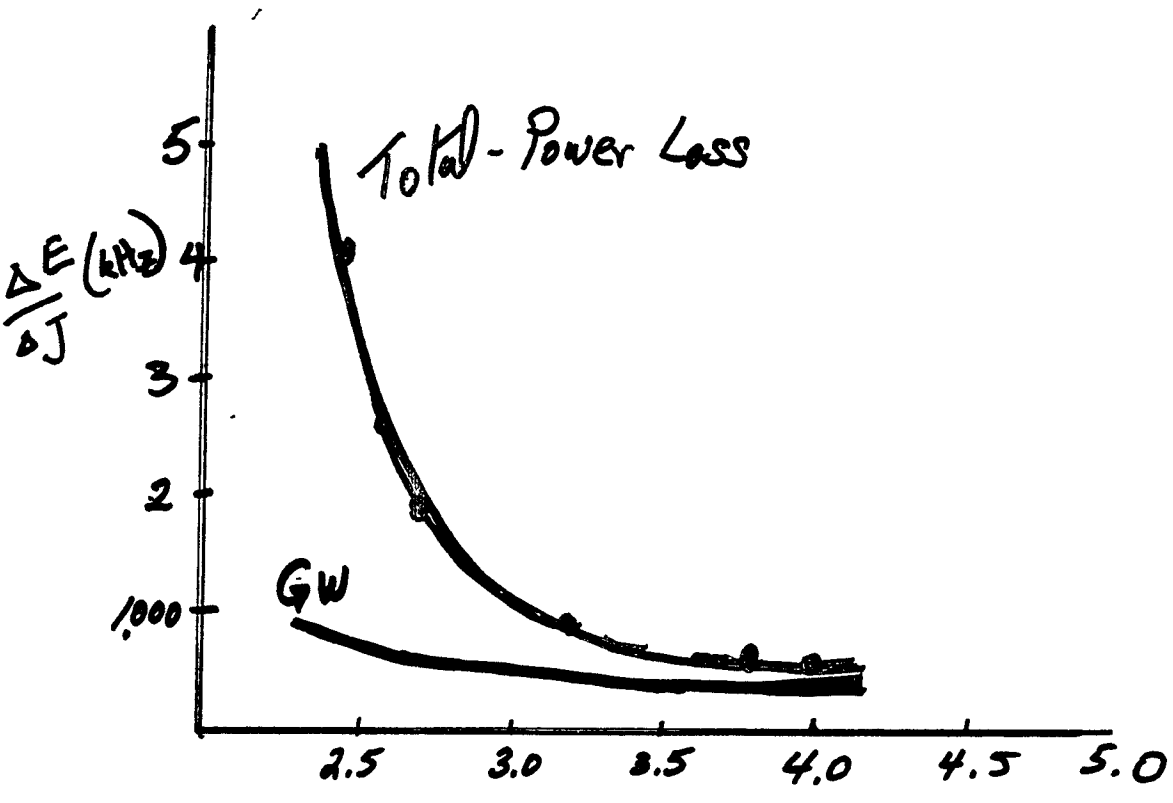

Swirl Instability

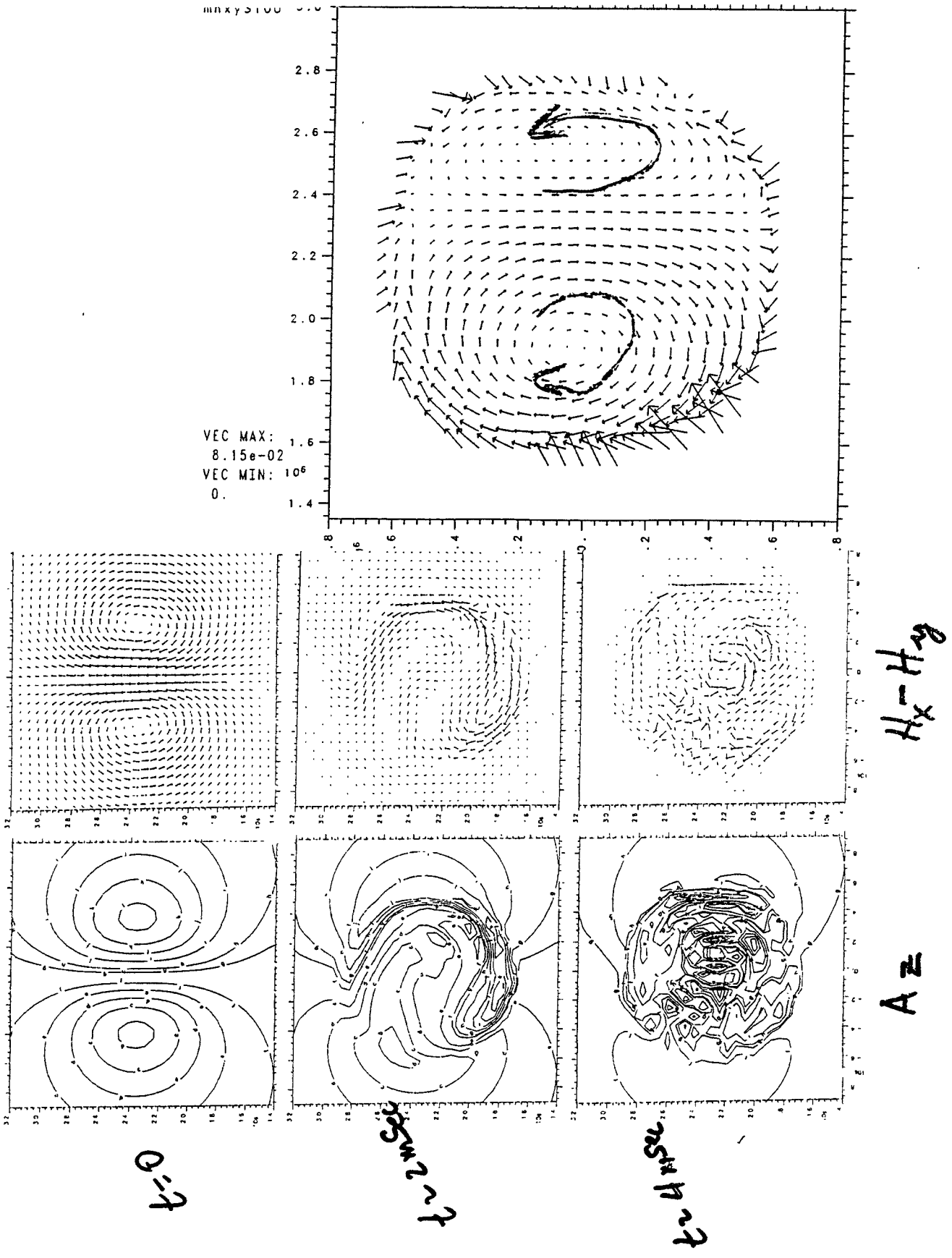

MHD

$$\frac{dA_i}{dt} = V^j\left(\frac{dA_j}{dx^i} - \frac{dA_i}{dx^j}\right)$$

$$u^\mu F_{\mu\nu} = 0 \; ; \quad \vec{E} = 0$$

$$\Rightarrow \quad \langle H^2 \rangle \sim \langle H_0^2 \rangle e^t$$

Equipartition Limit

$H \rightarrow 10^{17}$ gauss

Friday AM — Signal Processing and Data Analysis of Existing and Future Data I
January 31 — Chair: N. Robertson

8:00	S. Vitale(Trento)	Data Analysis for Resonant Detectors-AURIGA Data Analysis
8:25	Discussion	
8:35	W. Johnson(LSU)	Lessons Learned from Allegro and Others
9:00	Discussion	
9:10	Coffee Break	
9:25	P. Astone(Rome)	Interactive Method for the GW Periodic Sources Search
9:50	Discussion	
10:00	A. Wiseman(Caltech)	Future of Coalescing Binary Data Analysis
10:25	Discussion	
10:35	C. Cutler(Penn State)	GW Pulsar Searches
11:00	Discussion	

DATA ANALYSIS FOR RESONANT DETECTORS:

1) AURIGA data analysis

2) Signal Timing with μs Resolution (Experiment)

3) Background Measurement with bars and spheres (Theory)

M. Cerdonio, V. Crivelli-Visconti, A. Ortolan, G.A. Prodi, L. Taffarello, G. Vedovato, S. Vitale, and J. P. Zendri

AURIGA
100 mK 2 3 Tons

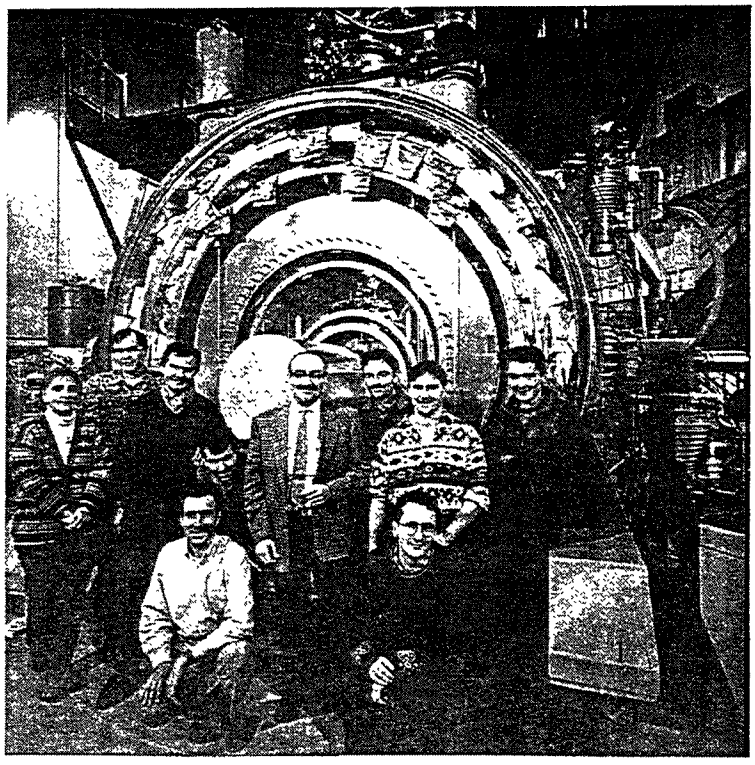

L. Baggio
M. Bonaldi
M. Cerdonio
A. Colombo
L. Conti
V. Crivelli Visconti
P. Falferi
P.L. Fortini
R. Mezzena
A. Ortolan
G.A. Prodi
L. Taffarello
G. Vedovato
S. Vitale
J.P. Zendri

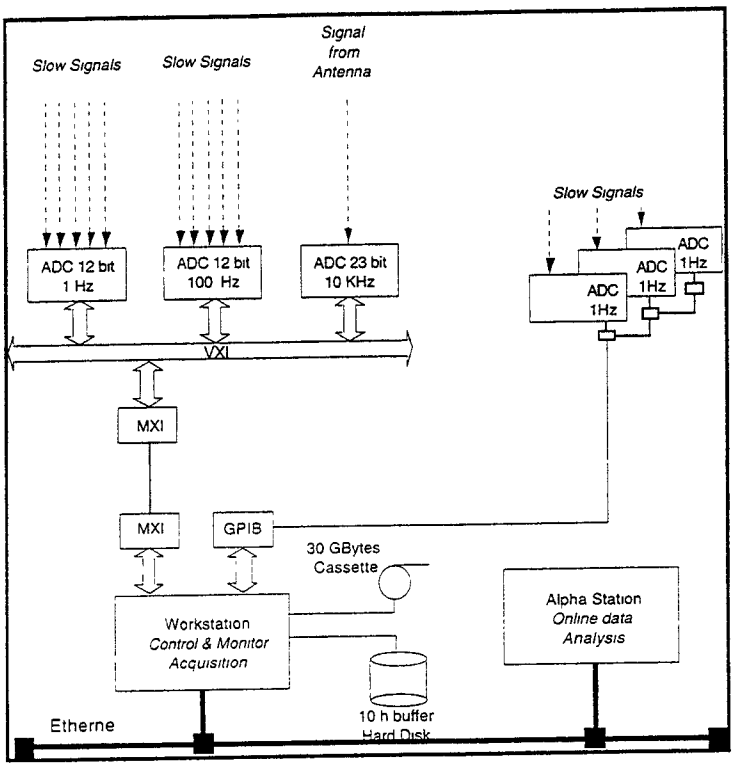

The AURIGA fully digital data acquisition and processing system

23-bit (18 linear)

5 kHz sampling rate

30 Gbytes cassettes raw data storage for full retrieval ability

[Phys Rev D50, 4737, (1994)]

Tested on AURIGA
+
Room Temperature Antenna

(Noise Spectrum->Scaled Replica of AURIGA at its Goal)

($\Delta\nu$ >10 Hz)

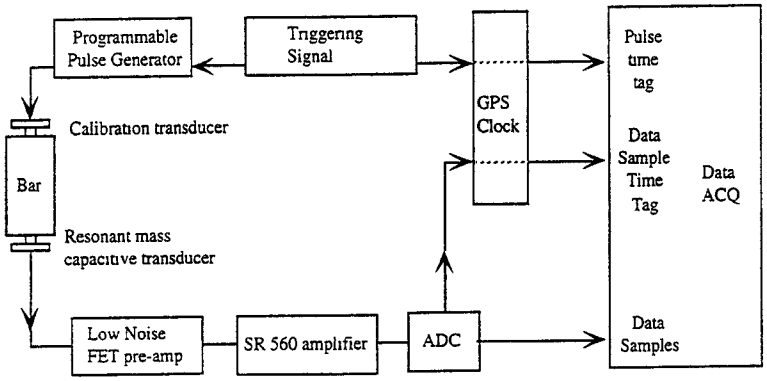

Template-Free Analysis: Signal Expanded in Statistically Independent Eigenfunctions

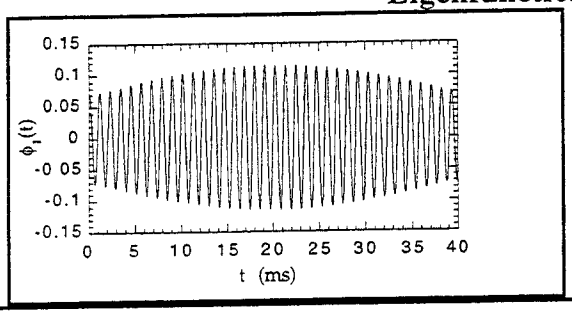

The lowest eigen-function (+ a $\pi/2$ phase shifted companion)

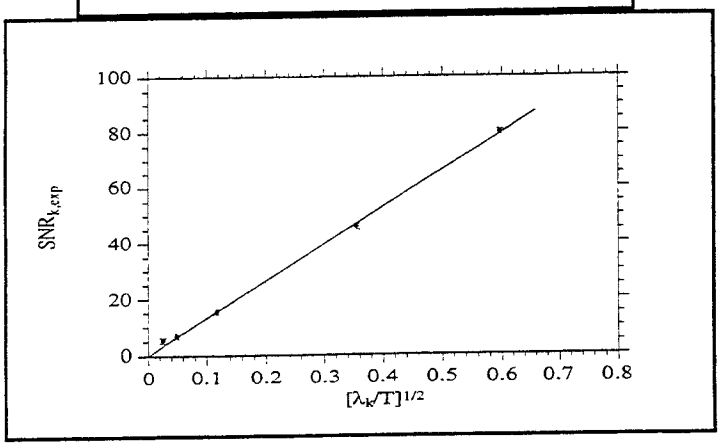

The rapid decay of the SNR

For Most Signal a Delta is a 90% faithful representation up to 50 Hz Bandwidth

Phys Rev D50, 4737 (1994)

"goodness of the fit" rejection of spuria

[Nucl. Phys. B48, 104 (1996)]

Wiener amplitude estimation: minimize the log-likelyhood (χ^2) function as a function of the amplitude A (and of other parameters θ):

$$\Lambda(\theta) = \frac{1}{2}\sum_{i,k=1}^{N} \mu_{ik}\left[x_i - Af(t_i,\theta)\right]\left[x_k - Af(t_k,\theta)\right]$$

minimum

$$\Lambda_{min} = \frac{1}{2}\left[\left(\sum_{i,k=1}^{N} \mu_{ik}x_i x_k\right) - \frac{A^2}{\sigma_A^2}\right] = \frac{1}{2}\left[N\frac{\overline{Y^2}}{\sigma_Y^2} - \frac{A^2}{\sigma_A^2}\right]$$

($\overline{Y^2}$ = m.s. of whitened data; σ_Y^2 = expected m.s)

$2\Lambda_{min}$ has to obey χ^2 statistics

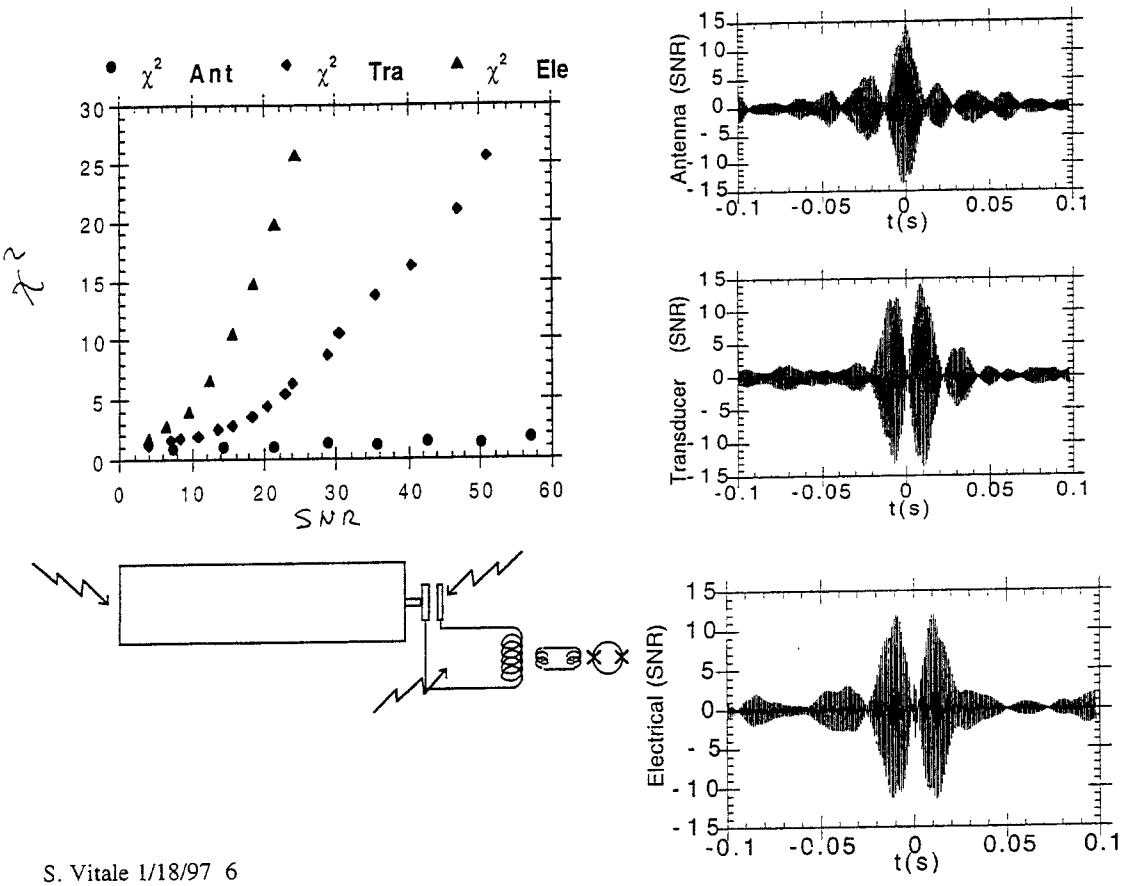

Antennas Arrays

optimal amplitude estimation:

$$A(\theta) = \frac{\sum_{\alpha=1}^{M} \frac{A_\alpha(\theta)}{\sigma_\alpha^2}}{\sum_{\alpha=1}^{M} \frac{1}{\sigma_\alpha^2}}$$

(M antennas)

log likelihood:

$$2\Lambda_{min} = \sum_{\alpha=1}^{M}\left[N_\alpha \frac{\overline{Y_\alpha^2}}{\sigma_{Y\alpha}^2} - \frac{A_\alpha^2}{\sigma_{A\alpha}^2}\right] + \sum_{\alpha=1}^{M}\left[\frac{(A_\alpha - A)^2}{\sigma_{A\alpha}^2}\right] =$$

each antenna has to give a good fit

$$= \sum_{\alpha=1}^{M} \chi_\alpha^2 (N_\alpha - 1) + \sum_{\alpha=1}^{M}\left[\frac{(A_\alpha - A)^2}{\sigma_{A\alpha}^2}\right]$$

the M amplitudes have to be consistent

Time of Arrival: Maximum of the Output of the Wiener Filter

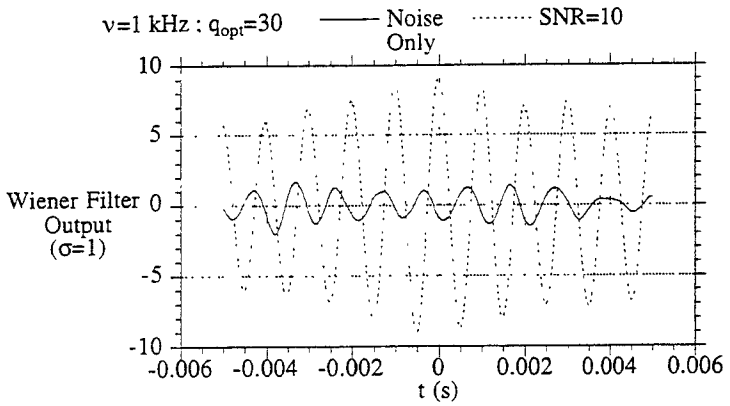

Two components:

Locating the time of each peak (phase timing)

Locating the highest peak (peak timing)

$$t_{arrival} = k\frac{T}{2} + t_{\phi}$$

Total Time of Arrival Distribution

SNR=6

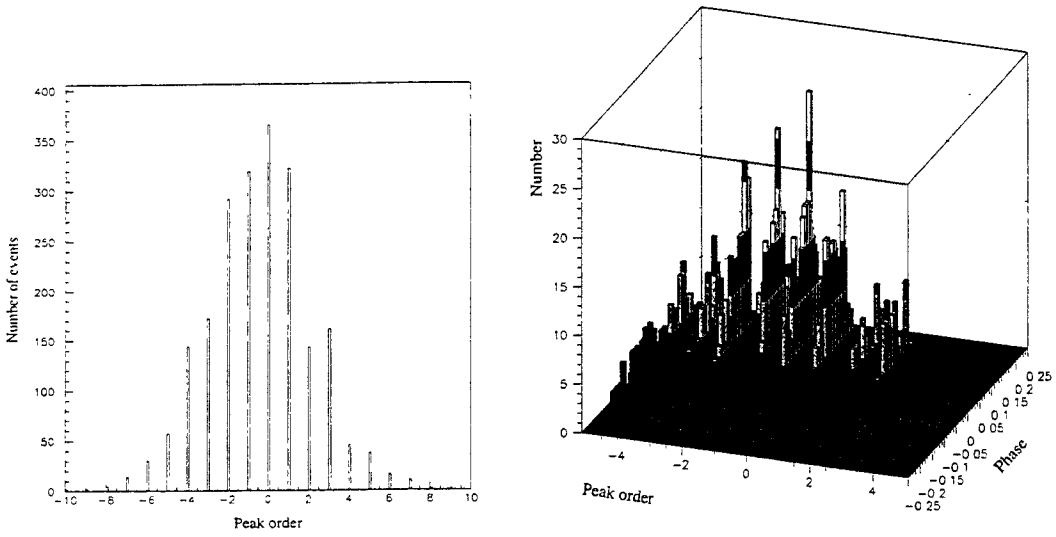

k, t_{ϕ} and Amplitude are Independent

Phase Timing
[Phys. Rev. Lett., 71, 4107 (1993)]

$$\sigma_{t_\phi} = \frac{T}{2\pi}\frac{1}{SNR} \approx \frac{173\mu s}{SNR} \quad @\ 920\ Hz$$

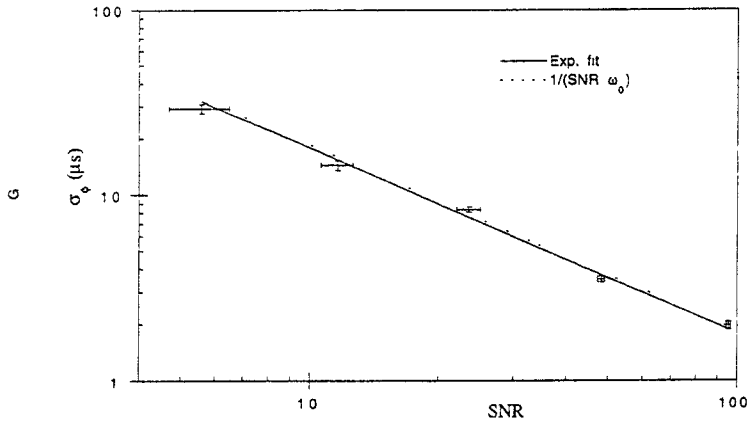

Peak Timing

Noise Autocorrelation: $R(t) \approx \sigma^2 e^{-\frac{t}{2\tau}} \cos(\omega_* t) \cos\left(\frac{2\pi}{T} t\right)$

Peak uncertainty:

$$\sigma_k = \begin{cases} \dfrac{2}{\omega_* T}\dfrac{1}{SNR} & \text{for} \quad \left(\dfrac{2\pi}{T\omega_*}\right)^2 << \pi^2 \dfrac{\tau}{T} \\ \dfrac{4\tau}{T}\dfrac{1}{SNR^2} & \text{for} \quad \left(\dfrac{2\pi}{T\omega_*}\right)^2 >> \pi^2 \dfrac{\tau}{T} \end{cases}$$

Under Damped <---> Over Damped

Beating Mode

When $\sigma_k << 1$ ->>>>>>> $\sigma_t \equiv \sigma_{t_\phi}$

The Room Temperature Antenna

Under Damped Beating Note

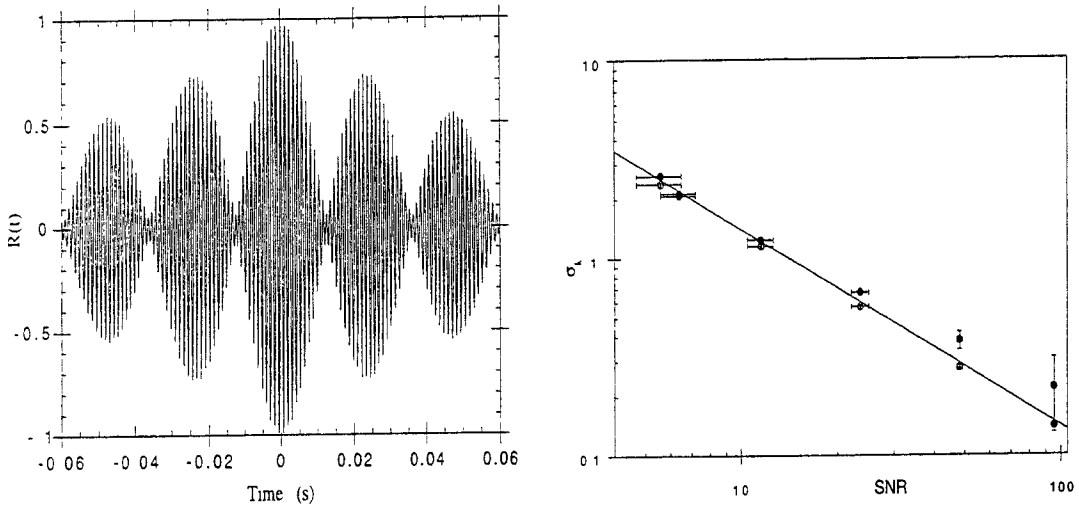

At SNR>20 $\sigma_t \approx 9\ \mu s$

Gravitational-Wave Stochastic Background Detection with Resonant-Mass Detectors.

[Phys Rev D '97]

Two Detectors Correlation (R distance)

$$\left\langle h^a(t)h^b(t')\right\rangle = \frac{1}{2\pi}\cdot\int_{-\infty}^{\infty} d\omega\cdot S(\omega)\, e^{-i\omega(t-t')}\times\Theta\left(\frac{\omega R}{c},\theta\right)$$

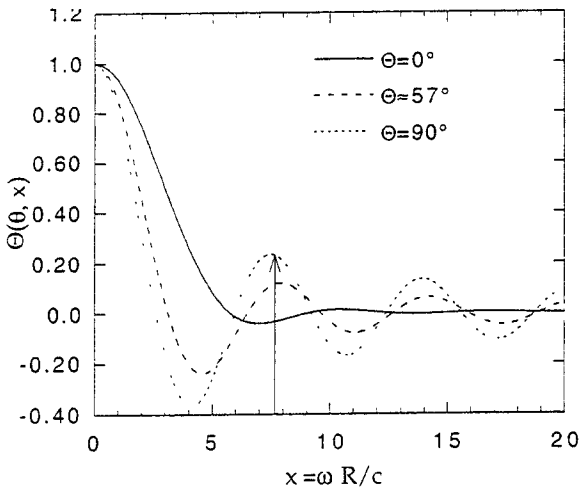

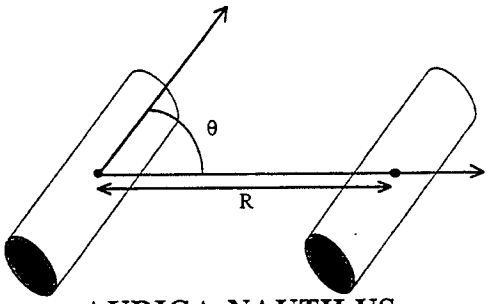

AURIGA-NAUTILUS:
Arrow: ωR/c for
ω=2π×920Hz R=400 km
57°: present value of θ

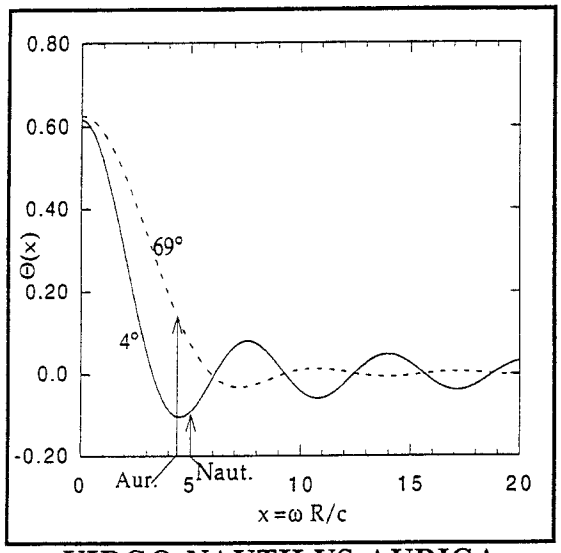

VIRGO-NAUTILUS-AURIGA

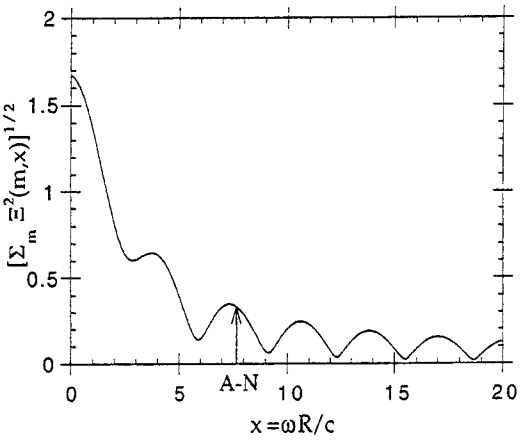

Two Spheres

The linearized estimation method with N detectors

$$h^a(t) = n^a(t) + As^a(t) \qquad \{1 \le a, b \le N\} \qquad \text{(s-> signal, n->noise)}$$

Bilinear unbiased estimate of minimum variance:

$$\hat{A}^2 = \sum_{a,b=1}^{N} \int_{-T}^{T} dt \int_{-T}^{T} dt'\, g_{ab}(t,t') h^a(t) h^b(t') \text{ with } \left\langle \hat{A}^2 \right\rangle = A^2$$

Solution for $As^a(t) << n^a(t)$ **:**

$$2 \int_{-T}^{T} dt'' \int_{-T}^{T} dt'''\, g_{ab}(t'',t''') R_n^a(t-t'')\, R_n^b(t'-t''') = -\frac{\lambda}{2} R_s^{ab}(t-t') \qquad a \neq b$$

$$g_{ab}(t,t') = 0 \qquad a = b$$

Table I
Estimated sensitivities of various detectors arrays.
$\Delta\omega_{pd} \approx 30$ Hz $\quad 2T = 1$ year

Detectors array	$\sigma_{\hat{A}^2}\left(\text{Hz}^{-1}\right)$	$\sigma_{\Omega_{GW}}$
AURIGA-NAUTILUS present orientation	2×10^{-49}	1.5×10^{-4}
AURIGA-NAUTILUS best orientation	10^{-49}	8.5×10^{-5}
AURIGA-NAUTILUS-VIRGO present orientation	1.3×10^{-49}	10^{-4}
AURIGA-NAUTILUS-VIRGO best orientation	8×10^{-50}	7×10^{-5}
VIRGO and One 38 ton sphere	2.5×10^{-50}	2×10^{-5}
Two 38 tons spheres at AURIGA and NAUTILUS sites	2×10^{-51}	2×10^{-6}

LESSONS LEARNED FROM ALLEGRO & others

(Applied to an 'Optical' Suspension)

WARREN JOHNSON
LOUISIANA STATE UNIV.

Goal : detect coalescing binary neutron stars

The natural target for interferometers

Shot noise is reduced at lower frequencies

Signal is higher at lower frequencies
--long time at low f causes signal strain h(f) to vary as $\sim(f)^{-1}$

Puts very large premium on low frequency sensitivity

Dominant problems: Mechanical

- Seismic transmission
- Non-thermal generation within suspension
- Thermal generation within suspension

Solution for 1&2: build a stable, steerable optics platform

with < 10^{-11} m/√Hz (f < 1 Hz) via active isolation

with < 10^{-16} m/√Hz, (f > 10 Hz) via passive isolation

Looking at a different mix of ingredients, using mostly ones proposed by people in this room, hoping to find a better recipe.

one remaining problem : thermal noise in final stages

solution : TBA [Glasgow, Stanford, MSU, ...]

Assume double pendulum mirror below platform

Actually need 2 more stages for final seismic isolation to 10^{-20} m/√Hz for f > 10 Hz

Thermally generated random forces must be very low, Equivalent Q's must be very high ≥ 10^9

Limits unknown ?

Simplistic Model 1

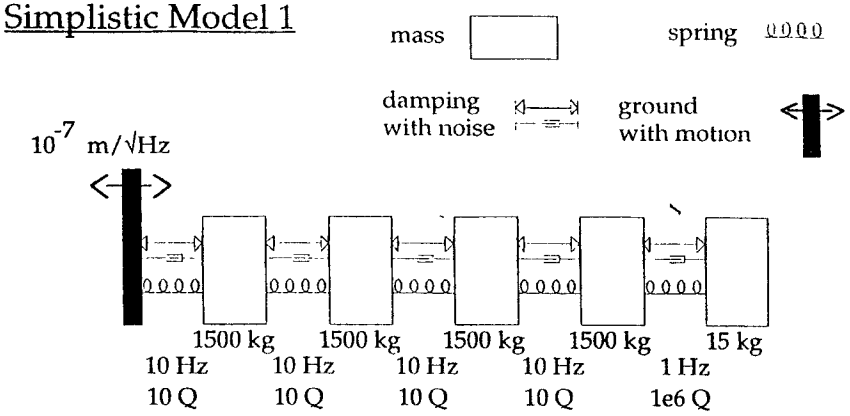

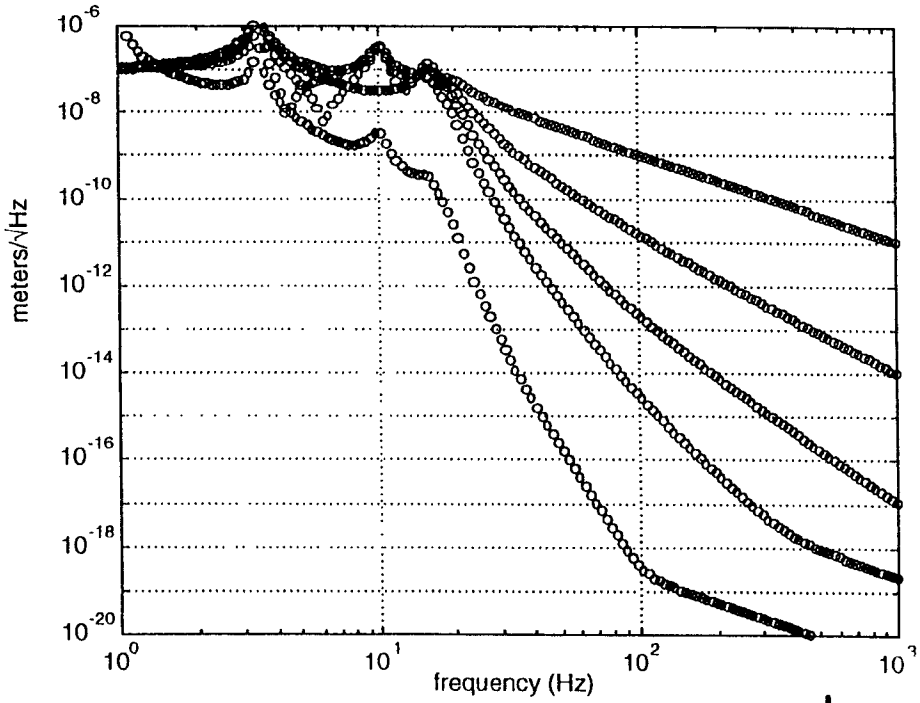

PLOT SIGNAL / NOISE ON SAME GRAPH

$$(SNR)^2 = \int_0^\infty df \frac{|\tilde{h}_s(\omega)|^2}{S_h(\omega)} = \int_0^\infty \frac{df}{\downarrow} \frac{|\sqrt{f}\,\tilde{h}(f)|^2}{|\sqrt{S_h}|^2}$$

$\times 10^{-22}$ $\frac{1}{\sqrt{Hz}}$

SIGNAL (NUMERATOR)

$= \sqrt{f}\,|\tilde{h}_s(\omega)|$

NOISE (DENOMINATOR)

$= \sqrt{S_h(\omega)}$

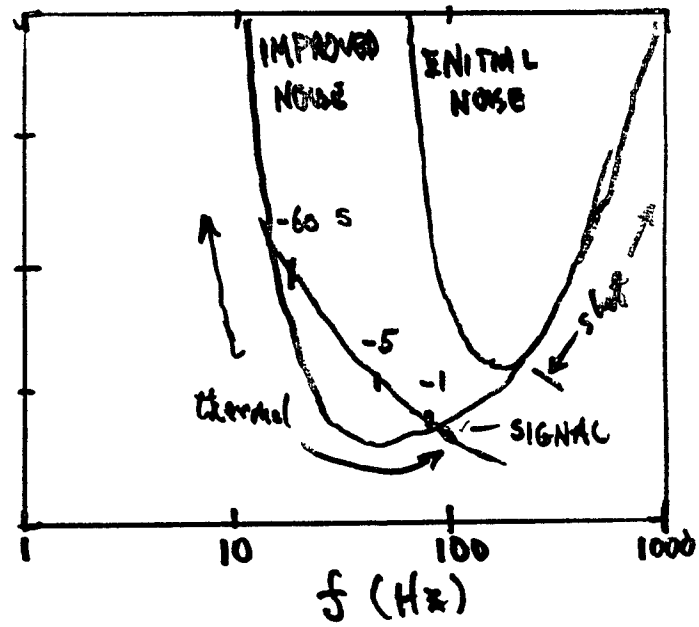

9 here, just detectable

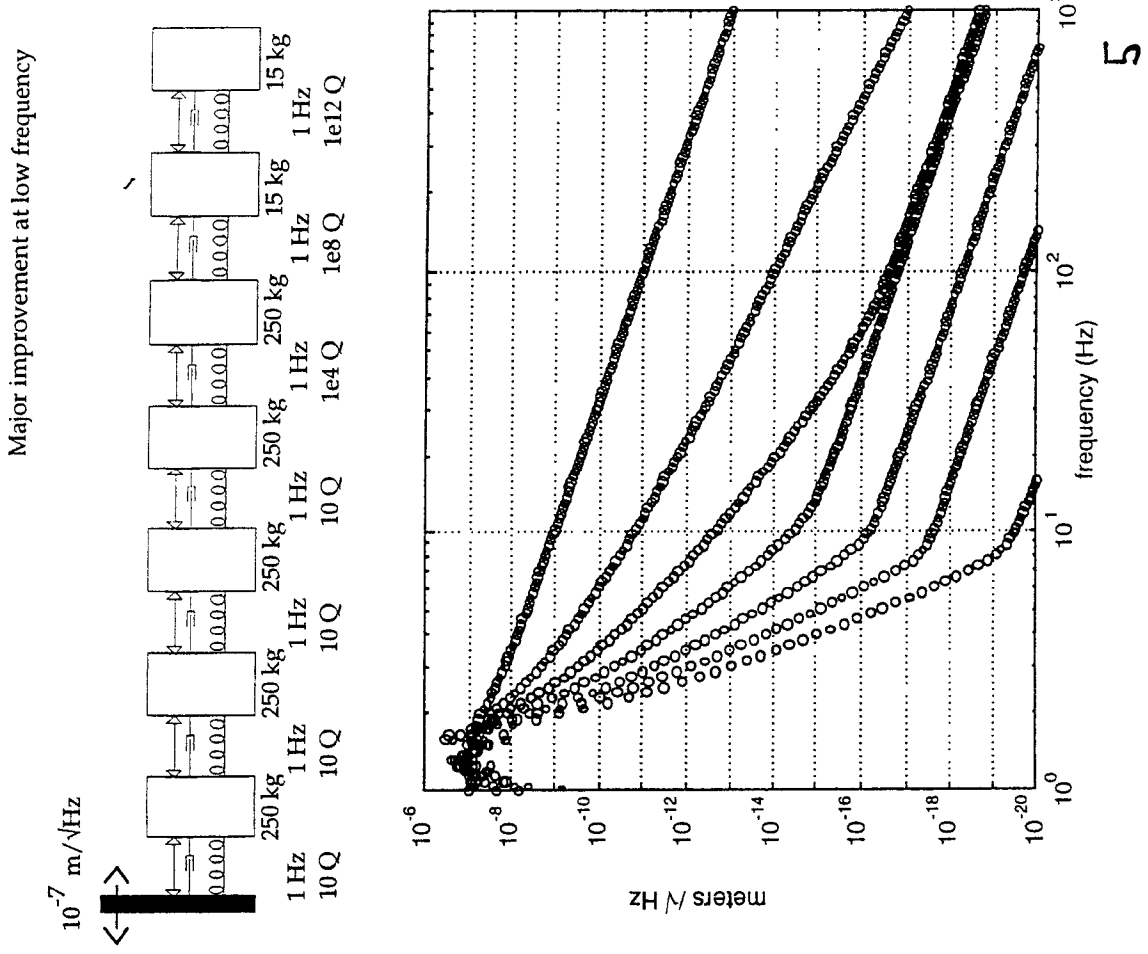

5

Simplistic Model 2

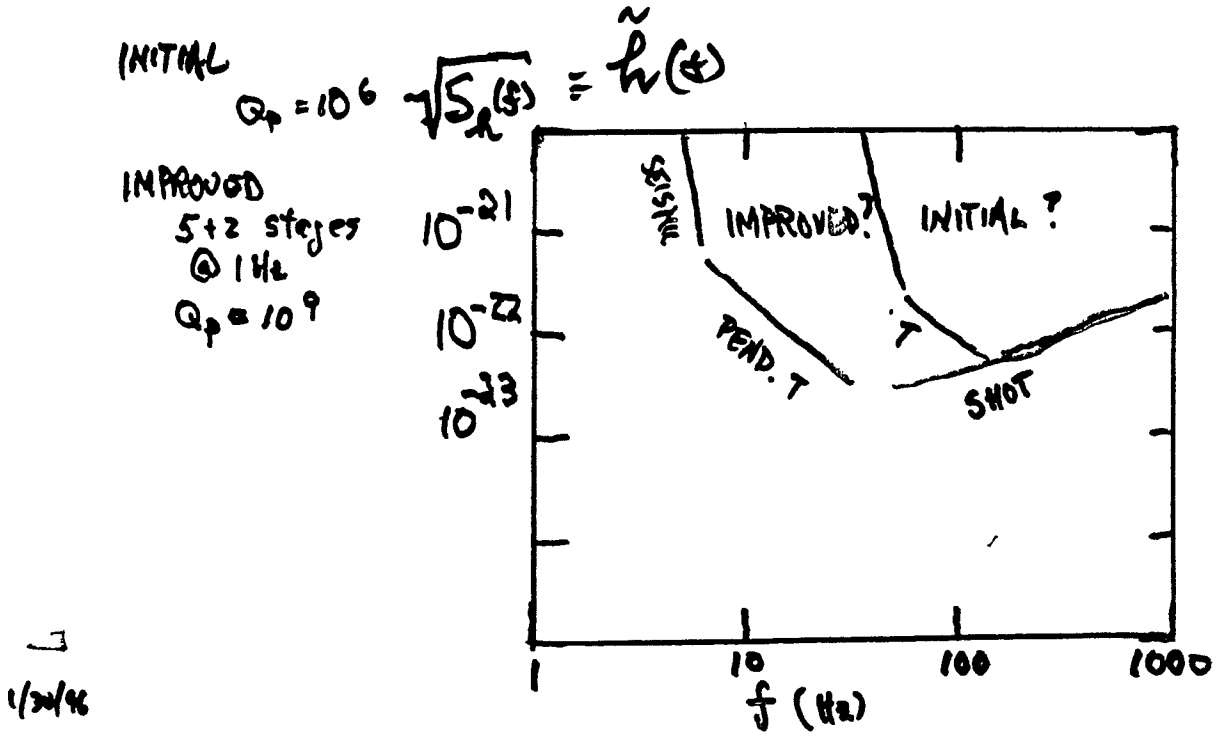

1/30/96

8

Proposal - a short pendulum suspension

The pendulum is too good to dismiss.

It has <u>proven best</u> for the mirrors, why not back a winner ?

Considered alternatives

Rubber springs under compression, like initial LIGO, were ruled out by their mass and stiffness at reasonable working load

X-pendulum ruled out by stiffness in other DOFs

Use of over-lapped pendula, to shorten total height while preserving indivual length, was calculate to be unstable to capsize.

So each stage is a disk shaped mass hung by a single wire from the stage above.

As proposed and developed by VIRGO collaboration

The wire has very low stiffness in 5 out of 6 DOF
so 5 out of 6 problems solved

The large axial (vertical) stiffness requires major effort to control.

Use 5 "large" stages and 2 smaller ones

Simplistic models suggest some requirements

all interferometers have used active isolation

but active isolation, at best, is useful only up to a "sensor limit" specific to its configuration

So active isolation's real function is to maintain angular alignment and cavity length within the needed range.

Passive isolation will superior in the signal frequency band. (excluding heroic developement of sensors).

Differences with VIRGO :

Has to meet all the system requirements for the US detectors :

1) Make it smaller

moderate mass in each stage (250 kgm)

moderate pendulum length (25 cm),

=> pendulum frequency = 1.0 Hz

==> stack height = (5+1) x (25+5 cm) = 1.8 m

double pendulum height + clearance ~ 0.8 m ?

Natural lower limit for mass is not obvious
how small can one go?

2) Use design and construction details suggested by resonant detector experience

Explicit normal mode control

Allow only high modes (> 2kHz)
- stiff masses (compact)
- stiff attachments
- smaller diameter tubes and wires require short lengths

Or require modes to be very low (< = 1 Hz)

Intermediate frequency modes are guilty until proven innocent

But cannot avoid some modes in the springs ("violin modes", etc), so make them low-mass which reduces their danger

All stresses levels far below yield (~ 25% of yield ?)

All loads carried by metal, not rubber

Expect metal under such moderate stress to have no micro-yield and creep and other non-thermal excitations

Must admit that the physics here is largely unknown, and that the safe stress level is just a guess

but cf Braginsky

which 'confirms' guess

Special attention to all joints

They are the suspicious locations for non-thermal noise : e.g., microyield, microslip, and upconversion

So weld, braze, or solder all joints, including all bolts

Put all loaded joints under compression, and fill them with a stiff, molecularly bonded "joint compound", like solder

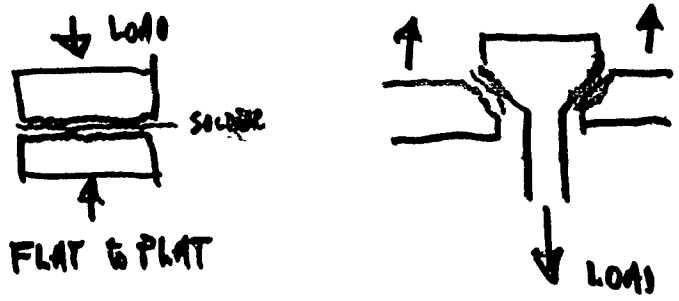

E.g. ordinary clamping method for wires has to be dangerous practice. Even when they do not hurt the Q, they may well be a source of "microslip" as the wire saws back and forth across the edge.

Suggests copper alloys for all parts

BeCu for suspension wires

ordinary copper for bulk

Wide variety of compatible brazing compounds and solders for all joints

In Sn melts near 100 °C
will bond to glass, SiO_2, Cu, ...

3) Use active control for all 5 large stages

Otherwise a compound pendulum will have enormous seismic motion

Electronics are probably better and cheaper than mechanicals , but only for low frequencies and low loads.

Requires 6 sensors and 6 actuators for every stage

Simpler if actuators act between stages

Use a geometry that makes mode orthogonalization (MIMO?) straightforward

For actuators - use magnets and coils

Evaluation required : which sensor is most reliable and most sensitive ?

optical ? (JILA ?)

capacitive ? (MIT ?)

LVDT ? (VIRGO?)

Sensors and actuators and feedback networks ought to be cheap, but what is realistic ? (does "mass" production reduce cost?)

Evaluation required : what is best inertial reference?
Proof mass in an accelerometer module?

Or the stage below?
This would cause all stages to ultimately follow the bottom stage, which becomes the final reference
It should be the quietest object around.
Does a such a staged servo system have better or worse dynamic range ?
Is servo stability a problem ?

4) Steer the bottom stage

Will require cavity length and alignment info from an optical system

Inertial reference is the flywheel, not the governor

Quiet and aligned stage should greatly reduce (or even eliminate?) servo requirements on the final mirror

Steering error depends on sensor drift and servo behavior
perhaps Δ(length) ~ 10^{-11} m ~ $10^{-5}\,\lambda$
and Δ(theta) ~ 10^{-11} m/0.3m ~ 3×10^{-10} radians
or better ?
what is requirement ?

5

6) Finally, the radical proposal : reconsider gas springs for vertical support

alternative to flexures

Mass comparison

Seems mechanically simpler (based on no experience)

Microphysics of gas support is absolutely reliable
no non-Gaussian noise mechanisms in the stressed gas
but metal membrane (bellows) must be considered

Thermal stability becomes a major question

But it is a straightforward engineering problem (no unknown physics)

Sensing of vertical height makes a fantastic thermometer, so use it.

Use heater for slow actuator, use magnet and coil for fast actuator

Drastically shorten thermal time constants
material - copper and helium
geometery - shorten conduction path

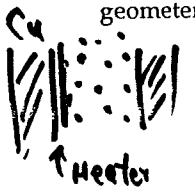

thermal diffusivity K

$\tau_{He\ (5m)} \sim \frac{(4m)^2}{0.3\ m^2/s} \sim 50s$

$\tau_{Cu} \sim \frac{(3m)^2}{1.2\ cm^2/s} \sim 10s$

Very low heat flow
Use good vacuum (free)
Use high reflectivity surfaces (cheap)
but optical problem ?
New cost : need temperature controlled radiation shield
expensive ?
how stable ?
could be light shield and absorber

$\frac{\dot{Q}}{A} = \frac{\sigma(T_2^4 - T_1^4)}{\frac{1}{e_1} + \frac{1}{e_2} - 1} \simeq e_1 \sigma 4T^3 \Delta T$!

$\dot{Q} \sim \left(25\ \frac{mW}{m^2}\right)\left(\frac{e_1}{.05}\right)\left(\frac{\Delta T}{.01K}\right) A$

$A \sim 0.5\ m^2$ $\quad C_p \sim \left(10^5\ \frac{J}{K}\right)\left(\frac{m}{250\ kg}\right)$

$\dot{T} = \frac{\dot{Q}}{C_p} \sim 10^{-7}\ \frac{K}{s}$ $\quad \Delta h \sim l_B \frac{\dot{T}\tau}{T_0}$

$\sim \frac{(.25m)\left(10^{-7}\frac{K}{s}\right)(50s)}{290K}$

$\rightarrow \Delta h \sim 4 \times 10^{-9}\ m$!

Heater, gas, and bellows appear to be excellent slow actuator

easy to fill (capillary)
long stroke
perfectly smooth !! motion

High conductivity and temperature stability are good things anyway

Is thermal drift a significant source of noise ?

Ignorant of vibration modes of a bellows
but internal constrained layer damping might control any problems

Possible stumbling blocks

All the other components (laser, input optics, etc) may require nearly comparable mechanical stability
The Murphy claims this is obvious

Sensors may require impossible pre-alignment

Sensor noise (as fedback force) might not cut off fast enough, and so overwhelm thermal noise at 10 Hz

Mechanical "1/f noise"
or is it only thermal drift ?
unknown physics at lower frequencies is possible

Support tower may amplify ground motion

Bellows may "crinkle"

Sensors, or feedback network, may be too difficult or too expensive

Height control may fail
from insufficient range in fast servo control
from complicated thermal dynamics

So far, there is not much in the way of good tests for a suspension system, besides using it in a real detector (which is an expensive).

It would be helpful if there was an inertial motion sensor (accelerometer) with internal noise less than 10^{-16} meters/$\sqrt{\text{Hz}}$ from 10 Hz to 1 kHz.

file gas_springs_1b

Short Pendulum - Gas Springs -- cross section, 3 stages

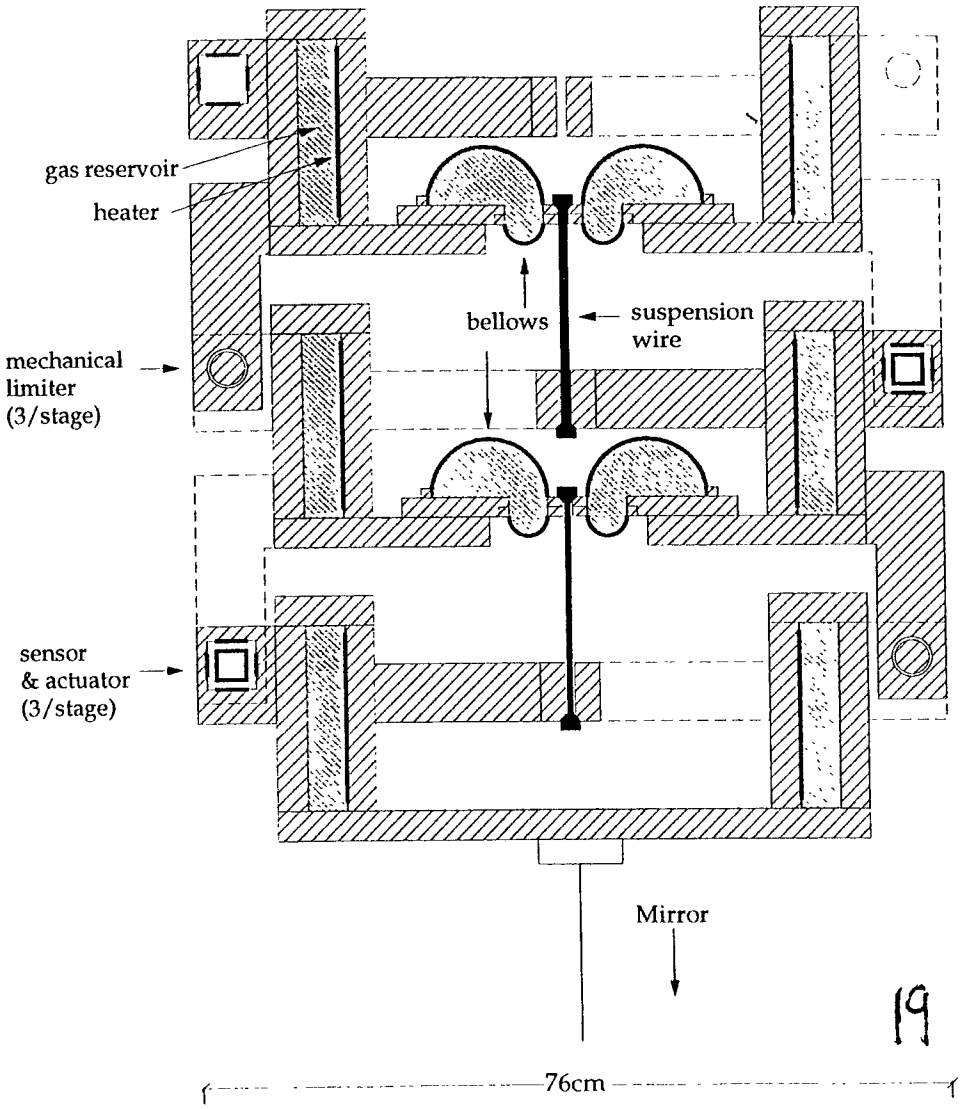

19

An interactive method for the gravitational wave periodic sources search

P. Astone
S. Frasca
M.A. Papa

Aspen Winter Conference
on gravitational waves
and their detection
Jan 26 - Feb. 1, 1997
Aspen, Colorado

Pulsars, $h_o = \sqrt{\frac{2 S_h}{t_m}}$ (Known source)

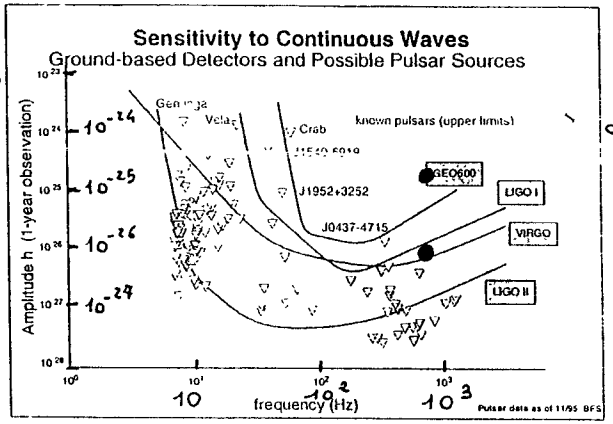

h_o 1 years of observation

Hz

(B.F. Schutz)

Explorer, $T = 2\,K$, $Q = 10^6$, $t_m = 1$ year

$h_o \sim 2.3 \cdot 10^{-25}$ (2 Hz around the resonances)

$h_o \sim 2 \cdot 10^{-24}$ (16 Hz between the resonances)

} We have ~4 years of data

Auriga
Nautilus, $T = 50\,mK$, $Q = 10^7$, $t_m = 1$ year

$h_o \sim 1.1 \cdot 10^{-26}$ Expected

⇝ Joint searches may really be helpful

Doppler effect
due to the Earth motion

$$\left|\dot{\nu}_{rev}\right|_{max} = \nu_0 \cdot 1.97 \cdot 10^{-11} \cos\beta_{ecl} \quad Hz/s$$

Earth revolut. (annual)

β_{ecl} = ecliptical latitude of the source

$$\left|\dot{\nu}_{rot}\right|_{max} = \nu_0 \cdot 11.2 \cdot 10^{-11} \cos\beta_{ter} \cos\delta \quad Hz/s$$

Earth rotation (sidereal)

β_{ter} = terrestrial latitude of the detector

δ = declination of the source

It can be used as a signature to identify true g.w. signals and to obtain information on the location of the source

Time modulation of the detected amplitude

due to the different orientation of the detector because of the Earth rotation

The effect can be used to identify true g.w. signals and to determine the source position and polarization

$$\Sigma = \Sigma_0 \cdot f(\vartheta, \epsilon, \varphi)$$

ϑ = angle between the direction of the wave and the direction of the antenna

ϵ = percentage of linearly polarized power

φ = polarization angle

- Intrinsical variation of the source frequency can be due to many factors and depends on the characteristics of the source itself.

- Huge amount of computation time needed to solve this detection problem in "standard" way, that is using one "very long" FFT, done with a very high frequency resolution $\delta\nu = 1/t_m$.

- Time precision and sampling frequency precision during the observation time are very crucial

Time precision

if $\epsilon_\nu = \frac{\Delta\nu}{\nu}$, $\tau = \frac{1}{\nu}$ ν = wave freq.

then $\Delta\tau = \epsilon_\nu \cdot \tau$

After the time t_m we have a phase error of

$\frac{\Phi}{2\pi} = t_m \cdot \Delta\nu = t_m \nu \epsilon_\nu$

If $\nu = 1\,kHz$, $\tau = 10^{-3}\,s$,

$t_m = 1\,year = 3.1 \cdot 10^7\,s$

and if we want $\frac{\Phi}{2\pi} \lesssim 0.1$ in 1 year

then we need $\epsilon_\nu \lesssim 3 \cdot 10^{-12}$

$(\Delta\nu \lesssim 3 \cdot 10^{-9}\,Hz)$

This means a $\Delta\tau \sim 10^{-4}\,s$/year

The frequency bin is $\delta\nu = \frac{1}{t_m} = 3 \cdot 10^{-8}\,Hz > \Delta\nu$

- Non-continuous observations

for resonant detectors we have reached duty cycles of the order of ~70% during one year.

- Time varying noise amplitude that causes a time varying sensitivity of the detector.
  - this can happen only in some bands or on the whole spectrum
  - one can exclude disturbed periods, but it may be difficult to decide what a "disturbed" period is...

- Presence of many non-stationary "spectral" disturbances that can partially mimic the signal of a periodic source
  - one must analyze and exclude all these disturbances

We plan to use a frequency domain data base (FD DB)

and software procedures operating on it

- "simple" spectral analysis
- "enhanced" analysis

The FD DB is composed taking the first half part of the FFT of 2N data

Each basic FFT in the Data base is completely characterized

Choice of the basic FFT element of the Data Base

One can use different criteria, depending on:

- the detector characteristics (it is important to have each FFT done over a time period during which the system is stationary)
- a priori information on the source

A reasonable choice, that we are using in our analysis of the Explorer data, is to consider the maximum expected Doppler shift

Frequency domain Data Base

Due to the Doppler effect the maximum sweeping in frequency is, at ~ 1 kHz:

during one year ~ **0.62 Hz**

during one day ~ **0.011 Hz**

Each FFT is taken over a time period of 0.6617 hours and covers the frequency range

$$900 - 927.5 \text{ Hz}$$

During this time we have

$$\Delta\nu_{Doppler} \lesssim 0.28 \text{ mHz}$$

smaller than the frequency step

$$\delta\nu = 0.42 \text{ mHz}$$

The choice **0.66 hours** for the basic element of the DB is good for signals at ~ 1kHz.

If the detector bandwidth is such that you can do the pulsar search in a very wide frequency range =>

the FDDB can be done with FFTs of different lengths

1 FFT done over 0.33h for 8 kHz searches
1 FFT 0.33h for 4 kHz searches
1 FFT 0.46 for 2 kHz searches

---

1 FFT done over 2.16h for 125Hz searches

(The amount of information is only a factor 2 bigger, compared to the use of only the first group of FFTs)

HEADER:
it is used for vetoing the experimental data

- Date
- Brownian noise, minus mode
- Brownian noise, plus mode
- frequencies, minus and plus
- decay times, minus and plus
- wide band noise
- calibration
- other information

In one year we have 13239 spectra

→ it is very important, during the analysis, to have all the information "at hand"

Simple spectral analysis

Power spectrum = $|FFT|^2$

A proper analysis of the spectra, 13239 in one year for detectors at ~ 1 mHz, will lead us to the detection of a possible continuous g. w., if the SNR is big enough

Explorer 1991
Search for Monochromatic Waves

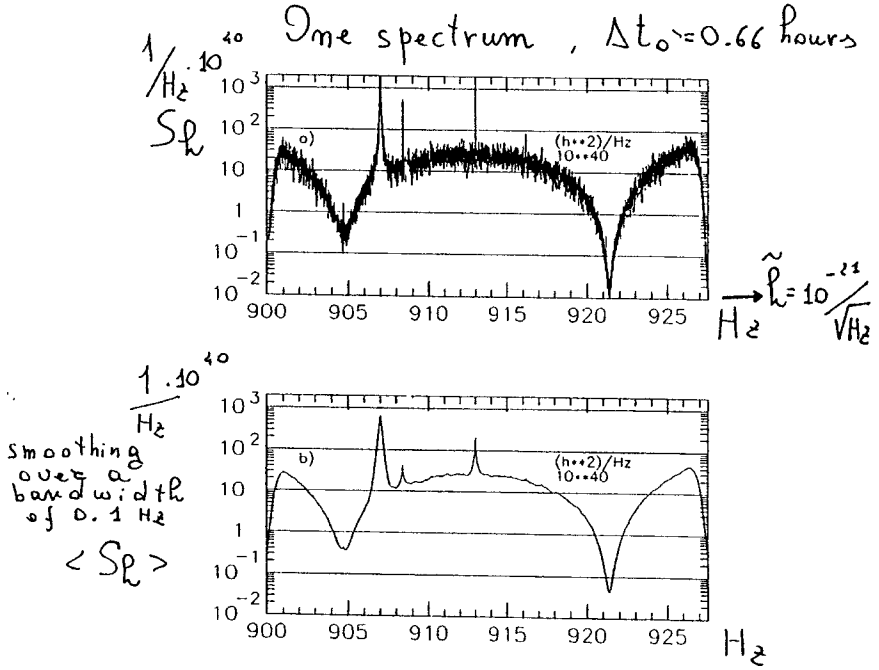

Figure 1 *a) One spectrum in the data base (1 august 1991) b) Its smoothing filter*

for $t_m = 0.66$ hours $\quad h_0 = \sqrt{\frac{2 S_h}{t_m}} = 3 \times 10^{-23}$ experimental

Procedure – Candidate lines REGISTRATION

in each spectrum of the Data base
The procedure $i = 1, 13239$ $j = 1, 65536$

reads $(\nu_{ji}, \tilde{h}^2_{ji})$ in the j channels of the i-spectrum

registers $(time_i, \nu_{ji}, \tilde{h}^2_{ji} - \langle \tilde{h}^2_i \rangle)$

if $\tilde{h}^2_{ji} \geq K \, \tilde{h}^2_{HIN\,i}$

(actually $K = 8$)

where $\tilde{h}^2_{HIN_i}$ is a MINIMUM value of the spectrum, evaluated again each time a new datum is registered. (register the LOCAL MAXIMA)

One file/year contains all these information that can be easily read by the analysis program

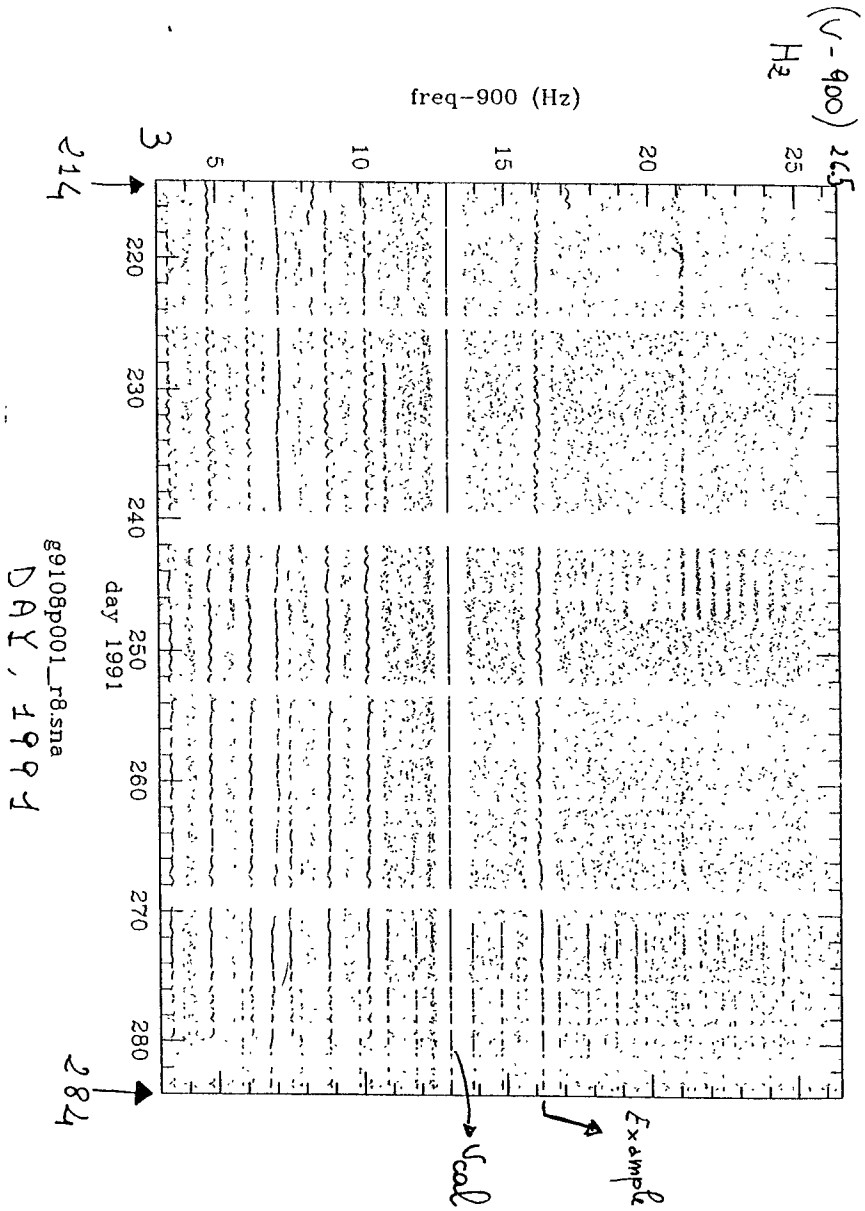

Simple spectral analysis

We analyze the frequency and amplitude patterns of each candidate spectral line in order to identify, or to exclude, a certain locus of points, as possible g. w. emitters.

Using ~ 20000 point sources

$\Delta\nu < 0.4$ mHz

(less than the frequency step in each spectrum)

$\Delta h^2 \lesssim 10\%$

We fit the frequency and the amplitude with the expected modulations from various sources.

The first step might consist in fitting the frequencies and chosing the direction which gives the best fit.

The energies are averaged as a function of the SIDEREAL TIME and we test if the fit for them, using the SAME direction, is satisfactory

The sensitivity of the spectral procedure:

It has a reduced sensitivity, compared to the "long" FFT

$$\left.\begin{aligned} h_0^{\text{"long"}} &= \sqrt{\frac{2\,S_h}{t_m}} \\ h_0 &= \sqrt{\frac{2\,S_h}{\sqrt{t_m \Delta t}}} \end{aligned}\right\} \Rightarrow \frac{h_0}{h_0^{\text{"long"}}} = \left(\frac{t_m}{\Delta t}\right)^{1/4}$$

if $t_m = \underline{\text{one year}}$, $\Delta t = 0.66\,h$ $\Rightarrow \underline{\dfrac{h_0}{h_0^{\text{"long"}}} \sim 10}$

- A Montecarlo, using the experimental data + simulated continuous signals, is in progress to confirm experimentally
- Compare the two sensitivities in terms of PROBABILITY OF DETECTION

Spectral line at 916.3 Hz
- frequency versus time -

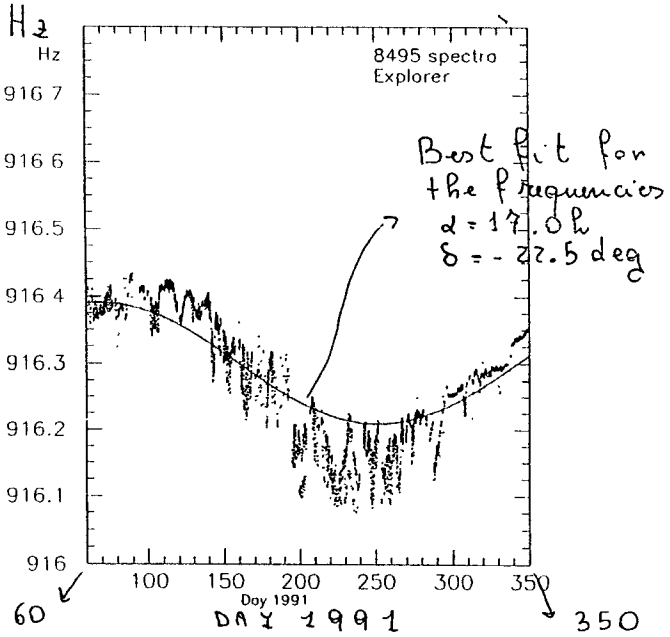

Figure 1: march-december 1991; 8495 spectra Experimental data, cleaned using ARMA filt+ thf 1 day, and expected if the source were at α=17 03 hours, δ=-22 5 degrees, that is the best fit for the frequencies

Example of the analysis procedure

Spectral line at 916.3
from the Explorer 1991 data base

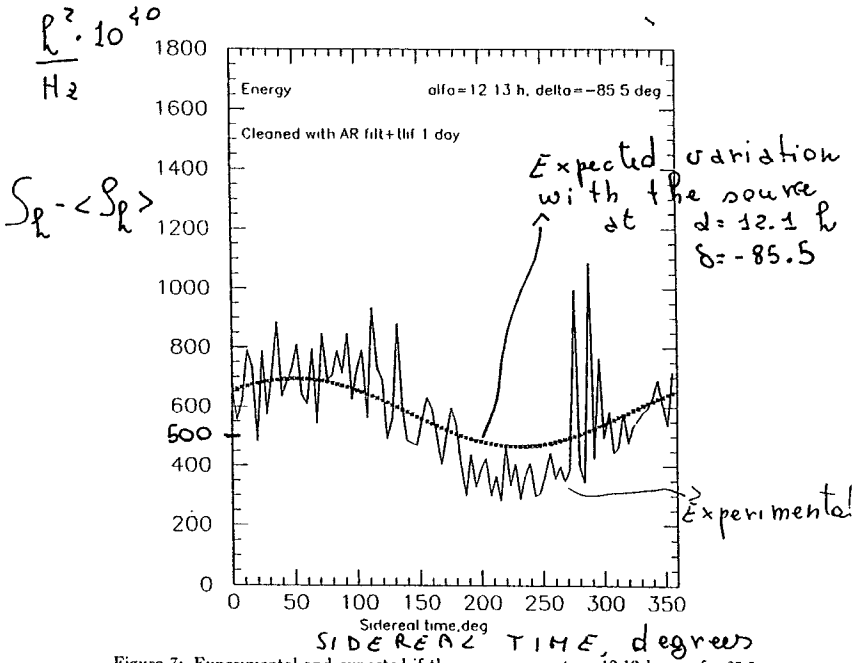

Figure 7: Experimental and expected if the source were at α=12.13 hours, δ=-85 5 degrees, that is the best fit for the energy

8495 spectra

$$h_0 \sim \left(500 \cdot 10^{-40} \cdot 0.4 \cdot 10^{-3}\right)^{1/2} \sim 5 \cdot 10^{-21}$$

noise experim. $\sim 3 \cdot 10^{-22} (8495)^{-1/4} \sim 3 \cdot 10^{-23}$

between the resonances

$$SNR = \frac{(5 \cdot 10^{-21})^2}{(3 \cdot 10^{-23})^2} \sim 3 \cdot 10^4$$

Enhanced spectral analysis

if there are a priori information on the source, or in case of interesting results with the "simple spectral analysis"

↑ In this case the "enhanced" analysis can be done using the information obtained with the "simple" analysis

(e.g. (source position, frequency
frequency decreasing, if observed)

Aim: increase the spectral resolution in the interesting sub-bands

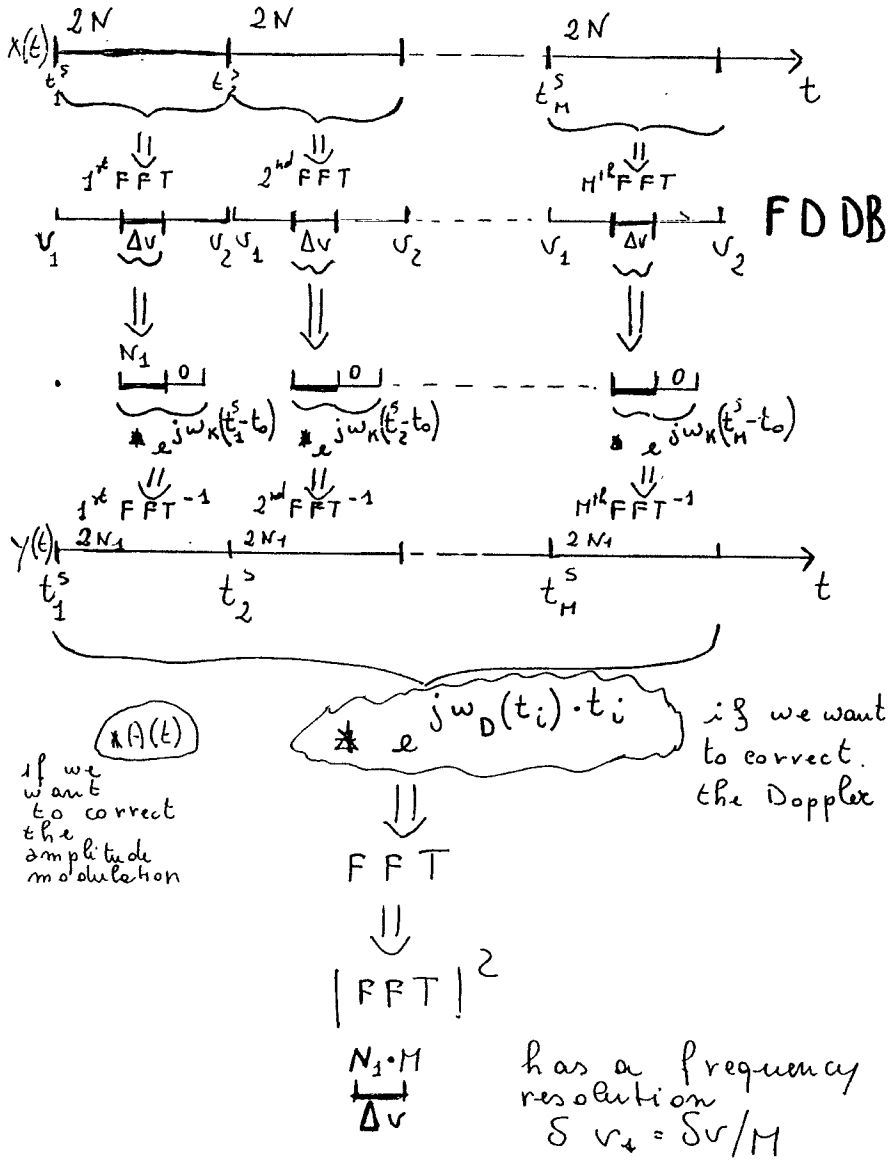

$\nu_1 = 900\,Hz$; $\nu_2 = 927.5\,Hz$; $\delta t = 18.18\,ms$; $\delta\nu = 0.4\,mHz$

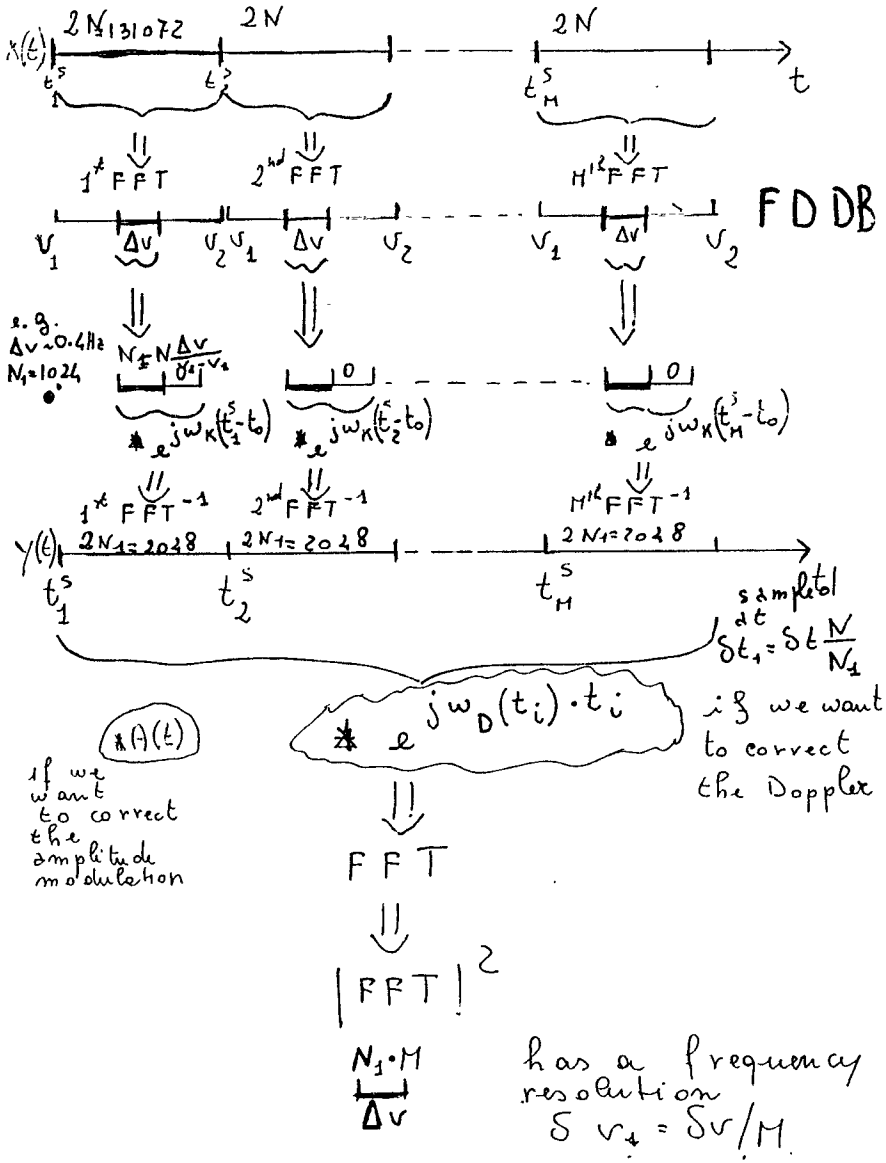

GW Pulsar Searches

T. Creighton, P. Brady, B. Schutz,
C. Cutler

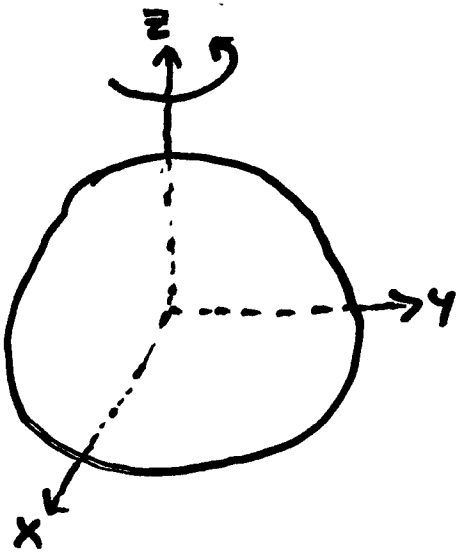

$$h = 2.1 \times 10^{-24} \frac{\varepsilon}{10^{-5}} \frac{I_{zz}}{10^{45}\ g\text{-}cm^2} \frac{10\ kpc}{r} \left(\frac{f_o}{1\ kHz}\right)^2$$

w/ $\varepsilon \equiv \dfrac{I_{xx} - I_{yy}}{I_{zz}}$

Neutron Stars

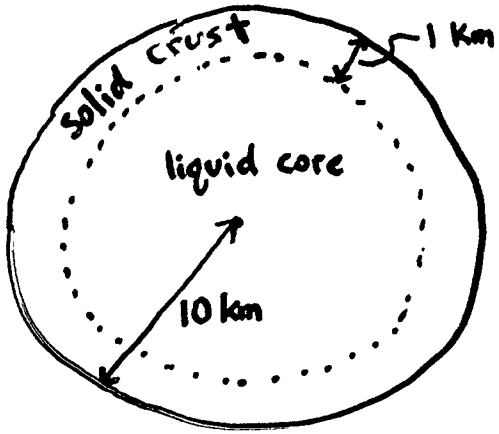

$\rho_{trans} = 2 \times 10^{14} \frac{g}{cm^3}$

$\frac{I_{solid}}{I_{total}} = 5\text{-}10\,\%$

Crust:

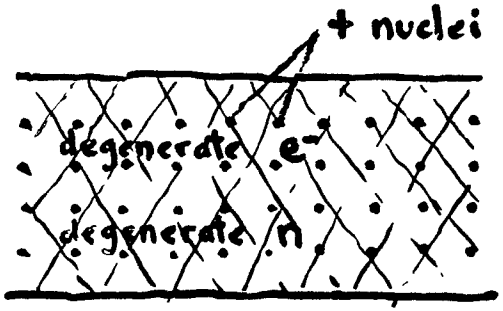

$\frac{\text{shear modulus}}{\text{bulk modulus}} \sim 10^{-2}$ "jello"

Rough Estimate of ε_{max}

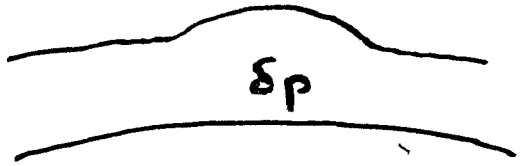

$$\delta\rho \sim \underbrace{\mu}_{\text{shear modulus}} \overbrace{\sigma}^{\text{strain}}$$

$$\delta\rho \sim \frac{\rho}{\bar{\rho}}\delta\rho \sim \rho\frac{\mu}{\bar{\rho}}\sigma$$

$$\Rightarrow \delta I \sim \int_{\text{crust}} \delta\rho\, r^2\, dV \sim \frac{\mu}{\bar{\rho}}\sigma \overbrace{\int_{\text{crust}} \rho\, r^2\, dV}^{I_{solid}}$$

$$\Rightarrow \varepsilon_{max} \sim \underbrace{\left(\frac{\mu}{\bar{\rho}}\right)}_{10^{-2}} \underbrace{\frac{I_{solid}}{I}}_{10^{-1}} \underbrace{\sigma_{max}}_{10^{-2}} \sim 10^{-5}$$

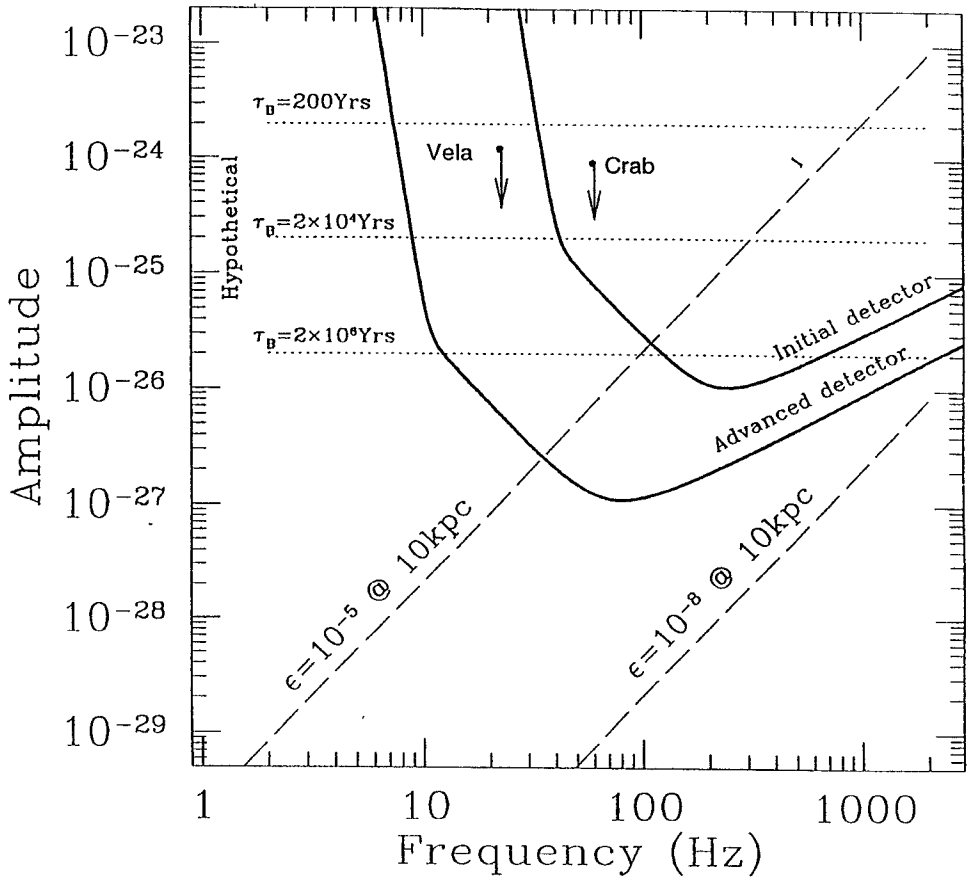

My Best Bet: Look for younger brothers of the Crab pulsar.

Type II SN rate $\approx \frac{1}{40\ \text{yrs}}$

⇒ Our galaxy has ~ 25 NS's younger than the Crab, but we don't know where they are or what spin periods they have!

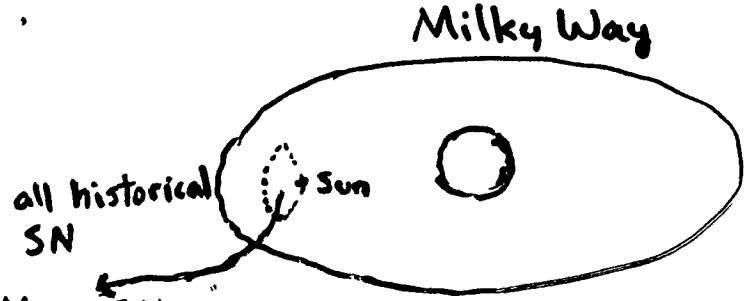

Yr	SN
1006	G327.6+14.6
1054	Crab
1181	3C58
1572	Tycho
1604	Kepler

If detector weren't on moving, spinning Earth & if NS weren't slowing down, then

$$h(t) = \sin(f_0 t)$$

⇒ just FFT the data stream.

But in reality

$$f_{GW}(t) = f_0\left(1 + \sum_k f_k t^k\right)\left(1 + \frac{\vec{v}\cdot\hat{n}}{c}\right)$$

$f_k \sim \left(\frac{1}{T_{pulsar}}\right)^k$; $\sim 10^{-2}$ for 1 year obs.

$\frac{\vec{v}\cdot\hat{n}}{c}$: $\sim 10^{-6}$ for rotati… ; $\sim 10^{-4}$ for orbit…

$f_0 \cdot (1\ \text{Yr}) \sim 10^{10}$ cycles

Given set of params $(f_1, .., f_n, \theta, \phi)$, we stretch the data: $t \to t'$

$$t' = \int_0^t \left(1 + \sum_k f_k t^k\right)\left(1 + \frac{\vec{v}\cdot\hat{n}}{c}\right) dt$$

and FFT the stretched data.

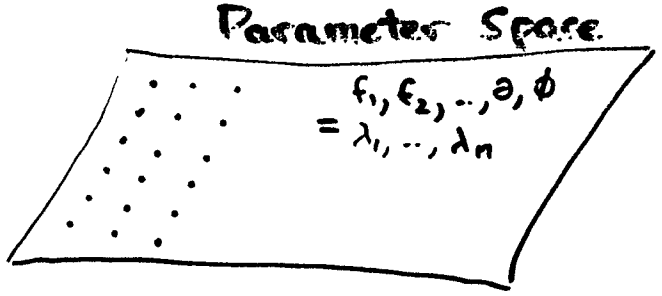

There's a natural metric g_{ab} on this param. space. It's meaning is, if template params are $(\lambda_1, .., \lambda_n)$ & true params are $(\lambda_1 + \Delta\lambda_1, .., \lambda_n + \Delta\lambda_n)$ then

$$(\%\ \text{lost } S/N) = \sum_{i,j} g_{ij}\, \Delta\lambda^i\, \Delta\lambda^j$$

$$\#\ \text{templates} \equiv N_p \sim \int \sqrt{g}\, dV$$

Each FFT requires $N \log_2 N$ operations with

$$N = f_{max}\, T_{obs}$$

$\Rightarrow$ Total # of operations

$$\sim N_p\, N \log_2 N$$

$$N_p(\tau_{pulsar}, T_{obs}, f_{max})$$

$$\text{Computing power} \sim \frac{N_p\, N \log N}{T_{obs}}$$

$$\Rightarrow T_{obs} = T_{obs}\left(\begin{matrix}\text{computing} \\ \text{power}\end{matrix}, \tau_{pulsar}, f_{max}\right)$$

Known Source Position

$f_{max} = 10^3$ Hz
$\tau_p \geq 40$ yr

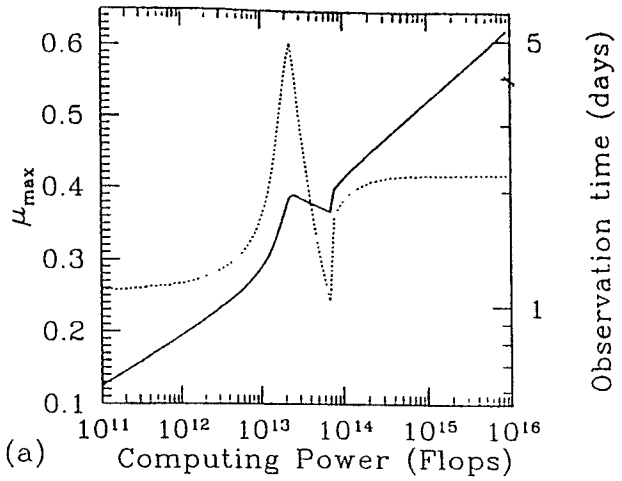

$f_{max} = 200$ Hz
$\tau_p \geq 10^3$ yr

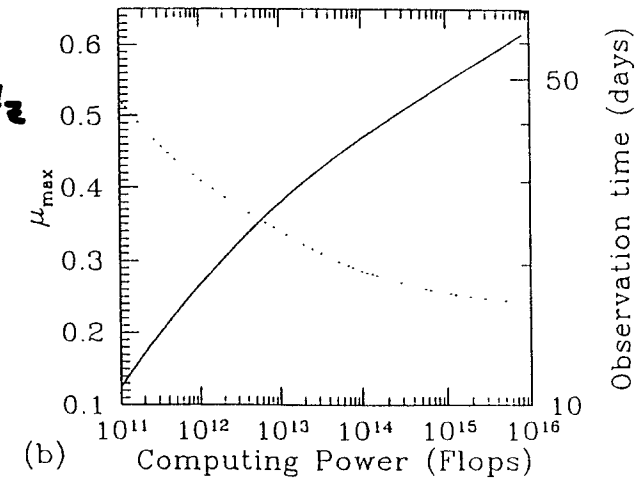

$f_{max} = 10^3$ Hz
$\tau_p \geq 40$ yr

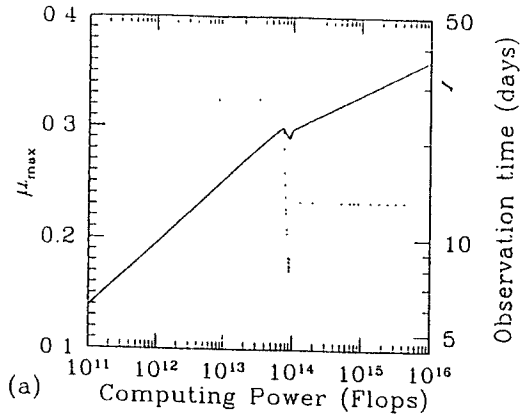

$f_{max} = 200$ Hz
$\tau_p \geq 10^3$ yr

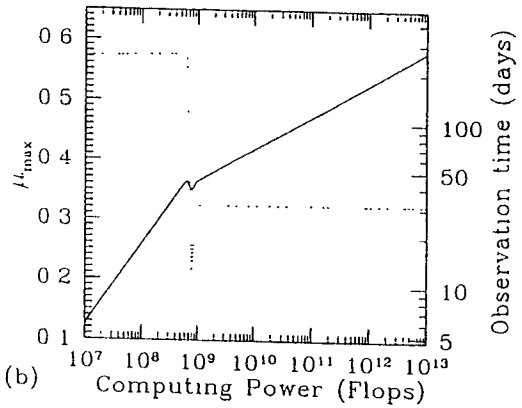

FIG. 8. The optimum observation time (thick solid line), and maximal mismatch (dotted line) as functions of available computational power for directed searches. Both graphs assume an overall statistical significance of 99% in the threshold (although the results are insensitive to the precise value). Each of the graphs

Hierarchical Search...

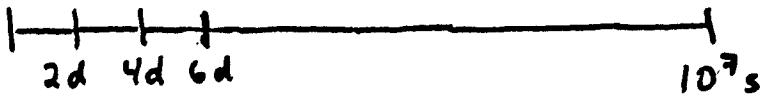

Search ~2d at a time, look for "suspects".

Probably need $S/N \sim 2\text{-}3$ in 2d.

$$\Rightarrow S/N \sim (2\text{-}3)\left(\frac{10^7 s}{2d}\right)^{1/2}$$

$$\sim 15\text{-}20 \text{ in } 10^7 s$$

With ∞ computing power, would still need $S/N \sim 8\text{-}10$ in 10^7s.

Friday PM — Signal Processing and Data Analysis of Existing and Future Data II
January 31 — Chair: M. Cerdonio

4:30	S. Finn(Northwestern)	Report on GWDAW Meeting
4:55	Discussion	
5:05	B. Allen(Caltech)	GRASP(Gravitational Radiation Analysis and Simulation Package)
5:30	Discussion	
6:00	Coffee Break	
6:15	P. Brady(Caltech)	Continuous Wave Sources: Hierarchical Searches and Stepping
6:40	Discussion	
6:50	M. Cerdonio(Padova)	(Almost) Isotropic Sky Coverage for GW Bursts of the Upcoming World Network of Interferometric and Bar Detectors
7:15	Discussion	

BRUCE ALLEN

Contents

4 GRASP Routines: Reading/using Caltech 40-meter prototype data

There is a good archive of data from the Caltech 40-meter prototype interferometer. Although the interferometer is only sensitive enough to detect events like binary inspiral within $\approx$ 10kpc (the distance to the galactic center) its output is nevertheless very useful in studying data analysis algorithms on real-world interferometer noise. This data was taken during the period from 1993 to 1996; for our purposes here we will concentrate on data taken during a one-week long observation run from November 14-21, 1994. The original data is contained on 11 exabyte tapes with about 46 total hours of data; the instrument was in lock about 88% of the time. The details of this run, the status of the instrument, and the properties of this data are well-described in theses by Gillespe [11] and Lyons [12].

The GRASP package includes routines for reading this data. The data is not read directly from the tapes themselves; the data instead must be read off the tapes and put onto disk (or into pipes) using a program called `extract`. The GRASP routines can then be used to read the resulting files. While the GRASP routines can be used without any further understanding of the data format, it is very helpful to understand this in more detail. Note that these data formats and the associated structures were defined years before GRASP was written; we did not choose this data format and should not be held accountable for its shortcomings.

4.1 The data format

Data is written onto the exabyte tapes in blocks about 1/2 megabyte in size. The format of the data on the tapes is as shown in Table 4.1. The tape begins with a main header (denoted "mh" in

mh	0's	0's	mh	0's	0's	mh	gh	0's	data	mh	gh	0's	data	···
1024		1024	1024		1024	1024			1024 × n	1024			1024 × n	···

Table 2: Format of Exabyte data tapes (first row: content, second row: length in bytes).

the table). This is followed by a set of zeros, padding the length of the header block to 1024 bytes. There is then an empty block of 1024 bytes containing zeros. This pattern is repeated until the first block containing actual data. This is signaled by the appearance of a main header, followed by a gravity header (denoted "gh" in the figure above). These two headers are padded with zeros to a length of 1024 bytes. This is then followed by a set of data (the length of this set is a multiple of 1024 bytes). Information about the length of the data sets is contained in the headers The data sets themselves consist of data from a total of 16 channels, each of which comes from a 12-bit A to D converter. Four of the 16 channels are fast (sample rates a bit slower than 10kHz) and the remaining 12 channels are slow (sample rates a bit slower than 1kHz). The ratio of sample rates is exactly 10 : 1. Within the blocks labeled "data", these samples are interleaved. The information content of the different channels is detailed on page 136 of Lyon's thesis [12], and is summarized in Table 4.1.

The program `extract` reads data off the tapes and writes them into files. One file is produced for each channel; typically these files are named `channel.0` → `channel.15`. The complete set of these files for the November 1994 run fits onto two Exabyte tapes (in the 8500c compressed format). The information in these files begins only at the moment when the useful data (starting with the gravity header blocks) begins to arrive. The format of the data in these `channel.*` files is shown in Table 4.1. Here the main headers are the same as before, however the headers that follow them

Channel Number	Description ≤ 14 November 94	Description ≥ 18 November 94
0	IFO output	IFO output
1	unused	magnetometer
2	unused	microphone
3	microphone	unused
4	dc strain	dc strain
5	mode cleaner pzt	mode cleaner pzt
6	seismometer	seismometer
7	unused	slow pzt
8	unused	power stabilizer
9	unused	unused
10	TTL locked	TTL locked
11	arm 1 visibility	arm 1 visibility
12	arm 2 visibility	arm 2 visibility
13	mode cleaner visibility	mode cleaner visibility
14	slow pzt	unused
15	arm 1 coil driver	arm 1 coil driver

Table 4: Channel assignments for the November 1994 data runs. Channels 0-3 are the "fast" channels, sampled at about 10 kHz; the remaining twelve are the "slow" channels, sampled at about 1KHz.

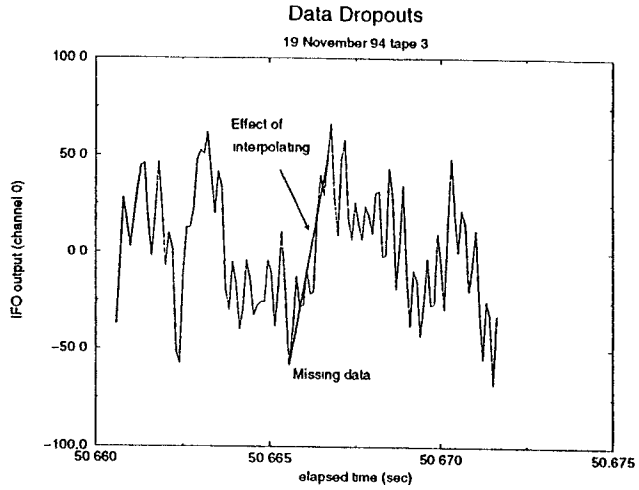

Figure 15: This shows the appearance of `channel.0` before and after the `extract` program was repaired (on 14 November 1996) to correctly extract data from the Exabyte data tapes. The old version of `extract` dropped the ten data points directly above the words "missing data"; in effect these were interpolated by the diagonal line (but with ten times the slope shown since everything in between was missing)

4.8 Example: animate program

This example uses the function `get_data()` described in the previous section to produce an animated display showing the time series output of the IFO in a lower window, and a simultaneously calculated FFT power spectrum in the upper window. This output from this program must be piped into a public domain graphing program called `xmgr`. This may be obtained from `ftp://ftp.teleport.com/pub/users/pturner/acegr`. Some sample output of `animate` is shown in Figure 16.

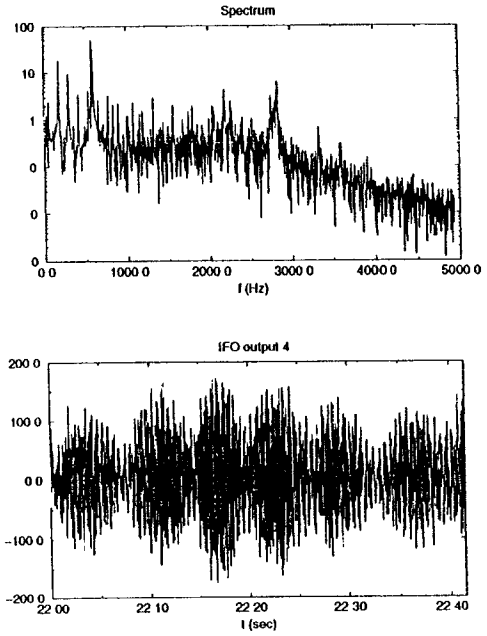

Figure 16: Snapshot of output from `animate`. This shows the (whitened) CIT 40-meter IFO a few seconds after acquiring lock, before the violin modes have damped down

After compilation, to run the program type:

```
animate | xmgr -pipe &
```

to get an animated display showing the data flowing by and the power spectrum changing, starting from the first locked data. You can also use this program with command-line arguments, for example

```
animate 100 4 500 7 900 1.5 | xmgr -pipe &
```

will show the data from time $t = 100$ to time $t = 104$ seconds, then from $t = 500$ to $t = 507$, then from $t = 900$ to $t = 901\ 5$. Notice that the sequence of start times must be increasing

4.12 Function: `normalize_gw()`

- `void normalize_gw(char *fname,int npoint,float srate,float *response)`

This routine generates an array of complex numbers $R(f)$ from the information in the swept sine file and an overall calibration constant. Multiplying this array of complex numbers by (the FFT of) `channel.0` yields the (FFT of the) differential displacement of the interferometer arms Δl, in meters: $\widetilde{\Delta l}(f) = R(f)\widetilde{C_0}(f)$. The units of $R(f)$ are meters/ADC-count.

The arguments are:

`fname`: Input. The name of the file in which the swept sine normalization data can be found.

`npoint`: Input. The number of points N of `channel.0` which will be used to calculate an FFT for normalization. Must be an integer power of 2.

`srate`: Input. The sample rate in Hz of `channel.0`.

`response`: Output. Pointer to an array `response[0..s]` with $s = N + 1$ in which $R(f)$ will be returned. By convention, $R(0) = 0$ so that `response[0]=response[1]=0`. Array elements `response[2i]` and `response[2i+1]` contain the real and imaginary parts of $R(f)$ at frequency $f =$ `israte`$/N$. The response at the Nyquist frequency `response[N]=0` and `response[N+1]=0` by convention.

The absolute normalization of the interferometer can be obtained from the information in the swept sine file, and one other normalization constant which we denote by Q. It is easy to understand how this works. In the calibration process, one of the interferometer end mirrors of mass m is driven by a magnetic coil. The equation of motion of the driven end mass is

$$m\frac{d^2}{dt^2}\Delta l = F(t) \tag{4.12.1}$$

where $F(t)$ is the driving force and Δl is the differential length of the two interferometer arms, in meters. Since the driving force $d(t)$ is proportional to the coil current and thus to the coil voltage, in frequency space this equation becomes

$$(-2\pi i f)^2\widetilde{\Delta l} = \text{constant} \times \tilde{V}_{\text{coil}} = \text{constant} \times \frac{\tilde{V}_{\text{IFO}}}{S^*(f)}. \tag{4.12.2}$$

We have substituted in equation (4 9 8) which relates $\tilde{V}_{\text{IFO}}$ and $\tilde{V}_{\text{coil}}$. The IFO voltage is directly proportional to the quantity recorded in `channel.0`: $V_{\text{IFO}} = \text{ADC} \times C_0$, with the constant ADC being the ratio of the analog-to-digital converters input voltage to output count.

Putting together these factors, the properly normalized value of Δl, in meters, may be obtained from the information in `channel.0`, the swept sine file, and the quantities given in Table 5 by

$$\widetilde{\Delta l} = R(f) \times \widetilde{C_0} \qquad \text{with} \quad R(f) = \frac{Q \times \text{ADC}}{-4\pi^2 f^2 S^*(f)}, \tag{4.12.3}$$

where the $\tilde{}$ denotes Fourier transform, and f denotes frequency in Hz. (Note that, apart from the complex conjugate on S, the conventions used in the Fourier transform drop out of this equation, provided that identical conventions (4.9 3,4.9 4) are applied to both Δl and to C_0). The constant quantity Q indicated in the above equations has been calculated and documented in a series of calibration experiments carried out by Robert Spero. In these calibration experiments, the interferometer's servo was left open-loop, and the end mass was driven at a single frequency, hard

Table 5: Quantities entering into normalization of the IFO output.

Description	Name	Value	Units
Gravity-wave signal (`channel.0`)	C_0	varies	ADC counts
A→D converter sensitivity	ADC	10/2048	$V_{IFO}\,(\text{ADC counts})^{-1}$
Swept sine calibration	S(f)	from file	$V_{IFO}\,(V_{coil})^{-1}$
Calibration constant	Q	1.428×10^{-4}	meter $Hz^2\,(V_{coil})^{-1}$

enough to move the end mass one-half wavelength and shift the interferences fringes pattern over by one fringe. In this way, the coil voltage required to bring about a given length motion at a particular frequency was established, and from this information, the value of Q may be inferred. During the November 1994 runs the value of Q was given by

$$Q = \frac{\sqrt{9.35\ \text{Hz}}}{k} = 1.428 \times 10^{-4} \frac{\text{meter Hz}^2}{V_{coil}} \qquad \text{where } k = 21399 \frac{V_{coil}}{\text{meter Hz}^{3/2}}. \tag{4.12.4}$$

4.13 Example: `power_spectrum` program

This example uses the function `normalize_gw()` to produce a normalized, properly calibrated power spectrum of the interferometer noise, using the gravity-wave signal from `channel.0`, the TTL-lock signal from `channel.10` and a swept-sine calibration curve.

The output of this program is a 2-column file; the first column is frequency and the second column is the noise in units of meters/$\sqrt{\text{Hz}}$.

A couple of comments are in order here:

1. Even though we only need the squared modulus, for pedagogic reasons, we explicitly calculate both the real and imaginary parts of $\widetilde{\Delta l}(f) = R(f)\widetilde{C}_0(f)$.

2. The fast Fourier transform of Δl, which we denote FFT[Δl], has the same units (meters!) as Δl. As can be immediately seen from *Numerical Recipes* equation (12.1.6) the Fourier transform $\widetilde{\Delta l}$ has units of meters-sec and is given by $\widetilde{\Delta l} = \Delta t\ \text{FFT}[\Delta l]$, where Δt is the sample interval. The (one-sided) power spectrum of Δl in meters/$\sqrt{\text{Hz}}$ is $P = \sqrt{\frac{2}{T}}\widetilde{\Delta l}$ where $T = N\Delta t$ is the total length of the observation interval, in seconds. Hence one has

$$P = \sqrt{\frac{2}{N\Delta t}}\,\Delta t\ \text{FFT}[\Delta l] = \sqrt{\frac{2\Delta t}{N}}\ \text{FFT}[\Delta l]. \tag{4.13.1}$$

   This is the reason for the factor which appears in this example.

3 To get a spectrum with decent frequency resolution, the time-domain data must be windowed (see the example program `calibrate` and the function `avg_spec()` to see how this works).

A sample of the output from this program is shown in Figure 18.

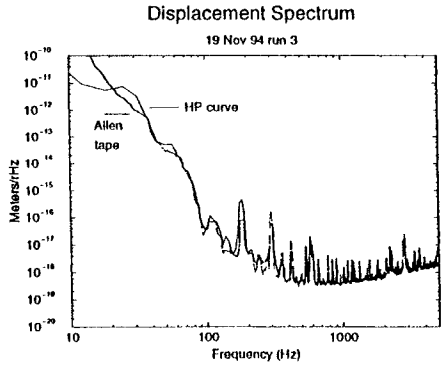

Figure 18: An example of a power spectrum curve produced with `power_spectrum`. The spectrum produced off a data tape (with 100 point smoothing) is compared to that produced by the HP spectrum analyzer in the lab

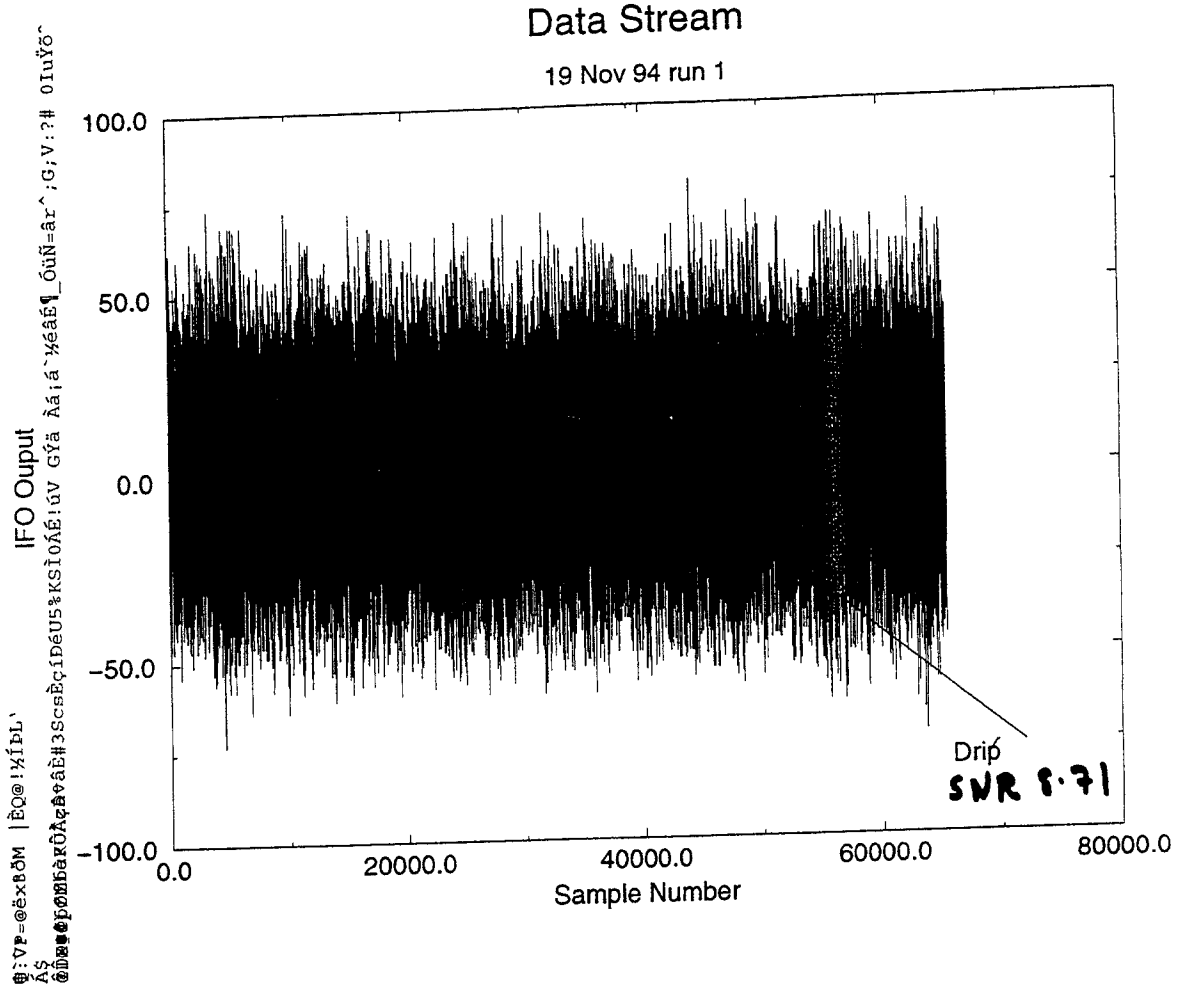
Data Stream
19 Nov 94 run 1
IFO Ouput
100.0
50.0
0.0
−50.0
−100.0
0.0
20000.0
40000.0
60000.0
80000.0
Sample Number
Drip
SNR 8.71

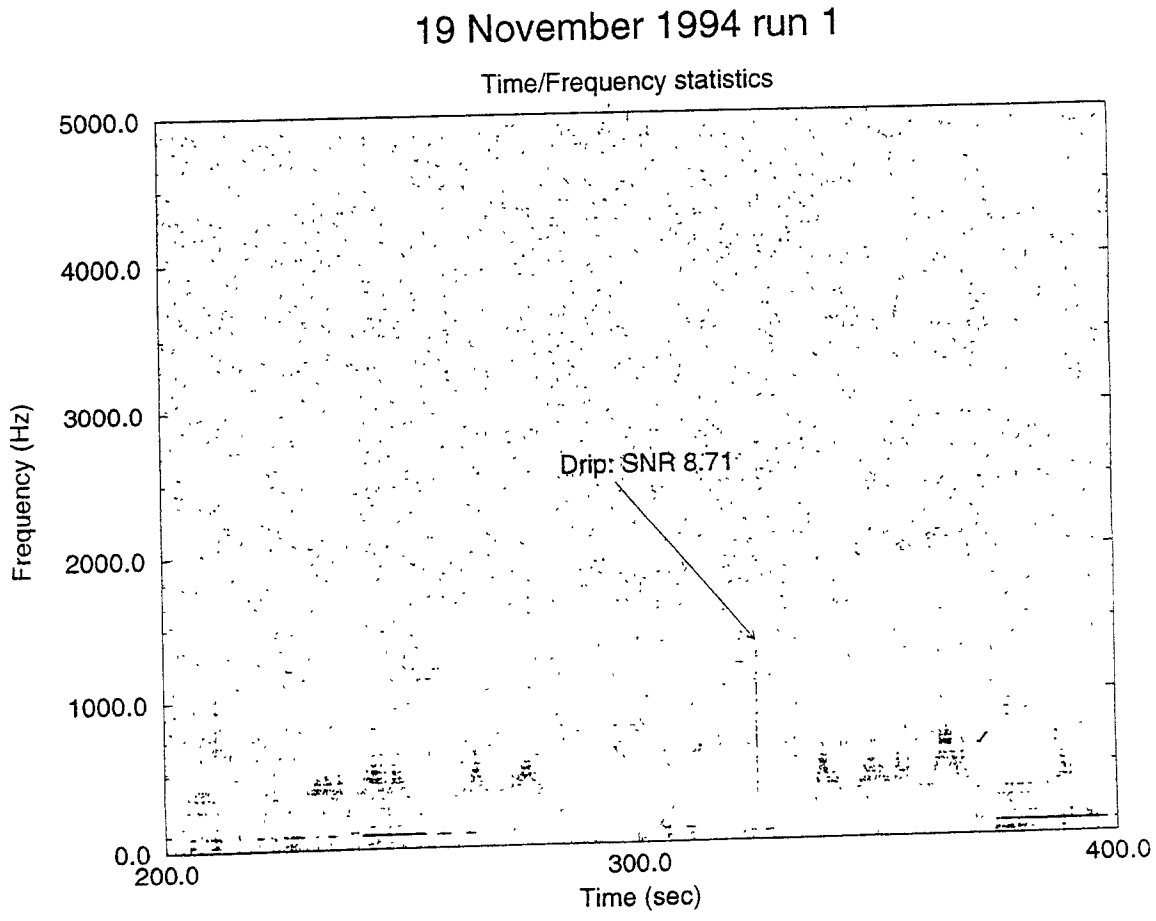
19 November 1994 run 1
Time/Frequency statistics
Frequency (Hz)
5000.0
4000.0
3000.0
2000.0
1000.0
0.0
200.0
300.0
400.0
Time (sec)
Drip: SNR 8.71

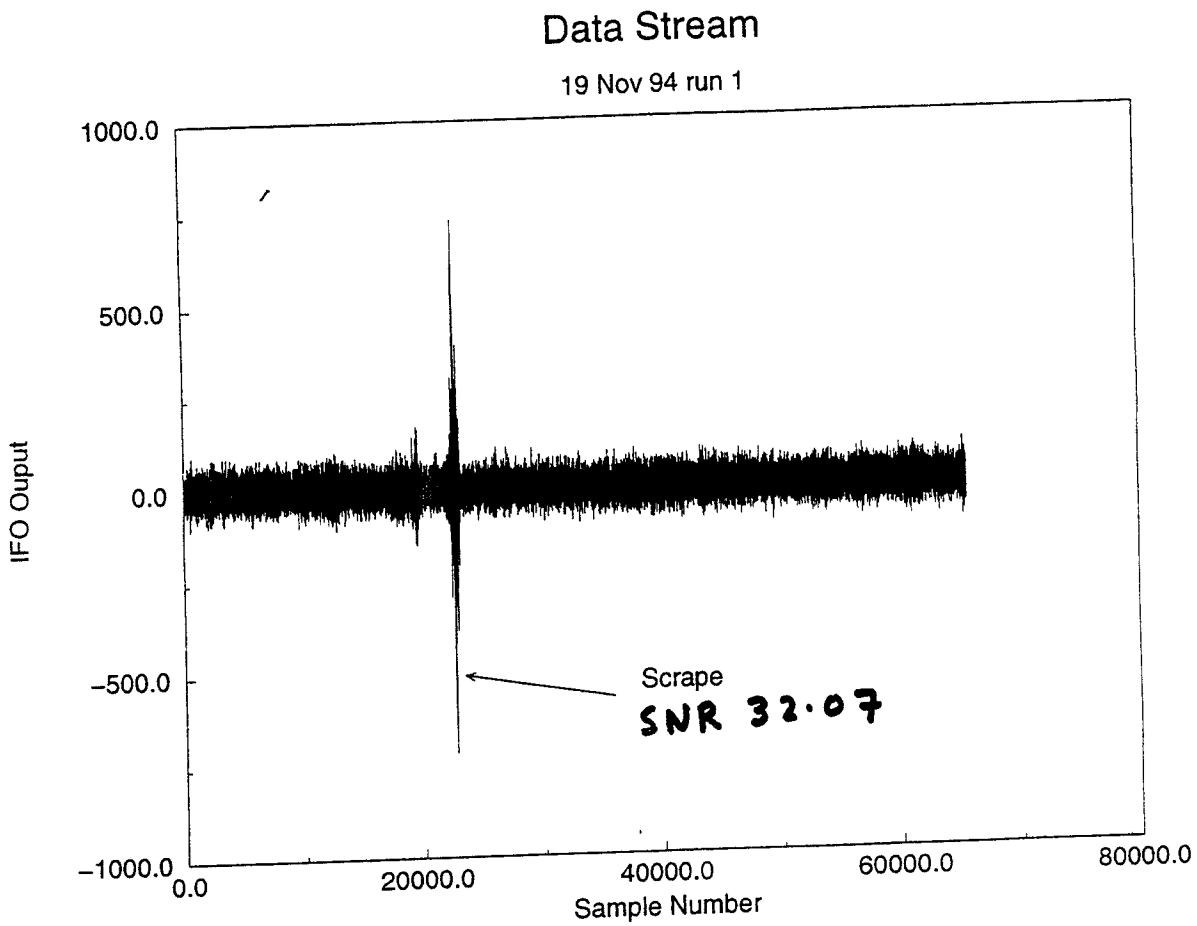
Data Stream
19 Nov 94 run 1
1000.0
500.0
0.0
-500.0
-1000.0
IFO Ouput
0.0
20000.0
40000.0
60000.0
80000.0
Sample Number
Scrape
SNR 32.07

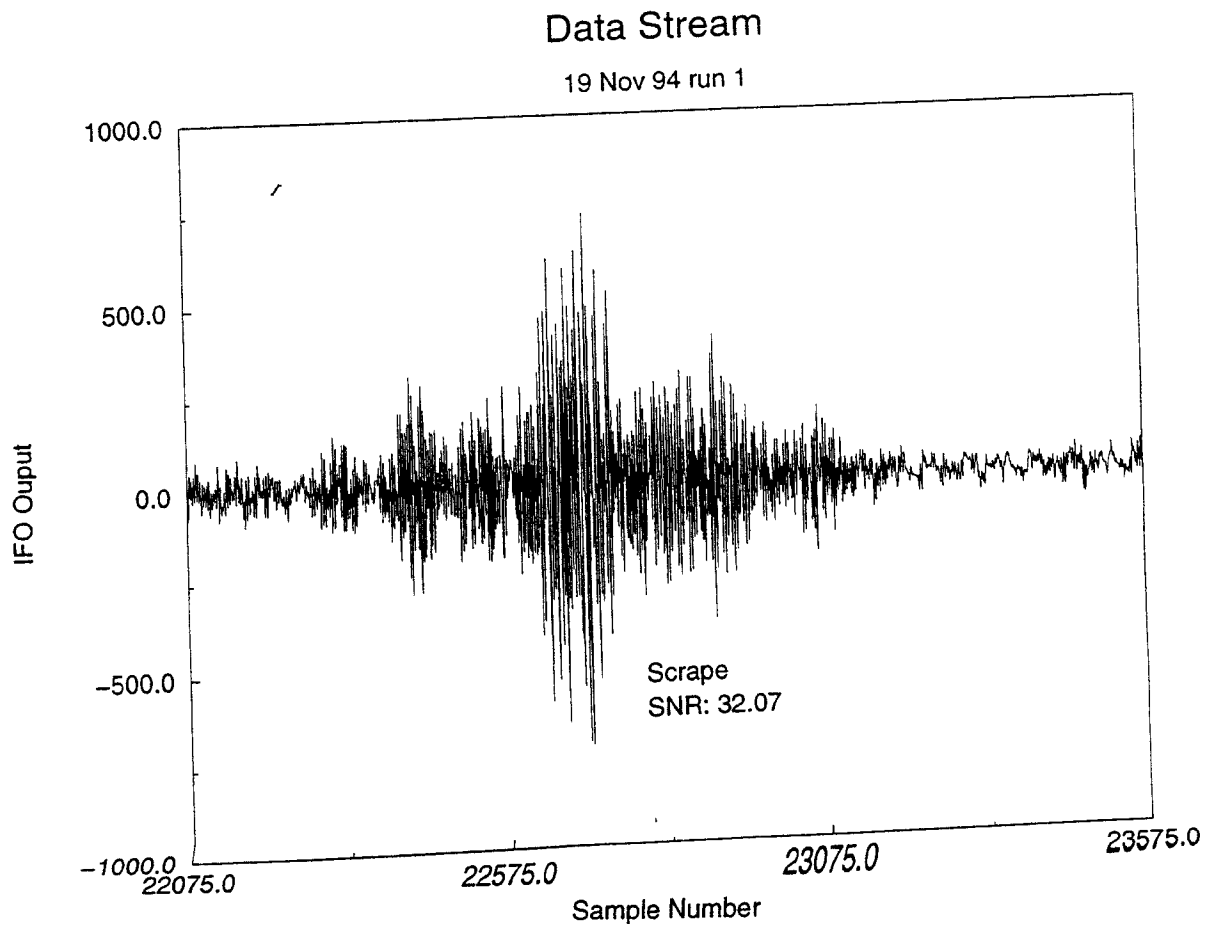
Data Stream
19 Nov 94 run 1
1000.0
500.0
0.0
-500.0
-1000.0
IFO Ouput
22075.0
22575.0
23075.0
23575.0
Sample Number
Scrape
SNR: 32.07

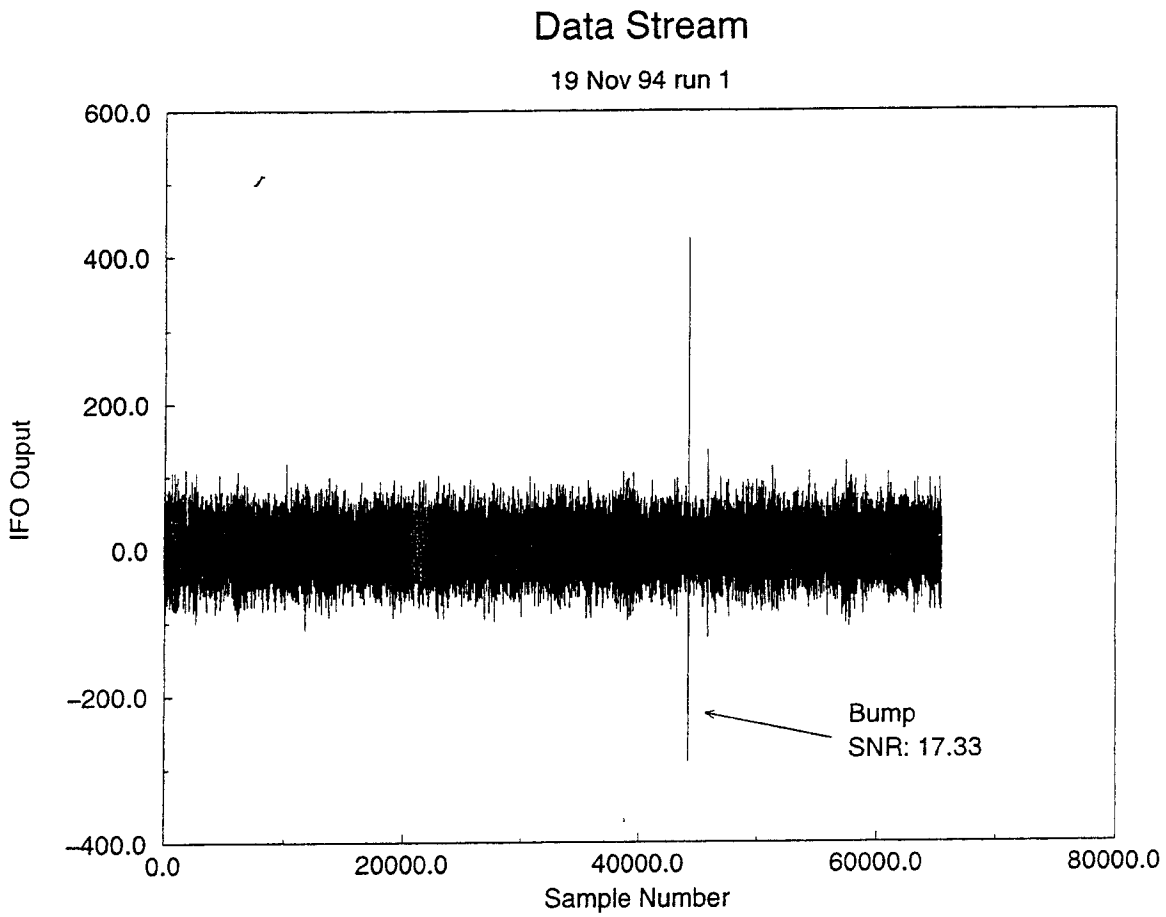
Data Stream
19 Nov 94 run 1
600.0
400.0
200.0
0.0
-200.0
-400.0
IFO Ouput
0.0
20000.0
40000.0
60000.0
80000.0
Sample Number
Bump
SNR: 17.33

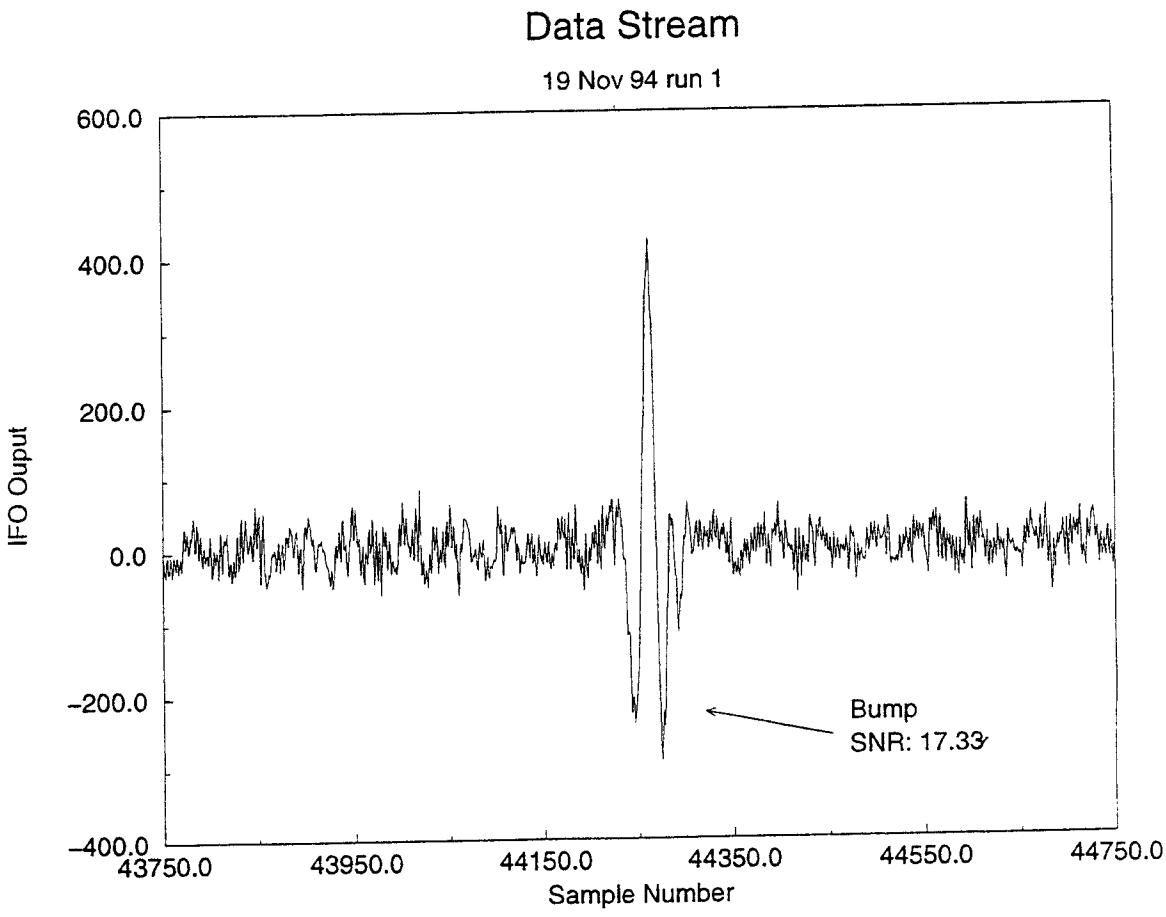
Data Stream
19 Nov 94 run 1
600.0
400.0
200.0
0.0
-200.0
-400.0
IFO Ouput
43750.0
43950.0
44150.0
44350.0
44550.0
44750.0
Sample Number
Bump
SNR: 17.33

3.30 Vetoing techniques

In an ideal world, the output of an interferometer would be a stationary signal described by Gaussian statistics (with very rare superposed binary inspiral chirps and other gravitational-wave signals). This is unfortunately not the case, as can be quickly determined by simply listening to the raw (whitened) interferometer output. Typically the output is a stationary-sounding hiss, interupted every few minutes by an obvious irregularity in the data stream These are typically "pops", "bumps", "clicks", "howlers", "scrapers" and other recognizable categories of noises. In at least some cases, there are "suspects" for these events. For example the pops and bumps might be problems in any of the hundreds of BNC cable connectors used in the instrument.

It is an unfortunate fact that the output of an optimal filter strongly reflects these events. As you have seen in the previous section, a delta-function-like impulse signal in the IFO ouput can cause a large signal in the optimal filter. And in practice, this happens all of the time - the outputs of optimal chirp filters are frequently triggered by identifiable events in the IFO data stream that are clearly not binary inspiral chirps. Distinguishing these events from real inspiral chirps is called *vetoing* We have found that two vetoing techniques work particularly well.

The first technique operates in the time domain, and is documented in the routine `is_gaussian()`. The idea is straightforward: if a chirp detector (optimal filter) is triggered, then we look in the data stream for an impulse event that might be responsible. Such events can be found by looking at the statistical distribution of the points in the time domain. If this distribution is significantly non-Gaussian then it indicates that some large transient event caused the filter to trigger, and the event is rejected.

The second technique is described here, and operates in the frequency domain It is a very stringent test, which determines if the hypothetical chirp which has been found in the data stream is consistent with a true binary inspiral chirp summed with Gaussian interferometer noise. If this is true, it should be possible to subtract the (best fit) chirp from the signal, and be left with a signal stream that is consistent with Gaussian IFO noise. One of the nice features of this technique is that it can be statistically characterized in a rigorous way.

Suppose that one of our optimal chirp filters $\tilde{Q}$ is triggered with a large SNR at time t_0. We will denote the signal value at this time by S:

Signal:

$$S = \int_{-f_{Ny}}^{f_{Ny}} df\, \frac{\tilde{h}(f)\tilde{T}^*(f)}{S_h(|f|)}\, e^{-2\pi i f t_0}. \tag{3.30.1}$$

(Here, f_{Ny} denotes the Nyqist frequency, one-half of the sampling rate) The chirp template T is normalized so that the expected value $\langle N^2\rangle = 1$:

Filter Norm:

$$\int_0^{f_{Ny}} df\, \frac{|\tilde{T}(f)|^2}{S_h(|f|)} = 1. \tag{3.30.2}$$

We are going to investigate if this signal is "really" due to a chirp by investigating the way in which S gets its contribution from different ranges of frequencies. To do this, break up the integration region in this integral into a set of p disjoint subintervals $\Delta f_1, \cdots, \Delta f_p$ whose union is the entire range of frequencies from DC to Nyquist. Here p is a small integer (for example, $p = 8$). This splitup can be performed using the GRASP function `splitup()`. The frequency intervals:

Freq Intervals:

$$\begin{aligned} \Delta f_1 &= \{f \mid 0 < f < f_1\} \\ \Delta f_2 &= \{f \mid f_1 < f < f_2\} \\ &\cdots \\ \Delta f_p &= \{f \mid f_{p-1} < f < f_{Ny}\}, \end{aligned} \tag{3.30.3}$$

are defined by the condition that the *expected signal contributions in each frequency band from a chirp are equal*:

defined by:

$$\int_{\Delta f_i} df\, \frac{|\tilde{T}(f)|^2}{S_h(|f|)} = \frac{1}{p}\int_0^{f_{Ny}} df\, \frac{|\tilde{T}(f)|^2}{S_h(|f|)} \tag{3.30.4}$$

Because the filter is optimal, this also means that the expected noise contributions in each band from the chirp is the same. The frequency subintervals Δf_i are fairly narrow in regions of frequency space where the interferometer is quiet, and they are fairly wide in regions where the IFO is noisy.

Now, define a set of p signal values, one for each frequency interval:

Signal:

$$S_i = \int_{-\Delta f_i \cup \Delta f_i} df\, \frac{\tilde{h}(f)\tilde{T}^*(f)}{S_h(|f|)}\, e^{-2\pi i f t_0} \quad \text{for } i = 1, \cdots, p. \tag{3.30.5}$$

We have included both the positive and negative frequency subintervals to ensure that the S_i are real. If the detector output is Gaussian noise plus a true chirp, then the expected value of each of these signal values is $\langle S_i\rangle = S/p$. In this case the values of $\Delta S_i \equiv S_i - S/p$ are independent normal random variables with a mean value of zero and a variance σ determined by the expected value of the noise-squared. Because of our choice of template normalization this is:

$$\sigma = \langle \Delta S_i^2\rangle = \langle N^2\rangle/p = 1/p. \tag{3.30.6}$$

Hence, in the presence of a true chirp and interferometer noise, the probability distribution of the ΔS_i is given by

$$P(\Delta S_1, \cdots, \Delta S_p) = \prod_{i=1}^{p} (2\pi\sigma)^{-1/2} e^{-\Delta S_i^2/2\sigma} = (2\pi\sigma)^{-p/2} e^{-(\Delta S_1^2 + \cdots + \Delta S_p^2)/2\sigma}. \tag{3.30.7}$$

Thus, if our optimal chirp filter is triggered by an event, we can check the contributions to the signal in each of p frequency subintervals, to determine if the distribution of frequency and the arrival times in the p distinct subintervals is consistent with "chirp + Gaussian noise".

Because the ΔS_i are independent random variables with zero mean and variance $1/p$, the sum of their squares is described by a χ^2 probability distribution. Define the statistic

Statistic:

$$r^2 = \sum_{i=1}^{p} (\Delta S_i)^2. \tag{3.30.8}$$

Then one can easily compute the probability distribution of r. The probability that $r > R$ in the presence of a true chirp signal is

Prob:

$$\begin{aligned} P(r > R) &= (2\pi\sigma)^{-p/2}\Omega_{p-1}\int_R^\infty r^{N-1} e^{-r^2/2\sigma} dr && (3.30.9) \\ &= \frac{1}{\Gamma(p/2)}\int_{R^2/2\sigma}^\infty x^{p/2-1} e^{-x} dx && (3.30.10) \\ &= Q(p/2, R^2/2\sigma), && (3.30.11) \end{aligned}$$

where Ω_p is the $p-$volume of a unit-radius $p-$sphere S^p. The incomplete gamma function Q is the same function that describes the likelyhood function in the traditional χ^2 test.

In practice (based on CIT 40-meter data) breaking up the frequency range into $p = 8$ intervals provides a very reliable veto for rejecting events that trigger an optimal filter, but which are not themselves chirps. The value of $Q(4, 10.0) = 0.0103\cdots$ so if $r^2 > 25$ then one can conclude that the likelyhood that a given trigger is actually due to a chirp is less than 1%; rejecting or vetoing such events will only reduce the "true event" rate by 1% However in practice it eliminates almost all other events that trigger an optimal filter; a noisy event that stimulates a binary chirp filter typically has $r^2 \approx 100$ or larger!

3.35 Some output from the optimal program

Some output from the optimal program follows:

```
...
max snr: 3.11 offset: 23623 data start: 180.00 sec. variance: 0.94044
max snr: 2.91 offset: 3311 data start: 185.17 sec. variance: 0.84484
...
max snr: 2.53 offset: 19041 data start: 309.26 sec. variance: 0.70333
max snr: 2.98 offset: 35711 data start: 314.43 sec. variance: 0.67523

Max SNR: 8.71 (offset 42109) variance 0.805030
   If impulsive event, offset 55624 or time 325.23
   If inspiral, template start offset 42109 (time 323.86) coalescence time 325.23
   Normalization: S/N=1 at 116.75 kpc
   Linear combination of max SNR: 0.9315 x phase_0 + 0.3638 x phase_pi/2
   Less than 1% probability that this is a chirp (p=0.000000).
   Distribution: s= 23, N>3s= 12 (expect 176), N>5s= 0 (expect 0)
   Distribution does not appear to have outliers...

max snr: 2.51 offset: 31183 data start: 324.77 sec. variance: 0.63028
max snr: 2.56 offset: 49909 data start: 329.94 sec. variance: 0.66853
...
max snr: 2.82 offset: 35080 data start: 3002.03 sec. variance: 0.77306
max snr: 2.61 offset: 33141 data start: 3007.20 sec. variance: 0.74268

Max SNR: 89.75 (offset 16678) variance 82.547005
   If impulsive event, offset 30193 or time 3015.43
   If inspiral, template start offset 16678 (time 3014.06) coalescence time 3015.43
   Normalization: S/N=1 at 128.49 kpc
   Linear combination of max SNR: -0.3955 x phase_0 + 0.9185 x phase_pi/2
   Less than 1% probability that this is a chirp (p=0.000000).
   Distribution: s= 29, N>3s= 157 (expect 176), N>5s= 30 (expect 0)
   Distribution has outliers! Reject

max snr: 3.24 offset: 22412 data start: 3017.54 sec. variance: 0.99474
max snr: 2.73 offset: 37777 data start: 3022.71 sec. variance: 0.75325
...
max snr: 2.80 offset: 5893 data start: 4140.89 sec. variance: 0.73240
max snr: 2.75 offset: 46932 data start: 4146.06 sec. variance: 0.69654

Max SNR: 6.08 (offset 30002) variance 0.883380
   If impulsive event, offset 43517 or time 4155.64
   If inspiral, template start offset 30002 (time 4154.27) coalescence time 4155.64
   Normalization: S/N=1 at 113.04 kpc
   Linear combination of max SNR: -0.4773 x phase_0 + 0.8787 x phase_pi/2
   POSSIBLE CHIRP!  with > 1% probability (p=0.024142).
   Distribution: s= 31, N>3s= 399 (expect 176), N>5s= 53 (expect 0)
   Distribution has outliers! Reject
```



```
max snr: 2.77 offset: 15985 data start: 4156.40 sec. variance: 0.72095
max snr: 2.69 offset: 47338 data start: 4161.57 sec. variance: 0.69708
...
```

This output shows three events that triggered an optimal filtering routine. The first and second of these events were rejected for different reasons. The first was rejected because if failed the frequency-distribution test. The second was rejected because it had 30 outlier points. The third failed for the same reason: it had 53 outlier points.

Next, we show some output when a fake chirp signal is injected into the data stream. This can be done for example by modifying optimal to read:

```
invMpc_inject=100.0;   /* To inject a signal at 10 kpc, set this to 100.0 */
time_inject(1.0,0.0,12345,invMpc_inject,chirp0,chirp90,data,response,output0,npoint);
```

This produces the following output:

```
...
Max SNR: 9.96 (offset 12345) variance 0.872624
   If impulsive event, offset 25860 or time 187.79
   If inspiral, template start offset 12345 (time 186.42) coalescence time 187.79
   Normalization: S/N=1 at 152.17 kpc
   Linear combination of max SNR: 0.9995 x phase_0 + -0.0304 x phase_pi/2
   POSSIBLE CHIRP!  with > 1% probability (p=0.421294).
   Distribution: s= 23, N>3s= 12 (expect 176), N>5s= 0 (expect 0)
   Distribution does not appear to have outliers...


Max SNR: 12.84 (offset 12345) variance 0.834527
   If impulsive event, offset 25860 or time 192.96
   If inspiral, template start offset 12345 (time 191.59) coalescence time 192.96
   Normalization: S/N=1 at 132.47 kpc
   Linear combination of max SNR: 0.9953 x phase_0 + 0.0973 x phase_pi/2
   POSSIBLE CHIRP!  with > 1% probability (p=0.949737).
   Distribution: s= 22, N>3s= 28 (expect 176), N>5s= 0 (expect 0)
   Distribution does not appear to have outliers...


Max SNR: 14.86 (offset 12345) variance 0.801640
   If impulsive event, offset 25860 or time 198.13
   If inspiral, template start offset 12345 (time 196.76) coalescence time 198.13
   Normalization: S/N=1 at 127.90 kpc
   Linear combination of max SNR: 0.9993 x phase_0 + -0.0372 x phase_pi/2
   POSSIBLE CHIRP!  with > 1% probability (p=0.999236).
   Distribution: s= 22, N>3s= 35 (expect 176), N>5s= 0 (expect 0)
   Distribution does not appear to have outliers...
...
```

The code is correctly finding the chirps, getting the distance and phase and time location of the chirps about as accurately as one would expect given the level of the IFO noise.

PATRICK BRADY CALTECH

Continuous Wave sources:

Hierarchical searches & stepping

- Why the data analysis problem will be difficult.
- Brief review of parameter space
- Data analysis strategies
  - Brute force
  - Brute force including "stepping"
  - Hierarchical strategies
- What next ?

Teviet Creighton + PRB
Curt Cutler
Bernie Schutz.

Why will the data analysis be difficult ?

Answer comes in two parts:

1) Strain amplitude from a pulsar

$$h_{pulsar} \lesssim 2\times10^{-24} \frac{\varepsilon}{10^{-5}} \frac{10\,\text{kpc}}{r} \left(\frac{f_0}{1\text{kHz}}\right)^2$$

Well below detector noise floor. Hope for detection is long observation times.

For periodic signal, $s(t)$, $\ldots$ square of the signal to noise $\ldots$

$$E(SNR)^2 = \frac{|\tilde{s}(f_0)|^2}{E[|\tilde{n}(f_0)|^2]} \propto T_{obs}$$

2)

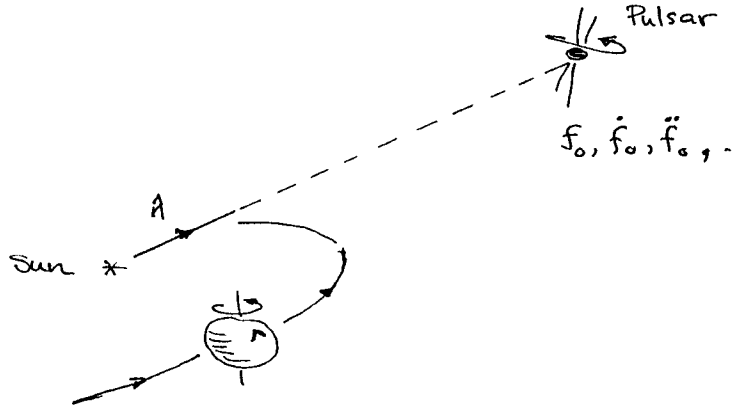

Long observation times ⇒ account for Doppler modulation

Initial & Advanced sensitivities : $T_{obs} = 10^7$ secs

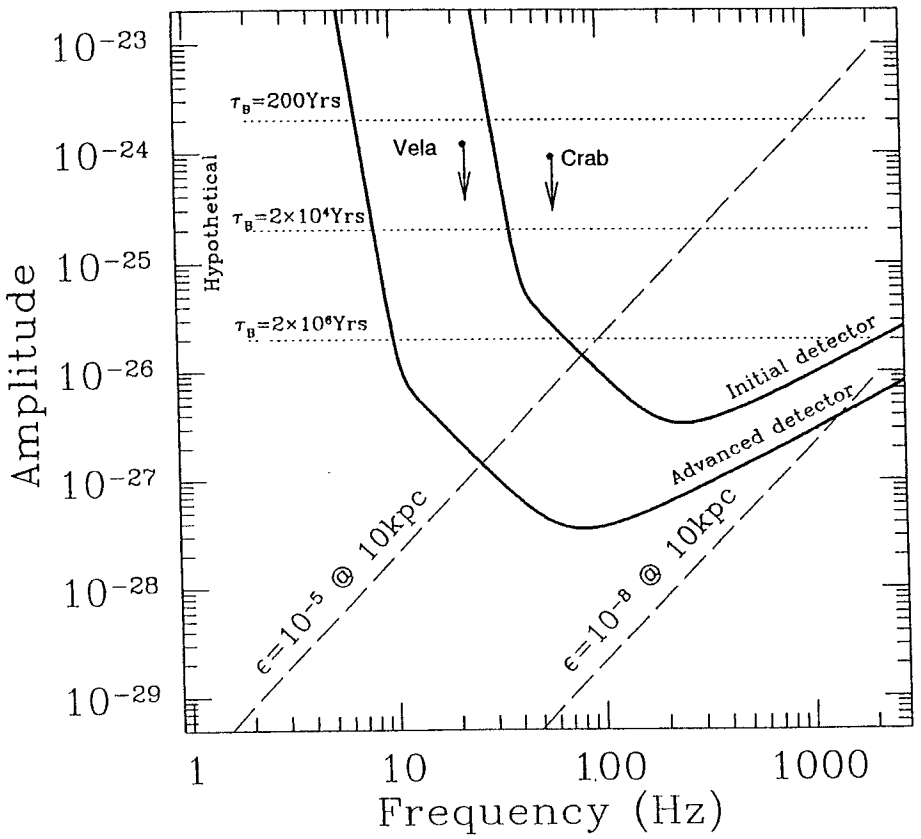

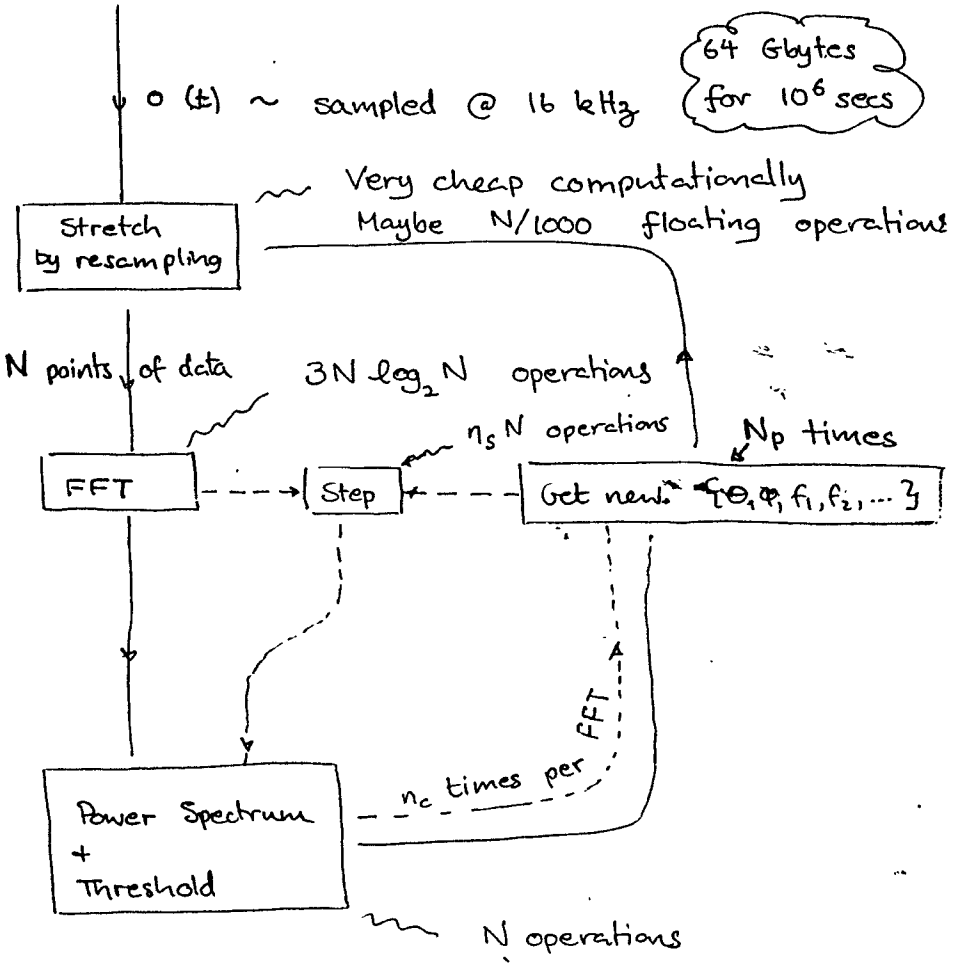

$$\frac{(\text{Cost})_{\text{brute force}}}{(\text{Cost})_{\text{stepping}}} \simeq \frac{N_p (3N \log_2 N + N)}{\frac{N_p}{n_c}(3N \log_2 N + n_c n_s N + (n_c+1)N}$$

$$\xrightarrow{n_c \to N_p} \sim \frac{3 \log_2 N + 1}{n_s + 1} \simeq \frac{90}{n_s+1}$$

What is stepping? (Bernard Schutz)

Suppose the vector $\underline{\underline{O}}$ represents total data to be analysed

$\{\Theta^{(1)}, \varphi^{(1)}, f_1^{(1)}, \ldots\}$ $\qquad$ $\{\Theta^{(2)}, \varphi^{(2)}, f_1^{(2)} \ldots\}$

↓

stretch $\qquad \underline{\underline{O}}^{(1)} = \underline{\underline{S}}^{(1)}\,\underline{\underline{O}}$ $\qquad$ $\underline{\underline{S}}^{(2)}\,\underline{\underline{O}}$

↓

FT $\qquad \tilde{\underline{\underline{O}}}^{(1)} = \underline{\underline{FT}} \cdot \underline{\underline{S}}^{(1)} \cdot \underline{\underline{O}}$ $\qquad$ $\tilde{\underline{\underline{O}}}^{(2)} = \underline{\underline{FT}} \cdot \underline{\underline{S}}^{(2)}\,\underline{\underline{O}}$

$$\tilde{\underline{\underline{O}}}^{(2)} = \left(\underline{\underline{FT}} \cdot \underline{\underline{S}}^{(2)} \cdot \underline{\underline{S}}^{-1} \cdot \underline{\underline{FT}}^{-1}\right) \tilde{\underline{\underline{O}}}^{(1)}$$

$$\boxed{\tilde{\underline{\underline{O}}}^{(2)} = \underline{\underline{\mathcal{G}}}^{21}\,\tilde{\underline{\underline{O}}}^{(1)}}$$

If $\underline{\underline{\mathcal{G}}}^{21}$ is nearly diagonal then going directly from $\tilde{\underline{\underline{O}}}^{(1)} \rightarrow \tilde{\underline{\underline{O}}}^{(2)}$ might be more efficient than going back to do a new FFT

Real part of one column of stepping kernel for 3 days.

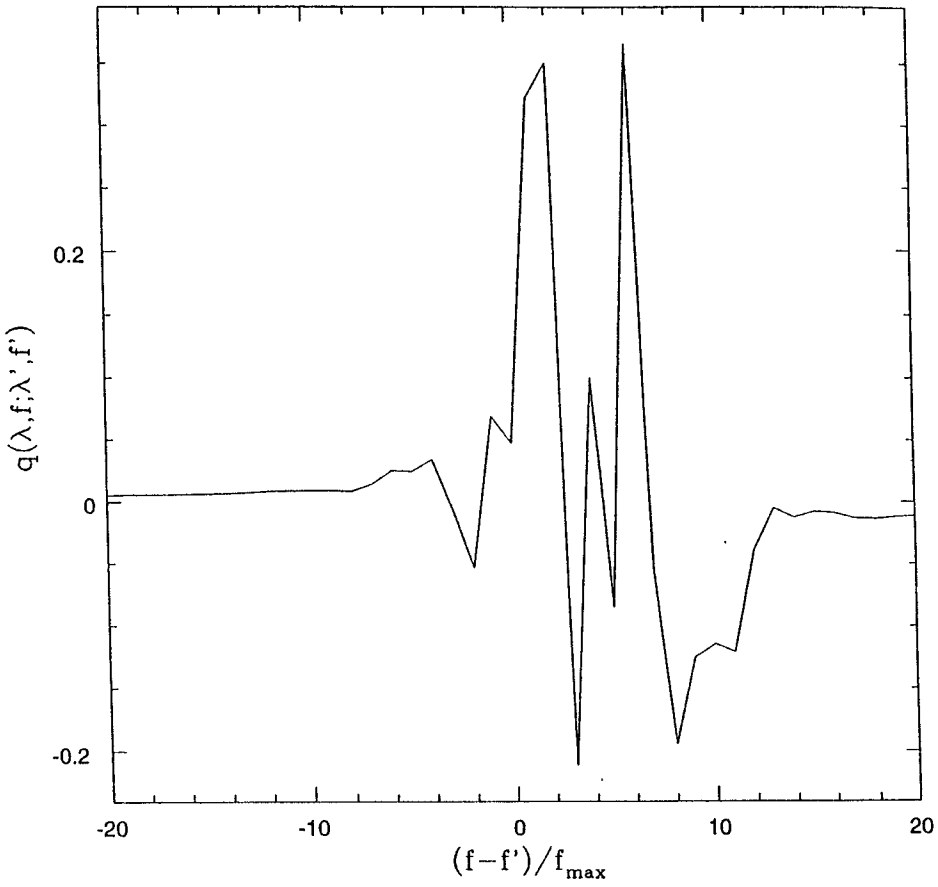

sources with frequencies $f_0 \leq 1\,\text{kHz}$

+ spindown age $\tau = \frac{f}{(df/dt)} \geq 40\ \text{Yrs}$

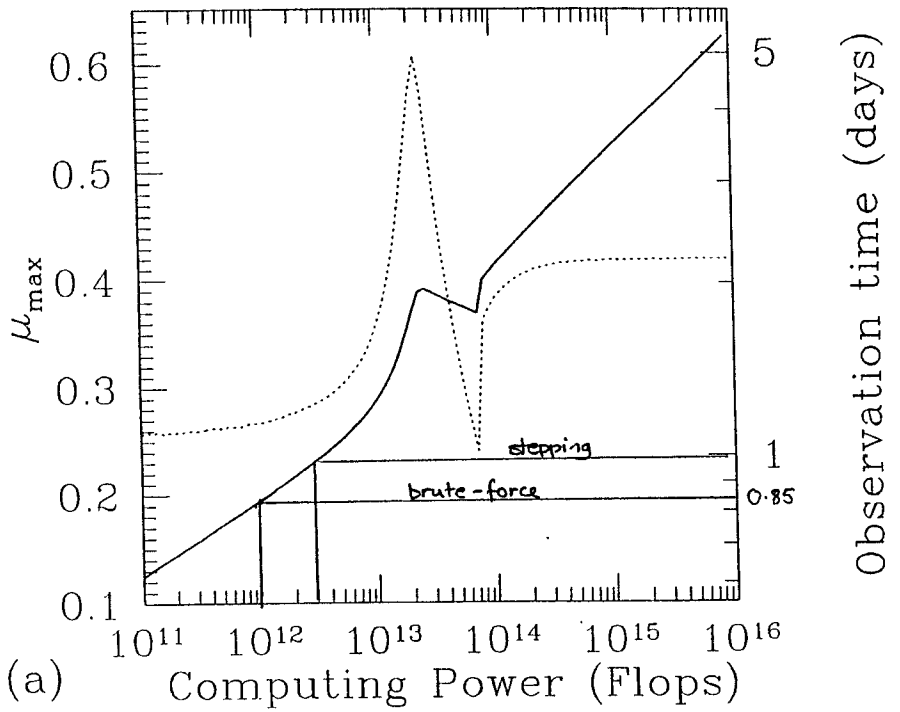

(a)

Hierarchical searches :

Search data stream of $T^{(2)}$ seconds in two stages

Stage 1 :

$\downarrow$ $O(t) \sim T^{(1)}$ seconds @ 16 kHz

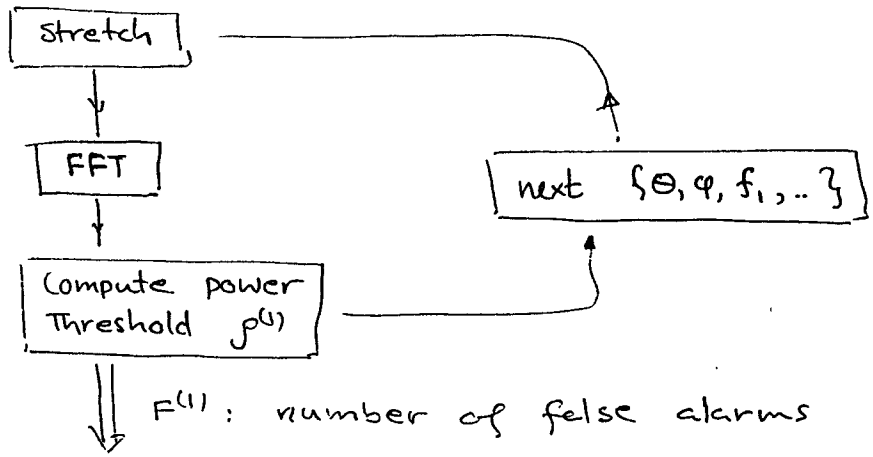

Stage 2 : Follow up false alarms only

$\downarrow$ $O(t) \sim T^{(2)}$ seconds @ 16 kHz

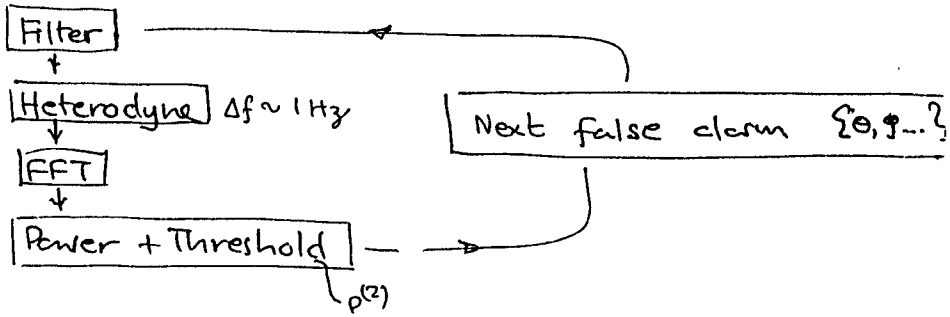

Now, maximize expected SNR of second stage

$$\Theta \propto \frac{T^{(2)}}{\left(\frac{\rho^{(2)}}{S_n(f)} - 1\right)}$$

subject to constraint

$$PT^{(2)} = N_{op}^{(1)} + N_{op}^{(2)}$$

$PT^{(2)}$: available computing power

$N_{op}^{(1)}$: number of floating point operations on 1st stage

$N_{op}^{(2)}$: floating point operations on 2nd stage

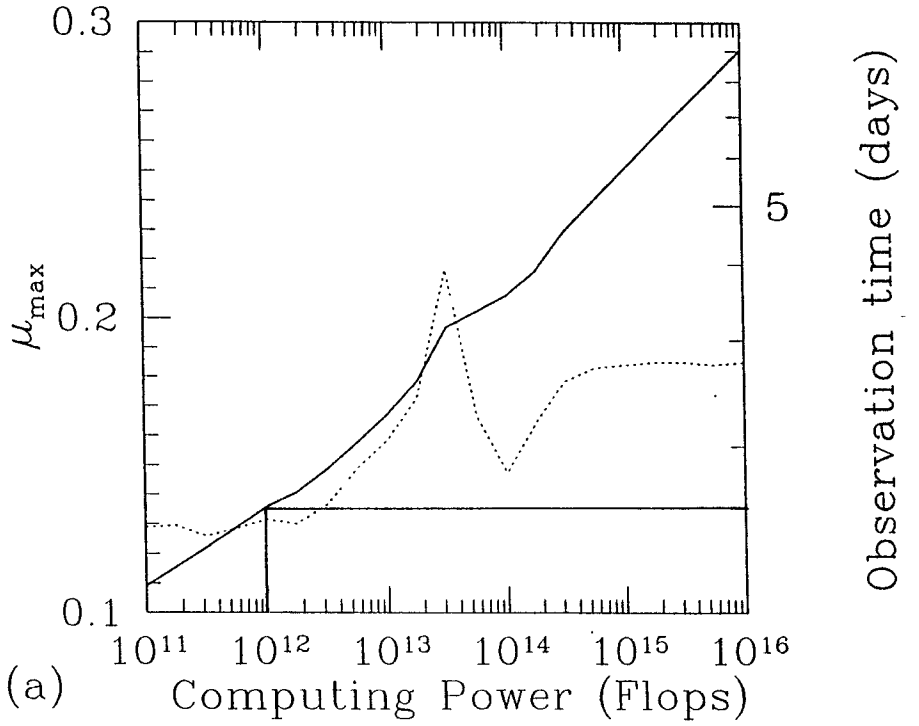

(a)

Future:

1. Alternative types of hierarchical search strategies — e.g.

2. Exploration of stepping — may be very efficient to step in spindown space

Conclusion: key to looking for continuous waves will be directed searches of portions of the sky — e.g. galactic plane.

MASSIMO CERDONIO

"ALMOST" ISOTROPIC SKY COVERAGE FOR G.W. BURSTS OF THE UPCOMING WORLD NETWORK OF INTERFEROMETRIC AND BAR DETECTORS

M.C., P.L. FORTINI, A. ORTOLAN, S. VITALE

motivation

- BY 2001 MANY DETECTORS VARIOUSLY LOCATED AND ORIENTED ON THE (ROTATING) EARTH SURFACE WILL BE OPERATING WITH COMPARABLE SENSITIVITY FOR MS BURST G.W. SIGNALS
- CURIOSITY: HOW TO "CORRELATE" THEIR OUTPUTS FOR A MOST EFFICIENT SEARCH AND A MOST CONFIDENT DETECTION

(VERY) PRELIMINARY ..... DON'T CHANGE YOUR P.M. JUST SAMPLE DATA FAST FOR LINE ANALYS

COINCIDENCE EFFICIENCY

Montecarlo 50000 signals
random direction, polarization, distance

$$\eta \simeq 0.4 \left(\frac{0.01}{\varepsilon_{GW}}\right)^{1/3} \left(\frac{h_{min}}{3\times10^{-20}}\right) \left(\frac{T}{4}\right) \left(\frac{d}{1\,Mpc}\right)$$

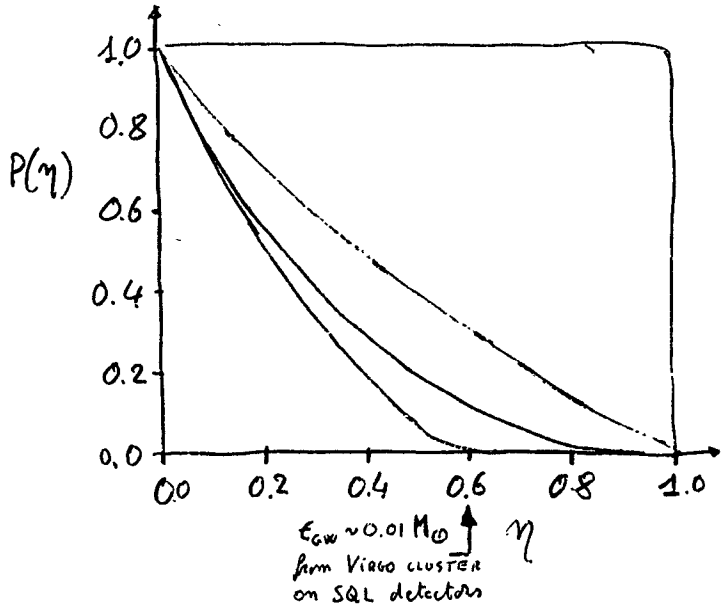

— AURIGA + NAUTILUS

— VIRGO + AURIGA , LIGO 1 + LIGO 2

— LIGO + VIRGO

— "GLOBAL" MULTI OBSERVATORY DETECTOR

ADAPT TO THE NETWORK

OF INTERFEROMETERS 2 LIGO
VIRGO
GEO
TAMA

AND BARS NAUTILUS
AURIGA
ALLEGRO
.....

THE SOLUTION OF THE "INVERSE PROBLEM" WORKED OUT (PRL 71, 4102 (1993)) FOR THE "6 BARS OBSERVATORY"

↓

usefull exercise to see how to get:
- ISOTROPIC SENSITIVITY
- VETOS AGAINST SIGNALS

RIEMANN TENSOR SYMM. ← { NON "TRACELESS"
NON "TRANSVERSE"
NON C-VELOCITY PROP.

get g.w. "signature" in the correlation

"6 bars" NETWORK

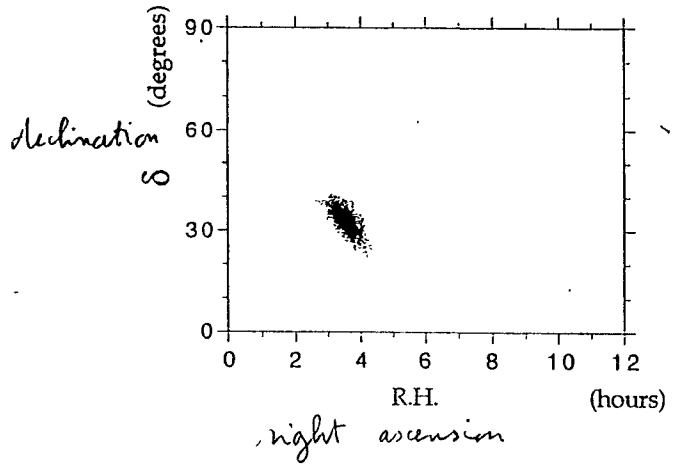

Fig. 1 Scatter plot of reconstructed positions of a source located at right ascension *R.A.* = 3*h* 35*m* and declination $\delta = 32°\ 18'$ over 3000 attemps. The incoming gravitational pulse is assumed linearly polarized with polarization angle $\psi = 30°$, the estimate of which has the same accuracy of the other two angles. The SNRs of the 6 BARS due to their different figure pattern, are respectively 4.5, 6, 1, 9, 10, 1.

DETECTORS ALONG THE AXIS OF THE REGULAR ICOSAEDRON

$SNR \equiv h_{pulse}/h_{min}$ SIGNAL $h_{pulse}\,\delta(t)$

an exercise ...

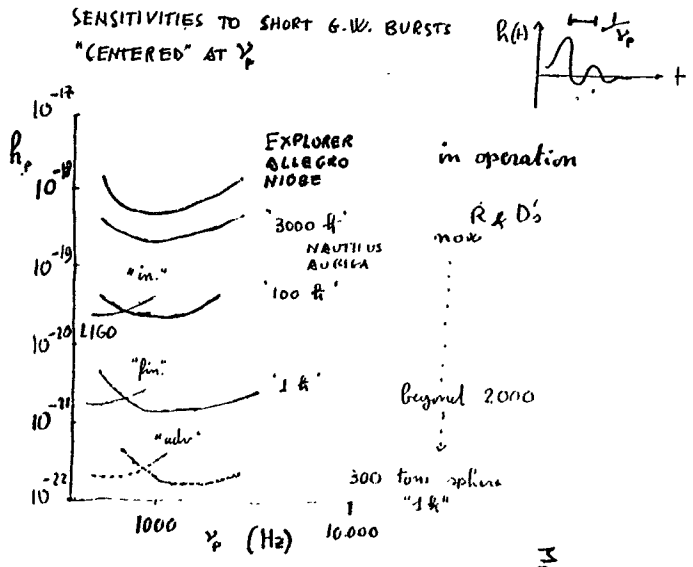

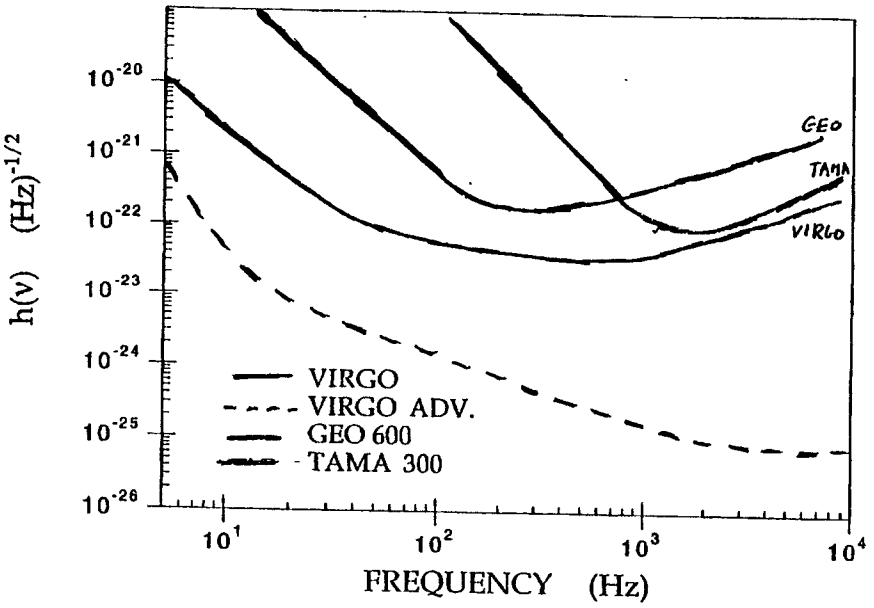

Maximum GEOMETRIC TUNED INPUT W/O1/2

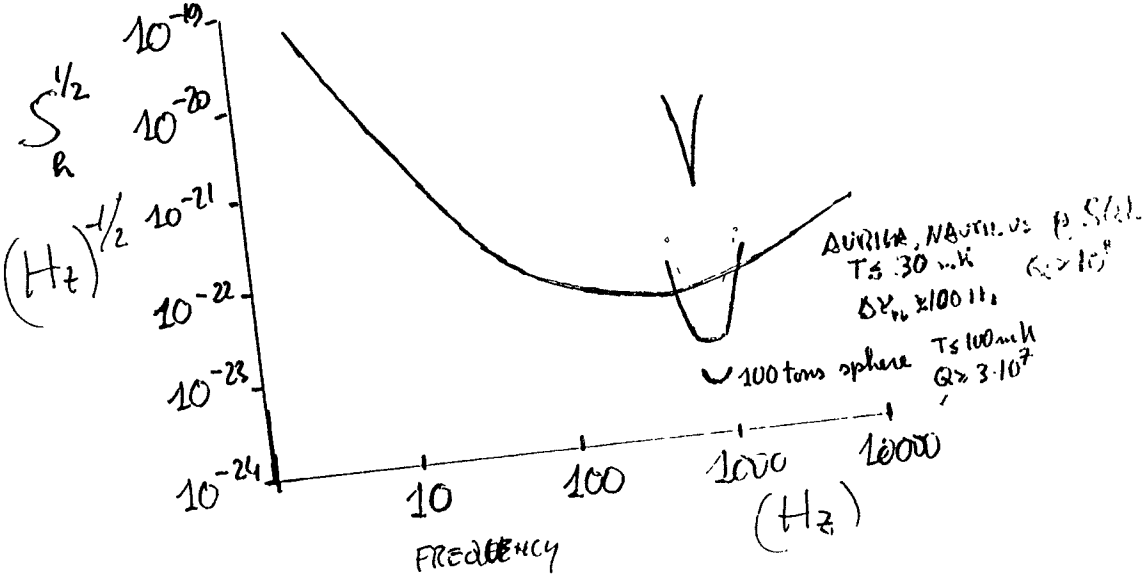

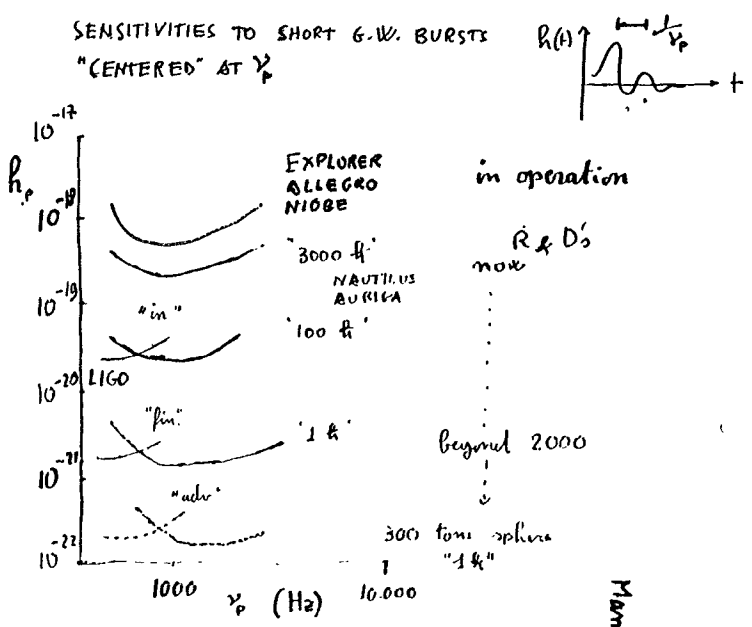
SENSITIVITIES TO SHORT G.W. BURSTS
"CENTERED" AT ν_p
h(t)
t
h_p
EXPLORER
ALLEGRO
NIOBE
in operation
R & D's
now
"3000 ft"
NAUTILUS
AURIGA
"100 ft"
"in"
LIGO
"1 k"
"fin"
beyond 2000
"adv"
300 tons sphere
"1 k"
1000
1
10.000
ν_p (Hz)

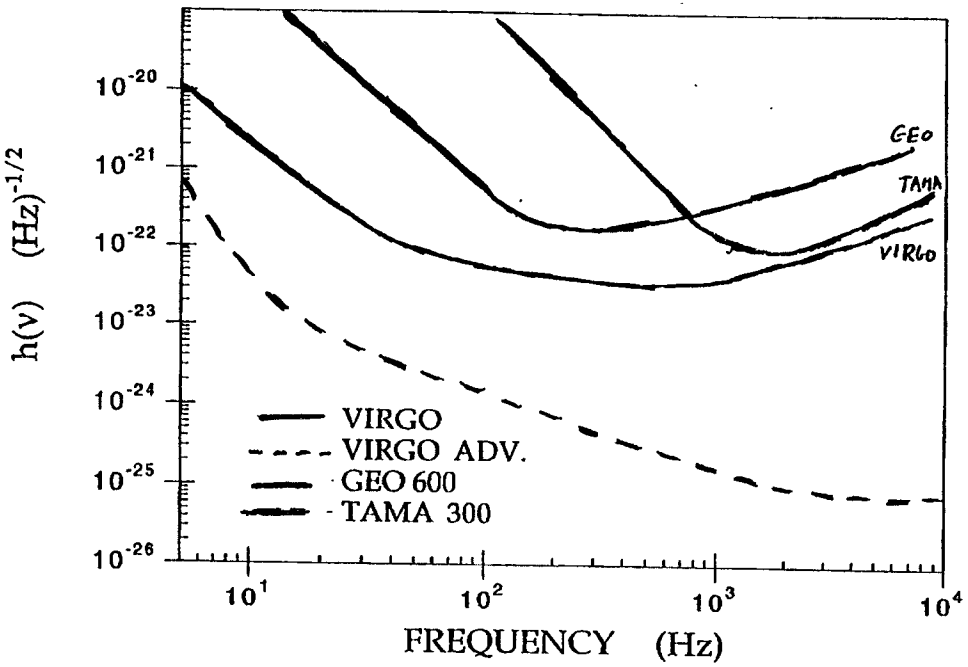
h(ν) (Hz)$^{-1/2}$
GEO
TAMA
VIRGO
VIRGO
VIRGO ADV.
GEO 600
TAMA 300
FREQUENCY (Hz)

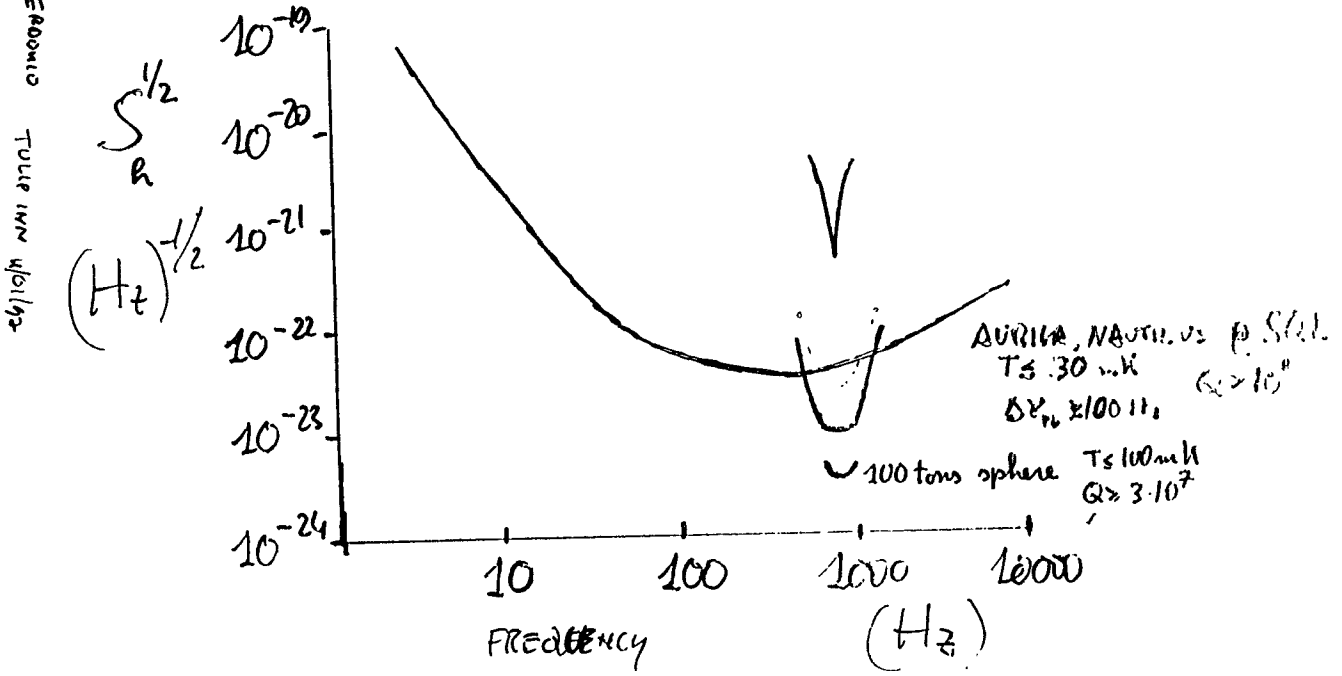
Maximum GEOMIO TULLIO INV. 1/0/93
$S_h^{1/2}$
$(Hz)^{-1/2}$
AURIGA, NAUTILUS & SOL.
T≤ 30 mK
Q≥ 10⁶
100 tons sphere
T≤ 100 mK
Q≥ 3·10⁷
FREQUENCY (Hz)

Intercontinental Network of Gravitational Waves Detectors

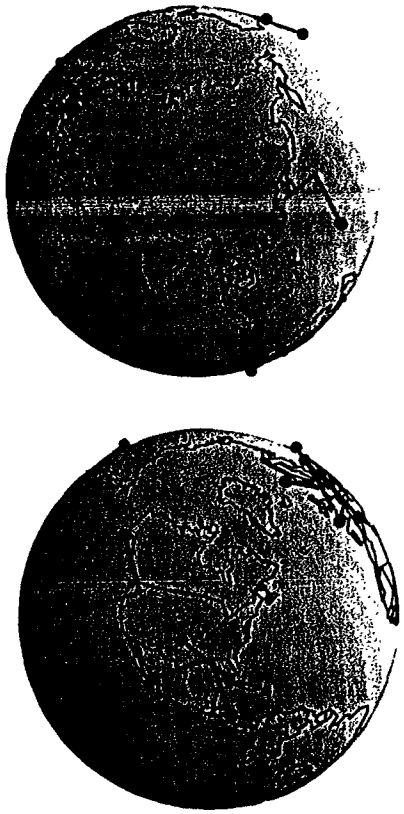

- AURIGA @ Legnaro (Italy)
- NAUTILUS @ Frascati (Italy)
- EXPLORER @ CERN (Switzerland)
- ALLEGRO@ Baton Rouge (USA)
- NIOBE @ Perth (Australia)
- VIRGO @ Pisa (Italy)
- LIGO1 @ Livingston LA (USA)
- LIGO2 @ Hanford WA (USA)
- TAMA300 @ Tokyo (Japan)
- GEO600 @ Hannover (Germany)

Searching for GW short (δ-like) bursts

Response of a gw detector at location $\mathbf{r}^\alpha$ and orientation $\mathbf{n}^\alpha$ ($\mathbf{m}^\alpha$) to a gw signal ($R_{0i0j} = {}^{TT}\dot{h}_{ij}/2c^2$) of amplitude h_b, incoming from the direction $\mathbf{k}$ and with polarizantion ψ

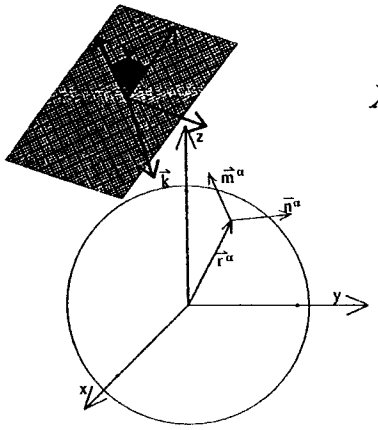

$$X^\alpha(t) = h_b\ F^\alpha(\vartheta,\varphi,\psi)\times \\ \times f(t - t_0 - \vec{r}^{\,\alpha}\cdot\vec{k}(\vartheta,\varphi))$$

(after Wiener filtering)

Figure pattern

$$F^\alpha(\vartheta,\varphi,\psi) = \begin{cases} R_{ij}\,(n^i n^j)^\alpha & \textit{Bars} \\ R_{ij}\,(n^i n^j - m^i m^j)^\alpha & \textit{Interf.} \end{cases}$$

R_{ij} polarization tensor with the distinctive properties of Transversality and Tracelessnes of the gw Riemann tensor

The inverse problem has to be solved

SEPARATE THE SEARCHING PROCEDURE

In general to search for a signal buried in additive gaussian noise, the classical procedure is to built a likelihood function and to maximize it over the signal space parameters (amplitude h_0, direction **k** and polarization ψ).

A less demanding computational procedure

- Estimate the arrival time (on at least 3 detectors of the network) and determine the direction **k**
- Shift all the detector responses by the corresponding delay time
- Solve the local inverse problem: estimate of total energy, direction and polarization of the burst
- Test of (at least one) distinctive Riemann simmetries of the burst ($R^i{}_l=0$, $k^j R^i{}_j=0$)

Arrival time estimate

Output of the optimal Wiener filter matched to a δ function at the detector input

$$X(t) \propto \int_{-\infty}^{+\infty} \frac{e^{i\omega t} d\omega}{S_h(\omega)}$$

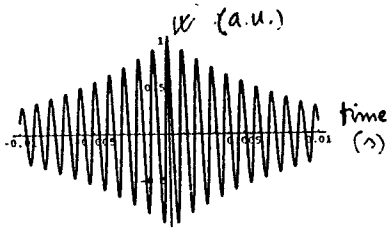

BAR

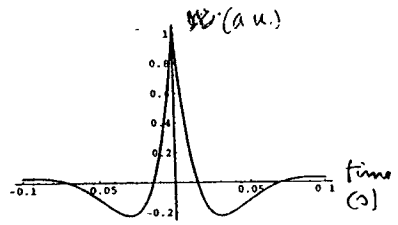

INTERFEROMETER

$$\sigma_t = \begin{cases} \dfrac{0.2\ ms}{SNR} & Bar \\ \dfrac{2\ ms}{SNR^2} & Interf. \end{cases} \qquad SNR = \frac{h_b}{h_{\min}}$$

- Notice: to solve peak ambiguity bar detectors require SNR≥10 and $\Delta\nu_{pd} \approx 50$ Hz
- Actual network: need burst with SNR≈ 4÷5 on 3 interferometes clustered in less than 42 ms

↳ the trigger

Solution of the local inverse problem

The 6 response of the detectors are linear combination of the independent element of the simmetric matrix R_{ij}

$$X^\alpha = R_{ij}(n^i n^j)^\alpha \qquad \textit{Bar}$$

$$X^\alpha = R_{ij}(n^i n^j - m^i m^j)^\alpha \quad \textit{Interf.}$$

$\Rightarrow$ each matrix element R_{ij} is a linear combination of the X^α

$$R_{ij} = \sum_\alpha C_{ij}^\alpha X^\alpha$$

(Note: the solution exists if the detector axes are not parallel and there is at least a bar in the network)

The 3 invariants of the matrix R under the rotation group:

- Linear $T \propto Tr(R)$: must be zero for a true gw burst
- Quadratic $E \propto Tr(R^2)$: total burst energy in the network
- Cubic $D \propto Tr(R^3)$: transversality of the wave (difficult to use)

If the detector outputs are pure gaussian stochastic processes with the same standard deviation h_{min}

- T is gaussian distributed with zero mean and standard deviation $\approx 3 \div 4\ h_{min}$
- E is χ^2 with 6 degree of freedom distributed with mean and standard deviation $\approx (4 \div 5\ h_{min})^2$

Reduction in the burst amplitude sensitivity of the network in respect to best orientation

- 4 interferometers (LIGO1,VIRGO,TAMA,GEO)
- 2 bars (AURIGA+25°,LSU–30°)

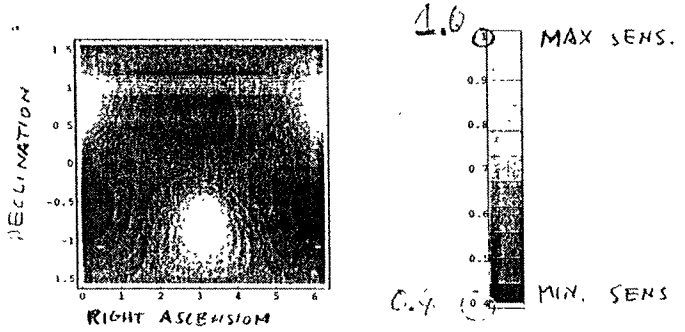

Average on polarizations

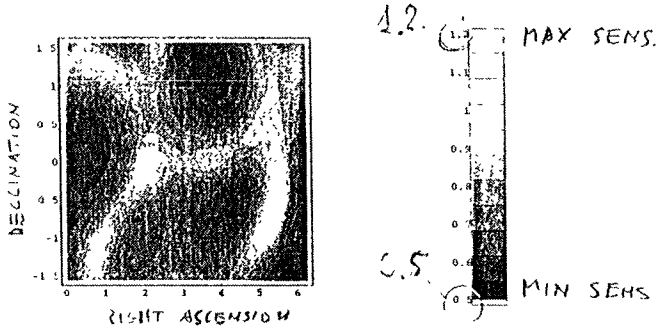

ψ=0 polarization

BURST SEARCHES: if, when and how ×3
share the data

∴ assumptions

- NO SET OF "SAME CONTINENT" DETECTORS IS EXPECTED TO GIVE CONVINCING COINCIDENCES ?????
- CORRELATIONS (= INT. COLLAB.) NEEDED
- RESPONSIBILITIES AND RIGHTS ABOUT CLAIMS MUST REMAIN DISTINCT (in particular for the teams producing the data)

∴ possible solution (a personal view)

- "FAST" DATA ACQUISITION AND FULL ARCHIVING
- SAME TIME FULL RELEASE (except periods of specified ill funct.) WITHOUT MANIPULATION TO EACH AND ALL THE TEAMS OF A SET LINKED BY A MOU → the INT. COLL.
- EACH TEAM OR SUBSET OF TEAMS OF THE INT. COLL. HAS A RIGHT TO PERFORM ITS OWN ANALYSIS
- EACH TEAM OR SUBSET OF TEAMS HAS A RIGHT TO MAKE CLAIMS (AND/OR "COUNTERCLAIMS") BASED ON THEIR OWN ANALYSIS

∴ by laws

- INITIALLY THE INT. COLL. MAY BE RESTRICTED TO...

Saturday AM A. Advanced Detectors in the Future
February 1 Chair: A. Giazotto

8:00	R. Stebbins(JILA)	A NASA-Led Version of LISA
8:30	Discussion	
8:40	M. Choptuik(UT-Austin)	Binary Black Hole Grand Challenge Update
9:10	Discussion	
9:20	Coffee Break	

B. Collaboration Formation for Advanced Detectors II
Chair: H. Ward

9:35	S. Finn(Northwestern)	Summary of Opinions Expressed at Meeting
10:05	Discussion	
10:15	P. Saulson(Syracuse)	Where Do We Go From Here?
10:40	Discussion	

A NASA-Led Version of LISA

Robin T. Stebbins
JILA - University of Colorado

Aspen Winter Conference on
Gravitational Waves and Their Detection
Aspen, CO
26 January - 1 February 1997

LISA mission concept

- Interferometric measurement over 5×10^6 km provides very high strain sensitivity from 10^{-4} to 1 Hz.
- Heliocentric orbit is a very benign environment.
- "Drag-free" design further reduces disturbances from the solar wind and photon pressure.
- Laser transponder scheme offset locks local laser to the received beam.
- Within each corner spacecraft of a triangular formation, lasers for both arms are intercompared by phase reference beams. Optical path differences, laser frequency noise and clock noise are determined.
- Third arm provides additional scientific information and redundancy. All three spacecraft are identical.

Extragalactic gravitational wave science

- Objective: To detect and study gravitational wave signals from sources involving massive black holes (MBHs) with masses of 10^3 to 10^8 $M_\odot$.
- Possible sources:
  - 5 or 10 $M_\odot$ black holes (BHs) or compact stars orbiting 10^5 to 10^7 $M_\odot$ MBHs.
  - MBH-MBH binaries formed by growth of several seed BHs in the same galactic nucleus.
  - MBH-MBH binaries formed by mergers of galaxies or pre-galactic structures that already contain MBHs.
  - Sudden formation of MBHs.
- It appears likely that at least one of these types of binaries can be detected and studied by LISA.

Galactic gravitational wave science

- Objective: To investigate the number and distribution of different types of short period binaries in our galaxy.
  - Neutron star binaries: hundreds will be detectable and their locations can be determined throughout the galaxy.
  - Close white dwarf binaries (CWDBs): thousands above about 1 mHz are expected to be resolvable.
  - Interacting white dwarf binaries (IWDBs): many will be observable, with several known except for possible frequency ambiguities.
  - Other compact binaries: BH-neutron star and BH-BH binaries are expected to be detectable.
  - CWDB background: below about 1 mHz, the very large number of CWDBs will give a confusion-limited background.

Fundamental physics and cosmology

- Objective: To test general relativity in the high field limit, and to search for cosmological information on gravitational background radiation.
  - If BH-MBH or MBH-MBH coalescence signals are seen, they will provide a unique test of general relativity at extremely high fields. Even slight deviations from the dynamical predictions of the theory would be detectable.
  - Cosmological background radiation could be detected near 10 mHz with a sensitivity of 10^{-10} to 10^{-11} of the closure density.

History

- Early NASA studies
- M3 - 4 spacecraft, proposed as a cooperative ESA/ NASA mission, studied for ESA only.
- Cornerstone - 6 spacecraft, ESA only. Selected for Horizons 2000 Programme. Launch in 2017.
- Goals of a NASA version
  - Cheaper - $300 M target
  - Faster - 2004 launch
  - Same science goals
  - Basis for a cooperative mission with ESA
- Team-X study, 14-17 Jan. '97

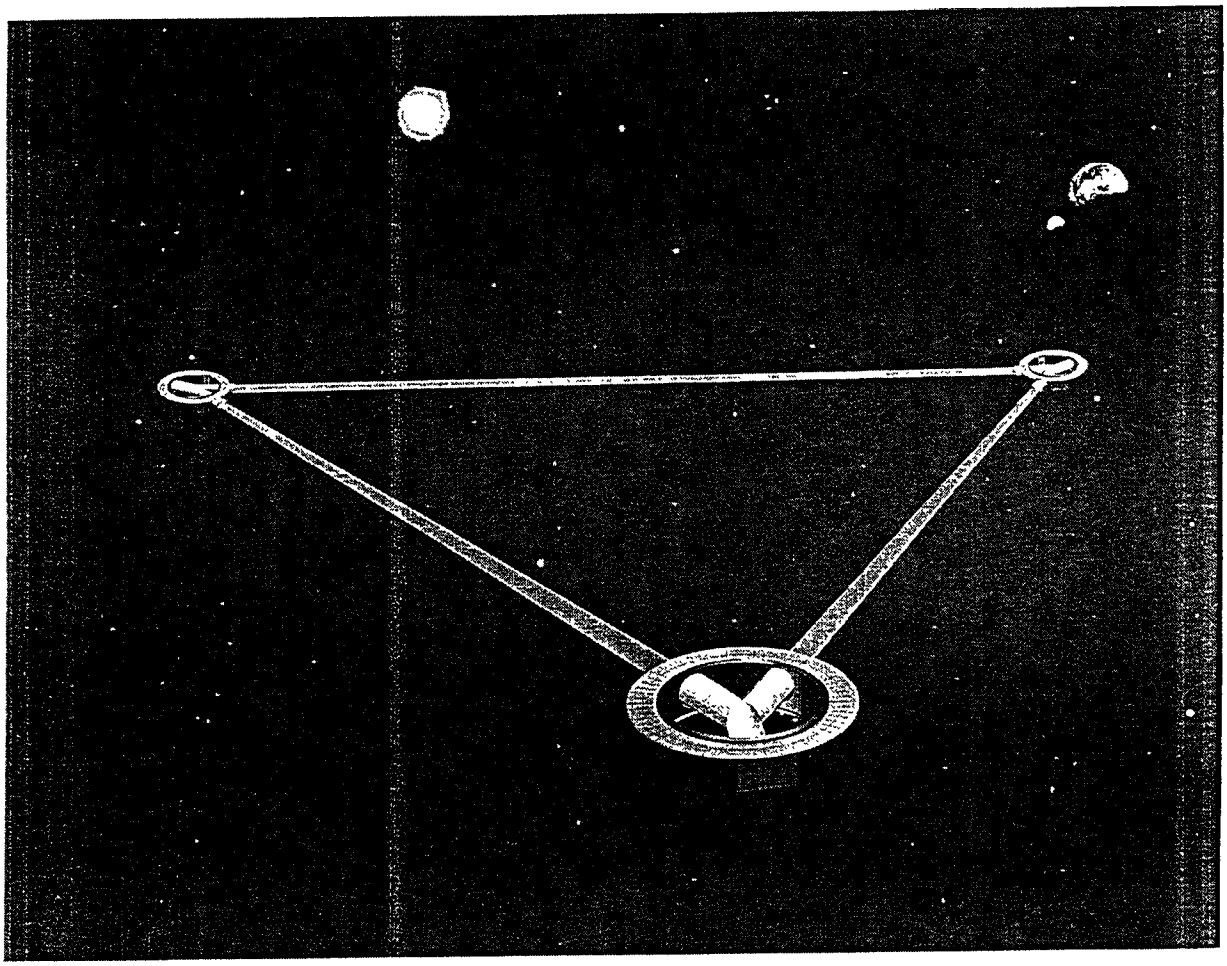

New Elements in the NASA Version of LISA

- 3 Corner spacecraft, full "science" redundancy
- Delta II 7925H
- Solar electric propulsion
- Phased array telecom
- Rely on European partners for drag-free sensor, lasers, FEEPs and telescope
- Team-X study
  - Specialists in propulsion, trajectory, launch vehicle, attitude control systems, command and data systems, instruments and operations, ground operations, telecom, structures, thermal engineering, power systems, spacecraft systems, and costing.
  - "Coordinated" engineering through spreadsheet web and discussion.
  - Databases, realism and models

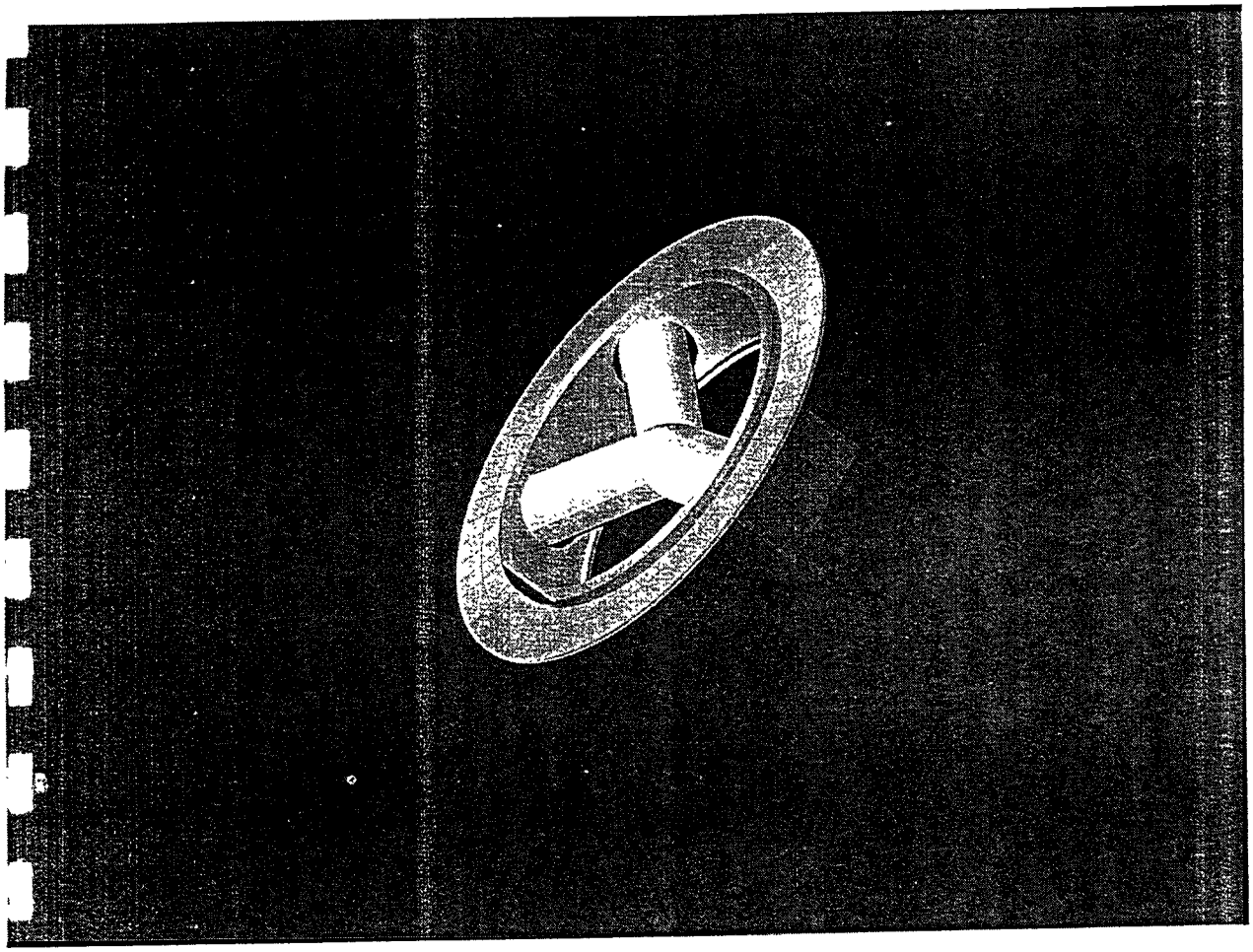

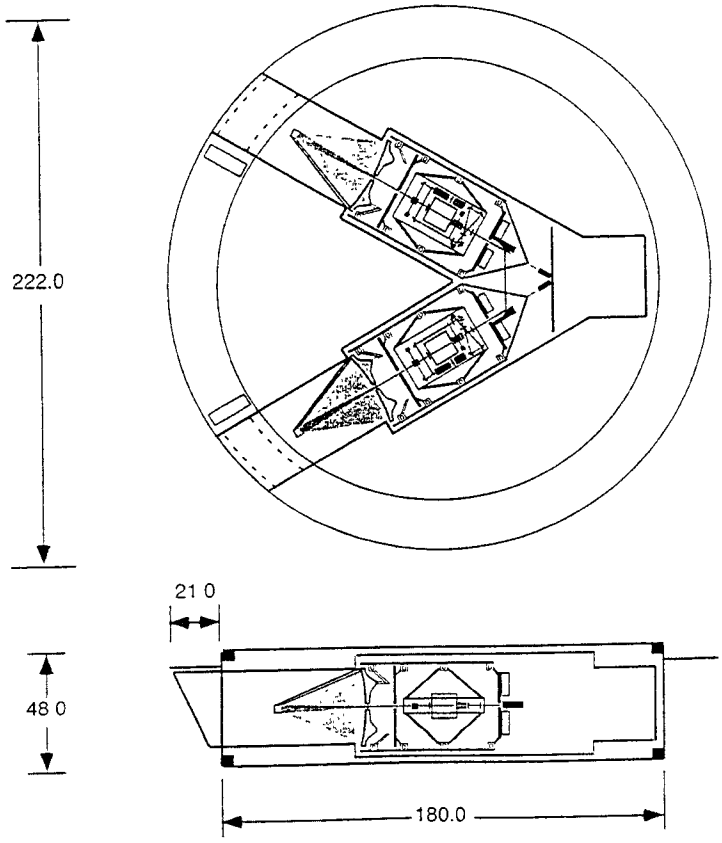
222.0
21 0
48 0
180.0

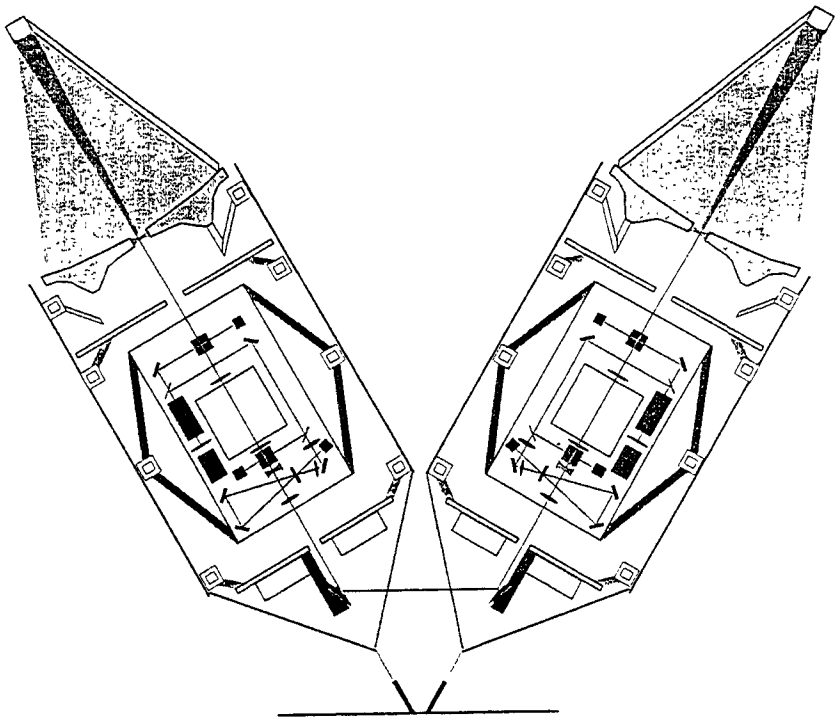

Sciencecraft - Structure

- Y-shaped payload
- Composite construction, rather than carbon-carbon
- Two optical benches with optics, modulator, drag-free sensor, laser stabilization cavity, photodiodes
- Two electronics disks with USO, capacitive sensing pre-amps, photodiode pre-amps
- Radiator disk with 4 lasers

Sciencecraft - Thermal

- Top and bottom shields, with appropriate coating
- Tensioned fiberglass bands
- Sciencecraft protected by the propulsion module during cruise.

Sciencecraft - Attitude and Position Control System (ACS)

- Science payload provides angle and displacement signals.
- Coarse and fine sun seekers
- Four star tracker heads, processing by sciencecraft computer (10 MIPS!).
- Fiber optic gyros for convenient rate information

Sciencecraft - Miscellaneous

- Command and Data (CDS) System
  - RS-6000 (15-20 MIPS)
  - VME crates
- Propulsion
  - FEEPs: cesium ion thrusters, 100 μN thrust, 0.1 μN noise (ESA/Centrospazio supplied)
  - Austrian alternative (Seibersdorf), based on indium (flight heritage as discharge system)
- Power
  - Fixed solar array on shield
  - 3.25 m^2
- Systems
  - 262 kg
  - 196 watts

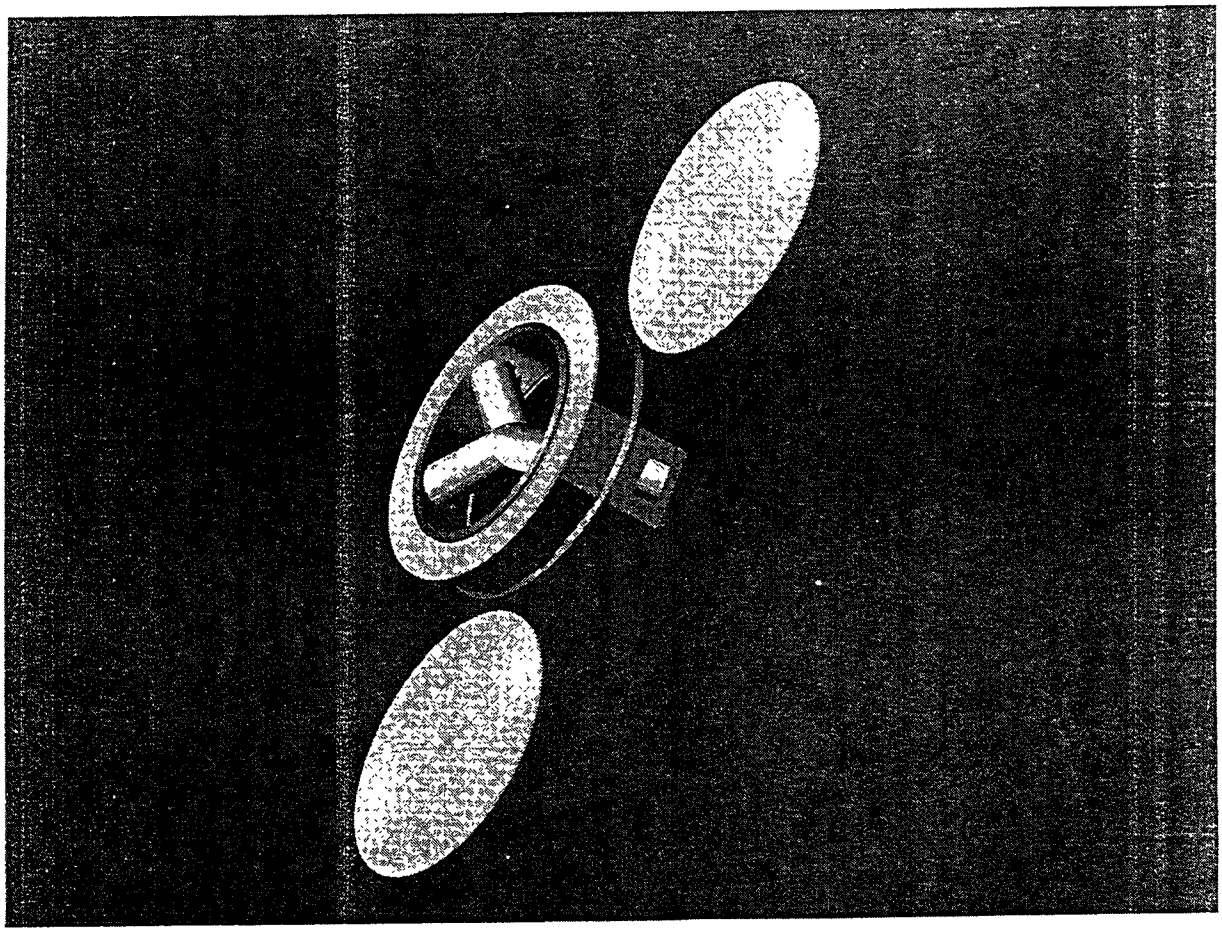

Propulsion Module - Propulsion

- 18 mN Hughes XIP 100 thrusters (xenon)
- Now in flight certification. Planned for 60 missions in next few years (station keeping for telecommunications satellites).
- 13 cm nozzle, 25 cm OD, 25 cm long
- 35 kg (including gimbals), 440 w
- Gimbals
- 23 kg fuel (vs. 134 kg for chemical)
- Hydrazine attitude control system, 8 nozzles, 5 kg fuel, 2 tanks, 10 kg hardware
- Saved 80 kg/spacecraft!

Propulsion Module - Miscellaneous I

- Structure
  - Composite ring
  - SEP engine vectored through CM, exhausting through ring
  - SEP engine gimbaled.
  - Pyro bolts for separation
- Telecom/ground - none
- Thermal - heaters for hydrazine tanks
- ACS - tip solar arrays
- CDH - On sciencecraft, control valves of attitude thrusters

Propulsion Module - Miscellaneous II

- Power
  - 2 flop-out panels, ~4 m^2
  - • Special power control unit
- Trajectory
  - 300/390 days propulsion
  - Problem: thrust angle/sciencecraft solar array
- Systems
  - Mass 175 kg
  - Power 573 w

Launch Vehicle

- Delta II 7935H
- Third stage STAR 48B
- Despin by PAM-D
- 9.5 ft. fairing
- C3 (hyperbolic excess energy) - 1.2 $(km/s)^2$
- Launch vehicle lift capacity - 1388.2 km
- With 30% mass margin, 2% (29 kg) over

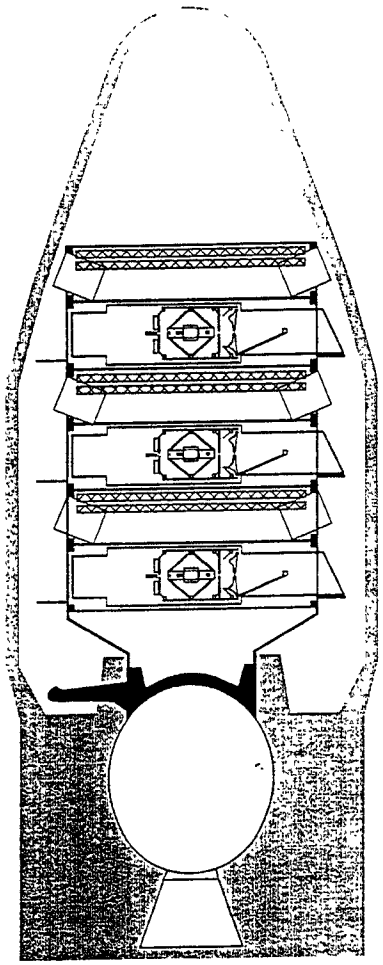

Costing

	Project Total	European Contributions	Net to NASA
	$M (1997)	$M (1997)	$M (1997)
Project Costs Through Phase D	$314	$52	$262
Reserves (17%)	$53	$9	$45
Project Total before Launch	$367	$61	$307
Launch Vehicle	$59		$59
Total with Reserves	$426	$61	$366
Phase E No Science, with Reserves	$25	$2	$22
Phase E Science, with Reserves	$14	$5	$9
Total Life Cycle Costs	$465	$68	$397

Schedule

- Phase A (industrial design study) 12 months, start Jan. '99.
- Phase B (engineering design) 18 months
- Phases C/D (construction) 24 months
- 1 July 2004 launch
- 13 mo. cruise
- 3 yr operations
- Consumables for 10 yrs.

Conclusions

- Status
  - We have conceptual design which is smaller, cheaper, faster and preserves the science.
  - The technology appears to be as ready as other missions in the Structure and Evolution of the Universe (SEU) theme.
  - The initial cost is about the right size, but needs some attention.
- What's Next
  - Seeking to be a recommended mission in the strategic plan for 2000-2005 by the SEU Subcommittee (SEUS, a.k.a. The Blandford Committee)
  - Further small studies and a Team-X update.

BINARY BLACK HOLE GRAND CHALLENGE UPDATE

- Formalisms
- The Initial Value Problem
- Black-Hole-Excising Techniques
- Computational Infrastructure
- Current State and Outstanding Problems

Matthew Choptuik, The University of Texas, Austin TX
Gravitational Waves and Their Detection
Aspen CO, Feb 1, 1997

Supported by NSF PHY9318152 (ARPA supplemented)

Binary Black Hole Grand Challenge Personnel

http://www.npac.syr.edu/projects/bh/

- UT Austin: MATZNER, BROWNE, CHOPTUIK, Huq, Hirschmann, Parashar; Nielsen, Liebling
- NCSA/Potsdam: SAIED, SAYLOR, SEIDEL, SHAPIRO, SMARR, Abrahams, Anninos, Baumgarte, Masso
- UNC Chapel Hill: EVANS, YORK; Rupright
- Cornell U: TEUKOLSKY, Cook, Scheel; Landry
- Syracuse U (NPAC): FOX, Haupt, Klasky
- U Pittsburgh: WINICOUR, Gomez, Marsa; Lehner
- Northwestern U: FINN, Kidder
- Penn State: LAGUNA, Papadopoulos
- Washington U: Suen (associate)
- University of South Africa: Bishop (associate)

The 3 + 1 (ADM) Formalism

- Pose general relativity as a dynamical theory (geometrodynamics).

  View geometry of spacetime as "time history" of the geometry of a spacelike hypersurface ("instant of time"), $\Sigma(t)$

- Geometry of spacetime is described by a 4-metric, ${}^{(4)}g_{\mu\nu}$
  Geometry of Σ is described by a 3-metric, g_{ij}

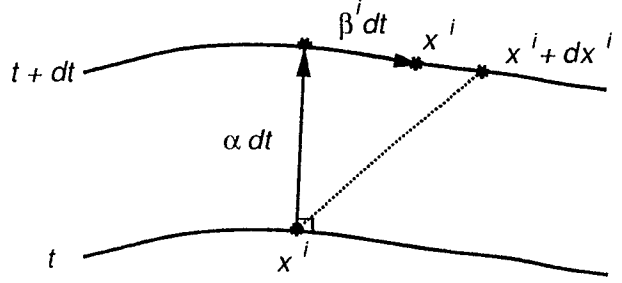

$$
\begin{aligned}
{}^{(4)}ds^2 &= {}^{(4)}g_{\mu\nu}dx^\mu\, dx^\nu \\
&= -\alpha^2\, dt^2 + g_{ij}\left(dx^i + \beta^i dt\right)\left(dx^j + \beta^j dt\right)
\end{aligned}
$$

- Two types of variables:

  1) Kinematical: lapse function, α and shift vector, β^i

  2) Dynamical. three metric, g_{ij}

The 3 + 1 (ADM) Formalism (cont.)

- Extrinsic curvature: K_{ij}

  Describes manner in which $\Sigma(t)$ is embedded in space-time. Can be viewed as the "velocity" of g_{ij}

$$K_{ij} = \frac{1}{2\alpha}\left(-\frac{\partial g_{ij}}{\partial t} + D_i\,\beta_j + D_j\,\beta_i\right)$$

  where D_i is the 3-covariant derivative: $D_i\, g_{ij} = 0$

- Einstein equations (vacuum):

$$G_{\mu\nu} = 0$$

  Constraint equations:

$$G_{0\nu} = 0$$

  Evolution equations:

$$\frac{\partial g_{ij}}{\partial t} = -2\alpha K_{ij} + D_i\,\beta_j + D_j\,\beta_i$$

$$\frac{\partial K_{ij}}{\partial t} = \mathcal{L}_\beta K_{ij} - D_i D_j \alpha + \alpha\left(R_{ij} - 2K_{ik}K^k{}_j + K_{ij}K\right)$$

  where R_{ij} is the 3-Ricci tensor, $K \equiv K^i{}_i$, and $\mathcal{L}_\beta$ is the Lie derivative along β^i.

Hyperbolic Formulations of Einstein's Equations

(York, Choquet-Bruhat, Abrahams, Bona, Masso)

- Standard 3+1 formulation of Einstein's equation yields set of PDEs which is generically non-hyperbolic.

  Possibility of ("gauge") information "propagating" at superluminal speeds: hampers black-hole excising techniques

- Hyperbolic formulation: Characteristic speeds are either 0 (some dynamical variables simply "Lie-dragged" along normal to hypersurfaces) or local light speed. Information only propagates along physical light cones.

  Hyperbolic formulations ("flux-conservative form") in principle allow techniques developed for fluid dynamics to be carried over to NR calculations

  Aids radiation extraction and formulation of boundary conditions (inner and outer)

- Einstein evolution equations:

$$\partial_t u + \partial_i F^i(u) = S(u)$$

  First order flux-conservative, hyperbolic form: $S(u)$ contains no spatial derivatives of dynamical variables, u.

- Possible disadvantage: lose some flexibility in choice of coordinates

The Initial Value Problem for Two Black Holes

(Ō Murchadha & York, Cook et al)

- Constraint equations

$$G_{0\nu} = 0$$

  are generically a system of 4 coupled, non-linear elliptic equations for $\{g_{ij}, K_{ij}\}$; setting up initial data for a general black hole collision is non-trivial

- Key problem: Which of the $\{g_{ij}, K_{ij}\}$ should be freely specified, which should be determined via solution of the constraints?

- General strategy: use conformal scaling and "spin-decomposition" of K_{ij}; constraints $\rightarrow$ system of quasi-linear elliptic equations for four potentials: $\{\psi, X^i\}$

- Momentum constraint can be solved analytically, Hamiltonian constraint requires numerical solution for ψ, typically using multi-grid technique.

$$g_{ij} = \psi^4 \, \hat{g}_{ij} = \psi^4 \, f_{ij}$$

The Initial Value Problem for Two Black Holes (cont.)

- State-of-the-art Hamiltonian Constraint Solver: (Cook). Uses special-purpose Čadež coordinates, (η, ξ, ϕ):

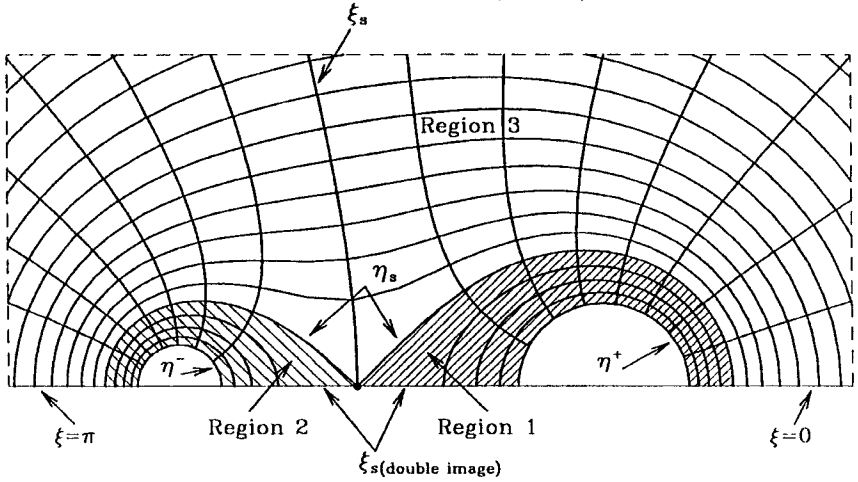

- Discretization is precisely $O(h^2)$, Richardson extrapolation can be applied to get $O(h^4)$ or better results. Solutions can be determined to essentially arbitrary accuracy

- Key remaining problem: How to generate realistic initial data—i.e. data for two holes with relatively small separation but representative of result of inspiral from wide separation.

Black Hole Excising Techniques

- Fundamental Problem: Black hole spacetimes contain physical singularities–apparently must be avoided at all costs in calculations

- Traditional Approach: Use coordinate freedom (choice of lapse and shift) to "freeze out" evolution in vicinity of physical singularity

- Spherically Symmetric Example: Choose coordinates r, t so that metric takes on "time-dependent-Schwarzschild" form:

$$ds^2 = -\alpha(r,t)^2\,dt^2 + \left(1 - \frac{2m(r,t)}{r}\right)^{-1} dr^2 + r^2\,d\Omega^2$$

Consider collapse of ball of matter to form black hole: when horizon formation is imminent, then near the Schwarzschild radius $r = R_S$

$$\alpha \to 0 \qquad \left(1 - \frac{2m(r,t)}{r}\right)^{-1} \to \infty$$

Physical singularity avoided, but coordinate singularity develops, code will crash on the order of black-hole dynamical time, $M = R_S/2$

Black Hole Excising Techniques (cont.)

- Excising Approach (Unruh): By definition, interior of black hole is out of causal contact with exterior spacetime. Simply remove regions inside event horizons from computational domain.

- Event horizon location not known until after computation is completed, use as inner boundary some surface known to lie within the event horizon (EH).

- Apparent horizon (AH): Two surface defined at some instant of time on which divergence of outgoing null rays vanishes—outgoing light rays emanating from surface "hover" at constant radius

- Assuming cosmic censorship, AH will always lie within EH, AH can be located at an instant of time by solving non-linear elliptic equation (finite-difference techniques (Thornburg, Huq) or spectral methods (NCSA/Wash-U, Cornell groups))

- Computational boundary is essentially a characteristic surface: modulo possible problems from non-hyperbolicity, don't need boundary conditions

- Efficacy of approach demonstrated in several spherically symmetric calculations (Seidel & Suen, Scheel et al, Marsa & Choptuik, Anninos et al); now implemented in 3D codes, some encouraging preliminary results (Potsdam/NCSA/Wash U)

Black Hole Excising Techniques (cont.)

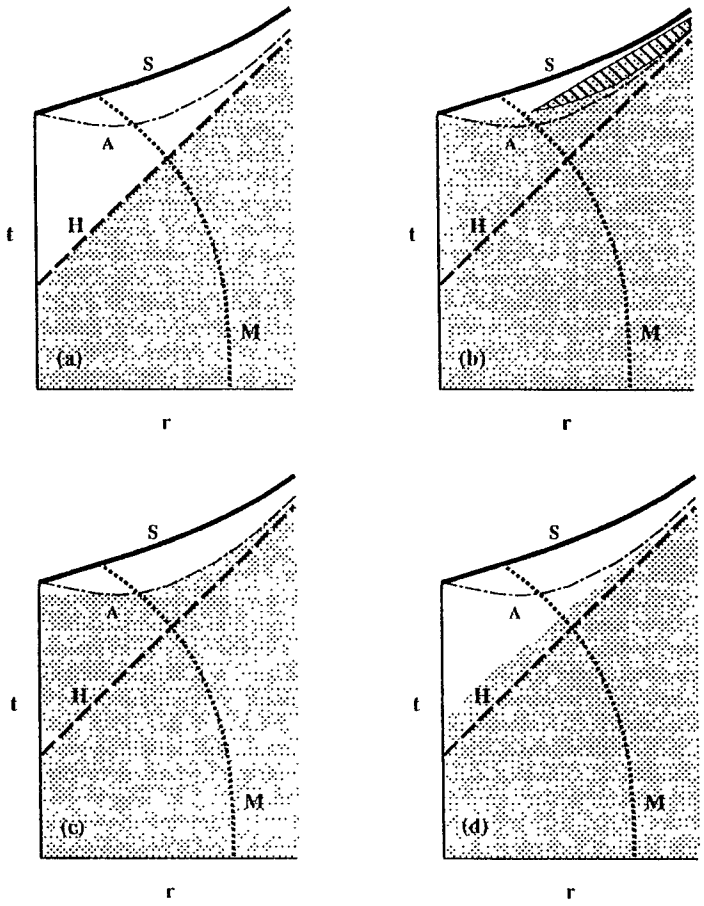

Black Hole Excising Techniques (cont.)

- Sample Calculation: Massless scalar field collapse onto a black hole (**Marsa & Choptuik**)

- Use Ingoing-Eddington-Finkelstein coordinates:

$$ds^2 = a^2 \left((2\beta - 1)\, dt + dr \right) (dt + dr) + r^2 d\Omega^2$$

Continuously track location of outer-most apparent horizon, "throw away" grid-points inside AH.

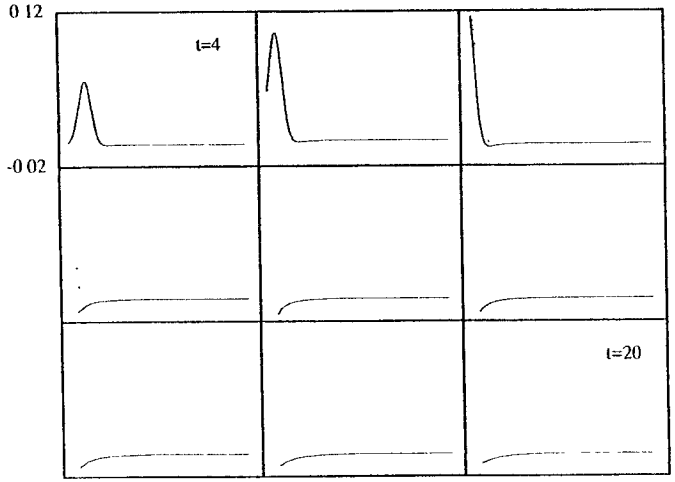

- Plot shows time series of scalar field amplitude $\phi(r,t)$ with apparent horizon at left of each frame; evolution can be continued essentially indefinitely. Mass of scalar field is approximately equal to initial black hole mass.

Computational Infrastructure

- Part of GC charge is to "push the envelope" vis a vis large-scale computation with particular emphasis on the effective use of massively parallel architectures.

- **Observation:** Our codes have tended to be remarkably homogeneous from a "high-level" point of view: Almost all have employed low order (second-order) finite difference techniques on single mesh, and have had the following structure:

```
Read (initial) state
for NUM_STEPS
  for NUM_UPDATES & maybe until convergence
    U (Grid Function(s)) -> Grid Function(s)
  end for
end for
Write (final) state
```

- Most of the hard work in developing a new code involves the construction of stable, accurate updates, **U**

- Also clear that significant dynamic range in black-hole problems such as binary coalescence means that adaptive-mesh-refinement (AMR) algorithms essential for efficient computation

- Ultimate goal: allow relativist to concentrate on developing stable, uni-grid code on serial architecture: parallelism and adaptivity to be "automatically" provided by the infrastructure

Computational Infrastructure: AMR

- Adopted AMR approach due to **Berger & Oliger** which achieves adaptivity via nested structure of individually-uniform grids:

Schematic Adaptive–Mesh Structure

2 : 1 Refinement in Space and Time

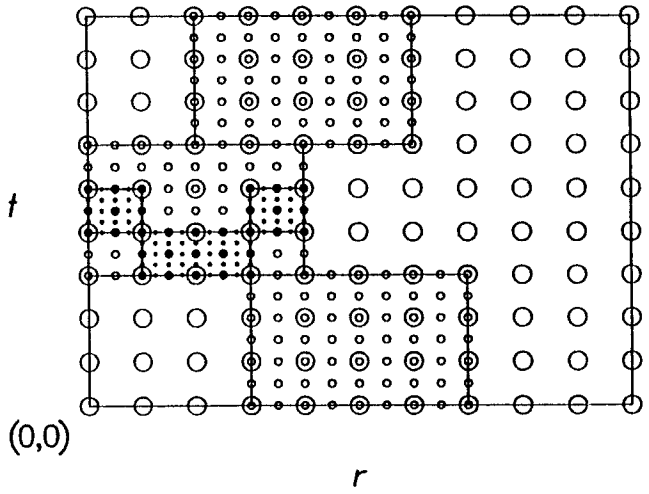

- Placement of component grids controlled dynamically via local truncation error estimates

Computational Infrastructure: DAGH

`http://wwwrel.ph.utexas.edu/Members/parashar/toolkit.html`

- Computer scientists on project (**Parashar, Browne**) have implemented MPI-based infrastructure which provides full support for

  (1) Parallelization (distributed-memory architectures) of regular, lattice-based calculations with local communication patterns (i.e. typical finite-difference codes)

  (2) Berger & Oliger style AMR

- System is called DAGH (Distributed Adaptive Grid Hierarchy), implemented in C++ (using MPI) but designed to easily interface with update routines written in Fortran 77, Fortran 90 or C.

- Key features:

  - Automatic dynamic partitioning and load distribution
  - Shadow grid hierarchy for memory-efficient truncation error estimates
  - Maintains data locality among different refinement levels (space-filling curves)

- Currently runs on IBM SP2, Cray T3D, Networked Workstations (RS6000, SGI)

Computational Infrastructure: Status

- Evaluation and de-bugging continues, but DAGH is already integral part of BBH GC effort, and has been adopted by other groups doing CFD, reservoir simulation, etc.
- Has been used extensively in uni-grid context, particularly by Cornell group working on SP-2, AMR for IVPs (neutron stars)
- Most benchmarks (not many exist!) show very good performance; in several preliminary cases, DAGH application ran faster than hand-coded MPI application
- Full AMR code for 2D linear wave-equation implemented (`Huq`, `Parashar`), currently being rigorously tested; will serve as basis for general AMR driver.
- I/O support remains outstanding issue; collaboration with NCSA groups underway, currently all I/O done through dedicated processors, `.hdf` support provided, hooks for other facilities in place

Current State of Main Code Effort

- Personnel involved in main code efforts (Cornell/Texas/Syracuse) recently agreed to focus effort on ADM code; Empire code (based on Choquet-Bruhat/York hyperbolic formalism) shelved.
- ADM code: Based on traditional 3+1 formalism, currently implemented in Fortran 90, runs on pretty well anything (C90, Power Challenge, SP-2, ...)
- Code implements black-hole excising, as well as "causal differencing" designed to ensure that numerical domain of dependence includes physical domain of dependence
- Resolution limited to 128^3 (unigrid) in both cases; significantly less (65^3) for quick-turnaround runs.
- Code currently *unstable* for single Schwarzschild hole, apparently due to treatment of inner boundary
- Lots of things to try, but nature of equations, differencing, "irregular" inner-boundary makes detailed stability analysis difficult

Additional Outstanding Problems (partial list)

- Choice of coordinate system: Almost certainly most important unsolved problem:
  - Black holes need to move through computational mesh while interiors of holes are simultaneously excised
  - We have essentially no experience with formulating coordinate conditions which will allow for such propagation while remaining non-singular
  - Intrinsic angular momentum of holes will only make matters worse
  - Differencing near horizons may need to be quite intricate to ensure convergent solution
- Will excising work in highly dynamic, asymmetric situations?
- Does horizon excising require a hyperbolic formulation?
- If so, can the problem of "coordinate shocks" (`Alcubierre`) be avoided?

Additional Outstanding Problems (cont.)

- How can we set up near-plunge initial data which is astrophysically realistic?
- How should outer boundary be handled: will AMR techniques and standard radiation extraction methods suffice, or must we match to a characteristic evolution to get an accurate estimate of gravitational radiation?
- AMR technology crucial if we want to solve this problem in the near future: will Berger & Oliger approach suffice, or will some more flexible approach be required?

Prognosis

- PROVIDED
  - Current and future stability problems are overcome expeditiously
  - A good coordinate prescription for generic translating, rotating is found
  - Some form of "outgoing" radiation conditions can be stably imposed at a reasonably finite radius

  THEN odds are good that we'll be able to crudely simulate inspiral within 18 mos. Waveform accuracy???

- Valuable infrastructure *is* being developed
- Nature of calculations is such that once stable, adaptive algorithm is in place, rapid increase in available computational capacity (which we can reasonably assume) will *quickly* lead to more realistic, and accurate simulations
- Have and will learn interesting things about strong-field gravity along the way